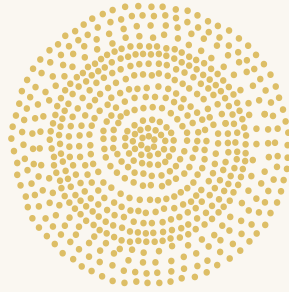


Living on the edge

The functional organization of metabotropic glutamate receptors
at excitatory synapses

Nicky Scheefhals



Living on the edge

The functional organization of metabotropic glutamate
receptors at excitatory synapses

Nicky Scheefhals

ISBN: 978-94-6458-535-3

DOI: 10.33540/1224

The studies described in this thesis were performed at the division of Cell Biology, Neurobiology and Biophysics at the Faculty of Science of Utrecht University in Utrecht, The Netherlands.

This work is supported by the Graduate Program of Quantitative Biology and Computational Life Sciences, part of the Netherlands Organisation for Scientific Research (NWO).

Printing of this thesis was kindly supported by my dear family, papa, mama, Lisa & Nick.

Cover design: Nicky Scheefhals

Layout: Nicky Scheefhals

Printed by Ridderprint

Copyright © Nicky Scheefhals, 2022

All rights reserved

Living on the edge

The functional organization of metabotropic glutamate
receptors at excitatory synapses

Leven op het randje

De functionele organisatie van metabotrope glutmaatreceptoren
in excitatoire synapsen
(met een samenvatting in het Nederlands)

Proefschrift

ter verkrijging van de graad van doctor aan de Universiteit Utrecht
op gezag van de rector magnificus, prof.dr. H.R.B.M. Kummeling,
ingevolge het besluit van het college voor promoties in het openbaar te
verdedigen op woensdag 5 oktober 2022 des middags te 2.15 uur

door

Nicky Scheefhals

geboren op 10 september 1991 te Utrecht

Promotor: Prof. dr. L.C. Kapitein
Copromotor: Dr. H.D. MacGillavry

Live on the edge and
enjoy the view

voor Floris en Mila

Content

1.	General introduction	8
2.	Functional organization of postsynaptic glutamate receptors	16
3.	Membrane trafficking and positioning of mGluRs at presynaptic and postsynaptic sites of excitatory synapses	46
4.	Shank proteins couple the endocytic zone to the postsynaptic density to control trafficking and signaling of metabotropic glutamate receptor 5	82
5.	mGluR5 is transiently confined in perisynaptic nanodomains to shape synaptic transmission	116
6.	ORANGE: A CRISPR/Cas9-based genome editing toolbox for epitope tagging of endogenous proteins in neurons	158
7.	General discussion	210
&	Addendum	230



1



General introduction

Nicky Scheefhals¹

¹Cell Biology, Neurobiology and Biophysics, Department of Biology, Faculty of Science,
Utrecht University, Utrecht, the Netherlands

The brain is a tremendously complex organ that consists of an intricate network of around 100 billion interconnected neurons (Azevedo et al., 2009; von Bartheld et al., 2016). Neurons are made up of three main compartments, the axon, soma and dendrites. The axon is a single long and thin process originating from the soma and facilitates signal transmission to other neurons through propagating action potentials. The dendrites are thicker and highly branched and receive and integrate the incoming signals from other neurons. Neurons communicate with each other via synapses, which are specialized structures at contact sites between the presynaptic axon and postsynaptic dendrite. At the presynapse, signal propagation down the axon (i.e. action potential) triggers the release of neurotransmitters into the synaptic cleft, upon which they can bind to neurotransmitter receptors on the postsynaptic dendrite converting the chemical signal into an electrical signal. The combined effect of multiple synapses receiving input can change the overall charge of the neuron leading to a temporary shift in membrane potential. At resting state, the cell membrane of a neuron is polarized and negatively charged. When the membrane potential is sufficiently decreased (i.e. depolarized) and reaches a threshold value, an action potential is triggered further relaying the signal (Figure 1). The type of neurotransmitter released determines whether neurons are excitatory or inhibitory and thus either decrease or increase the membrane potential. For example, excitatory neurons release the neurotransmitter glutamate and promote the firing of an action potential in the receiving neuron.

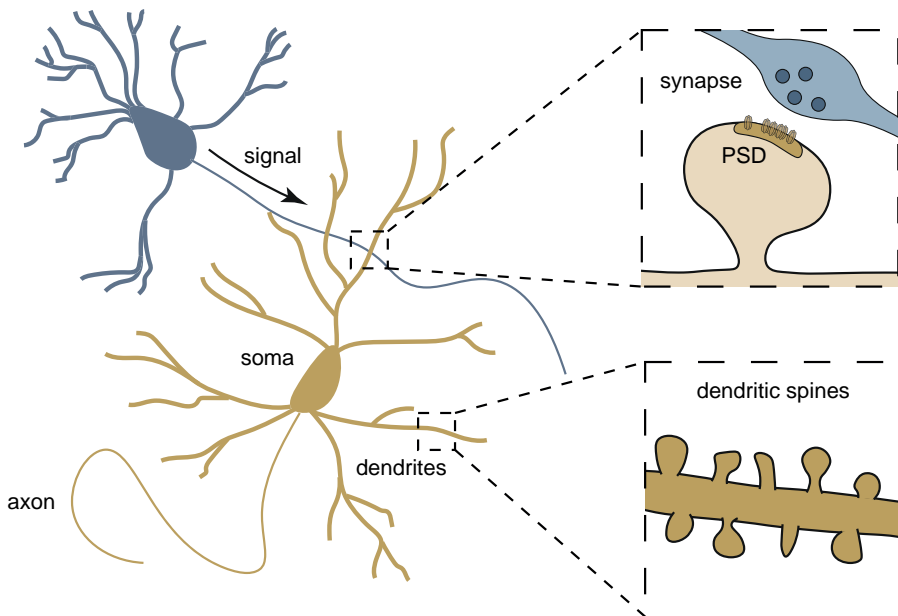


Figure 1. Neuronal communication at excitatory synapses.

Neurons make up our nervous system and consist of three main compartments: the axon, soma and multiple dendrites. The long, thin axon generates and conducts action potentials to transmit signals to other neurons. Here, the upper left neuron (blue) transmits a signal to the lower right neuron (yellow). After initiation, the action potential travels down the axon and reaches a synapse, through which the two neurons communicate, and causes the release of neurotransmitters from the presynaptic axon (blue). The presynaptic site contains vesicles filled with neurotransmitters that can be released into the synaptic cleft and bind to receptors on the postsynaptic dendrite (yellow). Multiple thicker, but shorter dendrites receive signals from other neurons and depending on the

Figure 1 continued on next page

Figure 1 continued

sum of total dendritic input can determine whether the neuron will fire an action potential further passing on the signal to other neurons. At excitatory synapses, the neurotransmitter glutamate can activate glutamate receptors that reside in the PSD, which in turn is typically located on small protrusions from the dendrite, called dendritic spines. Dendritic spines are found all along dendrites and separate and concentrate synaptic proteins from the dendritic shaft to compartmentalize signaling.

At excitatory synapses, the postsynaptic site is typically situated on a small protrusion formed on the dendritic branch, called the dendritic spine. For efficient glutamatergic signaling, it is critical that glutamate receptors are concentrated in the postsynaptic density (PSD), a complex macromolecular structure that contains numerous scaffolding proteins that anchor and position glutamate receptors close to the presynaptic site of release (Figure 1) (MacGillavry et al., 2011; Sheng and Hoogenraad, 2007). In the past few decades our view of synapse organization has changed dramatically from that of a static structure to a multiscale dynamic structure underlying synaptic transmission and plasticity. However, even though we have detailed information about the molecular constituents of the synapse, we know little about how these components are organized within the small confines of the synapse, and how changes in this organization alter synaptic signaling. This thesis aims at understanding the tight relation between nanoscale glutamate receptor positioning and signaling in the context of cognitive functioning. This chapter covers a concise introduction to the relevance of understanding the nanoscale structure-function relationship of glutamate receptors, whereas Chapter 2 and 3 cover elaborate introductions to the key topics presented in this thesis.

Nanoscale structure-function relationship of glutamate receptors

Glutamatergic signaling is mediated by ionotropic glutamate receptors (iGluRs) and metabotropic glutamate receptors (mGluRs). The iGluRs consist of three classes of receptors: α -amino-3-hydroxy-5-methyl-4-isoxazole propionic acid (AMPA), N-methyl-D-aspartate (NMDA), and kainate (KA) receptors. While iGluRs are ligand-gated ion channels that carry the majority of fast signal transmission across synapses, mGluRs modulate the efficacy of synaptic signaling on longer time scales. mGluRs belong to a large family of seven-transmembrane domain G-protein coupled receptors (GPCRs), and are subdivided in three groups based on sequence homology, pharmacology and downstream signaling pathways. Receptors belonging to each of these groups are expressed in the brain, but their expression differs greatly between brain regions and sub-cellular locations. Excitatory synapses of hippocampal neurons mainly express the group I mGluR subtypes mGluR1 and mGluR5. mGluR5 is the most highly expressed subtype throughout all regions of the hippocampus, especially in the CA1 area (Lujan et al., 1996). The focus of this thesis is on group I mGluRs, and mGluR5 in particular. Group I mGluRs link to G α q/11 G-proteins that activate phospholipase C (PLC) to form diacylglycerol (DAG) and inositol tris-phosphate (IP₃), which triggers the release of Ca²⁺ from internal stores, increasing Ca²⁺ concentration and activating PKC (Niswender and Conn, 2010). Moreover, activation of postsynaptic mGluRs was found to be critical for the induction of several forms of long-term synaptic plasticity that underlie learning and memory (Bashir et al., 1993; Bellone et al., 2008; Bortolotto et al., 1994; Hu et al., 2010).

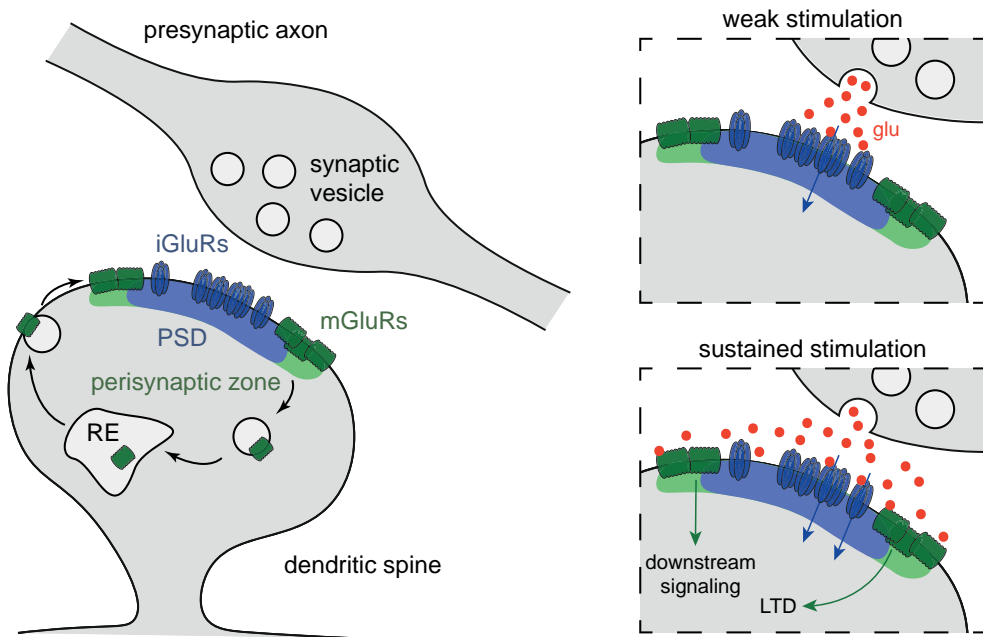


Figure 2. Functional organization of glutamate receptors.

iGluRs (dark blue) are concentrated within the PSD (blue), whereas mGluRs (dark green) are enriched in an annulus surrounding the PSD, called the perisynaptic zone (green). This nanoscale segregation of receptor types ensures that the local and temporal glutamate gradient caused by a single release event will only activate iGluRs (top panel), and that only repetitive or strong synaptic stimulation will also activate mGluRs initiating downstream signaling cascaded and long-term depression (LTD; bottom panel). On the left, a sequence of trafficking events is shown that maintains a surface pool of resensitized receptors: receptors are internalized via clathrin mediated endocytosis, can enter the endocytic recycling compartment (RE) and are recycled to the cell surface.

Receptor activation is regulated by their subsynaptic organization and alignment with the presynaptic active zone (Tang et al., 2016). Interestingly, while iGluRs concentrate in the core of the PSD that directly opposes the presynaptic vesicle release site (MacGillavry et al., 2013), mGluRs are enriched in the perisynaptic zone surrounding the PSD (Lujan et al., 1996; Nusser, 1994). This organization has direct implications for the activation of mGluRs. Kinetic models reveal that the local and temporal glutamate gradient caused by a single release event will only activate the opposing iGluRs, whereas sustained or high frequency stimulation is required to increase the glutamate concentration in the synaptic cleft to also activate the perisynaptic mGluRs (Figure 2) (Greget et al., 2011). To temporally restrict mGluR activity and protect against chronic mGluR over-stimulation, activated mGluRs are rapidly desensitized and internalized. Desensitization of mGluRs involves the phosphorylation of the intracellular loop by G-protein receptor kinases, uncoupling the receptor from the G-protein complex, which targets the receptor for internalization via clathrin-mediated endocytosis (Dhami and Ferguson, 2006). Once endocytosed, receptors can be recycled to the cell surface, critical to sustain a functional surface pool of receptors (Figure 2). Although it is evident that mGluRs are key to synaptic functioning, fundamental information on how mGluR are spatially and temporally controlled in and around synapses

is largely lacking. For example, even though many of the signaling events that underlie mGluR trafficking have been described in great detail, we know little about the mechanisms at excitatory synapses that spatially and temporally control recycling of synaptic mGluRs. Moreover, the dynamic positioning of mGluRs specifically at the perisynaptic zone has never been resolved. In Chapter 4, 5 and 6 we aim to answer these unresolved questions.

Scope of this thesis

Postsynaptic mGluRs are essential regulators of neuronal excitability and synaptic plasticity, underlined by the implication of deregulated mGluR signaling in diverse neurological disorders (Volk et al., 2015). In this thesis, I address fundamental questions about the spatiotemporal organization of mGluRs and how this particular organization tunes synaptic signaling. We used a combination of novel molecular tools, live-cell and super-resolution imaging and functional read-outs to directly examine the nanoscale structure-function relationship of mGluRs. This work presents exciting novel insights into the mechanisms that underlie the dynamic organization and functional regulation of the group I mGluRs at excitatory synapses.

In *Chapter 2* we elaborately discuss our current understanding of the functional distribution of glutamate receptors. We also discuss potential mechanisms that organize specific glutamate receptor types in distinct functional domains and how this would contribute to the regulation of synaptic transmission and plasticity.

In *Chapter 3* we present a complete overview of the currently known mechanisms underlying the trafficking and positioning of presynaptic and postsynaptic mGluRs at excitatory synapses. Furthermore, we highlight important outstanding questions and provide recommendations for future research that will further this field.

In *Chapter 4*, we show that agonist-induced internalization of mGluR5 is mediated by the endocytic zone (EZ), a stable platform to locally capture and recycle postsynaptic membrane proteins. Furthermore, we reveal that Shank proteins link essential components of the EZ to the PSD to regulate mGluR trafficking and signaling at excitatory synapses. Hence, if the coupling between the PSD and EZ is lost, mGluRs are no longer locally captured for efficient recycling and are allowed to diffuse away from the synapse leading to reduced surface expression and mGluR5-mediated signaling. These findings might have implications for the mechanisms underlying ASD, as a mutation in SHANK2 found in ASD disrupts these processes. This work presents exciting novel insights into the spatial and temporal control of mGluR activity, critical to the regulation of neuronal excitability and synaptic plasticity.

In *Chapter 5*, using super-resolution microscopy we uncovered an heterogeneous organization of mGluR5 in perisynaptic nanodomains, that likely determine receptor activation and function. Single-molecule tracking showed that mGluR5 is not stably anchored, but becomes transiently confined in these perisynaptic nanodomains. We found that the cytoplasmic tail of mGluR5 mediates perisynaptic confinement, but also prevents synaptic entry, which may represent transient binding to an interaction partner at the perisynaptic zone or other mechanisms that hinder mGluR5 diffusion. We developed an

inducible heterodimerization system to recruit mGluR5 to the synapse, which this led to increased synaptic calcium signaling. This reveals the importance of proper endogenous regulation of the dynamic positioning of mGluR5 to prevent synaptic entry and mGluR5 overactivation. These findings provide novel mechanistic insights into how the dynamic organization of mGluRs is regulated to tune synaptic signaling.

In **Chapter 6** we present ORANGE (Open resource for the application of neuronal genome editing), a CRISPR/Cas9-based approach to label endogenous proteins with fluorescent tags. The ORANGE toolbox contains a single template cloning vector, an easy to implement workflow for the generation of knock-in constructs and exchange of donor tags, as well as a broad library of ready-to-go knock-in constructs targeting over 30 genes for in depth investigation of diverse neuronal cell biological processes. We have validated ORANGE to great extent at the genomic and protein level and demonstrate its application using super-resolution microscopy.

Finally, **Chapter 7** concludes this thesis by placing the key findings in a broad perspective and defining critical research question and future perspectives.

References

- Azevedo, F.A., Carvalho, L.R., Grinberg, L.T., Farfel, J.M., Ferretti, R.E., Leite, R.E., Jacob Filho, W., Lent, R., and Herculano-Houzel, S. (2009). Equal numbers of neuronal and nonneuronal cells make the human brain an isometrically scaled-up primate brain. *J. Comp. Neurol.* 513, 532-541.
- Bashir, Z.I., Jane, D.E., Sunter, D.C., Watkins, J.C., and Collingridge, G.L. (1993). Metabotropic glutamate receptors contribute to the induction of long-term depression in the CA1 region of the hippocampus. *Eur. J. Pharmacol.* 239, 265-266.
- Bellone, C., Lüscher, C., and Mamei, M. (2008). Mechanisms of synaptic depression triggered by metabotropic glutamate receptors. *Cell. Mol. Life Sci.* 65, 2913-2923.
- Bortolotto, Z.A., Bashir, Z.I., Davies, C.H., and Collingridge, G.L. (1994). A molecular switch activated by metabotropic glutamate receptors regulates induction of long-term potentiation. *Nature* 368, 740-743.
- Dhami, G.K., and Ferguson, S.S.G. (2006). Regulation of metabotropic glutamate receptor signaling, desensitization and endocytosis. *Pharmacol. Ther.* 111, 260-271.
- Greget, R., Pernot, F., Bouteiller, J.M.C., Ghaderi, V., Allam, S., Keller, A.F., Ambert, N., Legendre, A., Sarmis, M., Haerberle, O., et al. (2011). Simulation of postsynaptic glutamate receptors reveals critical features of glutamatergic transmission. *PLoS ONE* e28380.
- Hu, J.H., Park, J.M., Park, S., Xiao, B., Dehoff, M.H., Kim, S., Hayashi, T., Schwarz, M.K., Huganir, R.L., Seeburg, P.H., et al. (2010). Homeostatic scaling requires group I mGluR activation mediated by Homer1a. *Neuron* 68, 1128-1142.
- Lujan, R., Nusser, Z., Roberts, J.D., Shigemoto, R., and Somogyi, P. (1996). Perisynaptic location of metabotropic glutamate receptors mGluR1 and mGluR5 on dendrites and dendritic spines in the rat hippocampus. *The Eur. J. Neurosci.* 8, 1488-1500.
- MacGillavry, H., Song, Y., Raghavachari, S., and Blanpied, T. (2013). Nanoscale scaffolding domains within the postsynaptic density concentrate synaptic ampa receptors. *Neuron* 78, 615-622.
- MacGillavry, H.D., Kerr, J.M., and Blanpied, T.A. (2011). Lateral organization of the postsynaptic density. *Mol. Cell. Neurosc.* 48, 321-331.
- Niswender, C.M., and Conn, P.J. (2010). Metabotropic Glutamate Receptors: Physiology, Pharmacology, and Disease. *Annu. Rev. Pharmacol. Toxicol.* 50, 295-322.
- Nusser, Z. (1994). Subsynaptic segregation of metabotropic and ionotropic glutamate receptors as revealed by immunogold localization. *Neuroscience* 61, 421-427.
- Sheng, M., and Hoogenraad, C.C. (2007). The postsynaptic architecture of excitatory synapses: a more quantitative view. *Ann. Rev. Biochem.* 76, 823-847.
- Tang, A., Chen, H., Li, T., Metzbower, S., MacGillavry, H., and TA, B. (2016). A trans-synaptic nanocolumn aligns neurotransmitter release to receptors. *Nature Publishing Group. Nature Publishing Group* 536, 210-214.
- Volk, L., Chiu, S.-L.L., Sharma, K., and Huganir, R.L. (2015). Glutamate synapses in human cognitive disorders. *Annu. Rev. Neurosci.* 38, 127-149.
- von Bartheld, C.S., Bahnéy, J., and Herculano-Houzel, S. (2016). The search for true numbers of neurons and glial cells in the human brain: A review of 150 years of cell counting. *J. Comp. Neurol.* 524, 3865-3895.



2



Functional organization of postsynaptic glutamate receptors

Nicky Scheefhals¹ and Harold D. MacGillavry¹

¹Cell Biology, Neurobiology and Biophysics, Department of Biology, Faculty of Science,
Utrecht University, Utrecht, the Netherlands.

Molecular and Cellular Neuroscience (2018), 91: 82-94

Abstract

Glutamate receptors are the most abundant excitatory neurotransmitter receptors in the brain, responsible for mediating the vast majority of excitatory transmission in neuronal networks. The AMPA- and NMDA-type ionotropic glutamate receptors (iGluRs) are ligand-gated ion channels that mediate the fast synaptic responses, while metabotropic glutamate receptors (mGluRs) are coupled to downstream signaling cascades that act on much slower timescales. These functionally distinct receptor sub-types are co-expressed at individual synapses, allowing for the precise temporal modulation of postsynaptic excitability and plasticity. Intriguingly, these receptors are differentially distributed with respect to the presynaptic release site. While iGluRs are enriched in the core of the synapse directly opposing the release site, mGluRs reside preferentially at the border of the synapse. As such, to understand the differential contribution of these receptors to synaptic transmission, it is important to not only consider their signaling properties, but also the mechanisms that control the spatial segregation of these receptor types within synapses. In this review, we will focus on the mechanisms that control the organization of glutamate receptors at the postsynaptic membrane with respect to the release site, and discuss how this organization could regulate synapse physiology.

Introduction

Synapses are the fundamental elements of neuronal networks that enable the processing, encoding, and retrieval of information in the brain, and pathological disruptions in synapse structure are broadly held to underlie the development of neurological disorders such as autism and schizophrenia (Volk et al., 2015). To maintain and adjust the efficiency of synaptic signaling, synapses are built from a broad array of components that assemble into large macromolecular machineries. At the presynaptic terminal, action potentials trigger the fast release of synaptic vesicles. Synaptic vesicles are docked at the active zone and primed for exocytosis by protein complexes containing e.g. Rab3-interacting molecules (RIM) and soluble N-ethylmaleimide-sensitive factor activating protein receptors (SNARE) (Sudhof, 2012). The release of glutamate is closely aligned with the postsynaptic receptors that are stably anchored in the opposing postsynaptic density (PSD), a complex molecular machine containing a plethora of scaffolding proteins and signaling molecules (Okabe, 2007; Sheng and Hoogenraad, 2007). How are these molecular complexes organized and precisely positioned to sustain synaptic transmission? In this review we will focus particularly on the functional distribution of glutamate receptors at the postsynaptic membrane.

Functional organization of postsynaptic glutamate receptors

Impact of glutamate receptor distribution on probability of receptor activation

At excitatory synapses, the postsynaptic effects of glutamate are mediated by different types of glutamate receptors; the ionotropic glutamate receptors (iGluRs) comprising AMPA- and NMDA- and kainate-type receptors, and the metabotropic glutamate receptors (mGluRs). The principal iGluRs, the AMPA and NMDA-type receptors act on millisecond timescales to mediate the majority of fast, basal synaptic transmission. In contrast, the postsynaptic

group I mGluRs, i.e. mGluR1 and mGluR5, respond much slower and have much longer-lasting physiological effects. Intriguingly, these functionally distinct receptor types are spatially segregated with respect to the presynaptic release site. While AMPA and NMDA receptors are highly enriched in the core of the PSD opposing the presynaptic release site, mGluRs are preferentially enriched in the perisynaptic domain, much further away from the vesicle release site, and seem to be largely excluded from the PSD (Baude et al., 1993; Lujan et al., 1996; Nusser et al., 1994) (Figure 1A). We define the perisynaptic domain as an annular ring of 100 – 200 nm surrounding the PSD, whereas the extrasynaptic domain is everything beyond the perisynaptic domain, and thus starts 100 – 200 nm away from the edge of the PSD (Figure 1B).

The spatial segregation of receptor types has important functional implications as the distinct localization with respect to the presynaptic release site is predicted to greatly impact the activation kinetics of these receptors types. As has been extensively investigated by numerous computational models that incorporate realistic features of glutamate release and synapse geometry single release events produce a very steep peak in synaptic cleft glutamate concentration, restricted to a small area (<100 nm) for only a brief period of time (~100 μ s) (Boucher et al., 2010; Franks et al., 2003; Raghavachari and Lisman, 2004; Uteshev and Pennefather, 1996; Xie et al., 1997; Xu-Friedman and Regehr, 2004). Importantly, the affinity of AMPARs for glutamate is relatively low and the number of glutamate molecules bound to AMPAR subunits determines the open probability of the receptor (Rosenmund et al., 1998). Initially it was thought that receptor activation requires binding of at least two glutamate molecules, however recently it was proposed that in the presence of auxiliary subunits binding of a single glutamate molecule might be sufficient for receptor activation (Coombs et al., 2017; Greger et al., 2017). However, binding of a single glutamate molecule was also shown to be sufficient to desensitize AMPARs (Robert and Howe, 2003), and although the rate of AMPAR desensitization upon binding of a single glutamate molecule is similar when bound to two to four glutamate molecules, the rate of glutamate dissociation is predicted to be slower with at least two glutamate molecules bound (Robert and Howe, 2003). As a result of these biophysical properties, computational models predict that the probability of AMPAR opening is highest near vesicle release sites, producing local hotspots (<0.03 μ m²) of maximally activated AMPARs that cover only a fraction of the total PSD area (~25% of an average PSD in a CA1 synapse) (Franks et al., 2003; Raghavachari and Lisman, 2004). Importantly, this suggests that not the absolute number, but the density of AMPARs with respect to the presynaptic release site determines the size of the synaptic response. Similarly, although to a lesser extent, the activation probability of NMDARs is also location-dependent. Even though NMDARs have a higher affinity for glutamate and desensitize slower than AMPARs (Erreger et al., 2005), the slow binding rate puts a considerable limit on the opening probability of NMDARs during the short-lived glutamate peak. This is particularly significant for GluN2B-containing NMDARs that are three times more likely to become activated when directly opposing the release site than when displaced more than 200 nm. In contrast, the activation probability of GluN2A-containing receptors falls below 50% only when displaced more than 300 nm from the release site (Santucci and Raghavachari, 2008). Indeed, receptor non-saturation has been demonstrated experimentally at different types of synapses, where increasing presynaptic release or focal application of exogenous glutamate resulted in larger amplitude responses (Liu et al., 1999; McAllister and Stevens, 2000; Pankratov and Krishtal, 2003).

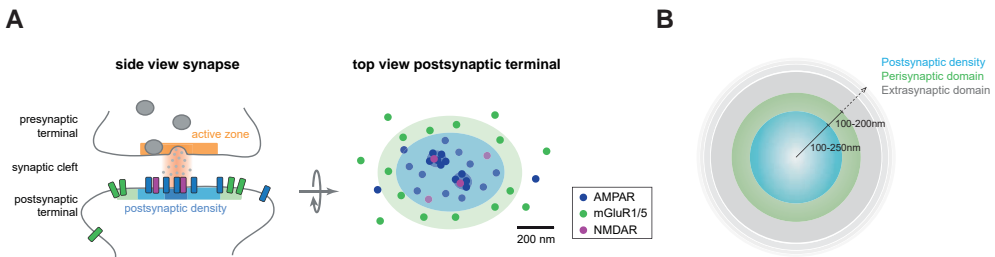


Figure 1. Subsynaptic segregation of glutamate receptor types at the postsynaptic membrane

(A) Side view of an excitatory synapse with an active zone (orange) at the presynaptic terminal and postsynaptic density (PSD) (blue), and perisynaptic domain (green) at the postsynaptic terminal (left). A single release event of glutamate is predicted to create a subsynaptic hotspot of maximally activated postsynaptic glutamate receptors (dark blue shaded area) aligned with the presynaptic vesicle release site. Top view of the lateral patterning of the postsynaptic membrane with a central PSD (blue) containing AMPA- (dark blue) and NMDA-type (pink) receptors, and a surrounding perisynaptic domain (green) enriched in mGluR1/5 (dark green) (right). Additionally, PSD components, most notably AMPARs, are organized in ~ 1 -3 distinct nanodomains per synapse (dark blue shaded area). (B) Top view of an excitatory postsynapse to make a clear distinction between the PSD, on average 500 - 1000 nm in diameter, the perisynaptic domain, an annulus of 100 - 200 nm surrounding the PSD, and the extrasynaptic domain, everything beyond the perisynaptic domain.

Even further displaced from the release site are the mGluRs, located at the perisynaptic domain surrounding the PSD, strongly constraining the activation probability of these receptors. The binding affinity of group I mGluRs for glutamate is comparable to AMPARs as measured in heterologous systems (Conn and Pin, 1997; Traynelis et al., 2010), and although one glutamate molecule is sufficient to activate mGluR5 dimers, occupation of both subunits is required for optimal activation (Kniazeff et al., 2004; Niswender and Conn, 2010). Thus, these biophysical properties predict that the low concentration of glutamate at the periphery of the synapse during single release events limits mGluR activation. Moreover, glutamate transporters co-localizing with mGluRs at the perisynaptic domain (Dehnes et al., 1998; He et al., 2000) compete for the residual glutamate that diffuses out of the synaptic cleft, which further enhances the rapid uptake of glutamate, and thereby virtually eliminating the probability of mGluRs to sense glutamate during single release events (Brasnjo and Otis, 2001). Functionally this would imply that mGluRs only respond when cleft glutamate concentration builds up such that it “spills over” to the perisynaptic domain, for instance during sustained high-frequency synaptic stimulation. Consistently, the activation kinetics of group I mGluRs are very fast (< 10 ms), and the deactivation time is slow (~ 50 ms) (Marcaggi et al., 2009; Rondard and Pin, 2015). Thus, also the intrinsic kinetic profile of mGluRs predicts that these receptors function as integrators of activity and are sensitive to high-frequency (> 20 Hz) pulses of release (Greget et al., 2011; Marcaggi et al., 2009). Indeed, at cerebellar synapses, trains of stimuli with a minimal frequency of 20 Hz are required to elicit mGluR1-mediated excitatory postsynaptic currents (EPSCs) (Tempia et al., 1998).

Taken together, the nanoscale segregation of glutamate receptor subtypes differentially determines their activation probabilities, providing synapses with a powerful means to encode synaptic activity patterns. In the following, we will present an overview of the literature on the molecular organization of excitatory synapses, focusing in particular on

the subsynaptic distribution of glutamate receptors at the postsynaptic membrane, and explore the potential physiological consequences of this organization and mechanisms that could control the entry and distribution of receptors in the synapse.

Subsynaptic segregation of glutamate receptor types

The activation of the distinct receptor subtypes and their contribution to synaptic transmission is controlled by their lateral distribution across the postsynaptic membrane. To better understand the functional organization of glutamate receptors at excitatory synapses, we will first discuss the distinct distribution patterns of the different postsynaptic glutamate receptors in relation to the presynaptic release site. Although glutamatergic synapses can vary tremendously in their structural, molecular and functional properties, we mainly focus on mature hippocampal excitatory synapses which have been most extensively studied in the context of the functional organization of glutamate receptors.

AMPA receptors (AMPAARs) are concentrated at the PSD opposing the presynaptic vesicle release site to ensure fast and efficient synaptic transmission (Figure 1A). Measuring the subsynaptic distribution of receptors has been challenging owing to the limited resolution of conventional light microscopy. Electron microscopy (EM) immunogold labeling techniques provide the highest achievable resolution and have been instrumental in precisely determining receptor distribution at synapses. At neocortical synapses, AMPAR localization was found preferentially at the edge of the PSD (Bernard et al., 1997; Kharazia and Weinberg, 1997), but generally AMPARs can be found anywhere in the PSD (Chen et al., 2008; Dani et al., 2010; Masugi-Tokita et al., 2007; Somogyi et al., 1998; Tang et al., 2016; Tarusawa et al., 2009), varying greatly between synapses and synapse types (MacGillavry et al., 2011). Also, variations in distribution between different AMPAR subtypes have been suggested. AMPARs form hetero-tetrameric complexes composed of different combinations of four subunits, i.e. GluA1-4. In the adult hippocampus, the most prevalent combinations are GluA1/2 and GluA2/3 heteromers, as well as GluA1 homomers (Lu et al., 2009; Wenthold et al., 1996). At hippocampal synapses, GluA1 tends to localize more towards the edge of the PSD, whereas GluA3 localizes significantly more central (Jacob and Weinberg, 2015). Peripheral localization of GluA1 was most prominent at small synapses, whereas at larger synapses GluA1 was localized more central, similar to GluA3 (Jacob and Weinberg, 2015). Super-resolution studies on individual synapses have corroborated the notion of receptor hotspots, demonstrating that AMPARs form distinct subsynaptic regions of high molecular density, of around 70 to 80 nm in diameter, hereinafter referred to as nanodomains (MacGillavry et al., 2013; Nair et al., 2013; Tarusawa et al., 2009). Most synapses were shown to contain one to three distinct nanodomains, each consisting of around 20 receptors (MacGillavry et al., 2013; Nair et al., 2013; Tang et al., 2016). Importantly, this heterogeneous organization was found to extend to presynaptic sites where key proteins involved in vesicle docking and priming, such as RIM1/2, also form distinct nanodomains within the presynaptic active zone that marked sites of preferred vesicle release. Additionally, these presynaptic nanodomains are spatially aligned with postsynaptic AMPAR nanodomains, forming a trans-synaptic molecular 'nanocolumn' (Biederer et al., 2017; Tang et al., 2016). This striking level of subsynaptic molecular organization provides a simple, but powerful mechanism to efficiently modulate the efficiency of synaptic transmission.

Like AMPARs, NMDARs are preferentially enriched at the PSD, but tend to localize more towards the center of the PSD (Chen et al., 2008; Kharazia and Weinberg, 1997;

Perez-Otano et al., 2006; Racca et al., 2000), potentially accompanied with reduced AMPAR densities (Chen et al., 2008). Functionally this is intriguing and might entail that the generally more central NMDARs allow the AMPARs to turn over quickly at the periphery of the PSD, accounting for dynamic modulation of synaptic transmission as suggested by mathematical models (Freche et al., 2011). However, this pattern is not universal among all synapses and synapse types. Clear clustered subsynaptic distributions of NMDARs, comparable to AMPAR nanodomains (Jezequel et al., 2017; MacGillavry et al., 2013), have been found at the center of the PSD (Chen et al., 2008), or either in central or peripheral regions of the PSD (Dani et al., 2010; Perez-Otano et al., 2006). Whether GluN2A- and GluN2B-containing receptors distribute differentially remains to be studied. In conclusion, both AMPARs and NMDARs are organized in higher density nanodomains within the PSD that may serve to optimize the open probability of these receptors by alignment with the presynaptic release site.

In stark contrast to AMPA and NMDA receptors, postsynaptic group I mGluRs (mGluR1/5) seem to be largely excluded from the PSD, but accumulate in the perisynaptic domain surrounding the PSD (Baude et al., 1993; Lujan et al., 1996; Nusser et al., 1994) (Figure 1A). Quantifications of immunogold labeling clearly demonstrate that the levels of mGluR1/5 significantly peak at the edge of the PSD (within 60 nm), but decrease further away from the PSD, reaching a uniform labeling density at the extrasynaptic dendritic membrane (Lujan et al., 1996). A more recent super-resolution study confirmed the perisynaptic accumulation of mGluR5 co-localizing with Norbin (Westin et al., 2014), a neuron-specific protein that interacts with and regulates the signaling properties of mGluR5 (Wang et al., 2009). Also, single-molecule tracking studies corroborate that a large fraction of the total mGluR5 pool is extrasynaptic and highly mobile (Aloisi et al., 2017; Renner et al., 2010; Sergé et al., 2002), but a small fraction can become reversibly immobilized at synaptic Homer clusters (~8%) (Aloisi et al., 2017; Renner et al., 2010; Sergé et al., 2002).

It is unknown whether mGluRs are distributed homogeneously throughout the perisynaptic domain, or are mGluRs perhaps enriched in local, perisynaptic nanodomains? Although speculative, such a non-random organization of mGluRs in nanodomains would aid in facilitating downstream signaling processes. It is becoming increasingly clear that clustering of receptors and their effectors in signaling platforms, or signalosomes, contributes to the efficacy and fidelity of signal transduction (Kasai and Kusumi, 2014). Many G-protein coupled receptors (GPCRs), including group I mGluRs (Francesconi et al., 2009; Kumari et al., 2013), have been found to localize in insoluble membrane domains, or lipid rafts, using biochemical approaches (Insel et al., 2005; Pontier et al., 2008). Such a local accumulation of receptor complexes could provide a platform for highly efficient and localized signal transduction, even when receptors and effectors are present at low numbers (Kusumi et al., 2012). A recent single-molecule tracking study confirmed the presence of GPCR signalosomes at the plasma membrane of non-neuronal cells. Using the $\alpha 2A$ -adrenergic receptor as a prototypical GPCR, this study found that receptors were confined at hotspots where they preferentially interacted with their cognate G-protein complexes (Sungkaworn et al., 2017). Thus, perhaps mGluRs are also organized in functional nanodomains together with its G-proteins and likely other signaling molecules. Indeed, immuno-labeling EM studies found that components of the mGluR signaling complex, including Gq-protein alpha subunits and phospholipase C beta (PLCb), are also localized in the perisynaptic domain (Nakamura et al., 2004; Tanaka et al., 2000). The perisynaptic domain also contains components of

the endocytic apparatus forming a stable endocytic zone (EZ) that is tightly linked to the PSD via specific protein-protein interactions (Blanpied et al., 2002; 2003; Lu et al., 2007). The EZ functions to locally internalize synaptic receptors, and acts as a mechanism for local retention of receptors for fast exchange between the synaptic and extrasynaptic receptor pool (Lu et al., 2007; Petrini et al., 2009). The close co-localization of the EZ and the perisynaptic mGluRs might facilitate the fast desensitization and local turn-over of receptors after activation to rapidly and dynamically respond to high-frequency inputs.

Downstream effects of glutamate receptor positioning

Regulation of synaptic transmission by subsynaptic AMPA receptor organization

The enrichment of AMPARs in nanodomains aligned with the presynaptic release site suggests that this subsynaptic pool of receptors contributes the most to synaptic responses, while receptors outside of nanodomains contribute only little. Computationally, this can be addressed systematically (MacGillavry et al., 2013; Nair et al., 2013; Tang et al., 2016), but experimentally it is highly challenging to specifically measure the contribution of receptors enriched in nanodomains. Nevertheless, as we will discuss here, the subsynaptic organization of AMPARs in nanodomains is predicted to influence both basal and plasticity-regulated synaptic transmission.

Important in this respect is the recent demonstration that spontaneous release events are distributed over a much larger area of the active zone than evoked synaptic responses (Tang et al., 2016), consistent with earlier suggestions that spontaneous and evoked release are mechanistically distinct events (Kavalali, 2015). Additionally, in contrast to spontaneous events, evoked vesicle fusion events were found to preferentially take place at subsynaptic hotspots marked by RIM1/2, that were transsynaptically aligned with postsynaptic nanodomains (Tang et al., 2016). Thus, evoked release is more likely to activate the receptors that are enriched in nanodomains, while spontaneous quantal events are likely to probe a larger fraction of the postsynaptic pool of receptors, including areas that are less dense in receptors. One prediction from this organization is that the variance in the peak amplitude of evoked EPSCs is much smaller than of mEPSCs (MacGillavry et al., 2013), which has indeed been confirmed experimentally (Freche et al., 2011). Alignment of presynaptic release with postsynaptic nanodomains thus gives rise to more reliable synaptic transmission (Figure 2).

How could changes in postsynaptic nanodomain organization affect synaptic responses? Since evoked release events are spatially aligned with postsynaptic nanodomains, evoked EPSCs are likely more directly influenced by changes in receptor organization than spontaneous events. As such, an increase in the number of postsynaptic receptor nanodomains is predicted to decrease the failure rate of evoked responses (Figure 2B), while an increase in nanodomain content (i.e. more receptors per nanodomain) would increase the amplitude of evoked responses (Figure 2C).

Given that spontaneous release events seem to take place at random positions, not preferentially aligned with postsynaptic nanodomains, changes in nanodomain organization are probably less directly associated with changes in mEPSCs. Nevertheless, computational simulations suggest that the amplitude of mEPSCs is highly dependent on the location relative to the receptor nanodomain, such that release events on non-clustered regions of the synapse are predicted to produce very modest, and likely undetectable mEPSCs and that

most of the recorded mEPSCs reflect “on-cluster” events (MacGillavry et al., 2013; Nair et al., 2013). Thus, similar as for evoked responses, changes in nanodomain content are predicted to alter mEPSC amplitude (Figure 2C). More speculative, one could predict that because spontaneous events ‘probe’ a larger fraction of the postsynaptic membrane, a change in the number of nanodomains per synapse, increases the probability that a spontaneous event activates receptors, and could be measured as a change in mEPSC frequency (Figure 2B). Thus, while a change in mEPSC frequency is generally interpreted as a change in presynaptic function or in the number of synaptic connections, perhaps it could also be interpreted as a change in the functional organization of postsynaptic receptors. For instance, the genetic removal of individual GluA2-containing AMPA receptors significantly reduced mEPSC frequency, but not amplitude, even though both the total number of synapses and measures of presynaptic function are not affected in (Lu et al., 2009). This might suggest that in the remaining fraction of functional synapses, GluA2-lacking AMPA receptors are still capable of populating subsynaptic nanodomains that can produce similar response amplitudes as normal synapses. It would be of interest to investigate how the subunit composition and levels of AMPARs at individual synapses is related to the molecular organization of synapses.

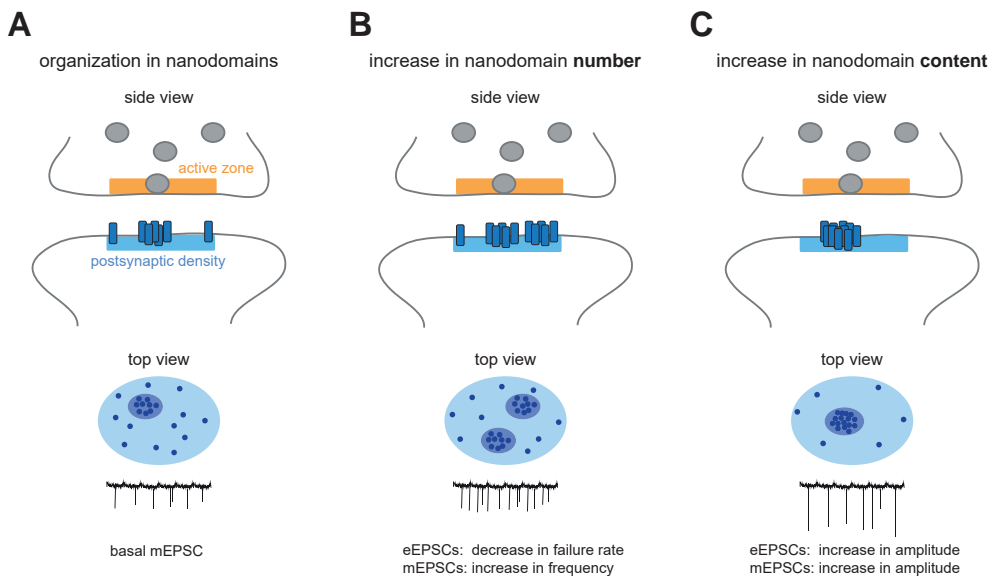


Figure 2. Physiological implications of AMPAR organization

(A) Overview of AMPAR organization in distinct nanodomains, aligned with the presynaptic release site in side view (top), top view (middle) and the hypothetical mEPSC trace (bottom), that is maintained throughout this figure. (B) An increase in the number of nanodomains per synapse is likely to increase the probability that a spontaneous event activates receptors, and could be measured as a decrease in the failure rate of evoked responses (eEPSCs), or an increase in mEPSC frequency. (C) An increase in the number of receptors in a nanodomain aligned with the presynaptic site of vesicle release is predicted to enhance synaptic transmission, which could be measured as an increase in the amplitude of eEPSCs or mEPSCs.

In a recent study, GluA1-containing AMPA receptors were selectively recruited to the PSD by an elegant optogenetic approach. Using this recruitment assay, it was shown that adding GluA1-containing AMPA receptors to existing synapses significantly

increased synaptic responses as measured by evoked EPSCs, glutamate uncaging, and mEPSC frequency, but did not affect the amplitude of mEPSCs (Sinnen et al., 2017). These experiments thus indicate that the global addition of receptors to a synapse does not necessarily increase quantal amplitude, and confirm predictions that adding receptors specifically to nanodomains aligned with presynaptic sites of vesicle release is required to enhance synaptic transmission (Liu et al., 2017). Also, it could indicate that the number of receptor slots in a nanodomain is limited, and is in most cases saturated, such that it cannot be further increased. Thus, it will be important to dissect the mechanisms that specifically control the integration of receptors in nanodomains after these receptors entered the synaptic membrane.

While the role of GluA1/2 receptors in synaptic transmission has been vigorously investigated, the contribution of GluA3 to synaptic transmission has long been regarded as non-essential. The deletion of GluA3-subunits has minimal effects on synaptic currents (Lu et al., 2009), and does not prevent the induction of long-term potentiation (LTP) and depression (LTD) (Meng et al., 2003; Reinders et al., 2016). However, recent studies on slice preparations from cerebellum (Gutierrez-Castellanos et al., 2017), and hippocampus (Renner et al., 2017) found that synaptic potentiation by increasing cyclic-AMP (cAMP) levels was completely abolished in GluA3 knock-out (KO) mice. It was furthermore shown that cAMP-mediated potentiation increased the open-channel probability of GluA3-containing AMPA receptors, thereby enhancing their contribution to the synaptic response. Thus, GluA3-containing AMPA receptors might form a distinct subpopulation of ‘silent’ AMPARs that become activated by modulatory inputs that activate cAMP signaling pathways. Interestingly, potentiation by cAMP had a drastic effect on mEPSC frequency, but no alterations in presynaptic function were observed, suggesting that the number of functional postsynaptic nanodomains was increased, or that the increased contribution of GluA3-containing AMPA receptors in pre-existing nanodomains ‘unsilenced’ these domains. In this respect it is interesting to note that ectopic expression of GluA3 can depress synaptic responses (Shi et al., 2001). Perhaps that these ectopically expressed, silent GluA3-containing AMPA receptors, exchange with AMPA receptors present in nanodomains, effectively silencing these receptor domains.

The strength of synaptic transmission is highly regulated by changes in synaptic activity patterns, and the dynamic trafficking of AMPARs to and from synapses underlies the expression of LTP and LTD (Huganir and Nicoll, 2013). Following on the discussion above, it is attractive to speculate that specifically altering the number or composition of nanodomains, or transsynaptic “modules” (Liu et al., 2017), underlies the expression of long-term plasticity. Consistent with this idea it was found that activity-induced potentiation of synapses involves an increase in the spatial alignment with presynaptic domains (Tang et al., 2016). It will be of great interest to further investigate how exactly synaptic potentiation affects postsynaptic receptor organization, and to test whether this involves an increase in the number of nanodomains, the number of receptors within nanodomains, an increase in effective alignment with the presynaptic release machinery, or a combination of these processes.

Modulation of synaptic transmission and plasticity by perisynaptic mGluRs

At the postsynaptic membrane, group I mGluRs are spatially segregated from the synaptic iGluRs in the PSD, at considerable distance from the hotspot of glutamate release (Figure 1A). Nevertheless, the activity of synaptic mGluRs has been shown to modulate synaptic

transmission and several forms of plasticity, and disruption of mGluR function has been implicated in neurological diseases, most notably Fragile X syndrome, the most common form of inherited intellectual disability (Bear et al., 2004; Lüscher and Huber, 2010). Group I mGluRs are GPCRs and can trigger a wide variety of effector systems. Group I mGluRs are canonically linked to Gαq/11 -proteins which activate PLC. PLC in turn, hydrolyzes the phospholipid PIP₂ (phosphatidylinositol 4,5-bisphosphate) to form diacylglycerol (DAG) and the soluble second-messenger IP₃ (inositol tris-phosphate). IP₃ activates IP₃ receptors on the endoplasmic reticulum (ER) triggering the release of Ca²⁺ from internal stores, which, together with DAG, activates protein kinase C (PKC) (Niswender and Conn, 2010). As a result of these signaling events, mGluR activity generally increases postsynaptic excitability through the modulation of several ion channels such as calcium-dependent and independent cationic channels, HCN channels, small-conductance K⁺ (SK) channels, and the regulation of NMDAR currents (Anwyl, 1999; Fitzjohn et al., 1996; Heidinger et al., 2002).

On longer time scales, the activity of mGluRs has been implicated in several forms of plasticity. Numerous studies have confirmed that mGluR5 is involved in the induction and expression of LTP, as shown by pharmacological blockade *in vitro* and *in vivo* (Balschun and Wetzel, 2002; Bashir et al., 1993a; Bortolotto et al., 1994; Francesconi et al., 2004; Neyman and Manahan-Vaughan, 2008), and by genetic deletion (Jia et al., 1998; Lu et al., 1997). These effects seem to reflect a metaplastic effect in which prior activation of mGluRs primes the induction of subsequent LTP by increasing the excitability (Cohen et al., 1999; Cohen et al., 1998), and even prolongs the expression of LTP by inducing local protein synthesis (Raymond et al., 2000). On the other hand, selective activation of group I mGluRs, or low-frequency synaptic stimulation, is sufficient to induce a form of synaptic depression that is independent of NMDARs, termed mGluR-LTD (Bashir et al., 1993b; Lüscher and Huber, 2010; Palmer et al., 1997). Unlike NMDAR-dependent depression, this form of LTD involves the protein synthesis-dependent endocytosis of AMPARs (Huber et al., 2000; Snyder et al., 2001; Waung and Huber, 2009).

The contribution of mGluRs to synaptic signaling and plasticity is likely to be not equal at all synapses. Using two-photon imaging of calcium transients in response to glutamate uncaging it was observed that these responses had much larger amplitudes in spines that contained a prominent ER structure (Holbro et al., 2009). Intriguingly, low-frequency stimulation of these ER-containing spines induced a long-lasting, mGluR-dependent depression of synaptic responses, while ER-lacking spines did not respond to this stimulus. This would suggest that mGluR activity is most prominent in a subset of spines that contain an ER. Interesting in this regard is that in the hippocampal CA1 region, the reported values of spines containing an ER has been variable (20-70%) (Holbro et al., 2009; Ng et al., 2014; Spacek and Harris, 1997), but considerably lower than in Purkinje neurons in the cerebellum, where virtually all spines contain an ER (Harris and Stevens, 1988; Wagner et al., 2011) and mGluR1-mediated signaling has a prominent role in synaptic transmission and plasticity. Interestingly in this respect is that mGluR activation itself can regulate ER complexity in dendrites (Cui-Wang et al., 2012), indicating that the activity of mGluRs and the ER are tightly coupled. Also, mGluR-mediated EPSCs, and mGluR-LTD could not be induced in directly coupled CA3-CA1 synapses, but was only apparent after activation of several (>7) inputs on a single CA1 neuron (Fan et al., 2010), additionally suggesting that mGluR-mediated responses can only be triggered in a subset of spines. Together, these results suggest that only in a subset of synapses, mGluRs are functionally coupled to the

ER to effectively modulate synaptic transmission. This would imply that ER-containing synapses carry most of the excitatory drive, and it will be important to determine how mGluRs functionally interact with the receptors in the core of the PSD, but also with compartments in the spines, such as the ER and spine apparatus. In conclusion, mGluRs can be regarded as sensors of synaptic activity providing critical feedback control, effectively gating the excitatory flow in neuronal networks.

Mechanisms underlying the subsynaptic positioning of glutamate receptors

Regulation of synaptic entry and retention of glutamate receptors

The distribution of glutamate receptors at synapses is highly heterogeneous, with a refined level of organization that has direct consequences for synaptic physiology. What underlies the entry of receptors into the PSD before they become stably anchored? Also, what mechanisms retain and position receptors once they entered the PSD? The trafficking of receptors into and away from the synaptic membrane is a highly regulated and dynamic process, and underlies the activity-dependent modulation of synaptic strength (Huganir and Nicoll, 2013; Kessels and Malinow, 2009). The level of receptors expressed at the synaptic membrane is governed by a series of vesicular trafficking steps and exocytosis of receptors from intracellular compartments (Kennedy and Ehlers, 2011; van der Sluijs and Hoogenraad, 2011; Wu et al., 2017), but lateral diffusion of receptors is the key final step by which receptors are inserted in the synaptic membrane (Makino and Malinow, 2009; Penn et al., 2017) (Figure 3A). Synaptic entry of receptors seems to be tightly regulated at the border of the PSD with specific receptors being selected by mechanisms that remain largely unknown.

How does the border of the PSD discriminate between receptor types to establish the remarkable nanoscale segregation of AMPARs and mGluRs? Here we will discuss potential mechanisms that could contribute to the formation and maintenance of the dynamic distribution of glutamate receptors at the synapse. To control receptor entry the PSD might act as a ‘gate keeper’ selecting receptors for entry based on specific properties, perhaps in an activity-regulated manner. Thus, we will make the distinction between processes that control the entry of receptors into the synapse, and processes that control the anchoring and positioning of receptors at distinct locations within the postsynaptic membrane (i.e. within or outside of subsynaptic nanodomains). Making this distinction might be important to understand and delineate processes that specifically control the (activity-induced) changes in the number of synaptic components, and processes that structurally (re-)organize the synapse or partition it into distinct nanodomains. We will specifically discuss the relative contribution of interactions of receptors with intracellular and extracellular protein complexes, steric hindrance due to molecular crowding, and cytoskeletal hindrance to the entry and retention of receptors. Here we will focus on AMPARs and mGluRs to narrow the scope of this review, as the AMPARs are the predominant iGluRs and are intriguingly different in their subsynaptic positioning compared to mGluRs.

Intracellular interactions with scaffolding proteins

At the synapse receptors can engage in a multitude of interactions with the numerous scaffolding proteins that form the PSD just below the membrane (Figure 3A). Indeed, decades of research have principally focused on identifying and characterizing protein-

protein interactions with intracellular scaffolding proteins (Okabe, 2007; Sheng and Hoogenraad, 2007). AMPARs can interact with scaffolding proteins via their PDZ ligand in their C-terminal domain (CTD). The GluA1 subunits have a long CTD containing a type-I PDZ ligand, whereas the GluA2/3 subunits have a short CTD with a type-II PDZ ligand. GluA1 can directly interact with the PDZ type I containing protein SAP97, whereas GluA2/3 can directly interact with the PDZ type II containing proteins PICK1 and GRIP/ABP (Anggono and Huganir, 2012). The differences in CTD have been ascribed to underlie the subunit-specific trafficking of AMPARs (Malinow and Malenka, 2002). In particular, it is broadly held that synaptic activity promotes the entry of GluA1-containing AMPA receptors, while GluA2/3 receptors can traffic constitutively to the synapse (Hayashi et al., 2000; Shi et al., 2001). Recent genetic studies, however, challenged this idea. It was demonstrated that removal of the GluA1 CTD, or even complete depletion of the AMPAR GluA1-3 subunits, did not prevent the induction of LTP or LTD (Granger and Nicoll, 2014; Granger et al., 2013). Interestingly, a more recent study in which the GluA1 and GluA2 CTD were genetically exchanged demonstrated that these tails are necessary and sufficient for plasticity-mediated receptor trafficking and hippocampal learning paradigms (Zhou et al., 2017). Thus, the CTDs of AMPAR subunits can differentially control the distribution and trafficking of AMPARs in and to synapses.

SAP97, a member of the membrane-associated guanylate kinase (MAGUK) family (also including PSD-95, PSD-93 and SAPI02), is a particularly interesting candidate to regulate the specific synaptic entry of GluA1 receptors, as SAP97 has been reported to concentrate at the edge of the PSD (DeGiorgis et al., 2006; Valtschanoff et al., 2000). Also, the two SAP97 isoforms, α SAP97 and β SAP97, were found to differentially regulate the targeting of GluA1 to the center or the periphery of the synaptic membrane respectively, as shown by dSTORM super-resolution imaging (Goodman et al., 2017). The palmitoylated α SAP97 isoform is stably anchored within the PSD and regulates the amount of synaptic binding sites for GluA1-containing AMPA receptors. On the other hand, the L27 domain-containing β SAP97 isoform is much more dynamic and regulates the cluster size and density of GluA1-containing AMPA receptors at the periphery of the PSD (Regalado et al., 2006; Waites et al., 2009). The α - and β SAP97 isoforms also differentially regulate synaptic transmission, with α SAP97 increasing and β SAP97 decreasing synaptic currents (Waites et al., 2009). Thus, the alternative splicing of the SAP97 N-terminus may be an important factor in the regulation of synaptic entry of AMPARs. Additionally, the S845 phosphorylation on the GluA1 subunit, which is a substrate of protein kinase A (PKA), has been shown to regulate the perisynaptic surface pool of GluA1 homomers, and dephosphorylation of S845 in turn removes the perisynaptic GluA1 homomers (He et al., 2009). Interestingly, these perisynaptic GluA1 homomers are implicated in the induction of PKA-dependent LTP, which might involve activity-induced recruitment of perisynaptic GluA1 homomers to synaptic sites (He et al., 2009; Park et al., 2016). On the other hand, genetic removal of the GluA1 PDZ ligand did not seem to affect synaptic targeting or CA1 hippocampal LTP (Kim et al., 2005), and the exact contribution of the GluA1 CTD and interaction with SAP97 isoforms to synaptic entry remains to be elucidated.

Once in the synapse, what scaffolding proteins could control the subsynaptic accumulation of AMPARs in nanodomains? By far the most prominent candidate is PSD-95, also part of the MAGUK family, that is highly enriched in the PSD. PSD-95 is stably anchored at the postsynaptic membrane via palmitoylation (Craven et al., 1999; El-Husseini et al., 2000),

and interacts with AMPAR auxiliary proteins, including the transmembrane AMPAR regulatory protein (TARP) family, to retain AMPARs at synaptic sites (Bats et al., 2007; Schnell et al., 2002). PSD-95 distribution within individual PSDs is highly heterogeneous, forming distinct subsynaptic nanodomains (Broadhead et al., 2016; Fukata et al., 2013; MacGillavry et al., 2013; Tang et al., 2016) that are enriched with AMPARs as found by EM (Chen et al., 2008), and super-resolution microscopy (MacGillavry et al., 2013; Nair et al., 2013; Tang et al., 2016). Thus, PSD-95 is likely to play a critical role in the immobilization of AMPARs in nanodomains. Indeed, immobilization of AMPARs within the synapse is found to be highly heterogeneous (Li and Blanpied, 2016; Nair et al., 2013) with restricted zones of diffusion (Ehlers et al., 2007; Kerr and Blanpied, 2012), where they can be retained for long periods of time (Adesnik et al., 2005). Furthermore, AMPARs within nanodomains are largely immobilized, whereas the AMPARs outside nanodomains are much more mobile (Nair et al., 2013). The mechanisms involved in the clustering of MAGUKs underlying the formation of AMPAR nanodomains, however, remain largely unexplored. Palmitoylation of MAGUKs might be crucial as it is involved in maintaining PSD-95 nanodomains (Fukata et al., 2013), and is essential for receptor binding (Jeyifous et al., 2016). Moreover, along with MAGUKs there are many other scaffolding proteins present in the PSD, such as Shanks, SAPAPs, and Homers, that together create a laminated structure providing a highly linked platform likely involved in the retention and subsynaptic positioning of receptors (Burette et al., 2012; Harris and Weinberg, 2012; Valtschanoff and Weinberg, 2001) (Figure 3A). As such, also these scaffolding molecules that reside in the deeper layers of the PSD and link to the cytoplasmic actin cytoskeleton, were found co-enriched in receptor nanodomains, suggesting a highly interlinked postsynaptic “super-complex” (Frank and Grant, 2017). To what extent each of these components simply constitute the nanodomain, or are instructive in the formation of the transsynaptic nanocolumn however, is as yet unknown.

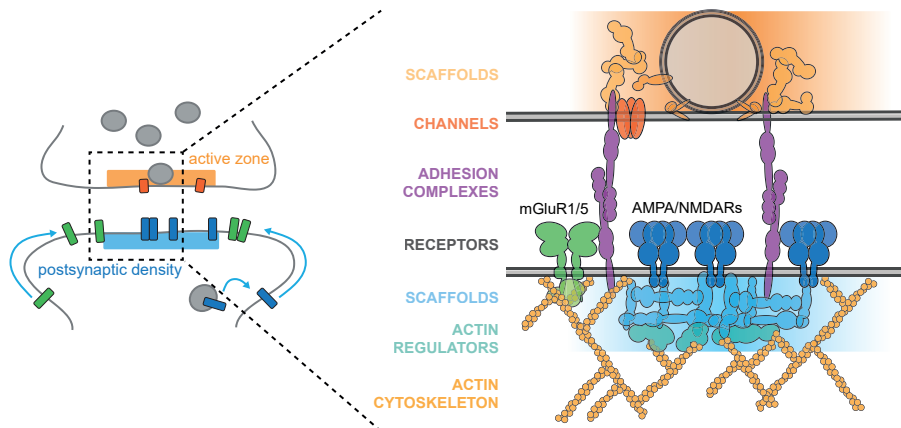
Unlike the well-studied AMPAR-scaffold interactions, identification of scaffolding proteins that regulate the lateral diffusion of mGluRs is largely lacking. Interestingly, similar to GluA1, mGluRs also contain a typical C-terminal type-I PDZ ligand known to interact with Shank and Tamalin (Kitano et al., 2002; Tu et al., 1999). However, this domain seems primarily involved in surface trafficking, and might not be involved in the positioning of the receptor (Kitano et al., 2002). The most prominent candidate, however, is the scaffolding protein Homer, which can interact with the CTD of group I mGluRs (Enz, 2012; Tu et al., 1999), and is generally proposed as the protein regulating the subsynaptic positioning of mGluRs. Indeed, Homer overexpression induces clustering of group I mGluRs in heterologous cell systems (Ciruela et al., 2000; Tadokoro et al., 1999), Homer and group I mGluRs co-localize at the light microscopy level (Tadokoro et al., 1999), move together in developing hippocampal neurons, and mGluR5 becomes more mobile when the binding with long Homer1b/c forms is disrupted by mutation or co-expression of Homer1a, a short Homer isoform that acts as dominant negative disrupting the interaction of mGluR5 with the longer Homer isoforms (Brakeman et al., 1997; Sergé et al., 2002; Xiao et al., 1998).

A recent study identified alterations in the mGluR5-Homer crosstalk in a new *Fmrl* KO mouse, a model for Fragile X syndrome (Aloisi et al., 2017). In these *Fmrl* KO mice, mGluR5 displayed increased mobility, specifically the small synaptic fraction, which was attributed to the disruption of the mGluR5-Homer1b/c interaction by overexpression of Homer1a (Aloisi et al., 2017). However, although these findings show that the small fraction of mGluR5 that was able to enter the PSD (8% of total mGluR5 pool) is dynamically

regulated by Homer, evidence for a role of Homer in clustering mGluRs at its preferred location within the perisynaptic domain is lacking. Moreover, given that Homer is highly enriched in the PSD, distant from the mGluRs that are concentrated in the perisynaptic domain, Homer might not be the prominent scaffold for mGluRs at perisynaptic sites. Rather, Homer might function as an adaptor protein, mediating mGluR signaling by forming a link between mGluR5 and downstream signaling pathways (Shiraishi-Yamaguchi and Furuichi, 2007). Intriguingly, the same study found that the loss of interaction between mGluR5 and Homer1b/c resulted in a tighter association between mGluR5 and NMDARs, associated with abnormal NMDAR functioning and plasticity (Aloisi et al., 2017). Importantly, this effect was rescued by knockdown of Homer1a. This supports the idea that a correct balance between the binding of long and short Homer forms to mGluR in specific physiological conditions are essential for proper mGluR signaling.

A

transient retention and steric hindrance



B

AMPA and mGluR1/5 receptor topology

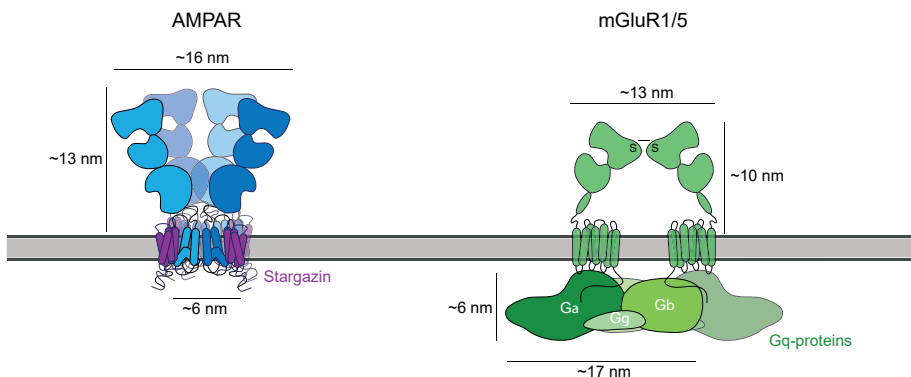


Figure 3. Mechanisms underlying the dynamic positioning of glutamate receptors

Figure 3 continued on next page

Figure 3 continued

(A) Side view of a synapse showing the subsynaptic distribution of the AMPA-, NMDA- and mGluR1/5-type receptors established by mechanisms regulating the synaptic entry and retention of these glutamate receptor types. The zoom of the synapse in side view reveals possible mechanisms underlying the distinct subsynaptic positioning of the glutamate receptor types; transient retention of glutamate receptors via intracellular interactions with scaffolding proteins and extracellular interactions with synaptic cleft proteins, and steric hindrance due to molecular crowding of the different synaptic components and cytoskeletal hindrance at the border of the PSD. (B) Side view of the tetrameric AMPAR (blue) in complex with Stargazin (magenta) based on (Greger et al., 2017) (left), and dimeric mGluR1/5 coupled to its cognate Gq-proteins (green) based on (Nishimura et al., 2010) (right). This figure shows the Y-shaped GluA2 homomer (Greger et al., 2017) and the closed-closed resting conformation of an mGluR dimer (Muto et al., 2007). Models are approached to scale.

Apart from Homer, a few other candidates could underlie the synaptic entry and retention of mGluRs. For instance, Norbin is an accessory protein of mGluRs shown to be important for mGluR surface expression and signaling (Wang et al., 2009), and was also found to accumulate in the perisynaptic domain (Westin et al., 2014). Thus, Norbin could potentially play an important role in regulating the availability and positioning of mGluRs modulating mGluR function in synapses. Additionally, other CTD interaction partners have been determined such as Calmodulin (Minakami et al., 1997), Filamin-A (Enz, 2002), Siah-1A (Ishikawa et al., 1999), Presol (Hu et al., 2012), Tamalin (Kitano et al., 2002), and Shank (Tu et al., 1999). However, whether these proteins play a role in mGluR positioning, rather than in regulating mGluR trafficking or signaling, remains to be established.

Extracellular interactions with synaptic cleft proteins

For AMPARs, the mechanisms underlying the targeting to and positioning at synapses have largely been ascribed to the intracellular tail of AMPARs (Shi et al, 2001; Anggono and Haganir, 2012; Shepherd and Haganir, 2007). Recent studies however suggest that the extracellular domain of AMPARs could also have an instructive role in subsynaptic targeting (Diaz-Alonso et al., 2017; Elegheert et al., 2016; Matsuda et al., 2016; Watson et al., 2017). AMPARs contain two extracellular domains, the ligand-binding domain (LBD) and the distant N-terminal domain (NTD) which encompass 50% of the receptor, extending 13 nm into the synaptic cleft. Removing the NTD from GluA1 was shown to prevent its synaptic targeting and impaired the maintenance of LTP (Diaz-Alonso et al., 2017; Watson et al., 2017). Moreover, the fusion of a GFP tag at the NTD (Diaz-Alonso et al., 2017; Granger et al., 2013; Greger et al., 2017), or coupling large quantum dots (Lee et al., 2017a), seemed to hamper the entry of GluA1 receptors, possibly by interfering with endogenous NTD interactions, but also see (Nabavi et al., 2014). Interestingly, the NTD sequence of different AMPAR subunits is highly variable. Indeed, deleting the NTD from GluA2 did not prevent synaptic entry (Diaz-Alonso et al., 2017), and replacing the GluA1 NTD with the GluA2 NTD promoted the synaptic entry of GluA1 receptors (Watson et al., 2017), suggesting that subunit-specific trafficking of AMPARs can in part be mediated by extracellular interactions. An interesting model in this respect would be that while the CTDs of AMPARs determine the trafficking to and from synapses, the NTD of AMPARs mediate the anchoring and positioning, and perhaps instruct the transsynaptic alignment of the receptors within the PSD with the vesicle release site at the presynaptic active zone.

How does the NTD mediate receptor positioning? Several proteins have been found to interact with the extracellular domain of different AMPAR subunits (Figure 3A), such as

N-cadherin (Saglietti et al., 2007), neuroligin-1 (Budreck et al., 2013), pentraxins (Farhy-Tselnicker et al., 2017; Lee et al., 2017b; O'Brien et al., 1999), LRRTMs (Schwenk et al., 2012), and the EphB2 receptor via ephrinBs (Dalva et al., 2000; Grunwald et al., 2001). However, their precise role in regulating synaptic entry or retention of AMPARs remains to be established (Biederer et al., 2017). Interestingly, the postsynaptic adhesion protein LRRTM2 was also found to form stable nanodomains (Chamma et al., 2016), and LRRTM2 knockdown resulted in decreased AMPAR-mediated synaptic currents (de Wit et al., 2009; Soler-Llavina et al., 2011), and might thus be an interesting candidate for the retention and subsynaptic positioning of AMPARs. Recent studies on GluD2 and kainate receptors found a similar requirement for NTD-dependent interactions in synaptic retention (Elegheert et al., 2016; Matsuda et al., 2016), suggesting that extracellular, and perhaps transsynaptic, interactions with glutamate receptors are a more general instructive mechanism to control synaptic entry and positioning.

Steric hindrance

In addition to direct biochemical interactions between receptors and other proteins, alternative, more indirect mechanisms are likely to contribute to the positioning of receptors. As the name implies, the PSD is an extremely densely packed structure with numerous synaptic proteins forming an intricate network just underneath the cell membrane (Burette et al., 2012; Sheng and Hoogenraad, 2007), and is thus likely to impose a physical barrier for receptors diffusing in the synaptic membrane (Figure 3A). Most directly, PSD-95 is attached to the membrane via palmitoylation and forms an intricate lateral structure close to the cytoplasmic face of the postsynaptic membrane. Indeed, computational modeling predicts that simply by molecular crowding, the PSD can trap receptors for hours, even in the absence of interactions (Santamaria et al., 2010). Additionally, using the heterogeneous distribution of PSD-95 as a template, measured experimentally with single-molecule localization microscopy, it was computationally predicted that receptor size contributes considerably to the extent that receptors can diffuse through the synapse and exchange with the extrasynaptic membrane. Importantly, also experimentally it was shown that while a single-pass transmembrane protein with one PDZ motif is efficiently targeted to the synapse, to the same extent as AMPARs, the much larger AMPAR was far less mobile (Li et al., 2016). Moreover, the diffusion properties of a single-pass transmembrane probe lacking an intracellular PSD-95 binding site was highly heterogeneous within individual synapses, and correlated inversely with the local density in PSD-95, i.e. mobility of this probe was significantly restricted in high-density PSD-95 nanodomains (Li and Blanpied, 2016). Thus, molecular crowding, in concert with molecular binding, can trap and limit the exit of receptors from the PSD and might as such favor the subsynaptic positioning of receptors in high-density scaffold nanodomains. Conversely, the PSD may act as an exclusion matrix or sieve that filters on molecular size to regulate receptor entry. This implies that different receptor subtypes must have different structures and geometries to contribute, probably in concert with scaffold interactions, to the distinct subsynaptic patterns of receptors (Figure 3B).

The transmembrane domain (TMD) of glutamate receptors contributes to steric hindrance in the molecular crowded PSD (Li et al., 2016). The AMPAR TMD sector forms a pore of approximately 5.5 nm in diameter (Sobolevsky et al., 2009), similar for different combinations of AMPAR subunits (Herguedas et al., 2016). On the other hand, mGluR forms dimers and each TMD consists of seven TM helices that each have a diameter of 3.5

nm (Muto et al., 2007). Thus, the TMD of an mGluR dimer is similar in size to an AMPAR tetramer. However, based on the crystal structures from group II mGluRs, highly similar in structure to group I mGluRs, several conformational states have been predicted that also affect the proximity of the two TMDs relative to each other (Muto et al., 2007). Interestingly, the distance between the TMDs of the mGluR dimer highly varies between the resting state (large) and the active state (small) of the receptor, varying the degree of steric hindrance in the synaptic membrane (Muto et al., 2007). This suggests that the regulation of synaptic entry and positioning of mGluRs is an activity-dependent process. Importantly, AMPARs additionally closely assemble with a variety of auxiliary subunits in the TMD that regulate AMPAR properties such as trafficking, expression, and functioning (Greger et al., 2017) (Figure 3B). Recent cryo-EM studies reveal that homo-tetrameric GluA2, also suggested for hetero-tetrameric AMPAR complexes (Kim et al., 2010), can interact with one to four Stargazins, with a preferred stoichiometry of one to two depending on Stargazin expression (Twomey et al., 2016; Zhao et al., 2016). In conclusion, although AMPARs and mGluRs differ broadly in the assembly of their TMD, the overall size of the TMD in the plane of the synaptic membrane contributing to steric hindrance appears to be highly similar.

Together with the TMD, the cytoplasmic CTD may also contribute to aggravating steric hindrance of the receptor types. The CTD of the GluA1 and GluA2/3 subunits are only 81 and 50 amino acid residues long respectively, whereas mGluR5a and mGluR5b have a very large CTD of 350 and 382 residues respectively. Unfortunately, because the CTDs are largely unfolded structures, the intracellular structures of mGluRs and the AMPAR/TARP complex have yet to be crystallized. However, the most striking difference between the two receptor types in their CTDs, is that unlike iGluRs, mGluRs are coupled to Gq-proteins. Gq-proteins assemble close to the cytoplasmic face of the synaptic membrane by interacting in the pocket formed between the second and third intracellular TM loops of mGluR (De Blasi et al., 2001) (Figure 3B). The Gq-proteins are composed of α -, β -, and γ -subunits with a total estimated size of 17.3 nm long, 17.3 nm wide and, 6.09 nm high based on the crystal structure (Nishimura et al., 2010). Even though the interaction with Stargazins also adds some bulk to the AMPAR CTD (Figure 3B), this is considerably less than the Gq-proteins interacting with the mGluR CTD. The differences suggest that the molecular size of the CTD in full assembly with its other constituents might contribute to the segregation of AMPAR and mGluRs, where the molecular crowded PSD acts as a size exclusion matrix regulating receptor entry. Interestingly, the full complex of Gq-proteins binds to the resting conformation of mGluRs, and upon activation the β - and γ -subunits uncouple, perhaps alleviating steric hindrance due to molecular crowding. This notion is supported by a study showing increased mobility of mGluR5 upon activation with its specific agonist DHPG (Sergé et al., 2002). This, in addition to the conformational changes upon activation, furthermore supports that the regulation of synaptic entry of mGluRs is an activity-dependent process.

The significant accumulation of synaptic cleft molecules could also hinder receptor entry via steric hindrance with the extracellular domain of receptors. AMPARs consist of two globular extracellular structures, the NTD and LBD, whereas mGluRs consist of one extracellular LBD and a small cysteine-rich region (Figure 3B). Interestingly, the density map of a tetrameric AMPAR can accommodate two dimeric crystal structures of the mGluR1 extracellular domain (Greger et al., 2017; Kunishima et al., 2000; Nakagawa et al., 2005). Although there are slight differences between the extracellular domains of

AMPA receptors and mGluRs, the overall conformation results in a high similarity in the secondary structure of these receptors and it is thus not likely that steric hindrance contributes to the segregation of these receptor types. Rather, adhesion molecules are suggested to be key to the transsynaptic alignment of the presynaptic vesicle release site with postsynaptic AMPAR nanodomains (Biederer et al., 2017; Tang et al., 2016). Several active zone proteins, such as Liprins, LAR, RIM, but also other pre- and postsynaptic components, are likely to be part of the lateral oligomerization forming a transsynaptic nanocolumn (Biederer et al., 2017). Also, some adhesion proteins specifically concentrate at the postsynaptic edge, such as SynCAM1 or more towards the center, such as EphB2 (Perez de Arce et al., 2015), or the classical synaptic adhesion molecule N-cadherin that initially localizes throughout the synaptic cleft, but at later stages forms distinct clusters at the edge (Elste and Benson, 2006; Uchida et al., 1996) providing a heterogeneous localization pattern possibly resembling the transsynaptic nanocolumns. Together, adhesion molecules can contribute to the retention and positioning of receptors by imposing diffusional barriers.

Cytoskeletal hindrance

The confinement of receptors within specific subsynaptic areas may also arise from structures that compartmentalize the synaptic membrane leading to steric hindrance counteracting free receptor diffusion and/or accumulations of receptor clusters (Kusumi et al., 2005). Modeling studies have sought to investigate the possibility that this can lead to the clustering of receptors by considering a boundary with small openings or a stochastic gate that allows receptor escape (Earnshaw and Bressloff, 2006; Holcman and Triller, 2006). Holcman and Triller (2006) modeled the PSD as two simplified compartments: a central region with both bound and unbound scaffolding molecules to receptors and a surrounding annulus that represents a fence formed by transmembrane proteins and submembranous cytoskeleton. By adding a small opening to this fence to allow for few receptors to escape, this model could reproduce fluorescence recovery after photobleaching (FRAP) data measured for AMPARs. However, these models treat the interior of the PSD as a homogeneous compartment, and therefore cannot explain the subsynaptic distribution of AMPARs. Rather, these models might be useful to consider the boundary of the PSD as a gatekeeper to receptor entry by varying the size of the small opening to better understand entry of different receptors.

The perisynaptic actin cytoskeleton could impose a diffusional barrier to receptor entry into the synapse. At the perisynaptic membrane actin is in close proximity to the cytoplasmic surface forming an intricate mesh-like structure of sub-membranous filaments, whereas actin is largely absent from the PSD (Burette et al., 2012; Frost et al., 2010; Morone et al., 2006; Westin et al., 2014) (Figure 3A). However, there is no clear evidence that the actin filamentous meshwork is enriched at the perisynaptic membrane. Thus, actin is likely not to be involved in the subsynaptic positioning of iGluRs, but might be involved in the exclusion of the larger mGluRs from the PSD and perhaps even in clustering mGluRs at perisynaptic sites. The actin-based membrane skeleton (MSK) may act as a gatekeeper or fence, but also transmembrane proteins attached to the MSK may behave as pickets that result in steric hindrance and nonspecific corralling of receptor diffusion at the perisynaptic domain, where only a few receptors 'hop the fence' of the PSD (Morone et al., 2006; Sako and Kusumi, 1994). Also, freely diffusing receptors may cluster when encountering these fences/pickets, a process called diffusion-limited aggregation (DLA). In support of this picket-fence model an EM study revealed that in non-neuronal cells the actin-based MSK

can partition the cell membrane limiting receptor diffusion within these compartments (Morone et al., 2006). The size of these MSK meshes was determined to range from 50 to 200 nm (Morone et al., 2006), which would also allow receptors to accumulate in the perisynaptic domain. Additionally, the recent finding that G-proteins are co-clustered with GPCRs at the cell surface defined by the actin cytoskeleton further support this notion (Sungkaworn et al., 2017). Although to date there is no ultrastructural evidence for actin meshes at the perisynaptic membrane, it is possible that the actin MSK is an important player in the gatekeeper role of the PSD, perhaps by forming a fence that only allows some receptors to pass.

Conclusions and future perspectives

The molecular organization of synapses is undoubtedly a critical determinant of the efficiency of synaptic transmission. The complexity of synapse organization has indeed been underlined by extensive genetic and biochemical approaches that over the past decades have resulted in a comprehensive “parts list” of synapses. Yet, how are these components properly assembled into the large macromolecular complexes that organize the glutamate receptors at the surface? Emerging evidence demonstrates that the structure and molecular organization of synapses is highly heterogeneous and organized in distinct subsynaptic nanodomains (Biederer et al., 2017), but we are only starting to understand how, within individual synapses, different proteins find their correct location. Undoubtedly, the overall assembly of synapses is directed by specific protein-protein interactions via well-defined protein interaction motifs (Kim and Sheng, 2004). These core biochemical processes give rise to the stable molecular complexes that effectively concentrate receptors at synaptic sites and couple these receptors to intracellular scaffolding, adaptor, and signaling proteins. At the same time, these mechanisms enable the dynamic modifications of synaptic structure in response to activity. However, while these mechanisms can explain the assembly and stoichiometry of specific components into molecular complexes, to date it is not fully understood how these mechanisms contribute to the spatial organization of molecules at the synapse, i.e. how proteins are positioned relative to each other within individual synapses. Moreover, apart from these classic biochemical operations, the contribution of biophysical processes such as steric hindrance, membrane composition (Tulodziecka et al., 2016), and phase transitions (Zeng et al., 2016) are only beginning to be explored in the context of synapse organization.

We have discussed potential mechanisms that could work globally to organize the synapse in functional domains and mechanisms that act on specific receptor subtypes, but many questions about the structural organization of synapses remain unanswered. What is the exact composition of a nanodomain? Is there a fixed number of proteins enriched in these domains and are there proteins that are exclusively found within the domain? Are AMPARs with different subunit compositions co-enriched in nanodomains? How do nanodomains develop? Are they present in early, newly formed PSDs, or do they form in response to specific activity patterns? Clearly, there is a strong need for experimental directions that can tag or disrupt specific aspects of synapse organization, without affecting overall synapse structure. Ongoing developments in super-resolution, single-molecule tracking, and EM tomography will be key in determining how synapses are built from their numerous components.

Alterations in glutamatergic synapse structure and function seem to represent a common hallmark of many cognitive disorders (Volk et al., 2015). Intriguingly, these disorders span a broad clinical spectrum, including intellectual disability, autism spectrum disorder, and schizophrenia, but all seem to stem from a common defect; synaptic dysfunction. Indeed, these disorders are frequently associated with loss of synapses, or changes in morphology of dendritic spines. Given that many disease-associated genes are components of the glutamate receptor-associated complexes or can regulate glutamate receptor function through the actin cytoskeleton, indicates that disruptions in the precise positioning of glutamate receptors can underlie the development of these diseases. Future directions aimed at understanding the spatial organization of glutamate receptors will therefore not only be indispensable for a deeper insight in the regulation of synaptic transmission and plasticity, but will also contribute to the identification of disease mechanisms.

Acknowledgements

We would like to thank Dr. Thomas Blanpied, Sai Sachin Divakaruni, Dr. Helmut Kessels, Feline Lindhout, Dieudonné van de Willige, and all members of the MacGillavry lab for discussions and critical reading of the manuscript. This work was supported by NWO (ALW-VENI 863.13.020, ALW-VIDI 171.029 and the Graduate Program of Quantitative Biology and Computational Life Sciences), the European Research Council (ERC-StG 716011), and a NARSAD Young Investigator Award.

References

- Adesnik, H., Nicoll, R.A., and England, P.M. (2005). Photoinactivation of native AMPA receptors reveals their real-time trafficking. *Neuron* 48, 977-985.
- Aloisi, E., Le Corf, K., Dupuis, J., Zhang, P., Ginger, M., Labrousse, V., Spatuzza, M., Georg Haberl, M., Costa, L., Shigemoto, R., Tappe-Theodor, A., Drago, F., Vincenzo Piazza, P., Mulle, C., Groc, L., Ciranna, L., Catania, M.V., and Frick, A. (2017). Altered surface mGluR5 dynamics provoke synaptic NMDAR dysfunction and cognitive defects in *Fmrl* knockout mice. *Nat. Commun.* 8, 1103.
- Anggono, V., and Huganir, R.L. (2012). Regulation of AMPA receptor trafficking and synaptic plasticity. *Curr. Opin. Neurobiol.* 22, 461-469.
- Anwyl, R. (1999). Metabotropic glutamate receptors: electrophysiological properties and role in plasticity. *Brain Res. Brain Res. Rev.* 29, 83-120.
- Balschun, D., and Wetzel, W. (2002). Inhibition of mGluR5 blocks hippocampal LTP *in vivo* and spatial learning in rats. *Pharmacol. Biochem. Behav.* 73, 375-380.
- Bashir, Z.I., Bortolotto, Z.A., Davies, C.H., Berretta, N., Irving, A.J., Seal, A.J., Henley, J.M., Jane, D.E., Watkins, J.C., and Collingridge, G.L. (1993a). Induction of LTP in the hippocampus needs synaptic activation of glutamate metabotropic receptors. *Nature* 363, 347-350.
- Bashir, Z.I., Jane, D.E., Sunter, D.C., Watkins, J.C., and Collingridge, G.L. (1993b). Metabotropic glutamate receptors contribute to the induction of long-term depression in the CA1 region of the hippocampus. *Eur. J. Pharmacol.* 239, 265-266.
- Bats, C., Groc, L., and Choquet, D. (2007). The interaction between Stargazin and PSD-95 regulates AMPA receptor surface trafficking. *Neuron* 53, 719-734.
- Baude, A., Nusser, Z., Roberts, J.D., Mulvihill, E., McIlhinney, R.A., and Somogyi, P. (1993). The metabotropic glutamate receptor (mGluR1 α) is concentrated at perisynaptic membrane of neuronal subpopulations as detected by immunogold reaction. *Neuron* 11, 771-787.
- Bear, M.F., Huber, K.M., and Warren, S.T. (2004). The mGluR theory of fragile X mental retardation. *Trends Neurosci.* 27, 370-377.
- Bernard, V., Somogyi, P., and Bolam, J.P. (1997). Cellular, subcellular, and subsynaptic distribution of AMPA-type glutamate receptor subunits in the neostriatum of the rat. *J. Neurosci.* 17, 819-833.
- Biederer, T., Kaeser, P.S., and Blanpied, T.A. (2017). Transcellular Nanoalignment of synaptic function. *Neuron* 96, 680-696.
- Blanpied, T.A., Scott, D.B., and Ehlers, M.D. (2002). Dynamics and regulation of clathrin coats at specialized endocytic zones of dendrites and spines. *Neuron* 36, 435-449.
- Blanpied, T.A., Scott, D.B., and Ehlers, M.D. (2003). Age-related regulation of dendritic endocytosis associated with altered clathrin dynamics. *Neurobiol. Aging* 24, 1095-1104.
- Bortolotto, Z.A., Bashir, Z.I., Davies, C.H., and Collingridge, G.L. (1994). A molecular switch activated by metabotropic glutamate receptors regulates induction of long-term potentiation. *Nature* 368, 740-743.
- Boucher, J., Kroger, H., and Sik, A. (2010). Realistic modelling of receptor activation in hippocampal excitatory synapses: analysis of multivesicular release, release location, temperature and synaptic cross-talk. *Brain Struct. Funct.* 215, 49-65.
- Brakeman, P.R., Lanahan, A.A., O'Brien, R., Roche, K., Barnes, C.A., Huganir, R.L., and Worley, P.F. (1997). Homer: a protein that selectively binds metabotropic glutamate receptors. *Nature* 386, 284-288.
- Brasnjó, G., and Otis, T.S. (2001). Neuronal glutamate transporters control activation of postsynaptic metabotropic glutamate receptors and influence cerebellar long-term depression. *Neuron* 31, 607-616.
- Broadhead, M.J., Horrocks, M.H., Zhu, F., Muresan, L., Benavides-Piccione, R., DeFelipe, J., Fricker, D., Kopanitsa, M.V., Duncan, R.R., Klenerman, D., Komiyama, N.H., Lee, S.F., and Grant, S.G. (2016). PSD95 nanoclusters are postsynaptic building blocks in hippocampus circuits. *Sci. Rep.* 6, 24626.
- Budreck, E.C., Kwon, O.B., Jung, J.H., Baudouin, S., Thommen, A., Kim, H.S., Fukazawa, Y., Harada, H., Tabuchi, K., Shigemoto, R., Scheiffele, P., and Kim, J.H. (2013). Neuroigin1 controls synaptic abundance of NMDA-type glutamate receptors through extracellular coupling. *Proc. Natl. Acad. Sci. U. S. A.* 110, 725-730.
- Burette, A.C., Lesperance, T., Crum, J., Martone, M., Volkman, N., Ellisman, M.H., and Weinberg, R.J. (2012). Electron tomographic analysis of synaptic ultrastructure. *J. Comp. Neurol.* 520, 2697-2711.
- Chamma, I., Letellier, M., Butler, C., Tessier, B., Lim, K.H., Gauthereau, I., Choquet, D., Sibarita, J.B., Park, S., Sainlos, M., and Thoumine, O. (2016). Mapping the dynamics and nanoscale organization of synaptic adhesion proteins using monomeric streptavidin. *Nat. Commun.* 7, 10773.
- Chen, X., Winters, C., Azzam, R., Li, X., Galbraith, J., Leapman, R., and Reese, T. (2008). Organization of the core structure of the postsynaptic density. *Proc. Natl. Acad. Sci. U. S. A.* 105, 4453-4458.

- Ciruela, F., Soloviev, M.M., Chan, W.Y., and McIlhinney, R.A. (2000). Homer-1c/Vesl-1L modulates the cell surface targeting of metabotropic glutamate receptor type alpha: evidence for an anchoring function. *Mol. Cell. Neurosci.* 15, 36-50.
- Cohen, A.S., Raymond, C.R., and Abraham, W.C. (1998). Priming of long-term potentiation induced by activation of metabotropic glutamate receptors coupled to phospholipase C. *Hippocampus* 8, 160-170.
- Cohen, A.S., Coussens, C.M., Raymond, C.R., and Abraham, W.C. (1999). Long-lasting increase in cellular excitability associated with the priming of LTP induction in rat hippocampus. *J. Neurophysiol.* 82, 3139-3148.
- Conn, P.J., and Pin, J.P. (1997). Pharmacology and functions of metabotropic glutamate receptors. *Annu. Rev. Pharmacol. Toxicol.* 37, 205-237.
- Coombs, I.D., MacLean, D.M., Jayaraman, V., Farrant, M., and Cull-Candy, S.G. (2017). Dual effects of TARP gamma-2 on glutamate efficacy can account for AMPA receptor autoinactivation. *Cell Rep.* 20, 1123-1135.
- Craven, S., El-Husseini, A., and Brecht, D. (1999). Synaptic targeting of the postsynaptic density protein PSD-95 mediated by lipid and protein motifs. *Neuron* 22, 497-509.
- Cui-Wang, T., Hanus, C., Cui, T., Helton, T., Bourne, J., Watson, D., Harris, K.M., and Ehlers, M.D. (2012). Local zones of endoplasmic reticulum complexity confine cargo in neuronal dendrites. *Cell* 148, 309-321.
- Dalva, M.B., Takasu, M.A., Lin, M.Z., Shamah, S.M., Hu, L., Gale, N.W., and Greenberg, M.E. (2000). EphB receptors interact with NMDA receptors and regulate excitatory synapse formation. *Cell* 103, 945-956.
- Dani, A., Huang, B., Bergan, J., Dulac, C., and Zhuang, X. (2010). Superresolution imaging of chemical synapses in the brain. *Neuron* 68, 843-856.
- De Blasi, A., Conn, P.J., Pin, J., and Nicoletti, F. (2001). Molecular determinants of metabotropic glutamate receptor signaling. *Trends Pharmacol. Sci.* 22, 114-120.
- de Wit, J., Sylwestrak, E., O'Sullivan, M.L., Otto, S., Tiglio, K., Savas, J.N., Yates 3rd, J.R., Comoletti, D., Taylor, P., and Ghosh, A. (2009). LRRTM2 interacts with Neurexin1 and regulates excitatory synapse formation. *Neuron* 64, 799-806.
- DeGiorgis, J.A., Galbraith, J.A., Dosemeci, A., Chen, X., and Reese, T.S. (2006). Distribution of the scaffolding proteins PSD-95, PSD-93, and SAP97 in isolated PSDs. *Brain Cell Biol.* 35, 239-250.
- Dehnes, Y., Chaudhry, F.A., Ullensvang, K., Lehre, K.P., Storm-Mathisen, J., and Danbolt, N.C. (1998). The glutamate transporter EAAT4 in rat cerebellar Purkinje cells: a glutamate-gated chloride channel concentrated near the synapse in parts of the dendritic membrane facing astroglia. *J. Neurosci.* 18, 3606-3619.
- Diaz-Alonso, J., Sun, Y.J., Granger, A.J., Levy, J.M., Blankenship, S.M., and Nicoll, R.A. (2017). Subunit-specific role for the amino-terminal domain of AMPA receptors in synaptic targeting. *Proc. Natl. Acad. Sci. U. S. A.* 114, 7136-7141.
- Earnshaw, B.A., and Bressloff, P.C. (2006). Biophysical model of AMPA receptor trafficking and its regulation during long-term potentiation/long-term depression. *J. Neurosci.* 26, 12362-12373.
- Ehlers, M., Heine, M., Groc, L., Lee, M., and Choquet, D. (2007). Diffusional trapping of GluR1 AMPA receptors by input-specific synaptic activity. *Neuron* 54, 447-460.
- Elgheert, J., Kakegawa, W., Clay, J.E., Shanks, N.F., Behiels, E., Matsuda, K., Kohda, K., Miura, E., Rossmann, M., Mitakidis, N., Motohashi, J., Chang, V.T., Siebold, C., Greger, I.H., Nakagawa, T., Yuzaki, M., and Aricescu, A.R. (2016). Structural basis for integration of GluD receptors within synaptic organizer complexes. *Science* 353, 295-299.
- El-Husseini, A., Craven, S., Chetkovich, D., Firestein, B., Schnell, E., Aoki, C., and Brecht, D. (2000). Dual palmitoylation of PSD-95 mediates its vesiculotubular sorting, postsynaptic targeting, and ion channel clustering. *J. Cell Biol.* 148, 159-172.
- Elste, A.M., and Benson, D.L. (2006). Structural basis for developmentally regulated changes in cadherin function at synapses. *J. Comp. Neurol.* 495, 324-335.
- Enz, R. (2002). The actin-binding protein Filamin-a interacts with the metabotropic glutamate receptor type 7. *FEBS Lett.* 514, 184-188.
- Enz, R. (2012). Structure of metabotropic glutamate receptor C-terminal domains in contact with interacting proteins. *Front. Mol. Neurosci.* 5, 52.
- Erreger, K., Dravid, S.M., Banke, T.G., Wyllie, D.J., and Traynelis, S.F. (2005). Subunit-specific gating controls rat NR1/NR2A and NR1/NR2B NMDA channel kinetics and synaptic signalling profiles. *J. Physiol.* 563, 345-358.
- Fan, W., Ster, J., and Gerber, U. (2010). Activation conditions for the induction of metabotropic glutamate receptor-dependent long-term depression in hippocampal CA1 pyramidal cells. *J. Neurosci.* 30, 1471-1475.
- Farhy-Tselnicker, I., van Casteren, A.C.M., Lee, A., Chang, V.T., Aricescu, A.R., and Allen, N.J. (2017). Astrocyte-secreted glypican 4 regulates release of neuronal pentraxin 1 from axons to induce functional synapse formation. *Neuron* 96 (428-445), e413.
- Fitzjohn, S.M., Irving, A.J., Palmer, M.J., Harvey, J., Lodge, D., and Collingridge, G.L. (1996). Activation of group

- mGluRs potentiates NMDA responses in rat hippocampal slices. *Neurosci. Lett.* 203, 211-213.
- Francesconi, W., Cammalleri, M., and Sanna, P.P. (2004). The metabotropic glutamate receptor 5 is necessary for late-phase long-term potentiation in the hippocampal CA1 region. *Brain Res.* 1022, 12-18.
- Francesconi, A., Kumari, R., and Zukin, R.S. (2009). Regulation of group I metabotropic glutamate receptor trafficking and signaling by the caveolar/lipid raft pathway. *J. Neurosci.* 29, 3590-3602.
- Frank, R.A., and Grant, S.G. (2017). Supramolecular organization of NMDA receptors and the postsynaptic density. *Curr. Opin. Neurobiol.* 45, 139-147.
- Franks, K.M., Stevens, C.F., and Sejnowski, T.J. (2003). Independent sources of quantal variability at single glutamatergic synapses. *J. Neurosci.* 23, 3186-3195.
- Freche, D., Pannasch, U., Rouach, N., and Holcman, D. (2011). Synapse geometry and receptor dynamics modulate synaptic strength. *PLoS One* 6, e25122.
- Frost, N.A., Shroff, H., Kong, H., Betzig, E., and Blanpied, T.A. (2010). Single-molecule discrimination of discrete perisynaptic and distributed sites of actin filament assembly within dendritic spines. *Neuron* 67, 86-99.
- Fukata, Y., Dimitrov, A., Boncompain, G., Vielemeyer, O., Perez, F., and Fukata, M. (2013). Local palmitoylation cycles define activity-regulated postsynaptic subdomains. *J. Cell Biol.* 202, 145-161.
- Goodman, L., Baddeley, D., Ambroziak, W., Waites, C.L., Garner, C.C., Soeller, C., and Montgomery, J.M. (2017). N-terminal SAP97 isoforms differentially regulate synaptic structure and postsynaptic surface pools of AMPA receptors. *Hippocampus* 27, 668-682.
- Granger, A.J., and Nicoll, R.A. (2014). LTD expression is independent of glutamate receptor subtype. *Front. Synaptic Neurosci.* 6, 15.
- Granger, A.J., Shi, Y., Lu, W., Cerpas, M., and Nicoll, R.A. (2013). LTP requires a reserve pool of glutamate receptors independent of subunit type. *Nature* 493, 495-500.
- Greger, I.H., Watson, J.F., and Cull-Candy, S.G. (2017). Structural and functional architecture of AMPA-type glutamate receptors and their auxiliary proteins. *Neuron* 94, 713-730.
- Greget, R., Pernot, F., Bouteiller, J.M., Ghaderi, V., Allam, S., Keller, A.F., Ambert, N., Legendre, A., Sarmis, M., Haeberle, O., Faupel, M., Bischoff, S., Berger, T.W., and Baudry, M. (2011). Simulation of postsynaptic glutamate receptors reveals critical features of glutamatergic transmission. *PLoS One* 6, e28380.
- Grunwald, I.C., Korte, M., Wolfer, D., Wilkinson, G.A., Unsicker, K., Lipp, H.P., Bonhoeffer, T., and Klein, R. (2001). Kinase-independent requirement of EphB2 receptors in hippocampal synaptic plasticity. *Neuron* 32, 1027-1040.
- Gutierrez-Castellanos, N., Da Silva-Matos, C.M., Zhou, K., Canto, C.B., Renner, M.C., Koene, L.M.C., Ozyildirim, O., Sprengel, R., Kessels, H.W., and De Zeeuw, C.I. (2017). Motor learning requires Purkinje cell synaptic potentiation through activation of AMPA-receptor subunit GluA3. *Neuron* 93, 409-424.
- Harris, K.M., and Stevens, J.K. (1988). Dendritic spines of rat cerebellar Purkinje cells: serial electron microscopy with reference to their biophysical characteristics. *J. Neurosci.* 8, 4455-4469.
- Harris, K.M., and Weinberg, R.J. (2012). Ultrastructure of synapses in the mammalian brain. *Cold Spring Harb Perspect Biol.* 4, 005587.
- Hayashi, Y., Shi, S.H., Esteban, J.A., Piccini, A., Poncer, J.C., and Malinow, R. (2000). Driving AMPA receptors into synapses by LTP and CaMKII: requirement for GluR1 and PDZ domain interaction. *Science* 287, 2262-2267.
- He, Y., Janssen, W.G., Rothstein, J.D., and Morrison, J.H. (2000). Differential synaptic localization of the glutamate transporter EAAC1 and glutamate receptor subunit GluR2 in the rat hippocampus. *J. Comp. Neurol.* 418, 255-269.
- He, K., Song, L., Cummings, L.W., Goldman, J., Huganir, R.L., and Lee, H.K. (2009). Stabilization of Ca²⁺-permeable AMPA receptors at perisynaptic sites by GluR1S845 phosphorylation. *Proc. Natl. Acad. Sci. U. S. A.* 106, 20033-20038.
- Heidinger, V., Manzerra, P., Wang, X.Q., Strasser, U., Yu, S.P., Choi, D.W., and Behrens, M.M. (2002). Metabotropic glutamate receptor 1-induced upregulation of NMDA receptor current: mediation through the Pyk2/Src-family kinase pathway in cortical neurons. *J. Neurosci.* 22, 5452-5461.
- Herguedas, B., Garcia-Nafria, J., Cais, O., Fernandez-Leiro, R., Krieger, J., Ho, H., and Greger, I.H. (2016). Structure and organization of heteromeric AMPA-type glutamate receptors. *Science* 352, aad3873.
- Holbro, N., Grunditz, A., and Oertner, T.G. (2009). Differential distribution of endoplasmic reticulum controls metabotropic signaling and plasticity at hippocampal synapses. *Proc. Natl. Acad. Sci. U. S. A.* 106, 15055-15060.
- Holcman, D., and Triller, A. (2006). Modeling synaptic dynamics driven by receptor lateral diffusion. *Biophys. J.* 91, 2405-2415.
- Hu, J.H., Yang, L., Kammermeier, P.J., Moore, C.G., Brakeman, P.R., Tu, J., Yu, S., Petralia, R.S., Li, Z., Zhang, P.W., Park, J.M., Dong, X., Xiao, B., and Worley, P.F. (2012). Presol dynamically regulates group I metabotropic glutamate receptors. *Nat. Neurosci.* 15, 836-844.

- Huber, K.M., Kayser, M.S., and Bear, M.F. (2000). Role for rapid dendritic protein synthesis in hippocampal mGluR-dependent long-term depression. *Science* 288, 1254-1257.
- Huganir, R.L., and Nicoll, R.A. (2013). AMPARs and synaptic plasticity: the last 25 years. *Neuron* 80, 704-717.
- Insel, P.A., Head, B.P., Patel, H.H., Roth, D.M., Bunday, R.A., and Swaney, J.S. (2005). Compartmentation of G-protein-coupled receptors and their signalling components in lipid rafts and caveolae. *Biochem. Soc. Trans.* 33, 1131-1134.
- Ishikawa, K., Nash, S.R., Nishimune, A., Neki, A., Kaneko, S., and Nakanishi, S. (1999). Competitive interaction of seven in absentia homolog-1A and Ca²⁺/calmodulin with the cytoplasmic tail of group I metabotropic glutamate receptors. *Genes Cells* 4, 381-390.
- Jacob, A.L., and Weinberg, R.J. (2015). The organization of AMPA receptor subunits at the postsynaptic membrane. *Hippocampus* 25, 798-812.
- Jeyifous, O., Lin, E.I., Chen, X., Antinone, S.E., Mastro, R., Drisdell, R., Reese, T.S., and Green, W.N. (2016). Palmitoylation regulates glutamate receptor distributions in postsynaptic densities through control of PSD95 conformation and orientation. *Proc. Natl. Acad. Sci. U. S. A.* 113, E8482-E8491.
- Jezequel, J., Johansson, E.M., Dupuis, J.P., Rogemond, V., Grea, H., Kellermayer, B., Hamdani, N., Le Guen, E., Rabu, C., Lepleux, M., Spatola, M., Mathias, E., Bouchet, D., Ramsey, A.J., Yolken, R.H., Tamouza, R., Dalmiau, J., Honnorat, J., Leboyer, M., and Groc, L. (2017). Dynamic disorganization of synaptic NMDA receptors triggered by autoantibodies from psychotic patients. *Nat. Commun.* 8, 1791.
- Jia, Z., Lu, Y., Henderson, J., Taverna, F., Romano, C., Abramow-Newerly, W., Wojtowicz, J.M., and Roder, J. (1998). Selective abolition of the NMDA component of long-term potentiation in mice lacking mGluR5. *Learn. Mem.* 5, 331-343.
- Kasai, R.S., and Kusumi, A. (2014). Single-molecule imaging revealed dynamic GPCR dimerization. *Curr. Opin. Cell Biol.* 27, 78-86.
- Kavalali, E.T. (2015). The mechanisms and functions of spontaneous neurotransmitter release. *Nat. Rev. Neurosci.* 16, 5-16.
- Kennedy, M.J., and Ehlers, M.D. (2011). Mechanisms and function of dendritic exocytosis. *Neuron* 69, 856-875.
- Kerr, J.M., and Blanpied, T.A. (2012). Subsynaptic AMPA receptor distribution is acutely regulated by actin-driven reorganization of the postsynaptic density. *J. Neurosci.* 32, 658-673.
- Kessels, H., and Malinow, R. (2009). Synaptic AMPA receptor plasticity and behavior. *Neuron* 61, 340-350.
- Kharazia, V.N., and Weinberg, R.J. (1997). Tangential synaptic distribution of NMDA and AMPA receptors in rat neocortex. *Neurosci. Lett.* 238, 41-44.
- Kim, E., and Sheng, M. (2004). PDZ domain proteins of synapses. *Nat. Rev. Neurosci.* 5, 771-781.
- Kim, C.H., Takamiya, K., Petralia, R.S., Sattler, R., Yu, S., Zhou, W., Kalb, R., Wenthold, R., and Huganir, R. (2005). Persistent hippocampal CA1 LTP in mice lacking the C-terminal PDZ ligand of GluR1. *Nat. Neurosci.* 8, 985-987.
- Kim, K.S., Yan, D., and Tomita, S. (2010). Assembly and stoichiometry of the AMPA receptor and transmembrane AMPA receptor regulatory protein complex. *J. Neurosci.* 30, 1064-1072.
- Kitano, J., Kimura, K., Yamazaki, Y., Soda, T., Shigemoto, R., Nakajima, Y., and Nakanishi, S. (2002). Tamalin, a PDZ domain-containing protein, links a protein complex formation of group I metabotropic glutamate receptors and the guanine nucleotide exchange factor cytohesins. *J. Neurosci.* 22, 1280-1289.
- Kniazeff, J., Bessis, A.S., Maurel, D., Ansanay, H., Prezeau, L., and Pin, J.P. (2004). Closed state of both binding domains of homodimeric mGlu receptors is required for full activity. *Nat. Struct. Mol. Biol.* 11, 706-713.
- Kumari, R., Castillo, C., and Francesconi, A. (2013). Agonist-dependent signaling by group I metabotropic glutamate receptors is regulated by association with lipid domains. *J. Biol. Chem.* 288, 32004-32019.
- Kunishima, N., Shimada, Y., Tsuji, Y., Sato, T., Yamamoto, M., Kumasaka, T., Nakanishi, S., Jingami, H., and Morikawa, K. (2000). Structural basis of glutamate recognition by a dimeric metabotropic glutamate receptor. *Nature* 407, 971-977.
- Kusumi, A., Nakada, C., Ritchie, K., Murase, K., Suzuki, K., Murakoshi, H., Kasai, R.S., Kondo, J., and Fujiwara, T. (2005). Paradigm shift of the plasma membrane concept from the two-dimensional continuum fluid to the partitioned fluid: high-speed single-molecule tracking of membrane molecules. *Annu. Rev. Biophys. Biomol. Struct.* 34, 351-378.
- Kusumi, A., Fujiwara, T.K., Chadda, R., Xie, M., Tsunoyama, T.A., Kalay, Z., Kasai, R.S., and Suzuki, K.G. (2012). Dynamic organizing principles of the plasma membrane that regulate signal transduction: commemorating the fortieth anniversary of Singer and Nicolson's fluid-mosaic model. *Annu. Rev. Cell Dev. Biol.* 28, 215-250.
- Lee, S.H., Jin, C., Cai, E., Ge, P., Ishitsuka, Y., Teng, K.W., de Thomaz, A.A., Nall, D., Baday, M., Jeyifous, O., Demonte, D., Dundas, C.M., Park, S., Delgado, J.Y., Green, W.N., and Selvin, P.R. (2017). Super-resolution imaging of synaptic and extra-synaptic AMPA receptors with different-sized fluorescent probes. *elife* 6.

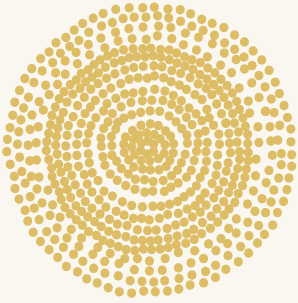
- Lee, S.J., Wei, M., Zhang, C., Maxeiner, S., Pak, C., Calado Botelho, S., Trotter, J., Sterky, F.H., Sudhof, T.C., 2017. Presynaptic neuronal Pentraxin receptor organizes excitatory and inhibitory synapses. *J. Neurosci.* 37, 1062-1080.
- Li, T.P., Blanpied, T.A., 2016. Control of transmembrane protein diffusion within the postsynaptic density assessed by simultaneous single-molecule tracking and localization microscopy. *Front. Synaptic Neurosci.* 8, 19.
- Li, T.P., Song, Y., MacGillavry, H.D., Blanpied, T.A., Raghavachari, S., 2016. Protein crowding within the postsynaptic density can impede the escape of membrane proteins. *J. Neurosci.* 36, 4276-4295.
- Liu, G., Choi, S., Tsien, R.W., 1999. Variability of neurotransmitter concentration and nonsaturation of postsynaptic AMPA receptors at synapses in hippocampal cultures and slices. *Neuron* 22, 395-409.
- Liu, K.K., Hagan, M.F., Lisman, J.E., 2017. Gradation (approx. 10 size states) of synaptic strength by quantal addition of structural modules. *Philos. Trans. R. Soc. Lond. Ser. B Biol. Sci.* 372.
- Lu, Y.M., Jia, Z., Janus, C., Henderson, J.T., Gerlai, R., Wojtowicz, J.M., Roder, J.C., 1997. Mice lacking metabotropic glutamate receptor 5 show impaired learning and reduced CA1 long-term potentiation (LTP) but normal CA3 LTP. *J. Neurosci.* 17, 5196-5205.
- Lu, J., Helton, T.D., Blanpied, T.A., Racz, B., Newpher, T.M., Weinberg, R.J., Ehlers, M.D., 2007. Postsynaptic positioning of endocytic zones and AMPA receptor cycling by physical coupling of dynamin-3 to Homer. *Neuron* 55, 874-889.
- Lu, W., Shi, Y., Jackson, A.C., Bjorgan, K., Doring, M.J., Sprengel, R., Seeburg, P.H., Nicoll, R.A., 2009. Subunit composition of synaptic AMPA receptors revealed by a single-cell genetic approach. *Neuron* 62, 254-268.
- Lujan, R., Nusser, Z., Roberts, J.D., Shigemoto, R., Somogyi, P., 1996. Perisynaptic location of metabotropic glutamate receptors mGluR1 and mGluR5 on dendrites and dendritic spines in the rat hippocampus. *Eur. J. Neurosci.* 8, 1488-1500.
- Lüscher, C., Huber, K.M., 2010. Group 1 mGluR-dependent synaptic long-term depression: mechanisms and implications for circuitry and disease. *Neuron* 65, 445-459.
- MacGillavry, H.D., Kerr, J.M., Blanpied, T.A., 2011. Lateral organization of the postsynaptic density. *Mol. Cell. Neurosci.* 48, 321-331.
- MacGillavry, H.D., Song, Y., Raghavachari, S., Blanpied, T.A., 2013. Nanoscale scaffolding domains within the postsynaptic density concentrate synaptic AMPA receptors. *Neuron* 78, 615-622.
- Makino, H., Malinow, R., 2009. AMPA receptor incorporation into synapses during LTP: the role of lateral movement and exocytosis. *Neuron* 64, 381-390.
- Malinow, R., Malenka, R.C., 2002. AMPA receptor trafficking and synaptic plasticity. *Annu. Rev. Neurosci.* 25, 103-126.
- Marcaggi, P., Mutoh, H., Dimitrov, D., Beato, M., Knopfel, T., 2009. Optical measurement of mGluR1 conformational changes reveals fast activation, slow deactivation, and sensitization. *Proc. Natl. Acad. Sci. U. S. A.* 106, 11388-11393.
- Masugi-Tokita, M., Tarusawa, E., Watanabe, M., Molnar, E., Fujimoto, K., Shigemoto, R., 2007. Number and density of AMPA receptors in individual synapses in the rat cerebellum as revealed by SDS-digested freeze-fracture replica labeling. *J. Neurosci.* 27, 2135-2144.
- Matsuda, K., Budisantoso, T., Mitakidis, N., Sugaya, Y., Miura, E., Kakegawa, W., Yamasaki, M., Konno, K., Uchigashima, M., Abe, M., Watanabe, I., Kano, M., Watanabe, M., Sakimura, K., Aricescu, A.R., Yuzaki, M., 2016. Transsynaptic modulation of kainate receptor functions by Clq-like proteins. *Neuron* 90, 752-767.
- McAllister, A.K., Stevens, C.F., 2000. Nonsaturation of AMPA and NMDA receptors at hippocampal synapses. *Proc. Natl. Acad. Sci. U. S. A.* 97, 6173-6178.
- Meng, Y., Zhang, Y., Jia, Z., 2003. Synaptic transmission and plasticity in the absence of AMPA glutamate receptor GluR2 and GluR3. *Neuron* 39, 163-176.
- Minakami, R., Jinnai, N., Sugiyama, H., 1997. Phosphorylation and calmodulin binding of the metabotropic glutamate receptor subtype 5 (mGluR5) are antagonistic *in vitro*. *J. Biol. Chem.* 272, 20291-20298.
- Morone, N., Fujiwara, T., Murase, K., Kasai, R.S., Ike, H., Yuasa, S., Usukura, J., Kusumi, A., 2006. Three-dimensional reconstruction of the membrane skeleton at the plasma membrane interface by electron tomography. *J. Cell Biol.* 174, 851-862.
- Muto, T., Tsuchiya, D., Morikawa, K., Jingami, H., 2007. Structures of the extracellular regions of the group II/III metabotropic glutamate receptors. *Proc. Natl. Acad. Sci. U. S. A.* 104, 3759-3764.
- Nabavi, S., Fox, R., Alfonso, S., Aow, J., Malinow, R., 2014. GluA1 trafficking and metabotropic NMDA: addressing results from other laboratories inconsistent with ours. *Philos. Trans. R. Soc. Lond. Ser. B Biol. Sci.* 369, 20130145.
- Nair, D., Hoyer, E., Petersen, J.D., Constals, A., Giannone, G., Choquet, D., Sibarita, J.B., 2013. Super-resolution imaging reveals that AMPA receptors inside synapses are dynamically organized in nanodomains regulated by PSD95. *J. Neurosci.* 33, 13204-13224.
- Nakagawa, T., Cheng, Y., Ramm, E., Sheng, M., Walz, T., 2005. Structure and different conformational states of

- native AMPA receptor complexes. *Nature* 433, 545-549.
- Nakamura, M., Sato, K., Fukaya, M., Araishi, K., Aiba, A., Kano, M., and Watanabe, M. (2004). Signaling complex formation of phospholipase C β 4 with metabotropic glutamate receptor type α and 1,4,5-trisphosphate receptor at the perisynapse and endoplasmic reticulum in the mouse brain. *Eur. J. Neurosci.* 20, 2929-2944.
- Neyman, S., and Manahan-Vaughan, D. (2008). Metabotropic glutamate receptor 1 (mGluR1) and 5 (mGluR5) regulate late phases of LTP and LTD in the hippocampal CA1 region *in vitro*. *Eur. J. Neurosci.* 27, 1345-1352.
- Ng, A.N., Doherty, A.J., Lombroso, P.J., Emptage, N.J., and Collingridge, G.L. (2014). Rapid regulation of endoplasmic reticulum dynamics in dendritic spines by NMDA receptor activation. *Mol. Brain* 7, 60.
- Nishimura, A., Kitano, K., Takasaki, J., Taniguchi, M., Mizuno, N., Tago, K., Hakoshima, T., and Itoh, H. (2010). Structural basis for the specific inhibition of heterotrimeric Gq protein by a small molecule. *Proc. Natl. Acad. Sci. U. S. A.* 107, 13666-13671.
- Niswender, C.M., and Conn, P.J. (2010). Metabotropic glutamate receptors: physiology, pharmacology, and disease. *Annu. Rev. Pharmacol. Toxicol.* 50, 295-322.
- Nusser, Z., Mulvihill, E., Streit, P., and Somogyi, P. (1994). Subsynaptic segregation of metabotropic and ionotropic glutamate receptors as revealed by immunogold localization. *Neuroscience* 61, 421-427.
- O'Brien, R.J., Xu, D., Petralia, R.S., Steward, O., Huganir, R.L., and Worley, P. (1999). Synaptic clustering of AMPA receptors by the extracellular immediate-early gene product Narp. *Neuron* 23, 309-323.
- Okabe, S. (2007). Molecular anatomy of the postsynaptic density. *Mol. Cell. Neurosci.* 34, 503-518.
- Palmer, M.J., Irving, A.J., Seabrook, G.R., Jane, D.E., and Collingridge, G.L. (1997). The group I mGlu receptor agonist DHPG induces a novel form of LTD in the CA1 region of the hippocampus. *Neuropharmacology* 36, 1517-1532.
- Pankratov, Y.V., and Krishtal, O.A. (2003). Distinct quantal features of AMPA and NMDA synaptic currents in hippocampal neurons: implication of glutamate spillover and receptor saturation. *Biophys. J.* 85, 3375-3387.
- Park, P., Sanderson, T.M., Amici, M., Choi, S.L., Bortolotto, Z.A., Zhuo, M., Kaang, B.K., and Collingridge, G.L. (2016). Calcium-permeable AMPA receptors mediate the induction of the protein kinase A-dependent component of long-term potentiation in the Hippocampus. *J. Neurosci.* 36, 622-631.
- Penn, A.C., Zhang, C.L., Georges, F., Royer, L., Breillat, C., Hosy, E., Petersen, J.D., Humeau, Y., and Choquet, D. (2017). Hippocampal LTP and contextual learning require surface diffusion of AMPA receptors. *Nature* 549, 384-388.
- Perez de Arce, K., Schrod, N., Metzbowler, S.W., Allgeyer, E., Kong, G.K., Tang, A.H., Krupp, A.J., Stein, V., Liu, X., Bewersdorf, J., Blanpied, T.A., Lucic, V., and Biederer, T. (2015). Topographic mapping of the synaptic cleft into adhesive nanodomains. *Neuron* 88, 1165-1172.
- Perez-Otano, I., Lujan, R., Tavalin, S.J., Plomann, M., Modregger, J., Liu, X.B., Jones, E.G., Heinemann, S.F., Lo, D.C., and Ehlers, M.D. (2006). Endocytosis and synaptic removal of NR3A-containing NMDA receptors by PACSIN1/syndapin1. *Nat. Neurosci.* 9, 611-621.
- Petrini, E.M., Lu, J., Cognet, L., Lounis, B., Ehlers, M.D., and Choquet, D. (2009). Endocytic trafficking and recycling maintain a pool of mobile surface AMPA receptors required for synaptic potentiation. *Neuron* 63, 92-105.
- Pontier, S.M., Percherancier, Y., Galandrin, S., Breit, A., Gales, C., and Bouvier, M. (2008). Cholesterol-dependent separation of the beta2-adrenergic receptor from its partners determines signaling efficacy: insight into nanoscale organization of signal transduction. *J. Biol. Chem.* 283, 24659-24672.
- Racca, C., Stephenson, F.A., Streit, P., Roberts, J.D., and Somogyi, P. (2000). NMDA receptor content of synapses in stratum radiatum of the hippocampal CA1 area. *J. Neurosci.* 20, 2512-2522.
- Raghavachari, S., and Lisman, J.E. (2004). Properties of quantal transmission at CA1 synapses. *J. Neurophysiol.* 92, 2456-2467.
- Raymond, C.R., Thompson, V.L., Tate, W.P., and Abraham, W.C. (2000). Metabotropic glutamate receptors trigger homosynaptic protein synthesis to prolong long-term potentiation. *J. Neurosci.* 20, 969-976.
- Regalado, M.P., Terry-Lorenzo, R.T., Waites, C.L., Garner, C.C., and Malenka, R.C. (2006). Transsynaptic signaling by postsynaptic synapse-associated protein 97. *J. Neurosci.* 26, 2343-2357.
- Reinders, N.R., Pao, Y., Renner, M.C., da Silva-Matos, C.M., Lodder, T.R., Malinow, R., and Kessels, H.W. (2016). Amyloid-beta effects on synapses and memory require AMPA receptor subunit GluA3. *Proc. Natl. Acad. Sci. U. S. A.* 113, E6526-E6534.
- Renner, M., Lacor, P.N., Velasco, P.T., Xu, J., Contractor, A., Klein, W.L., and Triller, A. (2010). Deleterious effects of amyloid beta oligomers acting as an extracellular scaffold for mGluR5. *Neuron* 66, 739-754.
- Renner, M.C., Albers, E.H., Gutierrez-Castellanos, N., Reinders, N.R., van Huijstee, A.N., Xiong, H., Lodder, T.R., and Kessels, H.W. (2017). Synaptic plasticity through activation of GluA3-containing AMPA-receptors. *elife* 6.

- Robert, A., Howe, J.R., 2003. How AMPA receptor desensitization depends on receptor occupancy. *J. Neurosci.* 23, 847-858.
- Rondard, P., Pin, J.P., 2015. Dynamics and modulation of metabotropic glutamate receptors. *Curr. Opin. Pharmacol.* 20, 95-101.
- Rosenmund, C., Stern-Bach, Y., Stevens, C.F., 1998. The tetrameric structure of a glutamate receptor channel. *Science* 280, 1596-1599.
- Saglietti, L., Dequidt, C., Kamieniarz, K., Rousset, M.C., Valnegri, P., Thoumine, O., Beretta, F., Fagni, L., Choquet, D., Sala, C., Sheng, M., Passafaro, M., 2007. Extracellular interactions between GluR2 and N-cadherin in spine regulation. *Neuron* 54, 461-477.
- Sako, Y., Kusumi, A., 1994. Compartmentalized structure of the plasma membrane for receptor movements as revealed by a nanometer-level motion analysis. *J. Cell Biol.* 125, 1251-1264.
- Santamaria, F., Gonzalez, J., Augustine, G.J., Raghavachari, S., 2010. Quantifying the effects of elastic collisions and non-covalent binding on glutamate receptor trafficking in the post-synaptic density. *PLoS Comput. Biol.* 6, e1000780.
- Santucci, D.M., Raghavachari, S., 2008. The effects of NR2 subunit-dependent NMDA receptor kinetics on synaptic transmission and CaMKII activation. *PLoS Comput. Biol.* 4, e1000208.
- Schnell, E., Sizemore, M., Karimzadegan, S., Chen, L., Brecht, D., Nicoll, R., 2002. Direct interactions between PSD-95 and stargazin control synaptic AMPA receptor number. *Proc. Natl. Acad. Sci. U. S. A.* 99, 13902-13907.
- Schwenk, J., Harmel, N., Brechet, A., Zolles, G., Berkefeld, H., Muller, C.S., Bildl, W., Baehrens, D., Huber, B., Kulik, A., Klocker, N., Schulte, U., Fakler, B., 2012. High-resolution proteomics unravel architecture and molecular diversity of native AMPA receptor complexes. *Neuron* 74, 621-633.
- Sergé, A., Fourgeaud, L., Hemar, A., Choquet, D., 2002. Receptor activation and homer differentially control the lateral mobility of metabotropic glutamate receptor 5 in the neuronal membrane. *J. Neurosci.* 22, 3910-3920.
- Sheng, M., Hoogenraad, C., 2007. The postsynaptic architecture of excitatory synapses: a more quantitative view. *Annu. Rev. Biochem.* 76, 823-847.
- Shepherd, J.D., Huganir, R.L., 2007. The cell biology of synaptic plasticity: AMPA receptor trafficking. *Annu. Rev. Cell Dev. Biol.* 23, 613-643.
- Shi, S., Hayashi, Y., Esteban, J.A., Malinow, R., 2001. Subunit-specific rules governing AMPA receptor trafficking to synapses in hippocampal pyramidal neurons. *Cell* 105, 331-343.
- Shiraishi-Yamaguchi, Y., Furuichi, T., 2007. The Homer family proteins. *Genome Biol.* 8, 206.
- Sinnen, B.L., Bowen, A.B., Forte, J.S., Hiester, B.G., Crosby, K.C., Gibson, E.S., Dell'Acqua, M.L., Kennedy, M.J., 2017. Optogenetic control of synaptic composition and function. *Neuron* 93 (646-660), e645.
- Snyder, E.M., Philpot, B.D., Huber, K.M., Dong, X., Fallon, J.R., Bear, M.F., 2001. Internalization of ionotropic glutamate receptors in response to mGluR activation. *Nat. Neurosci.* 4, 1079-1085.
- Sobolevsky, A.I., Rosconi, M.P., Gouaux, E., 2009. X-ray structure, symmetry and mechanism of an AMPA-subtype glutamate receptor. *Nature* 462, 745-756.
- Soler-Llavina, G.J., Fuccillo, M.V., Ko, J., Sudhof, T.C., Malenka, R.C., 2011. The neuroligin ligands, neuroligins and leucine-rich repeat transmembrane proteins, perform convergent and divergent synaptic functions *in vivo*. *Proc. Natl. Acad. Sci. U. S. A.* 108, 16502-16509.
- Somogyi, P., Tamas, G., Lujan, R., Buhl, E.H., 1998. Salient features of synaptic organisation in the cerebral cortex. *Brain Res. Brain Res. Rev.* 26, 113-135.
- Spacek, J., Harris, K.M., 1997. Three-dimensional organization of smooth endoplasmic reticulum in hippocampal CA1 dendrites and dendritic spines of the immature and mature rat. *J. Neurosci.* 17, 190-203.
- Sudhof, T.C., 2012. The presynaptic active zone. *Neuron* 75, 11-25.
- Sungkaworn, T., Jobin, M.L., Burneck, K., Weron, A., Lohse, M.J., Calebiro, D., 2017. Single-molecule imaging reveals receptor-G protein interactions at cell surface hot spots. *Nature* 550, 543-547.
- Tadokoro, S., Tachibana, T., Imanaka, T., Nishida, W., Sobue, K., 1999. Involvement of unique leucine-zipper motif of PSD-Zip45 (Homer 1c/vesl-1L) in group 1 metabotropic glutamate receptor clustering. *Proc. Natl. Acad. Sci. U. S. A.* 96, 13801-13806.
- Tanaka, J., Nakagawa, S., Kushiya, E., Yamasaki, M., Fukaya, M., Iwanaga, T., Simon, M.I., Sakimura, K., Kano, M., Watanabe, M., 2000. Gq protein alpha subunits Galphaq and Galpha11 are localized at postsynaptic extra-junctional membrane of cerebellar Purkinje cells and hippocampal pyramidal cells. *Eur. J. Neurosci.* 12, 781-792.
- Tang, A.H., Chen, H., Li, T.P., Metzbowler, S.R., MacGillavry, H.D., Blanpied, T.A., 2016. A trans-synaptic nanocolumn aligns neurotransmitter release to receptors. *Nature* 536, 210-214.
- Tarusawa, E., Matsui, K., Budisantoso, T., Molnar, E., Watanabe, M., Matsui, M., Fukazawa, Y., Shigemoto, R., 2009. Input-specific intrasynaptic arrangements of ionotropic glutamate receptors and their impact on postsynaptic responses. *J. Neurosci.* 29, 12896-12908.

- Tempia, F., Miniaci, M.C., Anchisi, D., and Strata, P. (1998). Postsynaptic current mediated by metabotropic glutamate receptors in cerebellar Purkinje cells. *J. Neurophysiol.* 80, 520-528.
- Traynelis, S.F., Wollmuth, L.P., McBain, C.J., Menniti, F.S., Vance, K.M., Ogden, K.K., Hansen, K.B., Yuan, H., Myers, S.J., and Dingledine, R. (2010). Glutamate receptor ion channels: structure, regulation, and function. *Pharmacol. Rev.* 62, 405-496.
- Tu, J.C., Xiao, B., Naisbitt, S., Yuan, J.P., Petralia, R.S., Brakeman, P., Doan, A., Aakalu, V.K., Lanahan, A.A., Sheng, M., and Worley, P.F. (1999). Coupling of mGluR/Homer and PSD-95 complexes by the Shank family of postsynaptic density proteins. *Neuron* 23, 583-592.
- Tulodziecka, K., Diaz-Rohrer, B.B., Farley, M.M., Chan, R.B., Di Paolo, G., Levental, K.R., Waxham, M.N., and Levental, I. (2016). Remodeling of the postsynaptic plasma membrane during neural development. *Mol. Biol. Cell* 27, 3480-3489.
- Twomey, E.C., Yelshanskaya, M.V., Grassucci, R.A., Frank, J., and Sobolevsky, A.I. (2016). Elucidation of AMPA receptor-starburst complexes by cryo-electron microscopy. *Science* 353, 83-86.
- Uchida, N., Honjo, Y., Johnson, K.R., Wheelock, M.J., and Takeichi, M. (1996). The catenin/ cadherin adhesion system is localized in synaptic junctions bordering transmitter release zones. *J. Cell Biol.* 135, 767-779.
- Uteshev, V.V., and Pennefather, P.S. (1996). A mathematical description of miniature postsynaptic current generation at central nervous system synapses. *Biophys. J.* 71, 1256-1266.
- Valtschanoff, J.G., and Weinberg, R.J. (2001). Laminar organization of the NMDA receptor complex within the postsynaptic density. *J. Neurosci.* 21, 1211-1217.
- Valtschanoff, J.G., Burette, A., Davare, M.A., Leonard, A.S., Hell, J.W., and Weinberg, R.J. (2000). SAP97 concentrates at the postsynaptic density in cerebral cortex. *Eur. J. Neurosci.* 12, 3605-3614.
- van der Sluijs, P., and Hoogenraad, C.C. (2011). New insights in endosomal dynamics and AMPA receptor trafficking. *Semin. Cell Dev. Biol.* 22, 499-505.
- Volk, L., Chiu, S.L., Sharma, K., and Haganir, R.L. (2015). Glutamate synapses in human cognitive disorders. *Annu. Rev. Neurosci.* 38, 127-149.
- Wagner, W., Brenowitz, S.D., and Hammer 3rd, J.A. (2011). Myosin-Va transports the endoplasmic reticulum into the dendritic spines of Purkinje neurons. *Nat. Cell Biol.* 13, 40-48.
- Waites, C.L., Specht, C.G., Hartel, K., Leal-Ortiz, S., Genoux, D., Li, D., Drisdell, R.C., Jeyifous, O., Cheyne, J.E., Green, W.N., Montgomery, J.M., and Garner, C.C. (2009). Synaptic SAP97 isoforms regulate AMPA receptor dynamics and access to presynaptic glutamate. *J. Neurosci.* 29, 4332-4345.
- Wang, H., Westin, L., Nong, Y., Birnbaum, S., Bendor, J., Brismar, H., Nestler, E., Aperia, A., Flajolet, M., and Greengard, P. (2009). Norbin is an endogenous regulator of metabotropic glutamate receptor 5 signaling. *Science* 326, 1554-1557.
- Watson, J.F., Ho, H., and Greger, I.H. (2017). Synaptic transmission and plasticity require AMPA receptor anchoring via its N-terminal domain. *elife* 6.
- Wang, M.W., and Huber, K.M. (2009). Protein translation in synaptic plasticity: mGluR-LTD, fragile X. *Curr. Opin. Neurobiol.* 19, 319-326.
- Wenthold, R.J., Petralia, R.S., Blahos II, J and Niedzielski, A.S. (1996). Evidence for multiple AMPA receptor complexes in hippocampal CA1/CA2 neurons. *J. Neurosci.* 16, 1982-1989.
- Westin, L., Reuss, M., Lindskog, M., Aperia, A., and Brismar, H. (2014). Nanoscopic spine localization of Norbin, an mGluR5 accessory protein. *BMC Neurosci.* 15, 45.
- Wu, D., Bacaj, T., Morishita, W., Goswami, D., Arendt, K.L., Xu, W., Chen, L., Malenka, R.C., and Sudhof, T.C. (2017). Postsynaptic synaptotagmins mediate AMPA receptor exocytosis during LTP. *Nature* 544, 316-321.
- Xiao, B., Tu, J.C., Petralia, R.S., Yuan, J.P., Doan, A., Breder, C.D., Ruggiero, A., Lanahan, A.A., Wenthold, R.J., and Worley, P.F. (1998). Homer regulates the association of group I metabotropic glutamate receptors with multivalent complexes of homer-related, synaptic proteins. *Neuron* 21, 707-716.
- Xie, X., Liaw, J.S., Baudry, M., and Berger, T.W. (1997). Novel expression mechanism for synaptic potentiation: alignment of presynaptic release site and postsynaptic receptor. *Proc. Natl. Acad. Sci. U. S. A.* 94, 6983-6988.
- Xu-Friedman, M.A., and Regehr, W.G. (2004). Structural contributions to short-term synaptic plasticity. *Physiol. Rev.* 84, 69-85.
- Zeng, M., Shang, Y., Araki, Y., Guo, T., Haganir, R.L., and Zhang, M. (2016). Phase transition in postsynaptic densities underlies formation of synaptic complexes and synaptic plasticity. *Cell* 166 (1163-1175), e1112.
- Zhao, Y., Chen, S., Yoshioka, C., Bacongus, L., and Gouaux, E. (2016). Architecture of fully occupied GluA2 AMPA receptor-TARP complex elucidated by cryo-EM. *Nature* 536, 108-111.
- Zhou, Z., Liu, A., Xia, S., Leung, C., Qi, J., Meng, Y., Xie, W., Park, P., Collingridge, G.L., and Jia, Z. (2018). The C-terminal tails of endogenous GluA1 and GluA2 differentially contribute to hippocampal synaptic plasticity and learning. *Nat. Neurosci.* 21, 50-62.

3



Membrane trafficking and positioning of mGluRs at presynaptic and postsynaptic sites of excitatory synapses

Nicky Scheefhals^{1,*}, Anna Bodzęta^{1,2,*}, Harold D. MacGillavry¹

*Equal contribution

¹Cell Biology, Neurobiology and Biophysics, Department of Biology, Faculty of Science, Utrecht University, Utrecht, the Netherlands

²Present address: Institute of Developmental and Neurobiology, Johannes Gutenberg-University Mainz, 55128 Mainz, Germany.

Neuropharmacology (2021), 200: 108799

Abstract

The plethora of functions of glutamate in the brain are mediated by the complementary actions of ionotropic and metabotropic glutamate receptors (mGluRs). The ionotropic glutamate receptors carry most of the fast excitatory transmission, while mGluRs modulate transmission on longer timescales by triggering multiple intracellular signaling pathways. As such, mGluRs mediate critical aspects of synaptic transmission and plasticity. Interestingly, at synapses, mGluRs operate at both sides of the cleft, and thus bidirectionally exert the effects of glutamate. At postsynaptic sites, group I mGluRs act to modulate excitability and plasticity. At presynaptic sites, group II and III mGluRs act as auto-receptors, modulating release properties in an activity-dependent manner. Thus, synaptic mGluRs are essential signal integrators that functionally couple presynaptic and postsynaptic mechanisms of transmission and plasticity. Understanding how these receptors reach the membrane and are positioned relative to the presynaptic glutamate release site are therefore important aspects of synapse biology. In this review, we will discuss the currently known mechanisms underlying the trafficking and positioning of mGluRs at and around synapses, and how these mechanisms contribute to synaptic functioning. We will highlight outstanding questions and present an outlook on how recent technological developments will move this exciting research field forward.

Introduction

The actions of glutamate in the brain are mediated by a remarkable large variety of receptors. The fast actions of glutamate are mediated by ionotropic glutamate receptors: the AMPA, NMDA-and KA-type receptors. These receptors are ligand-gated ion channels that allow fast excitatory synaptic transmission. The slower and long-lasting effects of glutamate are generally mediated by metabotropic glutamate receptors (mGluRs), a family of G-protein coupled receptors (GPCRs) that modulate various aspects of neuronal physiology, particularly excitability and plasticity (Reiner and Levitz, 2018; Scheefhals and MacGillavry, 2018). Thus, these receptors are potent modulators of critical aspects of neuronal functioning and are broadly considered to be vital drug targets in treating mental disorders such as anxiety, Parkinson's, autism spectrum disorders, and drug abuse (Crupi et al., 2019).

mGluRs belong to the class C of GPCRs that also includes the metabotropic GABA B receptor subunits. Class C GPCRs contain a particularly large extracellular domain that contains the agonist-binding Venus fly trap (VFT) domain and, in the case of mGluRs, a cysteine-rich domain (CRD) that connects to the highly conserved seven-pass transmembrane domain (TMD) (Figure 1A) (Pin and Bettler, 2016). Despite this common topology, the different mGluR subtypes are tremendously diversified in their biophysical properties, pharmacology, signaling profiles and expression patterns. Based on these characteristics, mGluRs can be divided in three main groups: group I mGluRs, (mGluR1 and 5) are coupled to G α q proteins, group II mGluRs (mGluR2 and 3) and group III mGluRs (mGluR4, 6, 7 and 8) are coupled to inhibitory Gai/o proteins (Figure 1B) (Niswender and Conn, 2010). The molecular diversity of mGluRs is further broadened by alternative splicing, generating isoforms with unique properties. And, although mGluRs are typically homodimers, recent studies identified several heterodimeric receptor combinations that potentially have distinct functions and properties (Doumazane et al., 2011; Levitz et al., 2016).

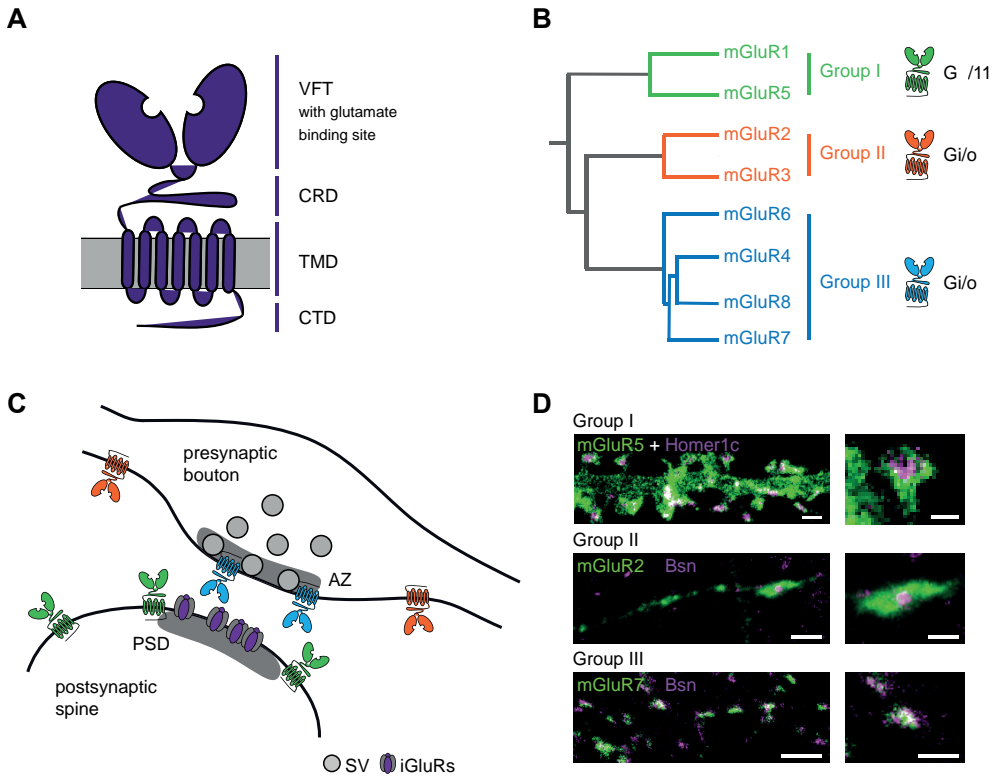


Figure 1. Structure organization and distribution of mGluRs

(A) Domain organization of mGluRs. ECD – extracellular domain, VFT - Venus fly trap domain with glutamate binding site, CRD – cysteine rich domain, TMD – transmembrane domain, ICD – intracellular domain. (B) Phylogenetic tree of the mGluR groups. (C) Schematic diagram of the distribution of mGluR types at the synapse. AZ – the active zone, iGluR – ionotropic glutamate receptors, PSD – the postsynaptic density, SV – synaptic vesicles. (D) STED images of mGluR distribution in hippocampal neurons. Group I mGluR5 co-stained with marker of postsynaptic density - Homer1c. Group II mGluR2 and group III mGluR7 co-stained with marker of the active zone – Bassoon (Bsn). Scale bar: 1 μ m, zooms: 500 nm.

mGluRs are widely expressed throughout the brain and are found at both presynaptic and postsynaptic sites of excitatory synapses. As such, mGluRs are ideally positioned to modulate virtually every aspect of synaptic transmission and plasticity. Here, we will discuss the current understanding of mGluR trafficking and positioning at excitatory synapses. Specifically, we will focus on how the precise (sub)synaptic distribution of mGluRs in neurons impacts their contribution to glutamatergic signaling in different ways. We will put particular emphasis on how mGluR trafficking and positioning contribute to synaptic functioning. This is important because although the biophysical properties of individual receptors principally dictate their activation kinetics, ultimately, the probability of receptor activation is determined by the distance these receptors are positioned relative to the release site of glutamate. Interestingly, while certain mGluRs are positioned close to, or even concentrated in the active zone, other receptors are localized at distinct distances from, or

even considerably far away from release sites, questioning how and when these receptors are activated. Additionally, for mGluRs the subcellular positioning, and the molecular environment of receptors largely influences their ability to engage local signaling effector molecules. For instance, while effectors close to the activated receptor can be modulated almost instantly, more distant effectors are less likely to contribute to the effects of receptor activation or respond with a delay. Thus, the mechanisms that control the trafficking and positioning of mGluRs at and around presynaptic and postsynaptic sites critically determine how this versatile group of glutamate receptors contributes to synaptic signaling and plasticity.

Cellular and subcellular distribution of mGluRs in neurons

The expression pattern and precise subcellular positioning of mGluRs are important determinants for their function. In situ hybridization and immunolabeling EM studies have been instrumental in mapping and quantifying the cellular and subcellular distribution of mGluRs in the brain at high resolution. These studies led to the general notion that different mGluR types are often co-expressed by individual neurons, but that the distribution within neurons is highly compartmentalized with different types of receptors targeted to different subcellular domains (Ferraguti and Shigemoto, 2006). Of note, mGluRs are also expressed by glia cells (Petralia et al., 1996) and can as such also be intricate components of the tripartite synapse regulating several aspects of synaptic transmission and plasticity. This will however not be discussed in this review.

Throughout the adult central nervous system, group I mGluRs have been found to localize almost exclusively at postsynaptic sites (Lujan et al., 1996; Lujan et al., 1997; Martin et al., 1992; Shigemoto et al., 1997; Shigemoto et al., 1993), although mGluR5 labeling has been found at presynaptic sites too (Romano et al., 1995). Strikingly, in dendritic spines the concentration of immunolabeling for both mGluR1 and mGluR5 is highest within an annular region (~100 nm) around the postsynaptic density (PSD), the perisynaptic domain, and rapidly drops further away in the extrasynaptic region (Baude et al., 1993; Lujan et al., 1996; Nusser et al., 1994). This perisynaptic enrichment seems more pronounced for mGluR1 than for mGluR5, with an estimated perisynaptic pool of 50% for mGluR1 compared to 25% for mGluR5 (Lujan et al., 1997). In hippocampal CA1 neurons the size of the perisynaptic pool of mGluR5 is highly heterogeneous across individual spines, with varying levels of perisynaptic enrichment and a significant population of spines lacking mGluR5 labeling (Lujan et al., 1997). The particular perisynaptic distribution likely has important consequences for receptor function. First, the concentration of glutamate is significantly lower in the perisynaptic region than in the center of the synapse. Second, being either in or just outside of the PSD could have tremendous consequences for a receptor's ability to connect to downstream effectors. Particularly, in the PSD numerous receptor types, scaffolds and signaling proteins are enriched within a sharply defined region. mGluR5 has also been found to localize in the nuclear membrane of neurons, regulating nuclear calcium signaling (Jong et al., 2005; O'Malley et al., 2003).

The expression patterns of the Group II mGluRs overlap and are both expressed in a number of brain regions and cell types, including Golgi cells of the cerebellum, dentate gyrus granule cells, the olfactory bulb, thalamus and cortex (Ohishi et al., 1993a; b; Petralia et al., 1996). mGluR2 and mGluR3 are found both in axons and dendrites of GABAergic

Golgi cells in the cerebellum and in the olfactory bulb (Hayashi et al., 1993; Neki et al., 1996a; b; Ohishi et al., 1994), but in the hippocampus mGluR2 and mGluR3 predominantly labeled axons (Petralia et al., 1996; Shigemoto et al., 1997; Tamaru et al., 2001). In axons, mGluR2/3 labeling was found along the axon but largely excluded from presynaptic terminals (Shigemoto et al., 1997; Yokoi et al., 1996).

Group III receptors are expressed throughout the brain and are consistently found at presynaptic sites, enriched at the active zone (AZ) of glutamatergic synapses (Bradley et al., 1996; Bradley et al., 1998; Corti et al., 2002; Kinoshita et al., 1996; Shigemoto et al., 1997; Shigemoto et al., 1996). An exception is mGluR6 which is exclusively expressed by ON-bipolar cells in the retina and is enriched at dendritic tips contacting photoreceptors (Nomura et al., 1994). mGluR4 and mGluR7 expression patterns in the brain seem to complement each other, with mGluR7 being the most widespread receptor in the adult nervous system. mGluR4 expression is abundant in granule cells in the cerebellum and the olfactory bulb, where mGluR7 levels are undetectable (Ohishi et al., 1995). mGluR7 expression is high in the cortex, hippocampus and several other forebrain regions (Kinzie et al., 1995). The expression pattern of mGluR8 seems to complement the pattern of mGluR2 in CA3 area and dentate gyrus (Shigemoto et al., 1997). The strong enrichment of mGluR4 and mGluR7 at the AZ suggests that specific anchors at the synapse position these receptors close to the release site. Additionally, mGluR4, mGluR7 and mGluR8 have also been found enriched in a subset of GABAergic synapses in the hippocampus (Corti et al., 2002; Ferraguti et al., 2005; Somogyi et al., 2003; Summa et al., 2013).

Altogether, these studies provide a general model where mGluRs are positioned in defined subcellular compartments (Figure 1C). In dendritic spines, group I mGluRs accumulate around the PSD, positioned to respond to strong synaptic stimulation protocols and modulate postsynaptic mechanisms of transmission and plasticity. In axons, group II mGluRs are widely distributed, but seemingly excluded from the AZ, while group III mGluRs are strongly enriched at the AZ. This suggests that group II and group III mGluRs likely respond differentially to glutamate release and can have differential effects on transmission.

Super-resolution studies of nanoscale mGluR distribution and dynamics

Apart from EM studies, single-molecule tracking (Aloisi et al., 2017; Goncalves et al., 2020; Renner et al., 2010; Sergé et al., 2002) and super-resolution techniques (Klotz et al., 2019; Siddig et al., 2020) provide additional insight in the mechanisms that underlie mGluR dynamics and distribution. In hippocampal neurons, a study using 3D structured illumination microscopy (3D-SIM) also revealed the perisynaptic enrichment of mGluR5, co-localizing with the mGluR5 accessory protein Norbin (Westin 2014). In seemingly contrast with this study and immuno-EM studies (Lujan et al., 1996), a study using direct stochastic optical reconstruction microscopy (dSTORM) found a homogeneous distribution of mGluR5 at the synaptic surface (Goncalves 2020). Moreover, a single-molecule tracking (SMT) study revealed that mGluR5 alternates between diffusive and confined states regulated by receptor activation and the scaffolding protein Homer (Sergé et al., 2002), but nevertheless mGluR5 was found to be highly mobile in both dendrites and spines (Goncalves 2020). Other SMT studies did reveal slower diffusion of mGluR5 at synaptic sites compared to extrasynaptic sites, and disrupted mGluR5 mobility was implicated in the pathology of Alzheimer's disease and Fragile X syndrome (Renner 2010; Aloisi 2017). A

recent study using stimulated emission depletion (STED) microscopy showed the exclusive postsynaptic localization of mGluR2 in ribbon synapses of inner hair cells in the cochlea (Klotz et al., 2019). Co-localization with the PSD marker PSD-95 revealed that mGluR2 is preferentially localized outside the PSD, while mGluR4 and mGluR8b co-localized strongly with the AZ marker CtBP2/RIBEYE. The subsynaptic localization of mGluR4 was studied in great detail in cerebellar granule cells using quantitative single-molecule localization microscopy (SMLM) (Siddig et al., 2020). This study found a high degree of enrichment of mGluR4 in the AZ and estimated that on average an AZ contains ~35 mGluR4 subunits. Within AZs, mGluR4 was found to be in close proximity to key molecular components regulating neurotransmitter release: Munc-18 (~30 nm coupling distance) and the Ca²⁺ channel CaV2.1 (~65 nm coupling distance), indicating that mGluR4 can directly or indirectly interact and modulate these AZ components. Super-resolution STED imaging of the subsynaptic distribution of presynaptic mGluRs in hippocampal neurons showed that mGluR2 localizes to the axon shaft and presynaptic boutons but was excluded from the AZ. In contrast, mGluR7 was found almost exclusively in the AZ (Figure 1D) (Bodzęta et al., 2020). Furthermore, SMT revealed that while mGluR2 was highly dynamic throughout the axon, mGluR7 was preferentially immobilized at AZs. Using domain-swapping experiments it was found that while intracellular interactions modulate mGluR2 mobility, mGluR7 seemed stabilized by its extracellular domain (Bodzęta et al., 2020).

Altogether, the overall distribution patterns for each of the different mGluR subtypes and their positioning in distinct subcellular compartments has been studied extensively in fixed preparations. Excitingly, recent advances in super-resolution technologies now allow live-cell investigation of receptor distribution and dynamics in neurons which will be important for extending our understanding of mGluR biology. Particularly, these directions will be of importance to reveal the mechanisms that underlie the dynamic organization of mGluRs at subsynaptic sites.

Secretory trafficking of mGluRs

Transmembrane proteins are synthesized, assembled, and processed through an ordered sequence of events along the secretory pathway. All mGluRs contain a signal peptide that drives the co-translational insertion of the newly formed receptor into the ER membrane. After adapting its proper conformation, the nascent receptor then exits the ER through the classic secretory system consisting of a series of organelles: the ER/Golgi intermediate compartment (ERGIC), cis-Golgi, Golgi apparatus (GA) and trans-Golgi network (TGN). Transport vesicles emanating from the Golgi then traffic to their destination by cytoskeleton-based transport to reach the membrane via exocytosis. The complex morphology of neurons imposes various challenges to this traditional organization. Unlike other cells, the secretory system in neurons has to correctly sort and distribute membrane proteins throughout its long, extended axon and the highly arborized somatodendritic compartment, putting unique demands on the organization of the secretory system (Kennedy and Hanus, 2019). Intriguingly, although neurons contain the same secretory compartments as other cells, the secretory system is organized differently. Neurons are equipped with a highly elaborate ER network that is continuous throughout the soma, axon and dendrites (Cui-Wang et al., 2012; Spacek and Harris, 1997). The Golgi compartment, however, is almost exclusively found in the soma, suggesting that newly synthesized receptors emanate primarily from the

soma (Horton and Ehlers, 2003), or through Golgi-like structures, termed Golgi outposts, present in dendrites (Horton and Ehlers, 2003; Mikhaylova et al., 2016; Pierce et al., 2001). Whether such elements are present in axons remains untested.

Proper regulation of each of these steps through the secretory pathway is essential for the correct delivery of functional receptors to the plasma membrane. However, while these processes have been well characterized for many synaptic transmembrane proteins, how mGluRs traffic through this intricate network of secretory organelles remains largely unknown. We will next discuss each of the steps in more detail and review what is currently known for mGluRs.

Protein folding and glycosylation

Newly synthesized transmembrane proteins are often glycosylated through a process termed N-linked glycosylation. Proper glycosylation is important for the correct folding, subsequent trafficking and ultimately the function of the protein (Helenius and Aebi, 2001). In this process, first a precursor mannose-rich oligosaccharide is attached to specific extracellular Asn residues. Then, mannose residues are trimmed before the protein can exit the ER and transit to the Golgi. In the Golgi, additional sugar chains are added to give rise to mature, complex glycan structures. For only a few mGluRs glycosylation and its effects on receptor function have been studied. For mGluR1 and mGluR5 a number of potential glycosylation sites were proposed. mGluR1b isolated from rat brain was indeed found to be fully glycosylated (Chan et al., 2001), but the exact sites of glycosylation have not been identified and although disruption of glycosylation severely diminished signaling downstream of mGluR1, surface expression was not affected (Mody et al., 1999). For mGluR5 six potential glycosylation consensus sites have been predicted. Initially only a single glycosylated site was confirmed biochemically (Bhave et al., 2003), but a more recent study indicated that five sites in the VFT domain are glycosylated and that glycosylation is critical for surface expression of mGluR5 (Nasrallah et al., 2018). Also, for mGluR3 several residues seem to be glycosylated (Muto et al., 2009), but the significance of glycosylation for the surface expression and function of group II mGluRs remains untested.

A recent study characterized the glycosylation of mGluR7 in great detail (Park et al., 2020). This study identified four Asn residues in the ECD that are linked to glycans and were found to be essential for the proper surface expression of mGluR7. Disruption of mGluR7 glycosylation led to the retention of the receptor in the ER. Conventionally, misfolded ER proteins are targeted for degradation by the ER-associated protein degradation pathway. However, deglycosylated mGluR7 was found to be targeted to the autophagolysosomal degradation pathway, that is independent of the ubiquitin proteasome system. Interestingly, two of these glycosylated residues were found to promote the interaction of mGluR7 with the adhesion molecule ELFN1, facilitating the correct localization of mGluR7 at presynaptic sites (Park et al., 2020). Thus, N-glycosylation seems to be a general feature of mGluRs and can have an important impact on receptor function but remains poorly characterized for most mGluR subtypes. It will be important to more systematically characterize the glycosylation patterns of individual mGluR subtypes and study the contribution of glycosylation to receptor trafficking and function in neurons.

Receptor dimerization

Dimerization of mGluRs has been studied using many different experimental approaches.

Traditional biochemical studies (Ray and Hauschild, 2000; Romano et al., 2001; Romano et al., 1996; Tsuji et al., 2000), time-resolved FRET assays in live cells (Doumazane et al., 2011), as well as quantitative fluorescence-based counting experiments (Lee et al., 2020; Levitz et al., 2016; Moller et al., 2018; Moreno Delgado et al., 2017) all consistently indicate that mGluRs form stable, disulphide-linked dimers on the plasma membrane. Dimerization is a requirement for full receptor activation (El Moustaine et al., 2012; Kammermeier and Yun, 2005). In the resting state of the receptor, dimers of mGluRs are in an open conformation. In the active state, after binding of glutamate, dimers change conformation to a closed state (Kniazeff et al., 2004; Levitz et al., 2016; Marcaggi et al., 2009). Generally, proper receptor dimerization is a requirement to pass the quality control system in the ER to transit along the secretory pathway. The assembly process of protomers into functional dimers remains poorly understood, but high-resolution mGluR structures and mutational analyses suggest that dimerization relies primarily on interactions between the hydrophobic interfaces of the VFT and interactions between the TMDs (El Moustaine et al., 2012; Koehl et al., 2019; Kunishima et al., 2000; Levitz et al., 2016). Interestingly, interactions between the TMDs play a predominant role in homodimerization of mGluR2 while for other mGluRs TMD interactions play only a moderate role in receptor dimerization (Gutzeit et al., 2019; Thibado et al., 2021). While mGluRs were long thought to be strict homodimeric receptors, a number of recent studies indicate that mGluRs are also able to form various heterodimer combinations (Doumazane et al., 2011; Habrian et al., 2019; Kammermeier, 2012; Lee et al., 2020; Levitz et al., 2016; Moreno Delgado et al., 2017; Pandya et al., 2016; Werthmann et al., 2020; Yin et al., 2014). Based on these studies, mostly in heterologous cells, it can be concluded that functional heterodimers form preferentially within group I, II or III mGluRs, but heterodimerization between group II and III mGluRs has also been found to occur. The functional relevance of these heterodimers for synaptic physiology remains to be explored, but a recent pharmacological study in the medial PFC (mPFC) showed that mGluR2/mGluR4 heterodimers selectively modulate synaptic transmission at specific thalamo-mPFC synapses but not at hippocampus-mPFC or amygdala-mPFC synapses (Xiang et al., 2021). A systematic single-cell sequencing study revealed that co-expression of mGluR subtypes is prevalent in the cortex (Lee et al., 2020), indicating that synapse-specific modulation of synaptic transmission by mGluR heterodimers could be a widespread phenomenon in the brain. Additionally, mGluRs can heterodimerize with other GPCR types e.g., mGluR2 can form dimers with the serotonin receptor (Gonzalez-Maeso et al., 2008), and mGluR5 was shown to interact with the dopamine receptor D1 (Sebastianutto et al., 2020).

ER export

ER exit is rate limiting for many receptors, including GPCRs (Petaja-Repo et al., 2000). For mGluRs, ER export has been best studied for group I mGluRs. mGluR1 dimerization was shown to take place in the ER and is independent of glycosylation (Robbins et al., 1999). Both the long and short isoforms of mGluR1 (mGluR1a and mGluR1b) contain a C-terminal ER retention signal (RRKK) (Chan et al., 2001). This sequence has a dominant effect on the surface trafficking and signaling capabilities of the short mGluR1b isoform (Chan et al., 2001; Francesconi and Duvoisin, 2002; Mary et al., 1998), but has little effect on the trafficking of the long mGluR1a isoform. Mutation analysis indicated that a region downstream of the retention signal in the long intracellular tail of mGluR1a neutralizes the

retention signal, overcoming ER retention (Chan et al., 2001). Additionally, when mGluR1a associates with mGluR1b, this region seems to also neutralize the retention motif in mGluR1b promoting the formation and surface trafficking of mGluR1a/b heterodimers (Kumpost et al., 2008; Techlovska et al., 2014), although see also (Remelli et al., 2008). Indeed, in the brain, mGluR1a is preferentially found in complex with mGluR1b, particularly in synaptic membranes (Techlovska et al., 2014). In contrast, for mGluR5 does not share a similar ER retention signal. In fact, although C-terminal interactions modulate mGluR5 ER exit and surface expression (Coutinho et al., 2001; Roche et al., 1999), these interactions do not seem to be dominant in controlling mGluR5 ER export (Chang and Roche, 2017). Rather the seventh transmembrane helix seems to be strictly required for surface expression of mGluR5 in both heterologous cell and neurons (Chang and Roche, 2017), further indicating that neurons evolved diversified mechanisms to control the secretory trafficking of mGluR subtypes and isoforms.

Once released from the ER, most receptors will be further processed by the somatic GA, or through non-somatic Golgi-like structures, and distributed throughout the cell in endosomes via long-range transport. Usually, long-range, directed transport is mediated by members of the kinesin superfamily that can selectively transport various cargoes via adaptor proteins (Kapitein and Hoogenraad, 2015). Indeed, mGluR1 has been shown to be transported by the molecular motor KIF5 (kinesin-1 heavy chain) in complex with the adaptor protein SNAP-23 along dendritic microtubules in hippocampal neurons (Raynaud et al., 2018). Similar information for other mGluRs is however lacking.

Membrane trafficking and anchoring of mGluRs

Ultimately, surface expression determines the density of receptors available for activation and the mechanisms that control the surface expression of mGluRs have been studied extensively (Suh et al., 2018). Particularly, the intracellular C-tails of mGluRs contain numerous interaction motifs and phosphorylation sites that are involved in receptor surface expression and trafficking (Enz, 2012), but recent evidence suggests that other receptor domains, most notably the extracellular domain are also involved in regulating receptor trafficking and function (Dunn et al., 2019a) (Figure 2).

The intracellular tail of mGluR5 contains several binding motifs that have been characterized to great extent. Perhaps the best studied group I mGluR-interacting protein is its adaptor protein Homer. The EVH1 domain of Homer binds to the proline-rich motif (PPxxFR) within the distal C terminus of group I mGluRs (Brakeman et al., 1997; Kato et al., 1998; Tu et al., 1999; Xiao et al., 1998). The short Homer1a isoform was first identified as an immediate early gene, whose expression is rapidly increased upon strong excitation or during LTP induction (Brakeman et al., 1997; Kato et al., 1997). The constitutively expressed long Homer isoforms (Homer1b/c, 2, and 3) contain a C-terminal coiled-coil multimerization domain that allows Homers to couple other PSD proteins, most notable Shank proteins, forming a large assembly platform in the PSD (Hayashi et al., 2009). In addition, the Homer EVH1 domain links group I mGluRs to effector proteins, such as the IP3 and ryanodine receptors modulating basal mGluR activity (Ango et al., 2001; Tu et al., 1998; Yuan et al., 2003), but also co-assembles mGluRs and NMDARs in the same complex (Moutin et al., 2012; Naisbitt et al., 1999). Homer1a lacks this coiled-coil domain and functions as a dominant negative regulator of mGluR signaling by disrupting the

binding between long Homer isoforms and mGluRs (Brakeman et al., 1997; Moutin et al., 2012; Xiao et al., 1998). As such, the Homer family of proteins modulate several aspects of group I mGluR biology, although findings have been contradictory. Long Homer isoforms were found to depress surface expression of mGluR1 and mGluR5 and retain receptors in intracellular clusters (Ango et al., 2002; Coutinho et al., 2001; Roche et al., 1999; Sergé et al., 2002), but other studies found that long Homer isoforms promote surface expression and synaptic targeting (Ango et al., 2000; Ciruela et al., 2000; Kammermeier, 2006; Tadokoro et al., 1999). Although studies do not unanimously agree, long Homer isoforms are generally proposed as the proteins regulating group I mGluR membrane trafficking and anchoring at postsynaptic sites (Figure 2A). Homer1a seems to have a relatively small effect on surface expression, but rather functions to acutely uncouple mGluRs from downstream signaling effectors (Sergé et al., 2002; Xiao et al., 1998).

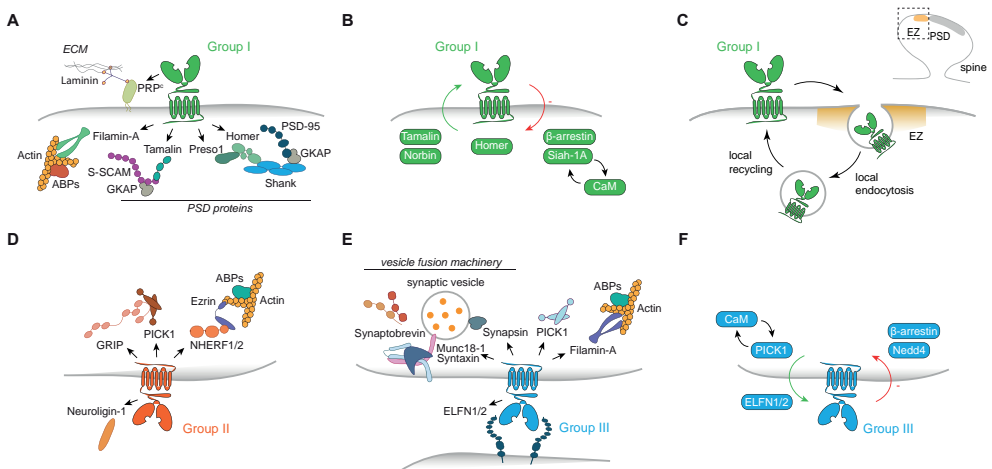


Figure 2. Spatial regulation of mGluRs

(A) Proteins that directly interact with group I mGluRs (green shaded) provide opportunities for bridging with different complexes potentially anchoring group I mGluRs (postsynaptic proteins: Filamin-A – Actin cytoskeleton – Actin binding proteins (ABPs), Tamalin – S-SCAM – GKAP, Preso1 – Homer – Shank – GKAP – PSD-95; and extracellular proteins: cellular prion protein (PRPc) – Laminin – extracellular matrix (ECM)). (B) Proteins that regulate group I mGluR surface expression; Tamalin and Norbin increase mGluR surface expression (green arrow), β -arrestin, Siah-1A binding and Calmodulin (CaM) unbinding decrease mGluR surface expression (red arrow), and Homer has been found to both increase and decrease mGluR surface expression. (C) The endocytic zone (EZ) is a compartmentalized receptor trafficking mechanism in spines, coupled to the PSD, that facilitates the local endocytosis and recycling of group I mGluRs to regulate receptor content. (D) Proteins that directly interact with group II mGluRs (orange shaded) provide opportunities for bridging with different complexes potentially anchoring group II mGluRs (presynaptic proteins: GRIP – PICK1, NHERF1/2 – Actin cytoskeleton – ABPs; and extracellular protein: Neurologin-1) (E) Proteins that directly interact with group III mGluRs (blue shaded) provide opportunities for bridging with different complexes potentially anchoring group III mGluRs (presynaptic proteins: Munc18 – Syntaxin – Synaptobrevin – synaptic vesicle, Synapsin – synaptic vesicle, Filamin-A – Actin cytoskeleton – ABPs; and postsynaptic protein: ELFN1/2) (F) Proteins that regulate group III surface expression; ELFN1/2, PICK1 binding and CaM unbinding increase mGluR surface expression (green arrow), and Nedd4 and β -arrestin decrease mGluR surface expression (red arrow).

Tamalin, Norbin and Preso1 are critical regulators of mGluR signaling and trafficking through interactions with the mGluR C-tail (Matosin et al., 2015a; Matosin et al., 2015b).

The scaffold protein Tamalin is autoinhibited through self-assembly of its PDZ domain and intrinsic ligand, which is disrupted by the presence and competitive binding of group I mGluRs (Kitano et al., 2002). The binding of the mGluR C-terminal SSSSL motif to the Tamalin PDZ domain liberates the intrinsic ligand for the motor protein receptor S-SCAM, facilitating mGluR cell surface trafficking and ligand-dependent internalization (Pandey et al., 2020; Sugi et al., 2007). Additionally, Tamalin links mGluRs to a complex of other proteins involved in postsynaptic organization and protein trafficking, including the ARF-specific guanine nucleotide exchange factor (GEF), that play a key role in the cell-surface expression and intracellular trafficking of group I mGluRs (Kitano et al., 2002; Kitano et al., 2003). However, even though Tamalin functions as a scaffolding molecule interacting with PDZ binding motifs of SAP90/PSD-95-associated proteins and likely assembles within the PSD (Kitano et al., 2003), Tamalin could be a candidate, but is thus far unknown to play a role in anchoring group I mGluRs. Rather, Tamalin has been proposed to play a critical role in mGluR trafficking to control the spatiotemporal surface expression modulating mGluR-dependent synaptic plasticity (Neyman et al., 2019; Pandey et al., 2020) (Figure 2A, B). Norbin binds to the proximal C-terminal part of mGluR5, but does not interfere with Homer binding to mGluR5. Norbin is an mGluR5 accessory protein and promotes mGluR5 surface expression and downstream signaling (Wang et al., 2009) (Figure 2B). Interestingly, using 3D-SIM and STED microscopy Norbin was found to localize to the perisynaptic domain, co-localizing with mGluR5 (Westin et al., 2014). However, whether the large degree of colocalization between Norbin and mGluR5 goes beyond underlining the importance of Norbin as a modulator of mGluR activity, and plays a role in mGluR anchoring, remains unknown. Presol is a multidomain scaffolding protein that can bind to group I mGluRs, as well as Homer and proline-directed kinases. The Presol binding to mGluR C-terminus is upstream of the Homer binding site, however the Presol-mGluR interaction does depend on the Homer binding site. Presol facilitates the binding of proline-directed kinases, such as CDK5/p35 and MEK/ERK, to mGluRs resulting in the phosphorylation of the Homer binding site in mGluR. In turn, Presol-dependent phosphorylation enhances mGluR-Homer binding, resulting in the negative regulation of activity-dependent mGluR signaling (Hu et al., 2012). In contrast to Tamalin and Norbin, Presol does not affect mGluR surface expression, but rather dynamically modulates the mGluR-Homer binding through anchoring proline-directed kinases in the vicinity of mGluRs that negatively regulate activity-dependent mGluR signaling (Figure 2A). Finally, Filamin-A, a large structural protein that crosslinks actin filaments, has been found to interact with several mGluRs, including mGluR5 and mGluR7 (Enz, 2002). Filamin-A could be an interesting candidate to position group I mGluRs in the perisynaptic domain by coupling receptors to the actin cytoskeleton that is prominent in spines (Figure 2A).

Relatively little is known about interactions with the C-tail of group II mGluRs. The intracellular domains of mGluR2 and mGluR3 have high sequence homology and contain a type I PDZ binding motif. However, yeast-two-hybrid and pull-down assays showed that PICK1 and glutamate receptor-interacting protein (GRIP) can interact via the PDZ binding motif only with mGluR3, but not mGluR2 (Hirbec et al., 2002). Another study using GST-pull down screening revealed interactions of group II mGluRs with the Na⁺/H⁺ exchanger regulatory factor 1 and 2 (NHERF-1 and -2) (Ritter-Makinson et al., 2017). Interestingly, NHERFs can interact with actin and could thus link mGluRs to the actin cytoskeleton, perhaps to anchor receptors at specific sites (Figure 2D). The apparent exclusion of mGluR2

from the presynaptic AZ suggests that specific mechanisms underlie receptor localization, but further studies are necessary to elucidate which molecular interactions contribute to group II mGluR positioning.

C-terminal interactions of group III mGluRs were studied in more detail. The C-tail of mGluR4 interacts with several exocytotic proteins such as Munc18-1, synapsins and syntaxins (Ramos et al., 2012). An early study using overexpression of mGluR7 suggested a dominant role for the C-tail of mGluR7 in axonal targeting (Stowell and Craig, 1999). Additionally, interactions between mGluR7 and PICK1 via PDZ binding motifs was shown to be important for targeting and clustering mGluR7 at presynaptic sites (Boudin et al., 2000) (Figure 2E). However, a study using a knock-in mouse with mGluR7 lacking the PDZ motif (Zhang et al., 2008) showed that the PDZ binding motif and interaction with PICK1 were not necessary for synaptic clustering but were essential for receptor function. A number of recent studies provided evidence that group III mGluRs interact in trans with the postsynaptic adhesion molecules ELFN1 and ELFN2 (Dunn et al., 2018; Dunn et al., 2019b; Tomioka et al., 2014). These interactions were shown to be important for the cell surface expression of mGluR7 (Dunn et al., 2019b; Tomioka et al., 2014) and interestingly, ELFNs act as allosteric modulators of group III receptor activity (Dunn et al., 2018; Stachniak et al., 2019) (Figure 2E, F). A recent study showed that a mutation in the VFT of mGluR7 associated with neurodevelopmental disorders reduces surface expression of the receptor in primary cortical neurons (Song et al., 2021). Altogether, there is growing number of evidence that ECD plays crucial role in surface expression of mGluR7.

Desensitization and endocytosis of mGluRs

In general, prolonged or repetitive activation of GPCRs leads to the rapid desensitization to prevent overaction of the receptor. Central in this process are the receptor-associated GPCR kinases (GRKs) that phosphorylate and terminate receptor activation in response to ligand binding (Gurevich and Gurevich, 2019). Receptor phosphorylation triggers the recruitment of β -arrestin which prevents further G-protein activation but also acts as an adaptor for components of the endocytic machinery (AP-2 and clathrin), leading to the sequestration and internalization of the receptor (Ferguson et al., 1996; Goodman et al., 1996; Laporte et al., 1999). For mGluRs, several other kinases have been shown to regulate receptor desensitization, including PKA, ERK, CaMKII, and PKC (Dhami and Ferguson, 2006). Finally, regulators of G protein signalling (RGS) act as GTPase activating proteins (GAPs) on G α proteins to terminate signaling (Saugstad et al., 1998).

Agonist-induced endocytosis of group I mGluRs

Agonist stimulation induces the rapid internalization of group I mGluRs that is primarily mediated by clathrin and dynamin (Dale et al., 2001; Mundell et al., 2002; Mundell et al., 2001), but can be modulated by a myriad of processes. First, GRK-mediated phosphorylation and β -arrestin recruitment trigger the recruitment of endocytic adaptor proteins that initiate clathrin-mediated endocytosis (Figure 2B). Several GRKs were shown to promote the desensitization and internalization of group I mGluRs in heterologous cells (Dale et al., 2000; Sallese et al., 2000; Sorensen and Conn, 2003). But, particularly GRK4, seems to have a physiological role in cerebellar neurons, where knockdown of GRK4 disrupted agonist-induced internalization of mGluR1 (Iacovelli et al., 2003; Sallese et al., 2000). Second, mGluR5 endocytosis was found to be modulated by the regulated binding of

calmodulin (CaM) in the mGluR5 C-tail (Minakami et al., 1997). Upon activation, mGluR5 triggers the activation of PKC that phosphorylates the CaM binding site, promoting the unbinding of CaM and subsequent endocytosis of mGluR5 (Choi et al., 2011; Lee et al., 2008). Interestingly, this regulatory feedback mechanism seems specific for mGluR5, as mGluR1 does not bind CaM (Choi et al., 2011). Third, the E3 ubiquitin ligase, seven in absentia homolog 1A (Siah-1A) competes with CaM for binding mGluR5 (Ishikawa et al., 1999) such that PKC phosphorylation of mGluR5 promotes Siah-1A binding by displacing CaM, leading to decreased mGluR5 surface expression (Ko et al., 2012; Moriyoshi et al., 2004) (Figure 2B). Furthermore, Siah-1A regulates mGluR5 trafficking through the endosomal pathway and accelerates lysosomal degradation of mGluR5 (Ko et al., 2012). Siah-1A was shown to indeed act as an E3 ubiquitin ligase for both mGluR1 and mGluR5, and ubiquitination underlies the efficient internalization of group I mGluRs (Gulia et al., 2017). Finally, the calcium-dependent kinase CaMKII was found to interact with mGluR5 and CaMKII-mediated phosphorylation promotes mGluR5 endocytosis (Jin et al., 2013a; Jin et al., 2013b; Raka et al., 2015).

Constitutive trafficking of Group I mGluRs

Apart from activity-dependent or ligand-induced endocytosis, receptors also undergo constitutive endocytosis in the absence of activity (Fourgeaud et al., 2003). The exact physiological function of this process remains unknown but might be required for maintaining a surface pool of ‘fresh’, resensitized receptors. Constitutive trafficking of mGluR5 in heterologous cells occurs at quite a high rate: almost the complete pool of receptors is recycled in ~3.5 hours (Trivedi and Bhattacharyya, 2012). Constitutive endocytosis of group I mGluRs was found to be independent of clathrin and dynamin (Fourgeaud et al., 2003; Mundell et al., 2001) and is instead mediated by caveolae (Francesconi et al., 2009) and dependent on Ral and PLD2 signaling (Bhattacharya et al., 2004). In neurons, agonist-independent internalization of mGluR5 was observed in both the dendritic spine and shaft and was also found to be independent of dynamin (Scheefhals et al., 2019).

Post-endocytic trafficking

After internalization, receptors enter the endosomal system, a complex system of different intracellular compartments that direct receptors to either undergo recycling to the cell surface or to late endosomes and lysosomes for degradation. In cell lines, it was shown that after agonist-induced internalization mGluR1 was preferentially targeted to recycling endosomes, and less to lysosomes (Pandey et al., 2014). Interestingly, receptor recycling was dependent on PP2A activity, indicating that receptor resensitization is a requirement for proper recycling to the cell surface (Pandey et al., 2014). Similarly, in hippocampal neurons, after agonist-induced internalization mGluR5 traffics preferentially through early endosomes to the recycling compartment before returning to the surface. Here, a small fraction of the internalized mGluR5 pool was targeted to lysosomes via late endosomes, suggesting the targeted breakdown of a subpopulation of internalized receptors (Scheefhals et al., 2019).

Endocytic trafficking of Group II and III mGluRs

In contrast to group I and III mGluRs, far less is known about the trafficking of group II mGluRs. Of interest, it was shown that in response to activation, mGluR3, but not mGluR2, desensitized the cAMP response in a GRK-dependent manner (Iacovelli et al., 2009;

Lennon et al., 2010). The resistance of mGluR2 to desensitization is a unique feature shared only by a few other GPCRs, including mGluR4 (Mathiesen and Ramirez, 2006), and is potentially relevant for mGluR2-mediated processes at presynaptic sites.

Constitutive and activity-dependent trafficking of group III mGluRs was studied most extensively for mGluR7. Studies from heterologous cells and neurons show that mGluR7 undergoes clathrin-independent, constitutive endocytosis and after internalization, mGluR7 is accumulated in Arf6-positive recycling endosomes (Lavezzari and Roche, 2007). Agonist stimulation induces the rapid internalization of mGluR7 (Pelkey et al., 2007; Suh et al., 2008) and many posttranslational modifications of mGluR7 have been reported that regulate mGluR7 trafficking and surface expression. Particularly, phosphorylation of mGluR7 by PKC is important for the stable expression of the receptor at the cell surface and its interaction with PICK1 and CaM (Suh et al., 2008). Reversely, activity-dependent dephosphorylation by protein phosphatases 1 (PP1) causes receptor internalization (Suh et al., 2013). Recently, Nedd4 and β -arrestin-dependent ubiquitination of mGluR7 were shown to regulate agonist-induced endocytosis (Lee et al., 2019) (Figure 2F). In addition, the covalent attachment of small ubiquitin-like modifiers (SUMO), or SUMOylation of mGluR7 has been suggested to be involved in activity-dependent receptor trafficking (Choi et al., 2016). Similarly, mGluR8 was also found to be a target of SUMOylation (Tang et al., 2005). However, a more recent study found that mGluR7 was not SUMO1-conjugated *in vivo* (Daniel et al., 2017). The exact relevance of these findings for synaptic functioning thus remain to be tested.

Local trafficking mechanisms at synapses

A wealth of information is available on the post-translational events and interactors that modulate mGluR trafficking. Nevertheless, many of these findings are based on overexpression studies in neurons and heterologous cells which could influence the trafficking pathways of receptors and surprisingly little is known about which of these mechanisms act locally at synaptic sites in neurons. Nevertheless, insight in the compartmentalized regulation of receptor trafficking is likely very important for a better understanding of how receptor surface levels and positioning are regulated at synapses. Local regulation of receptor trafficking has been studied most extensively in dendritic spines. Intriguingly, at postsynaptic sites clathrin-coated structures laterally coupled to the PSD mark the endocytic zone (EZ) (Blanpied et al., 2002). The EZ is physically coupled to the PSD via interactions with Homer, Dynamin and Shank proteins to facilitate the local uptake of synaptic receptors (Blanpied et al., 2002; Lu et al., 2007; Rácz et al., 2004; Scheefhals 2019). Ionotropic AMPA-type glutamate receptors have been shown to traffic through the EZ and disrupting the PSD-EZ interaction severely affected AMPA receptor levels at synapses (Petrini et al., 2009; Rosendale et al., 2017). The EZ is therefore generally thought to be a critical component in the regulation of synaptic transmission and plasticity and allows the synapse to autonomously control receptor content (Czondor et al., 2012). Once internalized at the EZ, glutamate receptors enter the local recycling mechanism that retains receptors in intracellular pools that can recycle back to the synaptic membrane in an activity-dependent manner (Park et al., 2006). Indeed, the local recycling of receptors via the EZ is essential for synaptic plasticity as uncoupling the EZ from the PSD depletes synaptic AMPA receptors and aborts activity-induced trafficking of receptors to the synaptic membrane during long-term potentiation (Lu et al., 2007; Petrini et al., 2009). While the EZ has been studied

almost exclusively in the context of AMPAR trafficking, more recently it was shown that also postsynaptic endocytosis and recycling of group I mGluRs relies on coupling of the EZ to the PSD (Scheefhals et al., 2019). Disrupting the PSD-EZ interaction reduced mGluR surface levels at synapses resulting in severely decreased mGluR5-mediated calcium responses and ERK1/2 activation (Scheefhals et al., 2019). These findings suggest that the postsynaptic EZ is an important mechanism to compartmentalize receptor recycling and locally balance the density of group I mGluRs to modulate neuronal functioning (Figure 2C). Even though the EZ plays such a central role in postsynaptic glutamate receptor trafficking, and disruptions in this structure might underlie cognitive deficits, insight in the molecular architecture and dynamics of this local trafficking mechanisms remain to be gained. A recent live-cell and super-resolution imaging study revealed that the EZ is remarkably long-lived and is assembled from a number of other key endocytic proteins that are dynamically organized at and around the clathrin lattice (Catsburg et al., 2021).

At presynaptic sites, receptor internalization has not been studied extensively. The G-protein coupled mu-opioid receptor was shown to undergo rapid ligand-induced internalization in axons and accumulated in a distinct population of endosomes marked by the retromer (Jullie et al., 2020). These retromer-marked endosomes were found to be enriched at synaptic boutons and provided a means of rapid receptor re-insertion in the axonal membrane. This vesicle cycle operates independently of the neurotransmitter vesicle cycle, indicating the existence of a dedicated machinery for the endosomal trafficking of presynaptic GPCRs that is mediated by the retromer complex. Further delineation of these processes would be of interest to determine how local trafficking mechanisms are organized in presynaptic boutons to sustain localized surface expression of receptors.

Functional roles of synaptic mGluRs

Role of presynaptic mGluRs in modulating neurotransmitter release

Presynaptic mechanisms that modulate the efficiency of neurotransmitter release are critical for the fine tuning of synaptic transmission. In this regard, presynaptic mGluRs are considered as essential auto-receptors that act as negative-feedback elements to depress glutamate release (Pinheiro and Mulle, 2008). Although group I mGluRs have been ascribed to modulate neurotransmitter release in different synapse types in the nervous system (Giribaldi et al., 2013; Luccini et al., 2007; Pittaluga, 2016), the group II and III mGluRs are studied most extensively in this context. The presynaptic group II and III mGluRs both couple to inhibitory G-proteins (Gai/o) (Tanabe et al., 1992). Activation of presynaptic mGluRs can depress synaptic transmission via several pathways: inhibition of voltage-gated Ca^{2+} -channels (VGCC), activation of K^+ channels, or by direct modulation of components of the release machinery such as Munc13, Munc18 and RIM-1 (de Jong and Verhage, 2009). Release can also be inhibited by action of $\text{G}\beta\gamma$ subunits that act on vesicular fusion machinery (Anwyl, 1999). Consequently, these receptors have been implicated in the acute, transient regulation of transmission as well as persistent forms of plasticity such as long-term depression (LTD) and long-term potentiation (LTP).

Determinants of activation for presynaptic mGluRs

Although both group II and group III mGluRs are co-expressed at presynaptic sites and can in principle couple to the same signaling pathways, the distribution of group II

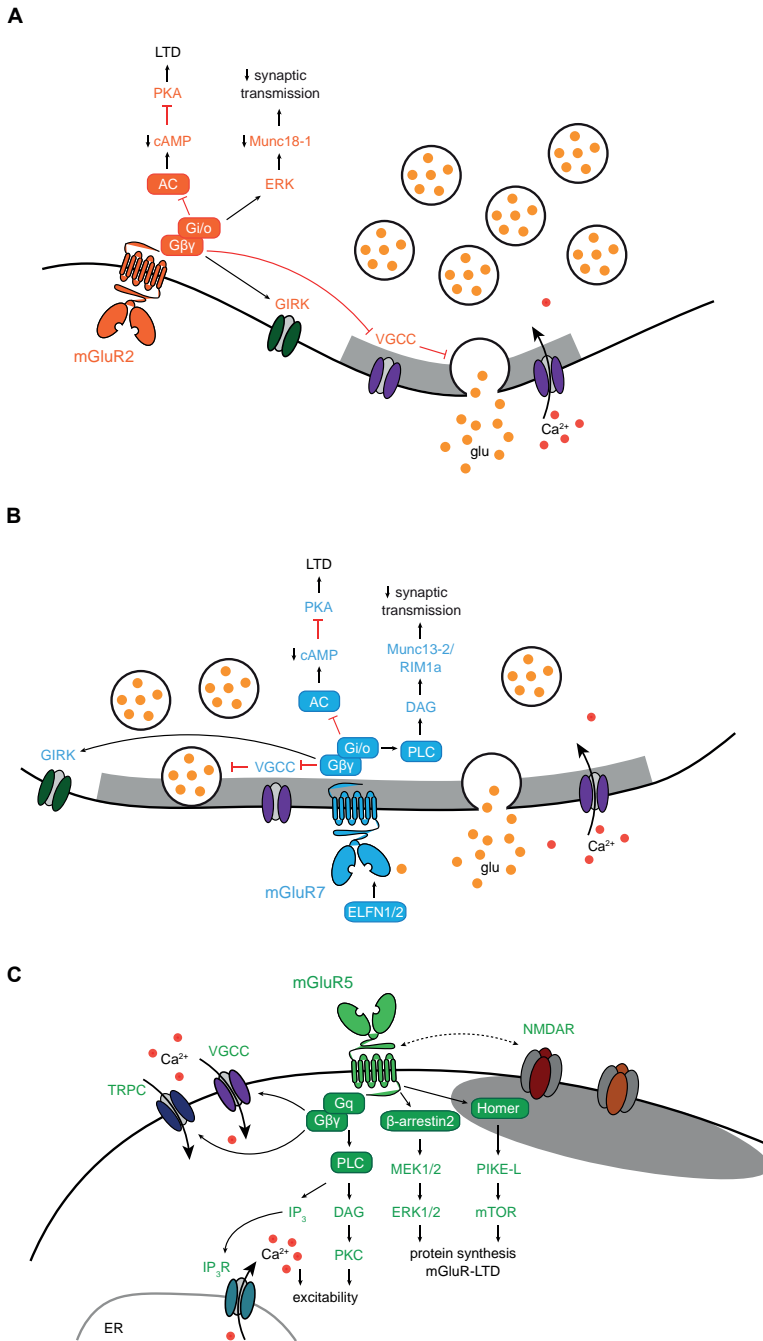


Figure 3. Main signaling pathways of mGluRs

(A - C) Main molecular components involved in the regulation of synaptic transmission by presynaptic group II mGluR2 (A) and group III mGluR7 (B) and postsynaptic group I mGluR5 (C). AC – adenylate cyclase, glu – glutamate, GIRK – G-protein-coupled inwardly-rectifying potassium channel, VGCC – voltage-gated calcium channel.

and III receptor relative to the presynaptic release site is highly segregated. Notably this distribution seems aligned with the differences in affinity of these receptors for glutamate. mGluR2 for instance has a moderate to high affinity for glutamate (0.5 - 20 μM) but is found primarily in the axonal shaft and at perisynaptic sites. The affinity of most group III mGluRs is somewhat lower (5 - 40 μM), however the EC₅₀ of mGluR7 for glutamate is exceptionally low (>500 μM) (Schoepp et al., 1999). Single release events produce only brief, 1 - 3 mM peaks in glutamate concentration in the synaptic cleft that rapidly decay in space and time. As a result, it has been proposed that presynaptic mGluRs preferentially respond to strong, high-frequency stimulation (HFS) patterns that result in high cleft concentration of glutamate or even spill-over activating perisynaptic receptors (Scanziani et al., 1997). However, there is a surprising scarcity of quantitative information on the activation kinetics of mGluRs in response to physiological synaptic stimuli.

Presynaptic actions of group II mGluRs

The depressing actions of mGluR2/3 activation on neurotransmitter release are primarily mediated by inhibition of adenylate cyclase (AC) activity and consequently reduced cAMP-mediated PKA activation (Nicholls et al., 2006; Tzounopoulos et al., 1998). In addition, mGluR2/3 activation also stimulates ERK-dependent pathways that lead for instance to phosphorylation of Munc18-1, directly impacting the release machinery (Schmitz et al., 2016) (Figure 3A). Stimulation of group II mGluRs with selective agonists acutely depresses transmission at excitatory synapses throughout the brain (Bushell et al., 1996; Capogna, 2004; Kilbride et al., 1998; Lovinger and McCool, 1995; Price et al., 2005). A role for group II mGluRs in persistent presynaptic LTD has also been found and has been most intensely studied at mossy fiber (MF)-CA3 synapses (Kobayashi et al., 1996; Yokoi et al., 1996). This form of LTD relies on a mGluR-dependent reduction in cAMP and decrease in PKA activity, but additionally requires the activity-dependent influx of presynaptic calcium (Tzounopoulos et al., 1998). The exact targets of PKA at presynaptic sites remain elusive, but the induction of LTD was blocked in Rab3a knock-out mice (Tzounopoulos et al., 1998), suggesting that PKA acts on targets that directly regulate transmitter release. However, the absolute requirement for group II mGluRs for mossy fiber LTD was recently challenged by findings that LTD was unaltered by a new selective and highly potent group II mGluR antagonist (Wostrack and Dietrich, 2009) and remained intact in mGluR2/3 double-knockout mice (Lyon et al., 2011).

Presynaptic actions of group III mGluRs

The inhibitory action of group III mGluRs on glutamate release has been shown in a broad variety of preparations. Stimulation of group III mGluRs blocks the stimulated release of glutamate from isolated nerve endings or synaptosomes (Millan et al., 2002; Rodriguez-Moreno et al., 1998) and autapses (O'Connor et al., 1999), depresses cAMP-induced vesicle cycling (Chavis et al., 1998), induces the PKC-dependent blockade of P/Q-type channels (Martin et al., 2007; Perroy et al., 2000) (Figure 3B), and potently depresses synaptic transmission at CA3-CA1 synapses in the hippocampus (Ayala et al., 2008; Baskys and Malenka, 1991; Gereau and Conn, 1995), as well as other synapses in the central nervous system (Pelkey et al., 2005; Perroy et al., 2002; Zhang et al., 2008). Also, short-term plasticity is significantly altered short-term plasticity at CA3-CA1 synapses in mGluR7 knockout mice (Bushell et al., 2002). Thus, all these lines of evidence are consistent with the

notion that these receptors act as autoreceptors at excitatory synapses. However, mGluR7 has also been suggested to be a heteroreceptor acting at inhibitory synapses in the CA1 region of the hippocampus to indirectly regulate excitatory drive in the hippocampus (Klar et al., 2015). Activation of group III mGluRs has also been found to potentiate transmission through activation of PKC and recruitment of Munc-13 (Martin et al., 2010) (Figure 3B). It was proposed that mGluR7 activation bidirectionally regulates transmission, inducing a rapid, short-lasting potentiation followed by a longer-lasting depression of synaptic responses (Martin et al., 2018).

At MF-stratum lucidum interneurons HFS or transient application of L-AP4 induces a prominent presynaptic form of LTD that is mediated by mGluR7 and the subsequent persistent downregulation of P/Q-type VGCCs (Pelkey et al., 2005; Pelkey et al., 2006). Interestingly, however, when induced after L-AP4 application, this same HFS protocol induces potentiation, or de-depression of synaptic responses that required cAMP-PKA signaling. Since L-AP4 induces the rapid internalization of mGluR7, it is thought that the surface expression of mGluR7 dictates the direction of plasticity, acting as a metaplastic switch at MF-SLIN synapses (Pelkey et al., 2005; Pelkey et al., 2008; Suh et al., 2008). Interestingly, a recent study in SC-CA2 synapses similarly suggested a gating role for group III mGluRs, based on findings that group III mGluR antagonists allow the induction of NMDAR-dependent LTP that is normally absent at these synapses (Dasgupta et al., 2020).

Transsynaptic control of mGluR activity

Of interest for the regulation of group III mGluR function at synapses is the increasing evidence that the extracellular domain of mGluRs forms a critical point of regulation, allowing for interactions with structural proteins that act as structural and allosteric modulators of GPCR activity (Dunn et al., 2019a). For example, the adhesion molecules ELFN1 and ELFN2 bind selectively to all group III mGluRs in trans and act as allosteric modulators of mGluR activity (Dunn et al., 2018; Dunn et al., 2019b; Tomioka et al., 2014). At synapses, ELFN proteins generally seem to stimulate mGluR activity, even under resting conditions of synaptic activity, providing constitutive depression of release (Dunn et al., 2019b; Stachniak et al., 2019; Sylwestrak and Ghosh, 2012). These actions of ELFNs are probably mediated by maintaining sufficient surface expression levels of mGluR7 and increasing its apparent affinity for glutamate (Dunn et al., 2019b). It is tempting to speculate that extracellular interactions are a more general mechanism regulating different aspects of mGluR biology, including (subsynaptic) positioning, mobility, and receptor activity. Recent evidence for extrasynaptic interactions has been reported for mGluR2, which was shown to interact with neuroligin 1 (Gjørølund et al., 2017), and for group I mGluRs that were shown to transduce intracellular signaling triggered by the laminin-bound prion protein (Beraldo et al., 2011). Additionally, prion proteins are suggested to form a dynamic platform for signaling modules to assemble at the surface, spatially restricting group I mGluRs and compartmentalizing downstream responses (Linden, 2017) (Figure 2A, D).

Role of postsynaptic mGluRs in synaptic transmission and plasticity

The particular perisynaptic partitioning of group I mGluRs, puts these receptors at a considerable distance away from the release site, effectively lowering the probability that these receptors become activated by synaptic release events. Nevertheless, postsynaptic mGluR signaling has been found to be involved in a plethora of processes that regulate

basal synaptic transmission and long-term plasticity. Once activated, group I mGluRs can trigger a wide variety of signaling pathways. Canonically, group I mGluRs couple to Gαq/11 proteins that activate the PLC pathway, leading to release of Ca²⁺ from internal stores and stimulation of PKC (Niswender and Conn, 2010). Apart from this principal pathway, group I mGluRs can engage a wide range of other effector proteins, including casein kinase 1, Cdk 5, as well as the PI3K-mTOR signaling and ERK-signaling pathways that stimulate protein translation (Banko et al., 2006; Hou and Klann, 2004; Liu et al., 2001; Ronesi and Huber, 2008). The ability of group I mGluRs to activate these G-protein-independent signaling pathways relies on specific adaptor proteins that differentially recruit signaling components. For instance, Homer proteins can recruit PIKE-L (phosphoinositide PI3-kinase enhancer) that couples to the PI3K-AKT-mTOR pathway (Rong et al., 2003), and b-arrestin2 couples mGluR5 to the ERK signaling pathway (Stoppel et al., 2017) (Figure 3C). Group I mGluRs also modulate several ion channels including K⁺ channels (Charpak et al., 1990), voltage-gated calcium channels (Kato et al., 2012), TRP channels (Gee et al., 2003), generally leading to an increased excitability (Anwyl, 1999; Fagni et al., 2000). Through these actions group I mGluRs can have broad and lasting effects on the excitability of a neuron but depending on the context, these receptors can also modulate local synaptic processes that lead to long-term changes in synaptic efficacy.

Modulation of NMDA receptors by group I mGluRs

Early studies in *Xenopus* oocytes demonstrated that group I mGluR activation can potentiate NMDAR activity (Kelso et al., 1992), presumably through an increase in NMDAR exocytosis (Lan et al., 2001b). Similarly, stimulation of group I mGluRs also potentiates NMDAR responses in the hippocampus (Aniksztejn et al., 1992; Benquet et al., 2002; Fitzjohn et al., 1996; Harvey and Collingridge, 1993; O'Connor et al., 1994) as well as other brain regions (Awad et al., 2000). In contrast, in other studies group I mGluRs were shown to depress NMDAR activity (Bertaso et al., 2010; Moutin et al., 2012; Perroy et al., 2008; Snyder et al., 2001; Wang et al., 1998; Yu et al., 1997). A clear explanation for these contradicting findings is still lacking but the effect of mGluR activity on NMDAR function seems to be highly dependent on the context, i.e., related to the synapse type that is investigated, interacting scaffolds and access to signaling pathways. For instance, group I mGluR activation potentiates NMDARs in the hippocampal CA1 region, but has a depressing effect on NMDAR currents in CA3 neurons (Grishin et al., 2004).

Likely related to these conflicting results, how group I mGluRs exert their modulatory effects on NMDAR activity remains poorly understood. Various modes of crosstalk between group I mGluRs and NMDARs have been described that could in principle mediate these effects. For instance, G-protein-mediated activation of PKC and Src were shown to be involved in modulating the gating properties and trafficking of NMDARs (Aniksztejn et al., 1992; Benquet et al., 2002; Harvey and Collingridge, 1993; Heidinger et al., 2002; Lan et al., 2001a). Another potential mode of crosstalk is through modulation of the Homer scaffold proteins. The interaction of Homer with Shank proteins (Tu et al., 1999) links group I mGluRs to the NMDAR that couples to Shank via its interaction with PSD-95. Interestingly, the activity-regulated short Homer1a isoform, lacks the coiled-coil domain and acts as a dominant-negative monomer that disrupts the structural link between mGluRs and NMDARs. Overexpression of Homer1a abolishes the potentiating effects of mGluRs on NMDAR activity (Sylantsev et al., 2013), suggesting there could be

a direct modulatory impact of mGluRs on NMDARs through this structural interaction (O'Neill et al., 2018). In an alternative, seemingly conflicting model, the Homer-Shank scaffold interaction prevents mGluR1/5 from exerting a modulatory role on the synaptic NMDAR and Homer1a-mediated disruption of this complex is required to allow crosstalk (Bertaso et al., 2010). Support for this notion comes from studies that show that Homer1a uncouples mGluR5 from perisynaptic sites, allowing direct interaction of mGluR5 with the NMDAR in the PSD (Aloisi et al., 2017; Moutin et al., 2012; Perroy et al., 2008). These seemingly conflicting mechanisms might in fact overlap at different time scales with the outcome being dependent on the properties of the particular cell and/or synapse type (O'Neill et al., 2018).

Modulation of NMDAR-dependent plasticity by mGluRs

At hippocampal SC-CA1 synapses, the most well-studied forms of long-term plasticity, LTD and LTP, are induced by the activation of NMDARs. Thus, the modulatory effects of group I mGluRs on NMDAR function suggest that mGluRs can also influence the expression of NMDAR-mediated forms of plasticity. Several studies have indeed implicated group I mGluRs in the regulation of NMDAR-dependent LTP in SC-CA1 synapses. Prior stimulation of mGluRs with agonists primes LTP induction (Bashir et al., 1993b; Bortolotto et al., 1994; Cohen and Abraham, 1996; Cohen et al., 1998), and PAMs enhance LTP at hippocampal SC-CA1 synapses (Ayala et al., 2009). Conversely, pharmacological blockade of group I mGluRs (Balschun and Wetzel, 2002; Bashir et al., 1993a; Bortolotto et al., 1994; Francesconi et al., 2004; Neyman and Manahan-Vaughan, 2008) and genetic deletion of mGluR5 (Jia et al., 1998; Lu et al., 1997) strongly reduce hippocampal LTP. Thus, co-activation of postsynaptic group I mGluRs and NMDARs seems to underlie the induction of LTP, and chemical co-activation of these receptors has even been found sufficient to induce LTP (Kotecha et al., 2003). In a recent, careful analysis evaluating the plasticity-inducing rules at SC-CA1 synapses it was shown that time-correlated pre- and postsynaptic spiking induced strong potentiation that was dependent on the coordinated calcium influx through NMDARs and VGCCs in spines and required group I mGluRs (Tigaret et al., 2016). Here, group I mGluRs were shown to be required for depressing SK channels that negatively affect NMDAR activity. Thus, also under more physiological synaptic stimulation protocols, mGluRs seem to work in close synergy with synaptic NMDARs to orchestrate synaptic transmission and plasticity.

Group I mGluR-dependent long-term depression

Activation of group I mGluRs by prolonged low-frequency stimulation protocols or direct application of DHPG, induces a persistent form of LTD: mGluR-LTD (Luscher and Huber, 2010). Interestingly, this form of LTD is mechanistically distinct from NMDAR-dependent LTD (Oliet et al., 1997). Most importantly, unlike NMDAR-LTD, mGluR-LTD relies on the rapid and local synthesis of new proteins in dendrites (Huber et al., 2000) that promote the internalization of AMPARs (Park et al., 2008; Waung et al., 2008). mGluR-LTD induction is dependent on the activation of Gαq signalling (Kleppisch et al., 2001), PI3K/mTOR signaling (Hou and Klann, 2004), ERK (Gallagher et al., 2004) and b-arrestins (Stoppel et al., 2017) that converge on local cap-dependent translation. Interestingly, the efficacy of mGluR-mediated LTD seems strongly determined by the availability of effectors. Using local glutamate uncaging protocols that induce mGluR-dependent LTD

at individual spines it was shown that only spines containing an ER were able to undergo LTD (Holbro et al., 2009).

Role of group I mGluRs in non-Hebbian plasticity

Apart from Hebbian, input-specific forms of plasticity, group I mGluRs have been found to play a dominant role in forms of non-Hebbian plasticity such as homeostatic scaling of synaptic strength and metaplasticity (Bockaert et al., 2021). This was first shown in dissociated cortical neurons, where synaptic downscaling by a chronic increase in network activity was prevented by pharmacological inhibition of group I mGluRs (Hu et al., 2010). Interestingly, this study showed that mGluR1/5-driven scaling was not initiated by synaptically released glutamate but was stimulated by the activity-induced increase in Homer1a expression (Hu et al., 2010), consistent with earlier observations that Homer1a expression stimulates agonist-independent signaling pathways downstream of mGluR5 (Ango et al., 2001). In a physiological context, downscaling of synapses is prominent during sleep, which is thought to desaturate synaptic strength and allow further learning during the awake phase. In a recent comprehensive study, it was shown that excitatory synapses undergo extensive remodeling during sleep, which was primarily driven by targeting of Homer1a to the synapse, and the consequent stimulation of group I mGluR activity (Diering et al., 2017). Homer1a-driven stimulation of mGluR1/5 activity was also shown to regulate visual experience-dependent weakening of synapses in the visual cortex (Chokshi et al., 2019), and has been extensively investigated in the context of reward-directed learning in drug addiction (Marton et al., 2015), as well as other psychiatric disorders (Szumlinski et al., 2006). Promisingly, stimulating constitutive activation of mGluR1/5 activity by introducing cell-permeable Homer1a was recently shown to have anti-depressant effects (Holz et al., 2019). This induction mechanism of mGluR1/5 signaling by intracellular Homer1a thus seems to be a particularly important mechanism in non-Hebbian forms of synaptic plasticity that has clear relevance for understanding physiological and pathological conditions.

Postsynaptic actions of group II mGluRs

Of note, group II mGluRs have also been reported to have postsynaptic effects. Group II agonists were shown to strongly enhance neuronal excitability in CA3 neurons (Ster et al., 2011). Moreover, stimulation of group II mGluRs induced the stable potentiation of SC-CA1 synapses that was mediated by modulation of NMDAR activity (Rosenberg et al., 2016). Interestingly, this form of mGluR-dependent LTP seemed to be independent of the classic form of HFS-induced SC-CA1 LTP. Rather, the activation of mGluR2/3 potentiated NMDARs and was proposed to act as a metaplasticity switch that gates the subsequent induction of NMDAR-mediated LTP (Rosenberg et al., 2016). Group II mGluRs were also shown to potentiate postsynaptic mGluR5 function in the prefrontal cortex (PFC) (Di Menna et al., 2018) and regulate AMPA receptor trafficking in PFC neurons (Wang et al., 2013). Interestingly, disruptions in mGluR3-mGluR5 crosstalk were found to underlie stress-induced cognitive deficits (Joffe et al., 2019), and stimulation of mGluR3 enhanced cognitive performance of mice in an mGluR5-dependent manner (Dogra et al., 2021), highlighting the relevance of this emerging notion of mGluR crosstalk for understanding psychiatric disorders. It thus seems that several mGluRs impact NMDAR-dependent processes and it would be important to further dissect the extent of glutamate receptor crosstalk at postsynaptic sites and unravel the mechanisms that mediate glutamate receptor cooperativity.

Conclusions and future directions for the field

Since the initial cloning of metabotropic glutamate receptors, tremendous efforts have led to an astonishing progress in our understanding of how mGluRs are trafficked and targeted to their subcellular destination in neurons. This fascinating family of glutamate receptors has evolved to fulfil a broad palette of cellular functions and regulate key aspects of neuronal functioning. We here discussed the various actions of these receptors at pre- and postsynaptic sites that are key for the regulation of synaptic transmission and plasticity, but it is important to note is that these receptors also signal in various other subcellular compartments, including the nucleus, and fulfil key roles in glial cells. This striking diversity in biological functions is determined by the various signaling pathways, heterodimerization with family members and other GPCRs, subcellular localization and crosstalk with ionotropic receptors. Grasping this functional complexity and incorporating this into existing models of synaptic transmission is one of the largest challenges of the moment and will greatly benefit from computational modeling efforts that can integrate different levels of complexity and make quantitative predictions. Moreover, defining the activation and deactivation kinetics of receptors in intact neuronal networks is important to connect the pharmacology and molecular biology of mGluRs to a circuit level understanding of brain functioning and animal behavior. This is for instance exemplified by the recent discovery of endogenous allosteric modulators such as the ELFN proteins, that significantly alter the pharmacological and functional profile of mGluRs at native synapses in the brain. To accurately probe receptor function within their native environment it will be important to continue ongoing exciting developments in fluorescence live-cell and super-resolution microscopy to study the nanoscale distribution and dynamics of glutamate receptors (Groc and Choquet, 2020). These techniques in turn will benefit from the development of optical sensors of receptor activation (Vilardaga et al., 2003), optogenetic tools to control receptor activation (Levitz et al., 2017; Levitz et al., 2013) or localization (Sinnen et al., 2017) and CRISPR/Cas9 technologies to label endogenous receptor complexes (Willems et al., 2020). Continuing research in these directions will provide a firm understanding of the dynamic processes that underlie the actions of mGluRs at and around synapses. This will not only result in a deeper insight in the regulatory roles of mGluRs in synaptic transmission and plasticity but will also reveal critical points in these processes that can be targeted in therapeutic approaches to treat neurological disorders.

Acknowledgements

Funding: This work was supported by the European Research Council [ERC-StG 716011; the Netherlands Organization for Scientific Research (Graduate Program of Quantitative Biology and Computational Life Sciences).

References

- Aloisi, E., Le Corf, K., Dupuis, J., Zhang, P., Ginger, M., Labrousse, V., Spatuzza, M., Georg Haberl, M., Costa, L., Shigemoto, R., Tappe-Theodor, A., Drago, F., Vincenzo Piazza, P., Mülle, C., Groc, L., Ciranna, L., Catania, M.V., and Frick, A. (2017). Altered surface mGluR5 dynamics provoke synaptic NMDAR dysfunction and cognitive defects in Fmr1 knockout mice. *Nat. Commun.* 8, 1103.
- Ango, F., Pin, J.P., Tu, J.C., Xiao, B., Worley, P.F., Bockaert, J., and Fagni, L. (2000). Dendritic and axonal targeting of type 5 metabotropic glutamate receptor is regulated by homer1 proteins and neuronal excitation. *J. Neurosci.* 20, 8710-8716.
- Ango, F., Prezeau, L., Muller, T., Tu, J.C., Xiao, B., Worley, P.F., Pin, J.P., Bockaert, J., and Fagni, L. (2001). Agonist-independent activation of metabotropic glutamate receptors by the intracellular protein Homer. *Nature* 411, 962-965.
- Ango, F., Robbe, D., Tu, J.C., Xiao, B., Worley, P.F., Pin, J.P., Bockaert, J., and Fagni, L. (2002). Homer-dependent cell surface expression of metabotropic glutamate receptor type 5 in neurons. *Mol. Cell. Neurosci.* 20, 323-329.
- Aniksztejn, L., Otani, S., and Ben-Ari, Y. (1992). Quisqualate metabotropic receptors modulate NMDA currents and facilitate induction of long-term potentiation through protein kinase C. *Eur. J. Neurosci.* 4, 500-505.
- Anwyl, R. (1999). Metabotropic glutamate receptors: electrophysiological properties and role in plasticity. *Brain Res Brain Res Rev* 29, 83-120.
- Awad, H., Hubert, G.W., Smith, Y., Levey, A.I., and Conn, P.J. (2000). Activation of metabotropic glutamate receptor 5 has direct excitatory effects and potentiates NMDA receptor currents in neurons of the subthalamic nucleus. *J. Neurosci.* 20, 7871-7879.
- Ayala, J.E., Chen, Y., Banko, J.L., Sheffler, D.J., Williams, R., Telk, A.N., Watson, N.L., Xiang, Z., Zhang, Y., Jones, P.J., Lindsley, C.W., Olive, M.F., and Conn, P.J. (2009). mGluR5 positive allosteric modulators facilitate both hippocampal LTP and LTD and enhance spatial learning. *Neuropsychopharmacology* 34, 2057-2071.
- Ayala, J.E., Niswender, C.M., Luo, Q., Banko, J.L., and Conn, P.J. (2008). Group III mGluR regulation of synaptic transmission at the SC-CA1 synapse is developmentally regulated. *Neuropharmacology* 54, 804-814.
- Balschun, D., and Wetzell, W. (2002). Inhibition of mGluR5 blocks hippocampal LTP *in vivo* and spatial learning in rats. *Pharmacol. Biochem. Behav.* 73, 375-380.
- Banko, J.L., Hou, L., Poulin, F., Sonenberg, N., and Klann, E. (2006). Regulation of eukaryotic initiation factor 4E by converging signaling pathways during metabotropic glutamate receptor-dependent long-term depression. *J. Neurosci.* 26, 2167-2173.
- Bashir, Z.I., Bortolotto, Z.A., Davies, C.H., Berretta, N., Irving, A.J., Seal, A.J., Henley, J. M., Jane, D.E., Watkins, J.C., and Collingridge, G.L. (1993a). Induction of LTP in the hippocampus needs synaptic activation of glutamate metabotropic receptors. *Nature* 363, 347-350.
- Bashir, Z.I., Jane, D.E., Sunter, D.C., Watkins, J.C., and Collingridge, G.L. (1993b). Metabotropic glutamate receptors contribute to the induction of long-term depression in the CA1 region of the hippocampus. *Eur. J. Pharmacol.* 239, 265-266.
- Baskys, A., and Malenka, R.C. (1991). Agonists at metabotropic glutamate receptors presynaptically inhibit EPSCs in neonatal rat hippocampus. *J. Physiol* 444, 687-701.
- Baude, A., Nusser, Z., Roberts, J.D., Mulvihill, E., McIlhinney, R.A., and Somogyi, P. (1993). The metabotropic glutamate receptor (mGluR1 α) is concentrated at perisynaptic membrane of neuronal subpopulations as detected by immunogold reaction. *Neuron* 11, 771-787.
- Benquet, P., Gee, C.E., and Gerber, U. (2002). Two distinct signaling pathways upregulate NMDA receptor responses via two distinct metabotropic glutamate receptor subtypes. *J. Neurosci.* 22, 9679-9686.
- Beraldo, F.H., Arantes, C.P., Santos, T.G., Machado, C.F., Roffe, M., Hajj, G.N., Lee, K.S., Magalhaes, A.C., Caetano, F.A., Mancini, G.L., Lopes, M.H., Americo, T.H., Magdesian, M.H., Ferguson, S.S., Linden, R., Prado, M.A., and Martins, V.R. (2011). Metabotropic glutamate receptors transduce signals for neurite outgrowth after binding of the prion protein to laminin gamma1 chain. *FASEB J* 25, 265-279.
- Bertaso, F., Roussignol, G., Worley, P., Bockaert, J., Fagni, L., and Ango, F. (2010). Homer1a-dependent crosstalk between NMDA and metabotropic glutamate receptors in mouse neurons. *PLoS One* 5, e9755.
- Bhattacharya, M., Babwah, A.V., Godin, C., Anborgh, P.H., Dale, L.B., Poulter, M.O., and Ferguson, S.S. (2004). Ral and phospholipase D2-dependent pathway for constitutive metabotropic glutamate receptor endocytosis. *J. Neurosci.* 24, 8752-8761.
- Bhave, G., Nadin, B.M., Brasier, D.J., Glauner, K.S., Shah, R.D., Heinemann, S.F., Karim, F., and Gereau, R.W.t. (2003). Membrane topology of a metabotropic glutamate receptor. *J. Biol. Chem.* 278, 30294-30301.
- Blanpied, T.A., Scott, D.B., and Ehlers, M.D. (2002). Dynamics and regulation of clathrin coats at specialized endocytic zones of dendrites and spines. *Neuron* 36, 435-449.

- Bockaert, J., Perroy, J., and Ango, F. (2021). The complex formed by group I metabotropic glutamate receptor (mGluR) and Homer1a plays a central role in metaplasticity and homeostatic synaptic scaling. *J. Neurosci.* 41, 5567-5578.
- Bodzęta, A., Berger, F., and MacGillavry, H.D. (2020). Distinct mechanisms underlie the subsynaptic mobility of presynaptic metabotropic glutamate receptor types to tune receptor activation. *BioRxiv*. <https://doi.org/10.1101/2020.07.06.188995>.
- Bortolotto, Z.A., Bashir, Z.I., Davies, C.H., and Collingridge, G.L. (1994). A molecular switch activated by metabotropic glutamate receptors regulates induction of long-term potentiation. *Nature* 368, 740-743.
- Boudin, H., Doan, A., Xia, J., Shigemoto, R., Huganir, R.L., Worley, P., and Craig, A.M. (2000). Presynaptic clustering of mGluR7a requires the PICK1 PDZ domain binding site. *Neuron* 28, 485-497.
- Bradley, S.R., Levey, A.I., Hersch, S.M., and Conn, P.J. (1996). Immunocytochemical localization of group III metabotropic glutamate receptors in the hippocampus with subtype-specific antibodies. *J. Neurosci.* 16, 2044-2056.
- Bradley, S.R., Rees, H.D., Yi, H., Levey, A.I., and Conn, P.J. (1998). Distribution and developmental regulation of metabotropic glutamate receptor 7a in rat brain. *J. Neurochem.* 71, 636-645.
- Brakeman, P.R., Lanahan, A.A., O'Brien, R., Roche, K., Barnes, C.A., Huganir, R.L., and Worley, P.F. (1997). Homer: a protein that selectively binds metabotropic glutamate receptors. *Nature* 386, 284-288.
- Bushell, T.J., Jane, D.E., Tse, H.W., Watkins, J.C., Garthwaite, J., and Collingridge, G.L. (1996). Pharmacological antagonism of the actions of group II and III mGluR agonists in the lateral perforant path of rat hippocampal slices. *Br. J. Pharmacol.* 117, 1457-1462.
- Bushell, T.J., Sansig, G., Collett, V.J., van der Putten, H., and Collingridge, G.L. (2002). Altered short-term synaptic plasticity in mice lacking the metabotropic glutamate receptor mGlu7. *ScientificWorldJournal* 2, 730-737.
- Capogna, M. (2004). Distinct properties of presynaptic group II and III metabotropic glutamate receptor-mediated inhibition of perforant pathway-CA1 EPSCs. *Eur. J. Neurosci.* 19, 2847-2858.
- Catsburg, L.A.E., Westra, M., Van Schaik, A.M.L., and MacGillavry, H.D. (2021). Dynamics and nanoscale organization of the postsynaptic endocytic zone at excitatory synapses. *bioRxiv*. <https://doi.org/10.1101/2021.02.18.431766>.
- Chan, W.Y., Soloviev, M.M., Ciruela, F., and McIlhinney, R.A. (2001). Molecular determinants of metabotropic glutamate receptor 1B trafficking. *Mol. Cell. Neurosci.* 17, 577-588.
- Chang, K., and Roche, K.W. (2017). Structural and molecular determinants regulating mGluR5 surface expression. *Neuropharmacology* 115, 10-19.
- Charpak, S., Gahwiler, B.H., Do, K.Q., and Knopfel, T. (1990). Potassium conductances in hippocampal neurons blocked by excitatory amino-acid transmitters. *Nature* 347, 765-767.
- Chavis, P., Mollard, P., Bockaert, J., and Manzoni, O. (1998). Visualization of cyclic AMP-regulated presynaptic activity at cerebellar granule cells. *Neuron* 20, 773-781.
- Choi, J.H., Park, J.Y., Park, S.P., Lee, H., Han, S., Park, K.H., and Suh, Y.H. (2016). Regulation of mGluR7 trafficking by SUMOylation in neurons. *Neuropharmacology* 102, 229-235.
- Choi, K.Y., Chung, S., and Roche, K.W. (2011). Differential binding of calmodulin to group I metabotropic glutamate receptors regulates receptor trafficking and signaling. *J. Neurosci.* 31, 5921-5930.
- Chokshi, V., Gao, M., Grier, B.D., Owens, A., Wang, H., Worley, P.F., and Lee, H.K. (2019). Input-specific metaplasticity in the visual cortex requires homer1a-mediated mGluR5 signaling. *Neuron* 104, 736-748 e736.
- Ciruela, F., Soloviev, M.M., Chan, W.Y., and McIlhinney, R.A. (2000). Homer-1c/Vesl-1L modulates the cell surface targeting of metabotropic glutamate receptor type 1alpha: evidence for an anchoring function. *Mol. Cell. Neurosci.* 15, 36-50.
- Cohen, A.S., and Abraham, W.C. (1996). Facilitation of long-term potentiation by prior activation of metabotropic glutamate receptors. *J. Neurophysiol.* 76, 953-962.
- Cohen, A.S., Raymond, C.R., and Abraham, W.C. (1998). Priming of long-term potentiation induced by activation of metabotropic glutamate receptors coupled to phospholipase C. *Hippocampus* 8, 160-170.
- Corti, C., Aldegheri, L., Somogyi, P., and Ferraguti, F. (2002). Distribution and synaptic localisation of the metabotropic glutamate receptor 4 (mGluR4) in the rodent CNS. *Neuroscience* 110, 403-420.
- Coutinho, V., Kavanagh, I., Sugiyama, H., Tones, M.A., and Henley, J.M. (2001). Characterization of a metabotropic glutamate receptor type 5-green fluorescent protein chimera (mGluR5-GFP): pharmacology, surface expression, and differential effects of Homer-1a and Homer-1c. *Mol. Cell. Neurosci.* 18, 296-306.
- Crupi, R., Impellizzeri, D., and Cuzzocrea, S. (2019). Role of metabotropic glutamate receptors in neurological disorders. *Front. Mol. Neurosci.* 12, 20.
- Cui-Wang, T., Hanus, C., Cui, T., Helton, T., Bourne, J., Watson, D., Harris, K.M., and Ehlers, M.D. (2012). Local zones of endoplasmic reticulum complexity confine cargo in neuronal dendrites. *Cell* 148, 309-321.

- Czondor, K., Mondin, M., Garcia, M., Heine, M., Frischknecht, R., Choquet, D., Sibarita, J.B., and Thoumine, O.R. (2012). Unified quantitative model of AMPA receptor trafficking at synapses. *Proc. Natl. Acad. Sci. U. S. A.* 109, 3522-3527.
- Dale, L.B., Bhattacharya, M., Anborgh, P.H., Murdoch, B., Bhatia, M., Nakanishi, S., and Ferguson, S.S. (2000). G protein-coupled receptor kinase-mediated desensitization of metabotropic glutamate receptor 1A protects against cell death. *J. Biol. Chem.* 275, 38213-38220.
- Dale, L.B., Bhattacharya, M., Seachrist, J.L., Anborgh, P.H., and Ferguson, S.S. (2001). Agonist-stimulated and tonic internalization of metabotropic glutamate receptor 1a in human embryonic kidney 293 cells: agonist-stimulated endocytosis is beta-arrestin1 isoform-specific. *Mol. Pharmacol.* 60, 1243-1253.
- Daniel, J.A., Cooper, B.H., Palvimo, J.J., Zhang, F.P., Brose, N., and Tirard, M. (2017). Analysis of SUMO1-conjugation at synapses. *Elife* 6.
- Dasgupta, A., Lim, Y.J., Kumar, K., Baby, N., Pang, K.L.K., Benoy, A., Behnisch, T., and Sajikumar, S. (2020). Group III metabotropic glutamate receptors gate long-term potentiation and synaptic tagging/capture in rat hippocampal area CA2. *Elife* 9.
- de Jong, A.P., and Verhage, M. (2009). Presynaptic signal transduction pathways that modulate synaptic transmission. *Curr. Opin. Neurobiol.* 19, 245-253.
- Dhami, G.K., and Ferguson, S.S. (2006). Regulation of metabotropic glutamate receptor signaling, desensitization and endocytosis. *Pharmacol. Ther.* 111, 260-271.
- Di Menna, L., Joffe, M.E., Iacovelli, L., Orlando, R., Lindsley, C.W., Mairesse, J., Gressens, P., Cannella, M., Caraci, F., Copani, A., Bruno, V., Battaglia, G., Conn, P.J., and Nicoletti, F. (2018). Functional partnership between mGlu3 and mGlu5 metabotropic glutamate receptors in the central nervous system. *Neuropharmacology* 128, 301-313.
- Diering, G.H., Nirujogi, R.S., Roth, R.H., Worley, P.F., Pandey, A., and Hagan, R.L. (2017). Homer1a drives homeostatic scaling-down of excitatory synapses during sleep. *Science* 355, 511-515.
- Dogra, S., Stansley, B.J., Xiang, Z., Qian, W., Gogliotti, R.G., Nicoletti, F., Lindsley, C.W., Niswender, C.M., Joffe, M.E., and Conn, P.J. (2021). Activating mGlu3 metabotropic glutamate receptors rescues schizophrenia-like cognitive deficits through metaplastic adaptations within the hippocampus. *Biol Psychiatry* 90 (6), 385-398.
- Doumazane, E., Scholler, P., Zwier, J.M., Trinquet, E., Rondard, P., and Pin, J.P. (2011). A new approach to analyze cell surface protein complexes reveals specific heterodimeric metabotropic glutamate receptors. *Faseb J.* 25, 66-77.
- Dunn, H.A., Orlandi, C., and Martemyanov, K.A. (2019a). Beyond the ligand: extracellular and transcellular G protein-coupled receptor complexes in physiology and pharmacology. *Pharmacol. Rev.* 71, 503-519.
- Dunn, H.A., Patil, D.N., Cao, Y., Orlandi, C., and Martemyanov, K.A. (2018). Synaptic adhesion protein ELFN1 is a selective allosteric modulator of group III metabotropic glutamate receptors in trans. *Proc. Natl. Acad. Sci. U. S. A.* 115, 5022-5027.
- Dunn, H.A., Zucca, S., Dao, M., Orlandi, C., and Martemyanov, K.A. (2019b). ELFN2 is a postsynaptic cell adhesion molecule with essential roles in controlling group III mGluRs in the brain and neuropsychiatric behavior. *Mol. Psychiatr.* 24, 1902-1919.
- El Moustaine, D., Granier, S., Doumazane, E., Scholler, P., Rahmeh, R., Bron, P., Mouillac, B., Baneres, J.L., Rondard, P., and Pin, J.P. (2012). Distinct roles of metabotropic glutamate receptor dimerization in agonist activation and G-protein coupling. *Proc. Natl. Acad. Sci. U. S. A.* 109, 16342-16347.
- Enz, R. (2002). The actin-binding protein Filamin-A interacts with the metabotropic glutamate receptor type 7. *FEBS Lett.* 514, 184-188.
- Enz, R. (2012). Structure of metabotropic glutamate receptor C-terminal domains in contact with interacting proteins. *Front. Mol. Neurosci.* 5, 52.
- Fagni, L., Chavis, P., Ango, F., and Bockaert, J. (2000). Complex interactions between mGluRs, intracellular Ca²⁺ stores and ion channels in neurons. *Trends Neurosci.* 23, 80-88.
- Ferguson, S.S., Downey 3rd, W.E., Colapietro, A.M., Barak, L.S., Menard, L., and Caron, M.G. (1996). Role of beta-arrestin in mediating agonist-promoted G protein-coupled receptor internalization. *Science* 271, 363-366.
- Ferraguti, F., Klausberger, T., Cobden, P., Baude, A., Roberts, J.D., Szucs, P., Kinoshita, A., Shigemoto, R., Somogyi, P., and Dalezios, Y. (2005). Metabotropic glutamate receptor 8-expressing nerve terminals target subsets of GABAergic neurons in the hippocampus. *J. Neurosci.* 25, 10520-10536.
- Ferraguti, F., and Shigemoto, R. (2006). Metabotropic glutamate receptors. *Cell Tissue Res.* 326, 483-504.
- Fitzjohn, S.M., Irving, A.J., Palmer, M.J., Harvey, J., Lodge, D., and Collingridge, G.L. (1996). Activation of group I mGluRs potentiates NMDA responses in rat hippocampal slices. *Neurosci. Lett.* 203, 211-213.
- Fourgeaud, L., Bessis, A.S., Rossignol, F., Pin, J.P., Olivo-Marin, J.C., and Hemar, A. (2003). The metabotropic glutamate receptor mGluR5 is endocytosed by a clathrin-independent pathway. *J. Biol. Chem.* 278, 12222-12230.
- Francesconi, A., and Duvoisin, R.M. (2002). Alternative splicing unmasks dendritic and axonal targeting signals in

- metabotropic glutamate receptor 1. *J. Neurosci.* 22, 2196-2205.
- Francesconi, A., Kumari, R., and Zukin, R.S. (2009). Regulation of group I metabotropic glutamate receptor trafficking and signaling by the caveolar/lipid raft pathway. *J. Neurosci.* 29, 3590-3602.
- Francesconi, W., Cammalleri, M., and Sanna, P.P. (2004). The metabotropic glutamate receptor 5 is necessary for late-phase long-term potentiation in the hippocampal CA1 region. *Brain Res.* 1022, 12-18.
- Gallagher, S.M., Daly, C.A., Bear, M.F., and Huber, K.M. (2004). Extracellular signal-regulated protein kinase activation is required for metabotropic glutamate receptor-dependent long-term depression in hippocampal area CA1. *J. Neurosci.* 24, 4859-4864.
- Gee, C.E., Benquet, P., and Gerber, U. (2003). Group I metabotropic glutamate receptors activate a calcium-sensitive transient receptor potential-like conductance in rat hippocampus. *J. Physiol* 546, 655-664.
- Gereau, R.W.t., and Conn, P.J. (1995). Multiple presynaptic metabotropic glutamate receptors modulate excitatory and inhibitory synaptic transmission in hippocampal area CA1. *J. Neurosci.* 15, 6879-6889.
- Giribaldi, F., Milanese, M., Bonifacino, T., Anna Rossi, P.I., Di Prisco, S., Pittaluga, A., Tacchetti, C., Puliti, A., Usai, C., and Bonanno, G. (2013). Group I metabotropic glutamate autoreceptors induce abnormal glutamate exocytosis in a mouse model of amyotrophic lateral sclerosis. *Neuropharmacology* 66, 253-263.
- Gjorlund, M.D., Carlsen, E.M.M., Konig, A.B., Dmytrieva, O., Petersen, A.V., Jacobsen, J., Berezin, V., Perrier, J.F., and Owczarek, C. (2017). Soluble ectodomain of neuroligin 1 decreases synaptic activity by activating metabotropic glutamate receptor 2. *Front Mol Neurosci* 10 (116).
- Goncalves, J., Bartol, T.M., Camus, C., Levet, F., Menegolla, A.P., Sejnowski, T.J., Sibarita, J.B., Vivaudou, M., Choquet, D., and Hossy, E. (2020). Nanoscale co-organization and coactivation of AMPAR, NMDAR, and mGluR at excitatory synapses. *Proc. Natl. Acad. Sci. U. S. A.* 117, 14503-14511.
- Gonzalez-Maeso, J., Ang, R.L., Yuen, T., Chan, P., Weisstaub, N.V., Lopez-Gimenez, J.F., Zhou, M., Okawa, Y., Callado, L.F., Milligan, G., Gingrich, J.A., Filizola, M., Meana, J.J., and Sealfon, S.C. (2008). Identification of a serotonin/glutamate receptor complex implicated in psychosis. *Nature* 452, 93-97.
- Goodman Jr., O.B., Krupnick, J.G., Santini, F., Gurevich, V.V., Penn, R.B., Gagnon, A.W., Keen, J.H., and Benovic, J.L. (1996). Beta-arrestin acts as a clathrin adaptor in endocytosis of the beta2-adrenergic receptor. *Nature* 383, 447-450.
- Grishin, A.A., Gee, C.E., Gerber, U., and Benquet, P. (2004). Differential calcium-dependent modulation of NMDA currents in CA1 and CA3 hippocampal pyramidal cells. *J. Neurosci.* 24, 350-355.
- Groc, L., and Choquet, D. (2020). Linking glutamate receptor movements and synapse function. *Science* 368.
- Gulia, R., Sharma, R., and Bhattacharyya, S. (2017). A critical role for ubiquitination in the endocytosis of glutamate receptors. *J. Biol. Chem.* 292, 1426-1437.
- Gurevich, V.V., and Gurevich, E.V. (2019). GPCR signaling regulation: the role of GRKs and arrestins. *Front. Pharmacol.* 10, 125.
- Gutzeit, V.A., Thibado, J., Stor, D.S., Zhou, Z., Blanchard, S.C., Andersen, O.S., and Levitz, J. (2019). Conformational dynamics between transmembrane domains and allosteric modulation of a metabotropic glutamate receptor. *Elife* 8.
- Habrian, C.H., Levitz, J., Vyklicky, V., Fu, Z., Hoagland, A., McCort-Tranchepain, I., Acher, F., and Isacoff, E.Y. (2019). Conformational pathway provides unique sensitivity to a synaptic mGluR. *Nat. Commun.* 10, 5572.
- Harvey, J., and Collingridge, G.L. (1993). Signal transduction pathways involved in the acute potentiation of NMDA responses by 1S,3R-ACPD in rat hippocampal slices. *Br. J. Pharmacol.* 109, 1085-1090.
- Hayashi, M.K., Tang, C., Verpilli, C., Narayanan, R., Stearns, M.H., Xu, R.M., Li, H., Sala, C., and Hayashi, Y. (2009). The postsynaptic density proteins Homer and Shank form a polymeric network structure. *Cell* 137, 159-171.
- Hayashi, Y., Momiyama, A., Takahashi, T., Ohishi, H., Ogawa-Meguro, R., Shigemoto, R., Mizuno, N., and Nakanishi, S. (1993). Role of a metabotropic glutamate receptor in synaptic modulation in the accessory olfactory bulb. *Nature* 366, 687-690.
- Heidinger, V., Manzerra, P., Wang, X.Q., Strasser, U., Yu, S.P., Choi, D.W., and Behrens, M. M. (2002). Metabotropic glutamate receptor 1-induced upregulation of NMDA receptor current: mediation through the Pyk2/Src-family kinase pathway in cortical neurons. *J. Neurosci.* 22, 5452-5461.
- Helenius, A., and Aebi, M. (2001). Intracellular functions of N-linked glycans. *Science* 291, 2364-2369.
- Hirbec, H., Perestenko, O., Nishimune, A., Meyer, G., Nakanishi, S., Henley, J.M., and Dev, K. K. (2002). The PDZ proteins PICK1, GRIP, and syntenin bind multiple glutamate receptor subtypes. Analysis of PDZ binding motifs. *J. Biol. Chem.* 277, 15221-15224.
- Holbro, N., Grunditz, A., and Oertner, T.G. (2009). Differential distribution of endoplasmic reticulum controls metabotropic signaling and plasticity at hippocampal synapses. *Proc. Natl. Acad. Sci. U. S. A.* 106, 15055-15060.
- Holz, A., Mulsch, F., Schwarz, M.K., Hollmann, M., Dobrossy, M.D., Coenen, V.A., Bartos, M., Normann, C., Biber, K., van Calker, D., and Serchov, T. (2019). Enhanced mGlu5 signaling in excitatory neurons promotes

- rapid antidepressant effects via AMPA receptor activation. *Neuron* 104, 338-352 e337.
- Horton, A.C., and Ehlers, M.D. (2003). Dual modes of endoplasmic reticulum-to-Golgi transport in dendrites revealed by live-cell imaging. *J. Neurosci.* 23, 6188-6199.
- Hou, L., and Klann, E. (2004). Activation of the phosphoinositide 3-kinase-Akt-mammalian target of rapamycin signaling pathway is required for metabotropic glutamate receptor-dependent long-term depression. *J. Neurosci.* 24, 6352-6361.
- Hu, J.H., Park, J.M., Park, S., Xiao, B., Dehoff, M.H., Kim, S., Hayashi, T., Schwarz, M.K., Haganir, R.L., Seeburg, P.H., Linden, D.J., and Worley, P.F. (2010). Homeostatic scaling requires group I mGluR activation mediated by Homer1a. *Neuron* 68, 1128-1142.
- Hu, J.H., Yang, L., Kammermeier, P.J., Moore, C.G., Brakeman, P.R., Tu, J., Yu, S., Petralia, R.S., Li, Z., Zhang, P.W., Park, J.M., Dong, X., Xiao, B., and Worley, P.F. (2012). Presol dynamically regulates group I metabotropic glutamate receptors. *Nat. Neurosci.* 15, 836-844.
- Huber, K.M., Kayser, M.S., and Bear, M.F. (2000). Role for rapid dendritic protein synthesis in hippocampal mGluR-dependent long-term depression. *Science* 288, 1254-1257.
- Iacovelli, L., Molinaro, G., Battaglia, G., Motolese, M., Di Menna, L., Alfiero, M., Blahos, J., Matriciano, F., Corsi, M., Corti, C., Bruno, V., De Blasi, A., and Nicoletti, F. (2009). Regulation of group II metabotropic glutamate receptors by G protein-coupled receptor kinases: mGlu2 receptors are resistant to homologous desensitization. *Mol. Pharmacol.* 75, 991-1003.
- Iacovelli, L., Salvatore, L., Capobianco, L., Picascia, A., Barletta, E., Storto, M., Mariggio, S., Sallese, M., Porcellini, A., Nicoletti, F., and De Blasi, A. (2003). Role of G protein-coupled receptor kinase 4 and beta-arrestin 1 in agonist-stimulated metabotropic glutamate receptor 1 internalization and activation of mitogen-activated protein kinases. *J. Biol. Chem.* 278, 12433-12442.
- Ishikawa, K., Nash, S.R., Nishimune, A., Neki, A., Kaneko, S., and Nakanishi, S. (1999). Competitive interaction of seven in absentia homolog-1A and Ca²⁺/calmodulin with the cytoplasmic tail of group I metabotropic glutamate receptors. *Gene Cell.* 4, 381-390.
- Jia, Z., Lu, Y., Henderson, J., Taverna, F., Romano, C., Abramow-Newerly, W., Wojtowicz, J.M., and Roder, J. (1998). Selective abolition of the NMDA component of long-term potentiation in mice lacking mGluR5. *Learn. Mem.* 5, 331-343.
- Jin, D.Z., Guo, M.L., Xue, B., Fibuch, E.E., Choe, E.S., Mao, L.M., and Wang, J.Q. (2013a). Phosphorylation and feedback regulation of metabotropic glutamate receptor 1 by calcium/calmodulin-dependent protein kinase II. *J. Neurosci.* 33, 3402-3412.
- Jin, D.Z., Guo, M.L., Xue, B., Mao, L.M., and Wang, J.Q. (2013b). Differential regulation of CaMKIIalpha interactions with mGluR5 and NMDA receptors by Ca(2+) in neurons. *J. Neurochem.* 127, 620-631.
- Joffe, M.E., Santiago, C.I., Stansley, B.J., Maksymetz, J., Gogliotti, R.G., Engers, J.L., Nicoletti, F., Lindsley, C.W., and Conn, P.J. (2019). Mechanisms underlying prefrontal cortex mGlu3/mGlu5-dependent plasticity and reversal learning deficits following acute stress. *Neuropharmacology* 144, 19-28.
- Jong, Y.J., Kumar, V., Kingston, A.E., Romano, C., and O'Malley, K.L. (2005). Functional metabotropic glutamate receptors on nuclei from brain and primary cultured striatal neurons. Role of transporters in delivering ligand. *J. Biol. Chem.* 280, 30469-30480.
- Jullie, D., Stoeber, M., Sibarita, J.B., Zieger, H.L., Bartol, T.M., Arttamangkul, S., Sejnowski, T.J., Hosy, E., and von Zastrow, M. (2020). A discrete presynaptic vesicle cycle for neuromodulator receptors. *Neuron* 105, 663-677 e668.
- Kammermeier, P.J. (2006). Surface clustering of metabotropic glutamate receptor 1 induced by long Homer proteins. *BMC Neurosci.* 7, 1.
- Kammermeier, P.J. (2012). Functional and pharmacological characteristics of metabotropic glutamate receptors 2/4 heterodimers. *Mol. Pharmacol.* 82, 438-447.
- Kammermeier, P.J., and Yun, J. (2005). Activation of metabotropic glutamate receptor 1 dimers requires glutamate binding in both subunits. *J. Pharmacol. Exp. Therapeut.* 312, 502-508.
- Kaptein, L.C., and Hoogenraad, C.C. (2015). Building the neuronal microtubule cytoskeleton. *Neuron* 87, 492-506.
- Kato, A., Ozawa, F., Saitoh, Y., Fukazawa, Y., Sugiyama, H., and Inokuchi, K. (1998). Novel members of the Ves1/Homer family of PDZ proteins that bind metabotropic glutamate receptors. *J. Biol. Chem.* 273, 23969-23975.
- Kato, A., Ozawa, F., Saitoh, Y., Hirai, K., and Inokuchi, K. (1997). vesl, a gene encoding VASP/Ena family related protein, is upregulated during seizure, long-term potentiation and synaptogenesis. *FEBS Lett.* 412, 183-189.
- Kato, H.K., Kassai, H., Watabe, A.M., Aiba, A., and Manabe, T. (2012). Functional coupling of the metabotropic glutamate receptor, InsP3 receptor and L-type Ca²⁺ channel in mouse CA1 pyramidal cells. *J. Physiol* 590, 3019-3034.
- Kelso, S.R., Nelson, T.E., and Leonard, J.P. (1992). Protein kinase C-mediated enhancement of NMDA currents by

- metabotropic glutamate receptors in *Xenopus* oocytes. *J Physiol* 449, 705-718.
- Kennedy, M.J., and Hanus, C. (2019). Architecture and dynamics of the neuronal secretory network. *Annu. Rev. Cell Dev. Biol.* 35, 543-566.
- Kilbride, J., Huang, L.Q., Rowan, M.J. and Anwyl, R. (1998). Presynaptic inhibitory action of the group II metabotropic glutamate receptor agonists, LY354740 and DCG-IV. *Eur. J. Pharmacol.* 356, 149-157.
- Kinoshita, A., Ohishi, H., Nomura, S., Shigemoto, R., Nakanishi, S., and Mizuno, N. (1996). Presynaptic localization of a metabotropic glutamate receptor, mGluR4a, in the cerebellar cortex: a light and electron microscope study in the rat. *Neurosci. Lett.* 207, 199-202.
- Kinzie, J.M., Saugstad, J.A., Westbrook, G.L., and Segerson, T.P. (1995). Distribution of metabotropic glutamate receptor 7 messenger RNA in the developing and adult rat brain. *Neuroscience* 69, 167-176.
- Kitano, J., Kimura, K., Yamazaki, Y., Soda, T., Shigemoto, R., Nakajima, Y., and Nakanishi, S. (2002). Tamalin, a PDZ domain-containing protein, links a protein complex formation of group I metabotropic glutamate receptors and the guanine nucleotide exchange factor cytohesins. *J. Neurosci.* 22, 1280-1289.
- Kitano, J., Yamazaki, Y., Kimura, K., Masukado, T., Nakajima, Y., and Nakanishi, S. (2003). Tamalin is a scaffold protein that interacts with multiple neuronal proteins in distinct modes of protein-protein association. *J. Biol. Chem.* 278, 14762-14768.
- Klar, R., Walker, A.G., Ghose, D., Grueter, B.A., Engers, D.W., Hopkins, C.R., Lindsley, C. W., Xiang, Z., Conn, P.J., and Niswender, C.M. (2015). Activation of metabotropic glutamate receptor 7 is required for induction of long-term potentiation at SC-CA1 synapses in the Hippocampus. *J. Neurosci.* 35, 7600-7615.
- Kleppisch, T., Voigt, V., Allmann, R., and Offermanns, S. (2001). G(alpha)q-deficient mice lack metabotropic glutamate receptor-dependent long-term depression but show normal long-term potentiation in the hippocampal CA1 region. *J. Neurosci.* 21, 4943-4948.
- Klotz, L., Wendler, O., Frischknecht, R., Shigemoto, R., Schulze, H., and Enz, R. (2019). Localization of group II and III metabotropic glutamate receptors at pre- and postsynaptic sites of inner hair cell ribbon synapses. *Faseb. J.* 33, 13734-13746.
- Kniazeff, J., Bessis, A.S., Maurel, D., Ansanay, H., Prezeau, L., and Pin, J.P. (2004). Closed state of both binding domains of homodimeric mGlu receptors is required for full activity. *Nat. Struct. Mol. Biol.* 11, 706-713.
- Ko, S.J., Iozaki, K., Kim, I., Lee, J.H., Cho, H.J., Sohn, S.Y., Oh, S.R., Park, S., Kim, D.G., Kim, C.H., and Roche, K.W. (2012). PKC phosphorylation regulates mGluR5 trafficking by enhancing binding of Siah-1A. *J. Neurosci.* 32, 16391-16401.
- Kobayashi, K., Manabe, T., and Takahashi, T. (1996). Presynaptic long-term depression at the hippocampal mossy fiber-CA3 synapse. *Science* 273, 648-650.
- Koehl, A., Hu, H., Feng, D., Sun, B., Zhang, Y., Robertson, M.J., Chu, M., Kobilka, T.S., Laeremans, T., Steyaert, J., Tarrasch, J., Dutta, S., Fonseca, R., Weis, W.I., Mathiesen, J.M., Skiniotis, G., and Kobilka, B.K. (2019). Structural insights into the activation of metabotropic glutamate receptors. *Nature* 566, 79-84.
- Kotecha, S.A., Jackson, M.F., Al-Mahrouki, A., Roder, J.C., Orser, B.A., and MacDonald, J.F. (2003). Co-stimulation of mGluR5 and N-methyl-D-aspartate receptors is required for potentiation of excitatory synaptic transmission in hippocampal neurons. *J. Biol. Chem.* 278, 27742-27749.
- Kumpost, J., Syrova, Z., Kulihova, L., Frankova, D., Bologna, J.C., Hlavackova, V., Prezeau, L., Kralikova, M., Hruskova, B., Pin, J.P., and Blahos, J. (2008). Surface expression of metabotropic glutamate receptor variants mGluR1a and mGluR1b in transfected HEK293 cells. *Neuropharmacology* 55, 409-418.
- Kunishima, N., Shimada, Y., Tsuji, Y., Sato, T., Yamamoto, M., Kumasaka, T., Nakanishi, S., Jingami, H., and Morikawa, K. (2000). Structural basis of glutamate recognition by a dimeric metabotropic glutamate receptor. *Nature* 407, 971-977.
- Lan, J.Y., Skeberdis, V.A., Jover, T., Grooms, S.Y., Lin, Y., Aranedo, R.C., Zheng, X., Bennett, M.V., and Zukin, R.S. (2001a). Protein kinase C modulates NMDA receptor trafficking and gating. *Nat. Neurosci.* 4, 382-390.
- Lan, J.Y., Skeberdis, V.A., Jover, T., Zheng, X., Bennett, M.V., and Zukin, R.S. (2001b). Activation of metabotropic glutamate receptor 1 accelerates NMDA receptor trafficking. *J. Neurosci.* 21, 6058-6068.
- Laporte, S.A., Oakley, R.H., Zhang, J., Holt, J.A., Ferguson, S.S., Caron, M.G., and Barak, L.S. (1999). The beta2-adrenergic receptor/betaarrestin complex recruits the clathrin adaptor AP-2 during endocytosis. *Proc. Natl. Acad. Sci. U. S. A.* 96, 3712-3717.
- Lavezzari, G., and Roche, K.W. (2007). Constitutive endocytosis of the metabotropic glutamate receptor mGluR7 is clathrin-independent. *Neuropharmacology* 52, 100-107.
- Lee, J., Munguba, H., Gutzeit, V.A., Singh, D.R., Krist, M., Dittman, J.S., and Levitz, J. (2020). Defining the homo- and heterodimerization propensities of metabotropic glutamate receptors. *Cell Rep.* 31, 107891.
- Lee, J.H., Lee, J., Choi, K.Y., Hepp, R., Lee, J.Y., Lim, M.K., Chatani-Hinze, M., Roche, P. A., Kim, D.G., Ahn, Y.S., Kim, C.H., and Roche, K.W. (2008). Calmodulin dynamically regulates the trafficking of the metabotropic

- glutamate receptor mGluR5. *Proc. Natl. Acad. Sci. U. S. A.* 105, 12575-12580.
- Lee, S., Park, S., Lee, H., Han, S., Song, J.M., Han, D., and Suh, Y.H. (2019). Nedd4 E3 ligase and beta-arrestins regulate ubiquitination, trafficking, and stability of the mGlu7 receptor. *Elife* 8.
- Lennon, S.M., Rivero, G., Matharu, A., Howson, P.A., Jane, D.E., Roberts, P.J., and Kelly, E. (2010). Metabotropic glutamate receptor mGlu2 is resistant to homologous agonist-induced desensitization but undergoes protein kinase C-mediated heterologous desensitization. *Eur. J. Pharmacol.* 649, 29-37.
- Levitz, J., Broichhagen, J., Leippe, P., Konrad, D., Trauner, D., and Isacoff, E.Y. (2017). Dual optical control and mechanistic insights into photoswitchable group II and III metabotropic glutamate receptors. *Proc. Natl. Acad. Sci. U. S. A.* 114, E3546-E3554.
- Levitz, J., Habrian, C., Bharill, S., Fu, Z., Vafabakhsh, R., and Isacoff, E.Y. (2016). Mechanism of assembly and cooperativity of homomeric and heteromeric metabotropic glutamate receptors. *Neuron* 92, 143-159.
- Levitz, J., Pantoja, C., Gaub, B., Janovjak, H., Reiner, A., Hoagland, A., Schoppik, D., Kane, B., Stawski, P., Schier, A.F., Trauner, D., and Isacoff, E.Y. (2013). Optical control of metabotropic glutamate receptors. *Nat. Neurosci.* 16, 507-516.
- Linden, R. (2017). The biological function of the prion protein: a cell surface scaffold of signaling modules. *Front. Mol. Neurosci.* 10, 77.
- Liu, F., Ma, X.H., Ule, J., Bibb, J.A., Nishi, A., DeMaggio, A.J., Yan, Z., Nairn, A.C., and Greengard, P. (2001). Regulation of cyclin-dependent kinase 5 and casein kinase 1 by metabotropic glutamate receptors. *Proc. Natl. Acad. Sci. U. S. A.* 98, 11062-11068.
- Lovinger, D.M., and McCool, B.A. (1995). Metabotropic glutamate receptor-mediated presynaptic depression at corticostriatal synapses involves mGluR2 or 3. *J. Neurophysiol.* 73, 1076-1083.
- Lu, J., Helton, T.D., Blanpied, T.A., Racz, B., Newpher, T.M., Weinberg, R.J., and Ehlers, M. D. (2007). Postsynaptic positioning of endocytic zones and AMPA receptor cycling by physical coupling of dynamin-3 to homer. *Neuron* 55, 874-889.
- Lu, Y.M., Jia, Z., Janus, C., Henderson, J.T., Gerlai, R., Wojtowicz, J.M., and Roder, J.C. (1997). Mice lacking metabotropic glutamate receptor 5 show impaired learning and reduced CA1 long-term potentiation (LTP) but normal CA3 LTP. *J. Neurosci.* 17, 5196-5205.
- Luccini, E., Musante, V., Neri, E., Brambilla Bas, M., Severi, P., Raiteri, M., and Pittaluga, A. (2007). Functional interactions between presynaptic NMDA receptors and metabotropic glutamate receptors co-expressed on rat and human noradrenergic terminals. *Br. J. Pharmacol.* 151, 1087-1094.
- Lujan, R., Nusser, Z., Roberts, J.D., Shigemoto and R., Somogyi, P. (1996). Perisynaptic location of metabotropic glutamate receptors mGluR1 and mGluR5 on dendrites and dendritic spines in the rat hippocampus. *Eur. J. Neurosci.* 8, 1488-1500.
- Lujan, R., Roberts, J.D., Shigemoto, R., Ohishi, H., and Somogyi, P. (1997). Differential plasma membrane distribution of metabotropic glutamate receptors mGluR1 alpha, mGluR2 and mGluR5, relative to neurotransmitter release sites. *J. Chem. Neuroanat.* 13, 219-241.
- Luscher, C., and Huber, K.M. (2010). Group 1 mGluR-dependent synaptic long-term depression: mechanisms and implications for circuitry and disease. *Neuron* 65, 445-459.
- Lyon, L., Borel, M., Carrion, M., Kew, J.N., Corti, C., Harrison, P.J., Burnet, P.W., Paulsen, O., and Rodriguez-Moreno, A. (2011). Hippocampal mossy fiber long-term depression in Grm2/3 double knockout mice. *Synapse* 65, 945-954.
- Marcaggi, P., Mutoh, H., Dimitrov, D., Beato, M., and Knopfel, T. (2009). Optical measurement of mGluR1 conformational changes reveals fast activation, slow deactivation, and sensitization. *Proc. Natl. Acad. Sci. U. S. A.* 106, 11388-11393.
- Martin, L.J., Blackstone, C.D., Haganir, R.L., and Price, D.L. (1992). Cellular localization of a metabotropic glutamate receptor in rat brain. *Neuron* 9, 259-270.
- Martin, R., Durroux, T., Ciruela, F., Torres, M., Pin, J.P., and Sanchez-Prieto, J. (2010). The metabotropic glutamate receptor mGlu7 activates phospholipase C, translocates munc-13-1 protein, and potentiates glutamate release at cerebrocortical nerve terminals. *J. Biol. Chem.* 285, 17907-17917.
- Martin, R., Ferrero, J.J., Collado-Alsina, A., Aguado, C., Lujan, R., Torres, M., and Sanchez-Prieto, J. (2018). Bidirectional modulation of glutamatergic synaptic transmission by metabotropic glutamate type 7 receptors at Schaffer collateral-CA1 hippocampal synapses. *J. Physiol* 596, 921-940.
- Martin, R., Torres, M., and Sanchez-Prieto, J. (2007). mGluR7 inhibits glutamate release through a PKC-independent decrease in the activity of P/Q-type Ca²⁺ channels and by diminishing cAMP in hippocampal nerve terminals. *Eur. J. Neurosci.* 26, 312-322.
- Marton, T.M., Hussain Shuler, M.G., and Worley, P.F. (2015). Homer 1a and mGluR5 phosphorylation in reward-sensitive metaplasticity: a hypothesis of neuronal selection and bidirectional synaptic plasticity. *Brain Res.* 1628,

- 17-28.
- Mary, S., Gomeza, J., Prezeau, L., Bockaert, J., and Pin, J.P. (1998). A cluster of basic residues in the carboxyl-terminal tail of the short metabotropic glutamate receptor 1 variants impairs their coupling to phospholipase C. *J. Biol. Chem.* 273, 425-432.
- Mathiesen, J.M., and Ramirez, M.T. (2006). The metabotropic glutamate receptor 4 is internalized and desensitized upon protein kinase C activation. *Br. J. Pharmacol.* 148, 279-290.
- Matosin, N., Fernandez-Enright, F., Fung, S.J., Lum, J.S., Engel, M., Andrews, J.L., Huang, X.F., Weickert, C.S., and Newell, K.A. (2015a). Alterations of mGluR5 and its endogenous regulators Norbin, Tamalin and Presol in schizophrenia: towards a model of mGluR5 dysregulation. *Acta Neuropathol.* 130, 119-129.
- Matosin, N., Fernandez-Enright, F., Lum, J.S., Andrews, J.L., Engel, M., Huang, X.F., and Newell, K.A. (2015b). Metabotropic glutamate receptor 5, and its trafficking molecules Norbin and Tamalin, are increased in the CA1 hippocampal region of subjects with schizophrenia. *Schizophr. Res.* 166, 212-218.
- Mikhaylova, M., Bera, S., Kobler, O., Frischknecht, R., and Kreutz, M.R. (2016). A dendritic Golgi satellite between ERGIC and retromer. *Cell Rep.* 14, 189-199.
- Millan, C., Lujan, R., Shigemoto, R., and Sanchez-Prieto, J. (2002). The inhibition of glutamate release by metabotropic glutamate receptor 7 affects both $[Ca^{2+}]_c$ and cAMP: evidence for a strong reduction of Ca^{2+} entry in single nerve terminals. *J. Biol. Chem.* 277, 14092-14101.
- Minakami, R., Jinnai, N., and Sugiyama, H. (1997). Phosphorylation and calmodulin binding of the metabotropic glutamate receptor subtype 5 (mGluR5) are antagonistic *in vitro*. *J. Biol. Chem.* 272, 20291-20298.
- Mody, N., Hermans, E., Nahorski, S.R., and Challiss, R.A. (1999). Inhibition of N-linked glycosylation of the human type I alpha metabotropic glutamate receptor by tunicamycin: effects on cell-surface receptor expression and function. *Neuropharmacology* 38, 1485-1492.
- Moller, T.C., Hotin, J., Clerie, C., Zwier, J.M., Durroux, T., Rondard, P., Prezeau, L., Royer, C.A., Pin, J.P., Margeat, E., and Kniazeff, J. (2018). Oligomerization of a G protein-coupled receptor in neurons controlled by its structural dynamics. *Sci. Rep.* 8, 10414.
- Moreno Delgado, D., Moller, T.C., Ster, J., Giraldo, J., Maurel, D., Rovira, X., Scholler, P., Zwier, J.M., Perroy, J., Durroux, T., Trinquet, E., Prezeau, L., Rondard, P., and Pin, J.P. (2017). Pharmacological evidence for a metabotropic glutamate receptor heterodimer in neuronal cells. *Elife* 6.
- Moriyoshi, K., Iijima, K., Fujii, H., Ito, H., Cho, Y., and Nakanishi, S. (2004). Seven in absentia homolog 1A mediates ubiquitination and degradation of group I metabotropic glutamate receptors. *Proc. Natl. Acad. Sci. U. S. A.* 101, 8614-8619.
- Moutin, E., Raynaud, F., Roger, J., Pellegrino, E., Homburger, V., Bertaso, F., Ollendorff, V., Bockaert, J., Fagni, L., and Perroy, J. (2012). Dynamic remodeling of scaffold interactions in dendritic spines controls synaptic excitability. *J. Cell Biol.* 198, 251-263.
- Mundell, S.J., Matharu, A.L., Pula, G., Holman, D., Roberts, P.J., and Kelly, E. (2002). Metabotropic glutamate receptor 1 internalization induced by muscarinic acetylcholine receptor activation: differential dependency of internalization of splice variants on nonvisual arrestins. *Mol. Pharmacol.* 61, 1114-1123.
- Mundell, S.J., Matharu, A.L., Pula, G., Roberts, P.J., and Kelly, E. (2001). Agonist-induced internalization of the metabotropic glutamate receptor 1a is arrestin- and dynamin- dependent. *J. Neurochem.* 78, 546-551.
- Muto, T., Tsuchiya, D., Morikawa, K., and Jingami, H. (2009). Site-specific unglycosylation to improve crystallization of the metabotropic glutamate receptor 3 extracellular domain. *Acta Crystallogr Sect F Struct Biol Cryst Commun* 65, 236-241.
- Naisbitt, S., Kim, E., Tu, J., Xiao, B., Sala, C., Valtschanoff, J., Weinberg, R., Worley, P., and Sheng, M. (1999). Shank, a novel family of postsynaptic density proteins that binds to the NMDA receptor/PSD-95/GKAP complex and cortactin. *Neuron* 23, 569-582.
- Nasrallah, C., Rottier, K., Marcellin, R., Compan, V., Font, J., Llebaria, A., Pin, J.P., Baneres, J.L., and Lebon, G. (2018). Direct coupling of detergent purified human mGlu5 receptor to the heterotrimeric G proteins Gq and Gs. *Sci. Rep.* 8, 4407.
- Neki, A., Ohishi, H., Kaneko, T., Shigemoto, R., Nakanishi, S., and Mizuno, N. (1996a). Metabotropic glutamate receptors mGluR2 and mGluR5 are expressed in two non-overlapping populations of Golgi cells in the rat cerebellum. *Neuroscience* 75, 815-826.
- Neki, A., Ohishi, H., Kaneko, T., Shigemoto, R., Nakanishi, S., and Mizuno, N. (1996b). Pre- and postsynaptic localization of a metabotropic glutamate receptor, mGluR2, in the rat brain: an immunohistochemical study with a monoclonal antibody. *Neurosci. Lett.* 202, 197-200.
- Neyman, S., Braunewell, K.H., O'Connell, K.E., Dev, K.K., and Manahan-Vaughan, D. (2019). Inhibition of the interaction between group I metabotropic glutamate receptors and PDZ-domain proteins prevents hippocampal long-term depression, but not long-term potentiation. *Front. Synaptic Neurosci.* 11, 13.

- Neyman, S., and Manahan-Vaughan, D. (2008). Metabotropic glutamate receptor 1 (mGluR1) and 5 (mGluR5) regulate late phases of LTP and LTD in the hippocampal CA1 region *in vitro*. *Eur. J. Neurosci.* 27, 1345-1352.
- Nicholls, R.E., Zhang, X.L., Bailey, C.P., Conklin, B.R., Kandel, E.R., and Stanton, P.K. (2006). mGluR2 acts through inhibitory Galpha subunits to regulate transmission and long-term plasticity at hippocampal mossy fiber-CA3 synapses. *Proc. Natl. Acad. Sci. U. S. A.* 103, 6380-6385.
- Niswender, C.M., and Conn, P.J. (2010). Metabotropic glutamate receptors: physiology, pharmacology, and disease. *Annu. Rev. Pharmacol. Toxicol.* 50, 295-322.
- Nomura, A., Shigemoto, R., Nakamura, Y., Okamoto, N., Mizuno, N., and Nakanishi, S. (1994). Developmentally regulated postsynaptic localization of a metabotropic glutamate receptor in rat rod bipolar cells. *Cell* 77, 361-369.
- Nusser, Z., Mulvihill, E., Streit, P., and Somogyi, P. (1994). Subsynaptic segregation of metabotropic and ionotropic glutamate receptors as revealed by immunogold localization. *Neuroscience* 61, 421-427.
- O'Connor, J.J., Rowan, M.J., and Anwyl, R. (1994). Long-lasting enhancement of NMDA receptor-mediated synaptic transmission by metabotropic glutamate receptor activation. *Nature* 367, 557-559.
- O'Connor, V., El Far, O., Bofill-Cardona, E., Nanoff, C., Freissmuth, M., Karschin, A., Airas, J.M., Betz, H., and Boehm, S. (1999). Calmodulin dependence of presynaptic metabotropic glutamate receptor signaling. *Science* 286, 1180-1184.
- O'Malley, K.L., Jong, Y.J., Gonchar, Y., Burkhalter, A., and Romano, C. (2003). Activation of metabotropic glutamate receptor mGlu5 on nuclear membranes mediates intranuclear Ca²⁺ changes in heterologous cell types and neurons. *J. Biol. Chem.* 278, 28210-28219.
- O'Neill, N., McLaughlin, C., Komiya, N., and Sylantsev, S. (2018). Biphasic modulation of NMDA receptor function by metabotropic glutamate receptors. *J. Neurosci.* 38, 9840-9855.
- Ohishi, H., Akazawa, C., Shigemoto, R., Nakanishi, S., and Mizuno, N. (1995). Distributions of the mRNAs for L-2-amino-4-phosphonobutyrate-sensitive metabotropic glutamate receptors, mGluR4 and mGluR7, in the rat brain. *J. Comp. Neurol.* 360, 555-570.
- Ohishi, H., Ogawa-Meguro, R., Shigemoto, R., Kaneko, T., Nakanishi, S., and Mizuno, N. (1994). Immunohistochemical localization of metabotropic glutamate receptors, mGluR2 and mGluR3, in rat cerebellar cortex. *Neuron* 13, 55-66.
- Ohishi, H., Shigemoto, R., Nakanishi, S., and Mizuno, N. (1993a). Distribution of the messenger RNA for a metabotropic glutamate receptor, mGluR2, in the central nervous system of the rat. *Neuroscience* 53, 1009-1018.
- Ohishi, H., Shigemoto, R., Nakanishi, S., and Mizuno, N. (1993b). Distribution of the mRNA for a metabotropic glutamate receptor (mGluR3) in the rat brain: an *in situ* hybridization study. *J. Comp. Neurol.* 335, 252-266.
- Oliet, S.H., Malenka, R.C., and Nicoll, R.A. (1997). Two distinct forms of long-term depression coexist in CA1 hippocampal pyramidal cells. *Neuron* 18, 969-982.
- Pandey, S., Mahato, P.K., and Bhattacharyya, S. (2014). Metabotropic glutamate receptor 1 recycles to the cell surface in protein phosphatase 2A-dependent manner in non-neuronal and neuronal cell lines. *J. Neurochem.* 131, 602-614.
- Pandey, S., Ramsakha, N., Sharma, R., Gulia, R., Ojha, P., Lu, W., and Bhattacharyya, S. (2020). The postsynaptic scaffolding protein tamalin regulates ligand-mediated trafficking of metabotropic glutamate receptors. *J. Biol. Chem.* 295, 8575-8588.
- Pandya, N.J., Klaassen, R.V., van der Schors, R.C., Slotman, J.A., Houtsmuller, A., Smit, A.B., and Li, K.W. (2016). Group 1 metabotropic glutamate receptors 1 and 5 form a protein complex in mouse hippocampus and cortex. *Proteomics* 16, 2698-2705.
- Park, D.H., Park, S., Song, J.M., Kang, M., Lee, S., Horak, M., and Suh, Y.H. (2020). N-linked glycosylation of the mGlu7 receptor regulates the forward trafficking and transsynaptic interaction with Elnf1. *FASEB J* 34 (11), 14977-14996.
- Park, M., Salgado, J.M., Ostroff, L., Helton, T.D., Robinson, C.G., Harris, K.M., and Ehlers, M. D. (2006). Plasticity-induced growth of dendritic spines by exocytic trafficking from recycling endosomes. *Neuron* 52, 817-830.
- Park, S., Park, J.M., Kim, S., Kim, J.A., Shepherd, J.D., Smith-Hicks, C.L., Chowdhury, S., Kaufmann, W., Kuhl, D., Ryazanov, A.G., Haganir, R.L., Linden, D.J., and Worley, P.F. (2008). Elongation factor 2 and fragile X mental retardation protein control the dynamic translation of Arc/Arg3.1 essential for mGluR-LTD. *Neuron* 59, 70-83.
- Pelkey, K.A., Lavezzi, G., Racca, C., Roche, K.W., and McBain, C.J. (2005). mGluR7 is a metaplastic switch controlling bidirectional plasticity of feedforward inhibition. *Neuron* 46, 89-102.
- Pelkey, K.A., Topolnik, L., Lacaille, J.C., and McBain, C.J. (2006). Compartmentalized Ca(2+) channel regulation at divergent mossy-fiber release sites underlies target cell-dependent plasticity. *Neuron* 52, 497-510.
- Pelkey, K.A., Topolnik, L., Yuan, X.Q., Lacaille, J.C., and McBain, C.J. (2008). State-dependent cAMP sensitivity of

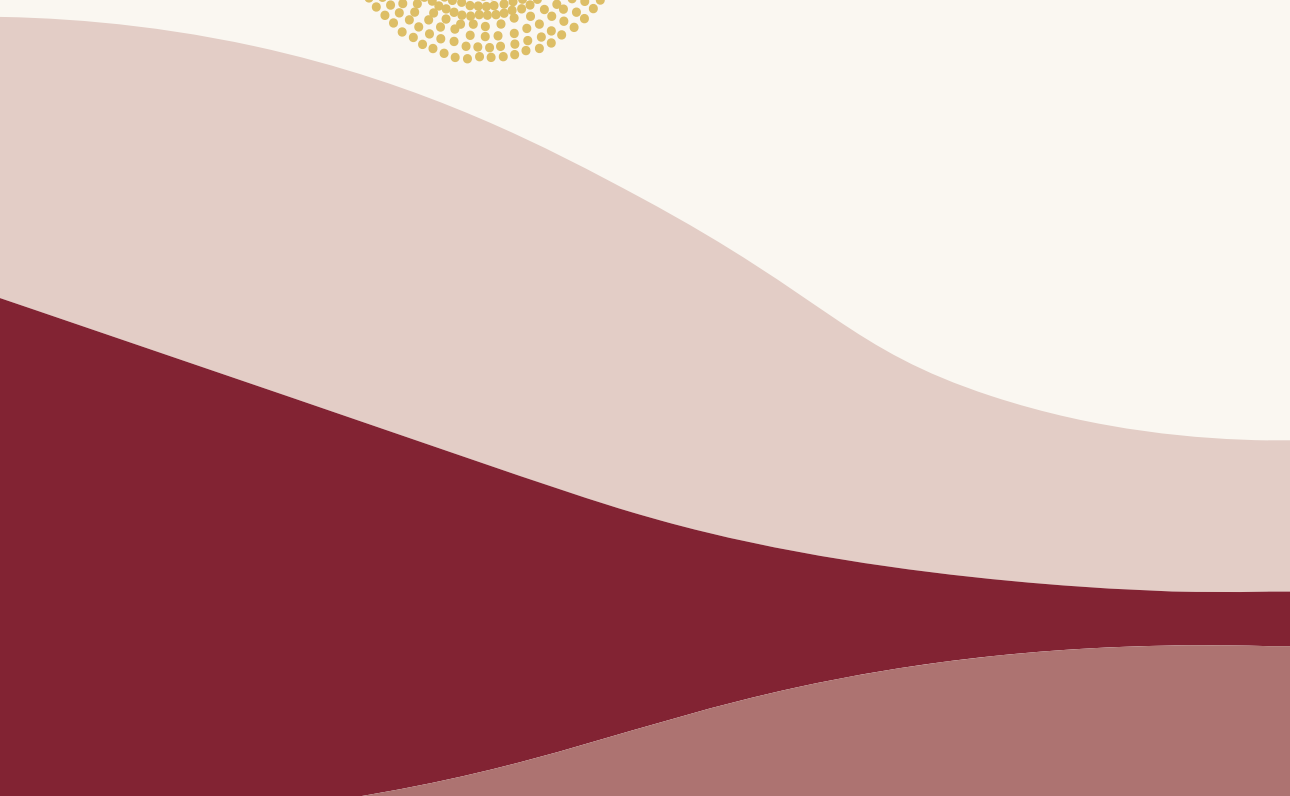
- presynaptic function underlies metaplasticity in a hippocampal feedforward inhibitory circuit. *Neuron* 60, 980-987.
- Pelkey, K.A., Yuan, X., Lavezari, G., Roche, K.W., and McBain, C.J. (2007). mGluR7 undergoes rapid internalization in response to activation by the allosteric agonist AMN082. *Neuropharmacology* 52, 108-117.
- Perroy, J., El Far, O., Bertaso, F., Pin, J.P., Betz, H., Bockaert, J., and Fagni, L. (2002). PICK1 is required for the control of synaptic transmission by the metabotropic glutamate receptor 7. *EMBO J.* 21, 2990-2999.
- Perroy, J., Prezeau, L., De Waard, M., Shigemoto, R., Bockaert, J., and Fagni, L. (2000). Selective blockade of P/Q-type calcium channels by the metabotropic glutamate receptor type 7 involves a phospholipase C pathway in neurons. *J. Neurosci.* 20, 7896-7904.
- Perroy, J., Raynaud, F., Homburger, V., Rousset, M.C., Telley, L., Bockaert, J., and Fagni, L. (2008). Direct interaction enables cross-talk between ionotropic and group I metabotropic glutamate receptors. *J. Biol. Chem.* 283, 6799-6805.
- Petaja-Repo, U.E., Hogue, M., Laperriere, A., Walker, P., and Bouvier, M. (2000). Export from the endoplasmic reticulum represents the limiting step in the maturation and cell surface expression of the human delta opioid receptor. *J. Biol. Chem.* 275, 13727-13736.
- Petralia, R.S., Wang, Y.X., Niedzielski, A.S., and Wenthold, R.J. (1996). The metabotropic glutamate receptors, mGluR2 and mGluR3, show unique postsynaptic, presynaptic and glial localizations. *Neuroscience* 71, 949-976.
- Petrini, E.M., Lu, J., Cognet, L., Lounis, B., Ehlers, M.D., and Choquet, D. (2009). Endocytic trafficking and recycling maintain a pool of mobile surface AMPA receptors required for synaptic potentiation. *Neuron* 63, 92-105.
- Pierce, J.P., Mayer, T., and McCarthy, J.B. (2001). Evidence for a satellite secretory pathway in neuronal dendritic spines. *Curr. Biol.* 11, 351-355.
- Pin, J.P., and Bettler, B. (2016). Organization and functions of mGlu and GABAB receptor complexes. *Nature* 540, 60-68.
- Pinheiro, P.S., and Mulle, C. (2008). Presynaptic glutamate receptors: physiological functions and mechanisms of action. *Nat. Rev. Neurosci.* 9, 423-436.
- Pittaluga, A. (2016). Presynaptic release-regulating mGlu1 receptors in central nervous system. *Front. Pharmacol.* 7, 295.
- Price, C.J., Karayannis, T., Pal, B.Z., and Capogna, M. (2005). Group II and III mGluRs-mediated presynaptic inhibition of EPSCs recorded from hippocampal interneurons of CA1 stratum lacunosum moleculare. *Neuropharmacology* 49 (Suppl. 1), 45-56.
- Raka, F., Di Sebastiano, A.R., Kulhawy, S.C., Ribeiro, F.M., Godin, C.M., Caetano, F.A., Angers, S., and Ferguson, S.S. (2015). Ca(2+)/calmodulin-dependent protein kinase II interacts with group I metabotropic glutamate and facilitates receptor endocytosis and ERK1/2 signaling: role of beta-amyloid. *Mol. Brain* 8, 21.
- Ramos, C., Chardonnet, S., Marchand, C.H., Decottignies, P., Ango, F., Daniel, H., and Le Marechal, P. (2012). Native presynaptic metabotropic glutamate receptor 4 (mGluR4) interacts with exocytosis proteins in rat cerebellum. *J. Biol. Chem.* 287, 20176-20186.
- Ray, K., and Hauschild, B.C. (2000). Cys-140 is critical for metabotropic glutamate receptor-1 dimerization. *J. Biol. Chem.* 275, 34245-34251.
- Raynaud, F., Homburger, V., Seveno, M., Vigy, O., Moutin, E., Fagni, L., and Perroy, J. (2018). SNAP23-Kif5 complex controls mGlu1 receptor trafficking. *J. Mol. Cell Biol.* 10, 423-436.
- Reiner, A., and Levitz, J. (2018). Glutamatergic signaling in the central nervous system: ionotropic and metabotropic receptors in concert. *Neuron* 98, 1080-1098.
- Remelli, R., Robbins, M.J., and McIlhinney, R.A. (2008). The C-terminus of the metabotropic glutamate receptor 1b regulates dimerization of the receptor. *J. Neurochem.* 104, 1020-1031.
- Renner, M., Lacor, P.N., Velasco, P.T., Xu, J., Contractor, A., Klein, W.L., and Triller, A. (2010). Deleterious effects of amyloid beta oligomers acting as an extracellular scaffold for mGluR5. *Neuron* 66, 739-754.
- Ritter-Makinson, S.L., Paquet, M., Bogenpohl, J.W., Rodin, R.E., Chris Yun, C., Weinman, E.J., Smith, Y., and Hall, R.A. (2017). Group II metabotropic glutamate receptor interactions with NHERF scaffold proteins: implications for receptor localization in brain. *Neuroscience* 353, 58-75.
- Robbins, M.J., Ciruela, F., Rhodes, A., and McIlhinney, R.A. (1999). Characterization of the dimerization of metabotropic glutamate receptors using an N-terminal truncation of mGluR1alpha. *J. Neurochem.* 72, 2539-2547.
- Roche, K.W., Tu, J.C., Petralia, R.S., Xiao, B., Wenthold, R.J., and Worley, P.F. (1999). Homer 1b regulates the trafficking of group I metabotropic glutamate receptors. *J. Biol. Chem.* 274, 25953-25957.
- Rodriguez-Moreno, A., Sistiaga, A., Lerma, J., and Sanchez-Prieto, J. (1998). Switch from facilitation to inhibition of excitatory synaptic transmission by group I mGluR desensitization. *Neuron* 21, 1477-1486.
- Romano, C., Miller, J.K., Hyrc, K., Dikranian, S., Mennerick, S., Takeuchi, Y., Goldberg, M.P., and O'Malley, K.L. (2001). Covalent and noncovalent interactions mediate metabotropic glutamate receptor mGlu5 dimerization. *Mol. Pharmacol.* 59, 46-53.

- Romano, C., Sesma, M.A., McDonald, C.T., O'Malley, K., Van den Pol, A.N., and Olney, J.W. (1995). Distribution of metabotropic glutamate receptor mGluR5 immunoreactivity in rat brain. *J. Comp. Neurol.* 355, 455-469.
- Romano, C., Yang, W.L., and O'Malley, K.L. (1996). Metabotropic glutamate receptor 5 is a disulfide-linked dimer. *J. Biol. Chem.* 271, 28612-28616.
- Ronesi, J.A., and Huber, K.M. (2008). Homer interactions are necessary for metabotropic glutamate receptor-induced long-term depression and translational activation. *J. Neurosci.* 28, 543-547.
- Rong, R., Ahn, J.Y., Huang, H., Nagata, E., Kalman, D., Kapp, J.A., Tu, J., Worley, P.F., Snyder, S.H., and Ye, K. (2003). PI3 kinase enhancer-Homer complex couples mGluRI to PI3 kinase, preventing neuronal apoptosis. *Nat. Neurosci.* 6, 1153-1161.
- Rosenberg, N., Gerber, U., and Ster, J. (2016). Activation of group II metabotropic glutamate receptors promotes LTP induction at schaffer collateral-CA1 pyramidal cell synapses by priming NMDA receptors. *J. Neurosci.* 36, 11521-11531.
- Rosendale, M., Julli, D., Choquet, D., and Perrais, D. (2017). Spatial and temporal regulation of receptor endocytosis in neuronal dendrites revealed by imaging of single vesicle formation. *Cell Rep.* 18, 1840-1847.
- Sallese, M., Salvatore, L., D'Urbano, E., Sala, G., Storto, M., Launey, T., Nicoletti, F., Knopfel, T., and De Blasi, A. (2000). The G-protein-coupled receptor kinase GRK4 mediates homologous desensitization of metabotropic glutamate receptor 1. *FASEB J.* 14, 2569-2580.
- Saugstad, J.A., Marino, M.J., Folk, J.A., Hepler, J.R., and Conn, P.J. (1998). RGS4 inhibits signaling by group I metabotropic glutamate receptors. *J. Neurosci.* 18, 905-913.
- Scanziani, M., Salin, P.A., Vogt, K.E., Malenka, R.C., and Nicoll, R.A. (1997). Use-dependent increases in glutamate concentration activate presynaptic metabotropic glutamate receptors. *Nature* 385, 630-634.
- Scheefhals, N., Catsburg, L.A.E., Westerveld, M.L., Blanpied, T.A., Hoogenraad, C.C., and MacGillavry, H.D. (2019). Shank proteins couple the endocytic zone to the postsynaptic density to control trafficking and signaling of metabotropic glutamate receptor 5. *Cell Rep.* 29, 258-269 e258.
- Scheefhals, N., and MacGillavry, H.D. (2018). Functional organization of postsynaptic glutamate receptors. *Mol. Cell. Neurosci.* 91, 82-94.
- Schmitz, S.K., King, C., Kortleven, C., Huson, V., Kroon, T., Kevenaar, J.T., Schut, D., Saarloos, I., Hoetjes, J.P., de Wit, H., Stiedl, O., Spijker, S., Li, K.W., Mansvelde, H. D., Smit, A.B., Cornelisse, L.N., Verhage, M., and Toonen, R.F. (2016). Presynaptic inhibition upon CB1 or mGlu2/3 receptor activation requires ERK/MAPK phosphorylation of Munc18-1. *EMBO J.* 35, 1236-1250.
- Schoepp, D.D., Jane, D.E., and Monn, J.A. (1999). Pharmacological agents acting at subtypes of metabotropic glutamate receptors. *Neuropharmacology* 38, 1431-1476.
- Sebastianutto, I., Goyet, E., Andreoli, L., Font-Ingles, J., Moreno-Delgado, D., Bouquier, N., Jahannault-Talignani, C., Moutin, E., Di Menna, L., Maslava, N., Pin, J. P., Fagni, L., Nicoletti, F., Ango, F., Cenci, M.A., and Perroy, J. (2020). D1-mGlu5 heteromers mediate noncanonical dopamine signaling in Parkinson's disease. *J. Clin. Invest.* 130, 1168-1184.
- Sergé, A., Fourgeaud, L., Hemar, A., and Choquet, D. (2002). Receptor activation and homer differentially control the lateral mobility of metabotropic glutamate receptor 5 in the neuronal membrane. *J. Neurosci.* 22, 3910-3920.
- Shigemoto, R., Kinoshita, A., Wada, E., Nomura, S., Ohishi, H., Takada, M., Flor, P.J., Neki, A., Abe, T., Nakanishi, S., and Mizuno, N. (1997). Differential presynaptic localization of metabotropic glutamate receptor subtypes in the rat hippocampus. *J. Neurosci.* 17, 7503-7522.
- Shigemoto, R., Kulik, A., Roberts, J.D., Ohishi, H., Nusser, Z., Kaneko, T., and Somogyi, P. (1996). Target-cell-specific concentration of a metabotropic glutamate receptor in the presynaptic active zone. *Nature* 381, 523-525.
- Shigemoto, R., Nomura, S., Ohishi, H., Sugihara, H., Nakanishi, S., and Mizuno, N. (1993). Immunohistochemical localization of a metabotropic glutamate receptor, mGluR5, in the rat brain. *Neurosci. Lett.* 163, 53-57.
- Siddig, S., Aufmkolk, S., Doose, S., Jobin, M.L., Werner, C., Sauer, M., and Calebiro, D. (2020). Super-resolution imaging reveals the nanoscale organization of metabotropic glutamate receptors at presynaptic active zones. *Sci Adv* 6, eaay7193.
- Sinnen, B.L., Bowen, A.B., Forte, J.S., Hiester, B.G., Crosby, K.C., Gibson, E.S., Dell'Acqua, M.L., and Kennedy, M.J. (2017). Optogenetic control of synaptic composition and function. *Neuron* 93, 646-660 e645.
- Snyder, E.M., Philpot, B.D., Huber, K.M., Dong, X., Fallon, J.R., and Bear, M.F. (2001). Internalization of ionotropic glutamate receptors in response to mGluR activation. *Nat. Neurosci.* 4, 1079-1085.
- Somogyi, P., Dalezios, Y., Lujan, R., Roberts, J.D., Watanabe, M., and Shigemoto, R. (2003). High level of mGluR7 in the presynaptic active zones of select populations of GABAergic terminals innervating interneurons in the rat hippocampus. *Eur. J. Neurosci.* 17, 2503-2520.
- Song, J.M., Kang, M., Park, D.H., Park, S., Lee, S., and Suh, Y.H. (2021). Pathogenic GRM7 mutations associated with neurodevelopmental disorders impair axon outgrowth and presynaptic terminal development. *J. Neurosci.*

- 41, 2344-2359.
- Sorensen, S.D., and Conn, P.J. (2003). G protein-coupled receptor kinases regulate metabotropic glutamate receptor 5 function and expression. *Neuropharmacology* 44, 699-706.
- Spacek, J., and Harris, K.M. (1997). Three-dimensional organization of smooth endoplasmic reticulum in hippocampal CA1 dendrites and dendritic spines of the immature and mature rat. *J. Neurosci.* 17, 190-203.
- Stachniak, T.J., Sylwestrak, E.L., Scheiffle, P., Hall, B.J., and Ghosh, A. (2019). Elnf1-Induced constitutive activation of mGluR7 determines frequency-dependent recruitment of somatostatin interneurons. *J. Neurosci.* 39, 4461-4474.
- Ster, J., Mateos, J.M., Grewe, B.F., Coiret, G., Corti, C., Corsi, M., Helmchen, F., and Gerber, U. (2011). Enhancement of CA3 hippocampal network activity by activation of group II metabotropic glutamate receptors. *Proc. Natl. Acad. Sci. U. S. A.* 108, 9993-9997.
- Stoppel, L.J., Auerbach, B.D., Senter, R.K., Preza, A.R., Lefkowitz, R.J., and Bear, M.F. (2017). beta-Arrestin2 couples metabotropic glutamate receptor 5 to neuronal protein synthesis and is a potential target to treat fragile X. *Cell Rep.* 18, 2807-2814.
- Stowell, J.N., and Craig, A.M. (1999). Axon/dendrite targeting of metabotropic glutamate receptors by their cytoplasmic carboxy-terminal domains. *Neuron* 22, 525-536.
- Sugi, T., Oyama, T., Muto, T., Nakanishi, S., Morikawa, K., and Jingami, H. (2007). Crystal structures of autoinhibitory PDZ domain of Tamalin: implications for metabotropic glutamate receptor trafficking regulation. *EMBO J.* 26, 2192-2205.
- Suh, Y.H., Chang, K., and Roche, K.W. (2018). Metabotropic glutamate receptor trafficking. *Mol. Cell. Neurosci.* 91, 10-24.
- Suh, Y.H., Park, J.Y., Park, S., Jou, I., Roche, P.A., and Roche, K.W. (2013). Regulation of metabotropic glutamate receptor 7 (mGluR7) internalization and surface expression by Ser/Thr protein phosphatase 1. *J. Biol. Chem.* 288, 17544-17551.
- Suh, Y.H., Pelkey, K.A., Lavezzari, G., Roche, P.A., Huganir, R.L., McBain, C.J., and Roche, K. W. (2008). Corequirement of PICK1 binding and PKC phosphorylation for stable surface expression of the metabotropic glutamate receptor mGluR7. *Neuron* 58, 736-748.
- Summa, M., Di Prisco, S., Grilli, M., Usai, C., Marchi, M., and Pittaluga, A. (2013). Presynaptic mGlu7 receptors control GABA release in mouse hippocampus. *Neuropharmacology* 66, 215-224.
- Sylantsev, S., Savtchenko, L.P., Ermolyuk, Y., Michaluk, P., and Rusakov, D.A. (2013). Spike-driven glutamate electrodiffusion triggers synaptic potentiation via a homer-dependent mGluR-NMDAR link. *Neuron* 77, 528-541.
- Sylwestrak, E.L., and Ghosh, A. (2012). Elnf1 regulates target-specific release probability at CA1-interneuron synapses. *Science* 338, 536-540.
- Szumliński, K.K., Kalivas, P.W., and Worley, P.F. (2006). Homer proteins: implications for neuropsychiatric disorders. *Curr. Opin. Neurobiol.* 16, 251-257.
- Tadokoro, S., Tachibana, T., Imanaka, T., Nishida, W., and Sobue, K. (1999). Involvement of unique leucine-zipper motif of PSD-Zip45 (Homer 1c/vesl-1L) in group 1 metabotropic glutamate receptor clustering. *Proc. Natl. Acad. Sci. U. S. A.* 96, 13801-13806.
- Tamaru, Y., Nomura, S., Mizuno, N., and Shigemoto, R. (2001). Distribution of metabotropic glutamate receptor mGluR3 in the mouse CNS: differential location relative to pre- and postsynaptic sites. *Neuroscience* 106, 481-503.
- Tanabe, Y., Masu, M., Ishii, T., Shigemoto, R., and Nakanishi, S. (1992). A family of metabotropic glutamate receptors. *Neuron* 8, 169-179.
- Tang, Z., El Far, O., Betz, H., and Scheschonka, A. (2005). Pias1 interaction and sumoylation of metabotropic glutamate receptor 8. *J. Biol. Chem.* 280, 38153-38159.
- Techlovská, S., Chambers, J.N., Dvorakova, M., Petralia, R.S., Wang, Y.X., Hajkova, A., Nova, A., Frankova, D., Prezeau, L., and Blahos, J. (2014). Metabotropic glutamate receptor 1 splice variants mGluR1a and mGluR1b combine in mGluR1a/b dimers *in vivo*. *Neuropharmacology* 86, 329-336.
- Thibado, J.K., Tano, J.Y., Lee, J., Salas-Estrada, L., Provasi, D., Strauss, A., Marcelo Lamim Ribeiro, J., Xiang, G., Broichhagen, J., Filizola, M., Lohse, M.J., and Levitz, J. (2021). Differences in interactions between transmembrane domains tune the activation of metabotropic glutamate receptors. *Elife* 10.
- Tigaret, C.M., Olivo, V., Sadowski, J.H., Ashby, M.C., and Mellor, J.R. (2016). Coordinated activation of distinct Ca(2+) sources and metabotropic glutamate receptors encodes Hebbian synaptic plasticity. *Nat. Commun.* 7, 10289.
- Tomioka, N.H., Yasuda, H., Miyamoto, H., Hatayama, M., Morimura, N., Matsumoto, Y., Suzuki, T., Odagawa, M., Odaka, Y.S., Iwayama, Y., Won Um, J., Ko, J., Inoue, Y., Kaneko, S., Hirose, S., Yamada, K., Yoshikawa, T., Yamakawa, K., and Aruga, J. (2014). Elnf1 recruits presynaptic mGluR7 in trans and its loss results in seizures. *Nat. Commun.* 5, 4501.

- Trivedi, R.R., and Bhattacharyya, S. (2012). Constitutive internalization and recycling of metabotropic glutamate receptor 5 (mGluR5). *Biochem. Biophys. Res. Commun.* 427, 185-190.
- Tsuji, Y., Shimada, Y., Takeshita, T., Kajimura, N., Nomura, S., Sekiyama, N., Otomo, J., Usukura, J., Nakanishi, S., and Jingami, H. (2000). Cryptic dimer interface and domain organization of the extracellular region of metabotropic glutamate receptor subtype 1. *J. Biol. Chem.* 275, 28144-28151.
- Tu, J.C., Xiao, B., Naisbitt, S., Yuan, J.P., Petralia, R.S., Brakeman, P., Doan, A., Aakalu, V.K., Lanahan, A.A., Sheng, M., and Worley, P.F. (1999). Coupling of mGluR/ Homer and PSD-95 complexes by the Shank family of postsynaptic density proteins. *Neuron* 23, 583-592.
- Tu, J.C., Xiao, B., Yuan, J.P., Lanahan, A.A., Leoffert, K., Li, M., Linden, D.J., and Worley, P. F. (1998). Homer binds a novel proline-rich motif and links group 1 metabotropic glutamate receptors with IP3 receptors. *Neuron* 21, 717-726.
- Tzounopoulos, T., Janz, R., Sudhof, T.C., Nicoll, R.A., and Malenka, R.C. (1998). A role for cAMP in long-term depression at hippocampal mossy fiber synapses. *Neuron* 21, 837-845.
- Vilardaga, J.P., Bunemann, M., Krasel, C., Castro, M., and Lohse, M.J. (2003). Measurement of the millisecond activation switch of G protein-coupled receptors in living cells. *Nat. Biotechnol.* 21, 807-812.
- Wang, H., Westin, L., Nong, Y., Birnbaum, S., Bendor, J., Brismar, H., Nestler, E., Aperia, A., Flajolet, M., and Greengard, P. (2009). Norbin is an endogenous regulator of metabotropic glutamate receptor 5 signaling. *Science* 326, 1554-1557.
- Wang, M.J., Li, Y.C., Snyder, M.A., Wang, H., Li, F., and Gao, W.J. (2013). Group II metabotropic glutamate receptor agonist LY379268 regulates AMPA receptor trafficking in prefrontal cortical neurons. *PloS One* 8, e61787.
- Wang, X.F., Daw, N.W., and Jin, X. (1998). The effect of ACPD on the responses to NMDA and AMPA varies with layer in slices of rat visual cortex. *Brain Res.* 812, 186-192.
- Waung, M.W., Pfeiffer, B.E., Nosyreva, E.D., Ronesi, J.A., and Huber, K.M. (2008). Rapid translation of Arc/Arg3.1 selectively mediates mGluR-dependent LTD through persistent increases in AMPAR endocytosis rate. *Neuron* 59, 84-97.
- Werthmann, R.C., Tzouros, M., Lamerz, J., Augustin, A., Fritzius, T., Trovo, L., Stawarski, M., Raveh, A., Diener, C., Fischer, C., Gassmann, M., Lindemann, L., and Bettler, B. (2020). Symmetric signal transduction and negative allosteric modulation of heterodimeric mGlu1/5 receptors. *Neuropharmacology*, 108426.
- Westin, L., Reuss, M., Lindskog, M., Aperia, A., and Brismar, H. (2014). Nanoscopic spine localization of Norbin, an mGluR5 accessory protein. *BMC Neurosci.* 15, 45.
- Willems, J., de Jong, A.P.H., Scheefhals, N., Mertens, E., Catsburg, L.A.E., Poorthuis, R. B., de Winter, F., Verhaagen, J., Meye, F.J., and MacGillavry, H.D. (2020). ORANGE: a CRISPR/Cas9-based genome editing toolbox for epitope tagging of endogenous proteins in neurons. *PLoS Biol.* 18, e3000665.
- Wostrack, M., and Dietrich, D. (2009). Involvement of Group II mGluRs in mossy fiber LTD. *Synapse* 63, 1060-1068.
- Xiang, Z., Lv, X., Lin, X., O'Brien, D.E., Altman, M.K., Lindsley, C.W., Javitch, J.A., Niswender, C.M., and Conn, P.J. (2021). Input-specific regulation of glutamatergic synaptic transmission in the medial prefrontal cortex by mGlu2/mGlu4 receptor heterodimers. *Sci. Signal.* 14.
- Xiao, B., Tu, J.C., Petralia, R.S., Yuan, J.P., Doan, A., Breder, C.D., Ruggiero, A., Lanahan, A.A., Wenthold, R.J., and Worley, P.F. (1998). Homer regulates the association of group 1 metabotropic glutamate receptors with multivalent complexes of homer-related, synaptic proteins. *Neuron* 21, 707-716.
- Yin, S., Noetzel, M.J., Johnson, K.A., Zamorano, R., Jalan-Sakrikar, N., Gregory, K.J., Conn, P.J., and Niswender, C.M. (2014). Selective actions of novel allosteric modulators reveal functional heteromers of metabotropic glutamate receptors in the CNS. *J. Neurosci.* 34, 79-94.
- Yokoi, M., Kobayashi, K., Manabe, T., Takahashi, T., Sakaguchi, I., Katsura, G., Shigemoto, R., Ohishi, H., Nomura, S., Nakamura, K., Nakao, K., Katsuki, M., and Nakanishi, S. (1996). Impairment of hippocampal mossy fiber LTD in mice lacking mGluR2. *Science* 273, 645-647.
- Yu, S.P., Sensi, S.L., Canzoniero, L.M., Buisson, A., and Choi, D.W. (1997). Membrane-delimited modulation of NMDA currents by metabotropic glutamate receptor subtypes 1/5 in cultured mouse cortical neurons. *J Physiol* 499 (Pt 3), 721-732.
- Yuan, J.P., Kiselyov, K., Shin, D.M., Chen, J., Shcheynikov, N., Kang, S.H., Dehoff, M.H., Schwarz, M.K., Seeburg, P.H., Muallem, S., and Worley, P.F. (2003). Homer binds TRPC family channels and is required for gating of TRPC1 by IP3 receptors. *Cell* 114, 777-789.
- Zhang, C.S., Bertaso, F., Eulenburg, V., Lerner-Natoli, M., Herin, G.A., Bauer, L., Bockaert, J., Fagni, L., Betz, H., and Scheschonka, A. (2008). Knock-in mice lacking the PDZ-ligand motif of mGluR7a show impaired PKC-dependent autoinhibition of glutamate release, spatial working memory deficits, and increased susceptibility to pentylenetetrazol. *J. Neurosci.* 28, 8604-8614.

4



Shank proteins couple the endocytic zone to the postsynaptic density to control trafficking and signaling of metabotropic glutamate receptor 5

Nicky Scheefhals¹, Lisa A.E. Catsburg¹, Margriet L. Westerveld¹, Thomas A. Blanpied², Casper C. Hoogenraad¹, and Harold D. MacGillavry¹

¹Cell Biology, Neurobiology and Biophysics, Department of Biology, Faculty of Science, Utrecht University, Utrecht, the Netherlands

²Department of Physiology, Program in Neuroscience, University of Maryland School of Medicine, Baltimore, MD 21201, USA.

Cell Reports (2019), 29: 258-269

Abstract

Activation of postsynaptic metabotropic glutamate receptors (mGluRs) modulates neuronal excitability and synaptic plasticity, while deregulation of mGluR signaling has been implicated in neurodevelopmental disorders. Importantly, overstimulation of mGluR is restricted by the rapid endocytosis of receptors after activation. However, how membrane trafficking of mGluRs at synapses is controlled remains poorly defined. We find that in hippocampal neurons, agonist-induced receptor internalization of synaptic mGluR5 is significantly reduced in Shank knockdown neurons. Interestingly, this is rescued by re-expression of wild-type Shanks, but not by mutants unable to bind Homer1b/c, Dynamin2 or Cortactin. Strikingly, these effects are paralleled by a reduction in synapses associated with an endocytic zone. Moreover, a mutation in SHANK2 found in ASD similarly disrupts these processes. Based on these findings, we propose that synaptic Shank scaffolds anchor the endocytic machinery to govern efficient trafficking of mGluR5 and to balance the surface expression of mGluRs to efficiently modulate neuronal functioning.

Introduction

At excitatory synapses of hippocampal neurons, the group I metabotropic glutamate receptors (mGluRs) mGluR1 and mGluR5 critically modulate synaptic transmission and plasticity (Scheefhals and MacGillavry, 2018). The contribution of mGluRs to glutamatergic signaling underlies cognitive functions and disrupted mGluR signaling has been implicated in neurological disorders including autism spectrum disorders (ASDs) (Lüscher and Huber, 2010). To prevent overstimulation, activated mGluRs are rapidly desensitized and internalized via clathrin-mediated endocytosis (Dhami and Ferguson, 2006). Despite the importance of controlled receptor trafficking at synapses, we know little about the mechanisms that control the endocytosis and recycling of synaptic mGluRs. Endocytosis of postsynaptic membrane proteins preferentially takes place at endocytic zones (EZs) (Rosendale et al., 2017). EZs are stable clathrin assemblies coupled to the postsynaptic density (PSD) via interactions with Homer1b/c and Dynamin3 (Blanpied et al., 2002; Lu et al., 2007; Racz et al., 2004). Disruption of PSD-EZ coupling reduces the synaptic population of AMPA receptors, and prevents plasticity-induced receptor insertion (Petrini et al., 2009). However, it remains untested whether mGluRs are locally endocytosed through EZs and recycle to the synaptic membrane.

The Shank family (Shank1, 2 and 3) is an integral part of the PSD, interacting with a multitude of synaptic proteins, as well as endocytic proteins, such as Dynamin2, Cortactin, Syndapin I, and Abpl (Kessels et al., 2001; McNiven et al., 2000; Naisbitt et al., 1999; Okamoto et al., 2001; Qualmann et al., 2004). Moreover, abrogated mGluR signaling has been found in Shank mutant models (Bariselli et al., 2016; Kouser et al., 2013; Lee et al., 2019; Verpelli et al., 2011), but how Shank proteins control mGluR function remains unknown. We hypothesized that Shank proteins recruit components of the endocytic machinery to facilitate local regulation of receptor internalization to control mGluR function. We found that agonist-induced internalization of mGluR5 is severely affected in Shank triple knockdown neurons and present evidence that mGluR5 is internalized through the EZ coupled to the PSD by Shank-mediated interactions. We propose that Shank proteins link

the EZ to the PSD to control trafficking of synaptic membrane proteins and to balance the density of receptors at the membrane to modulate neuronal functioning.

Results

Efficient internalization and intracellular sorting of activated mGluR5

To test whether activation of mGluR5 triggers endocytosis in hippocampal neurons, we live-labeled surface-expressed myc-mGluR5, and incubated neurons with the group I specific agonist DHPG. Surface expression of mGluR5 markedly decreased over time, which was best described by a single-exponential decay function with a rate constant of $0.077 \pm 0.03 \text{ min}^{-1}$, reaching a plateau at $42 \pm 7\%$ reduction (Figures 1A and B), consistent with previous reports (Lee et al., 2008). Internalized mGluR5 puncta largely overlapped with the early and recycling endosome markers anti-EEA1, GFP-Rab5, GFP-Rab11, and mRFP-TfR, but much less with the late endosome marker GFP-Rab7, and lysosomal marker GFP-LAMP1 (EEA1: $70 \pm 3\%$, Rab5: $80 \pm 3\%$, Rab11: $76 \pm 3\%$, TfR: 77 ± 4 , Rab7: $38 \pm 3\%$, LAMP1: $31 \pm 5\%$, $P < 0.001$; Figure 1C and D).

To image the surface expressed pool of mGluR5 in live cells, we tagged mGluR5 with an extracellular super-ecliptic pHluorin (SEP) tag (Figure 1E). We confirmed that fluorescence of this GFP variant is quenched at low pH, such as in endocytic vesicles, and only fluoresces at neutral pH (Supplementary Figure 1A). Application of DHPG induced a rapid decrease in SEP-mGluR5 intensity from dendritic spines (DHPG: $39.7 \pm 2.2\%$ at $t = 28$ minutes, vehicle: $14.0 \pm 1.6\%$, $P < 0.001$; Figure 1F and G). Imaging at reduced frame rates revealed no significant difference in observed signal reduction both after vehicle ($15.8 \pm 3.1\%$; Supplementary Figure 1B) and DHPG application ($37.8 \pm 3.5\%$; Supplementary Figure 1C). Thus, the observed reduction of SEP-mGluR5 intensity in unstimulated spines is not due to photobleaching, but likely reflects ongoing receptor internalization, consistent with other studies that estimated $\sim 20\%$ agonist-independent internalization over 30 minutes (Francesconi et al., 2009; Lee et al., 2008). In some, but not all experiments we noted that DHPG or vehicle application induced a transient increase in SEP-mGluR5 fluorescence intensity (f.e. Figure 1G). If observed, it was independent of the experimental conditions, and could potentially be attributed to the opening of the imaging chamber, briefly affecting the pH of the imaging buffer.

The DHPG-induced decrease in SEP-mGluR5 signal in dendrites was not significantly different from the vehicle control (DHPG: $26.0 \pm 4.7\%$, vehicle: $18.1 \pm 2.6\%$; Figure 1H). However these measurements do not directly measure endocytosis, but also reflect ongoing recycling, and lateral exchange of receptors on the membrane. To more directly determine whether mGluR5 can be internalized in dendrites, we tagged mGluR5 with an extracellular Halo-tag to label with AcidiFluor ORANGE, which only fluoresces at low pH (pH 5 - 6) (Isa et al., 2014) (Supplementary Figure 1D). Application of DHPG induced distinct, local increases in Halo-mGluR5 signal intensity, reflecting acidification of Halo-mGluR5 containing endocytic vesicles, both in spines and dendrites (Supplementary Figure 1E, F, G and H).

To test whether dynamin activity is required for agonist-induced mGluR5 internalization in spines, we treated neurons with dynasore, a potent inhibitor of Dynamin GTPase activity (Macia et al., 2006) before addition of DHPG. Dynasore significantly reduced DHPG-

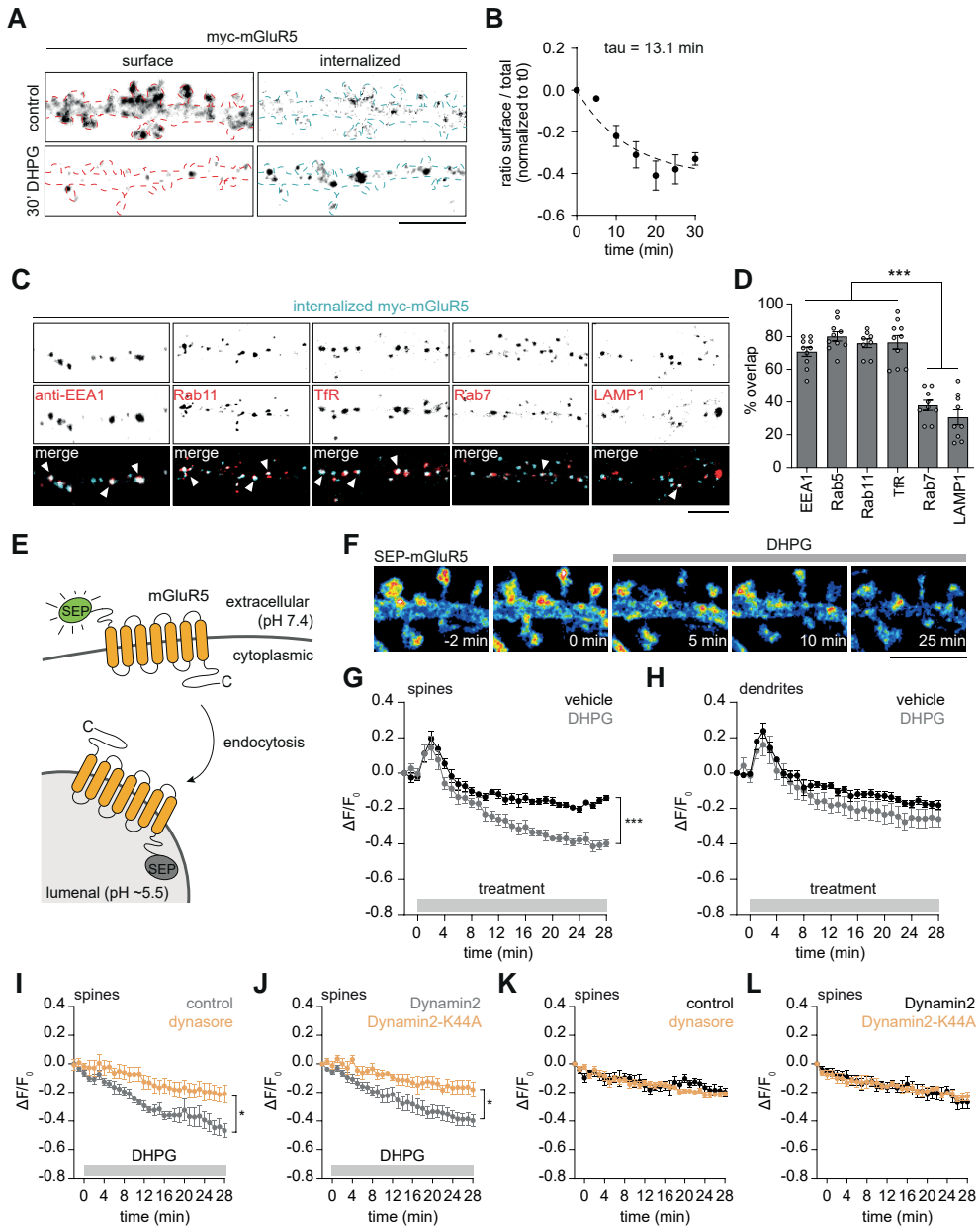


Figure 1. Efficient agonist-induced mGluR5 internalization in spines

(A) Dendrite stained for surface expressed (red outline) and internalized (cyan outline) myc-mGluR5 before (upper panels) and 30 minutes after (lower panels) DHPG treatment. Scale bar, 5 μ m. (B) Quantification of the ratio of surface over total myc-mGluR5 intensity at different time points after DHPG stimulation ($n = 8 - 20$). Dashed line represents single exponential fit. (C) Co-localization of internalized myc-mGluR5 (cyan) and indicated endosomal- and lysosomal markers (red). Arrowheads indicate examples of overlapping puncta. Scale bar, 5 μ m. (D) Quantification of overlap between internalized myc-mGluR5 puncta and indicated markers (EEA1: $n = 10$, Rab5: $n = 10$, Rab11: $n = 8$, TfR: $n = 10$, Rab7: $n = 9$, LAMP1: $n = 9$). (E) Schematic of SEP-tag fused

Figure 1 continued on next page

Figure 1 continued

to mGluR5. (F) Live-cell time-lapse imaging of a dendrite expressing SEP-mGluR5 stimulated with DHPG at $t = 0$. Scale bar, 5 μm . (G) Quantification of SEP-mGluR5 intensity over a 30-minute time period comparing application of vehicle (black; $n = 8$) and DHPG (grey; $n = 6$) at $t = 0$ in spines (H) and dendrites. (I) Quantification of SEP-mGluR5 intensity in spines over time after DHPG stimulation comparing control neurons (grey; $n = 6$) with neurons pre-treated with dynasore (orange; $n = 6$) and (J) in neurons co-transfected with Dyn2 (grey; $n = 6$) with neurons co-transfected with Dyn2-K44A (orange, $n = 6$). (K) Quantification of SEP-mGluR5 intensity in spines over time without the addition of DHPG comparing control neurons (black; $n = 6$) with neurons pre-treated with dynasore (orange; $n = 8$) and (L) in neurons co-transfected with Dyn2 (grey; $n = 6$) with neurons co-transfected with Dyn2-K44A (orange; $n = 6$). Data are represented as mean \pm SEM. * $P < 0.05$, *** $P < 0.001$.

induced mGluR5 internalization in spines (control: $46.9 \pm 5.1\%$, dynasore: $20.1 \pm 6.3\%$, $P < 0.05$; Figure 1I). Moreover, expression of a dominant-negative form of Dynamin2 (Dyn2), Dynamin2-K44A (Dyn2-K44A), also reduced DHPG-induced internalization of mGluR5 in spines (Dyn2: $39.8 \pm 4.3\%$, Dyn2-K44A: $18.0 \pm 5.5\%$, $P < 0.05$; Figure 1J). The slow decrease in fluorescence intensity of SEP-mGluR5 observed in spines without the application of DHPG was similar in dynasore-treated neurons and neurons expressing Dyn2-K44A, and not different from control neurons (Figure 1K and L). In dendrites, the decrease in SEP-mGluR5 signal, in both unstimulated and DHPG-stimulated neurons, was not affected by dynasore, or expression of Dyn2-K44A (Supplementary Figure 1I, J, K and L), suggesting that internalization in dendrites is dynamin-independent. Together, these results indicate that in dendritic spines, receptor activation triggers rapid, dynamin-dependent endocytosis of mGluR5, and that internalized receptors preferentially enter the recycling compartment.

Shank proteins are required for agonist-induced internalization of mGluR5 in spines

To test whether Shank proteins contribute to mGluR5 endocytosis, we used a triple miRNA knockdown construct to simultaneously reduce the expression of Shank1, Shank2 and Shank3 (mirShank) (Supplementary Figure 2A) (MacGillavry et al., 2016). Interestingly, DHPG-induced mGluR5 internalization was significantly reduced in Shank triple knockdown (hereafter Shank knockdown) neurons compared to control neurons (control: $43.8 \pm 2.2\%$, mirShank: $24.8 \pm 2.9\%$, $P < 0.001$; Figure 2A and B). In contrast, in dendrites of both control and Shank knockdown neurons DHPG-induced mGluR5 internalization was similar (control: $22.8 \pm 2.9\%$, mirShank: $18.8 \pm 3.5\%$, Figure 2C). Importantly, DHPG-induced mGluR5 internalization in spines was completely restored to control levels by re-expression of miRNA-resistant Shank1, SHANK2 or SHANK3 in Shank knockdown neurons (control: $35.3 \pm 1.8\%$, mirShank: $10.4 \pm 4.4\%$, mirShank::SHANK2: $36.4 \pm 2.6\%$, mirShank::SHANK3: $36.4 \pm 2.4\%$; Figure 2A and D; and control: $44.5 \pm 3.3\%$, mirShank: $24.8 \pm 2.7\%$, mirShank::Shank1: $43.4 \pm 2.9\%$; Supplementary Figure 2B and C). We did not find a significant change in agonist-induced mGluR5 internalization in neurons overexpressing SHANK2 (control: $46.6 \pm 4.0\%$, SHANK2 OE: $39.5 \pm 2.7\%$; Figure 2E), suggesting that endogenous Shank levels are sufficient to sustain agonist-induced endocytosis of mGluR5. Also, SEP-mGluR5 intensity was unchanged over a period of 30 minutes in the absence of DHPG between control and Shank knockdown neurons in spines (control: $18.6 \pm 1.7\%$, mirShank: $22.4 \pm 2.8\%$; Figure 2F) and dendrites (control: $11.9 \pm 2.7\%$, mirShank: $10.1 \pm 3.9\%$, Supplementary Figure 2D). Similarly, agonist-induced internalization of mGluR1 was also reduced in Shank knockdown neurons (control: $38.6 \pm$

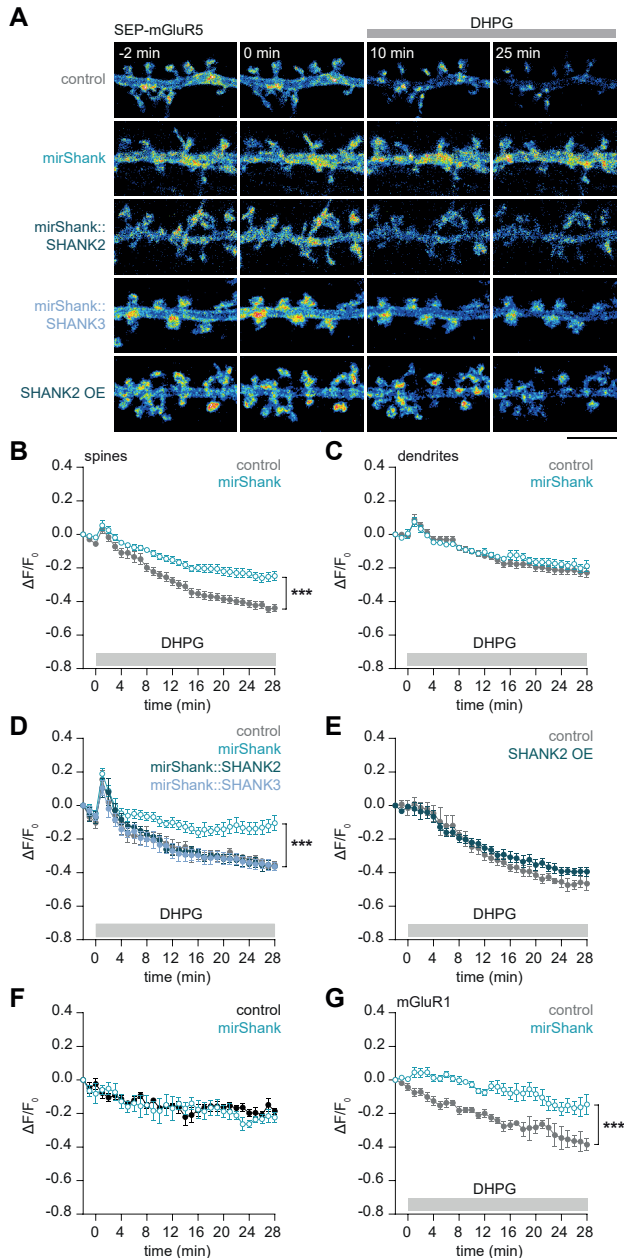


Figure 2. Shank knockdown reduces agonist-induced mGluR5 internalization in spines

(A) Live-cell time-lapse images of SEP-mGluR5 before and after DHPG stimulation (added at $t = 0$ min) in control, mirShank, mirShank::SHANK2, mirShank::SHANK3 and SHANK2 overexpression (OE) neurons. The dendrites are color-coded for the fluorescence intensity of SEP-mGluR5. Scale bar, 5 μm . (B) Quantification of SEP-mGluR5 intensity over time after the addition of DHPG in spines (C) and dendrites of control (grey; $n = 29$) and mirShank neurons (blue; $n = 34$). (D) Quantification of SEP-mGluR5 intensity in spines over time after the addition of DHPG comparing control (grey; $n = 7$), mirShank (blue; open circles; $n = 8$) and the

Figure 2 continued on next page

Figure 2 continued

mirShank::SHANK2 (n = 6) and mirShank::SHANK3 (n = 8) rescue neurons (shades of blue; closed circles), and (E) in control (grey; n = 4) compared to SHANK2 overexpression (OE; blue; n = 6) neurons. (F) Quantification of SEP-mGluR5 intensity in spines over time without the addition of DHPG comparing control (black; n = 5) and mirShank neurons (blue; n = 5). (G) Quantification of SEP-mGluR1 intensity in spines over time after the addition of DHPG in control (grey; n = 8) and mirShank neurons (blue; n = 6). Data are represented as mean \pm SEM. *** P < 0.001.

3.4, mirShank: $14.6 \pm 5.8\%$, P < 0.001; Figure 2G). Thus, agonist-induced internalization of mGluR1 and 5 in spines is modulated by synaptic Shank scaffolds.

Shank proteins couple the EZ to the PSD to mediate local endocytosis of mGluR5

We hypothesized that Shank proteins could play a central role in positioning the EZ by recruiting essential components of the endocytic machinery to the PSD (Figure 3A). As a first test, we measured the fraction of PSDs associated with an EZ in control and Shank knockdown neurons. Consistent with previous reports (Blanpied et al., 2002; Lu et al., 2007), we found that the majority of PSDs ($72 \pm 2\%$) were associated with an EZ marked by GFP-tagged clathrin light chain (GFP-CLC), but this was significantly reduced in Shank knockdown neurons ($44 \pm 2\%$, P < 0.001; Figure 3B and C). The density of GFP-CLC puncta along the dendrite was not different between control and Shank knockdown neurons (Supplementary Figure 3A). Also, immuno-labeled clathrin puncta were less frequently associated with synapses labeled with anti-Homer1b/c in Shank knockdown neurons compared to control neurons (untransfected: $72 \pm 3\%$, control: $78 \pm 3\%$, mirShank: $39 \pm 5\%$; Figure 3D). Importantly, the synaptic distribution of Homer1c-mCherry was not altered in Shank knockdown neurons (Supplementary Figure 3B, C and D).

To test whether specific interaction motifs in SHANK2 are required for coupling the EZ to the PSD, we determined the fraction of EZ-positive synapses in Shank knockdown neurons co-expressing miRNA-resistant wild-type SHANK2 (mirShank::SHANK2-WT; WT) and mutant forms of SHANK2 that lack the Dynamin2 (mirShank::SHANK2- Δ DYN; Δ DYN), Cortactin (mirShank::SHANK2- Δ COR; Δ COR), or Homer1b/c (mirShank::SHANK2-P1035L; P1035L) bindings sites. All mutants were effectively targeted to the PSD and did not alter synapse density (Supplementary Figure 3E, F and G), and were used as a marker of the PSD. Interestingly, whereas re-expression of wild-type SHANK2 completely restored the fraction of EZ-associated PSDs to control levels, the Dynamin2, Cortactin, or Homer1c binding site mutants were all unable to rescue this (WT: $66 \pm 3\%$, Δ DYN: $40.1 \pm 3\%$, Δ COR: $35.3 \pm 3\%$, P1035L: $42.2 \pm 2\%$, P < 0.001; Figure 3E and F). On the other hand, complete removal of the SHANK2 PDZ domain (Δ PDZ) did not alter the ability of SHANK2 to rescue the fraction of EZ-positive synapses ($66.1 \pm 2\%$, n = 10; Figure 3E and F). Also, the overall density of GFP-CLC puncta in dendrites was not different between conditions (Supplementary Figure 3H). Thus, these data indicate that SHANK2 binding to Homer1b/c, Cortactin, and Dynamin2 all contribute to positioning the EZ close to the PSD. Similar to SHANK2, re-expression of wild-type Shank1 and SHANK3 completely restored the fraction of EZ-associated PSDs (Shank1: $70.3 \pm 3\%$, SHANK2: $73.6 \pm 2\%$, SHANK3: $72.9 \pm 2\%$; Supplementary Figure 3I and J).

Among the numerous *de novo* mutations in the *SHANK2* gene identified in individuals with ASD, one particular nonsense mutation in *SHANK2* (T1127M) is located in the core of

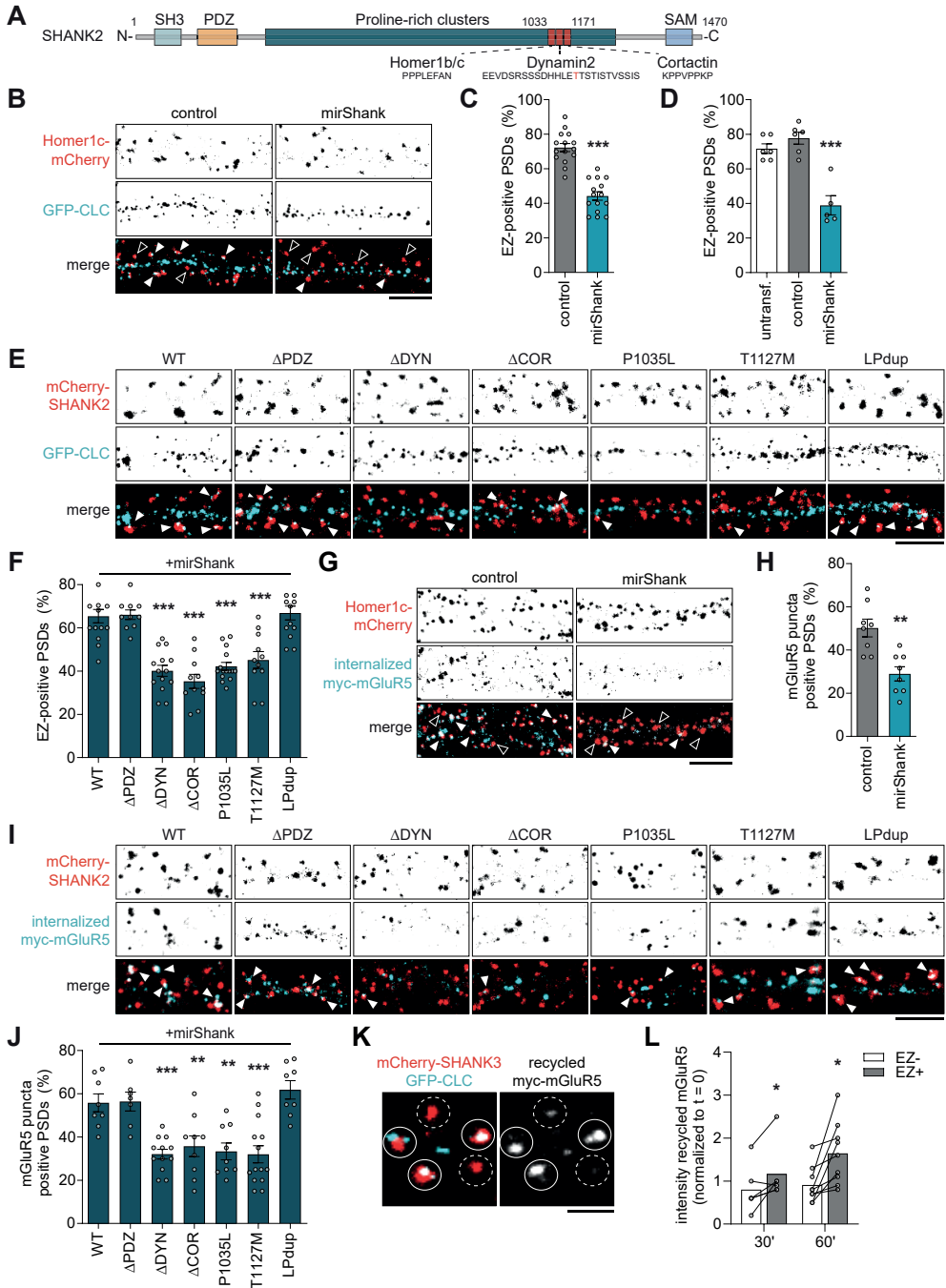


Figure 3. Shanks couple the EZ to the PSD to control mGluR5 trafficking in spines

(A) Domain structure of SHANK2. Proline-rich binding motifs for Homer1b/c, Dynamin2, and Cortactin are indicated. (B) Representative images of dendrites co-expressing GFP-CLC (cyan) and Homer1c-mCherry (red)

Figure 3 continued on next page

Figure 3 continued

in control and mirShank neurons. Indicated are examples of EZ-positive (filled arrowhead) and EZ-negative (open arrowheads) PSDs. Scale bar, 5 μm . (C) Quantification of the percentage of PSDs associated with a GFP-CLC marked EZ in control (n = 15) and mirShank (n = 15) neurons. (D) Quantification of PSDs associated with endogenous anti-clathrin in untransfected (n = 6) and transfected control (n = 6) and mirShank (n = 5) neurons. (E) Representative images of dendrites co-expressing mCherry-tagged SHANK2 rescue constructs (red) and GFP-CLC (cyan). Scale bar, 5 μm . (F) Quantification of the percentage of EZ-positive PSDs in neurons co-expressing mCherry-tagged SHANK2 rescue constructs (WT: n = 14, Δ PDZ: n = 10, Δ DYN: n = 14, Δ COR: n = 11, P1035L: n = 15, T1127M: n = 11, LPdup: n = 13). (G) Representative images showing internalized myc-mGluR5 (cyan) puncta 30 minutes after the application of DHPG in dendrites co-expressing Homer1b/c-mCherry (red) as a PSD-marker, in control and mirShank neurons. Indicated are examples of mGluR5 puncta positive PSDs (filled arrowhead) and mGluR5 puncta negative PSDs (open arrowheads). Scale bar, 5 μm . (H) Quantification of the percentage of mGluR5 puncta positive PSDs in control (n = 8) and mirShank (n = 8) neurons. (I) Representative images of dendrites co-expressing mCherry-tagged SHANK2 rescue constructs (red) and internalized myc-mGluR5 (cyan) 30 minutes after the application of DHPG. Scale bar, 5 μm . (J) Quantification of the percentage of mGluR5 puncta positive PSDs in neurons co-expressing mCherry-tagged SHANK2 rescue constructs (WT: n = 8, Δ PDZ: n = 7, Δ DYN: n = 12, Δ COR: n = 9, P1035L: n = 9, T1127M: n = 14, LPdup: n = 8). (K) Representative image of recycled myc-mGluR5 (right panel) at EZ-positive PSDs (white circles) and at EZ-negative PSDs (white dashed circles). EZs are marked by GFP-CLC (cyan) and PSDs are marked by mCherry-SHANK3 (red) (left panel). Scale bar, 2 μm . (L) Quantification of signal intensity of recycled myc-mGluR5 at EZ-negative and EZ-positive synapses after 30 (n = 6) and 60 (n = 9) minutes recycling. Data is normalized to myc-mGluR5 intensity at t = 0 min. Data are represented as mean \pm SEM. * P < 0.05, ** P < 0.01, *** P < 0.001.

the Dynamin2 binding site (Berkel et al., 2010). We confirmed that this SHANK2 variant was efficiently targeted to synapses (Supplementary Figure S3E) (Berkel et al., 2012), but this single point mutation rendered SHANK2 unable to rescue the loss of EZ-associated PSDs ($45.2 \pm 4\%$, P < 0.001; Figure 3E and F). Another *de novo* mutation found in SHANK2 in an individual with autism (L1008P1009dup; LPdup) was still able to rescue the loss of EZ-associated PSDs ($66.9 \pm 3\%$; Figure 3E and F).

To further test whether Shank proteins promote the local endocytosis of mGluR5, we determined the localization of internalized myc-mGluR5 with respect to the PSD. Interestingly, the fraction of synapses that overlapped with internalized mGluR5 puncta was significantly reduced in Shank knockdown neurons (control: $50.2 \pm 4\%$, mirShank: $29.0 \pm 3\%$, P < 0.01; Figure 3G and H). In neurons re-expressing wild-type SHANK2 this was completely restored, while SHANK2 mutants deficient in binding Homer1b/c, Cortactin, or Dynamin2 were unable to rescue this (WT: $55.8 \pm 4\%$, Δ DYN: $32.1 \pm 2\%$, Δ COR: $35.7 \pm 5\%$, P1035L: $33.4 \pm 4\%$, P < 0.001; Figure 3I and J). Also, in neurons re-expressing the ASD-associated SHANK2-T1127M mutant there was a significant reduction in synapse-associated mGluR5 puncta ($32 \pm 4\%$, P < 0.001; Figure 3I and J). On the other hand, re-expression of SHANK2- Δ PDZ and the ASD-associated SHANK2-LPdup mutant did not alter the ability of SHANK2 to rescue this (Δ PDZ: $56.4 \pm 4\%$, LPdup: $61.8 \pm 4\%$; Figure 3I and J). Thus, Shank proteins spatially restrict endocytosis of mGluR5 to perisynaptic sites by coupling the EZ to the PSD.

The EZ mediates local mGluR5 recycling

The reduction in EZ-associated synapses and the decrease in mGluR5 internalization in Shank knockdown neurons suggest that mGluR5 internalizes through the spine EZ coupled to the PSD via Shank intermediates. To further test whether mGluR5 can undergo recycling

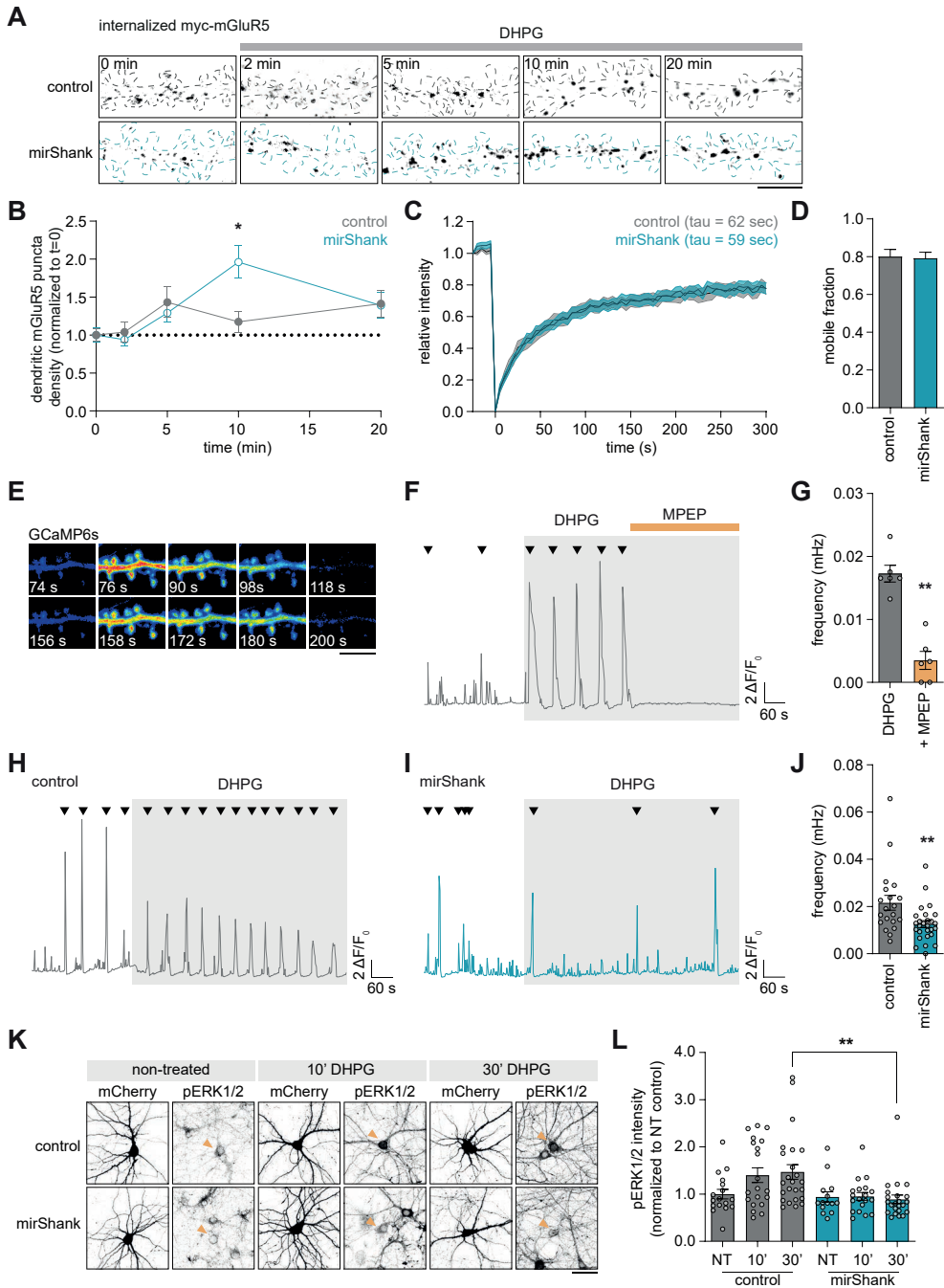


Figure 4. Shanks control mGluR5-mediated calcium signaling and ERK1/2 activity

(A) Dendrite stained for internalized myc-mGluR5 at different time points after DHPG stimulation in control (grey outline; upper panels) and mirShank (blue outline; lower panels) neurons. Scale bar, 5 μ m. (B) Quantification of internalized myc-mGluR5 puncta density in the dendritic shaft at different time points after DHPG stimulation

Figure 4 continued on next page

Figure 4 continued

in control (n = 18 – 24) and mirShank (n = 18 – 27) neurons, normalized to t = 0 per condition. (C) FRAP analysis of Venus-mGluR5 in spines of control (grey; n = 38 spines) and mirShank (blue; n = 38 spines) neurons. (D) Quantification of the mobile fraction of Venus-mGluR5 in spines of control and mirShank neurons. (E) Example of a dendrite expressing GCaMP6s stimulated with DHPG. Scale bar, 5 μ m. (F) Oscillatory response of GCaMP6s signal in response to the application of DHPG (grey; n = 22) and DHPG + MPEP (orange; n = 26). (G) Quantification of the frequency (mHz) of the GCaMP6s oscillations in response to DHPG and DHPG + MPEP (n = 6). (H) Oscillatory response of GCaMP6s signal in response to DHPG in control (grey), and (I) mirShank (blue) neurons. (J) Quantification of the frequency (mHz) of the GCaMP6s oscillations in response to DHPG in control (n = 20) and mirShank (n = 27) neurons. (K) Examples of control (upper panels) and mirShank (lower panels) neurons immuno-labeled for anti-pERK1/2 in non-treated (NT) and treated neurons with DHPG for 10 minutes (10') or 30 minutes (30'). Orange arrowheads indicate the mCherry expressing control and mirShank neurons used for quantification. Scale bar, 50 μ m. (L) Quantification of the average anti-pERK1/2 fluorescence intensity in the cell bodies of the transfected neurons of control (n = 17 – 24) and mirShank (n = 14 – 23) neurons with indicated treatment. Data is normalized to the average intensity of the non-treated control condition. Data are represented as mean \pm SEM. * P < 0.05, ** P < 0.01 and *** P < 0.001.

and whether this is facilitated by the EZ, we performed an antibody-based recycling assay to specifically label the recycled pool of receptors (Lu et al., 2007). Strikingly, the levels of recycled mGluR5 were significantly higher at EZ-positive synapses, with almost no detectable recycling at EZ-negative synapses (30': EZ+: 1.2 ± 0.3 , EZ-: 0.8 ± 0.2 , 60': EZ+: 1.6 ± 0.2 , EZ-: 0.9 ± 0.1 , P < 0.05; Figure 3K and L), consistent with the model that mGluR5 is internalized through the EZ to undergo local capture and recycling, reminiscent of AMPAR recycling (Lu et al., 2007).

Shank proteins control local trafficking of mGluR5 in spines

We found that Shank knockdown specifically reduced agonist-induced internalization of mGluR5 in spines, but not in dendrites and predicted that disrupting the coupling between the EZ and the PSD would favor mGluR5 internalization at extrasynaptic sites. The density of internalized mGluR5 puncta at the dendritic shaft under basal condition (t = 0 min) was similar in control and Shank knockdown neurons (Supplementary Figure 4A) and showed a similar increase 5 minutes after application of DHPG (Figure 4A and B). Strikingly, 10 minutes after treatment with DHPG the density of internalized mGluR5 puncta at the dendritic shaft was significantly increased in Shank knockdown neurons compared to t = 0 min (0': 1 ± 0.09 , 10': 2.0 ± 0.2 , P < 0.001) and significantly different from control neurons (10': 1.2 ± 0.1 , P = 0.01) (Figure 4A and B). This increase returned to control levels 20 minutes after treatment. Thus, in the absence of Shanks, activated receptors diffuse away from the synapse to internalize at extrasynaptic sites. This is expected to lead to a progressive reduction in surface mGluR5 levels at the synapse. Indeed, SEP-mGluR5 enrichment in spines was significantly reduced in Shank knockdown neurons, and fully rescued by re-expression of Shank1, SHANK2 and SHANK3 (control: 1.5 ± 0.1 , mirShank: 1.1 ± 0.04 , Shank1: 1.4 ± 0.04 , SHANK2: 1.5 ± 0.1 , SHANK3: 1.4 ± 0.04 , P < 0.001; Supplementary Figure 4B). Immunoblotting showed no reduction in mGluR5 proteins levels in Shank knockdown neurons (Supplementary Figure 4C and D). However, immuno-labeling of mGluR5 showed that total levels of endogenous mGluR5 were reduced in Shank knockdown neurons (control: 1 ± 0.05 , mirShank: 0.8 ± 0.03 , P < 0.01; Supplementary Figure 4E and F), which has been previously reported in Shank3 knockdown neurons (Verpelli et al., 2011).

Thus, disrupted mGluR5 recycling in Shank knockdown neurons leads to a reduction in the density of mGluR5 at the synaptic membrane.

Shank proteins are large multi-domain scaffolding proteins and have been suggested to anchor mGluR5 at the synapse through interactions with Homer1b/c (Tu et al., 1999). The reduced surface levels of mGluR5 in spines, and total levels of endogenous mGluR5 in Shank knockdown neurons could thus also be explained by a reduction in receptor binding sites at the PSD modulating mGluR5 stability. However, using fluorescence recovery after photobleaching (FRAP) experiments, we found that the rate of recovery as well as the total recovery of Venus-mGluR5 were similar in control and Shank knockdown neurons (Figure 4C and D), suggesting that Shank proteins do not directly contribute to the anchoring of mGluR5 at synaptic sites.

mGluR5-mediated calcium and ERK1/2 signaling is abrogated in Shank knockdown neurons

The density of mGluR5 on the membrane controls the activation of downstream signaling pathways (Choi et al., 2011; Nash et al., 2002) that can trigger the oscillatory release of Ca^{2+} from internal stores (Kawabata et al., 1996) and activate the extracellular signal-regulated kinase (ERK1/2) pathway (Mao et al., 2005). To test the functional impact of the defect in mGluR5 trafficking in Shank knockdown neurons, we first measured DHPG-induced Ca^{2+} oscillations using the fluorescent Ca^{2+} reporter GCaMP6s (Chen et al., 2013). Consistent with previous reports, we found that DHPG triggered the immediate onset of robust Ca^{2+} oscillations (Figure 4E and F). DHPG-induced oscillations were completely blocked by addition of the specific mGluR5 antagonist MPEP (DHPG: 17.3 ± 1.3 mHz, and DHPG + MPEP: 3.5 ± 1.4 mHz, $P < 0.001$; Figure 4F and G), confirming that these oscillations are mediated by the activation of mGluR5. Importantly, we found that the frequency of DHPG-induced calcium peaks was significantly reduced in Shank knockdown neurons (control 21.6 ± 3.1 mHz, mirShank 12.6 ± 1.5 mHz, $P < 0.01$; Figure 4H, I and J). Furthermore, we compared DHPG-induced phosphorylation of ERK1/2 (pERK1/2) in control and Shank knockdown neurons. Incubation with DHPG for 10 and 30 minutes increased ERK1/2 phosphorylation shown by immuno-labeling of pERK1/2 in a population of control neurons, which was significantly reduced in Shank knockdown neurons after 30 minutes DHPG treatment (10' DHPG: control: 1.4 ± 0.15 , mirShank: 0.95 ± 0.08 , and 30' DHPG: control: 1.47 ± 0.16 , mirShank: 0.89 ± 0.09 , $P < 0.01$; Figure 4K and L). Importantly, under basal conditions (non-treated; NT) the levels of ERK1/2 phosphorylation were similar between control and Shank knockdown neurons (NT: control: 1.00 ± 0.10 , mirShank: 0.94 ± 0.11 ; Figure 4J and K). These results indicate that Shank regulates mGluR5 signaling, substantiating an involvement of aberrant receptor trafficking in animal models of ASD with implicated deregulation of mGluR5 signaling.

Discussion

Modulation of glutamatergic signaling by group I mGluRs is essential for proper synaptic transmission and plasticity, and deregulated mGluR signaling is broadly held to underlie the molecular pathology of neurodevelopmental disorders (Lüscher and Huber, 2010).

However, fundamental aspects of mGluR signaling and trafficking at excitatory synapses are still poorly understood. Here we present a model in which coupling of the EZ to the PSD by Shank proteins enables local recycling of mGluRs, allowing the synapse to balance the density of mGluRs at the membrane to efficiently modulate neuronal functioning.

Our data show that Shank proteins selectively regulate activity-induced internalization of mGluR5 in spines. While DHPG-induced mGluR5 internalization is greatly affected in Shank knockdown neurons, in the absence of stimulation the levels of mGluR5 remain relatively constant in both control and Shank knockdown neurons. This suggests that in the absence of Shanks constitutive internalization of mGluR5 is not affected and continues to replace surface receptors. Thus, in the absence of efficient PSD-EZ coupling, synaptic receptors now escape this local endocytic sink and become internalized and recycled at extrasynaptic sites, slowly depleting the synaptic pool of receptors. Indeed, we found a significant increase in agonist-induced mGluR5 internalization in dendrites, and a significant decrease in surface mGluR5 levels in spines of Shank knockdown neurons. This also suggests that dendritic internalization of mGluR5 is regulated independent of Shanks. Moreover, blocking dynamin activity did not alter dendritic mGluR5 internalization, indicating that internalization of dendritic receptors is regulated by different mechanisms. We consistently found a small reduction in SEP-mGluR5 signal in the absence of agonist, both in spines and dendrites. This could reflect constitutive internalization of mGluR5, but ongoing recycling and lateral diffusion of receptors make it hard to interpret this directly. Nevertheless, previous studies found that mGluR5 undergoes constitutive internalization at a similar rate, but that this process is independent of clathrin and dynamin activity (Fourgeaud et al., 2003), and has been suggested to be mediated by the caveolin-mediated internalization pathway (Francesconi et al., 2009). Altogether, our results are consistent with the notion that the EZ captures synaptic receptors through spatially restricted, clathrin-mediated endocytosis and recycling, allowing the synapse to autonomously control its receptor content (Czondor et al., 2012).

Importantly, the reduction in surface mGluR5 levels in spines in Shank knockdown neurons was functionally reflected in a decrease in mGluR5-mediated calcium responses and ERK1/2 activation. Our experiments were focused on mGluR5, but we cannot exclude that other synaptic receptors or ion channels undergo aberrant trafficking when the EZ is uncoupled from the PSD. Indeed, glutamatergic transmission in general is reduced in Shank knockdown neurons (Arons et al., 2012; Duffney et al., 2013; Verpelli et al., 2011), Shank knockout mouse models (Bozdagi et al., 2010; Duffney et al., 2015; Kouser et al., 2013; Schmeisser et al., 2012), and in neurons expressing ASD-associated Shank mutations (Lee et al., 2019). Thus, disrupting the link between the PSD and the EZ could have much broader effects on the composition of the synaptic membrane and glutamatergic transmission.

Our results indicate that all three Shank isoforms, which share a similar domain structure, recruit important components of the endocytic machinery to the PSD. The interaction between Shank and Homer1b/c confers a direct molecular link to the EZ through Dynamin3. Indeed, abrogating this interaction through directed mutation (our data) or through dominant-negative approaches (Lu et al., 2007), significantly impairs EZ positioning. Shank proteins also seem to recruit Dynamin2 to the EZ, which likely provides the GTPase activity necessary for vesicle scission. Interestingly, we found that the Cortactin-binding motif in SHANK2 was also required for efficient mGluR5 internalization. Cortactin can also bind Dynamin2 and 3 directly (Gray et al., 2003), and has been implicated in

endocytosis and endo-lysosomal sorting of AMPARs (Parkinson et al., 2018). Importantly, expression of the Shank triple knockdown construct leads to a strong reduction in total Shank levels, but leaves ~20% of total Shank levels intact (MacGillavry et al., 2016). Thus, we cannot exclude that remaining Shank proteins still recruit other interacting proteins that contribute to the trafficking of synaptic receptors.

Consistent with our results that Shank proteins control mGluR trafficking and function, recent studies show that deficits in social behavior caused by the loss of Shank function could be rescued by group I mGluR positive allosteric modulators (Bariselli et al., 2016; Vicidomini et al., 2017). However, even though deregulated receptor functioning at excitatory synapses has been implicated to underlie physiological deficits in many disease models, the molecular mechanisms underlying this have not been resolved. Our results indicate that Shank proteins do not directly anchor receptors at the synapse but provide a stable molecular framework that permits the local uptake and trafficking of receptors via the EZ thereby governing a stable pool of synaptic receptors. That the ASD-associated T1127M mutation in SHANK2 disrupts this process further underlines the relevance of understanding the functional relationship between Shank proteins and mGluR signaling in the context of human neurodevelopmental disorders.

Materials and Methods

Key resources table

Please find the key resources table at the end of this chapter.

Lead contact and materials availability

Plasmids generated in this study are available on request. Further information and requests for resources and reagents should be directed to and will be fulfilled by the Lead Contact, Harold MacGillavry (h.d.macgillavry@uu.nl).

Experimental model and subject details

Animals

All animal experiments were performed in compliance with the guidelines for the welfare of experimental animals issued by the Government of The Netherlands (Wet op de Dierproeven, 1996) and European regulations (Guideline 86/609/EEC). All animal experiments were approved by the Dutch Animal Experiments Review Committee (Dier Experimenten Commissie; DEC), performed in line with the institutional guidelines of Utrecht University.

Primary neuronal cultures and transfections

Hippocampal cultures were prepared from embryonic day 18 (E18) Janvier Wistar rat brains (both genders) as described in (Cunha-Ferreira et al., 2018). Dissociated neurons were plated on coverslips coated with poly-L-lysine (37.5 µg/ml, Sigma-Aldrich) and laminin (1.25 µg/ml, Roche Diagnostics) at a density of 100,000 neurons per well of a 12-well plate. Cultures were grown in Neurobasal medium (NB) supplemented with 2% B27 (GIBCO), 0.5 mM glutamine (GIBCO), 15.6 µM glutamate (Sigma-Aldrich), and 1% penicillin/

streptomycin at 37°C in 5% CO₂. At DIV14-18 neurons were transfected with indicated constructs using Lipofectamine 2000 (Invitrogen). Before transfection 260 µl conditioned medium was transferred to a new culture plate and replaced with 260 µl NB with 0.5 mM glutamine. For each well, 1.8 µg DNA was mixed with 3.3 µl Lipofectamine 2000 in 200 µl NB, incubated for 30 min at RT and added to the neurons. After 45 – 60 minutes, neurons were briefly washed with NB and transferred to the new culture plate with conditioned medium supplemented with 260 µl NB with B27, glutamine, penicillin/ streptomycin and kept at 37°C in 5% CO₂ for 2-4 days (for overexpression) or 5-7 days (for Shank knockdown).

Method details

DNA constructs

The pRK5-SEP-mGluR5a, pRK5-Halo-mGluR5a and pRK5-myc-mGluR5a constructs were made using the pRK5-Venus-mGluR5a construct (a gift from Dr. Julie Perroy) as a template and the pRK5-SEP-mGluR1 construct was made by replacing mGluR5a with mGluR1 (clone image ID # 40080840). The human mCherry-SHANK2 expression plasmid was kindly provided by Dr. Simone Berkel (Berkel et al., 2012). The pSM155-GFP (or Cerulean3; Cer3), Shank triple-knockdown construct pSM155-mirShank-GFP (or Cer3), and mirShank::GFP-SHANK2 wild-type (: to indicate that the Shank miRNAs and GFP-tagged human SHANK2 are expressed simultaneously from a single expression cassette), mirShank::GFP-SHANK2-ΔCOR, and mirShank::GFP-SHANK2-P1035L mutant rescue constructs are described in (MacGillavry et al., 2016). In these constructs GFP was replaced by mCherry (from pmCherry-N1, Invitrogen). To make the mirShank::mCherry-SHANK2-ΔDYN (lacking the 25-amino acid dynamin-binding domain; Glu1114 - Ser1138) (Okamoto et al., 2001), mirShank::mCherry-SHANK2-ΔPDZ (lacking the 95-amino acid PDZ domain, Thr254 - Thr348), mirShank::mCherry-SHANK2-L1008P1009dup and mirShank::mCherry-SHANK2-T1127M constructs, primers were designed containing the desired mutations and 10 – 15 bp overhangs for Gibson assembly (NEBuilder HiFi DNA assembly cloning kit). The rat Shank1 and human SHANK3 expression plasmids were a gift from Dr. Morgan Sheng and Dr. Michael Schmeisser (Cochoy et al., 2015), respectively, and used as a template to make the pSM155-mirShank::mCherry-Shank1 and pSM155-mirShank::mCherry-SHANK3 rescue constructs. Dynamin2-GFP and Dynamin2-K44A-GFP (Addgene plasmid # 22301) were a gift from Dr. Pietro De Camilli (Ochoa et al., 2000), and in both constructs GFP was replaced by mCherry. GFP-CLC (rat clathrin light chain A1) was a gift from Dr. Mike Ehlers, LAMP1-GFP was a gift from Dr. Esteban Dell'Angelica (Addgene plasmid # 34831) (Falcon-Perez et al., 2005), and pGP-CMV-GCaMP6s was a gift from Dr. Douglas Kim (Addgene plasmid # 40753) (Chen et al., 2013). pCAG-PSD95.FingR-eGFP-CCR5TC (PSDFingR-GFP) was a gift from Dr. Don Arnold (Addgene plasmid # 46295) (Gross et al., 2013). The following constructs have been described before: Homer1c-mCherry (MacGillavry et al., 2013), GFP-Rab5, GFP-Rab7, mRFP-TfR (Hoogenraad et al., 2010), and tdTomato-Rab11 (Esteves da Silva et al., 2015). FUGW was a gift from David Baltimore (Addgene plasmid # 14883) (Lois et al., 2002). FUGW-mirShank-GFP was generated by replacing GFP with the Shank triple-knockdown cassette from pSM155-mirShank-GFP. All constructs were verified by sequencing.

Lentiviral particles were generated by transfecting the transfer plasmid together with the

packaging plasmids p.MDG2 (Addgene plasmid #12259) and psPAX2 (Addgene plasmid #12260) (gifts from Didier Trono) in HEK293T cells. The supernatant was collected two days after transfection and concentrated using tangential flow filtration (Amicon Ultra spin filters, Millipore #UFC910024).

Confocal imaging

Confocal images were taken with a Zeiss LSM 700 confocal laser-scanning microscope with a Plan-Apochromat 63x NA 1.40 oil objective. Images consist of a z-stack of 7-9 planes at 0.39 μm interval, and maximum intensity projections were generated for analysis and display. The pERK1/2 (Figure J and K) and anti-mGluR5 (Supplementary Figure 4B and C) images were taken with an EC Plan-Neofluar 40x NA 1.30 oil objective and consist of a z-stack of 9 planes at 0.67 μm interval to obtain maximum intensity projections of the entire neuron in the z-axis.

Antibody feeding assay

DIV18 neurons were transfected with myc-mGluR5 and endosomal markers as indicated and were live-labeled at DIV21 with mouse anti-c-myc (9E10, Santa Cruz Biotechnology, catalog # sc-40) diluted 1:200 in extracellular imaging buffer (120 mM NaCl, 3 mM KCl, 2 mM CaCl_2 , 2 mM MgCl_2 , 10 mM glucose, and 10 mM HEPES, pH adjusted to 7.35 with NaOH) for 30 minutes at RT, washed twice with imaging buffer, and incubated with 50 μM DHPG (Tocris) for the indicated time-points at 37°C. Cells were then fixed in 4% (w/v) paraformaldehyde (PFA) and 4% (w/v) sucrose in PBS for 10 minutes at RT, and washed three times with PBS supplemented with 100 mM glycine (PBS/Gly). To label the surface-expressed pool of receptors, cells were incubated with goat anti-mouse Alexa-647 (Thermo Fisher Scientific) diluted 1:200 in 5% (v/v) NGS in PBS/Gly for 30 minutes at RT, and washed three times with PBS/Gly. Then, to label the intracellular pool of receptors, cells were permeabilized with 0.25% (v/v) Triton X-100 and 5% (v/v) NGS in PBS/Gly for 5 minutes at RT, blocked with 10% (v/v) NGS in PBS/Gly for 30 minutes, and incubated with goat anti-mouse Alexa-488 (Thermo Fisher Scientific) diluted 1:200 in 5% (v/v) NGS in PBS/Gly for 30 minutes at RT. For co-labeling internalized mGluR5 with EEA1, cells were incubated with human anti-EEA1 (clone 4114; gift from M. Fritzler) diluted 1:500 in 5% (v/v) NGS in PBS/Gly for 2 hours at RT after the permeabilization and blocking steps, and detected with goat anti-human Alexa-568 (Thermo Fisher Scientific). Cells were washed three times with PBS/Gly, mounted in Mowiol mounting medium and imaged on a confocal system as described above.

For the Shank knockdown experiments DIV14 neurons were transfected with pSM155-Cer3 or mirShank::Cer3 together with myc-mGluR5 and Homer1c-mCherry. For the rescue experiments DIV14 neurons were transfected with indicated mirShank::mCherry-SHANK rescue constructs and myc-mGluR5. After 7 days (DIV21), neurons were live-labeled with anti-myc, stimulated with DHPG for 30 minutes, and the surface and internalized pools of myc-mGluR5 were visualized as described above.

For the density of internalized mGluR5 puncta in the dendritic shaft after treatment with DHPG for several points before fixation, DIV14 neurons were transfected with pSM155-mCherry or mirShank::mCherry and myc-mGluR5. After 7 days (DIV21), neurons were live-labeled with anti-myc, stimulated with DHPG for 0, 2, 5, 10 or 20 minutes, and the surface and internalized pools of myc-mGluR5 were visualized as described above.

Endocytic zone associated PSDs

For the Shank knockdown experiments DIV14 neurons were transfected with pSM155-Cer3 or mirShank::Cer3 together with GFP-CLC and Homer1c-mCherry. Alternatively, pSM155-Cer3 or mirShank::Cer3 transfected neurons were stained for endogenous clathrin with mouse anti-clathrin heavy chain (clone X22, Fisher Scientific) and Homer1, with rabbit anti-Homer1 (SySy), and visualized with goat anti-mouse Alexa-647 and goat anti-rabbit Alexa-488 antibodies. For the rescue experiments DIV14 neurons were transfected with indicated mirShank::mCherry-SHANK rescue constructs and GFP-CLC. After 7 days (DIV21), neurons were fixed with 4% PFA and 4% sucrose in PBS for 15 minutes, washed, mounted in Mowiol mounting medium and imaged on a confocal system as described above.

For the co-localization between the PSD and Homer1c in control and Shank knockdown neurons, DIV14 neurons were transfected with pSM155-Cer3 or mirShank::Cer3 together with Homer1c-mCherry and PSDFingR-GFP. For the rescue experiments DIV14 neurons were transfected with indicated mirShank::mCherry-SHANK2 rescue constructs and PSDFingR-GFP. After 7 days (DIV21) the neurons were fixed, mounted and imaged as described above.

Receptor recycling assay

Neurons were live labeled with anti-myc 1:200 in extracellular imaging buffer for 30 minutes at RT, washed twice with imaging buffer, and incubated with 50 μ M DHPG for 30 minutes at 37°C to induce receptor internalization. Remaining surface-bound anti-myc antibodies were blocked by incubating with HRP-conjugated swine anti-mouse (Agilent) antibodies diluted 1:100 for 30 minutes at RT. Cells were then washed twice and returned to 37°C to allow receptor recycling for the indicated time points. The recycled receptor pool was then labeled with goat anti-mouse Alexa-647 diluted 1:200 in 5% (v/v) NGS in PBS/Gly for 30 minutes at RT. Cells were washed three times with PBS/Gly, mounted in Mowiol mounting medium and imaged on a confocal system as described above.

Endogenous mGluR5 protein levels

DIV14 neurons were transfected with pSM155-mCherry or mirShank::mCherry and stained for endogenous surface and intracellular mGluR5 with rabbit anti-mGluR5 (Chemicon, catalog #ab5675) diluted 1:500 in 0.1% (v/v) Triton X-100 and 5% (v/v) NGS in PBS/Gly overnight at 4°C, and visualized with goat anti-rabbit Alexa-488 diluted 1:250 in 0.1% (v/v) Triton X-100 and 5% (v/v) NGS in PBS/Gly for 1 hour at RT. Cells were washed three times with PBS/Gly, mounted in Mowiol mounting medium and imaged on a confocal system as described above.

ERK1/2 phosphorylation assay

Neurons were transfected with pSM155-mCherry or mirShank::mCherry at DIV14. Tetrodotoxin (2 μ M; TTX) was added 12 hours before treatment. At DIV22 neurons were incubated with either 100 μ M DHPG diluted in extracellular imaging buffer for 10 or 30 minutes, or with extracellular imaging buffer only for non-treated control neurons. After the indicated time points the neurons were fixed in 4% PFA and 4% sucrose in PBS for 10 minutes at RT, followed by a quick wash with PBS/Gly, incubated with ice cold methanol (MeOH) for 10 minutes at -20°C and washed three times with PBS/Gly. The

pSM155-mCherry or mirShank::mCherry transfected neurons were stained for ERK1/2 phosphorylation with rabbit anti-pERK1/2 (Cell Signaling, catalog #9101) diluted in 0.1% (v/v) Triton X-100 and 5% (v/v) NGS in PBS/Gly overnight at 4°C, and visualized with goat anti-rabbit Alexa-A488 diluted in 0.1% (v/v) Triton X-100 and 5% (v/v) NGS in PBS/Gly for 1 hour at RT. Cells were washed three times with PBS/Gly, mounted in Mowiol mounting medium and imaged on a confocal system as described above.

Live-cell imaging

Live-cell imaging was performed on a spinning disk confocal system (CSU-X1-A1; Yokogawa) mounted on a Nikon Eclipse Ti microscope (Nikon) with Plan Apo VC 100x 1.40 NA, or Plan Apo 60x 1.30 NA oil objectives (Nikon) with excitation from Cobolt Calypso (491 nm), and Jive (561 nm) lasers, and emission filters (Chroma). The microscope was equipped with a motorized XYZ stage (ASI; MS-2000), Perfect Focus System (Nikon), Evolve 512 EM-CCD camera (Photometrics), and was controlled by MetaMorph 7.7.6 software (Molecular Devices). Neurons were maintained in a closed incubation chamber (Tokai hit: INUBG2E-ZILCS) at 37°C in 5% CO₂ in extracellular imaging buffer.

Live-cell imaging of SEP-tagged mGluR5

DIV14 neurons were transfected with SEP-mGluR5 or SEP-mGluR1 together with pSM155-mCherry, mirShank::mCherry, mirShank::mCherry-Shank1 rescue, mirShank::mCherry-SHANK2 rescue, mirShank::mCherry-SHANK3 rescue or mCherry-Shank2 overexpression constructs. After 7 days, live neurons were imaged on a spinning disk confocal system (described above). After a 2-minute base-line acquisition, internalization was induced by the addition of DHPG to a final concentration of 50 μM and the SEP-mGluR5 signal was imaged every 30 seconds for 30 minutes (61 frames). Dynasore (100 μM; Tocris) was added 2 minutes before acquisition. In the vehicle control extracellular imaging buffer was added to the incubation chamber after a 2-minute base-line acquisition in the same volume (40 μl to 360 μl) as DHPG. To control for photobleaching the SEP-mGluR5 signal was imaged every 5 minutes for 30 minutes (7 frames). Multiple Z-stacks (10 planes) were obtained, with 0.5 μm intervals to acquire 4.5 μm image stacks.

SEP pH sensitivity assay

DIV18 neurons were transfected with SEP-mGluR5 and imaged at DIV21 on a spinning disk confocal system (described above). First, neurons were maintained in extracellular imaging buffer with pH 7.35 to visualize the mGluR5 surface pool. Then, the buffer was exchanged for imaging buffer with pH 5.5 (identical to extracellular imaging buffer, except 10 mM HEPES was replaced by 15 mM MES). Then, the low-pH buffer was exchanged for a buffer with pH 7.35 containing ammonium chloride (NH₄Cl) (identical to extracellular imaging buffer, except for 70 mM NaCl, 50 mM NH₄Cl and 2 mM NaHCO₃ instead of 120 mM NaCl). To evaluate the change in fluorescence upon exchanging the buffers, each neuron was imaged consecutively for all three conditions and 6 time points at 30 second intervals were obtained per condition. Multiple Z-stacks (10 planes) were obtained, with 0.5 μm intervals to acquire 4.5 μm image stacks per time point. For analysis, MAX intensity projections were used to assess the SEP-mGluR5 intensity for all 6 time points per condition and the change in fluorescence over time and different conditions was plotted.

Live-cell imaging of AcidiFluor ORANGE Halo-tagged mGluR5

DIV18 neurons were transfected with Halo-mGluR5 and psm155-GFP, and imaged at DIV21 on a spinning disk confocal system (described above). Surface Halo-mGluR5 was labeled with 1.5 μM HaloTag AcidiFluor ORANGE (Goryo Chemical, cat#-GC310) for 20 minutes at 37°C in 5% CO_2 . Neurons were rinsed in extracellular imaging buffer to remove unbound dye. Halo-mGluR5 labeled with AcidiFluor ORANGE was imaged in extracellular imaging buffer at 100 ms exposure and 2 second interval for 5 minutes using the 561 excitation laser. Timelapses were taken of a single z-plane. After a 40 second baseline acquisition, internalization was induced by the application of DHPG to a final concentration of 100 μM . Then, after 280 seconds, imaging buffer was exchanged for a buffer with pH 7.35 containing NH_4Cl (described above) to quench the signal of internalized Halo-mGluR5 AcidiFluor ORANGE. Also, a Z-stack (10 planes) was obtained, with 0.5 μm intervals to acquire 4.5 μm image stacks of psm155-GFP, which was co-transfected for quantification purposes.

Fluorescence recovery after photobleaching

For fluorescence recovery after photobleaching (FRAP) experiments, DIV14 neurons were transfected with Venus-mGluR5 and pSM155-mCherry or mirShank::mCherry, and imaged on a spinning disk confocal system (described above). FRAP experiments were performed using the ILas2 system (Roper Scientific). Individual spines were photobleached with a targeted 488 nm laser and imaged every 5 seconds for fluorescence recovery for a period of 5 minutes.

Calcium imaging

DIV14 neurons were transfected with GCaMP6s together with pSM155-mCherry or mirShank::mCherry and imaged 5 – 7 days later. Calcium imaging was performed on a spinning disk confocal system (described above). GCaMP6s signal was imaged at 2 second intervals (0.5 Hz) with a z-stack stream (3 - 5 planes) at every time point. After 5 minutes baseline imaging, DHPG was added to 100 μM final concentration, and cells were imaged for another 5 - 10 minutes. MPEP (5 μM ; Tocris) was added 5 minutes after application of DHPG.

Western blot and imaging

DIV10 neurons were infected with FUGW or FUGW-mirShank lentivirus for 10 days. Neurons were directly lysed in SDS sample buffer containing DTT. Lysates were subjected to Tris-Glycine SDS-PAGE followed by transfer on PVDF membranes. Blots were blocked in 2% BSA in PBS-T (0.05% Tween20) followed by primary and IRDye-conjugated secondary antibody incubation (in 2% BSA in PBS-T). Western blots were scanned using Odyssey infrared imaging system (Li-COR Biosciences).

Quantification and statistical analysis

Quantification of endocytic zone associated PSDs

To quantify the fraction of synapses with an associated endocytic zone, circular regions with a fixed diameter (0.69 μm) were centered on the Homer1c-mCherry or mCherry-SHANK2 clusters to indicate synaptic regions. These regions were then transferred to the GFP-CLC or

anti-clathrin channel. A synapse was classified EZ-positive if the clathrin cluster overlapped partially or completely with the circular region. The fraction of EZ-positive synapses was calculated per neuron and averaged per condition over the total population of neurons. Furthermore, the density of clathrin puncta was determined along the dendrite (per 10 μm).

To quantify the percentage of PSDFingR-GFP puncta overlapping with indicated mCherry constructs, puncta were selected with circular regions in the mCherry channel and transferred to the PSDFingR-GFP channel. It was classified as overlapping if the PSDFingR cluster overlapped partially or completely with the circular region. Furthermore, the puncta density of the indicated mirShank::mCherry-SHANK2 rescue constructs was determined along the dendrite (per 20 μm).

Quantification of internalized mGluR5 puncta in spines and dendrites

The number of PSDs associated with an internalized mGluR5 puncta was determined similar as the fraction of endocytic zone positive PSDs. The density of internalized mGluR5 puncta in the dendritic shaft was determined by semi-automatic quantification. The dendritic shaft (20 μm in length) was selected and a threshold was set for each image. The selection was converted to an inverted binary image and a particle analysis was used to detect internalized mGluR5 puncta with a minimum size of 0.01 μm^2 . The baseline condition ($t = 0$) was similar between control and Shank knockdown neurons. Therefore, to show the relative increase in internalized mGluR5 puncta in the dendritic shaft over time the treatment conditions were normalized per batch to the average density of its corresponding baseline condition.

Quantification of SEP-mGluR5 internalization in spines and dendrites

MAX intensity projections of the Z-stacks were obtained and corrected for XY drift over time using the Fiji plugin "StackReg". To quantify the SEP-mGluR5 intensity over a time-period of 30 minutes circular regions of interest (spines or dendrites) were selected at $t = -2$ and the intensity was measured for all 61 time points. To obtain the change in relative fluorescence intensity ($\Delta F/F_0$) over time, background was subtracted and the intensity relative to $t = -2$ was computed. For visualization all values were subtracted by 1 and plotted at 1 minute intervals.

Quantification of AcidiFluor ORANGE Halo-tagged mGluR5 acidification in spines and dendrites

MAX intensity projections of the psm155-GFP Z-stacks were made and used to trace the neuron using Fiji software. This selection was then transferred to the AcidiFluor ORANGE Halo-mGluR5 channel to clearly indicate the outline of the neuron. A gaussian blur ($\sigma = 2$) was applied to the AcidiFluor ORANGE images, and a total of 6 neurons from 2 batches were manually screened for acidification events. To test the pH sensitivity of AcidiFluor ORANGE, imaging buffer was exchanged for a buffer containing NH_4Cl which quenched the signal. Representative images are shown at 4-10 second intervals. To visualize the change in relative fluorescence intensity over time, values were plotted as $\Delta F/F_0$ for the spine and dendrite.

Quantification of spine enrichment

To assess the spine enrichment of surface mGluR5, the SEP-mGluR5 intensity at $t = -2$

min from the live-cell base-line acquisition was quantified in control, mirShank and mirShank::Shank1, mirShank::SHANK2 and mirShank::SHANK3 rescue neurons as relative spine intensity over relative dendritic shaft intensity. For each neuron circular regions were traced on multiple dendritic spines to measure spine intensity and for each selected spine a circular region in the dendrite at the base of the spine was measured as dendritic shaft intensity. Background intensity was subtracted.

Quantification of immunofluorescence of endogenous mGluR5

For the analysis of endogenous total mGluR5 levels a dendritic stretch of 20 μm was selected and traced in the mCherry channel using Fiji software. This selection was then transferred to the anti-mGluR5 channel and the average intensity of the anti-mGluR5 fluorescence of the transfected neurons with indicated constructs was obtained. Per batch the average intensity was normalized to the average intensity of the control neurons.

Quantification of FRAP experiment

For FRAP analysis, the mean intensity of the bleached area was corrected for background values, as well as the bleaching that occurred during image acquisition. Data were normalized to control fluorescence averaged over 5 frames before bleaching. Individual recovery curves were fitted with a single-exponential function $I = A(1 - \exp(-Kt))$ to estimate the mobile fraction (A) and time constant tau.

Quantification of calcium experiment

For each neuron, the fluorescence intensity of GCaMP6s signal was measured in 10 - 20 ROIs along the dendrite, background subtracted and averaged. To obtain the mean amplitude and frequency of the calcium oscillations, events were detected with the MATLAB 'PeakFinder' function.

Quantification of ERK1/2 phosphorylation assay

For analysis the cell bodies were manually traced based on the mCherry channel using Fiji software. The average intensity of the anti-pERK1/2 fluorescence of the transfected neurons with indicated constructs was obtained for each condition and was normalized per batch to the average intensity of the non-treated control condition.

Statistical Analysis

Statistical significance was tested with a paired t-test (Figure 3L and 4G) or unpaired t-test (Figures 3C, and H, 4D, S3A and S4A, D and F) when comparing two groups with a normal distribution and a Mann Whitney test when comparing two groups without a normal distribution (Figure 4J and S3C). If multiple groups were compared (Figures 1D, 3D, F and J, S3G, H and J and S4B), statistical significance was tested with a one-way ANOVA followed by a Tukey's multiple comparison when comparing the mean of each column to the mean of every other column or a Dunnett's multiple comparison when comparing the mean of each column to the mean of a control column. When comparing multiple groups without a normal distribution, a Kruskal Wallis followed by a Dunn's multiple comparison was performed (Figure S3F). To test for an effect of treatment over time between different groups with matched values in time (Figures 1G-L, 2B-F, S1B, C and I-L, S2C and D and 4C), statistical significance was tested with a repeated measures two-way ANOVA followed

by a Tukey's multiple comparison when comparing more than two groups. To test for an effect of treatment over time between different groups without matched factors (Figure 4B and L), statistical significance was tested with a two-way ANOVA followed by a Tukey's multiple comparison when comparing more than two groups. The data table of Figure 2G contains some missing values, since during image acquisition some frames were out of focus and could not be taken into account for analysis, and a mixed effects ANOVA was performed. The effect was considered significant if the row factor (time or treatment), the column factor (condition) and the interaction (time x condition) effect were all significant (P-value below 0.05). In the text the P-values of the condition effects are reported. In the figures, * indicates significance based on the condition effect and when comparing more than two groups, * indicates significance based on the multiple comparison test. In all figures * was used to indicate a P-value < 0.05, ** for P < 0.01, and *** for P < 0.001. See Supplementary Table 2 for all P-values and statistical tests performed. Data are represented as mean \pm SEM. Reported n is number of neurons, which are indicated as scatters in the bar graphs. Each experiment was replicated in cultures from at least 2 independent preparations. Statistical analysis and graphs were prepared in GraphPad Prism and figures were generated in Adobe Illustrator CC.

Data and code availability

The published article includes all datasets generated or analyzed during this study. Tables S1 and S2 are available online: <https://doi.org/10.1016/j.celrep.2019.08.102>.

Acknowledgments

We would like to thank the MacGillavry lab for helpful discussions. This work was supported by the Netherlands Organization for Scientific Research (NWO-ALW-VENI to HDM and the Graduate Program of Quantitative Biology and Computational Life Sciences to NS), the Federation of European Biochemical Societies (FEBS Return-to-Europe Fellowship), the European Research Council (ERC-StG 716011), and the Brain and Behavior Research Foundation (NARSAD Young Investigator Award) to HDM.

Author Contributions

Conceptualization, Methodology, Validation and Formal Analysis, N.S. and H.D.M., Investigation, N.S., L.C., M.W. and H.D.M., Resources, H.D.M., C.C.H. and T.A.B., Writing - Original Draft & Editing, N.S. and H.D.M., Writing - Review, C.C.H. and T.A.B., Visualization, N.S. and H.D.M., Supervision, H.D.M., Funding Acquisition, H.D.M.

References

- Arons, M.H., Thynne, C.J., Grubruker, A.M., Li, D., Schoen, M., Cheyne, J.E., Boeckers, T.M., Montgomery, J.M., and Garner, C.C. (2012). Autism-associated mutations in ProSAP2/Shank3 impair synaptic transmission and neurexin-neuroligin-mediated transsynaptic signaling. *J. Neurosci.* 32, 14966-14978.
- Bariselli, S., Tzanoulinou, S., Glangetas, C., Prévost-Solié, C., Pucci, L., Vigiúé, J., Bezzi, P., O'Connor, E.C., Georges, F., Lüscher, C., and Bellone, C. (2016). SHANK3 controls maturation of social reward circuits in the VTA. *Nat. Neurosci.* 19, 926-934.
- Berkel, S., Marshall, C.R., Weiss, B., Howe, J., Roeth, R., Moog, U., Endris, V., Roberts, W., Szatmari, P., Pinto, D., et al. (2010). Mutations in the SHANK2 synaptic scaffolding gene in autism spectrum disorder and mental retardation. *Nat. Genet.* 42, 489-491.
- Berkel, S., Tang, W., Treviño, M., Vogt, M., Obenaus, H.A., Gass, P., Scherer, S.W., Sprengel, R., Schratz, G., and Rappold, G.A. (2012). Inherited and de novo SHANK2 variants associated with autism spectrum disorder impair neuronal morphogenesis and physiology. *Hum. Mol. Genet.* 21, 344-357.
- Blanpied, T.A., Scott, D.B., and Ehlers, M.D. (2002). Dynamics and regulation of clathrin coats at specialized endocytic zones of dendrites and spines. *Neuron* 36, 435-449.
- Bozdagi, O., Sakurai, T., Papapetrou, D., Wang, X., Dickstein, D.L., Takahashi, N., Kajiwara, Y., Yang, M., Katz, A.M., Scattoni, M.L., et al. (2010). Haploinsufficiency of the autism-associated Shank3 gene leads to deficits in synaptic function, social interaction, and social communication. *Mol. Autism* 1, 15.
- Chen, T.W., Wardill, T.J., Sun, Y., Pulver, S.R., Renninger, S.L., Baohuan, A., Schreiter, E.R., Kerr, R.A., Orger, M.B., Jayaraman, V., et al. (2013). Ultrasensitive fluorescent proteins for imaging neuronal activity. *Nature* 499, 295-300.
- Choi, K.Y., Chung, S., and Roche, K.W. (2011). Differential binding of calmodulin to group I metabotropic glutamate receptors regulates receptor trafficking and signaling. *J. Neurosci.* 31, 5921-5930.
- Cochoy, D.M., Kolevzon, A., Kajiwara, Y., Schoen, M., Pascual-Lucas, M., Lurie, S., Buxbaum, J.D., Boeckers, T.M., and Schmeisser, M.J. (2015). Phenotypic and functional analysis of SHANK3 stop mutations identified in individuals with ASD and/or ID. *Mol. Autism* 6, 23.
- Cunha-Ferreira, I., Chazeau, A., Buijs, R.R., Stucchi, R., Will, L., Pan, X., Adolfs, Y., van der Meer, C., Wolhuis, J.C., Kahn, O.I., et al. (2018). The HAUS Complex Is a Key Regulator of Non-centrosomal Microtubule Organization during Neuronal Development. *Cell Rep.* 24, 791-800.
- Czöndör, K., Mondin, M., Garcia, M., Heine, M., Frischknecht, R., Choquet, D., Sibarita, J.B., and Thoumine, O.R. (2012). Unified quantitative model of AMPA receptor trafficking at synapses. *Proc. Natl. Acad. Sci. USA* 109, 3522-3527.
- Dhami, G.K., and Ferguson, S.S. (2006). Regulation of metabotropic glutamate receptor signaling, desensitization and endocytosis. *Pharmacol. Ther.* 111, 260-271.
- Duffney, L.J., Wei, J., Cheng, J., Liu, W., Smith, K.R., Kittler, J.T., and Yan, Z. (2013). Shank3 deficiency induces NMDA receptor hypofunction via an actin-dependent mechanism. *J. Neurosci.* 33, 15767-15778.
- Duffney, L.J., Zhong, P., Wei, J., Matas, E., Cheng, J., Qin, L., Ma, K., Dietz, D.M., Kajiwara, Y., Buxbaum, J.D., and Yan, Z. (2015). Autism-like Deficits in Shank3-Deficient Mice Are Rescued by Targeting Actin Regulators. *Cell Rep.* 11, 1400-1413.
- Esteves da Silva, M., Adrian, M., Schätzle, P., Lipka, J., Watanabe, T., Cho, S., Futai, K., Wierenga, C.J., Kapitein, L.C., and Hoogenraad, C.C. (2015). Positioning of AMPA Receptor-Containing Endosomes Regulates Synapse Architecture. *Cell Rep.* 13, 933-943.
- Falcón-Pérez, J.M., Nazarian, R., Sabatti, C., and Dell'Angelica, E.C. (2005). Distribution and dynamics of Lamp1-containing endocytic organelles in fibroblasts deficient in BLOC-3. *J. Cell Sci.* 118, 5243-5255.
- Fourgeaud, L., Bessis, A.S., Rossignol, F., Pin, J.P., Olivo-Marin, J.C., and Hémar, A. (2003). The metabotropic glutamate receptor mGluR5 is endocytosed by a clathrin-independent pathway. *J. Biol. Chem.* 278, 12222-12230.
- Francesconi, A., Kumari, R., and Zukin, R.S. (2009). Regulation of group I metabotropic glutamate receptor trafficking and signaling by the caveolar/lipid raft pathway. *J. Neurosci.* 29, 3590-3602.
- Gray, N.W., Fourgeaud, L., Huang, B., Chen, J., Cao, H., Oswald, B.J., Hémar, A., and McNiven, M.A. (2003). Dynamin 3 is a component of the postsynapse, where it interacts with mGluR5 and Homer. *Curr. Biol.* 13, 510-515.
- Gross, G.G., Junge, J.A., Mora, R.J., Kwon, H.B., Olson, C.A., Takahashi, T.T., Liman, E.R., Ellis-Davies, G.C., McGee, A.W., Sabatini, B.L., et al. (2013). Recombinant probes for visualizing endogenous synaptic proteins in living neurons. *Neuron* 78, 971-985.
- Hoogenraad, C.C., Popa, I., Futai, K., Martinez-Sanchez, E., Wulf, P.S., van Vlijmen, T., Dortland, B.R., Oorschot, V., Govers, R., Monti, M., et al. (2010). Neuron specific Rab4 effector GRASP-1 coordinates membrane

- specialization and maturation of recycling endosomes. *PLoS Biol.* 8, e1000283.
- Isa, M., Asanuma, D., Namiki, S., Kumagai, K., Kojima, H., Okabe, T., Nagano, T., and Hirose, K. (2014). High-throughput screening system to identify small molecules that induce internalization and degradation of HER2. *ACS Chem. Biol.* 9, 2237-2241.
- Kawabata, S., Tsutsumi, R., Kohara, A., Yamaguchi, T., Nakanishi, S., and Okada, M. (1996). Control of calcium oscillations by phosphorylation of metabotropic glutamate receptors. *Nature* 383, 89-92.
- Kessels, M.M., Engqvist-Goldstein, A.E., Drubin, D.G., and Qualmann, B. (2001). Mammalian Abp1, a signal-responsive F-actin-binding protein, links the actin cytoskeleton to endocytosis via the GTPase dynamin. *J. Cell Biol.* 153, 351-366.
- Kouser, M., Speed, H.E., Dewey, C.M., Reimers, J.M., Widman, A.J., Gupta, N., Liu, S., Jaramillo, T.C., Bangash, M., Xiao, B., et al. (2013). Loss of predominant Shank3 isoforms results in hippocampus-dependent impairments in behavior and synaptic transmission. *J. Neurosci.* 33, 18448-18468.
- Lee, J.H., Lee, J., Choi, K.Y., Hepp, R., Lee, J.Y., Lim, M.K., Chatani-Hinze, M., Roche, P.A., Kim, D.G., Ahn, Y.S., et al. (2008). Calmodulin dynamically regulates the trafficking of the metabotropic glutamate receptor mGluR5. *Proc. Natl. Acad. Sci. USA* 105, 12575-12580.
- Lee, K., Vyas, Y., Garner, C.C., and Montgomery, J.M. (2019). Autism-associated Shank3 mutations alter mGluR expression and mGluR-dependent but not NMDA receptor-dependent long-term depression. *Synapse* 73, e22097.
- Lois, C., Hong, E.J., Pease, S., Brown, E.J., and Baltimore, D. (2002). Germline transmission and tissue-specific expression of transgenes delivered by lentiviral vectors. *Science* 295, 868-872.
- Lu, J., Helton, T.D., Blanpied, T.A., Rácz, B., Newpher, T.M., Weinberg, R.J., and Ehlers, M.D. (2007). Postsynaptic positioning of endocytic zones and AMPA receptor cycling by physical coupling of dynamin-3 to Homer. *Neuron* 55, 874-889.
- Lüscher, C., and Huber, K.M. (2010). Group 1 mGluR-dependent synaptic long-term depression: mechanisms and implications for circuitry and disease. *Neuron* 65, 445-459.
- MacGillavry, H.D., Song, Y., Raghavachari, S., and Blanpied, T.A. (2013). Nanoscale scaffolding domains within the postsynaptic density concentrate synaptic AMPA receptors. *Neuron* 78, 615-622.
- MacGillavry, H.D., Kerr, J.M., Kassner, J., Frost, N.A., and Blanpied, T.A. (2016). Shank-cortactin interactions control actin dynamics to maintain flexibility of neuronal spines and synapses. *Eur. J. Neurosci.* 43, 179-193.
- Macia, E., Ehrlich, M., Massol, R., Boucrot, E., Brunner, C., and Kirchhausen, T. (2006). Dynasore, a cell-permeable inhibitor of dynamin. *Dev. Cell* 10, 839-850.
- Mao, L., Yang, L., Tang, Q., Samdani, S., Zhang, G., and Wang, J.Q. (2005). The scaffold protein Homer1b/c links metabotropic glutamate receptor 5 to extracellular signal-regulated protein kinase cascades in neurons. *J. Neurosci.* 25, 2741-2752.
- McNiven, M.A., Kim, L., Krueger, E.W., Orth, J.D., Cao, H., and Wong, T.W. (2000). Regulated interactions between dynamin and the actin-binding protein cortactin modulate cell shape. *J. Cell Biol.* 151, 187-198.
- Naisbitt, S., Kim, E., Tu, J.C., Xiao, B., Sala, C., Valtschanoff, J., Weinberg, R.J., Worley, P.F., and Sheng, M. (1999). Shank, a novel family of postsynaptic density proteins that binds to the NMDA receptor/PSD-95/GKAP complex and cortactin. *Neuron* 23, 569-582.
- Nash, M.S., Schell, M.J., Atkinson, P.J., Johnston, N.R., Nahorski, S.R., and Challiss, R.A. (2002). Determinants of metabotropic glutamate receptor 5-mediated Ca²⁺ and inositol 1,4,5-trisphosphate oscillation frequency. Receptor density versus agonist concentration. *J. Biol. Chem.* 277, 35947-35960.
- Ochoa, G.C., Slepnev, V.I., Neff, L., Ringstad, N., Takei, K., Daniell, L., Kim, W., Cao, H., McNiven, M., Baron, R., and De Camilli, P. (2000). A functional link between dynamin and the actin cytoskeleton at podosomes. *J. Cell Biol.* 150, 377-389.
- Okamoto, P.M., Gamby, C., Wells, D., Fallon, J., and Vallee, R.B. (2001). Dynamin isoform-specific interaction with the shank/ProSAP scaffolding proteins of the postsynaptic density and actin cytoskeleton. *J. Biol. Chem.* 276, 48458-48465.
- Parkinson, G.T., Chamberlain, S.E.L., Jaafari, N., Turvey, M., Mellor, J.R., and Hanley, J.G. (2018). Cortactin regulates endo-lysosomal sorting of AMPARs via direct interaction with GluA2 subunit. *Sci. Rep.* 8, 4155.
- Petrini, E.M., Lu, J., Cognet, L., Lounis, B., Ehlers, M.D., and Choquet, D. (2009). Endocytic trafficking and recycling maintain a pool of mobile surface AMPA receptors required for synaptic potentiation. *Neuron* 63, 92-105.
- Qualmann, B., Boeckers, T.M., Jeromin, M., Gundelfinger, E.D., and Kessels, M.M. (2004). Linkage of the actin cytoskeleton to the postsynaptic density via direct interactions of Abp1 with the ProSAP/Shank family. *J. Neurosci.* 24, 2481-2495.
- Rácz, B., Blanpied, T.A., Ehlers, M.D., and Weinberg, R.J. (2004). Lateral organization of endocytic machinery in dendritic spines. *Nat. Neurosci.* 7, 917-918.

- Rosendale, M., Julli , D., Choquet, D., and Perrais, D. (2017). Spatial and Temporal Regulation of Receptor Endocytosis in Neuronal Dendrites Revealed by Imaging of Single Vesicle Formation. *Cell Rep.* 18, 1840-1847.
- Scheefhals, N., and MacGillavry, H.D. (2018). Functional organization of post-synaptic glutamate receptors. *Mol. Cell. Neurosci.* 91, 82-94.
- Schmeisser, M.J., Ey, E., Wegener, S., Bockmann, J., Stempel, A.V., Kuebler, A., Janssen, A.L., Udvardi, P.T., Shiban, E., Spilker, C., et al. (2012). Autistic-like behaviours and hyperactivity in mice lacking ProSAP1/Shank2. *Nature* 486, 256-260.
- Tu, J.C., Xiao, B., Naisbitt, S., Yuan, J.P., Petralia, R.S., Brakeman, P., Doan, A., Aakalu, V.K., Lanahan, A.A., Sheng, M., and Worley, P.F. (1999). Coupling of mGluR/Homer and PSD-95 complexes by the Shank family of postsynaptic density proteins. *Neuron* 23, 583-592.
- Verpelli, C., Dvoretzkova, E., Vicidomini, C., Rossi, F., Chiappalone, M., Schoen, M., Di Stefano, B., Mantegazza, R., Broccoli, V., Bockers, T.M., et al. (2011). Importance of Shank3 protein in regulating metabotropic glutamate receptor 5 (mGluR5) expression and signaling at synapses. *J. Biol. Chem.* 286, 34839-34850.
- Vicidomini, C., Ponzoni, L., Lim, D., Schmeisser, M.J., Reim, D., Morello, N., Orellana, D., Tozzi, A., Durante, V., Scalmani, P., et al. (2017). Pharmacological enhancement of mGlu5 receptors rescues behavioral deficits in SHANK3 knock-out mice. *Mol. Psychiatry* 22, 689-702.

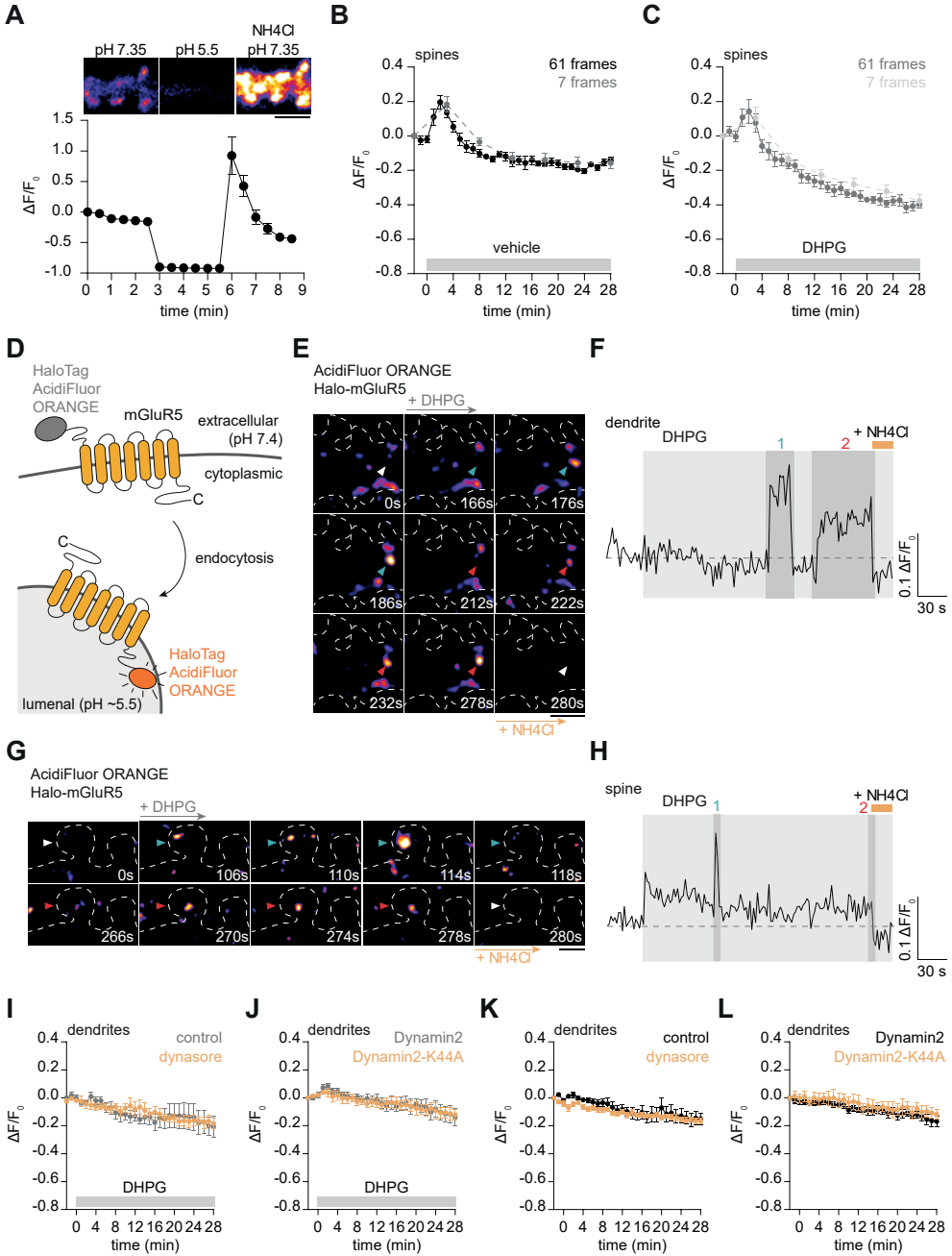


Figure S1, related to Figure 1. Characterization of SEP-mGluR5 fluorescence and evaluation of dendritic internalization

(A) Surface SEP-mGluR5 fluorescence intensity in imaging buffer with pH 7.35 ($t = 0 - 3$ min), is quenched at pH 5.5 ($t = 3 - 6$ min) and increased in fluorescence upon the application of imaging buffer containing NH_4Cl with pH 7.35 ($t = 6$ min) visualizing both surface and intracellular SEP-mGluR5 ($n = 6$). Scale bar, $2 \mu\text{m}$. (B) Quantification of SEP-mGluR5 intensity in spines over a 30-minute time period comparing the loss of SEP-mGluR5 intensity when imaged every 5 minutes (7 frames; dashed light grey line; $n = 12$) and when imaged every 30 seconds (61 frames; solid black line; $n = 8$) after application with vehicle and (C) after DHPG stimulation (7 frames; dashed light grey line; $n = 12$ and 61 frames; solid dark grey line; $n = 6$). The data sets from 61 frames shown in B and C are also shown in Figure 1G, as these figures describe different aspects of the same experiment. (D) Schematic of Halo-tag labeled with AcidiFluor ORANGE fused to mGluR5 to reveal acidification of Halo-mGluR5-containing endocytic vesicles. (E) Representative image of a dendrite expressing Halo-mGluR5 labeled with AcidiFluor ORANGE stimulated with DHPG (at $t = 40$ s) showing two acidification events, and quenching of the signal upon application of imaging buffer containing NH_4Cl with pH 7.35 ($t = 280$ s) at the dendritic shaft and (G) in a spine. Arrowheads indicate two acidification events (1; blue and 2; red). Scale bars, $2 \mu\text{m}$. (F) $\Delta F/F_0$ trace of the Halo-mGluR5 signal intensity, showing the baseline ($t = 0 - 40$ s), application of DHPG ($t = 42 - 178$ s; light grey), the acidification events shown in E and G (dark grey) and the application of NH_4Cl ($t = 280 - 300$ s; orange) at the dendritic shaft shown in E (indicated by arrowhead) and (H) in the spine shown in G (indicated by arrowhead). (I) Quantification of SEP-mGluR5 intensity in dendrites over time after DHPG stimulation comparing the time course of SEP-mGluR5 intensity in control neurons (grey; $n = 6$) with neurons pre-treated with dynasore (orange; $n = 6$) and (J) in neurons co-transfected with Dyn2 (grey; $n = 6$) with neurons co-transfected with the dominant negative Dyn2-K44A (orange; $n = 6$). (K) Quantification of SEP-mGluR5 intensity in dendrites over time without the addition of DHPG comparing the time course of SEP-mGluR5 intensity in control neurons (black; $n = 6$) with neurons pre-treated with dynasore (orange; $n = 8$) and (L) in neurons co-transfected with Dyn2 (grey; $n = 6$) with neurons cotransfected with the dominant negative Dyn2-K44A (orange; $n = 6$). Data are represented as mean \pm SEM.

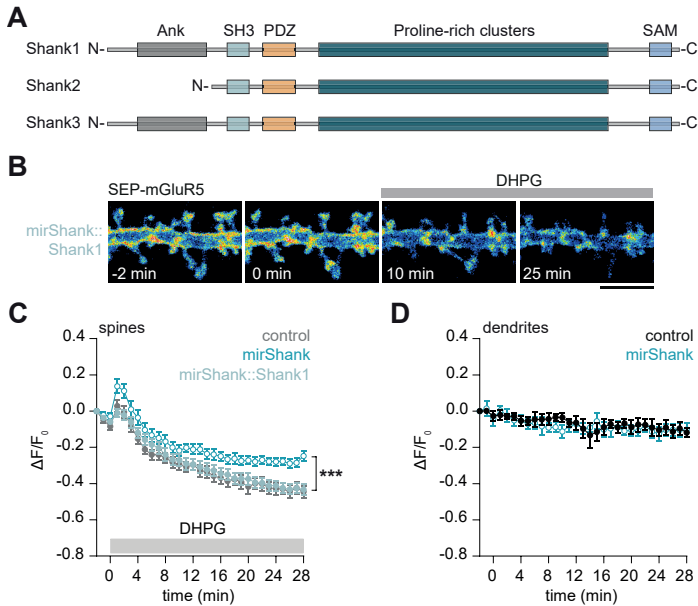


Figure S2, related to Figure 2. Re-expression of Shank1 rescues agonist-induced mGluR5 internalization in spines

(A) Domain structure of Shank1, Shank2 and Shank3. (B) Representative live-cell time-lapse image of SEP-mGluR5 before and after DHPG stimulation (added at $t = 0$ min) in mirShank::Shank1 neurons. Scale bar, 5 μm . (C) Quantification of SEP-mGluR5 intensity in spines over time after the addition of DHPG comparing the time course of SEP-mGluR5 intensity in control (grey; $n = 14$), mirShank (blue; open circles; $n = 17$) and mirShank::Shank1 rescue neurons (shade of blue; closed circles; $n = 22$). (D) Quantification of SEP-mGluR5 intensity in dendrites over time without the addition of DHPG comparing the time course of SEP-mGluR5 intensity in control (black; $n = 5$) and mirShank neurons (blue; $n = 5$). Data are represented as mean \pm SEM. ***, indicates $P < 0.001$.

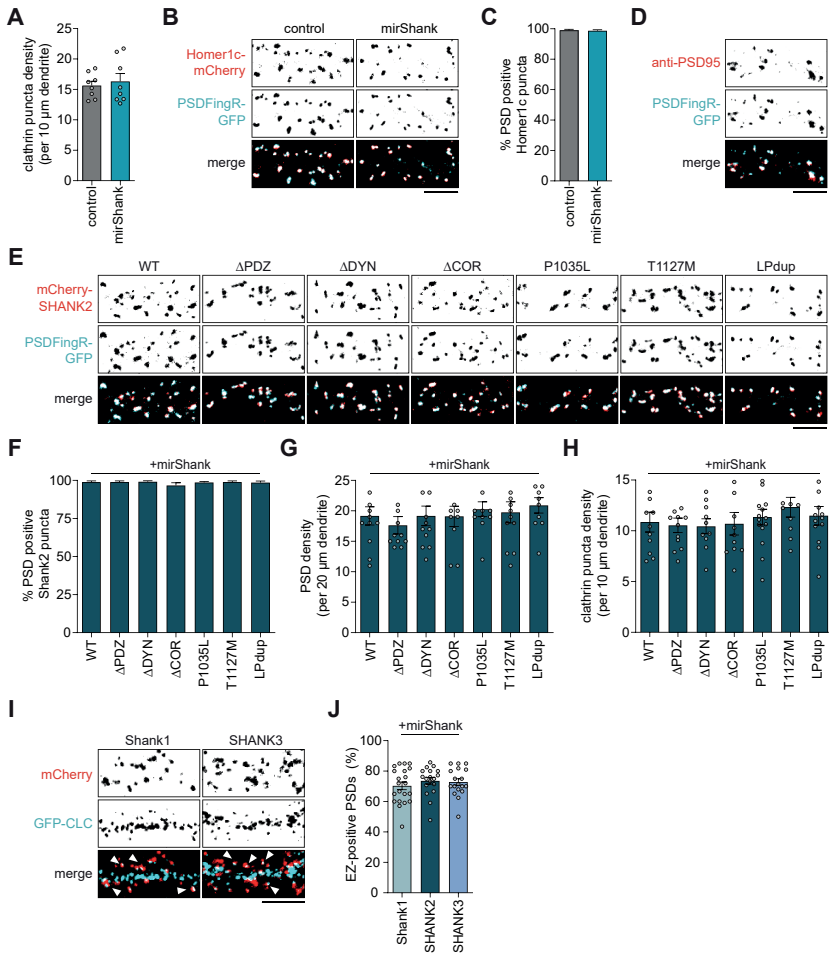


Figure S3, related to Figure 3. Clathrin puncta density in dendrites, mGluR5 spine enrichment and synaptic targeting of SHANK2 mutants

(A) Quantification of the density of GFP-CLC puncta along the dendrite (per 10 μm) in control (n = 8) and mirShank (n=8) neurons. (B) Representative images of dendrites co-expressing PSDFingR-GFP (cyan) and Homer1c-mCherry (red) in control and mirShank neurons. Scale bar, 5 μm . (C) Quantification of the percentage of Homer1c-mCherry puncta positive for PSDFingR-GFP, a marker of the PSD, in control (n = 10) and mirShank (n = 11) neurons. (D) Co-localization of PSDFingR-GFP (cyan) and immuno-labeled anti-PSD-95 (red). Scale bar, 5 μm . (E) Representative images of dendrites co-expressing mCherry-tagged SHANK2 rescue constructs (red) and PSDFingR-GFP (cyan). Scale bar, 5 μm . (F) Quantification of the percentage of mCherry-tagged WT and mutant SHANK2 puncta positive for PSDFingR-GFP, a marker of the PSD (WT: n = 12, Δ PDZ: n = 11, Δ DYN: n = 12, Δ COR: n = 10, P1035L: n = 11, T1127M: n = 12, LPdup: n = 10). (G) Quantification of the density of PSDs, marked by PSDFingR-GFP, along the dendrite (per 20 μm) in neurons co-expressing the mCherry-tagged SHANK2 rescue constructs (WT: n = 12, Δ PDZ: n = 11, Δ DYN: n = 12, Δ COR: n = 10, P1035L: n = 11, T1127M: n = 12, LPdup: n = 10). (H) Quantification of the density of GFP-CLC puncta along the dendrite (per 10 μm) in neurons co-expressing mCherry-tagged SHANK2 rescue constructs (WT: n = 11, Δ PDZ: n = 12, Δ DYN: n = 10, Δ COR: n = 11, P1035L: n = 15, T1127M: n = 10, LPdup: n = 13). (I) Representative images of dendrites co-expressing mCherry-tagged Shank1, SHANK2 and SHANK3 rescue constructs (red) and GFP-CLC (cyan). Scale bar, 5 μm . (J) Quantification of the percentage of EZ-positive PSDs in neurons co-expressing mCherry-tagged Shank1 (n = 21), SHANK2 (n = 18) and SHANK3 (n = 18) rescue constructs. Data are represented as mean \pm SEM.

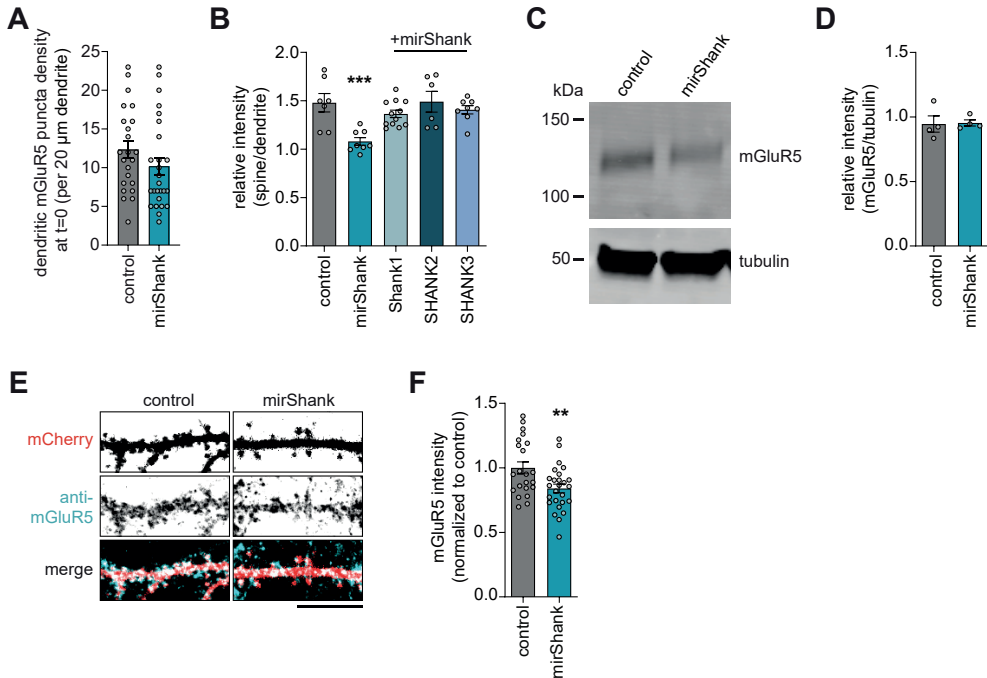


Figure S4, related to Figure 4. Shank proteins control surface and total expression of mGluR5

(A) Quantification of internalized myc-mGluR5 puncta density in dendrites of control ($n = 23$) and mirShank neurons ($n = 26$) at $t = 0$. (B) Quantification of SEP-mGluR5 intensity in spines over dendritic shaft of control ($n = 7$), mirShank ($n = 8$), mirShank::Shank1 ($n = 12$), mirShank::SHANK2 ($n = 6$) and mirShank::SHANK3 ($n = 9$) rescue neurons. (C) Western blot analysis of total lysates of neurons infected with GFP and GFP::mirShank and immuno-labelled for anti-mGluR5; tubulin was used as a loading control. (D) Quantification of anti-mGluR5 over tubulin intensity in control and mirShank neurons ($n = 3$). (E) Representative images of dendrites immuno-labeled for anti-mGluR5 (cyan) in mCherry-tagged control and mirShank neurons (red). Scale bar, 10 μ m. (F) Quantification of anti-mGluR5 intensity along the dendrite (20 μ m) in control ($n = 20$) and mirShank ($n = 27$) neurons, normalized to the average intensity of anti-mGluR5 fluorescence in the control condition. Data are represented as mean \pm SEM. **, indicates $P < 0.01$ and ***, indicates $P < 0.001$.

Key Resources Table

REAGENT or RESOURCE	SOURCE	IDENTIFIER
Antibodies		
Mouse anti-c-Myc (9E10) Monoclonal Antibody	Santa Cruz Biotechnology	Cat# sc-40; RRID: AB_627268
Human anti-EEA1 Antibody (clone 4114)	M. Fritzler	N/A
Rabbit anti-mGluR5 Antibody	Millipore	Cat# 06-451; RRID: AB_2313604
Rabbit anti-phospho-ERK1/2 Antibody	Cell Signaling	Cat# 9101; RRID: AB_331646
Mouse anti-PSD-95 Antibody	Neuromab	Cat# 75-028; RRID: AB_2292909
Mouse anti-Clathrin Heavy Chain (X22) Monoclonal Antibody	Thermo Fisher Scientific	Cat# MA1-065; RRID: AB_2083179
Rabbit anti-Homer1 Antibody	Synaptic Systems	Cat# 160 006; RRID: AB_2631222
Mouse anti-alpha-tubulin	Sigma-Aldrich	Cat# T6074, RRID: AB_477582
Goat anti-Human IgG (H+L) Secondary Antibody, Alexa Fluor 568	Thermo Fisher Scientific	Cat# A-21090; RRID: AB_2535746
Goat anti-Mouse IgG (H+L) Secondary Antibody, Alexa Fluor 647	Thermo Fisher Scientific	Cat# A-21236; RRID: AB_2535805
Goat anti-Mouse IgG (H+L) Secondary Antibody, Alexa Fluor 488	Thermo Fisher Scientific	Cat# A-11029; RRID: AB_2534088
Goat anti-Rabbit IgG (H+L) Secondary Antibody, Alexa Fluor 488	Thermo Fisher Scientific	Cat# A-11034; RRID: AB_2576217
Swine anti-mouse HRP-conjugated	Agilent	Cat# P0260; RRID: AB_263692
Goat Anti-Rabbit IgG Secondary Antibody, IRDye 680LT	LI-COR Biosciences	Cat# 827-11081; RRID: AB_10795015
Goat Anti-Mouse IgG Secondary Antibody, IRDye 800CW	LI-COR Biosciences	Cat# 827-08364; RRID: AB_10793856
Bacterial and Virus Strains		
Escherichia coli: BL21DE3	N/A	N/A
Chemicals, Peptides, and Recombinant Proteins		
Lipofectamine 2000	Thermo Fisher Scientific	Cat# 11668019
(S)-3,5-DHPG	Tocris	Cat# 805
Dynasore	Tocris	Cat# 2897
MPEP hydrochloride	Tocris	Cat# 1212
Tetrodotoxin citrate	Tocris	Cat# 1069
Polyvinyl alcohol mounting medium with DABCO®, antifading (Mowiol)	Sigma Aldrich	Cat# 10981
HaloTag® AcidiFluor™ORANGE Ligand	GORYO Chemical	Cat# GC310-01
Experimental Models: Cell Lines		
Human embryonic kidney 239T (HEK293T)	ATCC	Cat# CRL-3216; RRID: CVCL_0063
Experimental Models: Organisms/Strains		
Rattus norvegicus (Wistar; HanRj;WI)	RGD, Janvier labs	Cat# 13792727; RRID: RGD_13792727
Oligonucleotides		
See Table S1 for miRNA targeting sequences of Shank1, 2 and 3	N/A	N/A
ΔPDZ: deleted Thr254 – Thr348 with forward primer: ATTATTGAGGAGAAGAGGAATCTGGACCCCG	This paper	N/A
ΔPDZ: deleted Thr254 – Thr348 with reverse primer: CTTCTCCTCAATAATGCAGTCA	This paper	N/A

ΔDYN: deleted Glu1114 – Ser113 with forward primer: TTTGACGCCGTCGCCGACTCTGGGATCGAGACCCTGTCT TCCGAAGGTG	This paper	N/A
ΔDYN: deleted Glu1114 – Ser113 with reverse primer: CACATTCTCTCCACCTTCGGAAGACAGGGTCTCGATCCCA GAGTCGG	This paper	N/A
T1127M: mutagenesis with forward primer: AGCGACCACCACCTCGAGATGACCAGCACTATCTCCACC G	This paper	N/A
T1127M: mutagenesis with reverse primer: CGGTGGAGATAGTGCTGGTCATCTCGAGGTGGTGGTCGC T	This paper	N/A
L1008P1009: duplication with forward primer: GTGATTTTGCCATTGCCATCCGCATCCCTCC	This paper	N/A
L1008P1009: duplication with reverse primer: GGGATGCGGAATGGCAATGGCAAATCACCGC	This paper	N/A
Recombinant DNA		
pRK5-Venus-mGluR5a	Dr. J. Perroy	N/A
pRK5-SEP-mGluR5a	This paper	N/A
pRK5-myc-mGluR5a	This paper	N/A
pRK5-Halo-mGluR5a	This paper	N/A
pRK5-SEP-mGluR1	This paper	clone image ID # 40080840
pSM155-Cer3	(MacGillavry et al., 2015)	N/A
pSM155-mCherry	This paper	N/A
pSM155-GFP	(MacGillavry et al., 2015)	N/A
pSM155-mirShank::Cer3	(MacGillavry et al., 2015)	N/A
pSM155-mirShank::mCherry	This paper	N/A
pSM155-mirShank::GFP	(MacGillavry et al., 2015)	N/A
pSM155-mirShank::mCherry-Shank1	This paper	N/A
pSM155-mirShank::mCherry-SHANK2	This paper and (MacGillavry et al., 2015)	N/A
pSM155-mirShank::mCherry-SHANK3	This paper	N/A
pSM155-mirShank::mCherry-SHANK2-ΔPDZ	This paper	N/A
pSM155-mirShank::mCherry-SHANK2-ΔDYN	This paper	N/A
pSM155-mirShank::mCherry-SHANK2-ΔCOR	This paper and (MacGillavry et al., 2015)	N/A
pSM155-mirShank::mCherry-SHANK2-P1035L	This paper and (MacGillavry et al., 2015)	N/A
pSM155-mirShank::mCherry-SHANK2-T1127M	This paper	N/A
pSM155-mirShank::mCherry-SHANK2-Lpdup	This paper	N/A
pcDNA3.1- mCherry-Shank2	Dr. Simone Berkel (Berkel et al., 2012)	N/A
mCherry-Shank3	Dr. M. Schmeisser (Cochoy et al., 2015)	N/A
pEGFP-C2-GFP-Clathrin-light-Chain	Dr. Mike Ehlers	
pmCherry-N1-Homer1c-mCherry	(MacGillavry et al., 2013)	N/A
GFP-Rab5	(Hoogenraad et al., 2010)	N/A
GFP-Rab11	(Esteves da Silva et al., 2015)	N/A
TfR-SEP	(Hoogenraad et al., 2010)	N/A
GFP-Rab7	(Hoogenraad et al., 2010)	N/A

pEGFP-N3-LAMP1-mGFP	Dr. Esteban Dell'Angelica (Falcon-Perez et al., 2005)	http://n2t.net/addgene:34831 ; RRID: Addgene_34831
pEGFP-N1-Dynamin2-GFP	Dr. Pietro De Camilli (Ochoa et al., 2000)	N/A
pEGFP-N1-Dynamin2-K44A-GFP	Dr. Pietro De Camilli (Ochoa et al., 2000)	http://n2t.net/addgene:22301 ; RRID: Addgene_22301
pGP-CMV-GcaMP6s	Dr. Douglas Kim (Chen et al., 2013)	http://n2t.net/addgene:40753 ; RRID: Addgene_40753
pCAG_PSD95.FingR-eGFP-CCR5TC	Dr. Don Arnold (Gross et al., 2013)	http://n2t.net/addgene:46295 ; RRID: Addgene_46295
FUGW	Dr. David Baltimore	http://n2t.net/addgene:14883 ; RRID: Addgene_14883
FUGW-mirShank-GFP	This paper	N/A
p.MDG2	Didier Trono	http://n2t.net/addgene:12259 ; RRID: Addgene_12259
psPAX2	Didier Trono	http://n2t.net/addgene:12260 ; RRID: Addgene_12260
Software and Algorithms		
ImageJ	NIH	https://imagej.nih.gov/ij/ ; RRID: SCR_003070
Fiji	Fiji	http://fiji.sc ; RRID: SCR_002285
GraphPad Prism 8	GraphPad	https://www.graphpad.com/scientific-software/prism/ ; RRID: SCR_002798
Adobe Illustrator CC 2017	Adobe	https://www.adobe.com/products/illustrator.html ; RRID: SCR_010279
MATLAB 2018a	MATLAB	http://www.mathworks.com/products/matlab/ ; RRID: SCR_001622

5



mGluR5 is transiently confined in perisynaptic nanodomains to shape synaptic transmission

Nicky Scheefhals¹, Manon Westra¹ and Harold D. MacGillavry¹

¹Cell Biology, Neurobiology and Biophysics, Department of Biology, Faculty of Science,
Utrecht University, Utrecht, the Netherlands

Submitted, *under revisions*

Abstract

The dynamic subsynaptic organization of glutamate receptors is key to the regulation of synaptic transmission. However, testing the nanoscale structure-function relationship of glutamate receptors at synapses has been difficult. In particular, the unique perisynaptic distribution of postsynaptic metabotropic glutamate receptors (mGluRs) is predicted to directly shape synaptic function, but key mechanistic insight into how this distribution is regulated and impacts synaptic signaling remains untested. We used complementary super-resolution imaging approaches, and developed novel molecular tools to resolve and acutely manipulate the dynamic nanoscale distribution of the postsynaptic mGluR5 receptor. We found that mGluR5 is dynamically organized at distinct perisynaptic nanodomains that are preferentially localized close to, but not in the synapse, providing these receptors flexibility to control synaptic signaling. The C-terminal domain of mGluR5 critically controlled transient perisynaptic confinement and also prevented synaptic entry of mGluR5, even when forced to interact with synaptic scaffolds. We could overcome the synaptic exclusion of mGluR5 using an inducible interaction system, allowing directed manipulation of mGluR5 distribution. We found that mGluR5 recruitment to the synapse acutely increased synaptic calcium responses. Based on these findings, we propose that transient confinement of mGluRs in perisynaptic nanodomains allows flexible modulation of synaptic transmission.

Introduction

Precise modulation of glutamatergic synaptic transmission is critical for the execution of cognitive processes. Glutamatergic transmission is mediated by two types of postsynaptic glutamate receptors: the ionotropic glutamate receptors (iGluRs), including the AMPA and NMDA-type receptors, and the group I metabotropic glutamate receptors (mGluRs), mGluR1 and mGluR5. While iGluRs carry the majority of fast signal transmission across synapses, mGluRs modulate the efficacy of synaptic signaling on longer time scales by coupling to a variety of effector systems that collectively modulate synaptic transmission and plasticity (Reiner and Levitz, 2018; Scheefhals and MacGillavry, 2018). The contribution of mGluRs to glutamatergic signaling has been found to be critical for cognitive functions such as attention and learning and memory, and disrupted mGluR signaling has been implicated in diverse neurological disorders (Lüscher and Huber, 2010). Yet, the precise organization of mGluRs within the perisynaptic zone and the underlying mechanisms, critical to efficiently modulate synaptic transmission, are still poorly understood.

Key to the modulation of receptor activation is their subsynaptic organization and alignment with presynaptic vesicle release sites. iGluRs organize in nanodomains within the postsynaptic density (PSD), aligned with vesicle release sites within the presynaptic active zone, increasing the strength of a synaptic response (Biederer et al., 2017; Kellermayer et al., 2018; MacGillavry et al., 2013; Nair et al., 2013; Tang et al., 2016; Willems et al., 2020). In contrast, group I mGluRs are enriched in the perisynaptic zone, an annular ring of approximately 200 nm surrounding the PSD, considerably further away from vesicle release events (Baude et al., 1993; Lujan et al., 1996; Nusser, 1994). A single vesicle release event induces a very local and transient glutamate gradient only activating the opposing iGluRs due to the low affinity of AMPARs and mGluRs for glutamate (0.5 – 2mM) and the slow

glutamate binding rate of NMDARs (Niswender and Conn, 2010; Paoletti et al., 2013; Traynelis et al., 2010). Kinetic profiling of mGluR activation predicts that high frequency or repetitive stimulation is required for glutamate to reach sufficient concentrations in the synaptic cleft to also activate the perisynaptic mGluRs (Bodzęta et al., 2021a; Greget et al., 2011; Marcaggi et al., 2009). Hence, the spatial segregation of these functionally distinct receptor types allows for the precise temporal control of synaptic transmission and plasticity. The synaptic density and organization of receptors is not static, but highly dynamic, governed by processes that affect receptor mobility, such as lateral diffusion, endocytosis and exocytosis and immobilization to synaptic structures (Choquet and Triller, 2013; Triller and Choquet, 2005). Disrupted mGluR mobility has been implicated in neurological and neurodegenerative disorders (Aloisi et al., 2017; Renner et al., 2010; Shrivastava et al., 2013). Thus, an understanding of the dynamic organization of mGluRs is critical to provide new insights into the mechanisms underlying synaptic transmission in both physiological and pathophysiological conditions.

Here, we used complementary super-resolution imaging approaches and found that mGluR5 is largely excluded from the core of the PSD and is preferentially confined in perisynaptic nanodomains. Interestingly, we found that the C-terminal domain of mGluR5 mediates perisynaptic confinement, but also prevents synaptic entry of mGluR5, even when forced to interact with synaptic scaffolds. We acutely disrupted the distinct perisynaptic organization of mGluR5 and observed deregulated calcium signaling at spines.

Results

mGluR5 is enriched in spines but largely excluded from the synapse

To study the distribution of surface-expressed mGluR5 in neurons, we transfected hippocampal neurons with mGluR5 coupled to an extracellular super-ecliptic pHluorin (SEP) tag, additionally labelled with a cell impermeable GFP nanobody conjugated to Atto647N. The expression of mGluR5 was observed throughout neurons, but was most prominent in the dendritic shaft and spines (Figure 1A). mGluR5 was significantly enriched in spines compared to an mCherry fill (mGluR5: 1.49 ± 0.035 and mCherry: 0.74 ± 0.04 , Figure 1B, C), but significantly less enriched compared to the PSD scaffolding protein Homer1c (mGluR5: 1.49 ± 0.029 and Homer1c: 2.16 ± 0.066 ; Figure 1C, D). Homer1c overexpression to mark the PSD did not affect mGluR5 enrichment in spines (Figure 1C, light gray bars). Next, we used gated stimulated emission depletion (gSTED) microscopy to assess mGluR5 localization relative to the PSD. Foremost, we found that mGluR5 is largely excluded from the PSD, confirming early EM studies (Baude et al., 1993; Lujan et al., 1996; Nusser, 1994) (Figure 1E, F). Also, two-color gSTED imaging of mGluR5 and the PSD, labelled with anti-PSD-95, revealed minimal co-localization between mGluR5 and the PSD (Figure S1A-D).

Endogenous mGluR5 labelled with anti-mGluR5 was similarly excluded from synapses labelled with anti-PSD-95 compared to overexpressed mGluR5 (Figure S1E-H), and rather localized close to phalloidin staining F-actin, known to be enriched in the perisynaptic zone (Frost et al., 2010) (Figure S1I-K). Furthermore, we endogenously tagged mGluR5 with an extracellular GFP-tag using the ORANGE CRISPR/Cas9-based knock-in toolbox

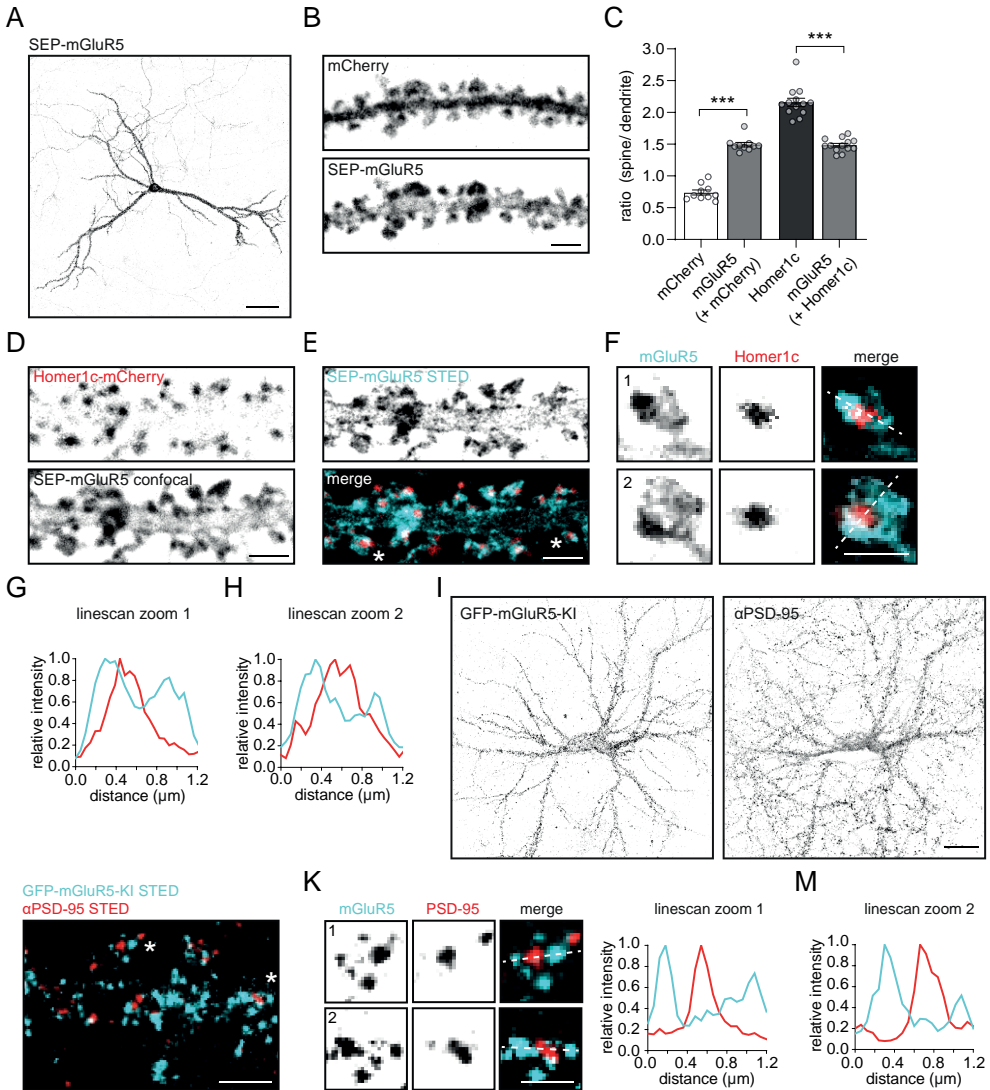


Figure 1. mGluR5 is enriched in spines but largely excluded from synapses in hippocampal neurons (A) Hippocampal neuron expressing SEP-mGluR5. Scale bar, 50 μ m. (B) Representative confocal image of dendrite expressing mCherry and SEP-mGluR5, surface-labelled with an anti-GFP nanobody Atto647N. Scale bar, 2 μ m. (C) Quantification of the ratio of spine over dendrite intensity of mCherry, surface SEP-mGluR5 co-expressing mCherry (n = 10, paired t-test), Homer1c-mCherry and surface SEP-mGluR5 co-expressing Homer1c-mCherry (n = 13, paired t-test). (D) Representative confocal image of dendrite expressing Homer1c-mCherry and SEP-mGluR5, surface-labelled with an anti-GFP nanobody Atto647N. Scale bar, 2 μ m. (E) gSTED imaging of SEP-mGluR5 surface-labelled with an anti-GFP nanobody Atto647N (cyan) and the merged image showing the relative localization to confocal resolved Homer1c-mCherry (red), shown in D. Scale bar, 2 μ m. (F) Zooms of dendritic spines indicated in E with asterisks. Scale bar, 1 μ m. (G) Linescan of spine 1 and (H) spine 2, indicated with dotted line in F. (I) Hippocampal neuron with an ORANGE GFP knock-in (KI) endogenously tagging mGluR5 at the N-terminus, enhanced with anti-GFP Alexa488 labeling (left), co-stained for anti-PSD-95 Alexa594 (right). Scale bar, 20 μ m (J) Representative two-color gSTED image of dendrite with GFP-mGluR5

Figure 1 continued on next page

Figure 1 continued

KI stained with anti-GFP Alexa488 to label surface-expressed receptors (cyan) and anti-PSD-95 Alexa594 (red). Scale bar, 2 μm . (K) Zooms of dendritic spines indicated in J with asterisks. Scale bar, 1 μm . (L) Linescan of spine 1 and (M) spine 2, indicated with dotted line in K. Data are represented as means \pm SEM. *** $p < 0.001$.

(Willems et al., 2020) (Figure 1I). gSTED imaging of the surface-labelled mGluR5 knock-in also revealed mGluR5 distribution throughout the dendrite, with preferential perisynaptic localization in spines (Figure 1J-M). Notably, the localization observed for mGluR5 is markedly different from other glutamate receptors, including AMPA receptors. GluA2, a subunit of the AMPA receptor family, co-localized with the PSD marked by Homer1c (Figure S1L-O) and localized in subsynaptic domains spatially segregated from mGluR5 shown with two-color gSTED microscopy (Figure S1P-S).

mGluR5 is organized in perisynaptic nanodomains

To resolve the nanoscale perisynaptic distribution of mGluR5 we used two-color single-molecule localization microscopy (SMLM) on neurons transfected with SEP-mGluR5, labelled with an anti-GFP nanobody coupled to Alexa647, and mEos3.2-tagged PSD_{FingR} to label the PSD (Gross et al., 2013) (Figure 2A, B and S2A). PSDs were identified using density-based spatial clustering of applications with noise (DBScan) (Ester et al., 1996) on the PSD_{FingR}-mEos3.2 localizations (Figure 2C). Consistent with our previous observations, we found that most mGluR5 localizations are within 200 nm from the PSD border (Figure 2D). To investigate this more closely, we mapped the localizations of mGluR5 and PSD_{FingR} in 8 incremental rings proportionally scaled to the PSD border to normalize for PSD size (Figure 2E and S2B) (Catsburg et al., 2021). As expected, almost all PSD_{FingR} molecules were found within the two inner synaptic rings and were almost absent from the surrounding rings. In contrast, we found that mGluR5 localizations were enriched in the three perisynaptic rings, compared to the synaptic and extrasynaptic rings (Figure 2F, also see Figure S2C for absolute number of localizations).

In these two-color SMLM experiments we observed that mGluR5 was not homogeneously distributed in the perisynaptic region. Indeed, using a density-based approach (DBScan) we found that mGluR5 is concentrated in subsynaptic nanodomains. These nanodomains were most frequently found within the perisynaptic region, with a median border-to-centroid distance from PSD to mGluR5 nanodomains of 240 nm (Figure 2G, H). The average area of individual mGluR5 nanodomains was $9.3 \times 10^3 \pm 0.7 \times 10^3 \text{ nm}^2$ (Figure 2I) and $131 \pm 3 \text{ nm}$ in length and $90 \pm 2 \text{ nm}$ in width (full width tenth maximum (FWTM); Figure 2J). The total mGluR5 nanodomain area per PSD slightly correlated with PSD area (Figure S2D). Thus, our two-color SMLM experiments revealed an unforeseen high degree of organization of mGluR5, demonstrating that mGluR5 is enriched in distinct nanodomains that preferentially localize in the perisynaptic zone.

The spatial distribution of mGluR5 diffusion at and around the synapse is highly heterogeneous

We observed a remarkable heterogeneous perisynaptic distribution of mGluR5, however we have little insight in whether mGluR5 is stably anchored at perisynaptic sites or only

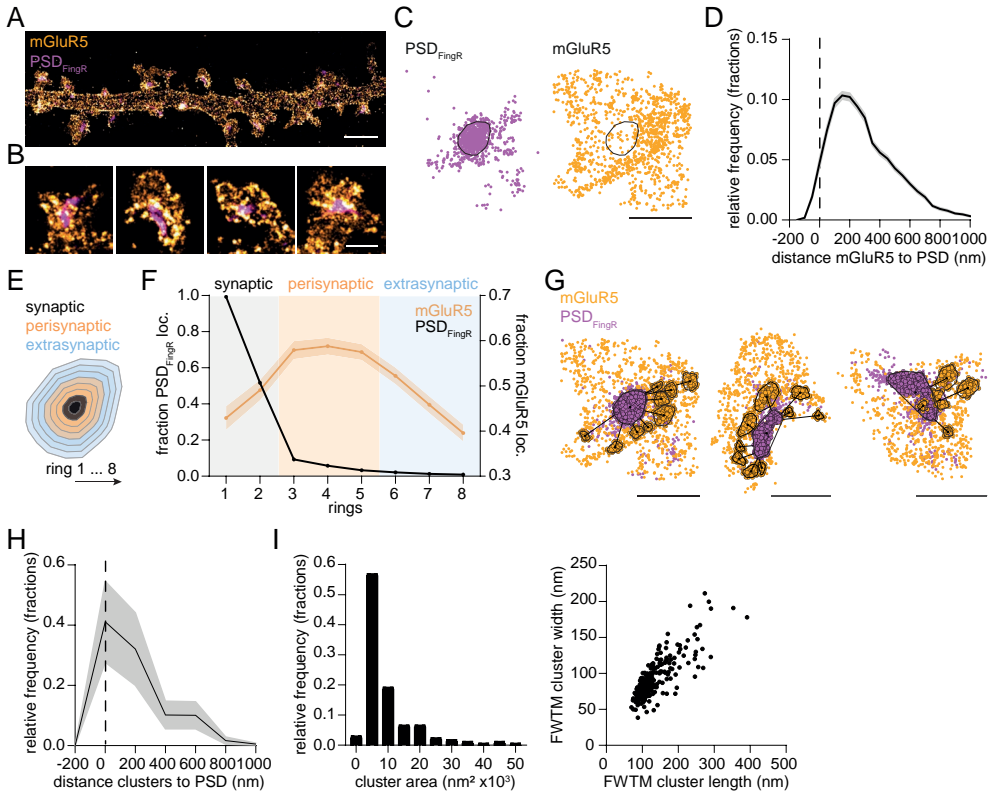


Figure 2. mGluR5 is organized in perisynaptic nanodomains

(A) Reconstruction of single-molecule localizations obtained for SEP-mGluR5 anti-GFP nanobody Alexa647 using dSTORM (orange hot) and PSD_{FingR}-mEos3.2 using PALM (cyan hot). Same dendritic region as shown in Figure S2A. Scale bar, 2 μ m. (B) Zooms of spines shown in A. Scale bar, 500 nm. (C) Representative spine with single-molecule localizations of PSD_{FingR} (cyan) and mGluR5 (orange) with indicated PSD border (black line) determined using DBScan. Scale bar, 500 nm. (D) Relative frequency distribution (fractions) of the distance of individual mGluR5 localizations to the PSD border ($n = 13$ neurons, 253 PSDs). (E) For each PSD, 8 rings, proportionally scaled based on its PSD border, defined the synapse (ring 1 and 2; black), perisynaptic zone (ring 3–5; orange) and extrasynaptic region (ring 6–8; blue). (F) Fraction of PSD_{FingR} (black; plotted on left y-axis) and mGluR5 (orange; plotted on right y-axis) localizations in rings 1 to 8. For each PSD, the number of localizations was normalized to the maximum number per ring, and the area per ring was calculated and corrected for. (G) Example spines with mGluR5 localizations (orange) belonging to clusters (black outline) as determined using DBScan, relative to PSD_{FingR} localizations (magenta). Scale bars, 500 nm. (H) Relative frequency distribution (fractions) of the distance from the center of mGluR5 clusters to the border of the PSD (as indicated in G by the black lines) ($n = 273$ clusters). (I) Relative frequency distribution (fractions) of the mGluR5 cluster area. (J) FWTM analysis comparing the width and length (in nm) of individual mGluR5 clusters. Data are represented as means \pm SEM.

transiently visits these perisynaptic nanodomains. Nevertheless, such information is critical to better understand how mGluR5 contributes to synaptic signaling. To address this, we used a single-molecule tracking (SMT) approach called universal point accumulation in nanoscale topography (uPAINT) (Giannone et al., 2010) to study the subsynaptic mobility of mGluR5. Neurons were co-transfected with SEP-mGluR5 and Homer1c-mCherry to mark the PSD (Figure 3A). SMT was performed using an anti-GFP nanobody coupled to

Atto647N that stochastically labelled individual SEP-tagged receptors, providing a map of mGluR5 mobility (Figure 3B). The diffusion coefficient of mGluR5 trajectories in spines were significantly lower than in dendrites (median D_{eff} spines: $0.022 \mu\text{m}^2/\text{s}$, dendrites: $0.036 \mu\text{m}^2/\text{s}$; Figure S3C, D). To further differentiate between mGluR5 diffusion at different synaptic subregions, we used the Homer1c-mCherry channel to mark the synaptic region (PSD mask), as well as an annulus surrounding the PSD by expanding the PSD mask with 200 nm to mark the perisynaptic zone. Importantly, we found that mGluR5 diffusion was similar in neurons expressing mCherry and Homer1c, indicating that Homer1c expression does not alter mGluR5 diffusion (Figure S3A-F). Trajectories were categorized as synaptic, perisynaptic or transient perisynaptic, all associating with the synapse and/or perisynaptic zone but to different extents (see M&M for details) (Figure S3G). Since we were interested in the mGluR5 dynamics within spines, trajectories without overlap with the synapse and/or perisynaptic zone were not included for further analysis. We found a large fraction of perisynaptic mGluR5 trajectories and a significantly smaller fraction of mGluR5 trajectories within the synapse (synaptic: 0.15 ± 0.01 , perisynaptic: 0.57 ± 0.01 , transient perisynaptic: 0.28 ± 0.01 ; Figure 3C, D and S3H), consistent with the mGluR5 distribution found using SMLM and gSTED microscopy. Interestingly, the large pool of perisynaptic mGluR5 diffused much slower compared to the mGluR5 trajectories that only transiently associated with the perisynaptic zone (median D_{eff} : synaptic: $0.014 \mu\text{m}^2/\text{s}$, perisynaptic: $0.023 \mu\text{m}^2/\text{s}$, transient perisynaptic: $0.042 \mu\text{m}^2/\text{s}$; Figure 3E, F), suggesting that mGluR5 surface mobility is specifically regulated at perisynaptic sites. The small fraction of mGluR5 within the synapse diffused at even lower rates, suggesting that although a small fraction of mGluR5 enters the PSD, these receptors are severely hindered in their diffusion.

Notably, most receptors that entered the perisynaptic zone remained there for the full duration of the observation time (here termed ‘captured’: 0.61 ± 0.01), or left the perisynaptic zone but returned to the perisynaptic zone (‘returned’: 0.29 ± 0.009). Only a very small fraction of perisynaptic tracks escaped the perisynaptic zone (‘escaped’: 0.11 ± 0.007 ; Figure 3G). Thus, corroborating our SMLM data, these observations suggest that there is an underlying mechanism that hinders free diffusion of mGluR5 specifically in the perisynaptic zone, effectively containing mGluR5 within the perisynaptic zone. Indeed, the MSD plots indicate that perisynaptic mGluR5 receptors undergo anomalous diffusion, in contrast to the transient perisynaptic mGluR5 trajectories that seem to undergo Brownian diffusion (Figure 3H).

mGluR5 is transiently confined in perisynaptic nanodomains

To further delineate how mGluR5 diffusion is locally controlled at perisynaptic sites, we next investigated the spatial distribution of mGluR5 immobilization and confinement. First, we classified mGluR5 trajectories as either mobile or immobile based on the ratio between the radius of gyration and the mean displacement per time step of individual trajectories (Golan and Sherman, 2017). We then mapped the immobile trajectories and mobile trajectories relative to the Homer1c PSD mask (Figure 4A, B and S4A, B). We found that the majority of mGluR5 trajectories was immobile (fraction of tracks: immobile: 0.65 and mobile: 0.35; Figure S4C), with an expected diffusion coefficient slower than the mobile trajectories (median D_{eff} immobile trajectories: $0.016 \mu\text{m}^2/\text{s}$ and mobile trajectories: $0.050 \mu\text{m}^2/\text{s}$; Figure S4D, E). Next, we sought to investigate whether the mobile mGluR5

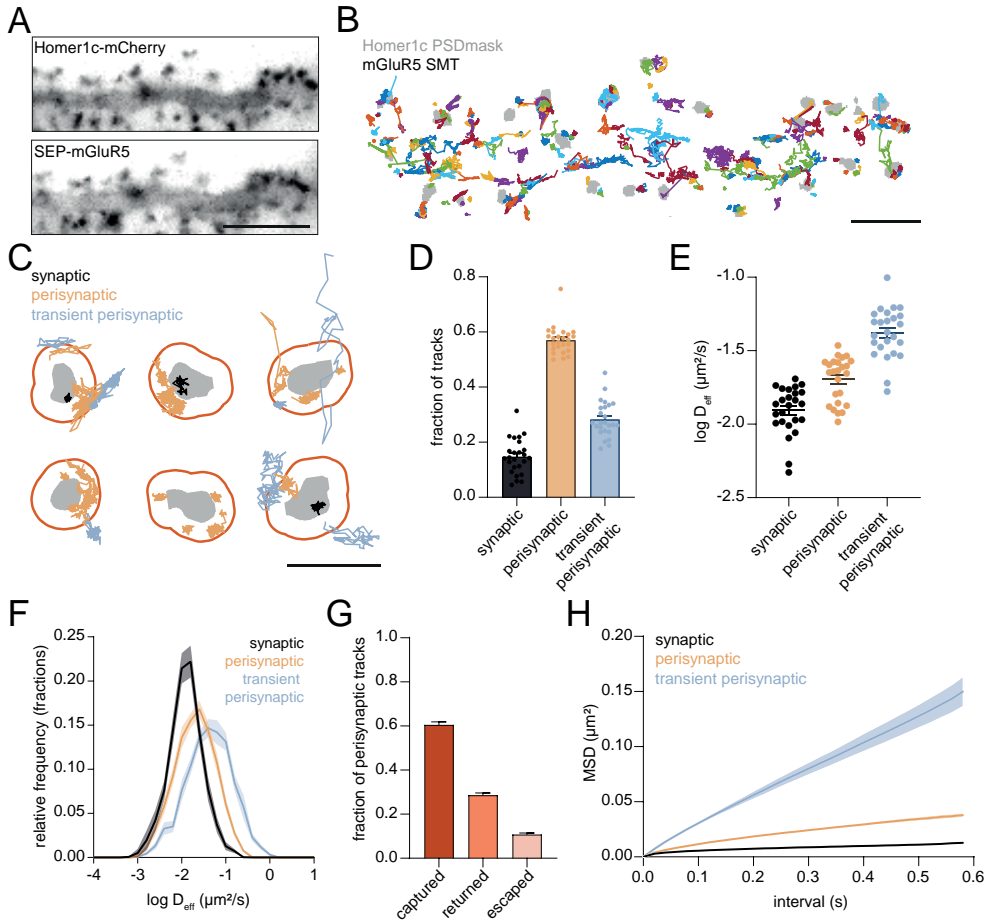


Figure 3. Distribution of mGluR5 diffusion in spines is heterogeneous

(A) Widefield of dendrite expressing Homer1c-mCherry and SEP-mGluR5. Scale bar, 5 μm . (B) Single-molecule trajectories (SMTs) of mGluR5 (each trajectory is assigned a random color) relative to the Homer1c PSD mask (grey) in the same dendrite as shown in A. Scale bar, 2 μm . (C) Example PSDs (grey) with their perisynaptic zone (orange ring) and mGluR5 SMTs color-coded for their subsynaptic localization. Scale bar, 1 μm . (D) Fraction of synaptic, perisynaptic and transient perisynaptic mGluR5 SMTs ($n = 25$ neurons). (E) Mean $\log D_{\text{eff}}$ per neuron of synaptic, perisynaptic and transient perisynaptic mGluR5 SMTs. (F) Relative frequency distributions of D_{eff} of individual synaptic, perisynaptic and transient perisynaptic mGluR5 SMTs. (H) Fraction of perisynaptic SMTs that stay within perisynaptic/synaptic region once entered (captured), exited at least once, but end up staying inside the perisynaptic/synaptic region (returned) and perisynaptic tracks that escaped the perisynaptic/synaptic region (escaped). (I) Mean MSD curve over time of synaptic, perisynaptic and transient perisynaptic mGluR5 SMTs. Data are represented as means \pm SEM.

trajectories undergo transient periods of confinement. We therefore estimated the confinement index L , which relates to the probability that a molecule undergoes confined diffusion in a region of radius R for a period of time t (Saxton, 1993; Simson et al., 1995). This analysis revealed that a substantial fraction of the mobile mGluR5 trajectories ($\sim 40\%$) undergoes transient confinement with single trajectories displaying alternating periods of free and confined diffusion. Using a critical threshold of confinement L_c we defined regions

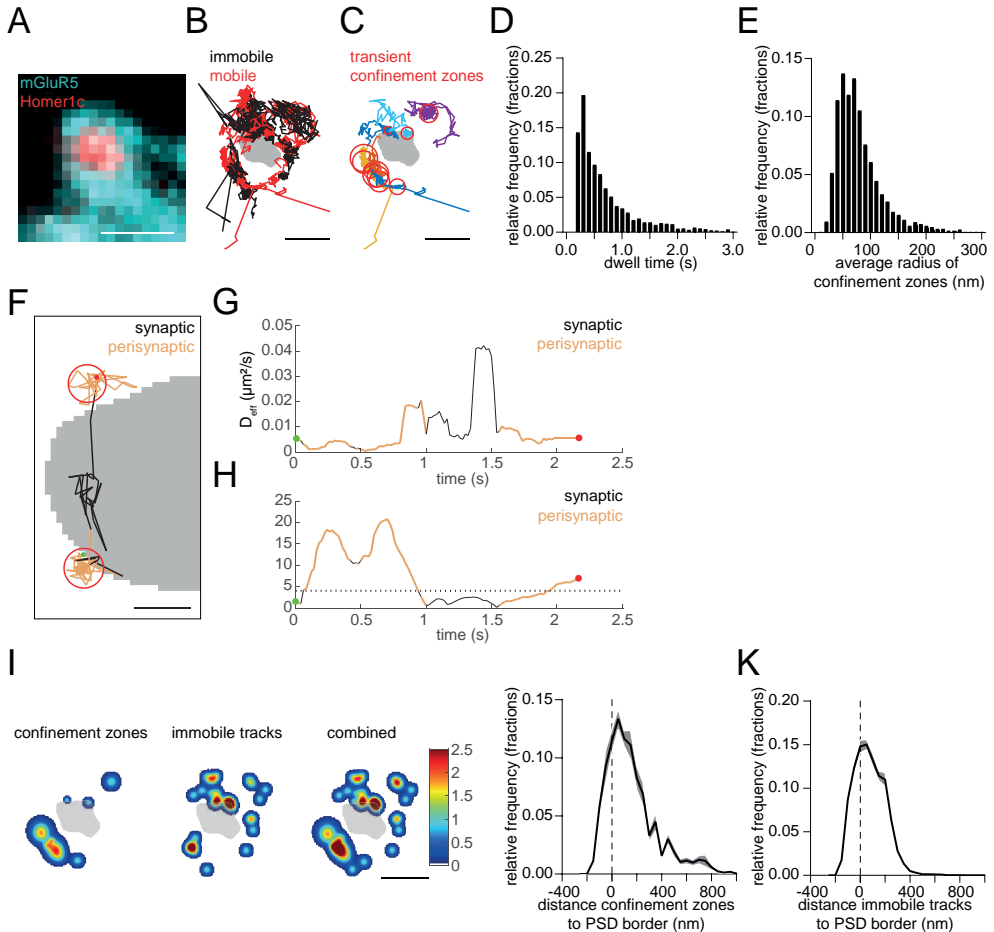


Figure 4. mGluR5 is transiently confined, but also immobilized at the perisynaptic zone

(A) Widefield image of a dendritic spine expressing SEP-mGluR5 (cyan) and Homer1c-mCherry (red). (larger ROI shown in Figure S4A). Scale bar, 1 μm . (B) The same spine as in A showing immobile (black) and mobile (red) SMTs of mGluR5 relative to the Homer1c PSD mask (larger ROI shown in Figure S4B). Scale bar, 500 nm. (C) Transient confinement zones (red circles) of the mobile trajectories (random colors) shown in B (larger ROI shown in Figure S4F). Scale bar, 500 nm. (D) Relative frequency plots of the dwell time (s) and (E) average radius of confinement zones for mGluR5 SMTs. (F) Example trajectory (assigned to perisynaptic fraction) that undergoes transient confinement in the perisynaptic zone, color-coded for entering the synapse (black) and perisynaptic zone (orange) and the confinement zones (red). The trajectory starts (green dot) and ends (red dot) in perisynaptic transient confinement zones. Scale bar, 100 nm. (G) The diffusion coefficient and (H) confinement index L over time for the trajectory shown in F, using the same color-coding. (I) The same example synapse as in A-C with hotspots of transient confinement zones, immobile tracks, and both images combined, color-coded for the frequency of confinement zones and/or immobile tracks (larger ROI shown in Figure S4I). Scale bar, 500 nm. (J) Relative frequency distribution of the distance of confinement zones of mGluR5 and (K) center of immobile mGluR5 trajectories to the border of the PSD ($= 0$ and indicated by dashed line). Data in this figure is the same dataset as used in Figure 3, as these figures show different aspects of the same experiment. Data are represented as means \pm SEM.

of confined diffusion, or confinement zones (Figure 4C and S4F). mGluR5 mobility was strongly reduced inside these confinement zones (median D_{eff} inside: $0.01 \mu\text{m}^2/\text{s}$ and outside: $0.068 \mu\text{m}^2/\text{s}$; Figure S4G, H). The average radius of confinement zones was 79.8 ± 0.97 nm, and receptors remained confined for 0.85 ± 0.03 s (Figure 4D, E). Interestingly, we frequently observed that trajectories undergo confinement specifically in the perisynaptic zone (Figure 4F-H). Indeed, when we mapped the peaks of confinement zones and centres of the immobile trajectories (see M&M for details), we detected clear hotspots of reduced mGluR5 mobility around synapses (Figure 4I and S4I). To quantify this, we determined the distance of the confinement zones to the PSD border. Strikingly we found that the vast majority of confinement zones was located within the perisynaptic zone, <100 nm from the PSD (Figure 4J). Similarly, immobile tracks were also enriched in the perisynaptic zone (Figure 4K). Together, these experiment reveal that the diffusion of mGluR5 around PSDs is highly heterogeneous and that mGluR5 is transiently confined primarily at perisynaptic zones, close to the border of the PSD.

The C-terminal domain of mGluR5 mediates perisynaptic confinement

The particular heterogeneous organization of mGluR5 dynamics suggests that specific mechanisms retain the receptor in the perisynaptic zone. The large intracellular C-terminal domain (CTD) of mGluR5a contains many protein interaction motifs and phosphorylation sites involved in surface expression and trafficking (Enz, 2012). However, whether the CTD of mGluR5 contributes to the spatial heterogeneity of surface mobility remains unknown. To test this, we generated a mutant lacking the last 314 C-terminal amino acids (SEP-mGluR5 Δ C) (Figure 5A). Truncation of the mGluR5 CTD did not impact surface expression (Figure S5A), as has been previously shown (Chang and Roche, 2017). We first used gSTED microscopy to assess the localization of surface-expressed mGluR5 Δ C relative to the PSD. Compared to mGluR5 wild-type (mGluR5WT), mGluR5 Δ C showed a similar exclusion from the PSD (Figure 5B-D). However, we found a significantly increased fraction of spines with a homogeneous distribution of mGluR5 Δ C (synaptic enrichment: WT: $11 \pm 2\%$ and Δ C: $7.1 \pm 2\%$, synaptic + perisynaptic enrichment: WT: $16 \pm 3\%$ and Δ C: $12 \pm 3\%$, perisynaptic enrichment: WT: $57 \pm 3\%$ and Δ C: $51 \pm 3\%$ and homogeneous distribution: WT: $16\% \pm 3$ and Δ C: $30\% \pm 5\%$; Figure 5D). Furthermore, the loss of the CTD resulted in the loss of mGluR5 enrichment in spines (WT: 1.47 ± 0.045 ; Δ C: 1.08 ± 0.032 ; Figure 5E and S5A).

To further investigate whether the CTD is involved in mediating mGluR5 confinement in the perisynaptic zone, we performed SMT. Significantly less mGluR5 Δ C trajectories were found to be perisynaptic, and more tracks were only transiently associated with the perisynaptic zone (Figure 5F). We also observed that mGluR5 Δ C tracks were more homogeneously distributed (Figure 5J). The diffusion coefficient was significantly increased for both perisynaptic and transient perisynaptic trajectories of mGluR5 Δ C (median D_{eff} perisynaptic: WT: $0.031 \mu\text{m}^2/\text{s}$ and Δ C: $0.056 \mu\text{m}^2/\text{s}$, median D_{eff} transient perisynaptic: WT: $0.069 \mu\text{m}^2/\text{s}$ and Δ C: $0.096 \mu\text{m}^2/\text{s}$), but not of synaptic mGluR5 Δ C trajectories (median D_{eff} synaptic: WT: $0.020 \mu\text{m}^2/\text{s}$ and Δ C: $0.026 \mu\text{m}^2/\text{s}$), compared to mGluR5WT (Figure 5G, J). Consistently, the fraction of immobile trajectories was significantly reduced for mGluR5 Δ C (WT: 0.64 ± 0.03 and Δ C: 0.44 ± 0.03 ; Figure 5K and S5B), as well as the fraction of mobile mGluR5 Δ C trajectories with transient confinement zones (WT: 0.43 ± 0.03 and Δ C: 0.25 ± 0.02 ; Figure 5L and S5C). Even when mGluR5 Δ C was transiently

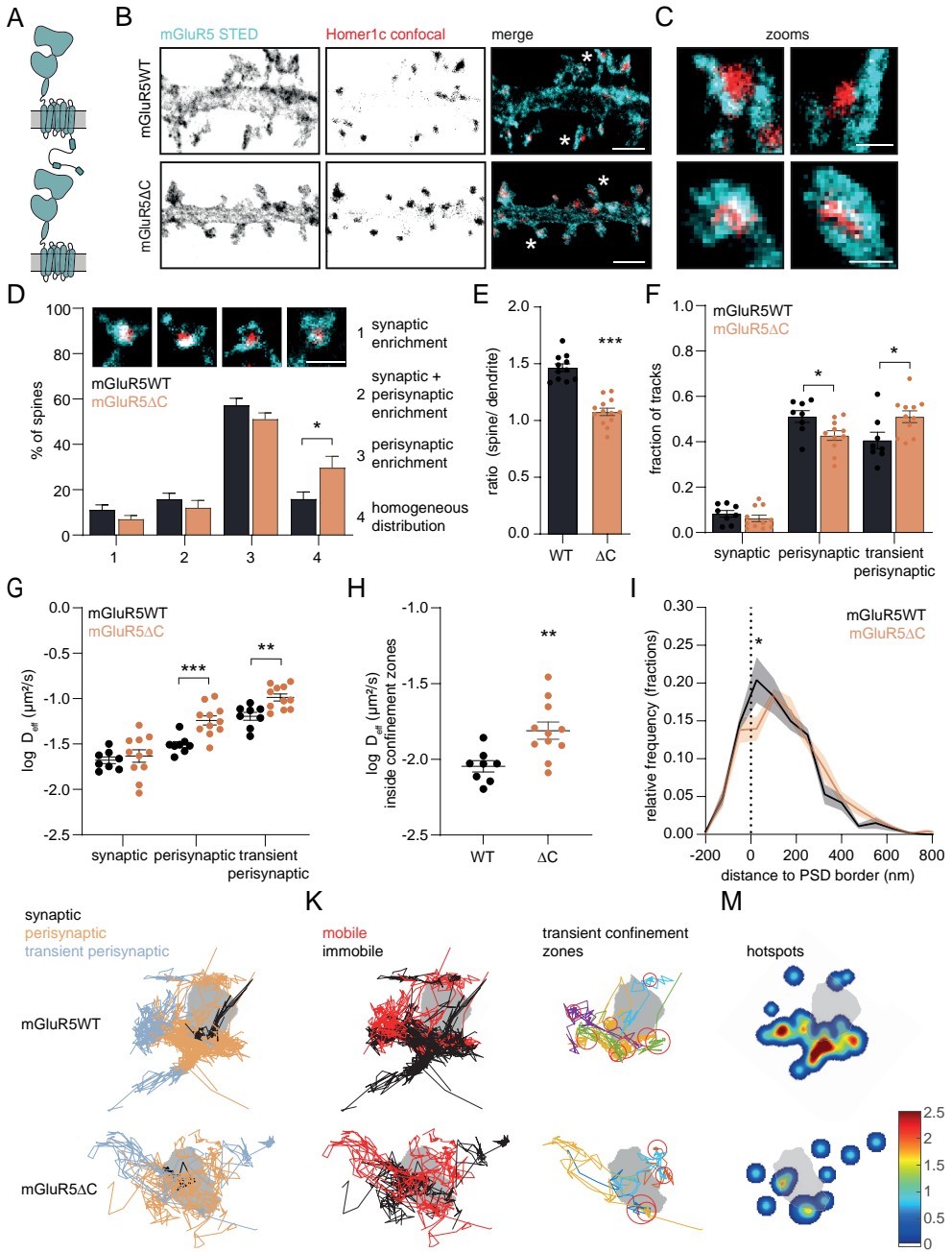


Figure 5. The C-terminal domain of mGluR5 mediates perisynaptic confinement

(A) Schematic of monomeric full-length mGluR5WT (top) and mGluR5 Δ C (bottom) lacking its C-terminal tail. (B) Representative gSTED images of dendrite expressing SEP-mGluR5WT and SEP-mGluR5 Δ C, additionally labeled with an anti-GFP nanobody Atto647N (cyan), and Homer1c-mCherry (red; confocal). Scale bar, 2 μ m. (C) Zooms of spines indicated in B with asterisks. Scale bar, 500 nm. (D) Quantification of mGluR5WT (black; n

Figure 5 continued on next page

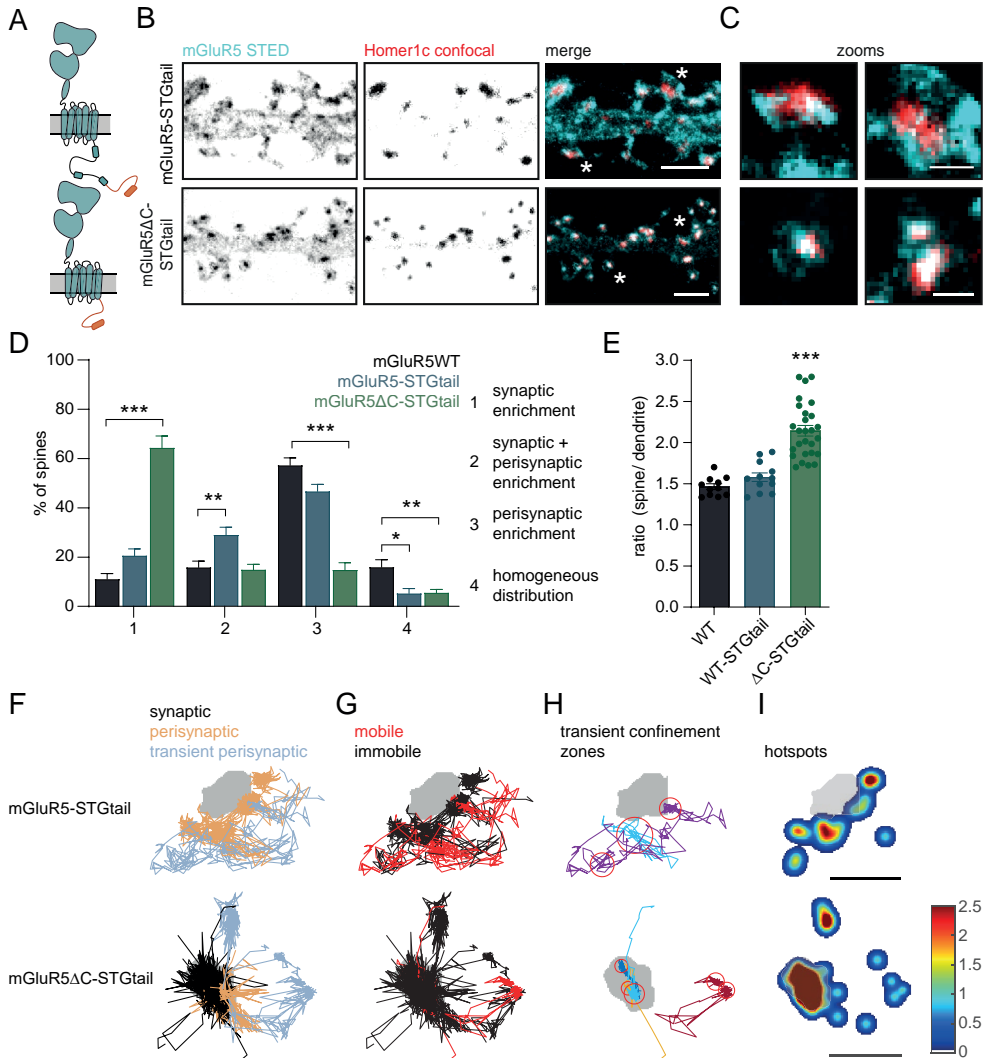
Figure 5 continued

= 16) and mGluR5 Δ C (orange; n = 14) localization in spines: (1) synaptic enrichment, (2) synaptic + perisynaptic enrichment, (3) perisynaptic enrichment and (4) homogeneous distribution (unpaired t-test for each category). On top are representative images of the different categories of mGluR5 localization (cyan), relative to Homer1c (red), at spines. Scale bar, 1 μ m. (E) Quantification of the ratio of spine over dendrite intensity of mGluR5WT (n = 11) and mGluR5 Δ C (n = 13; unpaired t-test). (F) Fraction of synaptic, perisynaptic and transient perisynaptic trajectories of mGluR5WT (n = 8) and mGluR5 Δ C (n = 11; unpaired t-test for each category). (G) Mean log D_{eff} per neuron of synaptic, perisynaptic and transient perisynaptic trajectories of mGluR5WT and mGluR5 Δ C (unpaired t-test for each category). (H) Mean log D_{eff} per neuron of trajectories inside confinement zones of mGluR5WT and mGluR5 Δ C (unpaired t-test). (I) Relative frequency distribution of the distance of confinement zones of mGluR5WT and mGluR5 Δ C to the border of the PSD (= 0 and indicated by dashed line) (two-way repeated measures ANOVA with Bonferroni's multiple comparisons test, at 25 nm distance from PSD border: p = 0.0003). (J) Example synapses of mGluR5WT and mGluR5 Δ C with trajectories color-coded for being synaptic (black), perisynaptic (orange) and transient perisynaptic (blue), (K) for being mobile (red) and immobile (black), (L) for being transiently confined trajectories (random colors) with corresponding confinement zones (red circles), and (M) hotspots of immobile tracks (shown in K) and confinement zones (shown in L), color-coded for their frequency. Scale bars, 500 nm. Data are represented as means \pm SEM. *p < 0.05, **p < 0.01 and ***p < 0.001.

confined, diffusion inside the confinement zones was significantly faster compared to mGluR5WT (median D_{eff} WT: 0.0094 $\mu\text{m}^2/\text{s}$ and Δ C: 0.015 $\mu\text{m}^2/\text{s}$; Figure 5H and S5D) and mGluR5 Δ C confinement zones were on average larger (radius WT: 76.7 \pm 2.3 nm and Δ C: 99.4 \pm 2.3 nm; Figure S5E). We found that the mGluR5 Δ C confinement zones were more homogeneously distributed and particularly showed less enrichment immediately adjacent to the PSD compared to mGluR5WT confinement zones (fraction confinement zones at 25 nm distance from PSD: WT: 0.20 \pm 0.03 and Δ C: 0.14 \pm 0.03; Figure 5I). Consistently, the map of mGluR5 Δ C confinement and immobility hotspots also revealed less pronounced areas of restricted mGluR5 diffusion in the perisynaptic zone (Figure 5M). These results further indicate that the mGluR5 CTD contributes to the transient confinement of mGluR5 in perisynaptic nanodomains.

The C-terminal domain of mGluR5 prevents synaptic entry

In stark contrast to AMPARs, mGluR5 seems to be transiently enriched in perisynaptic nanodomains, and almost completely excluded from the PSD. We therefore hypothesized that apart from mechanisms that confer perisynaptic retention of mGluR5, specific mechanisms prevent the synaptic entry of mGluR5. To begin to test this, we reasoned that we could target mGluR5 to the PSD by fusing mGluR5 to the CTD of Stargazin (STGtail), the AMPAR auxiliary protein that associates with PSD-95 to concentrate AMPARs in the PSD (Figure 6A) (Bats et al., 2007; Schnell et al., 2002). When we coupled the STGtail to a single transmembrane domain with an N-terminal SEP-tag (SEP-pDisp-STGtail), this construct was efficiently targeted to synapses marked by Homer1c-mCherry (Figure S6A-C). Surprisingly however, when mGluR5 was directly fused to the STGtail (mGluR5-STGtail), the receptor was still largely excluded from the PSD (Figure 6B-D). For mGluR5-STGtail we observed a modest but significant increase in the number of spines with synaptic and perisynaptic enrichments (mGluR5WT: 16 \pm 3% and mGluR5-STGtail: 29 \pm 3%; Figure 6D), showing that the attempt to recruit mGluR5 to the PSD by the addition of the STGtail was only successful in a few spines. This also resulted in a reduction of spines with a homogeneous distribution (mGluR5WT: 16 \pm 3% and mGluR5-STGtail: 5.3 \pm 2%; Figure 6D). Overall however, the distribution of mGluR5-STGtail was similar to mGluR5WT



5

(Figure 6B-D and Figure 5B-D), corroborated by the unchanged enrichment in spines (mGluR5WT: 1.47 ± 0.035 and mGluR5-STGtail: 1.58 ± 0.053 ; Figure 6E and S6D).

Considering that the mGluR5 CTD mediates perisynaptic confinement (Figure 5), we predicted that it may also play a critical role in preventing the synaptic entry of mGluR5. To test this idea we made a chimera construct replacing the CTD of mGluR5 for the STGtail: SEP-mGluR5 Δ C-STGtail (mGluR5 Δ C-STGtail) (Figure 6A). Interestingly, this mGluR5-Stargazin chimera was very efficiently recruited to the PSD, marked by Homer1c (Figure 6B,C). We found a 54% increase in the number of spines with synaptic enrichment, compared to mGluR5WT, and a decrease in spines with a perisynaptic distribution (mGluR5 Δ C-STGtail: synaptic enrichment: $64 \pm 5\%$, synaptic + perisynaptic enrichment: $15 \pm 2\%$, perisynaptic enrichment: $15 \pm 3\%$ and homogeneous distribution: $5.5 \pm 1\%$; Figure 6D). Furthermore, we observed a significant increase in spine enrichment of mGluR5 Δ C-STGtail (mGluR5 Δ C-STGtail: 2.14 ± 0.064 ; Figure 6E).

Similarly, SMT of mGluR5-STGtail showed that the addition of the STGtail did not affect the distribution of receptor diffusion (Figure 6F and Figure 5J). However, in the few instances that mGluR5-STGtail entered the PSD, it was more immobile compared to mGluR5WT (median synaptic D_{eff} mGluR5WT: $0.020 \mu\text{m}^2/\text{s}$ and mGluR5-STGtail: $0.015 \mu\text{m}^2/\text{s}$; Figure S6E). In contrast, the confinement zones and immobile trajectories of mGluR5 Δ C-STGtail were strongly enriched within the PSD (Figure 6G-I). Although not significant, synaptic mGluR5 Δ C-STGtail diffused at a slower rate compared to mGluR5WT, suggesting that the addition of the STGtail increased the retention in the PSD (median synaptic D_{eff} mGluR5 Δ C-STGtail: $0.014 \mu\text{m}^2/\text{s}$; Figure S6E). These results show that removing the mGluR5 CTD and increasing the affinity of mGluR5 for the PSD allow the entry and retention of mGluR5 in synapses, indicating that the mGluR5 CTD regulates both the retention and synaptic exclusion of mGluR5.

Inducible heterodimerization system allows robust and rapid recruitment of mGluR5 to the synapse

We hypothesized that the distinct segregation of ionotropic and metabotropic glutamate receptor types in different subsynaptic domains optimizes synaptic signaling. To better understand the functional relevance of mGluR5 nanodomains in the perisynaptic zone, we set out to develop a system to acutely control mGluR5 distribution to study the effect of mGluR5 positioning on synaptic signaling. To do so, we used the inducible FKBP-rapalog-FRB heterodimerization system, a reliable and robust tool to induce interactions between two proteins by the addition of rapalog (Clackson et al., 1998). To allow controlled recruitment of mGluR5 to the synaptic scaffold Homer1c we developed FRB-tagged mGluR5 and FKBP-tagged Homer1c constructs (Figure 7A). Indeed, the enrichment of mGluR5 in spines significantly increased upon the addition of rapalog (before: 1.5 ± 0.08 and 50 min after: 2.7 ± 0.2 ; Figure S7A-C). Importantly, Homer1c spine enrichment was not different between neurons incubated with rapalog and control neurons where a vehicle was added, indicating unidirectional recruitment of mGluR5 towards Homer1c, stably retained in the PSD. Live-cell imaging further demonstrated that mGluR5 accumulated within synapses over the time course of 40 minutes and we observed a clear re-distribution of mGluR5 into the PSD (Figure 7B-F). Together, these data show that this rapalog-inducible system can be employed to acutely and robustly re-locate mGluR5 to postsynaptic sites.

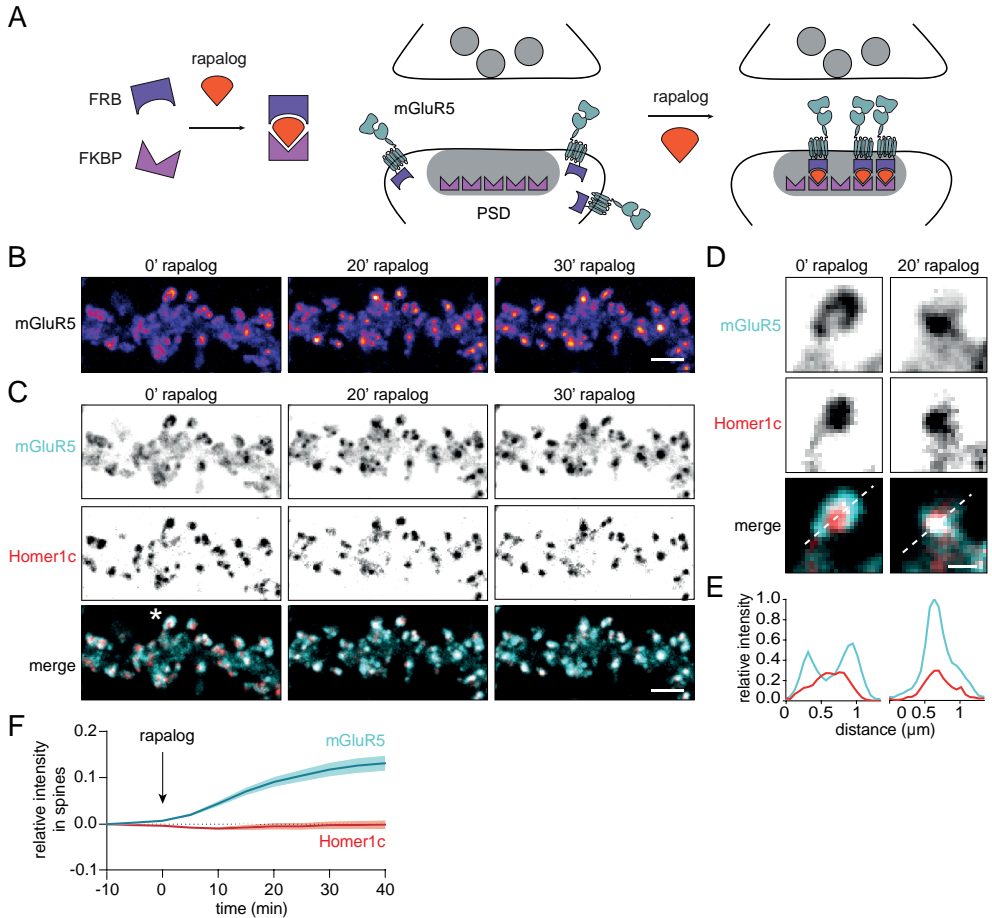


Figure 7. mGluR5 is efficiently recruited to the synapse using the inducible FKBP-rapalog-FRB heterodimerization system

(A) Schematic of the FKBP-rapalog-FRB heterodimerization system (left) and how this system is used to recruit mGluR5 to the PSD (right). (B) Live-cell time-lapse images of SEP-mGluR5-FRB before (0') and 20 and 30 minutes after rapalog application. The dendrites are color-coded for the fluorescence intensity of SEP-mGluR5-FRB. Scale bar, 2 μm . (C) Live-cell time-lapse images of the same dendrite as shown in B showing the relative localization SEP-mGluR5-FRB (cyan) and 2xFKBP-Homer1c-mCherry (red) before (0') and 20 and 30 minutes after rapalog application. Scale bar, 2 μm . (D) Zoom of spine indicated in C with asterisk before (0') and 20 minutes after rapalog application. Scale bar, 500 nm. (E) Line scans of the spine in D, indicated with dotted line, showing the localization of mGluR5 (cyan) relative to Homer1c (red) before (0') and 20 minutes after rapalog application. (F) Quantification of SEP-mGluR5-FRB (cyan) and 2xFKBP-Homer1c-mCherry (red) intensity in spines over time upon rapalog application at $t = 0$ ($n = 17$). Data are represented as means \pm SEM.

Synaptic recruitment of mGluR5 alters synaptic signaling

To investigate the spatiotemporal effects of mGluR distribution on synaptic function at individual synapses, we used the inducible FKBP-rapalog-FRB heterodimerization system to determine the effect of mGluR5 re-localization on synaptic signaling. Activation

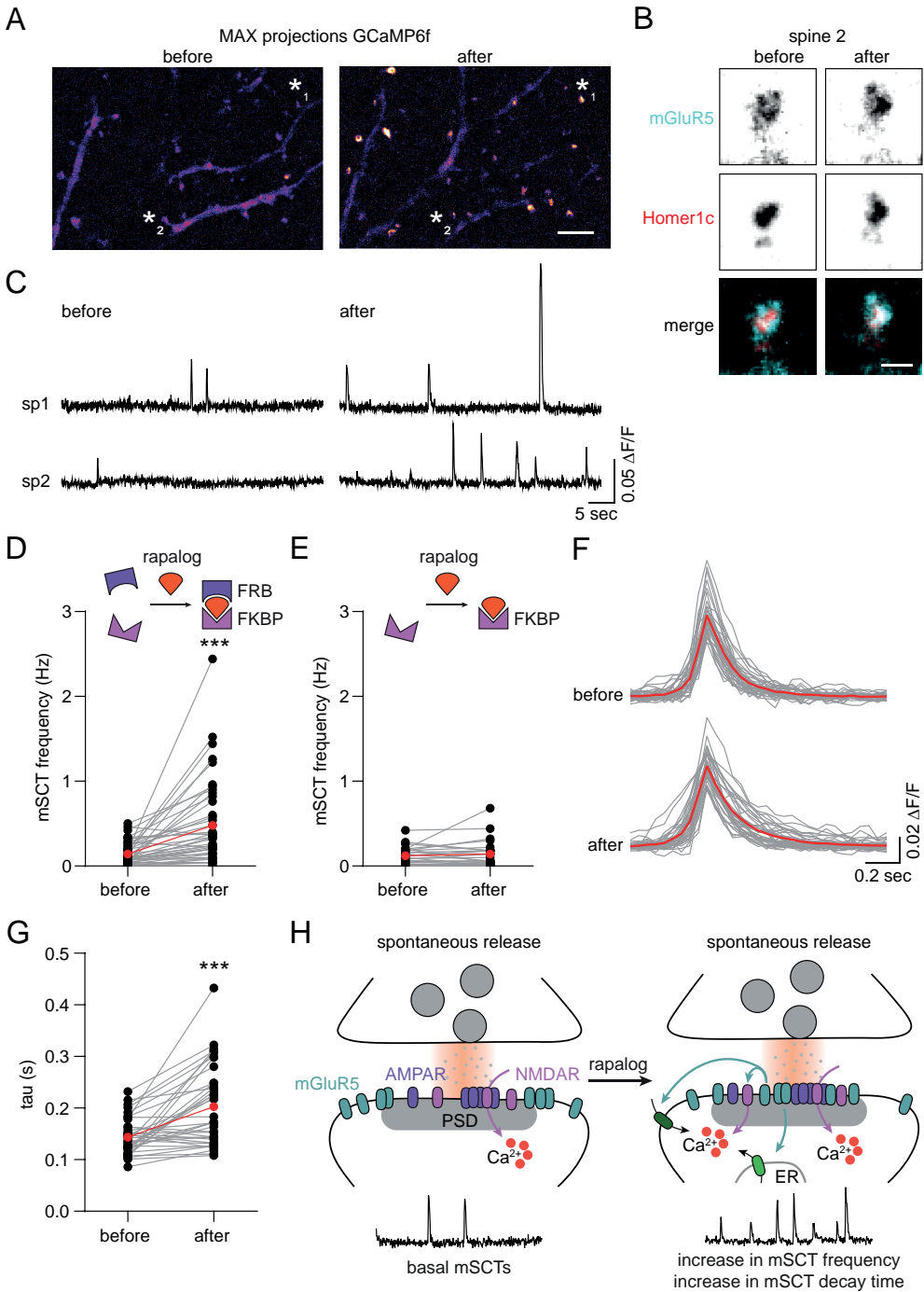


Figure 8. Synaptic recruitment of mGluR5 increases the frequency of spontaneous synaptic Ca²⁺ transients

(A) GCaMP6f max projection before (baseline) and after 30 minute rapalog application. Scale bar, 5 μm . (B) Zoom of spine 2 indicated in A with asterisk, expressing SNAP-mGluR5-FRB labeled with the cell-impermeable SNAPdye JF646 (cyan) and 2xFKBP-Homer1c-mCherry (red) before and 30 minutes after rapalog-induced recruitment. Scale bar, 1 μm . (C) $\Delta F/F_0$ traces of GCaMP6f signal from two spines indicated in A with asterisks before and after 30 minutes of rapalog-induced recruitment of mGluR5 to Homer1c. (D) Quantification of mSCT frequencies upon application of rapalog in neurons expressing SNAP-mGluR5-FRB and 2xFKBP-Homer1c-mCherry ($n = 43$ neurons, Wilcoxon matched-pairs signed rank test) and (E) in neurons expressing SNAP-mGluR5 and 2xFKBP-Homer1c-mCherry (control; $n = 37$ neurons, Wilcoxon matched-pairs signed rank test). (F) Average traces of all mSCTs per neuron (grey) and average mSCT trace of all neurons (red) before and after 30 minutes of rapalog. (G) Quantification of mSCT decay tau times (s) upon application of rapalog ($n = 37$ neurons, Wilcoxon matched-pairs signed rank test). (H) Model of deregulated calcium signaling upon mGluR5 recruitment to the synapse during during spontaneous synaptic activity. Means are indicated by the red lines.

of postsynaptic mGluRs induces spine Ca²⁺ levels via several routes: via IP3-sensitive intracellular stores (Niswender and Conn, 2010), modulation of voltage-gated calcium channels (VGCCs), NMDA receptors, or Ca²⁺-induced Ca²⁺ release (CICR) (Gerber et al., 2007; Kato et al., 2012; Skeberdis et al., 2001; Topolnik et al., 2006). Thus, as a functional read-out of mGluR5-mediated signaling we used the optical Ca²⁺ sensor GCaMP6f (Chen et al., 2013). We expressed GCaMP6f and imaged neurons at DIV21-23 in extracellular buffer containing 3 μM TTX and 0 mM Mg²⁺ to block action potentials and relieve the NMDA receptor pore block. GCaMP6f robustly reported miniature spontaneous Ca²⁺ transients (mSCTs) that were detected in individual dendritic spines without detected Ca²⁺ increases in the dendritic shaft or neighboring spines (Figure S8A-C), consistent with previous studies (Metzbower et al., 2019; Reese and Kavalali, 2015). We found a broad range of event frequencies per neuron, ranging from 0 to 25 events/ 50 seconds, with 90.6% of neurons exhibiting at least one event per 50 seconds. Next, we co-expressed GCaMP6f with SNAP-mGluR5-FRB and FBKP-Homer1c-mCherry and imaged GCaMP6f before and 30 minutes after the application of rapalog. In the maximum intensity projections of the obtained GCaMP6f streams (50 ms) we observed a clear increase in peak intensities at individual spines after a 30-minute rapalog incubation (Figure 8A-C). Indeed, quantification consistently showed that rapalog application caused a dramatic 3 to 4-fold increase in mSCT frequency (average mSCT frequency: before: 0.14 ± 0.02 Hz and after: 0.48 ± 0.08 Hz; Figure 8D and S8E), also when corrected for spine density (Figure S8D). The mean mSCT amplitude was not changed after the addition of rapalog (average $\Delta F/F_0$: before: 0.062 ± 0.003 and after: 0.062 ± 0.002 ; Figure S8F), but we did find significantly larger decay tau times (before: 0.14 ± 0.005 s and after: 0.20 ± 0.01 s; Figure 8F, G). To control for possible undesired side effects of rapalog on mSCT frequency and amplitude we performed the same experiment but with mGluR5 lacking the FRB domain. In this experiment we observed no differences in mSCT frequency (average mSCT frequency: before: 0.089 ± 0.02 Hz and after: 0.10 ± 0.02 Hz; Figure 8E and S8E) and amplitude (average $\Delta F/F_0$: before: 0.061 ± 0.004 and after: 0.060 ± 0.003 ; Figure S8G) before and after rapalog application. Altogether, these data support the model that the correct perisynaptic positioning of mGluR5 is critical for maintaining synaptic signaling, and that the acute recruitment of mGluR5 to the synapse results in aberrant synaptic calcium signaling (Figure 8H).

Discussion

The subsynaptic organization of group I mGluRs modulates their activation and subsequent downstream signaling, essential for proper synaptic transmission and plasticity. However, fundamental aspects of mGluR distribution and dynamics at excitatory synapses are still poorly understood. Here, we present mechanistic understanding of how the CTD of mGluR5 controls its dynamic organization in perisynaptic nanodomains, as well as preventing mGluR5 from entering the synapse, allowing mGluR5 to finely tune synaptic signaling.

Our localization and dynamic SMT data show that mGluR5 is enriched in the perisynaptic zone and largely absent from the PSD, consistent with early EM studies (Baude et al., 1993; Lujan et al., 1996; Nusser, 1994). Importantly, we observed that mGluR5 was not homogeneously distributed around the PSD, but assembled in distinct perisynaptic nanodomains, suggesting that specific mechanisms hinder mGluR5 diffusion at the perisynaptic zone. Consistently, our SMT data revealed that mGluR5 trajectories were enriched in the perisynaptic zone and were confined to domains with radii ranging from 40 up to 200 nm. Interestingly however, mGluR5 was only transiently trapped in these perisynaptic nanodomains, and rapidly exchanged between diffusive and confined states. Only a small fraction of mGluR5 seemed to be retained in the PSD, possibly by indirect steric hindrance, or molecular crowding mechanisms (Li et al., 2016; Renner et al., 2009). Thus, the enrichment of mGluR5 in perisynaptic nanodomains is the result of a highly dynamic equilibrium of diffusion states.

The transient confinement of mGluR5 may represent either binding and unbinding to an interaction partner or hindrance of movement of mGluRs due to other mechanisms. We found that the perisynaptic retention of mGluR5, but also the exclusion from the synapse is largely controlled by its CTD. Most importantly, the removal of the mGluR5 CTD resulted in a higher mobility in the perisynaptic zone and less transient confinement in perisynaptic nanodomains. Based on these data, we propose that the mGluR5 CTD is critical for the transient confinement of mGluR5 in perisynaptic nanodomains, possibly through stabilizing interactions at the perisynaptic zone. The CTD of mGluRs can interact with a variety of intracellular proteins, including the scaffolding protein Homer1b/c that links mGluRs to a larger synaptic complex (Das and Banker, 2006; De Blasi et al., 2001; Enz, 2012; Stowell and Craig, 1999; Tu et al., 1999). Much work generally propose Homer1b/c as the protein regulating the subsynaptic positioning of mGluRs (Ciruela et al., 2000; Kammermeier, 2006; Sergé et al., 2002; Tadokoro et al., 1999). In contrast, however we here show that Homer1c overexpression did not affect mGluR5 enrichment in spines nor did it affect mGluR5 diffusion. In fact, we found that mGluR5 localizes away from Homer1c, being present in the core of the PSD, and that forced recruitment of mGluR5 to Homer1c using the FKBP-heterodimerization-FRB system is required to recruit mGluR5 to the PSD. In previous work we demonstrated that Shank proteins, Homer1c-interacting scaffolds in the PSD, also do not anchor mGluRs at synaptic sites, but rather enable the local recycling of mGluRs and thereby balance the density of mGluRs at the synaptic membrane to modulate neuronal functioning (Scheefhals et al., 2019). Accordingly, we propose that Homer1c rather functions as an adaptor protein regulating mGluR signaling than that it anchors mGluR5 at synaptic sites. The mGluR5 CTD contains many other binding motifs and phosphorylation sites that might underlie the dynamic positioning of mGluRs (Bodzęta et al., 2021b; Enz, 2012). Also, other mechanisms such as phase separation, molecular

crowding or cytoskeletal hindrance might mediate the organizational properties of the mGluR5 CTD (Scheefhals and MacGillavry, 2018). Furthermore, we cannot exclude the possibility that other mGluR5 domains, including the extracellular N-terminal domain, are involved in receptor positioning (Bodżęta et al., 2021a; Dunn et al., 2019). For example, the enrichment of AMPARs at synaptic sites has been ascribed both to the C-terminal domain (Anggono and Huganir, 2012; Shepherd and Huganir, 2007; Shi et al., 2001), as well as the N-terminal domain (Díaz-alonso et al., 2017; Watson et al., 2017; Watson et al., 2021). Based on these findings we propose that at excitatory synapses functionally distinct glutamate receptor types are spatially segregated in subsynaptic domains, in part via intracellular interactions that can either promote or hinder the entry of receptors into the PSD. Our findings reveal that postsynaptic mGluR positioning is regulated by conceptually novel mechanisms that effectively retain mGluR5 close to the synapse, but segregated away from the core synaptic membrane, to efficiently modulate synaptic signaling.

The particular perisynaptic organization we observed for mGluR5 is likely to affect receptor activation and function. The perisynaptic mGluRs are perfectly situated to detect glutamate spillover from the synaptic cleft during sustained or high frequency stimulation and initiate downstream signaling. Furthermore, the perisynaptic nanodomains may function to concentrate signaling machineries optimizing the ability of mGluRs to connect to downstream signaling effectors. Such local accumulations of receptors and their effectors, in so-called signalosomes, have been shown to contribute to the efficiency and fidelity of signal transmission (Kasai and Kusumi, 2014; Kusumi et al., 2012). In support of this concept of perisynaptic signalosomes, the mGluR5 downstream signaling partners $G_{\alpha q}/G_{\alpha 11}$, $PLC\beta$, $DGL-\alpha$ and Norbin were found to closely parallel the organization of mGluR5 as they were either enriched in the perisynaptic zone or found to colocalize with mGluR5 (Katona et al., 2006; Nakamura et al., 2004; Olmo et al., 2016; Tanaka et al., 2000; Westin et al., 2014). In general, we observed that mGluR5 was not limited to one perisynaptic nanodomain, but formed multiple distinct domains in the perisynaptic zone. This opens the intriguing possibility that mGluRs assemble into distinct signalosomes that each consist of a specific subset of signaling molecules. The compartmentalization of downstream effectors of mGluRs might be of critical importance to regulate the initiation of downstream signaling and warrant the functional selectivity of mGluR1 and mGluR5. The perisynaptic zone also contains a stable endocytic zone (EZ) that functions to locally internalize and recycle synaptic receptors (Blanpied et al., 2002; Catsburg et al., 2021; Lu et al., 2007; Petrini et al., 2009). In particular, the tight coupling of the PSD to the EZ has been shown to govern efficient trafficking of mGluR5, regulating mGluR5 surface expression and signaling (Scheefhals et al., 2019). mGluR5 organized in perisynaptic nanodomains that localize in close vicinity of the EZ might be particularly well-suited for fast desensitization and local endocytosis and recycling after activation to rapidly respond to sustained synaptic activity.

We found that recruiting mGluR5 from the perisynaptic zone to the core of the PSD strikingly increased calcium events at synapses. These results indicate that increasing the availability of mGluR5 in the PSD for activation during spontaneous synaptic activity strongly deregulates synaptic calcium signaling. The increased mSCT frequency upon recruitment of mGluR5 to the synapse argues for a direct (Ca^{2+} influx through NMDARs) or indirect (downstream activation of Ca^{2+} release) contribution of mGluR5 to mSCTs. Even though increased mSCT frequency is expected to increase NMDA current magnitudes, our results

revealed no significant difference in mSCT amplitude indicating that mSCTs measured by GCaMP6f were not solely dependent on NMDA receptor activity. The increased mSCT frequency and decay times might reflect increased Ca^{2+} release from intracellular stores further shaping the mSCTs. Also, the number of mSCTs that were detectable and met by our detection criteria might be increased by Ca^{2+} release from internal stores (see M&M for details). Moreover, even though we performed the experiments in the absence of Mg^{2+} , the Ca^{2+} influx through NMDARs might not always be sufficient to generate mSCTs and further relies on activation of Ca^{2+} release from internal stores to amplify NMDA-mediated Ca^{2+} transients (Reese and Kavalali, 2015). We can also not exclude the possibility that other sources of Ca^{2+} entry, such as via VGCCs, also play a role here. It is nevertheless tempting to speculate that the induced synaptic enrichment of mGluR5 might to some extent induce the reported physical association between NMDA and mGluR5 initiated upon the activity-induced increase in Homer1a expression (Aloisi et al., 2017; Bertaso et al., 2010; Moutin et al., 2012).

Altogether, our data provide an unforeseen level of mechanistic understanding of how postsynaptic mGluRs are transiently retained in distinct perisynaptic nanodomains to control synaptic signaling. Further delineation of these mechanisms will shed new light on how glutamatergic signaling is regulated by the cooperative actions of different glutamate receptor subtypes. The functional implications of erroneous mGluR positioning further underlines the relevance of understanding the relation between mGluR trafficking and signaling in the context of cognitive functioning.

Materials and Methods

Experimental model and subject details

Animals

All animal experiments were performed in compliance with the guidelines for the welfare of experimental animals issued by the Government of the Netherlands (Wet op de Dierproeven, 1996) and European regulations (Guideline 86/609/EEC). All animal experiments were approved by the Dutch Animal Experiments Review Committee (Dier Experimenten Commissie; DEC), performed in line with the institutional guidelines of Utrecht University.

Primary neuronal cultures and transfections

Hippocampal cultures were prepared from embryonic day 18 (E18) Janvier Wistar rat brains (both genders) (Kapitein et al., 2010b). Dissociated neurons were plated on coverslips coated with poly-L-lysine (37.5 $\mu\text{g}/\text{ml}$, Sigma-Aldrich) and laminin (1.25 $\mu\text{g}/\text{ml}$, Roche Diagnostics) at a density of 100,000 neurons per well in a 12-well plate. Neurons were grown in Neurobasal medium (NB) supplemented with 2% B27 (GIBCO), 0.5 mM glutamine (GIBCO), 15.6 μM glutamate (Sigma-Aldrich), and 1% penicillin/ streptomycin (GIBCO) at 37°C in 5% CO_2 . Once per week, starting at 1 day *in vitro* (DIV1), half of the medium was refreshed with BrainPhys Neuronal Medium (BP, STEMCELL Technologies), supplemented with 2% NeuroCult SM1 (STEMCELL Technologies) and 1% penicillin/ streptomycin (GIBCO). At DIV3 (knock-in construct) or DIV11-16 neurons were transfected with indicated constructs using Lipofectamine 2000 (Invitrogen). Before transfection 300

μ l conditioned medium was transferred to a new culture plate. For each well, 1.8 μ g DNA was mixed with 3.3 μ l Lipofectamine 2000 in 200 μ l BP, incubated for 30 min at room temperature (RT) and added to the neurons. After 1 to 2 hours, neurons were briefly washed with BP and transferred to the new culture plate with conditioned medium supplemented with an additional 400 μ l BP with SM1 and penicillin/ streptomycin and kept at 37°C in 5% CO₂. All experiments were performed using neurons at DIV18-22. If neurons were kept longer than 6 days, medium was refreshed as described above.

Method details

DNA constructs

The pRK5-SEP-mGluR5a and pRK5-myc-mGluR5a are previously described (Scheefhals et al., 2019) and used as a template to make pRK5-SNAP-mGluR5a. To make pRK5-SEP-mGluR5a Δ C, primers were designed using Gibson Assembly (NEBuilder HiFi DNA assembly cloning kit) to remove the last 314 C-terminal amino acids of mGluR5a. The pDisp-SEP-TM-STGtail construct was a gift from Dr. Thomas A. Blanpied (Li et al., 2016) and the STGtail sequence was used to add to the C-terminal part of mGluR5a and mGluR5a Δ C (before the stopcodon) to make pRK5-SEP-mGluR5a-STGtail and pRK5-SEP-mGluR5a Δ C-STGtail. The FKBP and FRB containing expression plasmids were a gift from Lukas C. Kapitein (Kapitein et al., 2010a) and used to make pRK5-SNAP-mGluR5a-FRB, pRK5-SEP-mGluR5a-FRB and 2xFKBP-Homer1c-mCherry using Gibson Assembly. Homer1c-mCherry and pSM155-mCherry have been described before (Scheefhals et al., 2019). The pRK5-SEP-mGluR5a was used as a template to replace mGluR5a with GluA2 (flip, Q/R edited), previously described in (MacGillavry et al., 2013). GCaMP6f was a gift from Adam Cohen (Addgene plasmid # 58514) and PSD_{FingR}-mEos3.2 was a gift from Matthew J. Kennedy (Sinnen et al., 2017) and is based on (Dr. Don Arnold, Addgene plasmid # 46295) (Gross et al., 2013). The pAAV-GFP-mGluR5 CRISPR/Cas9 ORANGE knock-in construct was designed as described in (Willems et al., 2020). The GFP tag was inserted into the Grm5 gene using the following target sequence: 5' – GTGCACAGTCCAGTGAGAGG – 3', resulting in the N-terminal tagging of mGluR5.

Antibody and nanobody labeling

Neurons were fixed between DIV18-21 with 4% paraformaldehyde (PFA) and 4% sucrose in PBS for 10 minutes at RT, washed three times with PBS supplemented with 100 mM glycine (PBS/Gly), and blocked in 1-2% BSA in PBS/Gly for 30 minutes at RT. To label the surface-expressed pool of receptors, neurons were labeled with the GFP-booster Atto647N (Chromotek) diluted 1:200 in 1% BSA in PBS/Gly for 2 hours at RT or Fluotag-X4 anti-GFP Atto647N (Nanotag) diluted 1:250 in 1% BSA in PBS/Gly for 1 hour at RT. Neurons were then washed three times with PBS/Gly, mounted in Mowiol mounting medium (Sigma) and imaged on the Leica SP8 microscope as described below.

For the GFP-mGluR5 knock-in experiments (Figure 1K-O) neurons were fixed as described above and blocked with 10% NGS in PBS/Gly for 30 minutes at RT. To label the surface-expressed receptors neurons were incubated with rabbit anti-GFP (MBL) diluted 1:2000 in 5% NGS in PBS/Gly for 2 hours at RT and washed three times with PBS/Gly. Then, to label intracellular PSD-95, neurons were permeabilized in 0.25% Triton X-100 and 5% NGS in PBS/Gly for 10 minutes at RT, and incubated with mouse anti-PSD-95

(Neuromab) diluted 1:300 in 0.1% Triton X-100 and 5% NGS in PBS/Gly for 2 hours at RT or over night (O/N) at 4°C. Neurons were washed three times and incubated with anti-rabbit Alexa488 and anti-mouse Alexa594 (Thermo Fisher Scientific) diluted 1:250 in 0.1% Triton X-100 and 5% NGS in PBS/Gly for 1 hour at RT. Neurons were washed three times with PBS/Gly, mounted in Mowiol mounting medium (Sigma) and imaged on the Leica SP8 microscope as described below.

For two-color gSTED of SEP-mGluR5 and endogenous PSD-95 (Figure S1A-D), neurons were fixed and labelled as described above, except for the secondary antibodies used. Rabbit anti-mGluR5 and mouse anti-PSD-95 were visualized with anti-rabbit Atto647N (Sigma-Aldrich) and anti-mouse (Thermo Fisher Scientific) diluted 1:250. For two-color gSTED of endogenous mGluR5 and PSD-95 (Figure S1E-H) neurons were fixed as described above. Then neurons were blocked in 10% NGS and 0.1% Triton X-100 in PBS/Gly for 30 minutes at RT, incubated with rabbit anti-mGluR5 (Millipore) diluted 1:500 and mouse anti-PSD-95 (Neuromab) diluted 1:300 in 0.1% Triton X-100 and 5% NGS in PBS/Gly O/N at 4°C. Neurons were washed three times and incubated with anti-rabbit Atto647N (Sigma Aldrich) and anti-mouse Alexa594 (Thermo Fisher Scientific) diluted 1:250 in 0.1% Triton X-100 and 5% NGS in PBS/Gly for 1 hours at RT. For three-color gSTED of endogenous mGluR5, PSD-95 and actin (Figure S1I-K) neurons were fixed and blocked as described above. Then neurons were incubated with rabbit anti-mGluR5 (Alomone Labs) diluted 1:50 and mouse anti-PSD-95 (Neuromab) diluted 1:300 in 0.1% Triton X-100 and 5% NGS in PBS/Gly for 2 hours at RT. Neurons were washed three times and incubated with anti-rabbit Atto647N (Sigma Aldrich), anti-mouse Alexa488 (Thermo Fisher Scientific) diluted 1:250 and Phalloidin Alexa594 (Thermo Fisher Scientific) diluted 1:100 in 0.1% Triton X-100 and 5% NGS in PBS/Gly for 1 hours at RT. Note that we visualized the total pool of endogenous mGluR5 using both mGluR5 antibodies. For two-color STED of mGluR5 and GluA2 (Figure S1P-S) neurons were fixed as described above and blocked in 10% NGS in PBS/Gly for 30 minutes at RT. To label the surface-expressed receptors, neurons were incubated with rabbit anti-GFP (MBL) diluted 1:2000 and mouse anti-myc (Santa Cruz Biotechnology) diluted 1:500 in 5% NGS in PBS/Gly O/N at 4°C. Neurons were washed three times and incubated with anti-rabbit Atto647N (Sigma Aldrich) and anti-mouse Alexa594 (Thermo Fisher Scientific) diluted 1:250 in 5% NGS in PBS/Gly for 1 hours at RT. All neurons were washed three times with PBS/Gly after the incubation with secondary antibodies, mounted in Mowiol mounting medium (Sigma) and imaged on the Leica SP8 microscope as described below.

Confocal and STED microscopy

Imaging was performed with a Leica TCS SP8 STED 3x microscope using an HC PL APO 100x/NA 1.4 oil immersion STED WHITE objective. The 488, 590 and 647 nm wavelengths of pulsed white laser (80 MHz) were used to excite Alexa488, Alexa594 and Atto647N, respectively. To obtain gSTED images, Alexa488 was depleted with the 592 nm continuous wave depletion laser, and Alexa594 and Atto647N were depleted with the 775 nm pulsed depletion laser. We used an internal Leica HyD hybrid detector (set at 100% gain) with a time gate of $0.3 \leq t_g \leq 6$ ns. Images were acquired as Z-stacks using the 100x objective. Maximum intensity projections were obtained for image display and analysis. For the FKBP-rapalog-FRB heterodimerization assay DIV18-21 neurons transfected with SEP-mGluR5-FRB and 2xFKBP-Homer1c-mCherry were incubated with 1 μ M rapalog diluted

in extracellular imaging buffer or extracellular imaging buffer only (vehicle) for 50 minutes before fixation.

Single-molecule localization microscopy using dSTORM and PALM

Neurons were fixed at DIV21 with 4% PFA/sucrose in PBS for 10 minutes at RT, washed three times with PBS/Gly and blocked with 10% NGS in PBS/Gly for 15 minutes at RT. To label the surface-expressed pool of receptors, neurons were incubated with Fluotag-X4 anti-GFP Alexa647 (Nanotag) diluted 1:250 in PBS/Gly. Neurons were washed three times in PBS/Gly and stored in PBS at 4°C (dark) until use. Neurons were imaged in PBS containing 5 mM MEA, 5% w/v glucose, 700 µg/ml glucose oxidase, and 40 µg/ml catalase.

Dual-color SMLM data was acquired on the Nanoimager S from ONI (Oxford Nanoimaging; ONI), equipped with a 100x/NA 1.4 oil immersion objective (Olympus Plan Apo), with an effective pixel size of 117 nm, an XYZ closed-loop piezo stage, and with 405, 473, 561 and 640 nm wavelength excitation lasers. Fluorescence emission was detected using a sCMOS camera (ORCA Flash 4, Hamamatsu). Integrated filters were used to split far-red emission from blue-green-red emission, allowing simultaneous dual-color imaging. dSTORM and PALM were simultaneously performed using the 640 nm laser to bring Alexa647 to the dark state along with increasing power of the 405 nm laser to stochastically reactivate Alexa647 fluorophores and stochastically photoconvert PSD_{FingR}-mEos3.2 from green to red, combined with excitation of the photoconverted molecules by the 561 nm laser. Stacks of 10,000 to 20,000 images were acquired at 50 Hz with oblique illumination, which were processed using NimOS software from ONI. Before every acquisition, stacks of 30 frames were acquired with the 473 nm excitation laser to visualize SEP-mGluR5 and PSD-95_{FingR}-mEos3.2 expression. NimOS software from ONI was used for data processing and drift correction was performed. Before each imaging session, a bead sample was used to calibrate the system and align the two channels with a channel mapping precision >8 nm. The particle tables were exported to Matlab for analysis and images were rendered in NimOS software with 11.7 nm output pixels (sigma 1) and filtered on a minimum photocount of 300 and xy localization precision ≤ 30 nm for figure display.

Single-molecule tracking with uPAINT

uPAINT for Figure 3 and 4 was performed on the Nanoimager S from ONI (Oxford Nanoimaging; ONI), equipped with a 100x/NA 1.4 oil immersion objective (Olympus Plan Apo), an XYZ closed-loop piezo stage, and with 405, 471, 561 and 640 nm wavelength excitation lasers. Fluorescence emission was detected using a sCMOS camera (ORCA Flash 4, Hamamatsu). Stacks of 5000 frames were acquired at 50 Hz with oblique illumination. NimOS software from ONI was used for data analysis and drift correction was performed.

uPAINT for Figure 5 and 6 was performed on a Nikon Ti microscope with a Nikon 100x/NA 1.49 Apo TIRF objective, a Perfect Focus System, a 2.5x Optovar to achieve an effective pixel size of 64 nm and a DU-897D EMCDD camera (Andor). Imaging was performed with oblique laser illumination with a 405 nm diode laser (15mW; Power Technology), a 491 nm DPSS laser (50mW; Cobolt Calypso), a 561 nm DPSS laser (100mW; Cobolt Jive), and a 640 nm diode laser (35mW; Power Technology). Micromanager software was used to control all these components. 5000 frames were acquired at 50 Hz in TIRF. Acquired image stacks were analyzed using the ImageJ plug-in Detection of Molecules (DoM) v1.1.5 (https://github.com/ekatruxha/DoM_Utrecht) and drift correction was applied.

Neurons were imaged in extracellular imaging buffer containing 120 mM NaCl, 3 mM KCl, 10 mM HEPES, 2 mM CaCl_2 , 2 mM MgCl_2 and 10 mM glucose, pH adjusted to 7.35 with NaOH. The GFP-booster Atto647N (Chromotek) was added before image acquisition in a concentration of 1:150.000 to 1:50.000 in extracellular imaging buffer while blocking with 0.5-1.5 % BSA. Low concentrations of the GFP-booster were used to achieve temporal separation of fluorescence emission of mGluR5 molecules. Due to low dissociation rates of the nanobody, only being limited by photobleaching, we obtained long trajectories and used a minimum track length of 30 frames (20 ms interval) for visualization and quantification. PSD masks were created from a stack of 30 frames obtained for Homer1c-mCherry using the 561 nm excitation laser.

Live-cell spinning disk confocal imaging

The FKBP-rapalog-FRB heterodimerization assay and Ca^{2+} imaging were performed on a spinning disk confocal system (CSU-X1-A1 Yokogawa; Roper Scientific) mounted on an inverted Nikon Eclipse Ti microscope (Nikon) with a Plan Apo VC 100x 1.40 NA objective (Nikon) with excitation from 491 nm Cobolt Calypso (100 mW), 561 nm Cobolt Jive (100 mW), 642 nm Vortran Stradus (110 mW) lasers and emission filters (Chroma). The microscope is equipped with a motorized XYZ stage (ASI; MS-2000), Perfect Focus System (Nikon), and Prime BSI sCMOS camera (Photometrics), and controlled by MetaMorph software (Molecular Devices). During the image acquisition neurons were kept in extracellular imaging buffer (with or without MgCl_2) in a closed incubation chamber (INUBG2E-ZILCS; Tokai Hit) at 37°C in 5% CO_2 .

For the FKBP-rapalog-FRB heterodimerization assay neurons were transfected with SEP-mGluR5-FRB and 2xFKBP-Homer1c and imaged at DIV18-22. After a 10-minute baseline acquisition, recruitment of mGluR5 to Homer1c was induced by the addition of rapalog to a final concentration of 1 μM and the SEP-mGluR5 and Homer1c-mCherry signals were imaged every 5 minutes for another 40 minutes. Multiple Z stacks (7 planes) were obtained, with 0.5 μm intervals to acquire 3 μm image stacks.

For Ca^{2+} imaging neurons were transfected with SNAP-mGluR5-FRB, 2xFKBP-Homer1c-mCherry and GCaMP6f or SNAP-mGluR5, 2xFKBP-Homer1c-mCherry and GCaMP6f for control neurons. At DIV21-22, before each acquisition a coverslip with neurons was labelled with a SNAP JF646 cell impermeable dye (JF646i; Janelia/ Tocris) diluted 1:2000 in supplemented medium for 30 minutes followed by a single wash with extracellular buffer. Neurons were transferred to the closed 37°C/ 5% CO_2 imaging chamber containing extracellular imaging buffer without MgCl_2 and with 3 μM tetrodotoxin citrate (TTX; Tocris) to block action potentials and relieve the NMDA receptor pore block. At the start, Z stacks (7 planes) were obtained of the SNAP-mGluR5-FRB JF646i and 2xFKBP-Homer1c-mCherry channels, with 0.5 μm intervals to acquire 3 μm image stacks. This was shortly followed by a 50-second stream of the GCaMP6f signal, acquired at 50 ms intervals (20 Hz) (referred to as “before” rapalog). Then, rapalog was added to the imaging chamber to a final concentration of 1 μM and incubated for 30 minutes, the time we established is required for the synaptic recruitment of mGluR5 to reach a plateau. Again, this was followed by imaging stacks of SNAP-mGluR5 JF646i and Homer1c-mCherry and a stream of GCaMP6f (referred to as “after” rapalog). Maximum intensity projections were obtained of the mGluR5 and Homer1c stacks for image display and analysis.

Quantification and statistical analysis

Quantification of spine enrichment

To assess the spine enrichment of surface mGluR5 and mGluR5 variants, the SEP-mGluR5 Atto647N intensity from confocal images was quantified as mean spine intensity divided by mean dendritic shaft intensity. For each neuron, circular regions of interest (ROIs) were traced on multiple dendritic spines to measure spine intensity and for each selected spine an ROI in the dendrite at the base of the spine was measured as dendritic shaft intensity. Background intensity was subtracted. For Figure 1 and S7 the spine enrichment of mCherry and Homer1c-mCherry was determined using the same spine and dendrite ROIs as used for mGluR5.

STED imaging analysis

To assess the localization of mGluR5 relative to Homer1c, PSD-95, GluA2 or Phalloidin, line scans along spines were drawn using ImageJ software. To quantify the localization of mGluR5, mGluR5 Δ C, mGluR5WT-STGtail and mGluR5 Δ C-STGtail in spines, all images were scrambled and blinded. Per neuron, a minimum of 20 spines were selected based on the Homer1c channel and the localization of mGluR5 was determined using the merged image of confocal-resolved Homer1c and gSTED-resolved mGluR5 in ImageJ software. The localization of mGluR5 could be categorized as spines with 1) synaptic enrichments, 2) synaptic and perisynaptic enrichments, 3) perisynaptic enrichments or 4) a homogeneous distribution of mGluR5. Per category, the percentage of spines was plotted and the statistical significance was determined within each category and all conditions were compared to mGluR5WT.

Single-molecule localization analysis

The maximum projections of the 30 frames acquired in the green channel were used to select all spines and save these as separate ROIs using ImageJ software. The molecules from the ROIs were extracted and used for further analysis and were filtered on a localization precision <20 nm. Furthermore, molecules that were in the fluorescent state longer than 1 frame were filtered out by tracking with a radius of 58.5 nm (0.5 pixels). PSD_{FingR} clusters were identified using DBScan (Ester et al., 1996) executed in MATLAB. PSD_{FingR} clusters with a density >1200 molecules per μm (epsilon 0.35 and >50 localizations) were used for further analysis and the PSD border was defined using the alpha shape. The distance of individual localizations to the nearest PSD border (up to 1 μm distance) were computed and plotted as a frequency distribution. Rings were calculated as a fraction of the PSD border polyshape (is 1) defined by DBScan with two rings inside the PSD: 0-0.5 and 0.5-1 and 6 rings outside the PSD, with three rings approximating the perisynaptic zone: 1 - 1.5, 1.5 - 2 and 2 - 2.5 and three rings defining the extrasynaptic region: 2.5 - 3, 3 - 3.5 and 3.5 - 4. Per ring, the number of mGluR5 localizations was determined and the fraction of mGluR5 localizations per ring was calculated. To correct for the different sizes of ring 1 to 8, we further calculated the fraction of the area covered by each ring. The fraction of mGluR5 localizations was divided by the fraction of ring area, and normalized to 1. Then we also assessed the existence of mGluR5 clusters using DBScan and a density of >480 molecules per μm (epsilon 0.35 and >20 localizations). The border-to-centroid distance from PSD to mGluR5 cluster was calculated and plotted as a frequency distribution.

Single-molecule tracking analysis

Using MATLAB, molecules with a localization precision <50 nm were selected for analysis and background localizations were removed by outlining the neuron based on the obtained SEP-mGluR5 widefield image. Tracking was achieved using custom algorithms in MATLAB described previously (Lu et al., 2014). For tracks consisting of ≥ 4 frames the instantaneous diffusion coefficient was estimated. The first three points of the MSD with the addition of the value 0 at MSD(0) were used to fit the slope using a linear fit. Tracks with a negative slope were not used for further analysis. The diffusion coefficient was estimated based on the fit using the formula $MSD = 4D\Delta t$. Only tracks of at least 30 frames were selected for further analysis. Tracks were classified as immobile when the ratio between the radius of gyration and mean step size ($(\sqrt{\pi/2} \cdot \text{radius of gyration}) / (\text{mean stepsize})$) was smaller than 2.11 (Golan and Sherman, 2017).

The PSD mask was created based on the maximum intensity projection of Homer1c-mCherry. Peaks in intensity were detected after which a FWHM-like boundary was defined for each PSD. An expanded PSD mask of 200 nm around the PSD mask was created to define the perisynaptic zone. Tracks were assigned to the synaptic group if $\geq 80\%$ of the localizations of the track overlapped with the PSD. Perisynaptic tracks had to overlap $\geq 60\%$ with the perisynaptic zone and $< 80\%$ with the PSD, and transient perisynaptic tracks overlapped $> 0\%$ and $< 60\%$ with the perisynaptic zone. Entries and exits per perisynaptic trajectory were derived based on their overlap with the PSD mask. The perisynaptic tracks were categorized into three groups: captured, returned or escaped. The ‘captured’ tracks were the tracks that started within the (peri)synaptic region or entered this region but never left. The ‘returned’ tracks were at least once outside the (peri)synaptic region over the course of the track but ended up within the (peri)synaptic region. Lastly the ‘escaped’ group contains the tracks that crossed the perisynaptic region, but ended outside.

Transient confinement analysis on mobile trajectories was done in MATLAB using slightly modified scripts from a previously published MATLAB implementation (Menchón et al., 2012) based on the algorithm reported by (Meilhac et al., 2006; Simson et al., 1995). Briefly, transient confinement was detected in a trajectory based on the probability (ψ) of a molecule staying within a region of radius (R) for a period of time (t):

$$\log(\psi) = 0.2048 - 2.5117Dt/R^2$$

where D is the maximum of the instantaneous diffusion coefficients estimated for each sub-trajectory of Δt . This probability was translated into a confinement index L, the larger the value of L, the greater the probability that the observed part of the trajectory is not of Brownian origin. The regions where the confinement index is above the critical L for critical time T_c are identified as confinement zones. Parameters used in the analysis are: $L_c = 4$, $S_m = 15$, $\alpha = 0.5$, $T_c = 0.2$ s (10 frames). The confinement zones are further analyzed for size and duration of confinement and diffusion coefficient in and outside confinement zones.

Confinement maps were created based on the detected confinement radius for each confinement zone. Each confinement zone was stored as a 2D Gaussian with the radius as FWHM. The final matrix was plotted with a color-code, where higher values indicate confinement hotspots because there are multiple Gaussians on top of each other. For the immobile tracks the center of the track coordinates was determined and a 2D Gaussian with a fixed FWHM of 75 nm was plotted. The distance between a confinement zone and a PSD was defined as the shortest distance between the center of a confinement zone or immobile track to the nearest PSD border.

mGluR5-FRB to FKBP-Homer recruitment analysis

The maximum intensity projections were corrected for XY drift over time using the ImageJ plugin “StackReg.” We quantified the SEP-mGluR5-FRB recruitment to 2xFKBP-Homer1c-mCherry over a time-period of 40 minutes, after a 10-minute baseline period. The Homer1c timelapses were used to select ROIs using ImageJ. First, image noise was reduced by applying a gaussian blur with $\sigma = 1$ and background subtraction with a rolling ball of 50. Subsequently, the timelapse images were subjected to thresholding based on the $t = -10$ minute image to isolate all PSDs. Then, a mask followed by a selection of all PSDs was created for each timepoint and saved as ROIs. The raw timelapse images of Homer1c and mGluR5 were used to measure the signal intensity within the ROIs at the different time points. To obtain the change in relative fluorescence intensity ($\Delta F/F_0$) over time, the intensity relative to $t = -10$ minutes was calculated and for visualization all values were subtracted by 1. The increase in mGluR5 intensity upon rapalog application, measured within PSDs marked by Homer1c, was best explained by a one-phase association function, fitted using Graphpad Prism.

Ca²⁺ imaging analysis

To analyse the Ca²⁺ imaging data, a circular ROI was drawn around every spine within the field of view, clearly separated from the dendritic base and in focus, regardless of activity levels. Using ImageJ software, the mean intensity value within each ROI was measured for all 1000 frames (50 ms streams). Then, this data was analyzed using custom MATLAB scripts based on (Reese and Kavalali, 2015). Peaks of miniature spontaneous Ca²⁺ transients (mSCTs) were detected and measured if the 2-point slope was greater than $\text{meanslope} + 2 \cdot \text{STDslope}$, and amplitude greater than $0.035 \Delta F/F_0$. Using these and several other criteria described in more detail in Reese and Kavalali (2015), peaks were consistently detected, disregarding background noise or single high point artifacts. Then for each spine the mSCT frequency and for each peak the mSCT amplitude ($\Delta F/F_0$) was calculated. To measure average decay times, all $\Delta F/F_0$ values of detected peaks were loaded into Clampfit 10.3 (Molecular Devices) and average mSCT traces were made for each neuron by aligning all peaks before and all peak after rapalog application. Next, a single-exponential fit line was obtained from the decay phase of the average mSCT traces. The single-exponential fit lines were plotted in Graphpad Prism and the decay times (τ), the time in seconds required to decay to $(1/e)\Delta F$, were calculated. For measurements of mSCT frequency, τ , and amplitude spines with at least one mSCT before or after rapalog application were included and data is presented as the mean mSCT frequency (Hz) per neuron, mean mSCT τ (s) per neuron and mean mSCT amplitude ($\Delta F/F_0$) per neuron, respectively. While in the frequency analysis correcting for the variability in the number of ROIs (spines) in the field of view, all spines (also without activity) were included and data is presented as the mean mSCT frequency (Hz) per spine. To test the statistical significance of the change in mean decay times and amplitude upon rapalog application, only neurons that had at least one mSCT both before and after rapalog application could be used.

Statistical analysis

All statistical tests used and significance in this study are described in the main text and figure legends. Each experiment was replicated in cultures from at least 3 independent preparations of hippocampal neurons. The n indicated in the figure legends are the number

of neurons used for analysis, unless stated otherwise. Statistical analysis and graphs were prepared in GraphPad Prism and figures were generated in Adobe Illustrator CC.

Acknowledgments

We would like to thank all members of the MacGillavry lab and Eline Penners for helpful discussions and Arthur de Jong, Yolanda Gutierrez and Lisa A.E. Catsburg for critical reading of the manuscript. This work was supported by the Netherlands Organization for Scientific Research (the Graduate Program of Quantitative Biology and Computational Life Sciences) to N.S. and the European Research Council (ERC-StG 716011) to H.D.M..

Author Contributions

Conceptualization, Methodology, N.S. and H.D.M.; Validation & Formal Analysis, N.S. and M.W.; Investigation, N.S.; Resources, H.D.M.; Writing – Original Draft, N.S.; Writing – Review, H.D.M. and M.W.; Visualization, N.S.; Supervision, H.D.M.; Funding Acquisition, H.D.M. and N.S..

Declaration of Interest

The authors declare no competing interest.

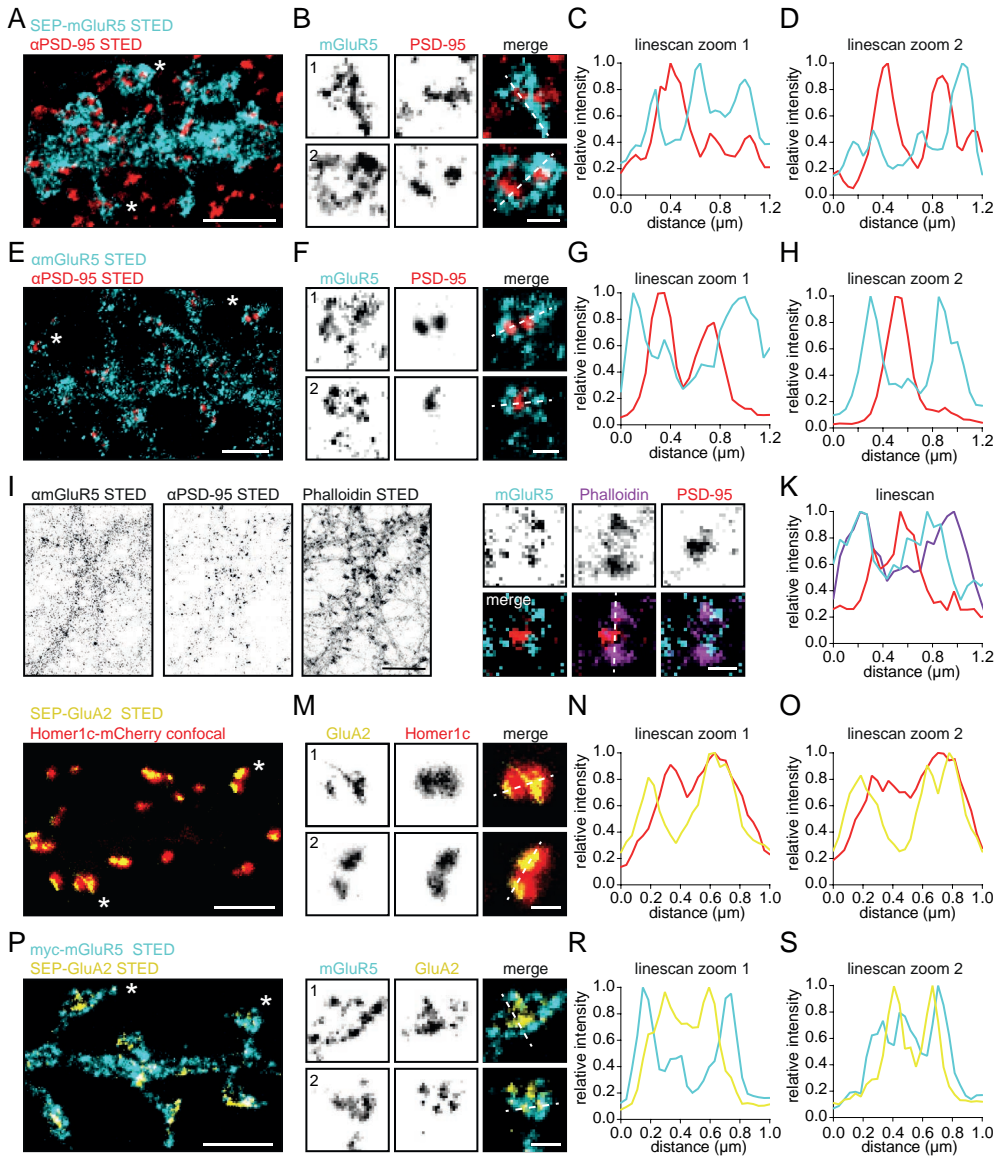
References

- Aloisi, E., Le Corf, K., Dupuis, J., Zhang, P., Ginger, M., Labrousse, V., Spatuzza, M., Georg Haberl, M., Costa, L., Shigemoto, R., et al. (2017). Altered surface mGluR5 dynamics provoke synaptic NMDAR dysfunction and cognitive defects in Fmrl knockout mice. *Nat. Commun.* 8, 1103.
- Anggono, V., and Huganir, R.L. (2012). Regulation of AMPA receptor trafficking and synaptic plasticity. *Curr. Opin. Neurobiol.* 22, 461-469
- Bats, C., Groc, L., and Choquet, D. (2007). The interaction between Stargazin and PSD-95 regulates AMPA receptor surface trafficking. *Neuron*. 53, 719-734.
- Baude, A., Nusser, Z., Roberts, J.D.B., Mulvihill, E., McIlhinney, R.A.J., and Somogyi, P. (1993). The metabotropic glutamate receptor (mGluR1) is concentrated at perisynaptic membrane of neuronal subpopulations as detected by immunogold reaction. *Neuron*. 11, 771-787.
- Bertaso, F., Roussignol, G., Worley, P., Bockaert, J., Fagni, L., and Ango, F. (2010). Homer1a-dependent crosstalk between NMDA and metabotropic glutamate receptors in mouse neurons. *PLoS One* 5, e9755.
- Biederer, T., Kaeser, P.S., and Blanpied, T.A. (2017). Transcellular Nanoalignment of Synaptic Function. *Neuron*. 96, 680-696.
- Blanpied, T.a., Scott, D.B., and Ehlers, M.D. (2002). Dynamics and regulation of clathrin coats at specialized endocytic zones of dendrites and spines. *Neuron*. 36, 435-449.
- Bodzęta, A., Berger, F., and MacGillavry, H.D. (2021a). Subsynaptic mobility of presynaptic mGluR types is differentially regulated by intra- and extracellular interactions. *bioRxiv*. <https://doi.org/10.1101/2020.07.06.188995>.
- Bodzęta, A., Scheefhals, N., and MacGillavry, H.D. (2021b). Membrane trafficking and positioning of mGluRs at presynaptic and postsynaptic sites of excitatory synapses. *Neuropharmacology* 200, 108799.
- Catsburg, L.A.E., Westra, M., van Schaik, A.M.L., and MacGillavry, H.D. (2021). Dynamics and nanoscale organization of the postsynaptic endocytic zone at excitatory synapses. *bioRxiv*. <https://doi.org/10.1101/2021.02.18.431766>.
- Chang, K., and Roche, K.W. (2017). Neuropharmacology Structural and molecular determinants regulating mGluR5 surface expression. *Neuropharmacology* 115, 10-19.
- Chen, T.-W., Wardill, T.J., Sun, Y., Pulver, S.R., Renninger, S.L., Baohan, A., Schreiter, E.R., Kerr, R.a., Orger, M.B., Jayaraman, V., et al. (2013). Ultrasensitive fluorescent proteins for imaging neuronal activity. *Nature*. 499, 295-300.
- Choquet, D., and Triller, A. (2013). The dynamic synapse. *Neuron*. 80, 691-703.
- Ciruella, F., Soloviev, M.M., Chan, W.Y., and McIlhinney, R.A. (2000). Homer-1c/Vesl-1L modulates the cell surface targeting of metabotropic glutamate receptor type 1alpha: evidence for an anchoring function. *Mol. Cell. Neurosci.* 15, 36-50.
- Clackson, T., Yang, W., Rozamus, L.W., Hatada, M., Amara, J.F., Rollins, C.T., Stevenson, L.F., Magari, S.R., Wood, S.a., Courage, N.L., et al. (1998). Redesigning an FKBP-ligand interface to generate chemical dimerizers with novel specificity. *Proc. Natl. Acad. Sci. U. S. A.* 95, 10437-10442.
- Das, S.S., and Banker, G.A. (2006). The role of protein interaction motifs in regulating the polarity and clustering of the metabotropic glutamate receptor mGluR1a. *J. Neurosci.* 26, 8115-8125.
- De Blasi, A., Conn, P.J., Pin, J.-P., and Nicoletti, F. (2001). Molecular determinants of metabotropic glutamate receptor signaling. *Trends Pharmacol. Sci.* 22, 114-120.
- Díaz-alonso, J., Sun, Y.J., Granger, A.J., Levy, J.M., Blankenship, S.M., and Nicoll, R.A. (2017). Subunit-specific role for the amino-terminal domain of AMPA receptors in synaptic targeting. *Proc. Natl. Acad. Sci. U. S. A.* 114, 7136-7141.
- Dunn, H.A., Orlandi, C., and Martemyanov, K.A. (2019). Beyond the Ligand: Extracellular and Transcellular G Protein-Coupled Receptor Complexes in Physiology and Pharmacology. *Pharmacol. Rev.* 71, 503-519.
- Enz, R. (2012). Structure of metabotropic glutamate receptor C-terminal domains in contact with interacting proteins. *Front. Mol. Neurosci.* 5, 52.
- Ester, M., Kriegel, H.-P., Sander, J., and Xu, X. (1996). A density-based algorithm for discovering clusters in large spatial databases with noise. *Proceedings of the Second International Conference on Knowledge Discovery and Data Mining*. AAAI Press. 226-31.
- Frost, N.a., Shroff, H., Kong, H., Betzig, E., and Blanpied, T.a. (2010). Single-molecule discrimination of discrete perisynaptic and distributed sites of actin filament assembly within dendritic spines. *Neuron*. 67, 86-99.
- Gerber, U., Gee, C.E., and Benquet, P. (2007). Metabotropic glutamate receptors: intracellular signaling pathways. *Curr. Opin. Pharmacol.* 7, 56-61.
- Giannone, G., Hossy, E., Levet, F., Constals, A., Schulze, K., Sobolevsky, A.I., Rosconi, M.P., Gouaux, E., Tampé, R., Choquet, D., and Cognet, L. (2010). Dynamic superresolution imaging of endogenous proteins on living cells

- at ultra-high density. *Biophys. J.* 99, 1303-1310.
- Golan, Y., and Sherman, E. (2017). Resolving mixed mechanisms of protein subdiffusion at the T cell plasma membrane. *Nat. Commun.* 8, 15851.
- Greget, R., Pernot, F., Bouteiller, J.M.C., Ghaderi, V., Allam, S., Keller, A.F., Ambert, N., Legendre, A., Sarmis, M., Haeblerle, O., et al. (2011). Simulation of postsynaptic glutamate receptors reveals critical features of glutamatergic transmission. *PLoS ONE* 6, e28380.
- Gross, G.G., Junge, J.A., Mora, R.J., Kwon, H.B., Olson, C.A., Takahashi, T.T., Liman, E.R., Ellis-Davies, G.C., McGee, A.W., Sabatini, B.L., et al. (2013). Recombinant probes for visualizing endogenous synaptic proteins in living neurons. *Neuron* 78, 971-985.
- Kammermeier, P.J. (2006). Surface clustering of metabotropic glutamate receptor 1 induced by long Homer proteins. *BMC Neurosci.* 7, 1.
- Kapitein, L.C., Schlager, M.A., Kuijpers, M., Wulf, P.S., van Spronsen, M., MacKintosh, F.C., and Hoogenraad, C.C. (2010a). Mixed microtubules steer dynein-driven cargo transport into dendrites. *Curr. Biol.* 20, 290-299.
- Kapitein, L.C., Yau, K.W., and Hoogenraad, C.C. (2010b). Microtubule dynamics in dendritic spines. *Methods Cell. Biol.* 97, 111-132.
- Kasai, R.S., and Kusumi, A. (2014). Single-molecule imaging revealed dynamic GPCR dimerization. *Curr Opin Cell. Biol.* 27, 78-86.
- Kato, H.K., Kassai, H., Watabe, A.M., Aiba, A., and Manabe, T. (2012). Functional coupling of the metabotropic glutamate receptor, InsP3 receptor and L-type Ca^{2+} channel in mouse CA1 pyramidal cells. *J. Physiol.* 590, 3019-3034.
- Katona, I., Urbán, G.M., Wallace, M., Ledent, C., Jung, K.M., Piomelli, D., Mackie, K., and Freund, T.F. (2006). Molecular composition of the endocannabinoid system at glutamatergic synapses. *J. Neurosci.* 26, 5628-5637.
- Kellermayer, B., Ferreira, J.S., Dupuis, J., Levet, F., Grillo-Bosch, D., Bard, L., Llinarès-Loyez, J., Bouchet, D., Choquet, D., Rusakov, D.A., et al. (2018). Differential Nanoscale Topography and Functional Role of GluN2-NMDA Receptor Subtypes at Glutamatergic Synapses. *Neuron* 100, 106-119.e107.
- Kusumi, A., Fujiwara, T.K., Chadda, R., Xie, M., Tsunoyama, T.a., Kalay, Z., Kasai, R.S., and Suzuki, K.G.N. (2012). Dynamic Organizing Principles of the Plasma Membrane that Regulate Signal Transduction: Commemorating the Fortieth Anniversary of Singer and Nicolson's Fluid-Mosaic Model. *Annu. Rev. Cell Dev. Biol.* 28, 215-250.
- Li, T.P., Song, Y., MacGillavry, H.D., Blanpied, T.a., and Raghavachari, S. (2016). Protein Crowding within the Postsynaptic Density Can Impede the Escape of Membrane Proteins. *J. Neurosci.* 36, 4276-4295.
- Lu, H.E., MacGillavry, H.D., Frost, N.A., and Blanpied, T.A. (2014). Multiple spatial and kinetic subpopulations of CaMKII in spines and dendrites as resolved by single-molecule tracking PALM. *J. Neurosci.* 34, 7600-7610.
- Lu, J., Helton, T.D., Blanpied, T.a., Rácz, B., Newpher, T.M., Weinberg, R.J., and Ehlers, M.D. (2007). Postsynaptic Positioning of Endocytic Zones and AMPA Receptor Cycling by Physical Coupling of Dynamin-3 to Homer. *Neuron*. 55, 874-889.
- Lujan, R., Nusser, Z., Roberts, J.D., Shigemoto, R., and Somogyi, P. (1996). Perisynaptic location of metabotropic glutamate receptors mGluR1 and mGluR5 on dendrites and dendritic spines in the rat hippocampus. *The Eur. J. Neurosci.* 8, 1488-1500.
- Lüscher, C., and Huber, K.M. (2010). Group 1 mGluR-Dependent Synaptic Long-Term Depression: Mechanisms and Implications for Circuitry and Disease. *Neuron* 65, 445-459.
- MacGillavry, H., Song, Y., Raghavachari, S., and Blanpied, T. (2013). Nanoscale scaffolding domains within the postsynaptic density concentrate synaptic ampa receptors. *Neuron*. 78, 615-622.
- Marcaggi, P., Mutoh, H., Dimitrov, D., Beato, M., and Knöpfel, T. (2009). Optical measurement of mGluR1 conformational changes reveals fast activation, slow deactivation, and sensitization. *Proc. Natl. Acad. Sci. U. S. A.* 106, 11388-11393.
- Meilhac, N., Le Guyader, L., Salomé, L., and Destainville, N. (2006). Detection of confinement and jumps in single-molecule membrane trajectories. *Phys. Rev. E. Stat. Nonlin. Soft Matter Phys.* 73, 011915.
- Menchón, S.a., Martín, M.G., and Dotti, C.G. (2012). APM_GUI: analyzing particle movement on the cell membrane and determining confinement. *BMC biophys.* 5, 4.
- Metzbower, S., Joo, Y., Benavides, D., and Blanpied, T. (2019). Properties of individual hippocampal synapses influencing NMDA-receptor activation by spontaneous neurotransmission. *eNeuro* 6, ENEURO.0419-18.2019.
- Moutin, E., Raynaud, F., Roger, J., Pellegrino, E., Homburger, V., Bertaso, F., Ollendorff, V., Bockaert, J., Fagni, L., and Perroy, J. (2012). Dynamic remodeling of scaffold interactions in dendritic spines controls synaptic excitability. *J. Cell Biol.* 198, 251-263.
- Nair, D., Hosy, E., Petersen, J.D., Constals, A., Giannone, G., Choquet, D., and Sibarita, J.-B. (2013). Super-resolution imaging reveals that AMPA receptors inside synapses are dynamically organized in nanodomains

- regulated by PSD95. *J. Neurosci.* 33, 13204-13224.
- Nakamura, M., Sato, K., Fukaya, M., Araishi, K., Aiba, A., Kano, M., and Watanabe, M. (2004). Signaling complex formation of phospholipase Cbeta4 with metabotropic glutamate receptor type 1alpha and 1,4,5-trisphosphate receptor at the perisynapse and endoplasmic reticulum in the mouse brain. *Eur. J. Neurosci.* 20, 2929-2944.
- Niswender, C.M., and Conn, P.J. (2010). Metabotropic Glutamate Receptors: Physiology, Pharmacology, and Disease. *Annu. Rev. Pharmacol. Toxicol.* 50, 295-322.
- Nusser, Z. (1994). Subsynaptic segregation of metabotropic and ionotropic glutamate receptors as revealed by immunogold localization. *Neuroscience* 61, 421-427.
- Olmo, I.G., Ferreira-Vieira, T.H., and Ribeiro, F.M. (2016). Dissecting the Signaling Pathways Involved in the Crosstalk between Metabotropic Glutamate 5 and Cannabinoid Type 1 Receptors. *Mol. Pharmacol.* 5, 609-619.
- Paoletti, P., Bellone, C., and Zhou, Q. (2013). NMDA receptor subunit diversity: impact on receptor properties, synaptic plasticity and disease. *Nat. Rev. Neurosci.* 14, 383-400.
- Petrini, E.M., Lu, J., Cognet, L., Lounis, B., Ehlers, M.D., and Choquet, D. (2009). Endocytic Trafficking and Recycling Maintain a Pool of Mobile Surface AMPA Receptors Required for Synaptic Potentiation. *Neuron.* 63, 92-105.
- Reese, A.L., and Kavalali, E.T. (2015). Spontaneous neurotransmission signals through store-driven Ca²⁺ transients to maintain synaptic homeostasis. *eLife* 4, 1-15.
- Reiner, A., and Levitz, J. (2018). Review Glutamatergic Signaling in the Central Nervous System : Ionotropic and Metabotropic Receptors in Concert. *Neuron* 98, 1080-1098.
- Renner, M., Lacor, P.N., Velasco, P.T., Xu, J., Contractor, A., Klein, W.L., and Triller, A. (2010). Deleterious Effects of Amyloid β Oligomers Acting as an Extracellular Scaffold for mGluR5. *Neuron* 66, 739-754.
- Renner, M.L., Cognet, L., Lounis, B., Triller, A., and Choquet, D. (2009). The excitatory postsynaptic density is a size exclusion diffusion environment. *Neuropharmacology* 56, 30-36.
- Saxton, M.J. (1993). Lateral diffusion in an archipelago. Single-particle diffusion. *Biophys. J.* 64, 1766-1780.
- Scheefhals, N., Catsburg, L.A.E., Westerveld, M.L., Blanpied, T.A., Hoogenraad, C.C., and Macgillavry, H.D. (2019). Shank Proteins Couple the Endocytic Zone to the Postsynaptic Density to Control Trafficking and Signaling of Metabotropic Glutamate Receptor 5. *Cell Rep.* 29, 258-269 e258.
- Scheefhals, N., and MacGillavry, H.D. (2018). Functional organization of postsynaptic glutamate receptors. *Mol. Cell. Neurosci.* 91, 82-94.
- Schnell, E., Sizemore, M., Karimzadegan, S., Chen, L., Bredt, D.S., and Nicoll, R.A. (2002). Direct interactions between PSD-95 and stargazin control synaptic AMPA receptor number. *Proc. Natl. Acad. Sci. U. S. A.* 99, 13902-13907.
- Sergé, A., Fourgeaud, L., Hémar, A., and Choquet, D. (2002). Receptor activation and homer differentially control the lateral mobility of metabotropic glutamate receptor 5 in the neuronal membrane. *J. Neurosci.* 22, 3910-3920.
- Shepherd, J.D., and Huganir, R.L. (2007). The Cell Biology of Synaptic Plasticity : AMPA Receptor Trafficking. *Annu. Rev. Cell Dev. Biol.* 23, 613-643.
- Shi, S.-H., Hayashi, Y., Esteban, J.A., and Malinow, R. (2001). Subunit-Specific Rules Governing AMPA Receptor Trafficking to Synapses in Hippocampal Pyramidal Neurons. *Cell* 105, 331-343.
- Shrivastava, A.N., Kowalewski, J.M., Renner, M., Bousset, L., Koulakoff, A., Melki, R., Giaume, C., and Triller, A. (2013). β -Amyloid and ATP-Induced Diffusional Trapping of Astrocyte and Neuronal Metabotropic Glutamate Type-5 Receptors. *Glia.* 61, 1673-86.
- Simson, R., Sheets, E.D., and Jacobson, K. (1995). Detection of temporary lateral confinement of membrane proteins using single-particle tracking analysis. *Biophys. J.* 74, 297-308.
- Sinnen, B.L., Bowen, A.B., Forte, J.S., Gibson, E.S., Acqua, M.L.D., and Kennedy, M.J. (2017). Optogenetic Control of Synaptic Composition and Function. *Neuron.* 93, 646-660 e645.
- Skeberdis, V.A., Lan, J., Opitz, T., Zheng, X., Bennett, M.V., and Zukin, R.S. (2001). mGluR1-mediated potentiation of NMDA receptors involves a rise in intracellular calcium and activation of protein kinase C. *Neuropharmacology* 40, 856-865.
- Stowell, J.N., and Craig, a.M. (1999). Axon/dendrite targeting of metabotropic glutamate receptors by their cytoplasmic carboxy-terminal domains. *Neuron.* 22, 525-536.
- Tadokoro, S., Tachibana, T., Imanaka, T., Nishida, W., and Sobue, K. (1999). Involvement of unique leucine-zipper motif of PSD-Zip45 (Homer 1c/vesl-1L) in group 1 metabotropic glutamate receptor clustering. *Proc. Natl. Acad. Sci. U. S. A.* 96, 13801-13806.
- Tanaka, J., Nakagawa, S., Kushiya, E., Yamasaki, M., Fukaya, M., Iwanaga, T., Simon, M.I., Sakimura, K., Kano, M., and Watanabe, M. (2000). Gq protein alpha subunits Galphaq and Galpha11 are localized at postsynaptic extra-junctional membrane of cerebellar Purkinje cells and hippocampal pyramidal cells. *Eur. J. Neurosci.* 12, 781-792.

- Tang, A., Chen, H., Li, T., Metzbower, S., MacGillavry, H., and TA, B. (2016). A trans-synaptic nanocolumn aligns neurotransmitter release to receptors. *Nature* 536, 210-214.
- Topolnik, L., Azzi, M., Morin, F., Kougioumoutzakis, A., and Lacaille, J.-C. (2006). mGluR1/5 subtype-specific calcium signalling and induction of long-term potentiation in rat hippocampal oriens/alveus interneurons. *The J. Physiol.* 575, 115-131.
- Traynelis, S.F., Wollmuth, L.P., McBain, C.J., Menniti, F.S., Vance, K.M., Ogden, K.K., Hansen, K.B., Yuan, H., Myers, S.J., and Dingledine, R. (2010). Glutamate receptor ion channels: structure, regulation, and function. *Pharmacol. Rev.* 62, 405-496.
- Triller, A., and Choquet, D. (2005). Surface trafficking of receptors between synaptic and extrasynaptic membranes: And yet they do move! *Trends Neurosci.* 28, 133-139
- Tu, J.C., Xiao, B., Naisbitt, S., Yuan, J.P., Petralia, R.S., Brakeman, P., Doan, A., Aakalu, V.K., Lanahan, A.a., Sheng, M., and Worley, P.F. (1999). Coupling of mGluR/Homer and PSD-95 complexes by the Shank family of postsynaptic density proteins. *Neuron* 23, 583-592.
- Watson, J.F., Ho, H., and Greger, I.H. (2017). Synaptic transmission and plasticity require AMPA receptor anchoring via its N-terminal domain. *eLife* 6.
- Watson, J.F., Pinggera, A., Ho, H., and Greger, I.H. (2021). AMPA receptor anchoring at CA1 synapses is determined by N-terminal domain and TARP γ 8 interactions. *Nat. Commun.* 12, 5083.
- Westin, L., Reuss, M., Lindskog, M., Aperia, A., and Brismar, H. (2014). Nanoscopic spine localization of Norbin, an mGluR5 accessory protein. *BMC Neurosci.* 15, 45.
- Willems, J., de Jong, A.P.H., Scheefhals, N., Mertens, E., Catsburg, L.A.E., Poorthuis, R.B., de Winter, F., Verhaagen, J., Meye, F.J., and MacGillavry, H.D. (2020). Orange: A CRISPR/Cas9-based genome editing toolbox for epitope tagging of endogenous proteins in neurons. *PLoS Biol.* 18, e3000665.

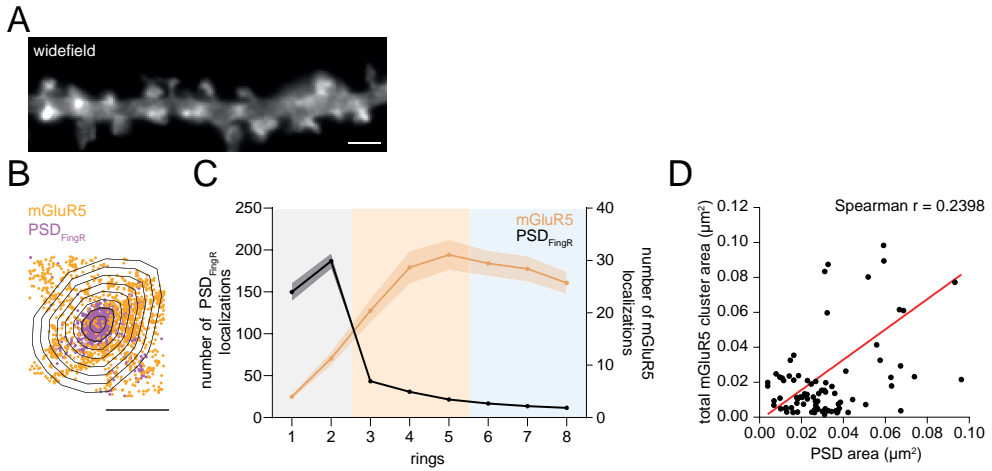
**Figure S1**

(A) Representative two-color gSTED image of dendrite with SEP-mGluR5 expression, with anti-GFP staining (cyan; Atto647N) to label surface-expressed receptors and co-stained for anti-PSD-95 (red; Alexa594). Scale bar, 2 μm. (B) Zooms of dendritic spines indicated in A with asterisks. Scale bar, 500 nm. (C) Linescan of spine 1 and (D) spine 2, indicated with dotted line in B. (E) Representative two-color gSTED image of dendrite endogenously stained for total mGluR5 (cyan; anti-mGluR5 Millipore Atto647N) and PSD-95 (red; Alexa594). Scale bar, 2 μm. (F) Zooms of dendritic spines indicated in E with asterisks. Scale bar, 500 nm. (G) Linescan of spine 1 and (H) spine 2, indicated with dotted line in F. (I) Representative three-color gSTED image of dendrite endogenously stained for total mGluR5 (cyan; anti-mGluR5 Alomone Atto647N), Phalloidin (magenta; Alexa594) and PSD-95 (red; Alexa488). Scale bar, 10 μm. (J) Zoom of dendritic spine stained for mGluR5 (cyan), Phalloidin (magenta)

Figure S1 continued on next page

Figure S1 continued

and PSD-95 (red). Scale bar, 500 nm. (K) Linescan of spine, indicated with dotted line in J. (L) Representative gSTED image of dendrite expressing SEP-GluA2, additionally labeled with anti-GFP nanobody Atto647N to visualize surface-expressed receptors (yellow), and Homer1c-mCherry (red; confocal). Scale bar, 2 μ m. (M) Zooms of dendritic spines indicated in L with asterisks. Scale bar, 500 nm. (N) Linescan of spine 1 and (O) spine 2, indicated with dotted line in M. (P) Representative two-color gSTED image of dendrite expressing myc-mGluR5 (cyan; anti-myc Alexa594 surface labeling) and SEP-GluA2 (yellow, anti-GFP Atto647N surface labeling). Scale bar, 2 μ m. (Q) Zooms of dendritic spines indicated in P with asterisks. Scale bar, 500 nm. (R) Linescan of spine 1 and (S) spine 2, indicated with dotted line in Q.

**Figure S2**

(A) Widefield image of dendrite expressing SEP-mGluR5 and PSD_{FingR}-mEos3.2 (green channel). Scale bar, 2 μm . (B) The rings from Figure 2E with the corresponding localizations of mGluR5 (orange) and PSD_{FingR} (cyan). Scale bar, 500 nm. (C) Absolute number of PSD_{FingR} (black; plotted on left y-axis) and mGluR5 (orange; plotted on right y-axis) localizations in rings 1 to 8. (D) Correlation between total mGluR5 cluster area and PSD area (in μm^2) (Correlation Spearman $r = 0.24$, $p = 0.03$). Data are represented as means \pm SEM.

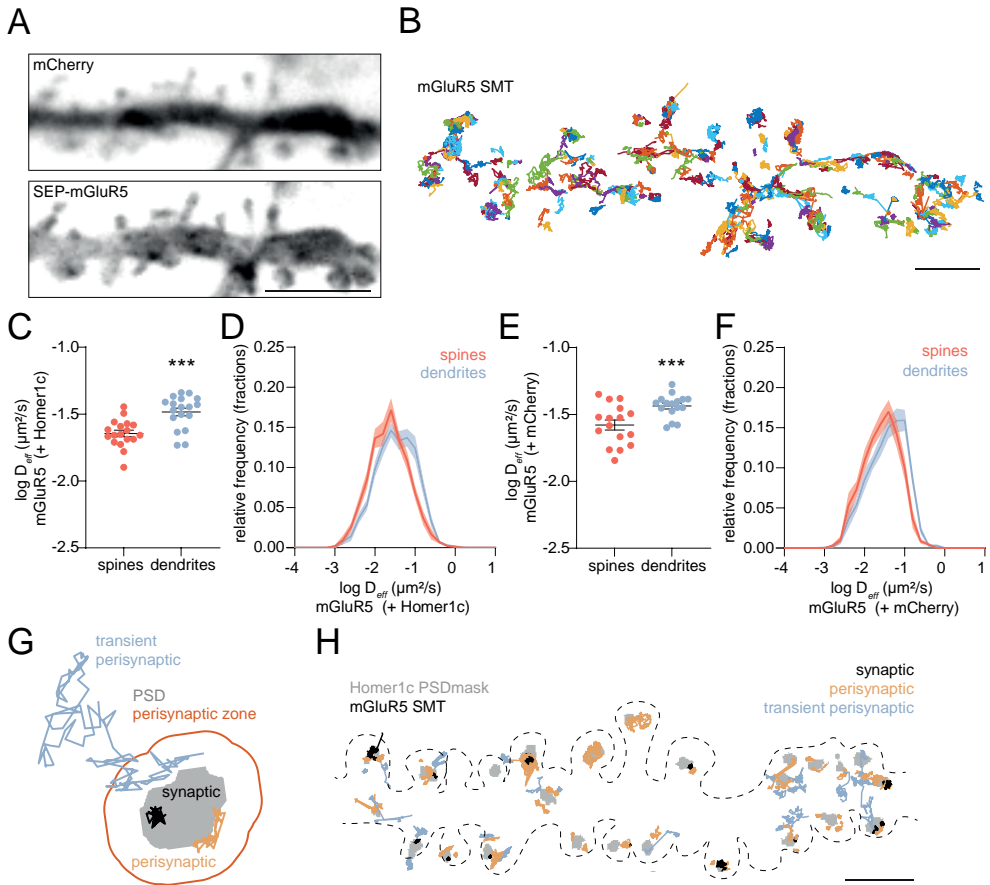
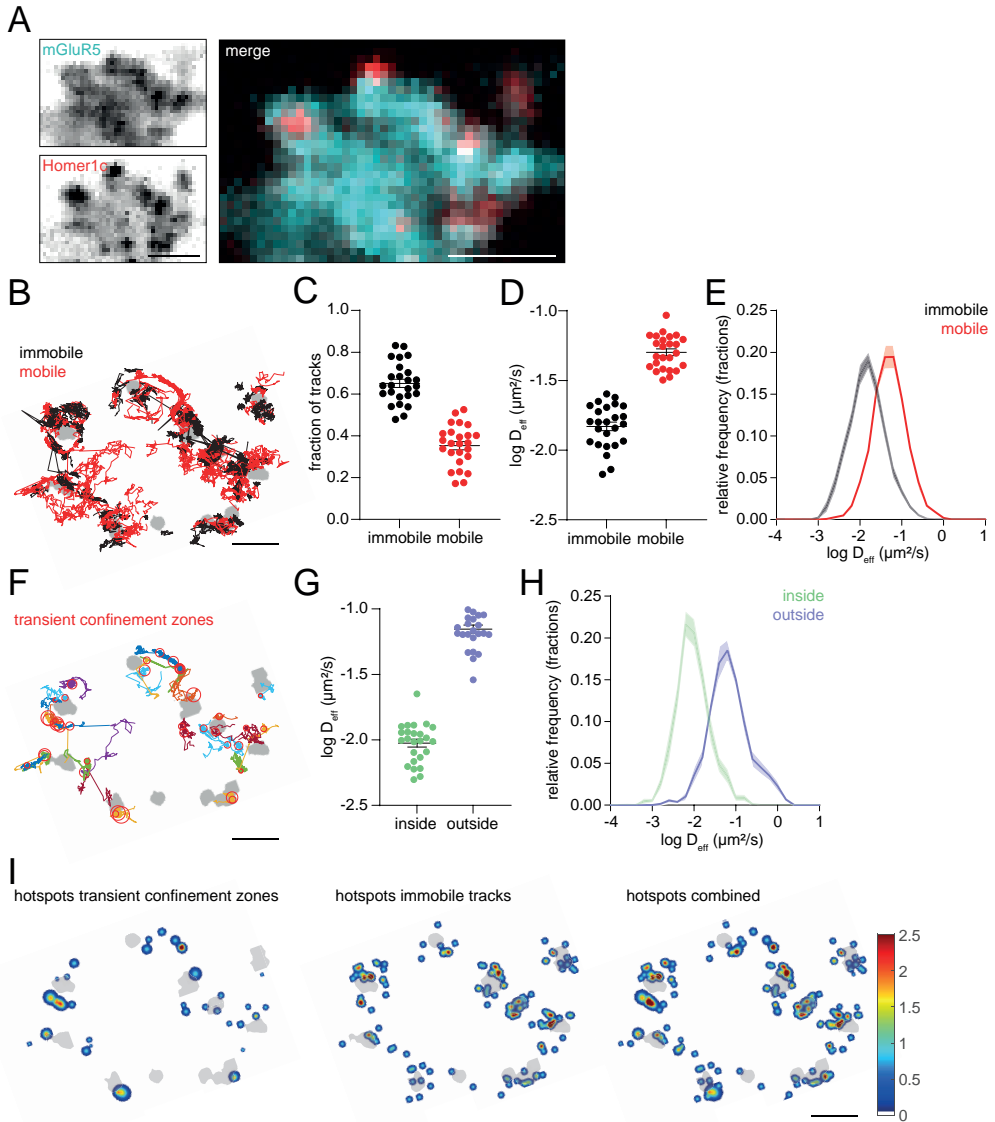
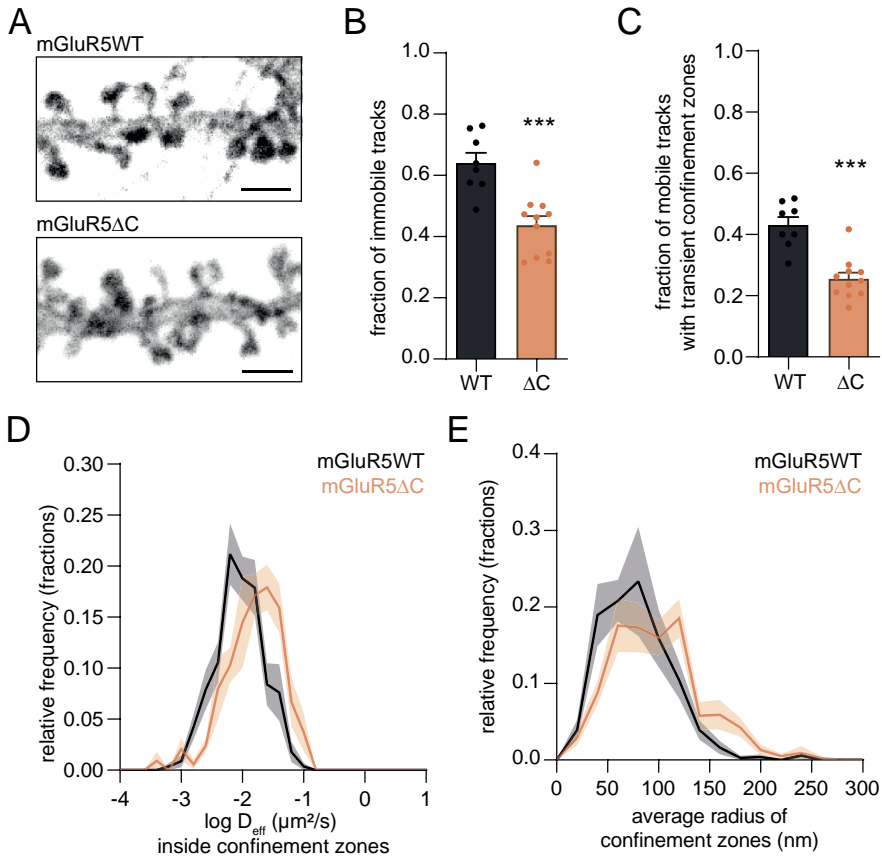


Figure S3

(A) Widefield image of dendrite expressing mCherry and SEP-mGluR5. Scale bar, 5 μm . (B) SMTs of mGluR5 (random colors) in the same dendrite as shown in A. Scale bar, 2 μm . (C) Mean $\log D_{\text{eff}}$ per neuron (paired t-test) and (D) relative frequency distributions of D_{eff} of mGluR5 trajectories in spines and dendrites co-transfected with Homer1c-mCherry ($n = 18$). (E) Mean $\log D_{\text{eff}}$ per neuron (paired t-test) and (F) relative frequency distributions of D_{eff} of mGluR5 trajectories in spines and dendrites co-transfected with mCherry ($n = 16$). (G) mGluR5 trajectories are assigned to different categories based on the degree of colocalization with the PSD (grey) and perisynaptic zone (orange): synaptic trajectories (black; $\geq 80\%$ overlap with PSD), perisynaptic trajectories (orange; $\geq 60\%$ overlap with the perisynaptic zone and $< 80\%$ overlap with PSD) and transient perisynaptic trajectories (blue; $> 0\%$, but $< 60\%$ overlap with the perisynaptic zone). (H) Synaptic (black), perisynaptic (orange) and transient perisynaptic (blue) SMTs of mGluR5 relative to the Homer1c PSD mask (grey) in the dendrite shown in Figure 3A and B. This dendrite is an example of the mGluR5 trajectories that are included for analysis, compared to the same dendritic stretch in Figure 3B with all obtained trajectories shown. Scale bar, 5 μm . Data are represented as means \pm SEM. *** $p < 0.001$.

**Figure S4**

(A) Widefield image of a dendrite expressing SEP-mGluR5 (cyan) and Homer1c-mCherry (red). Scale bar, 2 μm . (B) The same dendrite, with SMTs color-coded for immobile (black) and mobile (red) mGluR5 relative to the Homer1c PSD mask. Scale bar, 1 μm . (C) Fraction of immobile and mobile mGluR5 trajectories ($n = 25$ neurons). (D) Mean $\log D_{\text{eff}}$ per neuron and (E) relative frequency distributions of D_{eff} of immobile and mobile mGluR5 trajectories. (F) Transient confinement zones (red circles) of the mobile mGluR5 trajectories (random colors) shown in B. Scale bar, 1 μm . (G) Mean $\log D_{\text{eff}}$ per neuron and (H) relative frequency distributions of D_{eff} of mGluR5 trajectories inside (green) and outside (blue) confinement zones. (I) Hotspots of transient confinement zones (left), immobile track centers (middle) and both images combined (right), color-coded for the frequency of confinement zones and/or immobile tracks. Scale bar, 1 μm . Data are represented as means \pm SEM.

**Figure S5**

(A) Representative confocal images of dendrite with SEP-mGluR5WT (top) and SEP-mGluR5ΔC (bottom) expression, surface-labelled with an anti-GFP nanobody Atto647N. Scale bar, 2 μm . (B) Fraction of immobile trajectories of mGluR5WT ($n = 8$) and mGluR5ΔC ($n = 11$; unpaired- t -test). (C) Fraction of mobile trajectories with transient confinement zones for mGluR5WT and mGluR5ΔC (unpaired t -test). (D) Relative frequency distributions of D_{eff} of individual mGluR5WT and mGluR5ΔC trajectories inside confinement zones. (E) Relative frequency plot of the average radius of confinement zones for mGluR5WT and mGluR5ΔC trajectories. Data are represented as means \pm SEM. *** $p < 0.001$.

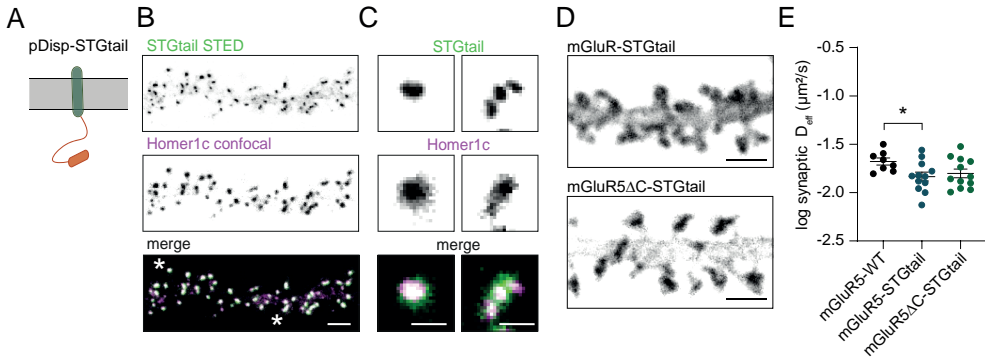


Figure S6

(A) Schematic of pDisp-TM-STGtail. (B) Representative gSTED image of dendrite expressing SEP-TM-STGtail, additionally labeled with an anti-GFP nanobody Atto647N (green), and Homer1c-mCherry (magenta; confocal). Scale bar, 2 μm. (C) Zooms of spines indicated in B with asterisks. Scale bar, 500 nm. (D) Representative confocal images of dendrite with SEP-mGluR5-STGtail (top) and SEP-mGluR5ΔC-STGtail (bottom) expression, surface-labelled with an anti-GFP nanobody Atto647N. Scale bar, 2 μm. (E) Mean log D_{eff} per neuron of synaptic trajectories of mGluR5WT, mGluR5-STGtail and mGluR5ΔC-STGtail. The mGluR5WT dataset shown E is also shown in Figure 5G, as these figures show different aspects of the same experiment. Data are represented as means \pm SEM. * $p < 0.05$.

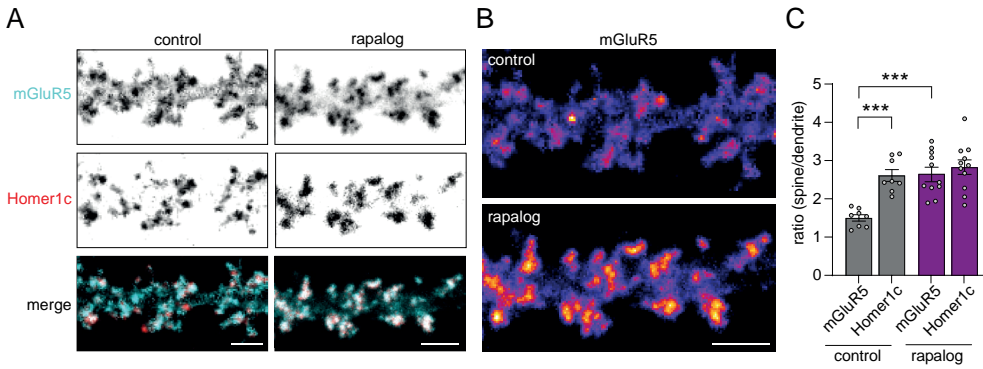


Figure S7

(A) Representative image of SEP-mGluR5-FRB and 2xFKBP-Homer1c-mcherry after vehicle (control) and rapalog application for 50 minutes. Scale bars, 2 μ m. (B) SEP-mGluR5-FRB color-coded for fluorescence intensity in control and rapalog neurons. Scale bar, 2 μ m. (C) Quantification of the ratio of spine over dendrite intensity of SEP-mGluR5-FRB and 2xFKBP-Homer1c-mCherry after vehicle (control; $n = 8$) and rapalog ($n = 11$) application for 50 minutes (one-way ANOVA with Tukey's multiple comparisons test). Data are represented as means \pm SEM. *** $p < 0.001$.

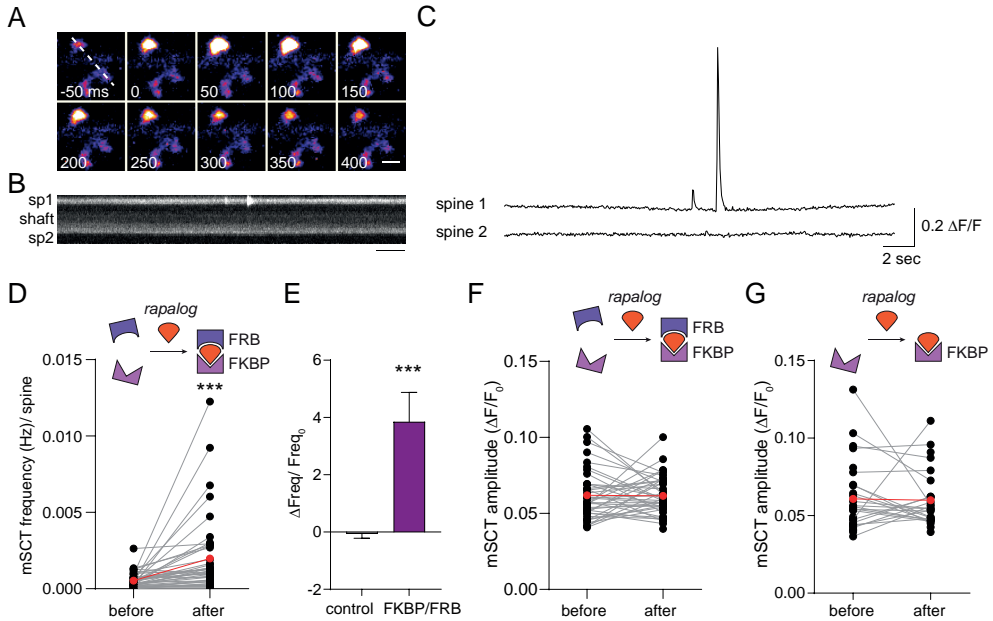
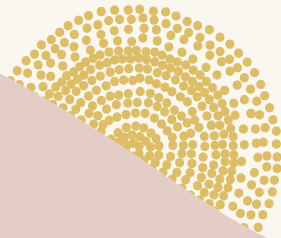


Figure S8

(A) Representative time-lapse of a spine with GCaMP6f expression showing one mSCT (scale bar, 1 μm), and (B) the kymograph showing two consecutive events at the same spine (sp1), and no detected Ca^{2+} increases at the dendritic shaft and neighboring spine (sp2). Scale bar, 2 sec. (C) The two successive mSCTs from spine 1 with different amplitudes and the absence of mSCTs in spine 2 (D) Quantification of mSCT frequencies upon application of rapalog in neurons expressing SNAP-mGluR5-FRB and 2xFKBP-Homer1c-mCherry, corrected for spine number ($n = 43$ neurons, Wilcoxon matched-pairs signed rank test). (E) mSCT frequencies per neuron before and after application of rapalog for 30 minutes in control (FKBP only) and FKBP/FRB neurons. The bar graph plots the change in mSCT frequency 30 minutes after rapalog application (ΔFreq), divided by the baseline value (Freq_0) (control: $n = 28$ and FKBP/FRB $n = 39$ neurons; Mann-Whitney test, only neurons included with minimum of one mSCT at baseline). (F) Quantification of mSCT amplitudes upon application of rapalog in neurons expressing SNAP-mGluR5-FRB and 2xFKBP-Homer1c-mCherry ($n = 39$ neurons, Wilcoxon matched-pairs signed rank test) and (G) in neurons expressing SNAP-mGluR5 and 2xFKBP-Homer1c-mCherry (control) ($n = 22$ neurons, Wilcoxon matched-pairs signed rank test). Means are indicated by the red lines. Data in E is represented as means \pm SEM. *** $p < 0.001$.

6



ORANGE: A CRISPR/Cas9-based genome editing toolbox for epitope tagging of endogenous proteins in neurons

Jelmer Willems^{1,*}, Arthur P. H. de Jong^{1,*}, Nicky Scheefhals¹, Eline Mertens¹, Lisa A. E. Catsburg¹, Rogier B. Poorthuis², Fred de Winter³, Joost Verhaagen³, Frank J. Meye², Harold D. MacGillavry¹

*These authors contributed equally to this work

¹Cell Biology, Neurobiology and Biophysics, Department of Biology, Faculty of Science, Utrecht University, Utrecht, the Netherlands

²Department of Translational Neuroscience, UMC Utrecht Brain Center, Utrecht University, Utrecht, the Netherlands,

³Laboratory for Neuroregeneration, Netherlands Institute for Neuroscience, Royal Netherlands Academy of Arts and Sciences, Amsterdam, the Netherlands

PLoS Biology (2020),18(4): 1-41

Abstract

The correct subcellular distribution of proteins establishes the complex morphology and function of neurons. Fluorescence microscopy techniques are invaluable to investigate subcellular protein distribution, but they suffer from the limited ability to efficiently and reliably label endogenous proteins with fluorescent probes. We developed ORANGE: Open Resource for the Application of Neuronal Genome Editing, which mediates targeted genomic integration of epitope tags in rodent dissociated neuronal culture, in organotypic slices, and *in vivo*. ORANGE includes a knock-in library for in-depth investigation of endogenous protein distribution, viral vectors and a detailed two-step cloning protocol to develop knock-ins for novel targets. Using ORANGE with (live-cell) superresolution microscopy, we revealed the dynamic nanoscale organization of endogenous neurotransmitter receptors and synaptic scaffolding proteins, as well as previously uncharacterized proteins. Finally, we developed a mechanism to create multiple knock-ins in neurons, mediating multiplex imaging of endogenous proteins. Thus, ORANGE enables quantification of expression, distribution, and dynamics for virtually any protein in neurons at nanoscale resolution.

Introduction

Neurons are highly complex cells with numerous functionally and structurally distinct subcellular compartments that are each composed of unique repertoires of molecular components. The correct targeting and localization of protein complexes and their spatial organization within subcellular domains underlies virtually every aspect of neuronal functioning. Thus, investigating the dynamic distribution of proteins in neurons is critical for a mechanistic understanding of brain function. Precise localization of individual protein species using fluorescence microscopy has become an essential technique in many fields of neuroscience and, in particular, for studies on synaptic function, in which protein mislocalization at scales less than 1 μm can already significantly affect synaptic efficacy (Biederer et al., 2017). Recently developed superresolution imaging methods now routinely achieve spatial resolution as low as tens of nanometers, allowing determination of protein distributions at the molecular scale (Sahl et al., 2017; Sigal et al., 2018). Consequently, these methods are highly sensitive to experimental alterations that affect protein organization, and efficient labeling techniques that accurately report the localization of endogenous proteins are critical.

Visualization of subcellular protein localization typically relies on antibody-based labeling approaches or overexpression of fluorescently tagged proteins, but both techniques have serious limitations (Schnell et al., 2012). Immunostaining largely relies on the availability of specific antibodies, which has severely hampered progress for many targets. Immunostaining also precludes labeling and visualization of protein dynamics in live cells, and penetration of antibodies in thick tissue samples is challenging. Additionally, it is often desirable to sparsely label individual cells to measure protein distribution at high contrast, which is difficult to achieve with immunostaining-based techniques. Expression of fluorescently tagged proteins overcomes many of these issues; however, exogenous expression of recombinant proteins can lead to mislocalization and can induce severe morphological and/or physiological artifacts. For instance, overexpression of synaptic proteins such as postsynaptic density

protein 95 (PSD95) and SH3 and multiple ankyrin repeat domains protein (Shank) have pronounced effects on synapse number, content, structure, and physiology (El-Husseini et al., 2000; Futai et al., 2007; Roussignol et al., 2005; Sala et al., 2001). Exorbitant expression levels can be circumvented by a replacement strategy in which a tagged protein is expressed in a knock-down or knock-out background (Schluter et al., 2006), but this will, at best, only approximate endogenous levels and is uncoupled from endogenous transcriptional or translational regulatory mechanisms. Recombinant antibody-based approaches have been developed for live-cell imaging of neuronal proteins, but they have so far been restricted to a few targets (Dong et al., 2019; Fukata et al., 2013; Gross et al., 2013; Mora et al., 2013; Nizak et al., 2003). The generation of fluorescently tagged knock-ins (for instance, in mouse lines) prevents these issues. However, the generation and maintenance of transgenic animals is costly and time consuming, making it an inefficient approach for high-throughput tagging of neuronal proteins. Also, generally, transgenic labeling leads to expression of tagged proteins in all cells, thus limiting the options for imaging in individual cells.

In view of the limitations of current techniques, we sought to develop a protein labeling strategy that meets the following criteria: (1) accurately reports a single protein species at endogenous protein levels and with spatiotemporal expression pattern; (2) can be rapidly developed and expanded to many proteins of interest; (3) does not interfere with protein localization and function; (4) can be applied in dissociated neuronal cultures, organotypic slice culture, and *in vivo*; (5) allows for sparse labeling of neurons; and (6) is compatible with (superresolution) light microscopy of live as well as fixed tissues. We reasoned that labeling of endogenous proteins with fluorescent tags using targeted gene-editing techniques would fulfill all these criteria.

Targeted gene editing using CRISPR/Cas9 facilitates the introduction of donor DNA at specific loci in the genome, effectively tagging endogenous proteins of interest (Knott and Doudna, 2018; Lee et al., 2018). For neuronal cells, several CRISPR/Cas9-based knock-in strategies have been developed, relying on different mechanisms to repair double-stranded breaks (DSBs) introduced by Cas9. One strategy is based on homology-directed repair (HDR) to insert donor DNA into the genomic locus (Mikuni et al., 2016; Uemura et al., 2016). However, HDR preferentially occurs during the S/G2 phases of the cell cycle and is significantly down-regulated in postmitotic cells (Orthwein et al., 2015). This limits the application of HDR in neurons, although successful integration can still be observed with highly elevated donor DNA levels or via a combination of donor cleavage and microhomology arms (Nishiyama et al., 2017; Yao et al., 2017). Additionally, in order to be efficient, HDR requires the addition of long homology arms to the donor DNA, which can be laborious to generate, considerably complicating the development of knock-in constructs.

Alternative strategies are based on nonhomologous end joining (NHEJ) to repair DSBs, which is active throughout the cell cycle, as well as in postmitotic cells, and can be used to insert donor DNA with high efficiency (Betermier et al., 2014; Gao et al., 2019; Suzuki et al., 2016). Based on NHEJ, the homology-independent targeted integration (HITI) method for endogenous protein tagging in postmitotic neurons was previously developed and outperformed HDR-based methods (Suzuki et al., 2016; Yao et al., 2017). We hypothesized that HITI would provide an accessible and scalable approach for the tagging of endogenous proteins in neurons, in dissociated neuronal cultures and organotypic cultures, and *in vivo*. However, applications of this method have so far been limited to a few target proteins (Matsuda and Oinuma, 2019; Spence et al., 2019; Suzuki

et al., 2016; Yao et al., 2017). In addition, designing and cloning of knock-in constructs, the compatibility of DNA delivery methods for various tissue preparations, and validation of NHEJ-based knock-in accuracy and efficiency have until now been quite challenging and have not been addressed systematically.

Here, based on HITI, we developed ORANGE, an Open Resource for the Application of Neuronal Genome Editing, which offers researchers the means to endogenously tag proteins of interest in neurons, allowing for the accurate investigation of protein expression, localization, and dynamics. This toolbox includes (1) a single template vector that contains the complete knock-in cassette, which can be adapted in two straightforward cloning steps to tag virtually any protein of interest, and (2) a library of readily usable knock-in constructs targeting a set of 38 proteins. This library encompasses a wide variety of proteins, including cytoskeletal components, signaling molecules, endosomal markers, presynaptic and postsynaptic scaffolds, adhesion complexes, and receptors. We show that this tagging strategy facilitates protein labeling in dissociated neuronal culture, in organotypic slice cultures, and *in vivo* with high accuracy and without overexpression artifacts. Moreover, we demonstrate that this toolbox facilitates live-cell and superresolution imaging of endogenous proteins to resolve their localization and dynamics in neurons at high spatial and temporal resolution. We furthermore show that ORANGE can be combined with the Cre-Lox system driving the conditional expression of genetically encoded reporters. Finally, we developed a Cre-dependent knock-in strategy for multiplex labeling of proteins within single cells. Altogether, we present a robust and easy-to-implement toolbox for the tagging and visualization of endogenous proteins in postmitotic neurons, allowing for in-depth investigation of diverse neuronal cell biological processes.

Results

ORANGE knock-in toolbox to fluorescently tag endogenous proteins in neurons

We first aimed to design a simple workflow to facilitate the rapid generation of knock-in constructs using conventional molecular cloning approaches. To this end, we designed a single CRISPR/Cas9 knock-in template vector (pORANGE) based on the original NHEJ-mediated HITI method (Suzuki et al., 2016). Our design allows for the flexible insertion of a unique 20-nucleotide target sequence that guides Cas9 to the genomic locus of interest and a donor sequence containing the knock-in sequence (e.g., green fluorescent protein [GFP]) that will be inserted in the targeted genomic locus (Figure 1A and S1 Fig). The generated knock-in construct contains all elements required for targeted CRISPR/Cas9-based genome editing: (1) a U6-driven expression cassette for the guide RNA (gRNA) targeting the genomic locus of interest, (2) the donor sequence containing the (fluorescent) tag, and (3) a Cas9 expression cassette driven by a universal β -actin promoter (Figure 1A). The donor sequence is generated by standard PCR, with primers introducing a short linker and Cas9 target sequences flanking the donor (Figure 1A). These target sequences are identical to the genomic target sequence. As a result, the gRNA used to create a genomic DSB is also used to remove the donor DNA from the plasmid, allowing for its genomic integration. Importantly, the orientation of the target sequence and protospacer adjacent motif (PAM) sites flanking the donor is inverted compared with the genomic sequence to guarantee that integration

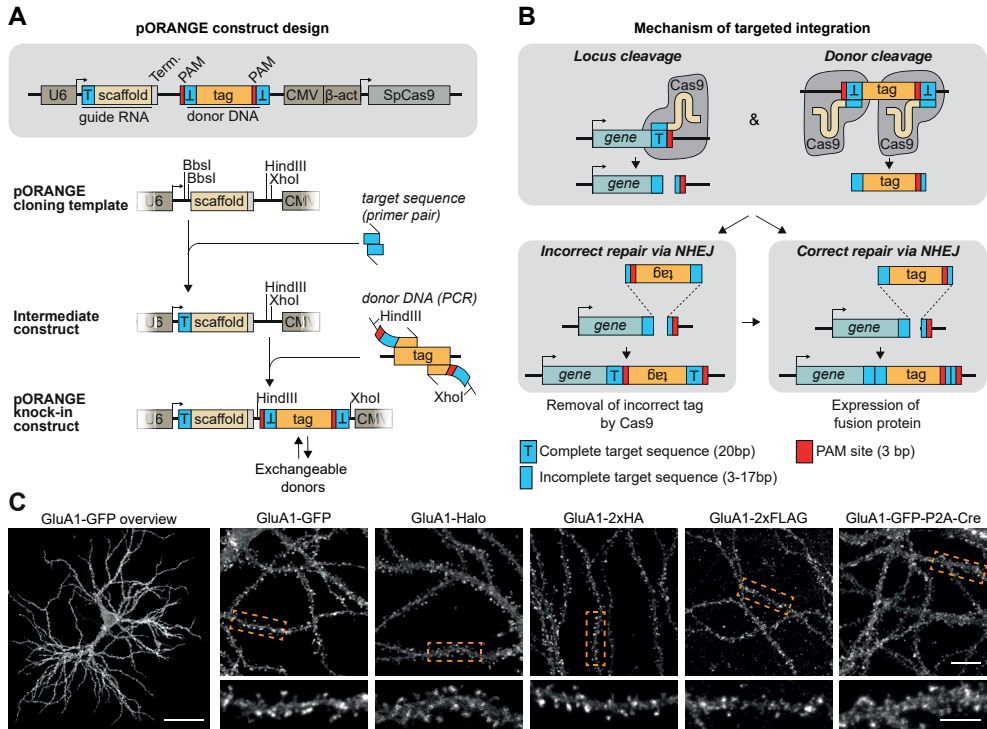


Figure 1. ORANGE: An easy-to-implement toolbox for endogenous tagging of proteins in neurons

(A) Overview of the pORANGE knock-in construct. To clone knock-in constructs, first a 20-bp target sequence for the genomic locus of interest is ligated in the guide RNA cassette. Then, the donor sequence containing the tag of interest is generated by PCR and inserted in the donor DNA cassette. (B) Mechanism of ORANGE-mediated gene targeting. (C) Examples of knock-in neurons expressing GluA1 tagged with GFP, HaloTag, small epitope tags (2x HA, 2x FLAG), or GFP-P2A-Cre recombinase. Dashed boxes indicate zooms. Scale bars, 40 μ m for the GluA1-GFP overview (far left), 10 μ m for individual overviews, and 5 μ m for the zooms. GFP, green fluorescent protein; NHEJ, nonhomologous end joining; ORANGE, Open Resource for the Application of Neuronal Genome Editing; T, target sequence; Term, termination sequence. PAM: protospacer adjacent motif; CMV, cytomegalovirus; β -act, β -actin; SpCas9, *Streptococcus pyogenes* Cas9, GluA, Glutamate receptor AMPA 1; HA, hemagglutinin.

occurs in the correct orientation (Figure 1B). For a detailed description of genomic target sequence selection, gRNA sequence, and donor PCR primer design, we refer to the design and cloning protocol in the Materials and methods section (also see S1 Fig). This approach is flexible because the donor sequence can be easily exchanged for different fluorophores, self-labeling enzymes like Halo, small epitope tags like hemagglutinin (HA) and FLAG, or larger donors like GFP-P2A-Cre to meet the specific demands for the experiment (Figure 1C). We found that this cloning strategy is easy to employ and enables the rapid and flexible generation of knock-in constructs.

Using the pORANGE template vector, we designed and generated a library providing knock-in constructs to endogenously label 38 proteins for fluorescence imaging (Figure 2, S2 Fig, and S5 Table). To cover the many areas of neuronal cell biology, we selected proteins representing various molecular processes, including cytoskeletal components, intracellular

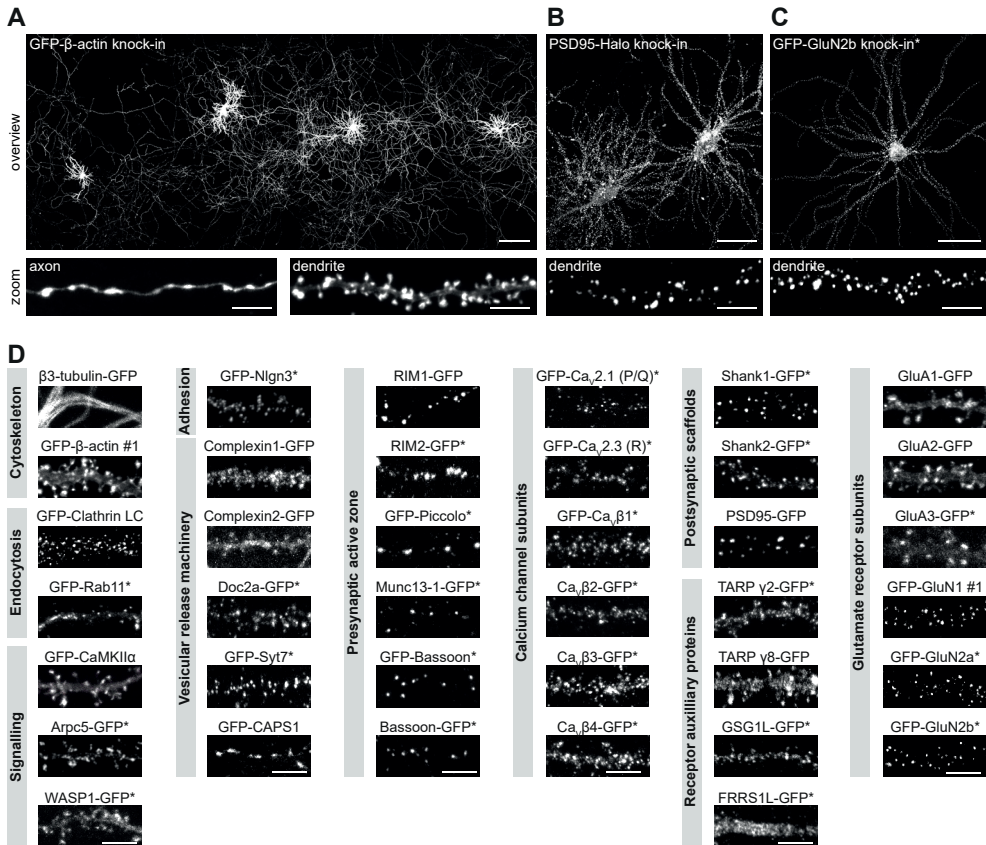


Figure 2. A versatile ORANGE knock-in library for endogenous tagging of proteins in neurons

(A) Example at low magnification showing four GFP- β -actin knock-in neurons (DIV 21). Zooms show an axon and dendrite, respectively. Scale bars: overview, 200 μ m; zoom, 5 μ m. (B) Example of two PSD95-Halo knock-in neurons (DIV 21). Zoom shows a single dendrite. Scale bars: overview, 40 μ m; zoom, 5 μ m. (C) Example of GFP-GluN2b knock-in neuron (DIV 21). Scale bars: overview, 40 μ m; zoom, 5 μ m. (D) Representative images of ORANGE knock-in neurons, categorized according to protein function or subcellular localization. Neurons were transfected at DIV 3 and imaged at DIV 21. Scale bars, 5 μ m. Asterisk indicates signal enhancement with anti-GFP staining (Alexa488 or Alexa647). GFP, green fluorescent protein; ORANGE, Open Resource for the Application of Neuronal Genome Editing; DIV, day *in vitro*; PSD95, postsynaptic protein 95; GluA, glutamate receptor AMPA 1; GluN, Glutamate receptor NMDA 1; LC, light chain; Rab11, ras-related protein 11; CaMKII α , Calcium/calmodulin-dependent protein kinase type II subunit alpha; Arpc5, actin-related protein 2/3 complex subunit 5; WASP1, Wiskott-Aldrich syndrome protein 1; Nlgn3, neuroligin 3; Doc2a, double C2-like domain-containing protein a; Syt7, Synaptotagmin 7; CAPS1, Calcium-dependent activator protein for secretion 1; RIM: Rab3-interacting molecule; Munc13, mammalian uncoordinated 13, CAV, voltage-dependent Ca²⁺-channel, Shank, SH3 and multiple ankyrin repeat domains protein; TARP, Transmembrane AMPAR regulatory protein; GSG1L, Germ cell-specific gene 1-like protein; FRRS1L, Ferric-chelate reductase 1-like protein.

signaling molecules, trafficking proteins, synaptic scaffolds, and receptor subunits. We were able to directly image the fluorescent GFP signal for many endogenously tagged proteins. However, for less abundant proteins (e.g., calcium channel subunits, presynaptic active zone proteins, and N-methyl-D-aspartate (NMDA) receptor subunits), amplification of the GFP tag with anti-GFP antibodies was required to visualize protein distribution (indicated with

an asterisk in Figure 2 and S2 Fig). Throughout this study, we refer to knock-in constructs as the name of the protein that is labeled: in N-terminally tagged proteins, the tag is in front of the protein name, and in C-terminally tagged proteins, the tag is after.

For several proteins in our library, no specific antibodies are available. In order to compare their subcellular distribution to what is reported in literature (S1 Table), we costained several knock-ins with pre- or postsynaptic markers and confirmed the expected distribution for all of the constructs we evaluated (S3 Fig). Together, our ORANGE toolbox includes a broad library of knock-in constructs and provides an efficient strategy to adapt or design constructs with relative ease using standardized cloning techniques.

Viral delivery of ORANGE to label endogenous proteins in dissociated neuronal cultures and organotypic slice cultures and *in vivo*

Adeno-associated virus (AAV)-based DNA delivery has become a valuable method of administration, especially for *in vivo* applications. To test whether this approach is compatible with ORANGE, we generated HaloTag knock-in constructs for PSD95 and Glutamate receptor AMPA 1 (GluA1) and subcloned these into AAV vectors. AAVs were injected in the cornu Ammonis region 1 (CA1) of the hippocampus in Cas9-P2A-GFP transgenic mice (Platt et al., 2014) (Figure 3A). After 4 weeks, acute slices were prepared and live-stained with Halo-JF646. This resulted in fast labeling deep into the tissue. For both PSD95 and GluA1, efficient knock-in labeling was observed in CA1, as well as in CA3 and subiculum, with additional labeling in the dentate gyrus (Figure 3C and 3D). At higher magnifications, we only observed neurons with punctate, synaptic expression of PSD95-Halo. Similarly, although to a lesser extent, GluA1-Halo was also highly enriched in dendritic spines, as expected (Figure 3E and G). Finally, we used superresolution gated stimulated-emission depletion (gSTED) imaging to resolve individual synapses at high resolution (Figure 3F and H).

Next, we tested whether ORANGE knock-ins could also be delivered using lentiviral (LV) vectors. We divided the ORANGE knock-in cassette over two LV constructs (S4A Fig) because the full cassette exceeds the packaging limit of LV particles. Also, premature coexpression of Cas9 and the gRNA during the production of viral particles in packaging cells would lead to removal of the donor DNA. Both in dissociated hippocampal cultures and in organotypic slice cultures, we observed knock-ins, showing that LVs can be used to successfully express ORANGE knock-ins (S4 Fig). Together, these results show that ORANGE is compatible with various modes of DNA delivery suitable for labeling in dissociated neuronal cultures, in organotypic slice cultures and *in vivo*, broadening the potential applications of this CRISPR/Cas9 genome editing toolbox.

ORANGE enables fast and accurate donor integration

To test the rate of donor integration and subsequent expression of tagged proteins with lipofection-based DNA delivery, we cotransfected dissociated hippocampal neurons at day *in vitro* (DIV) 3 with a β 3-tubulin-GFP knock-in construct and a construct for soluble mCherry expression (S5 Fig). Because of the high protein turnover rate of β 3-tubulin, integration of the donor should be rapidly observable by expression of the tagged protein. Successful labeling of β 3-tubulin was observed within 24 hours after transfection, albeit at relatively low efficiency ($1.1\% \pm 0.2\%$ β 3-tubulin GFP+/mCherry+ double positive cells).

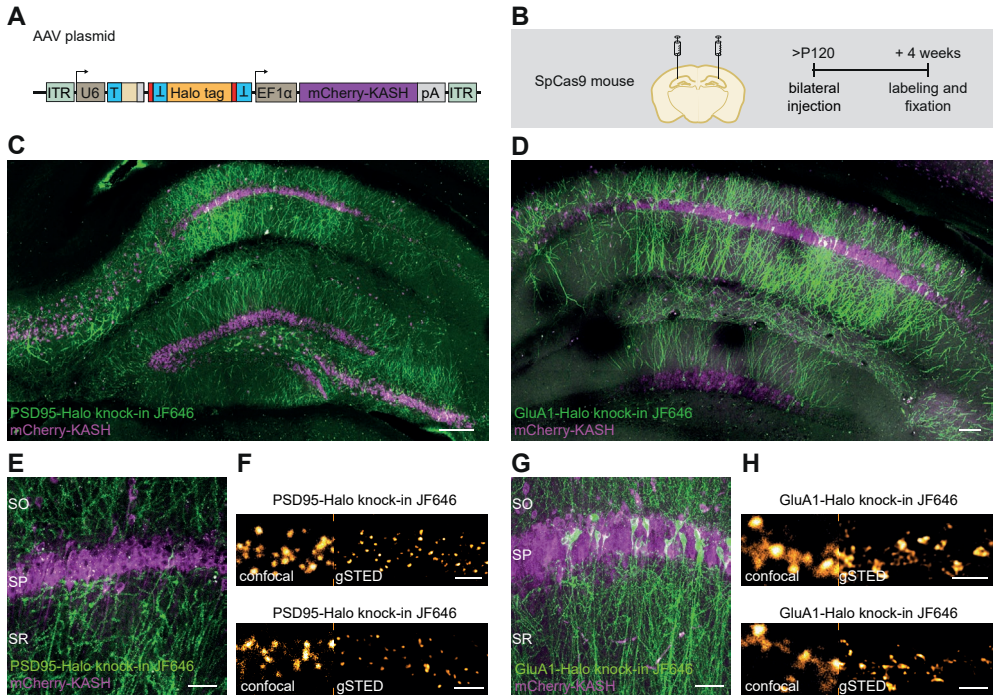


Figure 3. ORANGE mediates *in vivo* genome editing

(A) Overview of ORANGE AAV plasmid. (B) Workflow and time line for *in vivo* genome editing. (C and D) Confocal images of acute slices from SpCas9 mouse hippocampus injected with PSD95-Halo knock-in (C) and GluA1-Halo knock-in (D) AAV vectors visualized with Halo-JF646 ligand (green). Infected cells are positive for mCherry-KASH (magenta). Scale bar, 100 μ m. (E and G) Zooms for acute slices as shown in (C) and (D), respectively. Scale bar, 40 μ m. (F and H) Representative images of confocal and gSTED microscopy in acute slices. Shown are dendrites positive for PSD95-Halo (F) and GluA1-Halo knock-in (H). Scale bar, 2 μ m. AAV, adeno-associated virus; gSTED, gated stimulated-emission depletion; ORANGE, Open Resource for the Application of Neuronal Genome Editing; SO, stratum oriens; SP, stratum pyramidale; SR, stratum radiatum. SpCas9, *Streptococcus pyogenes* Cas9; PSD95, postsynaptic protein 95; GluA, Glutamate receptor AMPA, JF646 Janelia Fluor 646; KASH, Klarsicht, ANC-1, Syne Homology; ITR, inverted terminal repeat; T, target sequence; EF1 α , elongation factor 1 α ; pA, polyadenylation.

Labeling efficiency increased 10-fold over time and reached a plateau around 96 hours after transfection ($10.9\% \pm 0.1\%$ β 3-tubulinGFP+/mCherry+; S5 Fig), indicating that donor integration preferentially takes place within the first days after transfection.

Next, we determined the accuracy of genomic integration for our knock-in library using confocal microscopy. Expression patterns were in line with available literature (S1 Table), and we did not observe aberrant or diffuse expression of the integrated tag for any of the knock-in constructs in our library. This indicates that off-target integration, or unintended GFP expression directly from the knock-in plasmid, did not occur or is extremely rare (see Discussion).

To get a detailed overview of the precision of donor integration into the targeted genomic locus, we analyzed the genomic sequence after integration for 28 GFP knock-in constructs using next-generation sequencing (S6 Fig). We detected a high frequency of in-

frame integration of the GFP tag in the targeted locus for almost all knock-ins (S6B and C Fig). Besides correct integration, we found various insertions and deletions leading to frameshift mutations (S6B and D Fig). We noted that the frequency of indels was variable between different knock-ins, which is likely due to the difference in target sequences, which has been reported to highly determine the accuracy of Cas9-mediated cleavage and NHEJ-mediated repair (Shen et al., 2018; van Overbeek et al., 2016). Notably, the accuracy of donor integration did not correlate with the Doench on-target score (Doench et al., 2016) (Pearson r : -0.15 , R^2 : 0.02 , $P < 0.05$) or Bae out-of-frame score (Bae et al., 2014) (Pearson r : 0.25 , R^2 : 0.06 , $P > 0.05$) (S6E and F Fig). In conclusion, although out-of-frame integration occurs at varying frequencies as shown by next-generation sequencing, imaging of our knock-in library suggests that this does not result in a fluorescent signal or aberrant protein expression.

We noted that several of the knock-in constructs with lower in-frame integration, such as GFP- β -actin and GFP-Glutamate receptor NMDA 1 (GluN1), also had a low efficiency of knock-in expression in cultured neurons. To test whether this is gene specific or guide sequence specific, and in an attempt to generate more efficient knock-in constructs for these genes, we designed extra knock-in constructs for β -actin (GFP- β -actin #2) and GluN1 (GFP-GluN1 #2 and #3) by making use of alternative PAM sites (S7 Fig). All alternative PAM site variants resulted in successful GFP knock-ins in cultured neurons, with expected GFP expression patterns. Again, we did not observe neurons with aberrant distribution of GFP signal. For both genes, we found that various PAM sites along the same genomic region varied widely in their knock-in efficiency relative to the number of transfected neurons (GFP- β -actin knock-in #1: $0.42\% \pm 0.09\%$, #2: $7.4\% \pm 1.1\%$, Student t test, $P < 0.05$; GFP-GluN1 knock-in #1: $0.43\% \pm 0.04\%$, #2: $3.0\% \pm 0.7\%$, #3: $5.6\% \pm 0.4\%$, ANOVA, $P < 0.05$). These results show that knock-in efficiency is highly dependent on the target site used for integration.

ORANGE reliably labels proteins without overexpression artifacts

To further determine whether the integrated fluorescent tag reliably labels the endogenous target protein, we compared the localization of several knock-ins with specific antibody staining in confocal microscopy. First, we tested the knock-in construct for PSD95, a core postsynaptic scaffold molecule (Sheng and Hoogenraad, 2007) (Figure 4). We transfected dissociated hippocampal cultures with the PSD95-GFP knock-in construct well before synaptogenesis (DIV 3) and fixed the neurons at a mature stage (DIV 21) (Figure 4A-G). In all neurons with a detectable GFP signal, the GFP signal was found in a punctate pattern enriched in dendritic spines, characteristic for endogenous PSD95 expression. The GFP signal closely colocalized with immunolabeled PSD95 and showed a strong correlation with intensity of PSD95 immunostaining in PSD95-GFP knock-in neurons (Pearson r : 0.72 , R^2 : 0.51 , $P < 0.001$, $n = 550$ synapses from 11 neurons; Figure 4B). To test whether the knock-in affects total PSD95 levels, we used the PSD95 antibody staining to compare protein levels between PSD95-GFP knock-in and control neurons that were transfected with soluble GFP (GFP control). Although we observed that, in a subpopulation of PSD95 knock-in neurons, protein levels were modestly lower, PSD95 levels in PSD95-GFP knock-in neurons (relative fluorescence intensity: 0.84 ± 0.04 , $n = 17$ neurons) were on average comparable to GFP control neurons (0.98 ± 0.02 , $n = 15$ neurons, ANOVA, $P > 0.05$) (Figure 4C; inset). In contrast, overexpression of PSD95-GFP significantly increased

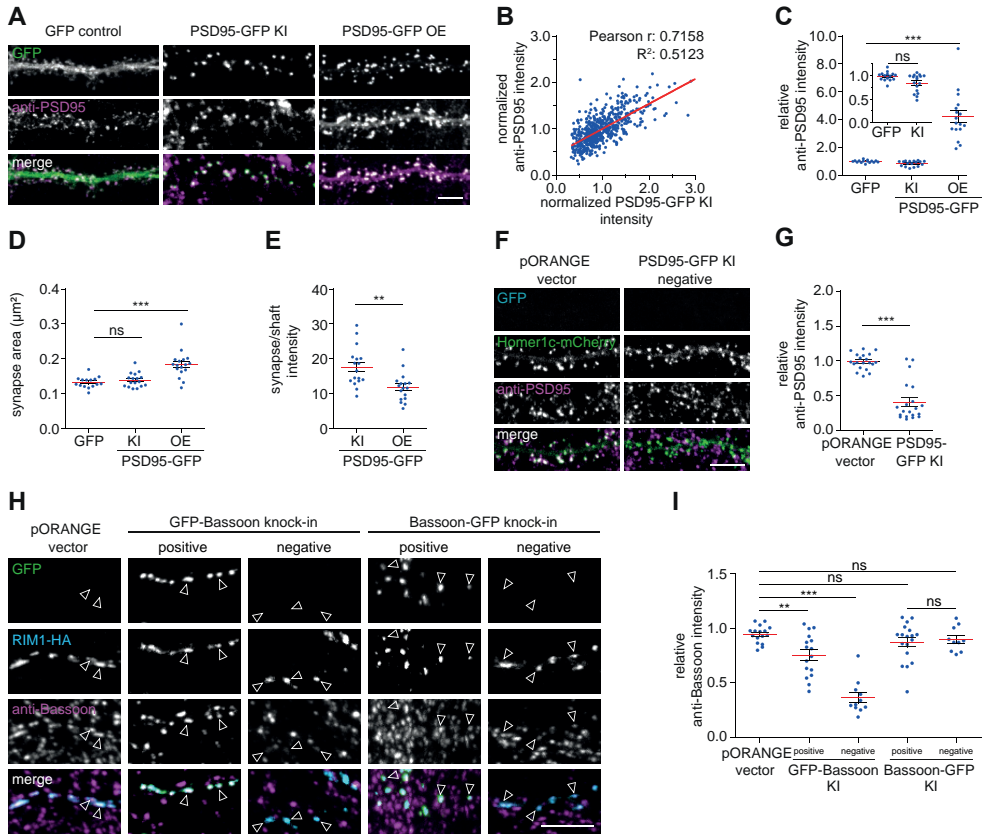


Figure 4. Validation of ORANGE labeling efficiency

(A) Representative images of dendrites transfected with soluble GFP, PSD95-GFP knock-in (KI) construct, or a PSD95-GFP overexpression construct (green) stained with anti-PSD95 (magenta, Alexa568). DIV 21. Scale bar, 5 μm . (B) Correlation between PSD95-GFP KI and anti-PSD95 staining intensity. (C) Quantification of synaptic PSD95 levels, (D) synapse area, and (E) PSD95 synapse/shaft intensity. (F) Representative images of dendrites coexpressing Homer1c-mCherry (green) and either the empty pORANGE template vector or PSD95-GFP KI construct (blue) stained with anti-PSD95 (magenta, Alexa647). DIV 21. Scale bar, 5 μm . (G) Quantification of PSD95 levels in transfected but KI-negative neurons. Data are represented as means \pm SEM. * $P < 0.05$, ** $P < 0.01$, *** $P < 0.001$, ANOVA or Student t test. Underlying data can be found in S1 Data. GFP, green fluorescent protein; KI, knock-in; ns, not significant; ORANGE, Open Resource for the Application of Neuronal Genome Editing; PSD95, postsynaptic protein 95; DIV, day *in vitro*; OE, overexpression; RIM1, Rab3-interacting molecule 1; HA, hemagglutinin.

synaptic PSD95 protein levels (relative fluorescence intensity: 4.2 ± 0.4 , $n = 17$ neurons, $P < 0.001$). Moreover, synapse size was significantly increased in neurons overexpressing PSD95 ($0.18 \pm 0.01 \mu\text{m}^2$) compared with GFP control neurons ($0.13 \pm 0.01 \mu\text{m}^2$, ANOVA, $P < 0.001$) but was unaffected in PSD95-GFP knock-in neurons ($0.14 \pm 0.001 \mu\text{m}^2$, $P > 0.05$; Figure 4D). Lastly, we found that PSD95 was significantly more enriched at synapses in PSD95 knock-in cells (ratio synapse/shaft intensity: 17.6 ± 1.4) compared with PSD95-overexpressing neurons (11.8 ± 1.0 , Student t test, $P < 0.01$; Figure 3E), indicating that a large fraction of overexpressed PSD95 mislocalized to the dendritic shaft.

Transfection of knock-in constructs did not always result in successful knock-in of GFP (S5-7 Fig). To determine whether in transfected but GFP knock-in-negative neurons integration of the GFP tag was simply not successful or integration introduced indels affecting protein expression, we cotransfected neurons with the PSD95-GFP knock-in construct with a Homer1c-mCherry overexpression construct to label synapses. We measured PSD95 levels in Homer1c-mCherry-positive neurons that did not show detectable PSD95-GFP signal (Figure 4F and G). In most of these GFP-negative neurons, PSD95 protein levels were significantly down-regulated (relative fluorescence intensity: 0.41 ± 0.06 , $n = 20$ neurons) compared with neurons cotransfected with the empty pORANGE template vector and Homer1c-mCherry (0.99 ± 0.02 , $n = 20$ neurons, Student t test, $P < 0.001$), suggesting partial or complete knock-out of the target protein in transfected but knock-in-negative neurons.

In addition to PSD95, we measured protein levels for several other proteins, including Shank2, Calcium/calmodulin-dependent protein kinase type II subunit alpha (CaMKII α), β -actin (S8 Fig), and the presynaptic active zone protein Bassoon (Figure 4H and I) in successful knock-in neurons as well as in knock-in-negative neurons. Additionally, taking advantage of the fact that Bassoon tolerates both N-terminal and C-terminal tagging (S1 Table) (Dresbach et al., 2003), we designed GFP-Bassoon and Bassoon-GFP knock-in constructs to compare the effect of tagging the same protein at different positions in the gene. Both N-terminal and C-terminal Bassoon knock-ins showed an identical, punctate expression pattern and colocalized with coexpressed Rab3-interacting molecule 1 (RIM1)-HA, a presynaptic marker (Figure 4H). This indicates that, for Bassoon, endogenous tagging either at the N-terminus or C-terminus does not interfere with protein localization. Using a specific Bassoon antibody, we found that, like PSD95, most knock-in neurons express Bassoon at endogenous levels. However, the N-terminal-tagged knock-in neurons showed a slightly larger fraction of neurons with reduced levels of Bassoon (relative fluorescence intensity: 0.75 ± 0.05 , $n = 16$ neurons, $P < 0.01$) compared with C-terminal-tagged (0.87 ± 0.04 , $n = 18$ neurons, $P > 0.05$) and control cells (0.94 ± 0.01 , $n = 16$ neurons). Notably, neurons transfected with (but negative for) the GFP-Bassoon knock-in showed significantly reduced levels of Bassoon (0.36 ± 0.04 , $n = 11$ neurons, $P < 0.001$), whereas transfection of the Bassoon-GFP knock-in did not affect protein levels in knock-in-negative neurons (0.90 ± 0.04 , $n = 10$ neurons, ANOVA, $P < 0.05$). Furthermore, we found that the GFP signal of the Shank2, CaMKII α , and β -actin knock-ins approximated endogenous levels but that the protein levels in knock-in-negative cells varied between constructs (S8 Fig). Thus, although a successful knock-in results in accurate detection of endogenously tagged proteins, erroneous integration may lead to partial knock-out of the targeted gene in knock-in-negative neurons depending on the protein and position of integration. Altogether, these data demonstrate that ORANGE enables successful integration of fluorescent tags at the targeted genomic locus, resulting in expression of fusion proteins, which reliably reports the localization of proteins of interest, without overexpression artifacts.

Live-cell imaging of endogenous protein dynamics

In addition to imaging fixed cells, the introduction of fluorescent tags allows for imaging of endogenous protein dynamics in living cells. To demonstrate this directly, we performed live-cell imaging on GFP- β -actin knock-in neurons. First, we confirmed that N-terminal

tagging of endogenous β -actin with GFP did not alter the actin network based on phalloidin staining of fixed neurons (S8 Fig). Second, we acquired time-lapse images of GFP- β -actin knock-in neurons showing the characteristic dynamic behavior of actin in dendritic spines (Hotulainen et al., 2009; Korobova and Svitkina, 2010) (Figure 5A). Jasplakinolide (Jasp), which stabilizes actin filaments and promotes actin polymerization, rapidly reduced dendritic spine dynamics (as measured by an increase in frame-to-frame correlation, 0.89 ± 0.01 , $n = 7$ neurons) compared with DMSO control (0.84 ± 0.01 , $n = 7$ neurons, Student t test, $P < 0.01$) (Figure 5B and C). We noted that the diffuse actin signal was depleted from the dendritic shafts after Jasp application, indicating that the enhanced actin polymerization incorporated free actin monomers from the dendritic shaft. We further evaluated this with a fluorescence recovery after photobleaching (FRAP) assay (Figure 5D). In control neurons, β -actin turnover was fast, with a large mobile pool (mobile fraction: 0.87 ± 0.01 , $n = 13$ neurons, Figure 5E and F), consistent with measures based on overexpressed β -actin (Zheng et al., 2010). As expected, addition of Jasp largely abolished turnover of spine β -actin (mobile fraction: 0.02 ± 0.01 , $n = 13$ neurons, Student t test, $P < 0.001$), indicating that Jasp induced integration of most GFP- β -actin in stable actin filaments. These experiments show that ORANGE knock-ins are compatible with live-cell imaging of endogenous protein dynamics in neurons.

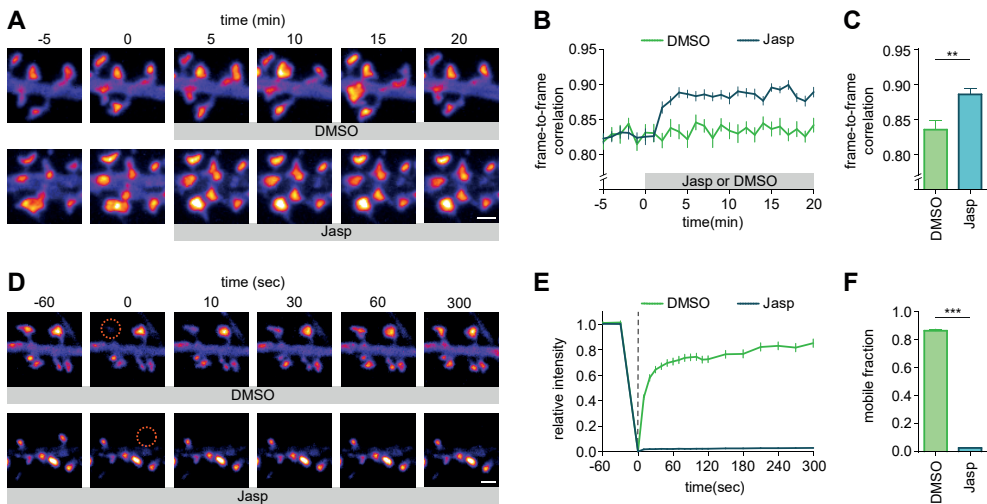


Figure 5. Live-cell imaging of intracellular endogenous protein dynamics

(A) Representative images of dendrites transfected with GFP- β -actin knock-in imaged over time. DMSO or Jasp was added at time point 0. DIV 21. Scale bar, 1 μ m. (B) Frame-to-frame correlation of pixel intensity over time for DMSO (green) or Jasp (blue) addition. (C) Quantification of mean frame-to-frame correlation averaged over the last five time points. (D) Representative images of FRAP experiment on dendrites transfected with GFP- β -actin knock-in vector. ROIs were bleached at time point 0 (orange circle). Recovery was followed over time. DIV 21. Scale bar, 1 μ m. (E) FRAP analysis of GFP- β -actin knock-in neurons treated with DMSO (control) or Jasp. ROIs were bleached at time point 0 (dotted line). (F) Quantification of mobile fraction calculated from the last five time points of each bleached ROI averaged per neuron. Data are represented as means \pm SEM. ** $P < 0.01$, *** $P < 0.001$, Student t test. Underlying data can be found in S1 Data. FRAP, fluorescence recovery after photobleaching; GFP, green fluorescent protein; Jasp, jasplakinolide; ORANGE, Open Resource for the Application of Neuronal Genome Editing; ROI, region of interest; DIV day *in vitro*.

Single-molecule imaging is a powerful tool to investigate the dynamics of individual molecules within living cells. We designed knock-in constructs targeting CaMKII α , an abundant neuronal Ca²⁺-activated signaling protein essential for learning and memory (Lisman et al., 2012). Confocal microscopy showed that the GFP-CaMKII α knock-in was primarily cytoplasmic with moderate enrichment in spines (Figure 2 and S2 Fig), consistent with previous studies (Mikuni et al., 2016; Shen and Meyer, 1999). We next replaced GFP for monomeric Eos 3.2 (mEos3.2), a photoconvertible protein compatible with single-molecule tracking based on photoactivated localization microscopy (PALM) (Frost et al., 2010; Lu et al., 2014) (S9A Fig). Individual mEos3.2-CaMKII α molecules were imaged to reconstruct a superresolved image of CaMKII α distribution (S9B Fig) and to map single-molecule trajectories in spines and dendrites over time (S9C and D Fig). From the trajectories, we calculated the mean-squared displacements (MSDs) to derive the diffusion coefficient for individual trajectories (S9E and F Fig), revealing two distinct dynamic CaMKII α populations: a mobile population (mean diffusion coefficient $0.145 \pm 0.049 \mu\text{m}^2/\text{s}$) and less-mobile population ($0.0140 \pm 0.0011 \mu\text{m}^2/\text{s}$, $n = 11$ neurons). Thus, genetic tagging with photoconvertible molecules such as mEos3.2 can be used for live-cell single-molecule tracking PALM experiments to resolve the distribution and dynamics of endogenous, intracellular proteins.

6

Superresolution imaging of endogenously expressed proteins in neurons

We envisioned that tagging endogenous proteins particularly presents advantages for superresolution imaging by facilitating labeling of proteins in a subset of neurons and overcoming many artifacts associated with antibody specificity or overexpression of recombinant proteins. Also, this combination would be interesting for studying recently identified proteins with unknown subcellular distribution.

First, we employed our GFP- β -actin and β 3-tubulin-GFP knock-in constructs to resolve and correlate their well-known subcellular organization in individual neurons using gSTED microscopy. Recent superresolution studies have demonstrated that the actin cytoskeleton forms ring-like structures that are periodically organized along axons as well as dendrites (D'Este et al., 2015; Han et al., 2017a; Xu et al., 2013). We tested whether we could resolve this particular organization of the actin cytoskeleton in individual β -actin knock-in neurons within dense, mature, dissociated hippocampal cultures. Using gSTED imaging, we observed distinct periodic actin structures in both the axon and dendrites (Figure 6A-E). In addition to resolving the actin network, we performed two-color gSTED imaging of β 3-tubulin-GFP knock-in neurons immunolabeled with anti- α -tubulin to resolve the neuronal microtubule network (S10A-C Fig). Thus, ORANGE combined with superresolution imaging is an easily accessible approach to resolve the subcellular distribution of endogenous proteins with high resolution.

Second, we took advantage of ORANGE to perform two-color gSTED imaging on synaptic proteins. To assess the performance of ORANGE knock-ins compared with conventional antibody staining in resolving subsynaptic protein organization using STED microscopy, we compared the localization of the PSD95-GFP knock-in signal with that of immunolabeled PSD95. Both confocal and gSTED images of individual synapses revealed a high degree of colocalization between the PSD95-GFP knock-in and anti-PSD95 staining (Figure 6F). Additionally, gSTED revealed that even at the subsynaptic level, the PSD95-

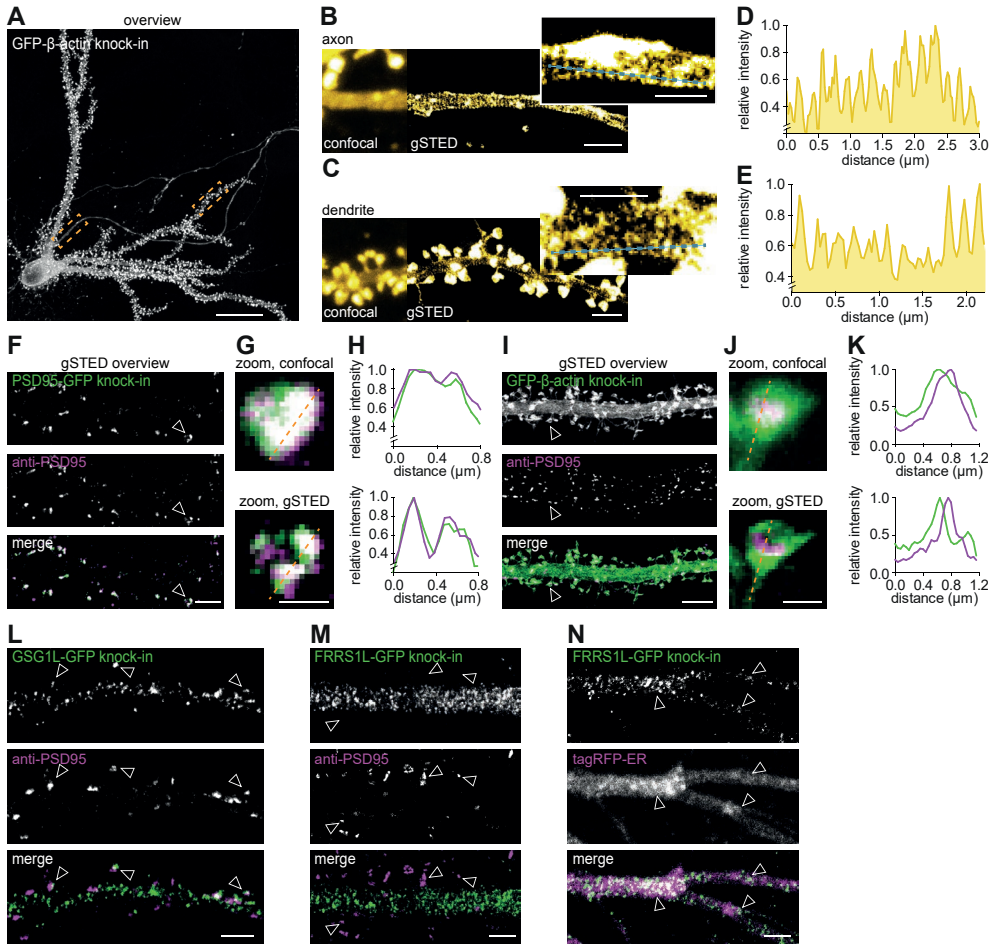


Figure 6. STED microscopy to resolve the subcellular distribution of endogenous proteins in individual neurons

(A) Representative gSTED image of a GFP- β -actin knock-in neuron (DIV 21) enhanced with anti-GFP (ATTO647N). Scale bar, 20 μ m. (B and C) Zooms of axon (B) and dendrite (C) as indicated with boxes in (A) comparing confocal and gSTED imaging. Scale bar, 2 μ m; insert scale is 1 μ m. (D and E) Line scans from zooms in (B) and (C), respectively. (F) Representative gSTED images of dendrites positive for PSD95-GFP knock-in stained with anti-GFP (green, ATTO647N) and anti-PSD95 staining (magenta, Alexa594). DIV 21. Scale bar, 2 μ m. (G) Zooms from (F) of individual synapses resolved with confocal and gSTED. Scale bar, 500 nm. (H) Line scans of confocal and gSTED images shown in (G). (I) Representative gSTED images of dendrites positive for GFP- β -actin knock-in stained with anti-GFP (green, ATTO647N) and anti-PSD95 (magenta, Alexa594). DIV 21. Scale bar, 2 μ m. (J) Zooms from (I) of individual spines resolved with confocal and gSTED. Scale bar, 500 nm. (K) Line scans of confocal and gSTED images shown in (J). (L and M) Representative gSTED images of dendrites positive for GSG1L-GFP (L) or FRRS1L-GFP knock-in (M) stained with anti-GFP (green, Alexa488) and anti-PSD95 (magenta, ATTO647N). DIV 21. Scale bar, 5 μ m. (N) Representative images of dendrites positive for FRRS1L-GFP knock-in enhanced with anti-GFP (gSTED, green) and coexpressed with tagRFP-ER (confocal, magenta). DIV 21. Scale bar, 2 μ m. GFP, green fluorescent protein; gSTED, gated STED; STED, stimulated-emission depletion; DIV, day *in vitro*; PSD95, postsynaptic protein 95; GSG1L, Germ cell-specific gene 1-like protein; FRRS1L, Ferric-chelate reductase 1-like protein; RFP, red fluorescent protein; ER, endoplasmic reticulum.

GFP knock-in and anti-PSD95 staining colocalized (Figure 6G and H). In contrast, two-color gSTED of GFP- β -actin knock-in and anti-PSD95 staining revealed that β -actin is enriched in dendritic spines but is largely excluded from the synapse (Figure 6I-K). The differential distribution of the PSD95-GFP and GFP- β -actin knock-ins was confirmed by quantifying the degree of colocalization with immunolabeled anti-PSD95 using two independent metrics: the Pearson's correlation coefficient (PCC) and Manders' overlap correlation (MOC) (Dunn et al., 2011; Manders et al., 1992), highlighting the need for superresolution techniques, such as STED (S10D and F Fig). Additionally, we found that CaMKII α is enriched in dendritic spines and only partially overlapped with PSD95 (S10G-J Fig).

Lastly, we studied the subcellular expression of proteins that have only recently been discovered. High-throughput proteomics studies have identified a number of novel components of the α -amino-3-hydroxy-5-methyl-4-isoxazolepropionic acid (AMPA) receptor complex that have different topologies and functions (Bissen et al., 2019; Schwenk et al., 2012). Information on the subcellular distribution of these components is sparse and largely based on overexpression, which is known to alter the trafficking and function of AMPA receptors at synapses. Here, we developed knock-in constructs for two AMPA receptor interactors: Germ cell-specific gene 1-like protein (GSG1L) and Ferric-chelate reductase 1-like protein (FRRS1L)/C9orf4. GSG1L has been recently shown to modulate AMPA receptor function (Gu et al., 2016; Shanks et al., 2012). Using gSTED imaging, we found that GSG1L localizes throughout the dendritic shaft and in dendritic spines, where it closely associates with synaptic PSD95 (Figure 6L). In contrast, FRRS1L was found to be excluded from synapses (Figure 6M) but showed a punctate distribution in the dendritic shaft, closely associated with the endoplasmic reticulum (ER) (Figure 6N). This is in line with a recent study showing that FRRS1L regulates AMPA receptor trafficking from the ER to control AMPA receptor surface expression (Brechet et al., 2017; Han et al., 2017b; Schwenk et al., 2019; Stewart et al., 2019). Altogether, these results demonstrate the potential of ORANGE to uncover the nanoscale organization of endogenous proteins, in particular those with unknown distribution due to lack of specific antibodies, in individually labeled neurons.

Dissection of endogenous NMDA receptor distribution and dynamics within individual synapses

Based on overexpression and antibody-labeling studies, the spatial organization of NMDA receptors at excitatory synapses has been proposed to be heterogeneous, with receptors accumulating in distinct subsynaptic nanodomains (Jezequel et al., 2017; Kellermayer et al., 2018; MacGillavry et al., 2013). However, because overexpression of individual receptor subunits could affect subunit stoichiometry and function of endogenous receptors (Shi et al., 2001), we combined ORANGE with superresolution techniques to dissect the distribution and dynamics of NMDA receptors. To visualize the total pool of NMDA receptors, we developed a knock-in construct to endogenously tag the obligatory GluN1 subunit with GFP (Figure 7A). Several studies have consistently estimated that the number of NMDA receptors at individual synapses is relatively low, ranging from 10 to 20 receptor complexes per synapse (Peng et al., 2004; Sheng and Hoogenraad, 2007). Despite these low copy numbers, we could detect concentrated dendritic clusters of GFP-GluN1, most of which colocalized with immunolabeled PSD95 (Figure 7A). Interestingly, we found that GFP-GluN1 intensity did not correlate with anti-PSD95 immunolabeling intensity (Figure 7B) (Pearson r : 0.19, R^2 :

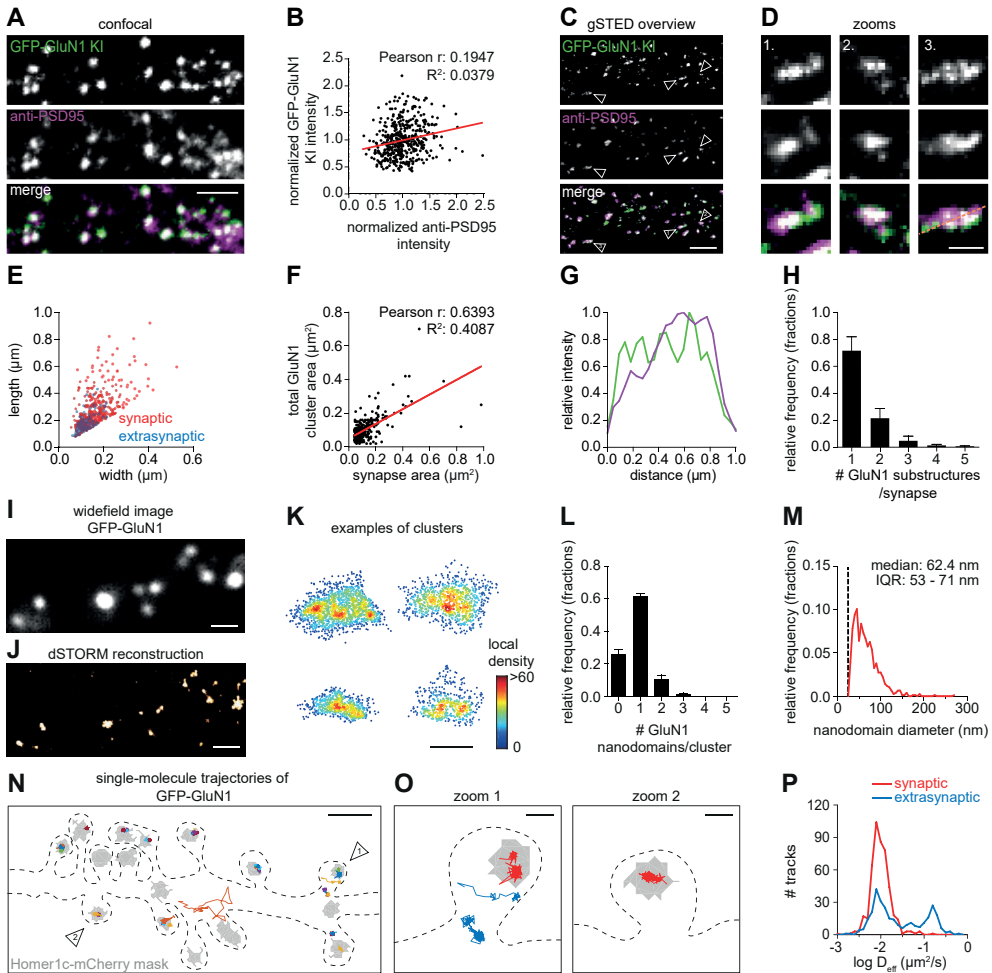


Figure 7. NMDA receptors concentrate in subsynaptic nanodomains and are highly immobilized in synapses

(A) Representative images of a dendrite positive for GFP-GluN1 KI (green) stained for PSD95 (magenta, Alexa647). Scale bar, 2 μm . (B) Correlation between GFP-GluN1 KI and anti-PSD95 staining intensity within individual GFP-GluN1 puncta. (C) Representative gSTED images of dendrites positive for GFP-GluN1 KI enhanced with anti-GFP (green, ATTO647N) and anti-PSD95 (magenta, Alexa594). DIV 21. Scale bar, 2 μm . (D) Zooms of individual synapses indicated in (C). Scale bar, 500 nm. (E) FWHM analysis of GFP-GluN1 structures comparing width and length of individual synaptic (red) and extrasynaptic (blue) GluN1 clusters. (F) Correlation between GFP-GluN1 cluster area and synapse area (based on anti-PSD95 staining) for individual synapses. (G) Line scan of synapse zoom 3 in (D). (H) Quantification of the number of GFP-GluN1 substructures per synapse. (I) Representative image of dendrite positive for GFP-GluN1 KI stained with anti-GFP (Alexa647). DIV 21. Scale bar, 1 μm . (J) Single-molecule dSTORM reconstruction of example shown in (I). Scale bar, 1 μm . (K) Examples of individual GFP-GluN1 clusters with single localizations plotted and color-coded based on the local density. Scale bar, 200 nm. (L) Quantification of number of GFP-GluN1 nanodomains per cluster. (M) Frequency distribution of GFP-GluN1 nanodomain size. Dotted line indicates nanodomain size cutoff. Bin size: 5 nm. (N) Representative example of GFP-GluN1 (anti-GFP nanobody conjugated to ATTO647N) single-molecule trajectories in a dendrite plotted with a random color and on top of a synapse mask (gray) based on Homer1c-mCherry widefield image. Dotted line indicates cell outline. DIV 21. Scale bar, 1 μm . (O) Zooms of

Figure 7 continued on next page

Figure 7 continued

individual spines indicated in (N) with example trajectories of synaptic (red) or extrasynaptic (blue) receptors. Scale bar, 200 nm. (P) Frequency distribution showing the diffusion coefficient of synaptic and extrasynaptic tracks. Data in bar plots are presented as means \pm SEM. Underlying data can be found in S1 Data. dSTORM, direct stochastic optical reconstruction microscopy; FWHM, Full Width at Half Maximum; GFP, green fluorescent protein; gSTED, gated stimulated-emission depletion; KI, knock-in; NMDA, N-methyl-D-aspartate; GluN, glutamate receptor NMDA; PSD95, postsynaptic protein 95; DIV, day *in vitro*.

0.038, $n = 450$ GluN1 clusters from nine neurons), consistent with earlier studies showing that the total number of NMDA receptors is largely invariable and does not scale with synapse size (Metzbower et al., 2019; Nimchinsky et al., 2004; Racca et al., 2000). Using gSTED imaging, we found that although most GFP-GluN1 clusters localized to synapses, some smaller extrasynaptic clusters could be detected (Figure 7C-E). Next, we measured the total GFP-GluN1 cluster area in individual synapses and found a slight correlation with synapse size (Pearson r : 0.64, R^2 : 0.4087, $n = 266$ synapses from three neurons; Figure 7F). Thus, our data suggest that the subsynaptic area covered by NMDA receptors, but not the total number of receptors, scales with synapse size. gSTED imaging of individual synapses also indicated that the subsynaptic distribution of GFP-GluN1 is heterogeneous (Figure 7B, G), with individual synapses containing one or more smaller GFP-GluN1 substructures (Figure 7H) ($n = 266$ synapses from three neurons).

To further investigate the subsynaptic distribution of NMDA receptors, we turned to single-molecule localization microscopy (SMLM). The GFP-GluN1 knock-in was immunolabeled with anti-GFP and Alexa647-coupled secondary antibodies for direct stochastic optical reconstruction microscopy (dSTORM) to reconstruct the spatial organization of NMDA receptors at individual synapses with nanometer precision (Figure 7I and J). Clusters of GFP-GluN1 receptors were identified using density-based spatial clustering of applications with noise (DBSCAN) (Ester et al., 1996). Next, all localizations within individual clusters were plotted and color-coded for the local density. These local density maps revealed that, within individual clusters, NMDA receptors form distinct nanodomains (Figure 7K), consistent with our gSTED data (Figure 7D). We found that the majority of GFP-GluN1 clusters contained one to three nanodomains with a median size of approximately 62 nm (IQR: 53–71 nm) ($n = 859$ GFP-GluN1 clusters from three neurons) (Figure 7L and M). Thus, these SMLM data indicate that endogenous NMDA receptors form distinct subsynaptic nanodomains.

To gain insight in the subsynaptic mobility of endogenously expressed NMDA receptors, we probed the diffusion kinetics of individual receptors using universal point accumulation in nanoscale topography (uPAINT) (Giannone et al., 2010). Stochastic labeling of individual GFP-tagged receptors with a GFP nanobody coupled to ATTO647N provided a map of individual receptor mobility along stretches of dendrites (Figure 7N and O). Most receptor trajectories mapped within the boundaries of the synapse. Strikingly, we found that these synaptic NMDA receptors were largely immobilized (median diffusion coefficient synaptic tracks: $0.0096 \mu\text{m}^2/\text{s}$, IQR: 0.0079 – 0.0122 , $n = 462$ tracks from 6 neurons), whereas on average, extrasynaptic receptors diffuse at higher rates ($0.0224 \mu\text{m}^2/\text{s}$, IQR: 0.0123 – 0.0419 , $n = 307$ tracks from 6 neurons) (Figure 7P). Altogether, by combining the ORANGE toolbox with superresolution microscopy, we show that NMDA receptors are enriched in the PSD, where they are highly immobilized and cluster in subsynaptic nanodomains.

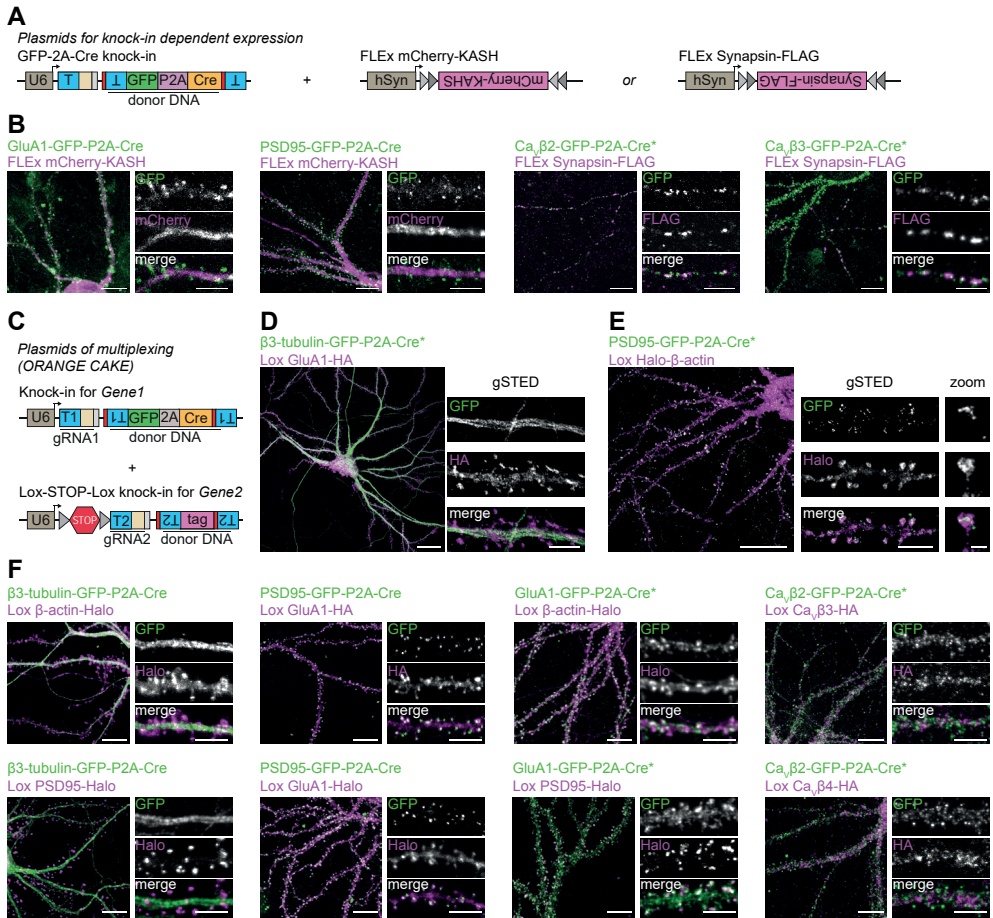


Figure 8. Cre-dependent coexpression and labeling of two proteins in single neurons

(A) Overview of plasmids used for Cre-dependent expression mCherry-KASH or Synapsin-FLAG in knock-in neurons. (B) Examples of GFP-P2A knock-in–driven expression of mCherry-KASH or Synapsin-FLAG (Alexa568) (magenta) for various knock-ins. DIV 21. Scale bars, 10 μ m and 5 μ m for the overviews and zooms, respectively. (C) Overview of plasmids used for multiplex knock-in of two proteins in single neurons (ORANGE CAKE). (D and E) Examples of β ₃-tubulin-GFP-P2A-Cre (green), Lox GluA1-HA (magenta, Alexa594) double knock-in, (D) and PSD95-GFP-P2A-Cre (green), Lox Halo- β -actin (magenta, JF549) double knock-in (E). Shown are overviews (confocal) and zooms (gSTED). DIV 21. Scale bars, 20 μ m for the overviews and 5 μ m (dendrites) and 500 nm (spine) for the zooms. (F) Examples of various combinations of GFP-P2A-Cre (green) and Lox (magenta) double knock-ins. HA was visualized by anti-HA staining (Alexa594), and Halo with Halo-JF549 ligand. DIV21. Scale bars, 10 μ m and 5 μ m for the overviews and zooms, respectively. Asterisk indicates enhancement with anti-GFP antibody (Alexa488). CAKE, conditional activation of knock-in expression; FLEx, flip-excision; GFP, green fluorescent protein; gRNA, guide RNA; gSTED, gated stimulated-emission depletion; ORANGE, Open Resource for the Application of Neuronal Genome Editing. KASH, Klarsicht, ANC-1, Syne Homology; DIV, day *in vitro*; HA, hemagglutinin; GluA, glutamate receptor AMPA; PSD95, postsynaptic protein 95; JF549, Janelia Fluor 549; T, target sequence; hSyn, human Synapsin; CaV, voltage-dependent Ca²⁺-channel.

Cre-dependent coexpression for multiplex labeling of two proteins in single neurons

We have shown that ORANGE mediates the integration of small epitope tags and fluorescent proteins in single genes (Figure 1). Tagging two proteins simultaneously in one neuron for dual-color imaging, however, is challenging using this approach. NHEJ-mediated integration of the donor sequence is homology independent, and therefore, the integration of independent donor sequences cannot be targeted to specific genes but occurs at random (Gao et al., 2019). Recently, NHEJ-based, targeted integration of Cre recombinase was used to disrupt the target gene and drive the expression of a second protein used as a reporter of a successful knock-out (Spence et al., 2019). Based on this, we reasoned that genomic integration of a fluorescent protein together with Cre recombinase could be used to trigger the expression of a second gRNA from an additional knock-in plasmid. This approach would facilitate the sequential integration of two donor sequences targeted to two genomic loci in a single neuron. To test this, we first developed knock-in constructs integrating a C-terminal GFP tag fused to a P2A-Cre sequence (GFP-P2A-Cre), leading to bicistronic expression of a GFP-fusion protein and Cre recombinase (Figure 8A). This yielded robust recombination and expression of flip-excision (FLEX) mCherry and Synapsin-FLAG (Figure 8B). We did, however, observe some cells that only expressed the FLEX construct without visible GFP signal, suggesting that either Cre expression is somewhat leaky or that very low levels of Cre are already sufficient to recombine FLEX switches.

Building on GFP-P2A-Cre knock-ins, we developed a pORANGE vector containing a Cre-dependent Lox-STOP-Lox sequence in the U6 promoter (Back et al., 2019), which blocks expression of the gRNA until Cre is expressed (Figure 8C). When combined with a GFP-P2A-Cre knock-in, this would mediate reliable dual-color knock-ins with NHEJ because the Lox-STOP-Lox gRNA is only expressed after GFP-P2A-Cre integration is completed and a functional protein has been produced from this allele (S11A Fig). Thus, this mechanism should prevent mix-up of donor sequences in the targeted loci. We dubbed this method conditional activation of knock-in expression (CAKE). Using ORANGE-CAKE, we developed multiplex knock-ins for a range of combinations and used these for dual-color confocal and gSTED microscopy of endogenous proteins (Figure 8D and F). As was observed for FLEX switches, we also observed occasional expression of Lox-STOP-Lox knock-ins without observable GFP signal (see Discussion). Additionally, for β 3-Tubulin-GFP-P2A-Cre and GluA1-GFP-P2A-Cre, we occasionally observed erroneous integration of donor DNA in the nontargeted locus (e.g., HaloTag labeling from the gene targeted with GFP-P2A-Cre) (S11B and C Fig, see Discussion). Importantly, we never observed expression of Lox-STOP-Lox knock-ins in cultures without expression of Cre recombinase. Together, these data show the feasibility of multiplex labeling in single cells using ORANGE-CAKE to study spatiotemporal protein expression of multiple proteins simultaneously in individual neurons.

Discussion

Mapping the subcellular distribution of proteins at high spatial resolution is fundamental to understand cell biological processes. Ongoing developments in superresolution imaging technologies have dramatically improved the spatial resolution, allowing the dissection of molecular organization of subcellular structures at nanometer precision. However, a major

obstacle remains the availability of a flexible strategy to efficiently and specifically label endogenous proteins, especially in neurons. Here, we developed ORANGE, a simple and scalable toolbox for epitope tagging of endogenous proteins using CRISPR/Cas9, and we provide a readily usable knock-in library that enables in-depth interrogation of protein distribution and dynamics in postmitotic neurons at high spatial resolution. Although CRISPR/Cas9-based tagging approaches have been developed for neurons, until now, large-scale applications of these methods have been limited. ORANGE offers a single template vector that only requires standard cloning methods. Moreover, we demonstrated that this approach is compatible with various generally used DNA delivery methods, including lipofection, electroporation, LVs, and AAVs, and thus can be used in dissociated neuronal cultures and organotypic slice cultures and *in vivo*. Instead of relying on antibodies that target individual proteins with varying levels of specificity and efficiency, the ORANGE toolbox utilizes fluorescent proteins that directly report protein localization, self-labeling enzymes, or epitope tags for which universal antibodies are available. Moreover, integration of Cre recombinase allowed for tagging of two endogenous proteins in single cells.

We demonstrated the level of accuracy of targeted genomic integration using ORANGE in several ways. First, we analyzed whether insertion of GFP was correct at the genomic level using next-generation sequencing. We detected high frequency of correct integration for many of the knock-ins, although the occurrence of indels is highly variable between individual targets. However, indels should not form a limitation for many purposes, including fluorescent imaging, because only neurons with detectable fluorescent signal are selected, and proteins with out-of-frame integration remain undetectable. At the network level, we expect that the effect of frameshift mutations is limited, especially when using lipofection, because more than 90% of cultured cells are not transfected and remain unedited. Importantly, we noted that the frequency of correct integration did not correlate with Doench on-target score (Doench et al., 2016) and Bae out-of-frame score (Bae et al., 2014), scores often used to select a target sequence with a high efficiency. Also, when testing knock-in constructs targeting different target sequences in the same gene, we found significant differences in knock-in efficiency, independent of the Doench and Bae scores. These scores are primarily developed based on knock-out outcomes, which might explain why these scores are not correlated with the accuracy or efficiency of donor integration.

Second, for all our targets, we found that the distribution of the GFP signal was consistent with previous reports of protein localization inferred from immunolabeling or biochemical fractionation experiments. Our results indicate that, when expressed, the tag accurately reports protein localization and does not affect protein levels in most knock-in-positive neurons. These results show that well-designed knock-ins do not affect localization of the targeted protein and that off-target expression of the donor tag is extremely rare. Multiple mechanisms within the design of knock-in construct prevent off-target expression. We selected target sequences with a high MIT score, meaning that the sequence is unique within the genome and that potential off-targets are intergenic or in introns. If off-target integration in protein-coding sequences does occur, the donor orientation will be random (i.e., 50% is in the inverted orientation). Additionally, in 66% of off-target integrations, the donor would be out of frame, and donor integration in a random location within a protein is likely to severely affect folding, leading to degradation of the targeted protein.

Third, with immunocytochemistry, we found that knock-ins were most often expressed at endogenous levels. However, in a few cases, we did observe that the tagged protein was expressed at slightly lower levels compared with the untagged protein in untransfected neurons. This might indicate that, in these neurons, one of the two alleles contains indels after genome editing and/or failed to integrate the donor DNA, consistent with estimates with the HITI method that 30%–50% of knock-in-positive cells show biallelic integration (Suzuki et al., 2016). We also showed that, for C-terminal tagging of PSD95, Shank2, and N-terminal Bassoon (but not C-terminal Bassoon knock-ins), knock-in-negative neurons are likely partial or complete knock-outs. This difference in protein levels, especially for C-terminal-tagged proteins, might be the result of different sensitivity to, for example, nonsense-mediated decay (Lindeboom et al., 2016). Ongoing advancements in CRISPR/Cas9 technology are likely to lead to new developments that increase the on-target integration efficiency and precision of this approach. For instance, Cas9 variants with higher specificity could decrease indel frequency (Kleinstiver et al., 2016; Slaymaker et al., 2016), and the knock-in efficiency and repair accuracy may be predicted based on the target sequence (Shen et al., 2018; van Overbeek et al., 2016). Also, alternative delivery methods such as ribonucleoproteins (RNPs) (Dewari et al., 2018) might increase the efficiency of DNA delivery.

An important advantage of our method is that targeted integration of common epitope tags circumvents the need for developing new specific antibodies. In particular, for proteins that are highly homologous in their amino acid sequence and for which generating specific antibodies is challenging, it is now possible to develop specific knock-in constructs that will report subcellular localization at unmatched specificity. As an example, we demonstrated successful knock-ins for RIM1 and RIM2, two highly homologous active zone proteins for which isoform-specific antibodies are not available. The knock-in constructs presented in our library are designed using the rat genome as a template. However, because of high gene homology, multiple of the knock-in constructs are compatible with the mouse genome (see S2 Table). For example, we have shown that our GluA1 knock-in works both in dissociated rat hippocampal cultures as well as in mouse organotypic hippocampal slice cultures and *in vivo* in mouse brain.

ORANGE is easily employed on targets yet to be characterized. Next-generation sequencing efforts and high-resolution proteomics studies continue to discover the implication of novel proteins in biological processes, but for many of these proteins, specific and efficient antibodies are lacking. For instance, we developed knock-in constructs for two AMPA receptor complex constituents, FRRS1L/C9orf4 and GSG1L, that have only recently been discovered in a high-resolution proteomics study (Schwenk et al., 2012). For both proteins, functional characterization is available (Gu et al., 2016; Han et al., 2017b; Schwenk et al., 2019; Shanks et al., 2012; Stewart et al., 2019), but high-resolution information on subcellular distribution was lacking because of the unavailability of specific antibodies. Thus, ORANGE allowed us to visualize and image these proteins at high resolution, showing that, whereas GSG1L is localized on the dendritic shaft and in dendritic spines, FRRS1L is preferentially targeted to the soma and dendritic shaft, seemingly associated with the ER.

The ability to tag endogenous proteins in sparse subsets of cells is particularly advantageous for superresolution approaches. Also, sparse labeling of cells increases contrast and provides internal negative controls because neighboring, nontargeted cells are unlabeled. The resolution of these approaches will detect any distortion in molecular

organization due to, for instance, overexpression artifacts, and therefore, these methods are highly sensitive to nonspecific labeling. We exploited the advantages of ORANGE to dissect the subcellular distribution of a number of neuronal proteins using different superresolution imaging approaches. We mapped the distribution of endogenous cytoskeletal elements, signaling proteins, and synaptic receptors. Our experiments demonstrate that endogenous CaMKII α has two distinct kinetic populations. Focusing on glutamate receptors, we found that endogenous NMDA receptors are highly immobilized at synaptic sites and enriched in distinct subsynaptic nanodomains. This particular distribution is likely to shape the efficiency of receptor activation by glutamate (Biederer et al., 2017), and therefore, dissection of the underlying molecular mechanisms is essential for our understanding of synapse physiology. Thus, ORANGE enables superresolution imaging and live-cell single-molecule tracking of neuronal proteins and thus provides a scalable approach to efficiently and reliably map the dynamic distribution of endogenous proteins at nanometer resolution.

Finally, we show that ORANGE can be used for multiplex labeling and dual-color imaging of endogenous proteins. Multiplex gene editing has remained a challenge in neuronal cells, and existing methods have relatively low efficacy (Mikuni et al., 2016) or are limited to specific combinations with small epitope tags (Gao et al., 2019). Our CAKE method of sequential genome editing using a GFP-P2A-Cre knock-in and a second Cre-dependent knock-in mediates flexible, multiplex editing for a wide range of combinations, without restrictions on donor DNA sequence. We did observe, however, that some GFP-P2A-Cre knock-ins had reduced GFP fluorescence compared with regular GFP knock-ins. Although it is currently unclear what the cause of this is, it is likely that the substantial increase in mRNA length reduces protein levels (Vogel et al., 2010). Therefore, the expression level of each knock-in should be carefully assessed for each target. For some GFP-P2A-Cre knock-ins, including β 3-tubulin and GluA1, we did observe occasional erroneous integration of the second, Cre-dependent knock-in. This is likely induced by rapid expression of Cre recombinase from these knock-ins after integration in the first allele, leading to activation of the Cre-dependent knock-in before the second allele has been edited. Indeed, we did already observe GFP expression from β 3-tubulin knock-ins after 24 hours, and it is not unlikely that this time span is insufficient to edit both alleles. Despite these current limitations, we feel that CAKE is a valuable tool to study the localization of multiple endogenous proteins in individual cells.

We believe that ORANGE is a simple and efficient genome editing toolbox that will rapidly advance many fields in biology through the in-depth investigation of protein distribution in cultured cell lines, primary cells, organotypic slice cultures, and animal models, but in particular, ORANGE presents one of the few possibilities to tag proteins in neurons. Further development of tools for cell type-specific targeting of epitope tags would allow interrogation of protein distribution in specialized neuron types in the brain. Apart from epitope tagging, our toolbox can, for example, be used for insertion of enzymes for proximity biotinylation (Roux et al., 2012), labeling of organelles for electron microscopy (Lam et al., 2015), or light-sensitive dimerization sequences for optical control over protein or organelle positioning (Sinnen et al., 2017; van Bergeijk et al., 2015). The unprecedented number of applications of ORANGE will undoubtedly deepen our molecular understanding of how the spatial distribution of endogenous proteins contributes to cell biological processes.

Materials and Methods

Ethics statement

All experiments were approved by the Dutch Animal Experiments Committee (Dier Experimenten Commissie [DEC] AVD1080020173404, AVD1080020173847, and AVD115002016797), performed in line with institutional guidelines of Utrecht University, and conducted in agreement with Dutch law (Wet op de Dierproeven, 1996) and European regulations (Directive 2010/63/EU). Timed pregnant Wistar rats were obtained from Janvier Labs. Wild-type male and female mice were used. Rosa26-Cas9 knock-in mice are originally from (Platt et al., 2014).

Antibodies and reagents

Primary antibodies used in this study are the following: rabbit anti-GFP (MBL Sanbio, 598, RRID AB_591819), rat anti-HA ([3F10], Sigma, 11867423001, RRID AB_390919), mouse anti-FLAG ([M2], Sigma, F3165, RRID AB_259529), mouse anti-PSD95 ([K28/43], Neuromab, 75-028, RRID AB_2307331), mouse anti-alpha-tubulin ([B-5-1-2], Sigma, T5168, RRID AB_477582), mouse anti-Bassoon ([SAP7F407], Enzo, ADI-VAM-PS003-F, RRID AB_10618753), mouse anti-Shank2 ([N23B/6], Neuromab, 75-088, RRID AB_2254586), mouse anti-CaMKII α ([6G9], Sigma, C265, RRID AB_2314080), and ATTO647N-conjugated anti-GFP nanobodies (GFPBooster-ATTO647N, Chromotek). Alexa488-, Alexa568-, Alexa594-, and Alexa647-conjugated secondary antibodies were from Life Technologies. ATTO647N-conjugated secondary antibodies were from Sigma. Alexa594- and Alexa647-conjugated phalloidin was from Life Technologies. Halo-ligands conjugated to Janelia fluorophore 549 (Halo-JF549) and 646 (Halo-JF646) were from Promega.

Dissociated neuronal cultures

Dissociated hippocampal cultures were prepared from embryonic day 18 (E18) rat brains of both genders, as described in (Cunha-Ferreira et al., 2018). Dissociated neurons were plated on Ø18-mm coverslips coated with poly-L-lysine (37.5 μ g/ml, Sigma-Aldrich) and laminin (1.25 μ g/ml, Roche Diagnostics) at a density of 100,000 neurons per well. Neurons were grown in Neurobasal medium (NB) supplemented with 1% penicillin and streptomycin (pen/strep), 2% B27, and 0.5 mM L-glutamine (all from Gibco) (NB-complete medium) at 37 °C in 5% CO₂. From DIV 1 onward, medium was refreshed weekly by replacing half of the medium with Brainphys neuronal medium supplemented with 2% NeuroCult SM1 neuronal supplement (STEMCELL Technologies) and 1% pen/strep (BP-complete medium).

Organotypic hippocampal slice cultures

Organotypic hippocampal slice cultures were prepared from wild-type mice at postnatal day 6–8. After decapitation, the brain was quickly removed and placed in ice-cold Gey's Balanced Salt Solution (GBSS) containing (mM) 137 NaCl, 5 KCl, 1.5 CaCl₂, 1 MgCl₂, 0.3 MgSO₄, 0.2 KH₂PO₄, and 0.85 Na₂HPO₄ and supplemented with 12.5 mM HEPES, 25 mM glucose, and 1 mM kynurenic acid (pH set at 7.2, osmolarity set at 320 mOsm, sterile filtered). The frontal part of the brain and the cerebellum were removed along the

transverse plane, and the hemispheres were then separated along the midline. Hippocampi were dissected and sliced perpendicularly to the long axis of the hippocampus with a thickness of 400 μm using a McIlwain Tissue Chopper. Slices were washed in culturing medium (consisting of 48% MEM, 25% HBSS, 25% horse serum, 30 mM glucose, and 12.5 mM HEPES, with pH set at 7.3–7.4 and osmolarity set at 325 mOsm) before being placed on Millicell cell culture inserts (Millipore) in 6-well plates containing culturing medium. Slices were kept at 37 °C with 5% CO₂ until use, and culturing medium was completely replaced twice per week.

Design and generation of ORANGE knock-in plasmids

Cloning of CRISPR/Cas9 knock-in vector pORANGE. To facilitate the generation of knock-in constructs, we developed a simple template vector (pORANGE). For this, we used pSpCas9(BB)-2A-Puro (PX459) V2.0 (Addgene 62988) and replaced SpCas9puro by SpCas9 from pAAV-nEFCas9 (Addgene 87115) flanked by the bipartite SV40 nuclear localization signal (NLS) sequences using the AgeI and EcoRI restriction sites, generating pSpCas9. To facilitate cloning of donor sequences, a multiple cloning site was inserted by annealing two complementary DNA oligos and ligation into the XbaI site of pSpCas9 generating pORANGE.

Design and cloning of ORANGE knock-in constructs.

To select regions within a protein of interest suitable for introducing a tag, we carefully examined known protein functions, domains, presence of signal peptides, binding ligands, and (if known) protein structure to minimize potential effects of the inserted tag sequence on protein function. For an overview of literature and design rationality given for each knock-in construct, see S1 Table. For most proteins, this resulted in tagging close to the start or stop codon or just behind the signal peptide. In some cases (including CaMKII α , Rab11, and β -actin knock-in #2), the genes were tagged just before the start codon. PAM sites in these identified regions were located in genomic sequences downloaded from the RGSC5.0/rn5 genome assembly through the UCSC genome browser gateway (<https://genome-euro.ucsc.edu/>). Target sequences were chosen, taking into consideration the MIT guide specificity score (Hsu et al., 2013). For some of the knock-ins, an extra G nucleotide was incorporated at the start of the target sequence to enhance transcription from the U6 promotor. We have no indication that this altered knock-in efficiency (for all protein target sites, target sequences, and gRNA scores, see S2 Table).

Next, oligos containing the 20-bp target sequences were annealed and ligated into the BbsI sites of pORANGE (Figure 1, S1). Donor sequences were designed to contain the fluorescent tag sequence (GFP or mEos3.2) flanked by two Cas9 target sites identical to the genomic target site. Importantly, to facilitate genomic integration of the donor sequence in the correct orientation, these target sites including PAM sequences were inserted as the reverse complement of the genomic target sequence (Figure 1A, S1). Additional linker sequences of at least three amino acids and additional base pairs to make the donor in frame after integration in the genome were introduced between the target sites and the tag sequence. Also, a start codon and new Kozak sequence or stop codon was introduced in the linker when proteins were tagged before the genomic start or stop codon, respectively. For the CaMKII α knock-in construct, the reverse integration of the incomplete target sequence introduces an additional start codon. Extra base pairs were introduced in the linker to

make this extra start codon in frame with the donor. To facilitate exchange of donor tags, in-frame BmtI and AfeI restriction sites were introduced in the linker for some, but not all, knock-in constructs. Primer oligos with overhangs containing all these features were designed to generate the complete donor sequence by PCR. (See S1 Figure for two example designs.) The donor sequences were PCR amplified from a GFP-containing plasmid as template and ligated into the multiple cloning site of the pORANGE vector containing the inserted target sequence to generate the complete knock-in construct. For all primers used to generate the knock-in donor inserts, see S3 Table. To replace GFP in the donor DNA, pORANGE plasmids were digested with BmtI and AfeI, and replacements were generated by primer ligation (in case of 2x HA or 2x FLAG) or PCR for larger donors.

For LV applications, the ORANGE system was split into two plasmids. To generate pFUGW-Cas9, SpCas9 (from pAAV-nEFCas9) was ligated into the AgeI and EcoRI sites of pFUGW (Addgene 14883). To generate the gRNA and donor containing LV plasmid, first, mCherry-KASH amplified from pAAV-mTubb3 (Addgene 87116) was ligated into the BshTI and EcoRI sites of pFUGW-Cas9 replacing Cas9, yielding pFUGW-mCherry-KASH. Then, the U6 promoter, gRNA, and the donor sequence were amplified by PCR from the pORANGE construct and inserted into the PacI site of pFUGW-mCherry-KASH using Gibson assembly (NEBuilder HiFi DNA assembly cloning kit).

For AAV vectors, we developed a pAAV backbone (pAAV-MCS-mCherry-KASH) containing a multiple cloning site, EF-1 α promoter, and mCherry-KASH using Gibson assembly. Knock-in cassettes containing the U6 promoter, gRNA, and donor DNA were subcloned by digesting pORANGE with PscI/MluI, which was ligated in the NcoI and SgsI sites of pAAV MCS mCherry-KASH.

To create Cre-dependent knock-ins for CAKE, we obtained an mU6 promoter containing a STOP sequence flanked by LoxP551 sites from Addgene (#113160) (Back et al., 2019) with PCR. pORANGE backbone was digested with PscI and BbsI to remove the original promoter, and Gibson assembly was used to ligate the PCR product to obtain pORANGE Lox. Knock-ins in pORANGE Lox are cloned with identical methods as regular knock-ins in pORANGE (discussed above).

For the expression of FLEx switches, the pFSW backbone with synapsin-1 promoter (a gift from Dr. Pascal Kaeser, Harvard Medical School) was digested with KpnI and PacI. Inverted mCherry-KASH and a FLEx switch based on Addgene #50955 (Lin et al., 2013) were generated by PCR and ligated with Gibson assembly to obtain pFSW-FLEx-mCherry-KASH. To replace mCherry-KASH with Synapsin-FLAG, Synapsin-1 with FLAG tag was generated by PCR from pCMV(pr)Synapsin-1Cherry-N1enti H81 (a gift from A. Jeromin, Allen Brain Institute, Seattle, United States), and ligated in the BmtI/BshTI restriction sites. pCaMK Homer1c-mCherry was cloned via amplification of Homer1c-mCherry from pCMV Homer1c-mCherry (MacGillavry et al., 2013) using PCR and ligation into the XhoI and MfeI sites of pCaMK mCherry-GluA1-CIBN (Addgene #89444) (Sinnen et al., 2017). All constructs were verified by sequencing.

Transfection of dissociated hippocampal cultures

Neurons were transfected at DIV 3 (for knock-in) or DIV 14–18 (for overexpression) using Lipofectamine 2000 reagent (Invitrogen). Briefly, for one Ø18-mm coverslip covered with 100,000 neurons, 1–2 μ g DNA was mixed with 3.3 μ l Lipofectamine in 200 μ l NB medium and incubated for 30 minutes at room temperature (RT). Next, 500 μ l conditioned medium

was transferred to a new culture plate and replaced by 300 μ l NB supplemented with 0.5 mM L-glutamine. The DNA mix was added to the neurons and incubated at 37 °C and 5% CO₂. After 90–120 minutes, neurons were transferred to the new culture plate with conditioned medium and 500 μ l new NB medium supplemented with L-glutamine, B27, and pen/strep and kept at 37 °C and 5% CO₂ for at least 3 days (for overexpression) and between 1–20 days for knock-in, depending on the experiment.

Electroporation of dissociated hippocampal neurons

For electroporation, hippocampal neurons were collected directly after dissection and dissociation in a 15-ml tube and centrifuged for 5 minutes at 200g. Neurons were resuspended in AMAXA transfection solution (Lonza) (3 \times 10⁵ neurons per sample), mixed with 8 μ g DNA, transferred to a gene pulser cuvette (Biorad), and electroporated using a Lonza Nucleofector 2b. Immediately after electroporation, fresh 37 °C NB medium supplemented with B27, L-glutamine, and pen/strep was added to the cuvette, after which the neurons were plated on a coated \varnothing 18-mm coverslip using a Pasteur pipette. Neurons were incubated at 37 °C and 5% CO₂ for 3 hours, after which all medium was replaced with fresh NB medium supplemented with B27, L-glutamine, and pen/strep.

HaloTag labeling of dissociated hippocampal cultures

HaloTag labeling was performed with cell-permeable Halo-JF549 or Halo-JF646 ligands. Prior to use, ligands were dissolved in DMSO to 200 μ M and stored in single-use aliquots at –20 °C. HaloTag ligands were added to culture medium at a final concentration of 200 nM, and cells were placed back in the incubator for 15 minutes. After rinsing the cells with culture medium, cells were fixed using 4% (w/v) paraformaldehyde (PFA) and 4% (w/v) sucrose in phosphate-buffered saline (PBS) (PFA/Suc).

Immunocytochemistry of dissociated hippocampal cultures

Immunocytochemistry was performed as described below, unless indicated otherwise. Hippocampal neurons were fixed using PFA/Suc for 10 minutes at RT and washed three times in PBS containing 0.1 M glycine (PBS/Gly). Neurons were blocked and permeabilized in blocking buffer (10% [v/v] normal goat serum [NGS] (Abcam) in PBS/Gly with 0.1% [v/v] Triton X100) for 1 hour at 37 °C. Next, coverslips were incubated with primary antibodies diluted in incubation buffer (5% [v/v] NGS in PBS/Gly with 0.1% [v/v] Triton X100) overnight at 4 °C. Coverslips were washed three times for 5 minutes with PBS/Gly and incubated with secondary antibodies diluted 1:400 in incubation buffer for 1 hour at RT. Coverslips were washed three times for 5 minutes in PBS/Gly, dipped in milliQ water (MQ), and mounted in Mowiol mounting medium (Sigma).

AAV production

AAV vectors serotype 5 encoding for GluA1-Halo or PSD95-Halo knock-ins were produced as described in detail in (Verhaagen et al., 2018) using helper plasmids obtained from (Grimm et al., 2003). In brief, HEK293T cells were plated 1 day before transfection in Dulbecco's Modified Earl's Medium (DMEM) supplemented with 10% fetal calf serum (FCS) and 1% pen/strep. At 2 hours before transfection, medium was exchanged with Iscove's Modified Dulbecco's Medium (IMDM) containing 10% FCS, 1% pen/strep, and 1% glutamine. Transfection was performed with polyethylenimine (PEI). At 1 day after

transfection, medium was exchanged with fresh IMDM with supplements. At 3 days after transfection, medium was aspirated, and cells were harvested using a cell scraper. After three freeze/thaw cycles and treatment with DNaseI, AAV vectors were purified using an iodixanol density gradient and ultracentrifugation (70 minutes, 69,000 rpm at 16 °C using rotor 70Ti [Beckman Coulter]). The fraction containing AAV particles was concentrated with centrifugation (3,220g, 15 minutes at RT) using an Amicon Ultra 15 column (Merck Millipore). Columns were washed 3 times using D-PBS containing 5% sucrose. AAV vectors were stored at -80 °C until use. Titters were measured using qPCR.

Stereotactic injection and staining of acute brain slices

AAV vectors were injected in 4- to 7-month-old Rosa26-Cas9 knock-in mice of either sex [27]. Mice were anaesthetized with an intraperitoneal injection of ketamine (75 mg/kg, Narketan; Vetoquinol BV) and dexmedetomidine (1 mg/kg, Dexdomitor; Orion Pharma). Analgesia was provided before the start of surgery (carprofen, 5 mg/kg, subcutaneous, Carporal; AST Farma BV). Mice were given eye cream (CAF; CEVA Sante Animale BW) and placed in a stereotactic frame (Kopf Instruments). Local anesthesia was applied by spraying lidocaine (100 mg/mL; Xylocaine, AstraZeneca BV), and two holes were drilled for entrance of the injection needles. AAV vectors, 500 nl, with a titer of 6.2×10^{11} gc/ml were injected bilaterally (-2.46 mm posterior to bregma, +/- 2.2 mm lateral from bregma, and -1.3 mm ventral from the skull, under a 10° angle) at 100 nl per minute with a syringe pump (Harvard Apparatus) connected to stainless steel needles (31G, Coopers Needleworks) targeted to the CA1 region of the hippocampus. Needles were left in place for 10 minutes following the injection. After surgery, mice were given atipamezole (2.5 mg/kg, intraperitoneal, SedaStop; AST Farma BV) and saline for rehydration. During the following 7 days, mice continuously received carprofen through their drinking water (0.027 mg/ml).

After 4 weeks, acute brain slices were obtained. Mice were first anaesthetized with isoflurane and decapitated. Brains were rapidly isolated, and 250- μ m-thick coronal slices were made on a vibratome (Leica VT1200 S) in ice-cold artificial cerebrospinal fluid (ACSF) containing (in mM) 124 NaCl, 26 NaHCO₃, 11 D-glucose, 2.5 KCl, 1 NaH₂PO₄, HEPES 5, 7 MgSO₄, and 0.5 CaCl₂. Subsequently, slices were transferred to an immersion-style holding chamber containing 124 NaCl, 26 NaHCO₃, 11 D-glucose, 2.5 KCl, 1 NaH₂PO₄, HEPES 5, 1 MgSO₄, and 2 CaCl₂, in which they recovered for at least 1 hour at RT. ACSF solutions were continuously bubbled with carbogen gas (95% O₂, 5% CO₂) and had an osmolarity of approximately 300 mOsm. After recovery, slices were stained for 1 hour with 250 nM Halo-JF646 ligand diluted in ACSF. Following rinsing with ACSF, slices were fixed overnight with 4% PFA, washed in PBS, and mounted with VectaShield (VectorLabs).

Lentivirus production and infection

For lentivirus production, HEK293T cells were maintained at a high growth rate in DMEM supplemented with 10% FCS and 1% pen/strep. At 1 day after plating, cells were transfected using PEI (Polysciences) with second-generation LV packaging plasmids (psPAX2 and 2MD2.G) and a pFUGW construct containing the desired insert at a 1:1:1 molar ratio. At 6 hours after transfection, cells were washed once with PBS, and medium was replaced with DMEM containing 1% pen/strep. At 48 hours after transfection, the supernatant was harvested and briefly centrifuged at 700g to remove cell debris. The supernatant was concentrated using Amicon Ultra 15 100K MWCO columns (Milipore),

and Cas9 and knock-in viruses were mixed at 1:1 and used immediately for infection. For cultured hippocampal neurons at DIV 2–4, 2–4 μl virus was added per well, and neurons were fixed at DIV 21–23 with 4% PFA/Suc for 10 minutes. For organotypic hippocampal slice cultures, virus was injected into the CA1 region at DIV 1 using an Eppendorf Femtojet injector. Slices were fixed at DIV 10 with 4% PFA in PBS for 30 minutes, washed 3 times for 10 minutes with PBS, and mounted with VectaShield (Vector Laboratories).

Next-generation sequencing of genomic sites of integration

Genomic DNA was isolated from electroporated neurons at DIV 4. Neurons were lysed in lysis buffer (100 mM Tris, 50 mM EDTA, 40 mM NaCl, 0.2% SDS [pH 8.5]) and incubated with 100 $\mu\text{g}/\text{ml}$ Proteinase K (Roche) at 55 °C for 2 hours, followed by 1 hour at 85 °C to inactivate Proteinase K. Genomic DNA was isolated by ethanol precipitation and dissolved in elution buffer (10 mM Tris [pH 8.0]) (Qiagen). Genomic PCR was performed to amplify the 5' and 3' junctions of the integrated donor (for PCR primers used, see S4 Table) using a touchdown PCR and Phusion HF polymerase (Thermo Fisher Scientific). Genomic primers were designed using NCBI Primer-Blast. Knock-ins analyzed were primarily selected based on flanking genomic sequence, and we failed to amplify multiple alleles because of sequence complexity (e.g., sequence repeats, high GC content, or potential secondary structure). Amplicons were only included if they resulted in a well-resolved band on agarose gel. PCR products were separated using agarose gel electrophoresis and subsequently purified using a gel extraction kit (Qiagen). Purified PCR products were pooled with, on average, 10 ng per amplicon and sent for Illumina Miseq 2 x 300 bp next-generation sequencing (Utrecht Sequencing Facility [USEQ], Utrecht, the Netherlands).

Sequencing results were analyzed using CRIS.py (Connelly and Pruett-Miller, 2019). Indel frequencies were plotted in a heatmap as the average percentage from the forward and reverse reads. The number of forward and reverse reads was averaged per junction for each knock-in and plotted. Indel and in-frame frequencies were also plotted compared with the Doench on-target score (Doench et al., 2016) and Bae out-of-frame score (Bae et al., 2014), respectively, obtained for each guideRNA sequence from UCSC genome browser gateway.

Confocal imaging

Confocal images were acquired with a Zeiss LSM 700. For dissociated hippocampal cultures, neurons were imaged with a 63x NA 1.40 oil objective. A Z-stack containing 7–12 planes at a 0.56- μm interval was acquired with 0.1- μm pixel size, and maximum intensity projections were made for analysis and display. Organotypic and acute slices were imaged with a 20x NA 0.8 objective. Z-stacks were acquired with varying intervals. Image analysis was primarily performed using FIJI software (Schindelin et al., 2012). Quantifications were performed in Excel 2016.

gSTED superresolution imaging

Imaging was performed with a Leica TCS SP8 STED 3x microscope using an HC PL APO 100x/NA 1.4 oil immersion STED WHITE objective. The 488-nm wavelength of pulsed white laser (80 MHz) was used to excite Alexa488, the 561-nm to excite Alexa568, the 590-nm to excite Alexa594, and the 647-nm to excite Alexa647-, JF646-, and ATTO647N-labeled proteins. Alexa594, Alexa647, JF646, and ATTO647N were depleted with the 775-nm pulsed depletion laser, and we used an internal Leica HyD hybrid detector (set at 100%

gain) with a time gate of $0.3 \leq \text{tg} \leq 6 \text{ ns}$. Images were acquired as Z-stack using the 100x objective. Maximum intensity projections were obtained for image display and analysis.

In vivo STED images were additionally subjected to deconvolution using Huygens deconvolution software. Deconvolution was performed using the CMLE deconvolution algorithm, with a maximum of 40 iterations and the signal-to-noise ratio (SNR) set at 7.

Quantification of knock-in efficiency

For quantification of knock-in efficiency over time, hippocampal neurons were transfected at DIV 3 with a 1:1 ratio mixture of pORANGE- β 3-tubulin-GFP knock-in and pSM155-mCherry. Coverslips were fixed 24, 48, 72, 96, 120, and 144 hours after transfection using 4% PFA/Suc for 10 minutes at RT, washed three times with PBS/Gly, and mounted in Mowiol mounting medium.

For testing GFP- β -actin and GFP-GluN1 knock-in efficiencies, hippocampal neurons were transfected at DIV 3 with a 1:1 ratio mixture of pCaMK-Homer1c-mCherry overexpression construct together with pORANGE-GFP- β -actin #1 or #2 or pORANGE-GFP-GluN1 #1, #2, or #3 knock-in constructs. Neurons were fixed at DIV 21 using 4% PFA/Suc for 10 minutes at RT, washed three times with PBS/Gly, and mounted in Mowiol mounting medium.

Neurons were imaged with confocal microscopy as described above. For both experiments, mCherry- or Homer1c-mCherry-positive (i.e., transfected) neurons were manually counted and scored as being knock-in positive or negative. At least 1,000 transfected neurons from two independent neuronal cultures were scored for each time point or experimental condition.

Quantification of synaptic PSD95 levels and enrichment and synapse size

Hippocampal neurons were transfected at DIV 3 with the pORANGE-PSD95-GFP knock-in construct or at DIV 15 with pSM155-PSD95-GFP overexpression plasmid (MacGillavry et al., 2013) or pSM155-GFP (MacGillavry et al., 2013). At DIV 21, neurons were fixed and stained with mouse anti-PSD95 antibody 1:200 and Alexa594-conjugated secondary antibodies as described above. Neurons were imaged with confocal microscopy as described above. For each neuron, 50 circular regions of interest (ROI) of 1 μm in diameter were drawn around PSD95-GFP-positive synapses. For each ROI, the mean intensity of the GFP signal and anti-PSD95 staining was measured, background was subtracted, and values were normalized to the mean intensity value of all ROIs for both individual channels. Normalized intensity values for the PSD95-GFP knock-in signal and anti-PSD95 signal of individual synapses were plotted. In total, 550 synapses from 11 neurons divided over two independent neuronal cultures were used in the quantification.

To determine relative synaptic PSD95 content, PSD95 staining intensity in 22 circular ROIs of 1 μm in diameter around synapses per transfected (knock-in, overexpression, or GFP control) neuron was measured. Similarly, an equal number of ROIs were drawn around PSD95 puncta of nearby nontransfected neurons within the same image. Intensities of the anti-PSD95 channel were measured, and background was subtracted. Relative PSD95 content was quantified as the average anti-PSD95 intensity in synapses of a transfected neuron divided by those of the nontransfected neurons. To measure synapse size, a threshold was applied to the GFP signal (for PSD95-GFP knock-in and overexpression neurons) or anti-PSD95 signal (for GFP control), and individual synapses were detected using FIJI “Analyze Particles” with a detection size of 0.04-Infinity (μm^2) with a detection circularity

of 0–1. Measured values were plotted as averages per analyzed neuron. To analyze synaptic enrichment of PSD95, circular ROIs were drawn within synapses and on the dendritic shaft. Mean GFP intensity was measured, background was subtracted, and values were averaged per neuron. Plotted ratio is the average intensity of synaptic GFP signal divided by that of the dendritic shaft. For each condition, at least 15 neurons from two independent neuronal cultures were analyzed.

To compare PSD95 levels in transfected but knock-in-negative neurons, neurons were transfected with a 1:1 ratio of pHomer1c-mCherry and the pORANGE empty vector or pHomer1c-mCherry and pPSD95-GFP knock-in construct at DIV 3. At DIV 21, neurons were fixed and stained for endogenous PSD95 as described above. Homer1c-mCherry-positive neurons were used to locate transfected neurons and to draw ROIs around synapses. For both conditions, 20 neurons from two independent neuronal cultures were analyzed.

Quantification of Bassoon, Shank2, CaMKII α , and F-actin levels

For Bassoon, neurons were transfected at DIV 3 with a 1:1 ratio of RIM1-HA under a synapsin promoter (overexpression construct) (de Jong et al., 2018) and pORANGE template vector (control), pORANGE-GFP-Bassoon knock-in, or pORANGE-Bassoon-GFP knock-in. For Shank2, CaMKII α , and β -actin, neurons were transfected with a 1:1 ratio of pHomer1c-mCherry (overexpression) and pORANGE template vector (control) or pORANGE-Shank2-GFP knock-in, pORANGE-GFP-CaMKII α knock-in, pORANGE-GFP- β -actin knock-in #1, or pORANGE-GFP- β -actin knock-in #2. Neurons were stained as described above. For β -actin, the neurons were stained with Phalloidin-Alexa594 (Invitrogen) diluted 1:200 in blocking buffer for 1 hour at RT. Coverslips were washed three times for 5 minutes in PBS/Gly and mounted in Mowiol mounting medium. For Bassoon, neurons were stained with anti-GFP (1:2,000) and anti-Bassoon (1:1,000) and anti-HA (1:200) antibodies as described above. For Shank2 and CaMKII α , neurons were stained with anti-Shank2 (1:200) or anti-CaMKII α (1:200) antibodies, respectively. Neurons were imaged with confocal microscopy as described above. Per transfected neuron, both knock-in positive and negative, 20 circular ROIs of 1 μ m in diameter were manually drawn around synapses based on Homer1c or RIM signal. Similarly, an equal number of ROIs were drawn around puncta of nearby nontransfected neurons within the same image based on the antibody staining. To measure relative protein levels, antibody or phalloidin labeling intensities of individual ROI measurements were background subtracted and averaged for each neuron. The average intensity in the transfected neuron relative to the nontransfected neuron from the same image is plotted. For each condition, between 10 and 18 neurons from at least two independent neuronal cultures were analyzed.

Live-cell imaging of β -actin dynamics

Imaging was performed on a spinning disk confocal system (CSU-X1-A1; Yokogawa) mounted on a Nikon Eclipse Ti microscope (Nikon) with Plan Apo VC 100x 1.40 NA oil objective (Nikon) with excitation from Cobolt Calypso (491 nm) and emission filters (Chroma). The microscope was equipped with a motorized XYZ stage (ASI; MS-2000), Perfect Focus System (Nikon), and Prime BSI sCMOS camera (Photometrics) and was controlled by MetaMorph software (Molecular Devices). Neurons were maintained in a closed incubation chamber (Tokai hit: INUBG2E-ZILCS) at 37 °C in 5% CO₂ in 200 μ l of conditioned medium.

For studying actin dynamics upon Jasp treatment, neurons were transfected with pORANGE-GFP- β -actin knock-in #2 construct at DIV 3 and imaged at DIV 21–23 on a spinning disk confocal system (described above). Every 1 minute, a Z-stack was obtained in a range of 5.5 μm (12 planes with 0.5- μm intervals). After 5 minutes baseline imaging (6 frames), 100 μl /30 μM of Jasp (10 μM final concentration) or DMSO diluted in conditioned medium was added to the incubation chamber. Imaging was continued for another 20 minutes (21 frames) after addition. For analysis, maximum intensity projections were obtained, and drift was corrected. Background was subtracted in FIJI software using a rolling ball radius of 3.15 μm . For each neuron, four ROIs of variable sizes containing at least one spine each were drawn. Integrated densities (InDen) were measured for each frame. Frame-to-frame differences were obtained by subtracting each frame (tx) from the previous (tx–1) using a macro developed by Jacob Pruess. Frame-to-frame differences of the selected ROIs were measured and subtracted from the InDen at tx and normalized to the InDen tx to obtain the frame-to-frame correlation for each ROI at each time point, such that correlation = $(\text{InDen tx} - [\text{InDen tx} - \text{InDen tx} - 1]) / \text{InDen tx}$. Frame-to-frame correlation was plotted over time. For statistical analysis, the frame-to-frame correlation of the last five time points for each ROI was averaged per cell. For each condition, measurements from 28 ROIs from seven neurons divided over two independent neuronal cultures were used in the analysis.

For FRAP experiments, neurons were transfected with the GFP- β -actin knock-in #2 construct at DIV 3 and imaged at DIV 21–23 on a spinning disk confocal system (described above). FRAP experiments were performed using the ILas2 system (Roper Scientific). Experiments were performed in the presence of 10 μM Jasp or DMSO added to the imaging chamber 5 minutes before the start of the acquisition. After 2 minutes baseline imaging (single Z-plane, five frames with 30-second intervals), six ROIs with a fixed diameter of 1.26 μm containing dendritic spines were bleached using a targeted laser. Imaging during fluorescence recovery was continued for 5 minutes (13 frames with 10-second intervals followed by six frames with 30-second intervals). For analysis, acquisitions were corrected for drift. For each ROI, mean intensities were measured for every time point and corrected for background using the averaged intensity of two background ROIs. For each ROI, intensities were normalized to the averaged intensities of the frames before bleaching and normalized to zero based on the intensity from the first frame after bleaching. Normalized intensities were plotted over time. The mobile fraction of protein was calculated by averaging the normalized intensity of the last five frames for each neuron. For each condition, five neurons divided over two independent neuronal cultures were used in the analysis.

Preparation of dissociated hippocampal cultures for gSTED

Hippocampal neurons were transfected with indicated knock-in constructs at DIV 3 and fixed at DIV 21. Dual-color gSTED imaging (as described above) was performed on PSD95-GFP, GFP- β -actin #1, GFP-GluN1 #1, GFP-CaMKII α , GSG1L-GFP, and FRRS1L-GFP knock-in neurons stained with anti-GFP and anti-PSD95. pORANGE FRRS1L-GFP was cotransfected with pSyn tagRFP-ER (Lindhout et al., 2019). (Dual-color) gSTED imaging was additionally performed on extracted cytoskeleton of the GFP- β -actin and β 3-tubulin-GFP knock-in neurons. At DIV 7 (β 3-tubulin-GFP knock-in) and DIV 21 (GFP- β -actin knock-in), the neuronal cytoskeleton was extracted using extraction buffer (PEM80-buffer [80 mM PIPES, 1 mM EGTAs, 2 mM MgCl₂ (pH 6.9)], 0.3% Triton-X, 0.1% glutaraldehyde) for 1 minute at RT. Next, neurons were fixed with PFA/Suc for 10 minutes at RT, washed

three times for 5 minutes with PBS/Gly, and subsequently incubated with 1 mg/ml sodium borohydride in PBS for 7 minutes at RT. Coverslips were washed 3 times for 5 minutes with PBS/Gly. The GFP signal was enhanced with anti-GFP staining. The β 3-tubulin-GFP knock-in was additionally stained for α -tubulin diluted 1:1,000. Anti-GFP primary antibodies were stained with Alexa488- or ATTO647N-conjugated secondary antibodies, and anti-PSD95 and anti- α -tubulin were stained with the Alexa594- or ATTO647N-conjugated secondary antibody (all as described above). To label surface receptors, GFP-GluN1 knock-in neurons were stained with anti-GFP prior to permeabilization and subsequent anti-PSD95 staining.

Quantification of colocalization gSTED

Using ImageJ software, a line scan of interest was drawn to obtain pixel intensity data to assess the degree of colocalization between two structures along that line. To quantify the degree of colocalization between two structures, entire images showing parts of the dendritic tree of a knock-in neuron were used for analysis. First, all dendritic spines (positive for both proteins: PSD95-GFP knock-in and anti-PSD95 staining or GFP- β -actin knock-in and anti-PSD95 staining) were selected by drawing ROIs in ImageJ. Next, the ROIs were combined to clear the outside of the ROIs to remove all background from surrounding neurons or dendritic shafts. Then, the ImageJ plug-in “JaCoP” (Just Another Colocalization Plug-in) was used to calculate the PCC and MOC. For the MOC, the thresholding was done manually. These analyses were performed on both the confocal and STED maximum projections of the exact same regions (of a neuron). In total, 10 PSD95-GFP knock-in and seven GFP- β -actin knock-in neurons were analyzed from two independent experiments.

Confocal and STED quantifications of NMDA receptors

Neurons were transfected at DIV 3 with the pORANGE-GFP-GluN1 knock-in #1 construct. Neurons were fixed at DIV 21 and stained with anti-PSD95 as described above. Neurons were imaged with confocal microscopy as described above. For each neuron, 50 circular ROIs of 1 μ m in diameter were drawn around GFP-GluN1-positive synapses. For each ROI, the mean intensity of the GFP signal and anti-PSD95 staining was measured, background was subtracted, and values were normalized to the mean intensity value of all ROIs for both individual channels. Normalized intensity values for the GFP-GluN1 knock-in signal and anti-PSD95 signal of individual synapses were plotted. In total, 450 synapses from nine neurons divided over two independent neuronal cultures were used in the analysis.

The FIJI plug-in Full Width at Half Maximum (FWHM) macro developed by John Lim was used to measure the FWHM from intensity profiles using Gaussian fitting. Line scans were drawn along the width and length of identified GluN1 substructures (by setting an appropriate brightness/contrast) to obtain the FWHM of the length and width of these substructures. Subsequently, these substructures were categorized as synaptic or extrasynaptic based on the colocalization with PSD95. For image display, the length was plotted against the width for each cluster. In all, 479 GFP-GluN1 clusters (387 synaptic, 92 extrasynaptic) from three neurons were analyzed.

For the quantification of total GluN1 cluster area per synapse, and correlation with synapse area, the same images were used as for the quantification of the FWHM of the GluN1 substructures. Specifically, the STED resolved images were used for the quantification of GluN1 cluster area, whereas the confocal images were used to quantify the area of the

PSD, using PSD95 as a marker. First, an ROI was drawn around the knock-in neuron of interest to clear the outside of the ROI, removing all background. Subsequently, the image was subjected to thresholding to isolate the objects of interest from the background and watershedding to separate overlapping objects. Then, all objects (GluN1 clusters and PSDs) were detected using “Analyze Particles” with a detection size of 0.02-Infinity (μm^2) for GluN1 substructures and 0.04-Infinity (μm^2) for PSDs, and all with a detection circularity of 0–1.

SMLM and detection

dSTORM imaging was performed on a Nikon Ti microscope equipped with a Nikon 100x NA 1.49 Apo total internal reflection fluorescence (TIRF) oil objective, a Perfect Focus System. Effective pixel size is 65 nm. Oblique laser illumination was achieved using a custom illumination pathway with a 60-mW, 405-nm-diode laser (Omicron); a 200-mW, 491-nm-diode laser (Omicron); and a 140-mW, 641-nm-diode laser (Omicron). Emission light was separated from excitation light with a quad-band polychroic mirror (ZT405/488/561/640rpc, Chroma) and additional band-pass emission filters (ET 525/595/700, Chroma). Fluorescence emission was acquired using an ORCA-Flash 4.0v2 CMOS camera (Hamamatsu). Lasers were controlled using Omicron software, whereas all other components were controlled by μ Manager software (Edelstein et al., 2010).

Live-cell SMLM imaging experiments were performed on a Nikon Ti microscope equipped with a 100x NA 1.49 Apo TIRF oil objective, a Perfect Focus System, and an additional 2.5x Optovar to achieve an effective pixel size of 64 nm. Oblique laser illumination was achieved using a custom illumination pathway with an AA acousto-optic tunable filter (AA opto-electronics); a 15-mW, 405-nm-diode laser (Power Technology); a 100-mW, 561-nm-DPSS laser (Cobolt Jive); and a 40-mW, 640-nm-diode laser (Power Technology). Emission light was separated from excitation light with a quad-band polychroic mirror (ZT405/488/561/640rpc, Chroma) and additional band-pass emission filters (ET 525/595/700, Chroma). Fluorescence emission was acquired using a DU-897D EMCCD camera (Andor). All components were controlled by μ Manager software (Edelstein et al., 2010).

Acquired image stacks were analyzed using the ImageJ plug-in Detection of Molecules (DoM) v1.1.5 (Yau et al., 2014). Briefly, each image was convoluted with a 2D Mexican hat-type kernel that matches the microscope’s point spread function. Spots were detected by thresholding the images and localized by fitting a 2D Gaussian function using unweighted nonlinear least-squares fitting with the Levenberg–Marquardt algorithm. Drift correction was applied by calculating the spatial cross-correlation function between intermediate superresolved reconstructions.

Single-molecule tracking PALM and analysis

Neurons were transfected with the mEos3.2-CaMKII α knock-in construct at DIV 3 and imaged at DIV 21–23. Neurons were imaged in extracellular imaging buffer (10 mM HEPES, 120 mM NaCl, 3 mM KCl, 2 mM CaCl₂, 2 mM MgCl₂, 10 mM glucose [pH 7.35]) at RT. mEos3.2 molecules were photoconverted from green to red fluorescence using simultaneous 405-nm and 561-nm illumination using TIRF. Stacks of 5,000–7,000 frames were acquired at 50 Hz. PALM reconstruction was made in DoM, plotting localizations based on their localization precision, rendered with a pixel size of 10 × 10 nm. Molecules localized with precision <25 nm were used for further analysis. Tracking was accomplished using custom tracking algorithms in MATLAB (MathWorks) using a tracking radius of 512

nm. For tracks consisting of ≥ 4 frames, the instantaneous diffusion coefficient was estimated as described (Lu et al., 2014). The first three points of the MSD versus elapsed time (t) plot were used to fit the slope using linear fitting adding a value of 0 at MSD(0). Tracks with a negative slope ($< 8\%$) were ignored. The diffusion coefficient D_{eff} was then calculated using $\text{MSD} = 4D_{\text{eff}} t$. Individual tracks were plotted using MATLAB, and each was given a random color. All single-molecule trajectories from all acquisitions were used to visualize a frequency distribution. On this, we fitted two Gaussian distributions to identify the two kinetic populations. Mean values for the two fits were calculated per analyzed neuron and plotted. In total, 11 neurons from two independent experiments were included in the analysis.

dSTORM imaging and analysis

Hippocampal neurons were transfected at DIV 3 with the GFP-GluN1 knock-in construct #1 and fixed on DIV 21. Neurons were surface stained with anti-GFP 1:2,000 and Alexa647-conjugated secondaries as described above. Neurons were postfixed in 4% PFA/Suc for 5 minutes, additionally washed 3 times with PBS/Gly, and kept in PBS at 4 °C until imaging. dSTORM imaging was performed in PBS containing 10–50 mM MEA, 5% w/v glucose, 700 $\mu\text{g}/\text{ml}$ glucose oxidase, and 40 $\mu\text{g}/\text{ml}$ catalase. GFP-GluN1 knock-in-positive neurons were located on GFP signal. For dSTORM, the sample was illuminated (in TIRF) with continuous 647-nm laser light and gradually increasing intensity of 405-nm laser light. Stacks of 10,000–15,000 frames were acquired at 50 Hz. dSTORM reconstruction was made in DoM, plotting localizations based on their localization precision, rendered with a pixel size of 10×10 nm. Molecules with a localization precision < 15 nm were selected for further analysis. Next, blinking events longer than one frame were filtered out by tracking (tracking radius of 130 nm). GluN1 clusters were identified using the DBSCAN algorithm (Ester et al., 1996) implemented in MATLAB. Subsequently, the alpha shape was used as the cluster border. Clusters with a density of $> 5,000$ molecules per micrometer were used for further analysis. For each individual cluster, molecules were plotted and color-coded according to the local density (MacGillavry et al., 2013), defined as the number of molecules within a radius of 5 times the mean nearest neighbor distance of all molecules within the cluster. Molecules with a local density value > 40 were considered to be enriched in a nanodomain. Nanodomains were isolated using MATLAB functions `linkage()` and `cluster()`. The polygon circumventing molecules belonging to individual nanodomains was used to calculate the diameter of the nanodomain. Nanodomains containing < 5 localizations and diameter < 30 nm were rejected. In total, 859 clusters from three neurons from two independent experiments were analyzed.

uPAINT and analysis

Neurons transfected with the GFP-GluN1 knock-in construct #1 and pCamk Homer1c-mCherry at DIV 3 were imaged at DIV 21–23 in extracellular imaging buffer supplemented with 0.8% BSA. GFP-GluN1-positive neurons were identified by GFP signal, and ATTO647N-conjugated anti-GFP nanobodies (GFPBooster-ATTO647N, Chromotek) were bath applied to a final dilution of 1:50,000. Imaging was conducted at a 50-Hz frame rate with 640-nm excitation laser illumination (in TIRF). Molecules fitted with a precision < 50 were tracked with tracking radius of 512 nm and diffusion coefficient determined for tracks > 30 frames. A cell mask was drawn manually to filter out localizations outside neurons

due to nonspecifically bound nanobody. Tracking and estimation of the instantaneous diffusion was performed as described for the PALM imaging. Synapses were identified based on widefield Homer1c-mCherry signal as described (Li and Blanpied, 2016). Synaptic tracks were defined as tracks in which 80% of the localizations were located within the border of the synapse. All others were considered extrasynaptic. In total, 6 neurons from three independent experiments were analyzed.

Statistics

Statistical significance was tested with a Student t test when comparing two groups. A P value below 0.05 was considered significant. If multiple groups were compared, statistical significance was tested with a one-way ANOVA followed by a Bonferroni's multiple comparison. In all figures, * was used to indicate a P value < 0.05, ** for P < 0.01, and *** for P < 0.001. Reported n is number of neurons, and each experiment was replicated in neuronal cultures from at least two independent preparations. Statistical analysis and graphs were prepared in GraphPad Prism, and figures were generated in Adobe Illustrator CC.

Additional Resources

Plasmids from this study will be made available through Addgene (see S5 Table).

Supporting Information

The following data is available online.

S1 Table. Design rationale for each ORANGE knock-in.

<https://doi.org/10.1371/journal.pbio.3000665.s012>

S2 Table. Target sequences for ORANGE knock-ins.

<https://doi.org/10.1371/journal.pbio.3000665.s013>

S3 Table. Donor PCR primers.

<https://doi.org/10.1371/journal.pbio.3000665.s014>

S4 Table. Genomic PCR primers.

<https://doi.org/10.1371/journal.pbio.3000665.s015>

S5 Table. Overview ORANGE constructs with Addgene IDs.

<https://doi.org/10.1371/journal.pbio.3000665.s016>

S1 Data. Raw data.

<https://doi.org/10.1371/journal.pbio.3000665.s017>

Acknowledgments

We want to thank all members of the MacGillavry lab for discussions. We want to thank Corette J. Wierenga for providing organotypic hippocampal slice cultures and Onur Basak

for helpful discussions. We want to thank Anna Akhmanova, Lukas C. Kapitein, and Corette J. Wierenga for critical reading of the manuscript.

Author Contributions

Conceptualization: Jelmer Willems, Arthur P. H. de Jong, Nicky Scheefhals, Harold D. MacGillavry.

Formal analysis: Jelmer Willems, Arthur P. H. de Jong, Nicky Scheefhals, Harold D. MacGillavry.

Funding acquisition: Harold D. MacGillavry.

Investigation: Jelmer Willems, Arthur P. H. de Jong, Nicky Scheefhals, Eline Mertens, Lisa A. E. Catsburg, Rogier B. Poorthuis, Harold D. MacGillavry.

Methodology: Jelmer Willems, Arthur P. H. de Jong, Nicky Scheefhals, Harold D. MacGillavry.

Resources: Fred de Winter, Joost Verhaagen, Frank J. Meye, Harold D. MacGillavry.

Supervision: Harold D. MacGillavry.

Validation: Jelmer Willems, Arthur P. H. de Jong, Nicky Scheefhals, Harold D. MacGillavry.

Visualization: Jelmer Willems, Arthur P. H. de Jong, Nicky Scheefhals, Harold D. MacGillavry.

Writing – original draft: Jelmer Willems, Arthur P. H. de Jong, Nicky Scheefhals, Harold D. MacGillavry.

Writing – review & editing: Jelmer Willems, Arthur P. H. de Jong, Nicky Scheefhals, Harold D. MacGillavry.

References

- Back, S., Necarsulmer, J., Whitaker, L.R., Coke, L.M., Koivula, P., Heathward, E.J., Fortuno, L.V., Zhang, Y., Yeh, C.G., Baldwin, H.A., et al. (2019). Neuron-Specific Genome Modification in the Adult Rat Brain Using CRISPR-Cas9 Transgenic Rats. *Neuron* 102, 105-119 e108.
- Bae, S., Kweon, J., Kim, H.S., and Kim, J.S. (2014). Microhomology-based choice of Cas9 nuclease target sites. *Nat. Methods* 11, 705-706.
- Betermier, M., Bertrand, P., and Lopez, B.S. (2014). Is non-homologous end-joining really an inherently error-prone process? *PLoS Genet.* 10, e1004086.
- Biederer, T., Kaeser, P.S., and Blanpied, T.A. (2017). Transcellular nanoalignment of synaptic function. *Neuron* 96, 680-696.
- Bissen, D., Foss, F., and Acker-Palmer, A. (2019). AMPA receptors and their minions: auxiliary proteins in AMPA receptor trafficking. *Cell. Mol. Life Sci.* 76, 2133-2169.
- Brechet, A., Buchert, R., Schwenk, J., Boudkkazi, S., Zolles, G., Siquier-Pernet, K., Schaber, I., Bildl, W., Saadi, A., Bole-Feysot, C., et al. (2017). AMPA-receptor specific biogenesis complexes control synaptic transmission and intellectual ability. *Nat. Commun.* 8, 15910.
- Connelly, J.P., and Pruett-Miller, S.M. (2019). CRIS.py: A Versatile and High-throughput Analysis Program for CRISPR-based Genome Editing. *Sci. Rep.* 9, 4194.
- Cunha-Ferreira, I., Chazeau, A., Buijs, R.R., Stucchi, R., Will, L., Pan, X., Adolfs, Y., van der Meer, C., Wolthuis, J.C., Kahn, O.L., et al. (2018). The HAUS Complex Is a Key Regulator of Non-centrosomal Microtubule Organization during Neuronal Development. *Cell Rep.* 24, 791-800.
- D'Este, E., Kamin, D., Gottfert, F., El-Hady, A., and Hell, S.W. (2015). STED nanoscopy reveals the ubiquity of subcortical cytoskeleton periodicity in living neurons. *Cell Rep.* 10, 1246-1251.
- de Jong, A.P.H., Roggero, C.M., Ho, M.R., Wong, M.Y., Brautigam, C.A., Rizo, J., and Kaeser, P.S. (2018). RIM C2B Domains Target Presynaptic Active Zone Functions to PIP2-Containing Membranes. *Neuron* 98, 335-349 e337.
- Dewari, P.S., Southgate, B., McCarten, K., Monogarov, G., O'Duibhir, E., Quinn, N., Tyrer, A., Leitner, M.C., Plumb, C., Kalantzaki, M., et al. (2018). An efficient and scalable pipeline for epitope tagging in mammalian stem cells using Cas9 ribonucleoprotein. *Elife* 7.
- Doench, J.G., Fusi, N., Sullender, M., Hegde, M., Vaimberg, E.W., Donovan, K.F., Smith, I., Tothova, Z., Wilen, C., Orchard, R., et al. (2016). Optimized sgRNA design to maximize activity and minimize off-target effects of CRISPR-Cas9. *Nat. Biotechnol.* 34, 184-191.
- Dong, J.X., Lee, Y., Kirmiz, M., Palacio, S., Dumitras, C., Moreno, C.M., Sando, R., Santana, L.F., Sudhof, T.C., Gong, B., et al. (2019). A toolbox of nanobodies developed and validated for use as intrabodies and nanoscale immunolabels in mammalian brain neurons. *Elife* 8.
- Dresbach, T., Hempelmann, A., Spilker, C., tom Dieck, S., Altmann, W.D., Zuschratter, W., Garner, C.C., and Gundelfinger, E.D. (2003). Functional regions of the presynaptic cytomatrix protein bassoon: significance for synaptic targeting and cytomatrix anchoring. *Mol. Cell. Neurosci.* 23, 279-291.
- Dunn, K.W., Kamocka, M.M., and McDonald, J.H. (2011). A practical guide to evaluating colocalization in biological microscopy. *Am J Physiol Cell. Physiol.* 300, C723-742.
- Edelstein, A., Amodaj, N., Hoover, K., Vale, R., and Stuurman, N. (2010). Computer control of microscopes using microManager. *Curr. Protoc. Mol. Biol.* Chapter 14, Unit14 20.
- El-Husseini, A., Schnell, E., Chetkovich, D., Nicoll, R., and Brecht, D. (2000). PSD-95 involvement in maturation of excitatory synapses. *Science* 290, 1364-1368.
- Ester, M., Kriegel, H.-P., Sander, J., and Xu, X. (1996). A density-based algorithm for discovering clusters a density-based algorithm for discovering clusters in large spatial databases with noise. *Proceedings of the Second International Conference on Knowledge Discovery and Data Mining.* AAAI Press. 226-31.
- Frost, N.A., Shroff, H., Kong, H., Betzig, E., and Blanpied, T.A. (2010). Single-molecule discrimination of discrete perisynaptic and distributed sites of actin filament assembly within dendritic spines. *Neuron* 67, 86-99.
- Fukata, Y., Dimitrov, A., Boncompain, G., Vielemeyer, O., Perez, F., and Fukata, M. (2013). Local palmitoylation cycles define activity-regulated postsynaptic subdomains. *J. Cell. Biol.* 202, 145-161.
- Futai, K., Kim, M.J., Hashikawa, T., Scheiffele, P., Sheng, M., and Hayashi, Y. (2007). Retrograde modulation of presynaptic release probability through signaling mediated by PSD-95-neurologin. *Nat. Neurosci.* 10, 186-195.
- Gao, Y., Hisey, E., Bradshaw, T.W.A., Erata, E., Brown, W.E., Courtland, J.L., Uezu, A., Xiang, Y., Diao, Y., and Soderling, S.H. (2019). Plug-and-Play Protein Modification Using Homology-Independent Universal Genome Engineering. *Neuron*. Epub 2019/07/06.
- Giannone, G., Hossy, E., Levett, F., Constals, A., Schulze, K., Sobolevsky, A., Rosconi, M.P., Gouaux, E., Tampe,

- R., Choquet, D., and Cognet, L. (2010). Dynamic super-resolution imaging of endogenous proteins on living cells at ultra high density. *Biophys. J.* 99, 1303-1310.
- Grimm, D., Kay, M.A., and Kleinschmidt, J.A. (2003). Helper virus-free, optically controllable, and two-plasmid-based production of adeno-associated virus vectors of serotypes 1 to 6. *Mol. Ther.* 7, 839-850.
- Gross, G.G., Junge, J.A., Mora, R.J., Kwon, H.B., Olson, C.A., Takahashi, T.T., Liman, E.R., Ellis-Davies, G.C., McGee, A.W., Sabatini, B.L., et al. (2013). Recombinant probes for visualizing endogenous synaptic proteins in living neurons. *Neuron* 78, 971-985.
- Gu, X., Mao, X., Lussier, M.P., Hutchison, M.A., Zhou, L., Hamra, F.K., Roche, K.W., and Lu, W. (2016). GSG1L suppresses AMPA receptor-mediated synaptic transmission and uniquely modulates AMPA receptor kinetics in hippocampal neurons. *Nat. Commun.* 7, 10873.
- Han, B., Zhou, R., Xia, C., and Zhuang, X. (2017a). Structural organization of the actin-spectrin-based membrane skeleton in dendrites and soma of neurons. *Proc. Natl. Acad. Sci. U. S. A.* 114, E6678-E6685.
- Han, W., Wang, H., Li, J., Zhang, S., and Lu, W. (2017b). Ferric Chelate Reductase 1 Like Protein (FRRS1L) Associates with Dynein Vesicles and Regulates Glutamatergic Synaptic Transmission. *Front. Mol. Neurosci.* 10, 402.
- Hotulainen, P., Llano, O., Smirnov, S., Tanhuanpaa, K., Faix, J., Rivera, C., and Lappalainen, P. (2009). Defining mechanisms of actin polymerization and depolymerization during dendritic spine morphogenesis. *J. Cell Biol.* 185, 323-339.
- Hsu, P.D., Scott, D.A., Weinstein, J.A., Ran, F.A., Konermann, S., Agarwala, V., Li, Y., Fine, E.J., Wu, X., Shalem, O., et al. (2013). DNA targeting specificity of RNA-guided Cas9 nucleases. *Nat. Biotechnol.* 31, 827-832.
- Jezequel, J., Johansson, E.M., Dupuis, J.P., Rogemond, V., Grea, H., Kellermayer, B., Hamdani, N., Le Guen, E., Rabu, C., Lepleux, M., et al. (2017). Dynamic disorganization of synaptic NMDA receptors triggered by autoantibodies from psychotic patients. *Nat. Commun.* 8, 1791.
- Kellermayer, B., Ferreira, J.S., Dupuis, J., Levet, F., Grillo-Bosch, D., Bard, L., Linares-Loyez, J., Bouchet, D., Choquet, D., Rusakov, D.A., et al. (2018). Differential nanoscale topography and functional role of GluN2-NMDA receptor subtypes at glutamatergic synapses. *Neuron* 100, 106-119 e107.
- Kleinstiver, B.P., Pattanayak, V., Prew, M.S., Tsai, S.Q., Nguyen, N.T., Zheng, Z., and Joung, J.K. (2016). High-fidelity CRISPR-Cas9 nucleases with no detectable genome-wide off-target effects. *Nature* 529, 490-495.
- Knott, G.J., and Doudna, J.A. (2018). CRISPR-Cas guides the future of genetic engineering. *Science* 361, 866-869.
- Korobova, F., and Svitkina, T. (2010). Molecular architecture of synaptic actin cytoskeleton in hippocampal neurons reveals a mechanism of dendritic spine morphogenesis. *Mol. Biol. Cell* 21, 165-176.
- Lam, S.S., Martell, J.D., Kamer, K.J., Deerinck, T.J., Ellisman, M.H., Mootha, V.K., and Ting, A.Y. (2015). Directed evolution of APEX2 for electron microscopy and proximity labeling. *Nat. Methods* 12, 51-54.
- Lee, S.H., Kim, S., and Hur, J.K. (2018). CRISPR and Target-Specific DNA Endonucleases for Efficient DNA Knock-in in Eukaryotic Genomes. *Mol. Cells* 41, 943-952.
- Li, T.P., and Blanpied, T.A. (2016). Control of Transmembrane Protein Diffusion within the Postsynaptic Density Assessed by Simultaneous Single-Molecule Tracking and Localization Microscopy. *Front. Synaptic Neurosci.* 8, 19.
- Lin, J.Y., Knutsen, P.M., Muller, A., Kleinfeld, D., and Tsien, R.Y. (2013). ReaChR: a red-shifted variant of channelrhodopsin enables deep transcranial optogenetic excitation. *Nat. Neurosci.* 16, 1499-1508.
- Lindeboom, R.G., Supek, F., and Lehner, B. (2016). The rules and impact of nonsense-mediated mRNA decay in human cancers. *Nat. Genet.* 48, 1112-1118.
- Lindhout, F.W., Cao, Y., Kevenaar, J.T., Bodzeta, A., Stucchi, R., Boumpoutsari, M.M., Katrukha, E.A., Altelaar, M., MacGillavry, H.D., and Hoogenraad, C.C. (2019). VAP-SCRN1 interaction regulates dynamic endoplasmic reticulum remodeling and presynaptic function. *EMBO J.* 38, e101345.
- Lisman, J., Yasuda, R., and Raghavachari, S. (2012). Mechanisms of CaMKII action in long-term potentiation. *Nat. Rev. Neurosci.* 13, 169-182.
- Lu, H.E., MacGillavry, H.D., Frost, N.A., and Blanpied, T.A. (2014). Multiple spatial and kinetic subpopulations of CaMKII in spines and dendrites as resolved by single-molecule tracking PALM. *J. Neurosci.* 34, 7600-7610.
- MacGillavry, H.D., Song, Y., Raghavachari, S., and Blanpied, T.A. (2013). Nanoscale scaffolding domains within the postsynaptic density concentrate synaptic AMPA receptors. *Neuron* 78, 615-622.
- Manders, E.M., Stap, J., Brakenhoff, G.J., van Driel, R., and Aten, J.A. (1992). Dynamics of three-dimensional replication patterns during the S-phase, analysed by double labelling of DNA and confocal microscopy. *J. Cell. Sci.* 103 (Pt 3), 857-862.
- Matsuda, T., and Oinuma, I. (2019). Imaging endogenous synaptic proteins in primary neurons at single-cell resolution using CRISPR/Cas9. *Mol. Biol. Cell* 30, 2838-2855.
- Metzbower, S.R., Joo, Y., Benavides, D.R., and Blanpied, T.A. (2019). Properties of Individual Hippocampal Synapses Influencing NMDA-Receptor Activation by Spontaneous Neurotransmission. *eNeuro* 6.

- Mikuni, T., Nishiyama, J., Sun, Y., Kamasawa, N., and Yasuda, R. (2016). High-Throughput, High-Resolution Mapping of Protein Localization in Mammalian Brain by *In Vivo* Genome Editing. *Cell* 165, 1803-1817.
- Mora, R.J., Roberts, R.W., and Arnold, D.B. (2013). Recombinant probes reveal dynamic localization of CaMKIIalpha within somata of cortical neurons. *J. Neurosci.* 33, 14579-14590.
- Nimchinsky, E.A., Yasuda, R., Oertner, T.G., and Svoboda, K. (2004). The number of glutamate receptors opened by synaptic stimulation in single hippocampal spines. *J. Neurosci.* 24, 2054-2064.
- Nishiyama, J., Mikuni, T., and Yasuda, R. (2017). Virus-Mediated Genome Editing via Homology-Directed Repair in Mitotic and Postmitotic Cells in Mammalian Brain. *Neuron* 96, 755-768 e755.
- Nizak, C., Monier, S., del Nery, E., Moutel, S., Goud, B., and Perez, F. (2003). Recombinant antibodies to the small GTPase Rab6 as conformation sensors. *Science* 300, 984-987.
- Orthwein, A., Noordermeer, S.M., Wilson, M.D., Landry, S., Enchev, R.I., Sherker, A., Munro, M., Pinder, J., Salsman, J., Dellaire, G., et al. (2015). A mechanism for the suppression of homologous recombination in G1 cells. *Nature* 528, 422-426.
- Peng, J., Kim, M.J., Cheng, D., Duong, D.M., Gygi, S.P., and Sheng, M. (2004). Semiquantitative proteomic analysis of rat forebrain postsynaptic density fractions by mass spectrometry. *J. Biol. Chem.* 279, 21003-21011.
- Platt, R.J., Chen, S., Zhou, Y., Yim, M.J., Swiech, L., Kempton, H.R., Dahlman, J.E., Parnas, O., Eisenhaure, T.M., Jovanovic, M., et al. (2014). CRISPR-Cas9 knockin mice for genome editing and cancer modeling. *Cell* 159, 440-455.
- Racca, C., Stephenson, F.A., Streit, P., Roberts, J.D., and Somogyi, P. (2000). NMDA receptor content of synapses in stratum radiatum of the hippocampal CA1 area. *J. Neurosci.* 20, 2512-2522.
- Roussignol, G., Ango, F., Romorini, S., Tu, J.C., Sala, C., Worley, P.F., Bockaert, J., and Fagni, L. (2005). Shank expression is sufficient to induce functional dendritic spine synapses in aspiny neurons. *J. Neurosci.* 25, 3560-3570.
- Roux, K.J., Kim, D.I., Raida, M., and Burke, B. (2012). A promiscuous biotin ligase fusion protein identifies proximal and interacting proteins in mammalian cells. *J. Cell. Biol.* 196, 801-810.
- Sahl, S.J., Hell, S.W., and Jakobs, S. (2017). Fluorescence nanoscopy in cell biology. *Nat. Rev. Mol. Cell. Biol.* 18, 685-701.
- Sala, C., Piech, V., Wilson, N.R., Passafaro, M., Liu, G., and Sheng, M. (2001). Regulation of dendritic spine morphology and synaptic function by Shank and Homer. *Neuron* 31, 115-130.
- Schindelin, J., Arganda-Carreras, I., Frise, E., Kaynig, V., Longair, M., Pietzsch, T., Preibisch, S., Rueden, C., Saalfeld, S., Schmid, B., et al. (2012). Fiji: an open-source platform for biological-image analysis. *Nat. Methods* 9, 676-682.
- Schluter, O.M., Xu, W., and Malenka, R.C. (2006). Alternative N-terminal domains of PSD-95 and SAP97 govern activity-dependent regulation of synaptic AMPA receptor function. *Neuron* 51, 99-111.
- Schnell, U., Dijk, F., Sjollem, K.A., and Giepmans, B.N. (2012). Immunolabeling artifacts and the need for live-cell imaging. *Nat. Methods* 9, 152-158.
- Schwenk, J., Boudkkazi, S., Kocylowski, M.K., Brechet, A., Zolles, G., Bus, T., Costa, K., Kollwe, A., Jordan, J., Bank, J., et al. (2019). An ER Assembly Line of AMPA-Receptors Controls Excitatory Neurotransmission and Its Plasticity. *Neuron* 104, 680-692 e689.
- Schwenk, J., Harmel, N., Brechet, A., Zolles, G., Berkefeld, H., Muller, C.S., Bildl, W., Baehrens, D., Huber, B., Kulik, A., et al. (2012). High-resolution proteomics unravel architecture and molecular diversity of native AMPA receptor complexes. *Neuron* 74, 621-633.
- Shanks, N.F., Savas, J.N., Maruo, T., Cais, O., Hirao, A., Oe, S., Ghosh, A., Noda, Y., Greger, I.H., Yates, J.R., 3rd, and Nakagawa, T. (2012). Differences in AMPA and kainate receptor interactomes facilitate identification of AMPA receptor auxiliary subunit GSG1L. *Cell Rep.* 1, 590-598.
- Shen, K., and Meyer, T. (1999). Dynamic control of CaMKII translocation and localization in hippocampal neurons by NMDA receptor stimulation. *Science* 284, 162-166.
- Shen, M.W., Arbab, M., Hsu, J.Y., Worstell, D., Culbertson, S.J., Krabbe, O., Cassa, C.A., Liu, D.R., Gifford, D.K., and Sherwood, R.I. (2018). Predictable and precise template-free CRISPR editing of pathogenic variants. *Nature* 563, 646-651.
- Sheng, M., and Hoogenraad, C. (2007). The postsynaptic architecture of excitatory synapses: a more quantitative view. *Annu. Rev. Biochem.* 76, 823-847.
- Shi, S., Hayashi, Y., Esteban, J.A., and Malinow, R. (2001). Subunit-specific rules governing AMPA receptor trafficking to synapses in hippocampal pyramidal neurons. *Cell* 105, 331-343.
- Sigal, Y.M., Zhou, R., and Zhuang, X. (2018). Visualizing and discovering cellular structures with super-resolution microscopy. *Science* 361, 880-887.
- Sinnen, B.L., Bowen, A.B., Forte, J.S., Hiester, B.G., Crosby, K.C., Gibson, E.S., Dell'Acqua, M.L., and Kennedy, M.J. (2017). Optogenetic Control of Synaptic Composition and Function. *Neuron* 93, 646-660 e645.

- Slymaker, I.M., Gao, L., Zetsche, B., Scott, D.A., Yan, W.X., and Zhang, F. (2016). Rationally engineered Cas9 nucleases with improved specificity. *Science* 351, 84-88.
- Spence, E.F., Dube, S., Uezu, A., Locke, M., Soderblom, E.J., and Soderling, S.H. (2019). *In vivo* proximity proteomics of nascent synapses reveals a novel regulator of cytoskeleton-mediated synaptic maturation. *Nat. Commun.* 10, 386.
- Stewart, M., Lau, P., Banks, G., Bains, R.S., Castroflorio, E., Oliver, P.L., Dixon, C.L., Kruer, M.C., Kullmann, D.M., Acevedo-Arozena, A., et al. (2019). Loss of *Frrs11* disrupts synaptic AMPA receptor function, and results in neurodevelopmental, motor, cognitive and electrographical abnormalities. *Dis. Model Mech.* Epub 2019/01/30.
- Suzuki, K., Tsunekawa, Y., Hernandez-Benitez, R., Wu, J., Zhu, J., Kim, E.J., Hatanaka, F., Yamamoto, M., Araoka, T., Li, Z., et al. (2016). *In vivo* genome editing via CRISPR/Cas9 mediated homology-independent targeted integration. *Nature* 540, 144-149.
- Uemura, T., Mori, T., Kurihara, T., Kawase, S., Koike, R., Satoga, M., Cao, X., Li, X., Yanagawa, T., Sakurai, T., et al. (2016). Fluorescent protein tagging of endogenous protein in brain neurons using CRISPR/Cas9-mediated knock-in and in utero electroporation techniques. *Sci. Rep.* 6, 35861.
- van Bergeijk, P., Adrian, M., Hoogenraad, C.C., and Kapitein, L.C. (2015). Optogenetic control of organelle transport and positioning. *Nature* 518, 111-114.
- van Overbeek, M., Capurso, D., Carter, M.M., Thompson, M.S., Frias, E., Russ, C., Reece-Hoyes, J.S., Nye, C., Gradia, S., Vidal, B., et al. (2016). DNA Repair Profiling Reveals Nonrandom Outcomes at Cas9-Mediated Breaks. *Mol. Cell* 63, 633-646.
- Verhaagen, J., Hobo, B., Ehlert, E.M.E., Eggers, R., Korecka, J.A., Hoyng, S.A., Attwell, C.L., Harvey, A.R., and Mason, M.R.J. (2018). Small Scale Production of Recombinant Adeno-Associated Viral Vectors for Gene Delivery to the Nervous System. *Methods Mol. Biol.* 1715, 3-17.
- Vogel, C., Abreu Rde, S., Ko, D., Le, S.Y., Shapiro, B.A., Burns, S.C., Sandhu, D., Boutz, D.R., Marcotte, E.M., and Penalva, L.O. (2010). Sequence signatures and mRNA concentration can explain two-thirds of protein abundance variation in a human cell line. *Mol. Syst. Biol.* 6, 400.
- Xu, K., Zhong, G., and Zhuang, X. (2013). Actin, spectrin, and associated proteins form a periodic cytoskeletal structure in axons. *Science* 339, 452-456.
- Yao, X., Wang, X., Hu, X., Liu, Z., Liu, J., Zhou, H., Shen, X., Wei, Y., Huang, Z., Ying, W., et al. (2017). Homology-mediated end joining-based targeted integration using CRISPR/Cas9. *Cell Res.* 27, 801-814.
- Yau, K.W., van Beuningen, S.F., Cunha-Ferreira, I., Cloin, B.M., van Battum, E.Y., Will, L., Schatzle, P., Tas, R.P., van Krugten, J., Katrukha, E.A., et al. (2014). Microtubule minus-end binding protein CAMSAP2 controls axon specification and dendrite development. *Neuron* 82, 1058-1073.
- Zheng, C.Y., Petralia, R.S., Wang, Y.X., Kachar, B., and Wenthold, R.J. (2010). SAP102 is a highly mobile MAGUK in spines. *J. Neurosci.* 30, 4757-4766.

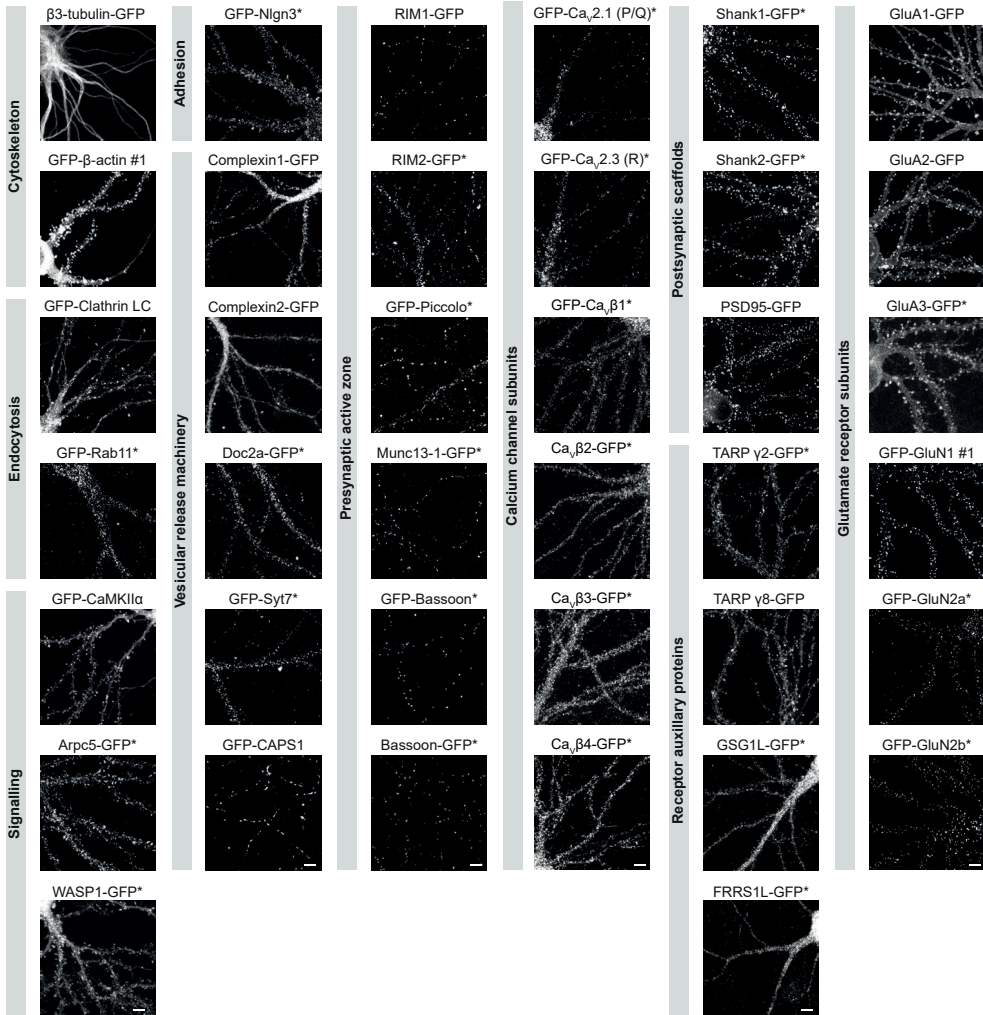


Figure S2. ORANGE CRISPR/Cas9 knock-in library (related to Figure 2)

Representative images of cultured hippocampal knock-in neurons. Examples shown are used for zooms shown in Figure 2D. DIV 21. Asterisk indicates signal enhanced using anti-GFP antibodies (Alexa488 or Alexa647). Scale bar, 5 μ m. GFP, green fluorescent protein; ORANGE, Open Resource for the Application of Neuronal Genome Editing.

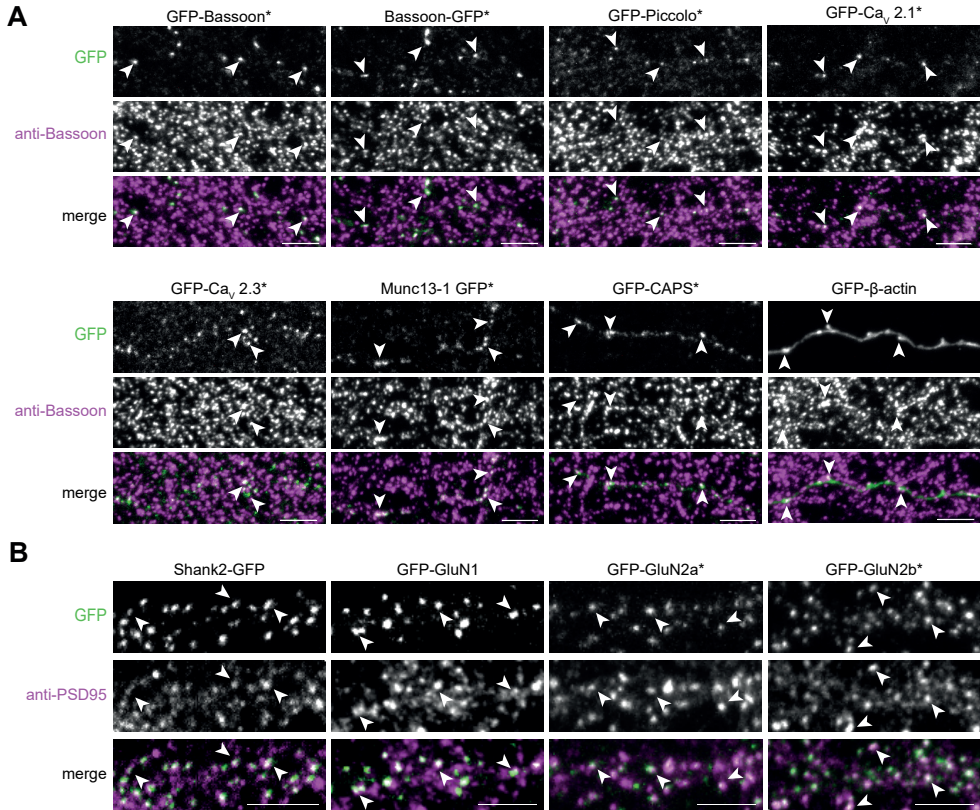


Figure S3. Localization of ORANGE knock-ins relative to synaptic markers (related to Figure 2)

(A) Examples of GFP knock-in (green) relative to anti-Bassoon staining (magenta, Alexa647) as presynaptic marker or (B) anti-PSD95 staining (magenta, Alexa647) as postsynaptic marker in cultured hippocampal neurons. Asterisk indicates signal enhancement using anti-GFP antibodies (Alexa488). Scale bars, 5 μ m. Arrows indicate examples of GFP-positive objects. GFP, green fluorescent protein; ORANGE, Open Resource for the Application of Neuronal Genome Editing.

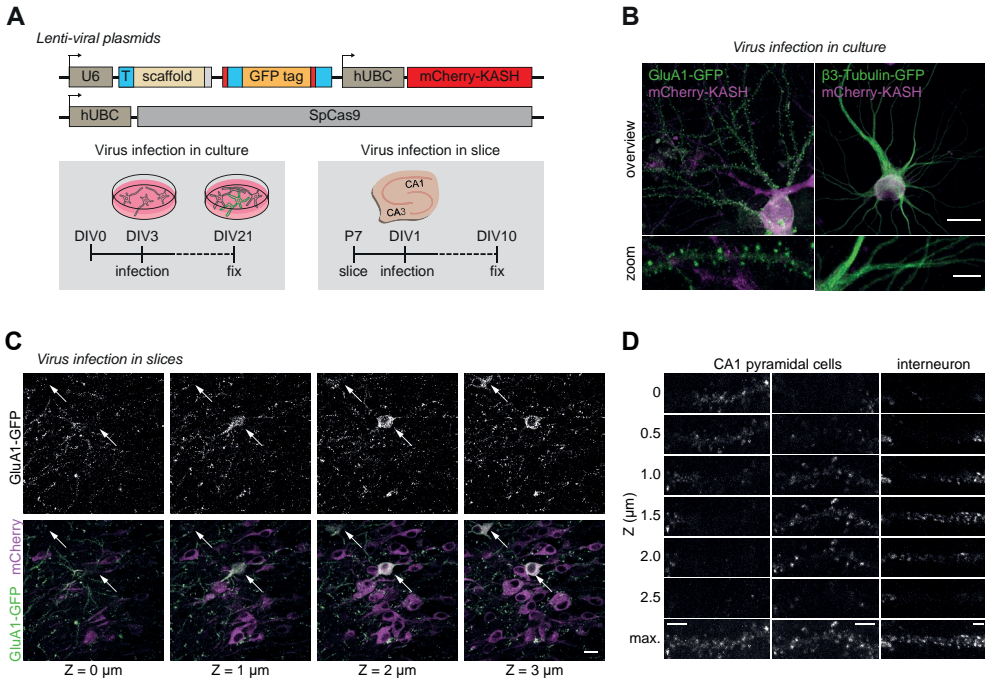


Figure S4. ORANGE knock-ins in dissociated neuronal culture and organotypic slices using a dual-lentiviral approach (related to Figure 3)

(A) Overview of lentiviral constructs and timeline showing age of infection and fixation. (B) Representative images of infected (magenta) primary rat hippocampal neurons positive for GluA1-GFP knock-in or $\beta 3$ -tubulin-GFP knock-in (green). Scale bars, 20 μm and 5 μm for the overview and zooms, respectively. (C) Representative images of GluA1-GFP knock-in in organotypic hippocampal slices from mice. Shown are a series of individual 1- μm planes from a Z-stack. Arrows indicate GFP-positive cells. Scale bar, 20 μm . (D) Representative zooms of GluA1-GFP knock-in dendrites from a CA1 pyramidal cell and an aspiny interneuron. Shown are individual 0.5- μm planes from a Z-stack and the maximum projection (max). Scale bar, 2 μm . GFP, green fluorescent protein; ORANGE, Open Resource for the Application of Neuronal Genome Editing; GluA1, Glutamate receptor AMPA 1; CA1, Cornu Ammonis region 1.

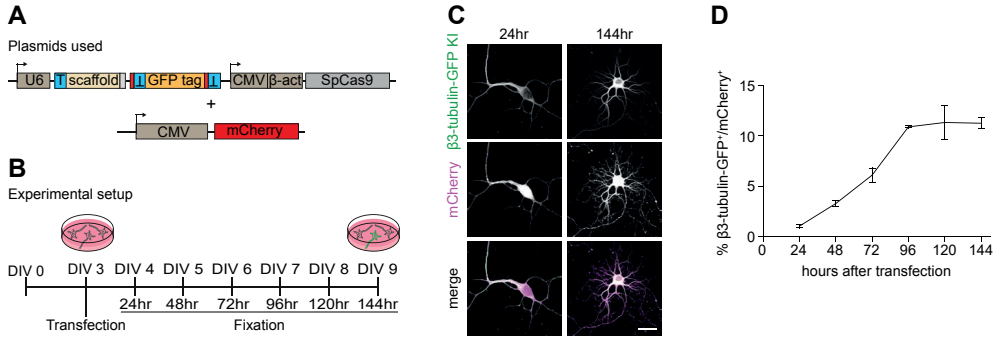


Figure S5. Efficiency of ORANGE knock-in over time in cultured neurons (related to Figure 4)

(A) Schematic overview of knock-in and mCherry reporter plasmids and (B) experimental setup. (C) Representative images of β 3-tubulin-GFP knock-in (green) cotransfected with an mCherry fill (magenta) fixed 24 hours (DIV 4) and 144 hours (DIV 9) after transfection. Scale bar, 20 μ m. (D) Quantification of β 3-tubulin-GFP knock-in efficiency over time as percentage of transfected (mCherry-positive) neurons. Data are represented as means \pm SEM. Underlying data can be found in S1 Data. GFP, green fluorescent protein; ORANGE, Open Resource for the Application of Neuronal Genome Editing; DIV, day *in vitro*.

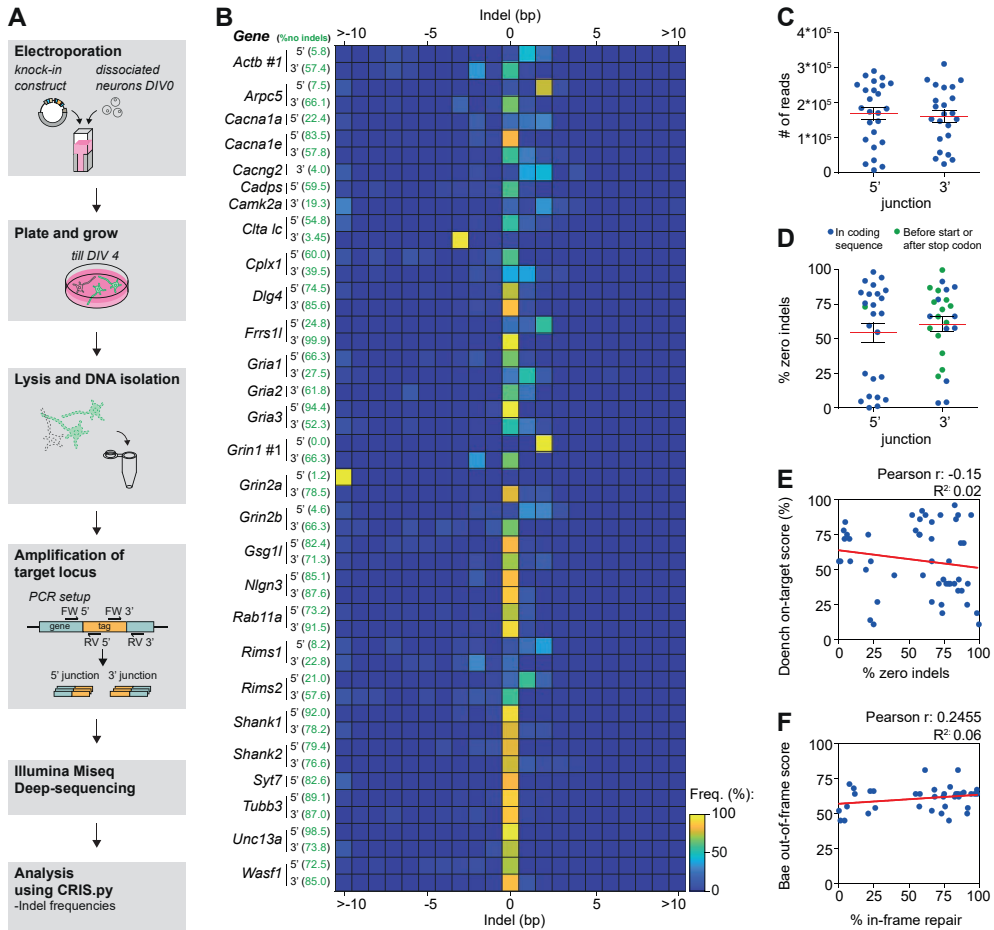


Figure S6. Next-generation sequencing of donor integration at targeted locus (related to Figure 4)

(A) Schematic overview of experimental setup. Neurons were electroporated immediately after dissociation and cultured until DIV 4. Genomic DNA was isolated, and the 5' and 3' junctions of integration were amplified with PCR, pooled, and subjected to next-generation sequencing. (B) Heatmap summarizing the sequencing results for 5' and 3' junction amplicons of the indicated knock-ins. Heatmap is color-coded for the frequency of indel size, as analyzed using CRIS.py. For a few genes, we were only able to amplify one of the two junctions with PCR. (C) Average number of reads obtained with deep sequencing for all successfully analyzed knock-ins (mean 5': $1.69 \times 10^5 \pm 0.18 \times 10^5$, 3': $1.57 \times 10^5 \pm 0.16 \times 10^5$). (D) Accuracy of knock-in plotted for each junction. Plotted points indicate percentage of zero indels from all knock-ins in (B) (mean 5': $54.2\% \pm 7.0\%$, 3': $60.7\% \pm 5.4\%$). Green points indicate minor mutations that do not influence the reading frame for this particular integration (e.g., frame shift after stop codon). (E) Correlation graph between zero indel frequency per amplicon and Doench on-target score of the gRNA target sequence. (F) Correlation graph between correct reading frame integration frequency and Bae out-of-frame score of the gRNA target sequence. Data are presented as means \pm SEM. Underlying data can be found in S1 Data. gRNA, guide RNA; DIV, day *in vitro*.

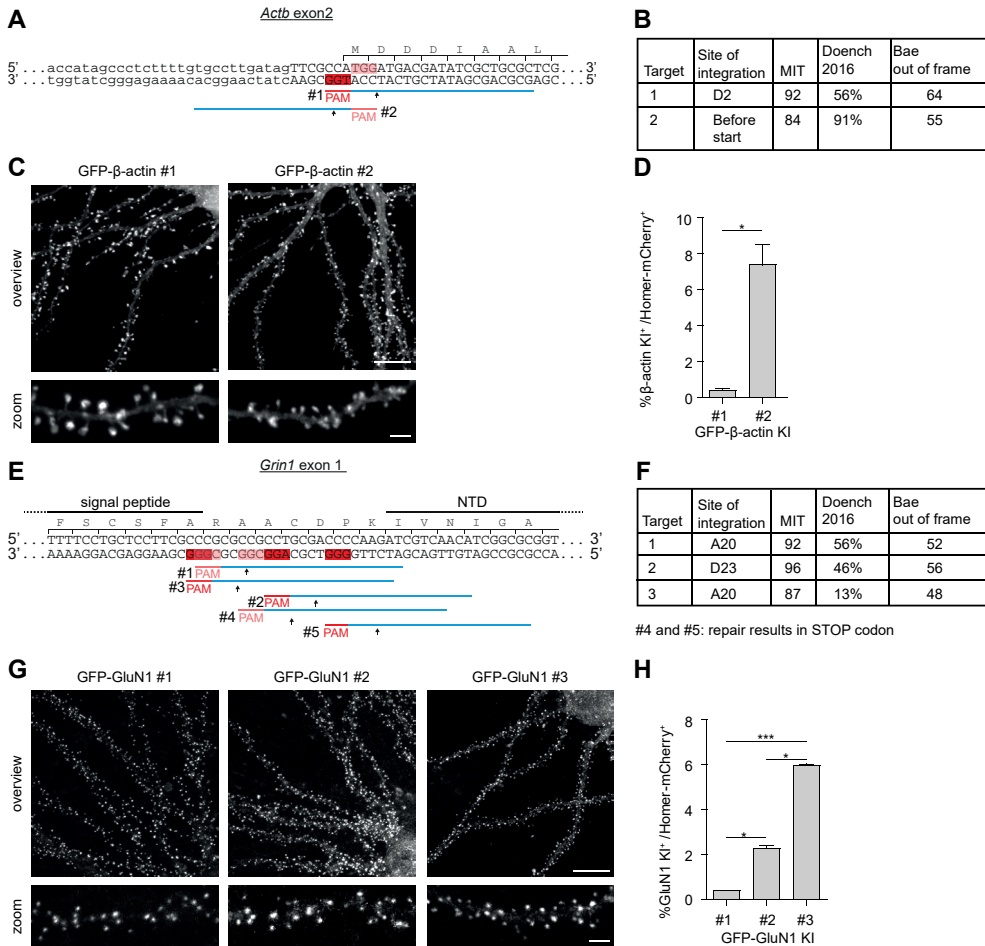


Figure S7. Comparison of integration efficiency at different PAM sites in the same gene (related to Figure 4)

(A and E) Genomic regions of the *Actb* and *Grin1* genes around the targeted integration site are shown. The PAM (red line and red shaded boxes) and target sequences (blue) are shown below for each of the tested knock-ins. Intron sequences are in lowercase, and exon sequences are in uppercase. Additional protein information is shown above the sequence. (B and F) Tables containing information about the site of integration at the protein level and MIT, Doench, and Bae scores of the individual guide RNA sequences (determined based on rat genomic sequence from the UCSC RGC5.0/rn5 genome assembly). (C and G) Representative images of neurons transfected with the various β-actin (C) or GluN1 (G) knock-in constructs targeting the PAM sites shown in (A) and (E), respectively. Scale bars, 10 μm and 2 μm for the overviews and zooms, respectively. (D and H) Knock-in efficiency determined as the percentage of GFP-β-actin (D) or GFP-GluN1 (H)-positive neurons coexpressing Homer1c-mCherry. Data are presented as means ± SEM. * $P < 0.05$, *** $P < 0.001$, ANOVA or Student t test. Underlying data can be found in S1 Data. GFP, green fluorescent protein; PAM, protospacer adjacent motif; *Actb*, Actin Beta; *Grin1*, glutamate ionotropic receptor NMDA type subunit 1; UCSC, University of California Santa Cruz; GluN1, Glutamate receptor NMDA 1.

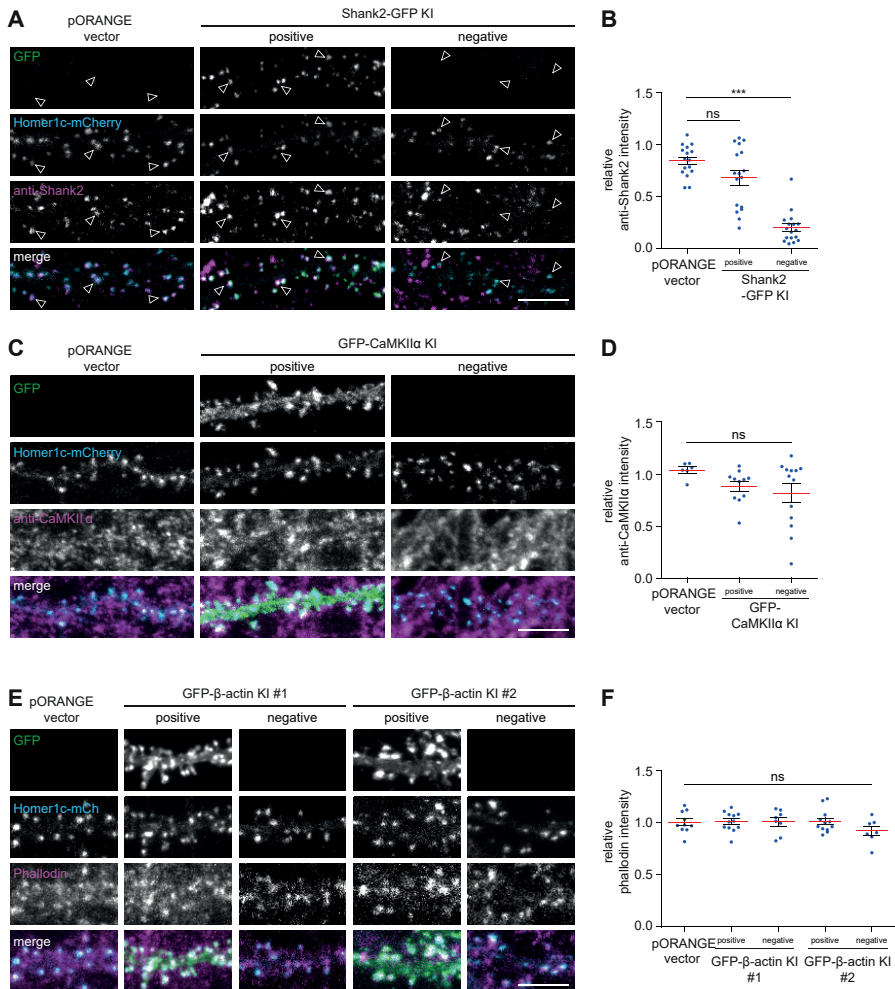


Figure S8. Quantification of Bassoon, Shank2, CaMKII α , and F-actin levels in knock-in neurons (related to Figure 4).

(A) Representative images of neurons transfected with Homer1c-mCherry (cyan) together with pORANGE empty vector as control or Shank2-GFP knock-in (green). Neurons were stained with anti-Shank2 (magenta, Alexa647). (C) Images of neurons transfected with Homer1c-mCherry (cyan) together with pORANGE empty vector as control GFP-CaMKII α knock-in (green). Neurons were stained with anti-CaMKII α (magenta, Alexa647). (E) Neurons transfected with Homer1c-mCherry together with pORANGE empty vector as control, GFP- β -actin knock-in #1 or GFP- β -actin knock-in #2 (green). Neurons were stained for F-actin using phalloidin (magenta, Alexa647). Scale bar, 5 μ m. (B, D, and F) Quantification of protein levels relative to transfected neurons. (B) Relative fluorescence intensity: control: 0.84 ± 0.04 , $n = 16$ neurons, Shank2-GFP knock-in: 0.67 ± 0.07 , $n = 17$ neurons, $P > 0.05$, knock-in negative: 0.20 ± 0.04 , $n = 17$ neurons, $P < 0.01$, ANOVA. (D) Control: 1.04 ± 0.03 , $n = 6$ neurons, GFP-CaMKII α knock-in: 0.88 ± 0.05 , $n = 11$ neurons, $P > 0.05$, knock-in negative: 0.82 ± 0.09 , $n = 13$ neurons, $P > 0.05$, ANOVA. (F) Control: 1.00 ± 0.03 , $n = 10$ neurons, GFP- β -actin knock-in #1: 1.01 ± 0.03 , $n = 12$ neurons, $P > 0.05$, knock-in #1 negative: 1.01 ± 0.04 , $n = 8$ neurons, $P > 0.05$, GFP- β -actin knock-in #2: 1.01 ± 0.03 , $n = 12$ neurons, $P > 0.05$, knock-in #2 negative: 0.92 ± 0.04 , $n = 7$ neurons, $P > 0.05$, ANOVA. Data are presented as means \pm SEM. *** $P < 0.001$, ANOVA. Underlying data can be found in S1 Data. GFP, green fluorescent protein; ns, not significant; ORANGE, Open Resource for the Application of Neuronal Genome Editing; SHANK2, SH3 and multiple ankyrin repeat domains protein 2; CaMKII α , Calcium/calmodulin-dependent protein kinase type II subunit alpha.

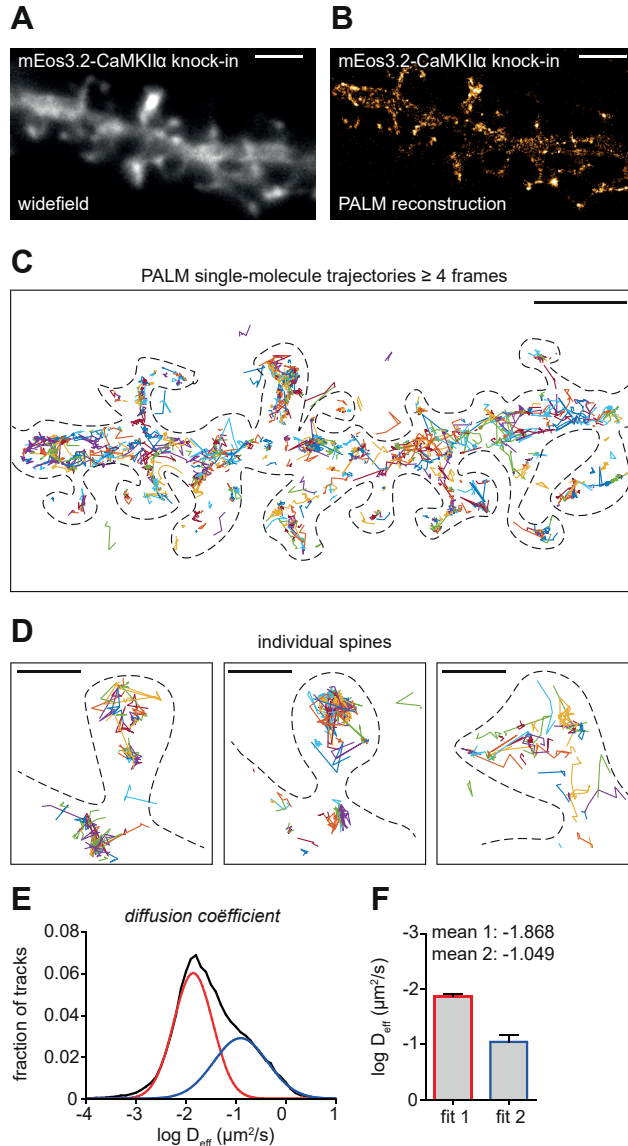


Figure S9. Live-cell superresolution PALM imaging of endogenous CaMKII α dynamics (related to Figure 5)

(A) Example of a dendrite expressing mEos3.2-CaMKII α knock-in. Scale bar, 2 μm . (B) Single-molecule PALM reconstruction of dendrite shown in (A). Scale bar, 2 μm . (C) Individual single-molecule trajectories. Scale bar, 2 μm . Dotted line indicates cell outline. (D) Representative zooms of single-molecule trajectories in individual spines. Scale bar, 200 nm. (E) Frequency distribution of diffusion coefficients derived from single-molecule trajectories (black line). Mixed Gaussian fits (red and blue) indicate two kinetic populations. (F) Quantification of mean diffusion coefficient for each of the two kinetic populations. Data are presented as means \pm SEM. Underlying data can be found in S1 Data. PALM, photoactivated localization microscopy; CaMKII α , Calcium/calmodulin-dependent protein kinase type II subunit alpha; mEos3.2, monomeric Eos 3.2.

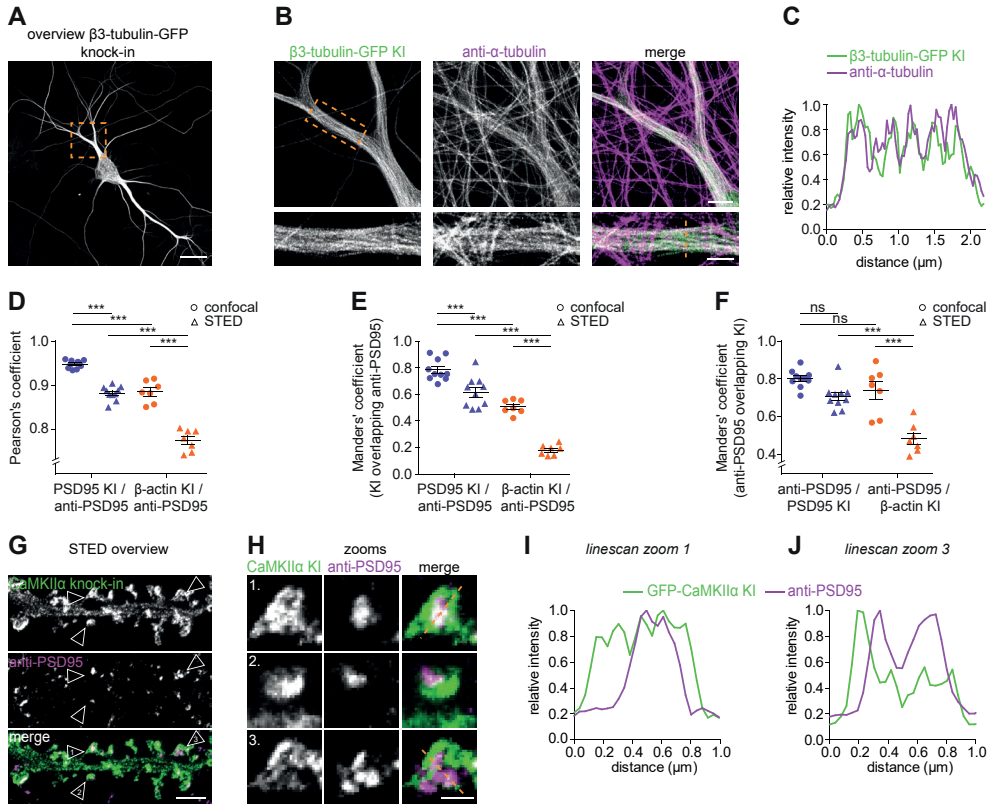
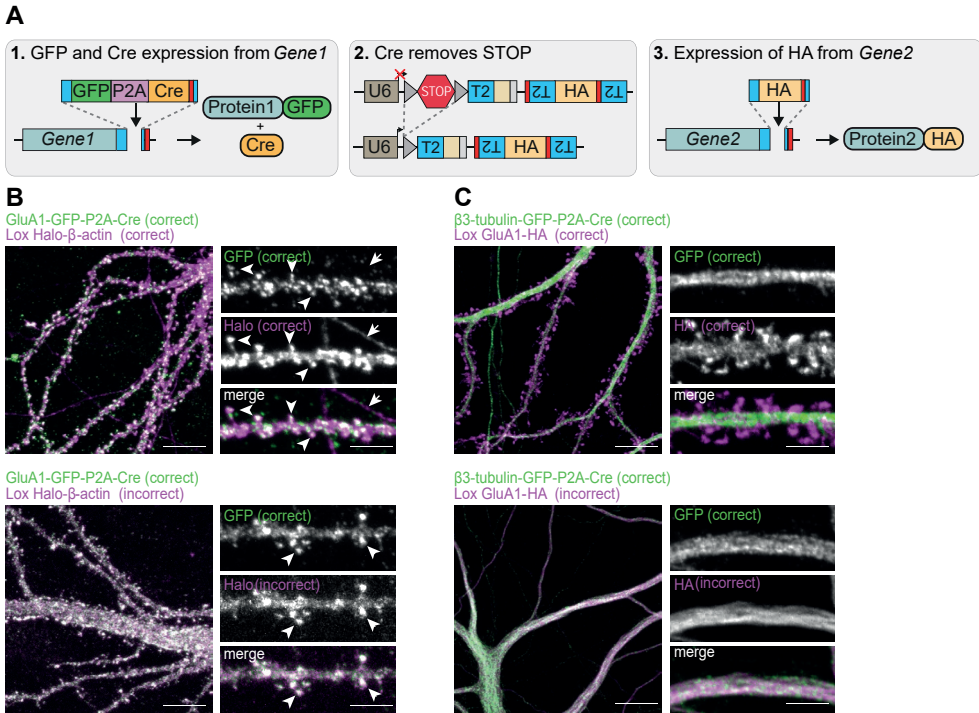


Figure S10. gSTED imaging and colocalization analysis (related to Figure 6)

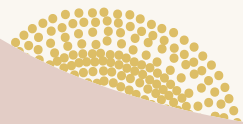
(A) Representative gSTED overview image and zooms (B) of β 3-tubulin-GFP knock-in neurons (DIV 7) extracted and stained with anti-GFP (green, ATTO647N) and anti- α -tubulin (magenta, Alexa594). Scale bars, 20 μ m, 4 μ m, and 2 μ m for the overview and zooms, respectively. (C) Intensity profile along the line indicated in (B). (D) PCC quantifying colocalization between PSD95-GFP or GFP- β -actin knock-in signal with anti-PSD95 staining intensity. Related to Figure 6F-K. (E and F) Manders' correlation of PSD95-GFP or GFP- β -actin knock-in overlapping with PSD95 staining (M1) (E) or anti-PSD95 staining overlapping with PSD95-GFP or GFP- β -actin knock-in (M2) (F) related to Figure 6F-K. Average values: (PSD95, confocal: median PCC = 0.95, M1 = 0.78, M2 = 0.80, STED: PCC = 0.88, ANOVA, $P < 0.001$, M1 = 0.62, $P < 0.001$, M2 = 0.71, $P > 0.05$, $n = 10$ neurons) (β -actin, confocal: median PCC = 0.88, $P < 0.001$, M1 = 0.50, $P < 0.001$, M2 = 0.74, $P > 0.05$, STED: median PCC = 0.78, ANOVA, $P < 0.001$, M1 = 0.18, $P < 0.001$, M2 = 0.48, $P < 0.001$, $n = 7$ neurons). (G and H) gSTED of dendrites and zooms positive for GFP-CaMKII α knock-in stained with anti-GFP (green, ATTO647N) and anti-PSD95 (magenta, Alexa594). Scale bars, 2 μ m and 500 nm for (G) and (H), respectively. (I and J) Line scans of individual spines indicated in (H). Data are represented as means \pm SEM. *** $P < 0.001$. ANOVA. Underlying data can be found in S1 Data. GFP, green fluorescent protein; gSTED, gated stimulated-emission depletion; ns, not significant; PCC, Pearson's correlation coefficient; DIV, day *in vitro*; PSD95, postsynaptic density protein 95; CaMKII α , Calcium/calmodulin-dependent protein kinase type II subunit alpha.



S11 Fig. Multiplex labeling using CAKE (related to Figure 8)

(A) Mechanism of sequential knock-in activation using CAKE. (B) Example of correct dual-color labeling (top) and incorrect dual-color labeling (bottom) with GluA1-GFP-P2A-Cre and Lox Halo β -actin. Arrowheads indicate dendritic spines, and arrow indicates the axon. (C) Example of correct dual-color labeling (top) and incorrect dual-color labeling (bottom) with β 3-tubulin-GFP-P2A-Cre and Lox GluA1-HA. Scale bar is 10 μ m for overview and 5 μ m for zooms. CAKE, conditional activation of knock-in expression; GFP, green fluorescent protein; GluA1, Glutamate receptor AMPA 1; HA, hemagglutinin.

7



General discussion

Nicky Scheefhals¹

¹Cell Biology, Neurobiology and Biophysics, Department of Biology, Faculty of Science,
Utrecht University, Utrecht, the Netherlands

Postsynaptic group I mGluRs are broadly held to be critical modulators of neuronal excitability and synaptic plasticity, and disrupted mGluR signaling has been implicated in severe neurological disorders. Nevertheless, critical information is lacking as to how mGluRs are spatially and temporally controlled in and around synapses to tune synaptic transmission. Therefore, the aim of this thesis was to uncover how mGluR5 activity is regulated at excitatory synapses. In *Chapter 2 (review)* we summarized our current understanding of the functionally distinct postsynaptic ionotropic and metabotropic glutamate receptors (mGluRs), and mechanisms that act to spatially segregate these receptor types in subsynaptic domains. In *Chapter 3 (review)* we further discussed mechanisms underlying the trafficking and positioning of both presynaptic and postsynaptic mGluRs at and around synapses, and the implications for synaptic functioning. In *Chapter 4* we showed that the endocytic zone (EZ) serves to locally internalize and recycle mGluR5 at synapses, regulated by the tight association with the postsynaptic density (PSD) via Shank proteins, additionally governing mGluR5 signaling. In *Chapter 5* we presented a model in which the cytoplasmic tail of mGluR5 controls its dynamic organization in perisynaptic nanodomains, as well as restricts mGluR5 from entering the synapse, providing flexibility to control synaptic signaling. In *Chapter 6* we presented the ORANGE toolbox for epitope tagging of endogenous proteins using CRISPR/Cas9-based technology, with ample applications, including the in-depth characterization of protein distribution in neurons. In this chapter, I will discuss the key findings of this thesis in light of current literature and emphasize on future research directions and potential clinical implications.

Novel insights in synaptic trafficking of mGluRs

Trafficking of synaptic glutamate receptors, especially in the context of synaptic plasticity, has been subject of intense investigation (Brown et al., 2005; Ehlers, 2000; Park et al., 2004; Park et al., 2006). However, the vast majority of work has been focused on AMPAR trafficking. In contrast, the steps that underlie the trafficking of synaptic mGluRs are poorly understood. In *Chapter 4* we provide novel insights in the endocytic trafficking and signaling of mGluR5 following receptor activation. In general, endocytosed receptors are either recycled to the membrane or targeted for degradation by lysosomes. We observed that activation of mGluR5 with its specific agonist DHPG triggers rapid internalization via clathrin-mediated endocytosis and that mGluR5 traffics preferentially through early endosomes to the recycling compartment before returning to the surface in dendritic spines. It is well known that a stable EZ adjacent to the PSD serves to locally capture and recycle specific postsynaptic membrane proteins in spines (Blanpied et al., 2002; Kennedy and Ehlers, 2006; Racz et al., 2004). Here we show that the internalization of mGluR5 is also facilitated by the PSD-EZ coupling, which has important implications for our understanding of the regulation of mGluR activity and signaling and therefore the maintenance of synaptic integrity (Figure 1). Consistent with the idea that internalization via the EZ promotes the local recycling of synaptic receptors, we established that the levels of recycled mGluR5 were significantly higher at EZ-positive synapses. Even though the EZ has been functionally linked to the regulation of synaptic glutamate receptors, so far only a few proteins; Homer, Dynamin-3, Oligophrenin-1, Endophilin-B2, and CPG2, have been implicated in coupling the EZ to the PSD (Cottrell et al., 2004; Loeblich et al., 2016; Lu et al., 2007; Nakano-Kobayashi et al., 2014). We show that Shank proteins are also critical intermediates in

coupling the PSD to the EZ, which was dependent on its Homer, Dynamin and Cortactin binding sites (Figure 1). Disruption of the PSD-EZ coupling in Shank knockdown (KD) neurons reduced agonist-induced internalization of mGluR5 in dendritic spines, leading to loss of mGluR5 from the synaptic membrane, and prevented mGluR5-mediated calcium signaling. This is in line with previous research showing that PSD-EZ uncoupling reduces the synaptic population of AMPARs and prevents plasticity-induced receptor insertion, also indicating loss of this local recycling mechanism in spines (Petrini et al., 2009). We focused on trafficking of mGluR5, but we cannot exclude that other synaptic membrane proteins such as ion channels, receptors, or perhaps even adhesion molecules undergo aberrant trafficking when the EZ is uncoupled from the PSD, also affecting glutamatergic transmission.

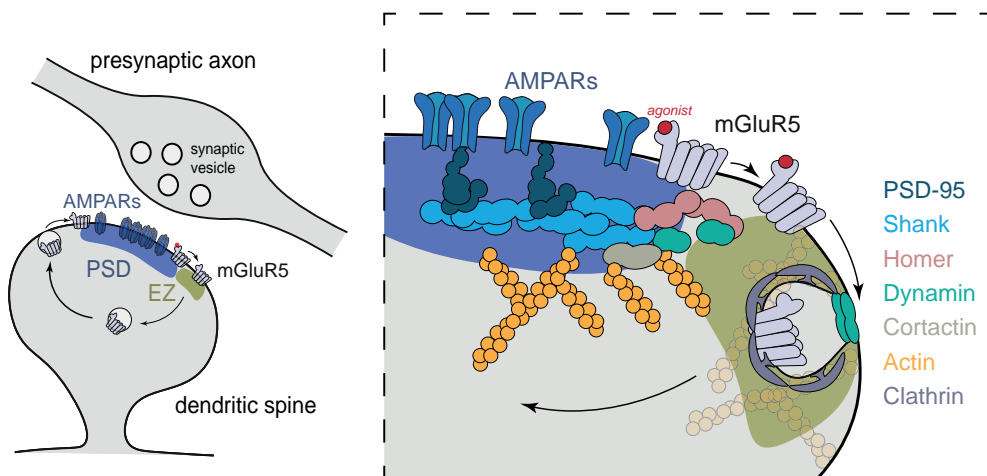


Figure 1. Local recycling of mGluR5 via the EZ, mediated by Shank proteins

Endocytosis of mGluR5 is facilitated by the EZ, which also serves to locally capture and recycle mGluRs. Moreover, Shank proteins have the ability to recruit the essential components of the endocytic machinery, including Homer, Dynamin and Cortactin, to the PSD to facilitate local regulation of mGluR internalization. This model is presented in Chapter 4.

The molecular composition of the EZ itself remains largely elusive. Given that the EZ plays such a central role in synaptic glutamate receptor trafficking, it would be of great interest to gain insight in the molecular architecture of this enigmatic structure. For instance, because each of its components could have distinct functions in different stages of endocytosis, it would be of interest to determine the accumulation of these components at the EZ in time and space. A recent study from the lab (Catsburg et al) investigated the organization of proteins with specific time-dependent roles in endocytosis at the EZ. They observed that proteins contributing to the early phase of endocytosis mostly accumulate specifically at the periphery of the EZ. While other endocytic proteins, mostly involved in the later phase of endocytosis including vesicle scission, were more widely and centrally distributed at the EZ (Catsburg et al., 2022), consistent with observations at clathrin sheets in non-neuronal cells (Sochacki et al., 2017). Also, while some endocytic proteins such as CPG2 were found to contribute more generally to receptor internalization, others such as

Endophilin-B2 were found specifically required for activity-induced, but not constitutive internalization (Loebrich et al., 2016). Remarkably, the EZ undergoes activity-induced remodeling to accommodate long-term changes in synaptic strength (Catsburg et al., 2022). This suggests that reorganization of the EZ induced upon distinct synaptic activity patterns facilitates changes in endocytic rate of receptors modulating long-term synaptic plasticity, a hypothesis that would be interesting to test. Together, these results demonstrate a requirement for spine-localized endocytic trafficking in regulating the synapse proximate receptor content, a principal mechanism for the dynamic regulation of synaptic strength (Czöndör et al., 2012). Such compartmentalized trafficking of specific receptor types may present a general paradigm for the regulation of synaptic membrane organization and composition, explaining how individual spines can remodel at the micron scale during synaptic plasticity.

Unforeseen high degree of organization of mGluR5 at the perisynaptic zone

Despite several studies reporting on the dynamic distribution of mGluRs in neurons both in physiological and pathophysiological conditions (Aloisi et al., 2017; Goncalves et al., 2020; Renner et al., 2010; Sergé et al., 2002; Shrivastava et al., 2013; Westin et al., 2014), a clear understanding of the subsynaptic distribution and dynamics of mGluR5 in mature hippocampal neurons was still missing. In *Chapter 5*, using complementary super-resolution microscopy techniques, we found that the spatial and temporal nanoscale organization of mGluR5 is much more heterogeneous than has been recognized before. Remarkably, we found that mGluR5 is organized in perisynaptic nanodomains that are preferentially localized close to, but not inside the PSD (Figure 2), likely resulting from an equilibrium between diffusive and confined states (Sergé et al., 2002). Indeed, we observed that mGluR5 transiently visits these perisynaptic nanodomains. This is largely contrasting a recent study that reported a homogenous distribution of mGluR5 in spines and a lack of diffusional trapping in the vicinity of the PSD (Goncalves et al., 2020). Nonetheless, the authors of this study did observe that mGluR5 was largely excluded from AMPAR clusters, which is more in line with our data and early EM studies (Nusser et al., 1994) and contrasts their conclusion on the random distribution of mGluR5. For AMPA and NMDA receptors it has been firmly established that they are stabilized and enriched in synaptic nanodomains (Hruska et al., 2022; Kellermayer et al., 2018; MacGillavry et al., 2013; Nair et al., 2013; Willems et al., 2020). This nanoscale segregation of glutamate receptor types suggest distinct mechanisms by which they are spatially segregated within the postsynaptic membrane.

mGluR5 is not uniquely present at perisynaptic sites, but also broadly localizes throughout the dendritic shaft and spines. The geometry of the spine, a thin spine neck that connects the spine head to the dendritic shaft, limits the passage of membrane proteins, which also aids in compartmentalizing processes such as endocytic trafficking and recycling described in *Chapter 4*. Indeed, mGluR5 is enriched in spines, but we additionally observed reduced lateral diffusion of mGluR5 in spines compared to that in the dendritic shaft (*Chapter 5*). Likely, this is due to the perisynaptic confinement zones we identified, but in addition lateral diffusion might be restricted by the spatial constraints imposed by spine shape (Adrian et al., 2017). Indeed, mGluR5 diffusion has been shown to be specifically reduced in the spine neck, indirectly regulated by synaptopodin that locally regulates the organization of the F-actin cytoskeleton (Wang et al., 2016). We did however, not further explore mGluR5

dynamics at the dendritic shaft, even though mGluRs are largely present at extrasynaptic sites. The dendritic shaft contains a heterogeneous pool of mGluRs regulated by different processes influencing receptor dynamics, including directed cell-surface trafficking (Sergé et al., 2003; Sugi et al., 2007) and organization at GABAergic inhibitory synapses located on the dendritic shaft. Interestingly, at inhibitory synapses mGluRs are localized inside synapses (Hanson and Smith, 1999; Mansouri et al., 2015), perhaps providing new insights that aid in identifying a unifying model underlying the dynamic positioning of mGluRs at different dendritic sites. For instance, the generally suggested mGluR scaffolding molecules Homer and Shank are not present at inhibitory synapses, suggesting that simple receptor-scaffold interactions are not the only mechanisms retaining mGluRs. Distinct features of excitatory and inhibitory synapses, such as their composition and density, may in addition regulate receptor entry and retention. For example, excitatory synapses are characterized by the prominent mesh-like and dense PSD hindering receptor diffusion, whereas inhibitory synapses are much thinner sheet-like structures close to the postsynaptic membrane (Tao et al., 2018), possibly allowing the entry of mGluRs. Interestingly, Glycine receptors and GABA receptors, the two main types of inhibitory receptors, as well as their postsynaptic scaffolding protein Gephyrin, organize in nanodomains which are differentially spatially organized and show activity-dependent regulation at inhibitory synapses (Pennacchietti et al., 2017; Specht et al., 2013; Yang et al., 2021). Hence, characterizing mGluR organization at the dendritic shaft, including at inhibitory synapses, will further our understanding of the tight relation between the nanoscale mGluR receptor positioning and signaling.

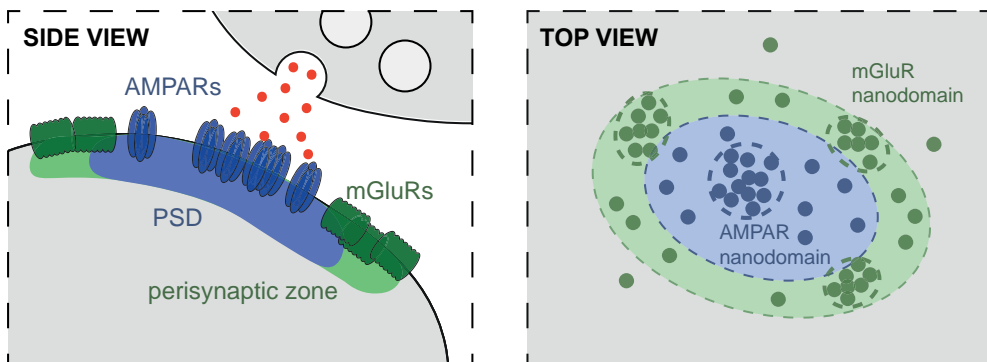


Figure 2. mGluR5 is organized in perisynaptic nanodomains

The side view of the synapse shows that ionotropic AMPA receptors (blue) are concentrated in the postsynaptic density (PSD; light blue), whereas mGluRs (green) are enriched in an annulus surrounding the PSD, named the perisynaptic zone (light green). The top view of the postsynaptic site illustrates the heterogeneous distribution of AMPARs and mGluRs forming nanodomains at their preferred site of localization. The finding that mGluRs are organized in perisynaptic nanodomains is established in Chapter 5 using super-resolution microscopy techniques.

The importance of the spatio-temporal characteristics of mGluRs are not limited to neurons. mGluRs are also expressed in astrocytes, the most numerous type of glial cell in the brain. Astrocytes sense glutamate spillover from synapses and in response evoke intracellular Ca^{2+} release via mGluRs, which contributes to the modulation of synaptic transmission. Strikingly, an mGluR-selective diffusion barrier compartmentalizes mGluR in specific subcellular domains in astrocyte processes, resulting in highly localized mGluR-

mediated Ca^{2+} signaling allowing for the local control of synaptic activity (Arizono et al., 2014; Arizono et al., 2012; Lee and Parpura, 2016). These studies further underline the relevance of understanding the interplay between mGluR dynamics and synaptic signaling, also in the context of neuron-astrocyte communication.

Regulation of synaptic exclusion and perisynaptic transient retention of mGluRs

Understanding the tight relation between nanoscale glutamate receptor positioning at synapses and efficiency of synaptic transmission is undoubtedly very important. Yet, how glutamate receptors are properly organized at the surface by the complex macromolecular synaptic structure is not fully understood. We are only starting to understand how different proteins obtain their distinct location within individual synapses. In *Chapter 5* we show that mGluRs are also heterogeneously distributed at synapses, with a refined level of organization that has direct implications for synaptic physiology. However, unlike AMPAR and NMDARs, mGluRs are largely excluded from the PSD and concentrate in the perisynaptic zone. How does the PSD border discriminate between these receptor types and establish this remarkable nanoscale segregation? What are the selection criteria for entry into the PSD? Is this based on specific receptor properties, perhaps also regulated in an activity-dependent manner? And what mechanisms anchor and position mGluRs once they reach the border of the PSD? It seems quite clear that the processes involved in determining synaptic entry and anchoring of receptors at distinct synaptic sites are tightly regulated, however to date the mechanisms remain largely unknown. In *Chapter 2* we elaborately discuss potential mechanisms that act on specific receptor subtypes and organize the synapse in functional domains.

In *Chapter 5* we show that the mGluR5 cytoplasmic tail domain (CTD) controls its dynamic organization in perisynaptic nanodomains, as well as restricts mGluR5 from entering the synapse. Surely, CTD protein interactions, for a large part, direct the trafficking and anchoring of mGluR5 at the synaptic membrane (Bodżęta et al., 2021b). However, our results indicate that two of the most often proposed mGluR scaffolding molecules, Shank and Homer, are most likely not contributing to the organization of mGluR5 in perisynaptic nanodomains. To rule out the popular, but simplified notion that Shank proteins anchor mGluRs at the synapse (Tu et al., 1999), we performed fluorescence recovery after photobleaching (FRAP) experiments and observed no effect of the Shank KD on mGluR5 stability (*Chapter 4*). Thus, rather than Shank proteins contributing to the anchoring of mGluRs at synaptic sites, our results indicate that Shank proteins play an essential role in synaptic receptor recycling. The prominent scaffolding protein Homer1b/c localizes in the core of the PSD, away from the perisynaptic mGluR5 nanodomains, and Homer1c expression does not affect mGluR5 enrichment or diffusion in spines (*Chapter 5*). We generated a mutant lacking the entire mGluR5 CTD, but for follow-up experiments it will be insightful to truncate motifs, or smaller domains, mediating interactions with specific proteins to identify the key regulator of mGluR positioning. We further discuss possible mGluR CTD interacting proteins that might control the spatial regulation of mGluR5 in *Chapter 3*.

An interesting observation is that AMPARs are transiently stabilized at the perisynaptic EZ, suggesting interactions with endocytic machinery components that influence the lateral diffusion of receptors (Petrini et al., 2009). For mGluR5 this may be regulated via β -arrestin since activated mGluR5 is desensitized by the recruitment of β -arrestin that targets the

receptor for internalization via clathrin-mediated endocytosis, but also acts as an adaptor for the endocytic machinery components AP-2 and Clathrin (Ferguson et al., 1996; Goodman et al., 1996; Laporte et al., 1999). AP-2, like Clathrin, localizes to the EZ and is known to bind to cytosolic receptor domains and might partake in the perisynaptic positioning of mGluRs (Catsburg et al., 2022; Laporte et al., 1999). Many questions remain however; do mGluR5 nanodomains colocalize with the perisynaptic EZ? And does the endocytic machinery play an active role in stabilizing synaptic mGluRs or do other mechanisms ensure the positioning close to the EZ enabling fast turnover of receptors?

Mechanisms, other than protein-protein interactions, that might mediate the organizational properties of the mGluR5 CTD include phase separation, molecular crowding, lipid organization or cytoskeletal hindrance. Interactions between components of the PSD have been found to induce phase separation further favoring complex formation into liquid-like droplets, mimicking the PSD (Zeng et al., 2018; Zeng et al., 2016). For example, Stargazin binding to PSD-95 through its CTD also triggered the condensation of other components of the PSD via liquid-liquid phase separation (LLPS), suggested to trap AMPARs at synapses (Zeng et al., 2019). Perhaps, the mGluR CTD has similar molecular properties as the inhibitory scaffolding protein Gephyrin, which was found to be actively repelled from reconstituted PSD assemblies through LLPS (Zeng et al., 2018). Furthermore, the PSD is very densely packed with proteins likely imposing a diffusional barrier to receptors. Indeed, molecular crowding has been shown to trap and prevent the exit of receptors, including AMPARs (Li and Blanpied, 2016; Li et al., 2016; MacGillavry et al., 2011; Renner et al., 2009; Santamaria et al., 2010). Conversely, the molecular crowded PSD might act as an exclusion matrix preventing the entry of mGluR5 with its large CTD, further implying distinct regulation of different receptor types varying in their molecular size and geometries contributing to their differential subsynaptic positioning (*Chapter 2*). Not only proteins close to the cytoplasmic face of the postsynaptic membrane, but also the lipid bilayer itself is likely to impose diffusional barriers to receptor diffusion. The lipid composition can compartmentalize protein complexes, but also determines the membrane viscosity further regulating the lateral diffusion of receptors (Sako and Kusumi, 1994; Westra et al., 2021). In particular that of mGluRs given their large size and complex membrane topology, namely seven transmembrane helices that span the membrane that, together with its CTD, couple to bulky Gq-proteins which assemble close to the membrane (De Blasi et al., 2001; Nishimura et al., 2010). Perisynaptic actin could also act as a gatekeeper, imposing a diffusional barrier to receptor entry into the PSD (Burette et al., 2012; Frost et al., 2010; Morone et al., 2006). Furthermore, the actin filamentous meshwork may compartmentalize proteins at the perisynaptic membrane. Indeed, another GPCR co-clustered with its cognate G-proteins at the cell membrane which was defined by the actin-based membrane skeleton (Sungkaworn et al., 2017), but also the mobility of presynaptic mGluR2 was increased upon depolymerization of the actin cytoskeleton (Bodzeta et al., 2021a). It would be interesting for future studies to look at the contribution of these specific mechanisms to receptor positioning.

Evidently, the N-terminal domain (NTD) of mGluRs could also hinder receptor entry via steric hindrance or anchoring via extracellular interactions with synaptic cleft proteins. To date many presynaptic and postsynaptic components, in particular adhesion molecules, have been shown to be part of the lateral oligomerization forming the transsynaptic nanocolumn, key to the alignment of postsynaptic receptors with the presynaptic active zone (Biederer et al., 2017; Tang et al., 2016). For instance, presynaptic group III subtype mGluR7

is stably anchored at the active zone which relied on its extracellular domain likely due to interactions with the adhesion molecule ELFN1/2 (Bodzęta et al., 2021a). Interestingly, the adhesion protein SynCAM1 is specifically enriched at the postsynaptic edge (Perez de Arce et al., 2015). Also, mGluRs induce intracellular signaling upon binding of the prion glycoprotein (PrPC) bound to the extracellular matrix protein Laminin peptide (Ln- γ 1) (Beraldo et al., 2011). PrPC, tethered to the membrane and bound to laminin is suggested to crosslink and spatially restrict proteins, including the neural cell adhesion molecule NCAM and mGluRs, forming dynamic signaling modules (Linden, 2017). However, the exact role of the mGluR extracellular domain in regulating synaptic entry or retention remains to be established. In *Chapter 2* we further discuss the contribution of alternative mechanisms such as steric hindrance, receptor structure and cytoskeletal hindrance to the regulation of synaptic entry and retention of glutamate receptors.

Super-resolution imaging and genome editing to fast-forward the neuroscience field

The main reason to the surprising lack of information on the basic mechanisms underlying the organization of the densely packed, sub-micrometer scale synapse has been the limited resolution of conventional light microscopy techniques. Over the past few years, advances in super-resolution imaging techniques allowed us to overcome this classical barrier of the diffraction limit of light microscopy and resolve synapse organization with nanometer precision. A commonality of the majority of studies discussed in the section above is their use of advanced super-resolution microscopy techniques, including single-molecule tracking in live cells. The latter is also a major advantage over using electron microscopy (EM), which to date provides the highest resolution possible, but is inherently unsuitable for live-cell imaging as EM relies on invasive fixation procedures. To employ the different super-resolution imaging techniques, including stimulated emission depletion (STED) microscopy, photoactivated localization microscopy (PALM), stochastic optical reconstruction microscopy (STORM) and universal point accumulation in nanoscale topography (uPAINT) we used in *Chapter 5*, we rely on engineered fluorescent proteins and organic dyes with specific properties to visualize the protein of interest. Clearly, there is a strong need for technological developments that can tag or manipulate specific aspects of synapse organization and function without disrupting overall synapse architecture. Our approach in *Chapter 4 and 5* largely relied on the overexpression of mGluR5 and even though we minimized overexpression artifacts by selecting neurons with moderate expression levels, it is preferred to look at endogenous proteins. In *Chapter 6* we developed the ORANGE (Open Resource for the Application of Neuronal Genome Editing) toolbox, which is a CRISPR/Cas9 technology that allows for the tagging of endogenous proteins in neurons. We validated our knock-in approach by targeting over 30 genes, including many synaptic proteins. Tagging endogenous proteins together with ongoing progress in super-resolution techniques and EM presents a very powerful approach to study how functional synapses are built. This is nicely demonstrated in *Chapter 6* where we resolved the subcellular organization of ORANGE knock-ins using super-resolution STED and STORM imaging, for example visualizing the periodic actin rings in dendrites and NMDA receptor synaptic nanodomains. Moreover, ORANGE is a valuable approach to study recently identified proteins with unknown localization and opens up a wide range of applications of great importance to the neuroscience field and beyond.

A role of nanodomains in the compartmentalization of downstream signaling

In neurons, mGluRs couple to intracellular signaling cascades modulating the efficacy of synaptic signaling. Consequently, the regulation of mGluR activity critically controls neuronal communication, and therefore needs to be tightly regulated. In *Chapter 5* we developed an inducible dimerization system to overcome endogenous regulation of mGluR5 positioning and acutely re-localize mGluR5 to the synapse. Strikingly, this led to a severe deregulation of synaptic calcium signaling. This implies the functional relevance of the proper dynamic positioning of mGluR5 in perisynaptic nanodomains and indicates that preventing synaptic entry is critical for restricting mGluR5 overactivation. But why are mGluRs not homogeneously distributed in an annulus surrounding the PSD? And what is the functional relevance of more than one nanodomain in the perisynaptic zone?

Inside nanodomains a higher density of mGluR5 is maintained which inherently leads to concentrated and enhanced mGluR-mediated downstream signaling. Local confinements of receptors together with its downstream effectors, known as signalosomes, increase the efficiency and fidelity of synaptic signaling (Kasai and Kusumi, 2014; Kusumi et al., 2012). Interestingly, Gαq/Gα11 extensively colocalize with group I mGluRs in Purkinje cells (PCs) and hippocampal neurons and PLCβ is enriched in the perisynaptic region of dendritic spines of PCs, as shown by immunogold EM (Nakamura et al., 2004; Tanaka et al., 2000). This supports the concept of a perisynaptic signalosome and suggests that activation of perisynaptic mGluRs is mediated by its cognate G-proteins, leading to subsequent activation of the downstream canonical pathway, including PLC. But also, DGL-α, an enzyme downstream of non-canonical mGluR5 signaling leading to the formation of the endocannabinoid 2-AG ligand, was found to closely parallel the organization of mGluR5. They showed, using immuno-EM, that DGL-α was compartmentalized in a 60 nm annulus surrounding the PSD and was completely absent from the PSD in hippocampal neurons (Katona et al., 2006; Olmo et al., 2016). Lastly, 3D structured illumination microscopy (3D-SIM) revealed that mGluR5 co-localized with the mGluR5 accessory protein Norbin at the perisynaptic zone (Westin et al., 2014).

mGluRs distributed over multiple nanodomains might be an efficient way to segregate downstream signaling by forming distinct signalosomes. Also, the functional selectivity of the different group I mGluRs, mGluR1 and mGluR5, might only be possible by segregating these receptors in different nanodomains at perisynaptic sites. For example, the initiation of 2-AG formation is almost exclusively mediated by mGluR5 activation, even though both receptors are coupled to the same G-protein dependent pathway activating PLC to form DAG, the precursor of 2-AG (Katona and Freund, 2008). In *Chapter 5* we focused on the group I subtype mGluR5a, however there are multiple splice variants of mGluR1 and mGluR5. These isoforms particularly differ in their C-terminus and thus likely differentially determine their subsynaptic positioning (Ferraguti and Shigemoto, 2006; Willard and Koochekpour, 2013). Moreover, although mGluR5 preferentially forms homodimers, recent work confirmed that mGluRs can also form heterodimers with mGluR1 (Lee et al., 2020), allowing cooperative signaling (Sevastyanova and Kammermeier, 2014). Thus, further delineating the subsynaptic organization of different group I mGluR isoforms and their preferential enrichment with effector proteins will provide insights in how functional selectivity can be warranted, even within the small confines of dendritic spines.

Functional implications of mGluRs organized in perisynaptic nanodomains

In the overall assembly of synapses, protein-protein interactions create a stable molecular complex effectively concentrating receptors, but at the same time allow for dynamic remodeling of synaptic structure in response to activity. In *Chapter 5* we show that mGluR5 is highly dynamic and transiently visits perisynaptic nanodomains. Moreover, we show that erroneous mGluR positioning during basal synaptic transmission leads to deregulation of synaptic calcium signaling. However, whether there is activity-induced reorganization of mGluR nanodomains remains to be investigated. mGluR dynamics are increased upon activation with the group I specific agonist DHPG, possibly representing uncoupling of Gq-proteins alleviating steric hindrance (Sergé et al., 2002). Alternatively, this might also represent the action of the immediate early gene *Homer1a*. *Homer1a* expression is increased during neuronal activity (Brakeman et al., 1997), and acts as a dominant negative regulator of mGluR signaling by disrupting the interaction between mGluR and the constitutively expressed longer isoforms *Homer1b/c* (Xiao et al., 1998). Interestingly, through the *Homer*-containing PSD complex mGluR5 can physically interact with NMDARs (Scannevin and Huganir, 2000; Tu et al., 1999). However, in the presence of *Homer1a* this complex is disrupted permitting the re-localization of mGluR5 in close proximity to NMDARs, allowing the functional crosstalk between mGluRs and NMDARs (Aloisi et al., 2017; Bertaso et al., 2010; Moutin et al., 2012). Specifically, disrupting the link between long *Homer* isoforms and mGluR5 led to increased mGluR5 mobility, as well as increased localization of mGluR5 and NMDARs inside synapses (Aloisi et al., 2017). Using bioluminescence resonance energy transfer (BRET) to study the proximity between proteins, it was observed that the presence of *Homer1a* triggered colocalization of mGluR5 and NMDARs in spines (Moutin et al., 2012). Furthermore, in the presence of *Homer1a* co-immunoprecipitation experiments revealed a direct interaction between NMDARs and the group I mGluR G-protein β subunits, indicating direct modulation of NMDARs by mGluRs (Bertaso et al., 2010). In the extension of the experiments performed in *Chapter 5*, single-molecule localization microscopy would be a more direct way to reveal whether mGluR5 translocates from the perisynaptic domain to the synapse, colocalizing with NMDARs, during sustained neuronal activity or overexpression of *Homer1a*. And to address whether this involves remodeling of entire nanodomains or whether only a few mGluRs are required to enter the synapse and modulate synaptic transmission.

In *Chapter 5* we show that the artificial recruitment of mGluR5 to the synapse results in a strikingly increased frequency of miniature spontaneous calcium transients (mSCTs) in spines. Even though we have not resolved the nature of this signaling, we could argue that this situation mimics the physical interaction between mGluR5 and NMDARs triggered by activity-induced *Homer1a* expression. During spontaneous neurotransmitter release, mSCTs require NMDA receptor activity (Reese and Kavalali, 2015). Surprisingly, however, the studies that reported increased mGluR5/NMDAR partnership during activity-induced *Homer1a* expression revealed mGluR5-mediated inhibition of NMDA currents (Aloisi et al., 2017; Bertaso et al., 2010; Moutin et al., 2012). The functional interaction between mGluRs and NMDARs has revealed to be highly complex as mGluRs also potentiate NMDAR responses in the hippocampus (Aniksztejn et al., 1992; Benquet et al., 2002; Fitzjohn et al., 1996; Harvey and Collingridge, 1993; O'Connor et al., 1994). Intriguingly, whereas mGluRs potentiate NMDA currents in the hippocampal CA1 region, mGluRs depress NMDA currents in CA3 neurons (Grishin et al., 2004). On top of that, mGluR1 and

mGluR5 also activate distinct signaling systems differentially controlling NMDAR function (Benquet et al., 2002). Hence, this makes the interpretation of our data even more complex, as we used primary hippocampal cultures containing a mixture of, amongst others CA1 and CA3, neuronal cell types. To corroborate mGluR-mediated inhibition of NMDARs in our system, a follow-up study should investigate whether NMDARs can still be potentiated upon Glycine-induced LTP when mGluR5 is recruited to the core of the synapse by our inducible FKBP-rapalog-FRB heterodimerization system.

Even though we observed an increase in mSCT frequency, the mSCT amplitude was unaffected by synaptic recruitment of mGluR5. GCaMP6f has often been used to measure mSCTs (Sinnen et al., 2016; Tang et al., 2016), however the degree of variability in mSCT amplitudes mediated by NMDAR activity was surprisingly low both between and within spines (Metzbower et al., 2019). This suggests that the amount of NMDAR-mediated Ca^{2+} influx is largely independent of NMDAR number. Alternatively, our results might indicate that the mSCTs are not solely dependent on NMDA receptor activity and might be generated by a signaling process downstream of Ca^{2+} entry. An interesting hypothesis could be that increased mSCT frequency is reflected by increased mGluR5 downstream signaling leading to Ca^{2+} release from smooth endoplasmic reticulum (SER) present in spines, differentially shaping the time course of mSCTs (Spacek and Harris, 1997). Indeed, we found significantly larger decay tau times supporting the idea that increased release of Ca^{2+} from SER generated more mSCTs upon mGluR5 recruitment to the synapse. Future experiments pharmacologically blocking specific sources of calcium influx should reveal the source responsible for the observed increase in mSCTs, such as blocking extracellular Ca^{2+} influx through NMDARs, AMPARs and L-type Ca^{2+} channels, but also blocking Ca^{2+} -induced Ca^{2+} release (CICR) from internal stores. Altogether, our data and that of others reveal that mGluR5 signaling is regulated by dynamic changes in mGluR5 positioning, that on the one hand prevent overstimulation during weak synaptic activity, but on the other hand scale synaptic excitability during sustained activity.

Translational concepts of mGluR5 in synaptic diseases

Remarkably, only in a very few reported instances deleterious mutations have been found in the GRM genes (coding mGluRs) that are related to neurodevelopmental disorders, which are not proven to play a causal role in disease. Specifically for ASD or ID no reports have implicated GRM mutations despite the fact that disrupted mGluR5 signaling has consistently been involved in the development of ASD and ID (Soto et al., 2014). Interestingly, while in some mouse models of ASD or ID (e.g. *Fmr1*^{-/-} and *Irsps53*^{-/-} mice) suppression of mGluR5 activity normalizes social interaction deficits (Aguilar-Valles et al., 2015; Bear et al., 2004; Chung et al., 2015; Michalon et al., 2012; Tian et al., 2015), in other models, positive modulation of mGluR5 restores synaptic and behavioral deficits (e.g. *Tsc2*^{+/-}, and *Shank2*^{-/-} mice) (Auerbach et al., 2011; Lin et al., 2014; Won et al., 2012). Thus, a proper balance in mGluR5 activity is critical for the regulation of neuronal communication underlying social behaviors. In *Chapter 4* we provide evidence that at the molecular level, specific mGluR trafficking events are disrupted in the absence of the Shank scaffolding molecules. Loss of individual Shank family members has previously been associated with alterations in mGluR signaling and function underlying human neurological disorders (Verpelli et al., 2011). Indeed, this is supported by our experiments demonstrating that a mutation in SHANK2

found in autism disrupts mGluR trafficking. Promising, social deficits in SHANK3 deficient mice could be rescued by restoring SHANK3 expression in adult mice (Mei et al., 2016), indicating that behavioral aspects associated with the loss of Shanks can be restored, even beyond development in adulthood. More general, furthering our understanding of how mutations in human synaptic genes lead to neurodevelopmental disorders such as ASD is critical for the development of refined pharmacological interventions.

One of the main goals of this thesis was to better understand the tight relation between dynamic mGluR positioning and signaling in the context of cognitive functioning. Even more so, because altered mGluR dynamics have been implicated in the pathophysiology of neurological disorders, including Fragile X syndrome (FXS) and Alzheimer's disease (Aloisi et al., 2017; Renner et al., 2010; Shrivastava et al., 2013). FXS is caused by the loss of the translational repressor FMRP protein, in particular leading to exaggerated mGluR5 signaling and synthesis of LTD-proteins depressing AMPAR activity (Huber et al., 2002). Hippocampal neurons of *Fmr1* KO mice showed increased lateral diffusion of mGluR5 specifically at synaptic sites, suggested to be due to disruptions in the mGluR5-Homer association. In turn, this increased the mGluR5-NMDAR association leading to NMDAR dysfunction (Aloisi et al., 2017; Giuffrida et al., 2005). Hence, a therapeutic approach could be designed to restore the mGluR5-Homer and mGluR5-NMDAR interactions, which might present a promising treatment option for FXS. Alzheimer's disease (AD) is characterized by β -amyloid ($A\beta$) oligomers, that can induce synaptotoxicity by binding to the plasma membrane via PrPC. In neurons, $A\beta$ was found to reduce the lateral diffusion and accumulation of mGluR5 at excitatory synapses resulting in elevated intracellular Ca^{2+} levels (Renner et al., 2010). A follow-up study revealed hyperactivity in astrocytes potentiated by mGluR5 enriched in astrocyte processes surrounding $A\beta$ plaques further leading to diffusional trapping and clustering of mGluR5 in both neurons and astrocytes (Shrivastava et al., 2013). These studies show that the toxic effect of $A\beta$ oligomers are largely executed through immobilizing mGluRs at the synaptic membrane disrupting synaptic signaling. So also here, it might be advantageous to consider mGluR5 as a target for the pharmacological treatment of AD.

Concluding remarks

The complex molecular architecture of neuronal synapses is fundamental to the maintenance of efficient synaptic signaling, and ultimately underlies processes such as learning and memory. While the precise positioning of glutamate receptors is predicted to shape synaptic transmission and plasticity, we know little about the mechanisms that underlie the spatiotemporal control of mGluRs at excitatory synapses. In this thesis we used a combination of novel molecular tools, super-resolution imaging and functional read-outs to resolve the dynamic distribution and trafficking of mGluR5 and the implications for its activation. Since mGluRs are key to synaptic functioning, these novel findings open the door to numerous future studies. These are exciting times for neuroscientists as we are really at the start of employing techniques allowing the direct visualization and manipulation of endogenous proteins to study specific aspects of synapse architecture, including glutamate receptors. Genome editing techniques such as our ORANGE toolbox aid in achieving this (Chapter 6). We achieved N-terminal tagging of mGluR5 allowing the investigation of the surface-expressed endogenous receptor pool, providing exciting new possibilities to

study mGluR5 biology. This includes employing different neurobiological model systems, such as *in vivo* applications and human induced pluripotent stem cells (iPSCs) (Linda et al., 2018). In addition, studying mGluR5 in human iPSCs allows for better translation of disruptions in the nanoscale structure-function relation of mGluR5 to human neurological disorders. The current challenge in the field of synapse biology is the option to tag or disrupt multiple proteins at once, which is in development as we speak (Droogers et al., 2022), to study the endogenous co-distribution of proteins in a single neuron. Together with cutting-edge single-molecule imaging techniques all these advances will enable us to reveal the mechanisms underlying the dynamic synaptic structure positioning glutamate receptors crucial for a deeper insight in the regulation of synaptic signaling and plasticity in both health and disease.

References

- Adrian, M., Kusters, R., Storm, C., Hoogenraad, C.C., and Kapitein, L.C. (2017). Probing the Interplay between Dendritic Spine Morphology and Membrane-Bound Diffusion. *Biophys. J.* 113, 2261-2270.
- Aguilar-Valles, A., Matta-Camacho, E., Khoutorsky, A., Gkogkas, C., Nader, K., Lacaille, J.C., and Sonenberg, N. (2015). Inhibition of Group I Metabotropic Glutamate Receptors Reverses Autistic-Like Phenotypes Caused by Deficiency of the Translation Repressor eIF4E Binding Protein 2. *J. Neurosci.* 35, 11125-11132.
- Aloisi, E., Le Corf, K., Dupuis, J., Zhang, P., Ginger, M., Labrousse, V., Spatzuza, M., Georg Haberl, M., Costa, L., Shigemoto, R., et al. (2017). Altered surface mGluR5 dynamics provoke synaptic NMDAR dysfunction and cognitive defects in Fmrl knockout mice. *Nat. Commun.* 8, 1103.
- Aniksztejn, L., Otani, S., and Ben-Ari, Y. (1992). Quisqualate Metabotropic Receptors Modulate NMDA Currents and Facilitate Induction of Long-Term Potentiation Through Protein Kinase C. *Eur. J. Neurosci.* 4, 500-505.
- Arizono, M., Bannai, H., and Mikoshiba, K. (2014). Imaging mGluR5 dynamics in astrocytes using quantum dots. *Curr. Protoc. Neurosci.* 66, 2.21.21-22.21.18.
- Arizono, M., Bannai, H., Nakamura, K., Niwa, F., Enomoto, M., Matsu-ura, T., Miyamoto, A., Sherwood, M.W., Nakamura, T., and Mikoshiba, K. (2012). Receptor-Selective Diffusion Barrier Enhances Sensitivity of Astrocytic Processes to Metabotropic Glutamate Receptor Stimulation. *Glia* 218, 1-11.
- Auerbach, B.D., Osterweil, E.K., and Bear, M.F. (2011). Mutations causing syndromic autism define an axis of synaptic pathophysiology. *Nature* 480, 63-68.
- Bear, M.F., Huber, K.M., and Warren, S.T. (2004). The mGluR theory of fragile X mental retardation. *Trends Neurosci.* 27, 370-377.
- Benquet, P., Gee, C.E., and Gerber, U. (2002). Two distinct signaling pathways upregulate NMDA receptor responses via two distinct metabotropic glutamate receptor subtypes. *J. Neurosci* 22, 9679-9686.
- Beraldo, F.H., Arantes, C.P., Santos, T.G., Machado, C.F., Roffe, M., Hajj, G.N., Lee, K.S., Magalhães, A.C., Caetano, F.A., Mancini, G.L., et al. (2011). Metabotropic glutamate receptors transduce signals for neurite outgrowth after binding of the prion protein to laminin $\gamma 1$ chain. *Faseb J.* 25, 265-279.
- Bertaso, F., Roussignol, G., Worley, P., Bockaert, J., Fagni, L., and Ango, F. (2010). Homer1a-dependent crosstalk between NMDA and metabotropic glutamate receptors in mouse neurons. *PLoS One* 5, e9755.
- Biederer, T., Kaeser, P.S., and Blanpied, T.A. (2017). Transcellular Nanoalignment of Synaptic Function. *Neuron.* 96, 680-696.
- Blanpied, T.A., Scott, D.B., and Ehlers, M.D. (2002). Dynamics and regulation of clathrin coats at specialized endocytic zones of dendrites and spines. *Neuron.* 36, 435-449.
- Bodźęta, A., Berger, F., and MacGillavry, H.D. (2021a). Subsynaptic mobility of presynaptic mGluR types is differentially regulated by intra- and extracellular interactions. *bioRxiv*. <https://doi.org/10.1101/2020.07.06.188995>.
- Bodźęta, A., Scheefhals, N., and MacGillavry, H.D. (2021b). Membrane trafficking and positioning of mGluRs at presynaptic and postsynaptic sites of excitatory synapses. *Neuropharmacology* 200, 108799.
- Brakeman, P.R., Lanahan, a.a., O'Brien, R., Roche, K., Barnes, C.a., Huganir, R.L., and Worley, P.F. (1997). Homer: a protein that selectively binds metabotropic glutamate receptors. *Nature* 386, 284-288.
- Brown, T.C., Tran, I.C., Backos, D.S., and Esteban, J.A. (2005). NMDA receptor-dependent activation of the small GTPase Rab5 drives the removal of synaptic AMPA receptors during hippocampal LTD. *Neuron* 45, 81-94.
- Burette, A.C., Lesperance, T., Crum, J., Martone, M., Volkman, N., Ellisman, M.H., and Weinberg, R.J. (2012). Electron tomographic analysis of synaptic ultrastructure. *J. Comp. Neurol.* 520, 2697-2711.
- Catsburg, L.A., Westra, M., van Schaik, A.M., and MacGillavry, H.D. (2022). Dynamics and nanoscale organization of the postsynaptic endocytic zone at excitatory synapses. *Elife* 11.
- Chung, W., Choi, S.Y., Lee, E., Park, H., Kang, J., Park, H., Choi, Y., Lee, D., Park, S.G., Kim, R., et al. (2015). Social deficits in IRSp53 mutant mice improved by NMDAR and mGluR5 suppression. *Nat. Neurosci.* 18, 435-443.
- Cottrell, J.R., Borok, E., Horvath, T.L., and Nedivi, E. (2004). CPG2: a brain- and synapse-specific protein that regulates the endocytosis of glutamate receptors. *Neuron* 44, 677-690.
- Czöndör, K., Mondin, M., Garcia, M., Heine, M., Frischknecht, R., Choquet, D., Sibarita, J.-B., and Thoumine, O.R. (2012). Unified quantitative model of AMPA receptor trafficking at synapses. *Proc. Natl. Acad. Sci. U. S. A.* 109, 3522-3527.
- De Blasi, A., Conn, P.J., Pin, J.-P., and Nicoletti, F. (2001). Molecular determinants of metabotropic glutamate receptor signaling. *Trends Pharmacol. Sci.* 22, 114-120.
- Droogers, W.J., Willems, J., MacGillavry, H.D., and de Jong, A.P. (2022). Multiplex labeling and manipulation of endogenous neuronal proteins using sequential CRISPR/Cas9 gene editing. *bioRxiv*, 2022.2001.2002.474730.
- Ehlers, M.D. (2000). Reinsertion or degradation of AMPA receptors determined by activity-dependent endocytic

- sorting. *Neuron* 28, 511-525.
- Ferguson, S.S., Downey, W.E., 3rd, Colapietro, A.M., Barak, L.S., Ménard, L., and Caron, M.G. (1996). Role of beta-arrestin in mediating agonist-promoted G protein-coupled receptor internalization. *Science* 271, 363-366.
- Ferraguti, F., and Shigemoto, R. (2006). Metabotropic glutamate receptors. *Cell and Tissue Research* 326, 483-504.
- Fitzjohn, S.M., Irving, A.J., Palmer, M.J., Harvey, J., Lodge, D., and Collingridge, G.L. (1996). Activation of group I mGluRs potentiates NMDA responses in rat hippocampal slices. *Neurosci. Lett.* 203, 211-213.
- Frost, N.a., Shroff, H., Kong, H., Betzig, E., and Blanpied, T.a. (2010). Single-molecule discrimination of discrete perisynaptic and distributed sites of actin filament assembly within dendritic spines. *Neuron* 67, 86-99.
- Giuffrida, R., Musumeci, S., D'Antoni, S., Bonaccorso, C.M., Giuffrida-Stella, A.M., Oostra, B.A., and Catania, M.V. (2005). A reduced number of metabotropic glutamate subtype 5 receptors are associated with constitutive homer proteins in a mouse model of fragile X syndrome. *J. Neurosci.* 25, 8908-8916.
- Goncalves, J., Bartol, T.M., Camus, C., Levet, F., and Paula, A. (2020). Nanoscale co-organization and coactivation of AMPAR, NMDAR, and mGluR at excitatory synapses. *Proc. Natl. Acad. Sci. U. S. A.* 117, 14503-14511.
- Goodman, O.B., Jr., Krupnick, J.G., Santini, F., Gurevich, V.V., Penn, R.B., Gagnon, A.W., Keen, J.H., and Benovic, J.L. (1996). Beta-arrestin acts as a clathrin adaptor in endocytosis of the beta2-adrenergic receptor. *Nature* 383, 447-450.
- Grishin, A.A., Gee, C.E., Gerber, U., and Benquet, P. (2004). Differential calcium-dependent modulation of NMDA currents in CA1 and CA3 hippocampal pyramidal cells. *J. Neurosci.* 24, 350-355.
- Hanson, J.E., and Smith, Y. (1999). Group I metabotropic glutamate receptors at GABAergic synapses in monkeys. *J. Neurosci.* 19, 6488-6496.
- Harvey, J., and Collingridge, G.L. (1993). Signal transduction pathways involved in the acute potentiation of NMDA responses by 1S,3R-ACPD in rat hippocampal slices. *Br. J. Pharmacol.* 109, 1085-1090.
- Hruska, M., Cain, R.E., and Dalva, M.B. (2022). Nanoscale rules governing the organization of glutamate receptors in spine synapses are subunit specific. *Nat. Commun.* 13, 920.
- Huber, K.M., Gallagher, S.M., Warren, S.T., and Bear, M.F. (2002). Altered synaptic plasticity in a mouse model of fragile X mental retardation. *Proc. Natl. Acad. Sci. U. S. A.* 99, 7746-7750.
- Kasai, R.S., and Kusumi, A. (2014). Single-molecule imaging revealed dynamic GPCR dimerization. *Curr. Opin. Cell. Biol.* 27, 78-86.
- Katona, I., and Freund, T.F. (2008). Endocannabinoid signaling as a synaptic circuit breaker in neurological disease. *Nature Medicine.* 14, 923-930.
- Katona, I., Urbán, G.M., Wallace, M., Ledent, C., Jung, K.M., Piomelli, D., Mackie, K., and Freund, T.F. (2006). Molecular composition of the endocannabinoid system at glutamatergic synapses. *J. Neurosci.* 26, 5628-5637.
- Kellermayer, B., Ferreira, J.S., Dupuis, J., Levet, F., Grillo-Bosch, D., Bard, L., Linarès-Loyez, J., Bouchet, D., Choquet, D., Rusakov, D.A., et al. (2018). Differential Nanoscale Topography and Functional Role of GluN2-NMDA Receptor Subtypes at Glutamatergic Synapses. *Neuron* 100, 106-119.e107.
- Kennedy, M.J., and Ehlers, M.D. (2006). Organelles and Trafficking Machinery for Postsynaptic Plasticity. *Annu. Rev. Neurosci.* 29, 325-362
- Kusumi, A., Fujiwara, T.K., Chadda, R., Xie, M., Tsunoyama, T.a., Kalay, Z., Kasai, R.S., and Suzuki, K.G.N. (2012). Dynamic Organizing Principles of the Plasma Membrane that Regulate Signal Transduction: Commemorating the Fortieth Anniversary of Singer and Nicolson's Fluid-Mosaic Model. *Annu. Rev. Cell Dev. Biol.* 28, 215-250.
- Laporte, S.A., Oakley, R.H., Zhang, J., Holt, J.A., Ferguson, S.S., Caron, M.G., and Barak, L.S. (1999). The beta2-adrenergic receptor/betaarrestin complex recruits the clathrin adaptor AP-2 during endocytosis. *Proc. Natl. Acad. Sci. U. S. A.* 96, 3712-3717
- Lee, J., Munguba, H., Gutzeit, V.A., Singh, D.R., Kristt, M., Dittman, J.S., and Levitz, J. (2020). Defining the Homo- and Heterodimerization Propensities of Metabotropic Glutamate Receptors. *Cell Rep.* 31, 107605.
- Lee, W., and Parpura, V. (2016). Spatio-temporal characteristics of metabotropic glutamate receptor 5 traffic at or near the plasma membrane in astrocytes. *Glia* 64, 1050-1065.
- Li, T.P., and Blanpied, T.A. (2016). Control of Transmembrane Protein Diffusion within the Postsynaptic Density Assessed by Simultaneous Single-Molecule Tracking and Localization Microscopy.
- Li, T.P., Song, Y., MacGillavry, H.D., Blanpied, T.a., and Raghavachari, S. (2016). Protein Crowding within the Postsynaptic Density Can Impede the Escape of Membrane Proteins. *J. Neurosci.* 36, 4276-4295.
- Lin, C.W., Chen, C.Y., Cheng, S.J., Hu, H.T., and Hsueh, Y.P. (2014). Sarm1 deficiency impairs synaptic function and leads to behavioral deficits, which can be ameliorated by an mGluR allosteric modulator. *Front. Cell. Neurosci.* 8, 87.
- Linda, K., Fiuzza, C., and Nadif Kasri, N. (2018). The promise of induced pluripotent stem cells for neurodevelopmental disorders. *Prog. Neuropsychopharmacol. Biol. Psychiatry* 84, 382-391.

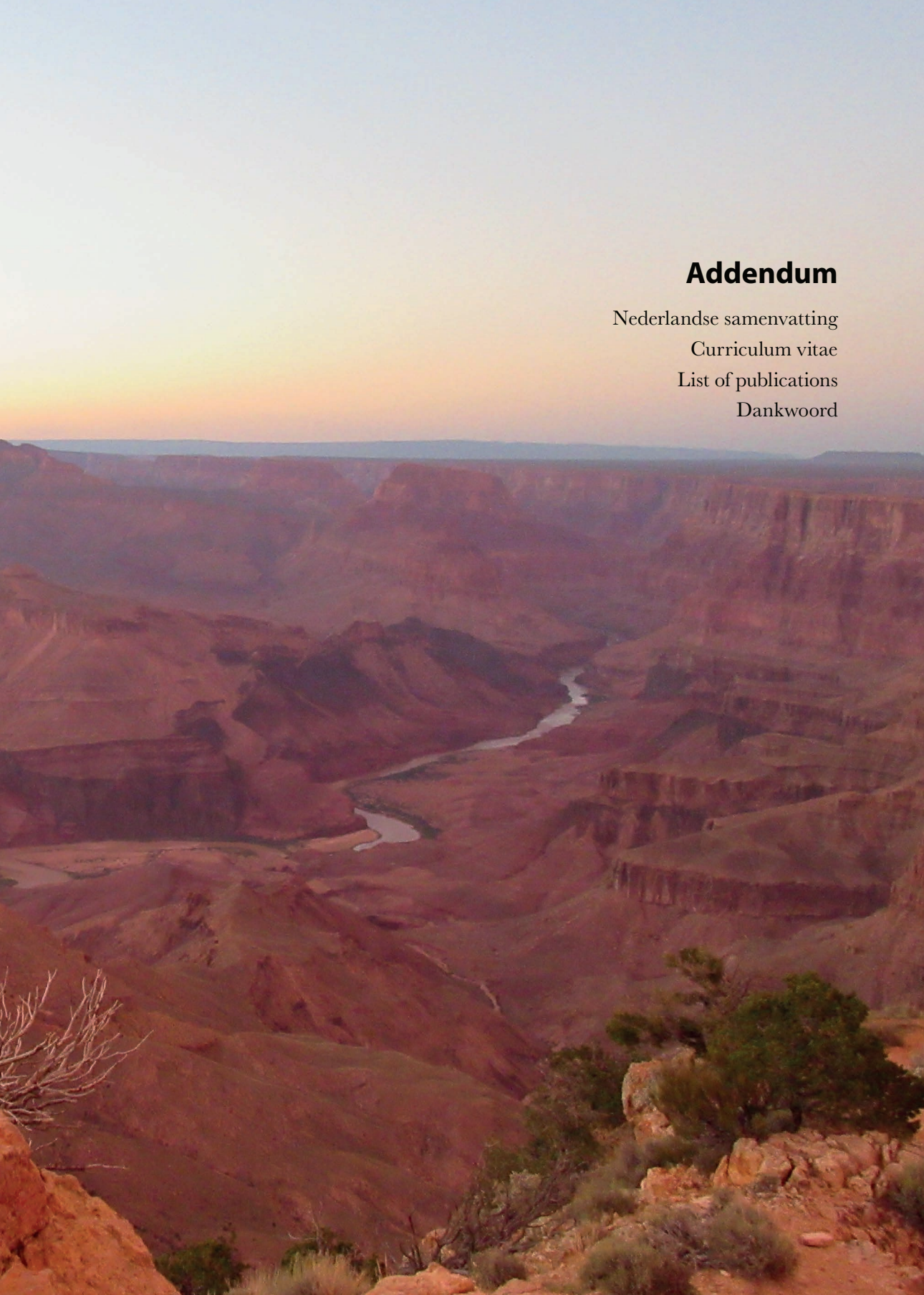
- Linden, R. (2017). The Biological Function of the Prion Protein: A Cell Surface Scaffold of Signaling Modules. *Front. Mol. Neurosci.* 10, 77.
- Loeblich, S., Benoit, M.R., Konopka, J.A., Cottrell, J.R., Gibson, J., and Nedivi, E. (2016). CPG2 Recruits Endophilin B2 to the Cytoskeleton for Activity-Dependent Endocytosis of Synaptic Glutamate Receptors. *Curr. Biol.* 26, 296-308.
- Lu, J., Helton, T.D., Blanpied, T.A., Racz, B., Newpher, T.M., Weinberg, R.J., and Ehlers, M.D. (2007). Postsynaptic positioning of endocytic zones and AMPA receptor cycling by physical coupling of dynamin-3 to Homer. *Neuron* 55, 874-889.
- MacGillavry, H., Song, Y., Raghavachari, S., and Blanpied, T. (2013). Nanoscale scaffolding domains within the postsynaptic density concentrate synaptic ampa receptors. *Neuron* 78, 615-622.
- MacGillavry, H.D., Kerr, J.M., and Blanpied, T.A. (2011). Lateral organization of the postsynaptic density. *Mol. Cell. Neurosci.* 48, 321-331.
- Mansouri, M., Kasugai, Y., Fukazawa, Y., Bertaso, F., Raynaud, F., Perroy, J., Fagni, L., Kaufmann, W.a., Watanabe, M., Shigemoto, R., and Ferraguti, F. (2015). Distinct subsynaptic localization of type 1 metabotropic glutamate receptors at glutamatergic and GABAergic synapses in the rodent cerebellar cortex. *Eur. J. Neurosci.* 41, 157-167.
- Mei, Y., Monteiro, P., Zhou, Y., Kim, J.A., Gao, X., Fu, Z., and Feng, G. (2016). Adult restoration of Shank3 expression rescues selective autistic-like phenotypes. *Nature* 530, 481-484.
- Metzbower, S., Joo, Y., Benavides, D., and Blanpied, T. (2019). Properties of individual hippocampal synapses influencing NMDA-receptor activation by spontaneous neurotransmission. Properties of individual hippocampal synapses influencing NMDA-receptor activation by spontaneous neurotransmission. *eNeuro* 6, ENEURO.0419-18.2019.
- Michalon, A., Sidorov, M., Ballard, T.M., Ozmen, L., Spooren, W., Wettstein, J.G., Jaeschke, G., Bear, M.F., and Lindemann, L. (2012). Chronic pharmacological mGlu5 inhibition corrects fragile X in adult mice. *Neuron* 74, 49-56.
- Morone, N., Fujiwara, T., Murase, K., Kasai, R.S., Ike, H., Yuasa, S., Usukura, J., and Kusumi, A. (2006). Three-dimensional reconstruction of the membrane skeleton at the plasma membrane interface by electron tomography. *J. Cell Biol.* 174, 851-862.
- Moutin, E., Raynaud, F., Roger, J., Pellegrino, E., Homburger, V., Bertaso, F., Ollendorff, V., Bockaert, J., Fagni, L., and Perroy, J. (2012). Dynamic remodeling of scaffold interactions in dendritic spines controls synaptic excitability. *J. Cell Biol.* 198, 251-263.
- Nair, D., Hosy, E., Petersen, J.D., Constals, A., Giannone, G., Choquet, D., and Sibarita, J.-B. (2013). Super-Resolution Imaging Reveals That AMPA Receptors Inside Synapses Are Dynamically Organized in Nanodomains Regulated by PSD95. *J. Neurosci.* 33, 13204-13224.
- Nakamura, M., Sato, K., Fukaya, M., Araishi, K., Aiba, A., Kano, M., and Watanabe, M. (2004). Signaling complex formation of phospholipase Cbeta4 with metabotropic glutamate receptor type alpha and 1,4,5-trisphosphate receptor at the perisynapse and endoplasmic reticulum in the mouse brain. *Eur. J. Neurosci.* 20, 2929-2944.
- Nakano-Kobayashi, A., Tai, Y., Nadif Kasri, N., and Van Aelst, L. (2014). The X-linked mental retardation protein OPHN1 interacts with Homer1b/c to control spine endocytic zone positioning and expression of synaptic potentiation. *J. Neurosci.* 34, 8665-8671.
- Nishimura, A., Kitano, K., Takasaki, J., Taniguchi, M., Mizuno, N., Tago, K., Hakoshima, T., and Itoh, H. (2010). Structural basis for the specific inhibition of heterotrimeric G q protein by a small molecule. *Proc. Natl. Acad. Sci. U. S. A.* 107, 13666-13671.
- Nusser, Z., Mulvihill, E., Streit, P., and Somogyi, P. (1994). Subsynaptic segregation of metabotropic and ionotropic glutamate receptors as revealed by immunogold localization. *Neuroscience* 61, 421-427.
- O'Connor, J.J., Rowan, M.J., and Anwyl, R. (1994). Long-lasting enhancement of NMDA receptor-mediated synaptic transmission by metabotropic glutamate receptor activation. *Nature* 367, 557-559.
- Olmo, I.G., Ferreira-Vieira, T.H., and Ribeiro, F.M. (2016). Dissecting the Signaling Pathways Involved in the Crosstalk between Metabotropic Glutamate 5 and Cannabinoid Type 1 Receptors. *Mol. Pharmacol.* 5, 609-619.
- Park, M., Penick, E.C., Edwards, J.G., Kauer, J.A., and Ehlers, M.D. (2004). Recycling endosomes supply AMPA receptors for LTP. *Science* 305, 1972-1975.
- Park, M., Salgado, J.M., Ostroff, L., Helton, T.D., Robinson, C.G., Harris, K.M., and Ehlers, M.D. (2006). Plasticity-induced growth of dendritic spines by exocytic trafficking from recycling endosomes. *Neuron* 52, 817-830.
- Pennacchietti, F., Vascon, S., Nieuw, T., Rosillo, C., Das, S., Tyagarajan, S.K., Diaspro, A., Del Bue, A., Petrini, E.M., Barberis, A., and Cella Zanacchi, F. (2017). Nanoscale Molecular Reorganization of the Inhibitory Postsynaptic Density Is a Determinant of GABAergic Synaptic Potentiation. *J. Neurosci.* 37, 1747-1756.

- Perez de Arce, K., Schrod, N., Metzbower, S.W.R., Allgeyer, E., Kong, G.K.-W., Tang, A.-H., Krupp, A.J., Stein, V., Liu, X., Bewersdorf, J., et al. (2015). Topographic Mapping of the Synaptic Cleft into Adhesive Nanodomains. *Neuron* 88, 1165-1172.
- Petrini, E.M., Lu, J., Cognet, L., Lounis, B., Ehlers, M.D., and Choquet, D. (2009). Endocytic trafficking and recycling maintain a pool of mobile surface AMPA receptors required for synaptic potentiation. *Neuron* 63, 92-105.
- Racz, B., Blanpied, T.A., Ehlers, M.D., and Weinberg, R.J. (2004). Lateral organization of endocytic machinery in dendritic spines. *Nat. Neurosci.* 2004/08/24 ed.
- Reese, A.L., and Kavalali, E.T. (2015). Spontaneous neurotransmission signals through store-driven Ca^{2+} transients to maintain synaptic homeostasis. *eLife* 4, 1-15.
- Renner, M., Lacor, P.N., Velasco, P.T., Xu, J., Contractor, A., Klein, W.L., and Triller, A. (2010). Deleterious Effects of Amyloid β Oligomers Acting as an Extracellular Scaffold for mGluR5. *Neuron* 66, 739-754.
- Renner, M.L., Cognet, L., Lounis, B., Triller, A., and Choquet, D. (2009). The excitatory postsynaptic density is a size exclusion diffusion environment. *Neuropharmacology* 56, 30-36.
- Sako, Y., and Kusumi, A. (1994). Compartmentalized structure of the plasma membrane for receptor movements as revealed by a nanometer-level motion analysis. *J. Cell Biol.* 125, 1251-1264.
- Santamaria, F., Gonzalez, J., Augustine, G.J., and Raghavachari, S. (2010). Quantifying the Effects of Elastic Collisions and Non-Covalent Binding on Glutamate Receptor Trafficking in the Post-Synaptic Density. *PLoS Comput. Biol.* 6, e1000780.
- Scannevin, R.H., and Huganir, R.L. (2000). Postsynaptic organization and regulation of excitatory synapses. *Nat. Rev. Neurosci.* 1, 133-141.
- Sergé, A., Furgeaud, L., Hémar, A., and Choquet, D. (2002). Receptor activation and homer differentially control the lateral mobility of metabotropic glutamate receptor 5 in the neuronal membrane. *J. Neurosci.* 22, 3910-3920.
- Sergé, A., Furgeaud, L., Hémar, A., and Choquet, D. (2003). Active surface transport of metabotropic glutamate receptors through binding to microtubules and actin flow. *J. Cell. Sci.* 116, 5015-22.
- Sevastyanova, T.N., and Kammermeier, P.J. (2014). Cooperative signaling between homodimers of metabotropic glutamate receptors 1 and 5. *Mol. Pharmacol.* 86, 492-504.
- Shrivastava, A.N., Kowalewski, J.M., Renner, M., Bousset, L., Koulakoff, A., Melki, R., Giaume, C., and Triller, A. (2013). β -Amyloid and ATP-Induced Diffusional Trapping of Astrocyte and Neuronal Metabotropic Glutamate Type-5 Receptors. *Glia.* 61, 1673-86.
- Sinnen, B.L., Bowen, A.B., Gibson, E.S., and Kennedy, M.J. (2016). Local and Use-Dependent Effects of β -Amyloid Oligomers on NMDA Receptor Function Revealed by Optical Quantal Analysis. *J. Neurosci.* 36, 11532-11543.
- Sochacki, K.A., Dickey, A.M., Strub, M.P., and Taraska, J.W. (2017). Endocytic proteins are partitioned at the edge of the clathrin lattice in mammalian cells. *Nat. Cell. Biol.* 19, 352-361.
- Soto, D., Altafaj, X., Sindreu, C., and Bayés, A. (2014). Glutamate receptor mutations in psychiatric and neurodevelopmental disorders. *Commun. Integr. Biol.* 7, e27887.
- Spacek, J., and Harris, K.M. (1997). Three-dimensional organization of smooth endoplasmic reticulum in hippocampal CA1 dendrites and dendritic spines of the immature and mature rat. *J. Neurosci.* 17, 190-203.
- Specht, C.G., Izeddin, I., Rodriguez, P.C., El Beheiry, M., Rostaing, P., Darzacq, X., Dahan, M., and Triller, A. (2013). Quantitative nanoscopy of inhibitory synapses: counting gephyrin molecules and receptor binding sites. *Neuron* 79, 308-321.
- Sugi, T., Oyama, T., Nakanishi, S., and Jingami, H. (2007). Crystal structures of autoinhibitory PDZ domain of Tamalin : implications for metabotropic glutamate receptor trafficking regulation. *EMBO J.* 26, 2192-2205.
- Sungkaworn, T., Jobin, M.-L., Burnecki, K., Weron, A., Lohse, M.J., and Calebiro, D. (2017). Single-molecule imaging reveals receptor-G protein interactions at cell surface hot spots. *Nature* 550, 543-547.
- Tanaka, J., Nakagawa, S., Kushiya, E., Yamasaki, M., Fukaya, M., Iwanaga, T., Simon, M.I., Sakimura, K., Kano, M., and Watanabe, M. (2000). Gq protein alpha subunits Galphaq and Galpha11 are localized at postsynaptic extra-junctional membrane of cerebellar Purkinje cells and hippocampal pyramidal cells. *Eur. J. Neurosci.* 12, 781-792.
- Tang, A., Chen, H., Li, T., Metzbower, S., MacGillavry, H., and TA, B. (2016). A trans-synaptic nanocolumn aligns neurotransmitter release to receptors. *Nature* 536, 210-214.
- Tao, C.-L., Liu, Y.-T., Sun, R., Zhang, B., Qi, L., Shivakoti, S., Tian, C.-L., Zhang, P., Lau, P.-M., Zhou, Z.H., and Bi, G.-Q. (2018). Differentiation and Characterization of Excitatory and Inhibitory Synapses by Cryo-electron Tomography and Correlative Microscopy. *J. Neurosci.* 38, 1493-1510.
- Tian, D., Stoppel, L.J., Heynen, A.J., Lindemann, L., Jaeschke, G., Mills, A.A., and Bear, M.F. (2015). Contribution of mGluR5 to pathophysiology in a mouse model of human chromosome 16p11.2 microdeletion. *Nat. Neurosci.* 18, 182-184.

- Tu, J.C., Xiao, B., Naisbitt, S., Yuan, J.P., Petralia, R.S., Brakeman, P., Doan, A., Aakalu, V.K., Lanahan, A.A., Sheng, M., and Worley, P.F. (1999). Coupling of mGluR/Homer and PSD-95 complexes by the Shank family of postsynaptic density proteins. *Neuron* 23, 583-592.
- Verpelli, C., Dvoretzkova, E., Vicidomini, C., Rossi, F., Chiappalone, M., Schoen, M., Di Stefano, B., Mantegazza, R., Broccoli, V., Böckers, T.M., et al. (2011). Importance of Shank3 protein in regulating metabotropic glutamate receptor 5 (mGluR5) expression and signaling at synapses. *J. Biol. Chem.* 286, 34839–34850.
- Wang, L., Dumoulin, A., Renner, M., Triller, A., and Specht, C.G. (2016). The Role of Synaptopodin in Membrane Protein Diffusion in the Dendritic Spine Neck. *PLoS One.* 11, e0148310.
- Westin, L., Reuss, M., Lindskog, M., Aperia, A., and Brismar, H. (2014). Nanoscopic spine localization of Norbin, an mGluR5 accessory protein. *BMC Neurosci.* 15, 45.
- Westra, M., Gutierrez, Y., and MacGillavry, H.D. (2021). Contribution of Membrane Lipids to Postsynaptic Protein Organization. *Front. Synaptic Neurosci.* 13, 790773.
- Willard, S.S., and Koochekpour, S. (2013). Glutamate, glutamate receptors, and downstream signaling pathways. *Int. J. Biol. Sci.* 9, 948-59.
- Willems, J., de Jong, A.P.H., Scheefhals, N., Mertens, E., Catsburg, L.A.E., Poorthuis, R.B., de Winter, F., Verhaagen, J., Meys, F.J., and MacGillavry, H.D. (2020). Orange: A CRISPR/Cas9-based genome editing toolbox for epitope tagging of endogenous proteins in neurons. *PLoS Biol.* 18, e3000665.
- Won, H., Lee, H.R., Gee, H.Y., Mah, W., Kim, J.I., Lee, J., Ha, S., Chung, C., Jung, E.S., Cho, Y.S., et al. (2012). Autistic-like social behaviour in Shank2-mutant mice improved by restoring NMDA receptor function. *Nature* 486, 261-265.
- Xiao, B., Tu, J.C., Petralia, R.S., Yuan, J.P., Doan, A., Breder, C.D., Ruggiero, A., Lanahan, A., Wenthold, R.J., and Worley, P.F. (1998). Homer regulates the association of group 1 metabotropic glutamate receptors with multivalent complexes of homer-related, synaptic proteins. *Neuron* 21, 707-716.
- Yang, X., Le Corrion, H., Legendre, P., Triller, A., and Specht, C.G. (2021). Differential regulation of glycinergic and GABAergic nanocolumns at mixed inhibitory synapses. *EMBO Rep.* 22, e52154.
- Zeng, M., Chen, X., Guan, D., Xu, J., Wu, H., Tong, P., and Zhang, M. (2018). Reconstituted Postsynaptic Density as a Molecular Platform for Understanding Synapse Formation and Plasticity. *Cell* 174, 1172-1187.e1116.
- Zeng, M., Di, J., Ye, F., Ji, Z., Nicoll, R.A., Ye, F., Chen, X., Xu, J., Ji, Z., and Nicoll, R.A. (2019). Phase Separation-Mediated TARP/ MAGUK Complex Condensation and AMPA Receptor Synaptic Transmission. *Neuron* 104, 529-543.
- Zeng, M., Shang, Y., Araki, Y., Guo, T., Haganir, R.L., and Zhang, M. (2016). Phase Transition in Postsynaptic Densities Underlies Formation of Synaptic Complexes and Synaptic Plasticity. *Cell* 166, 1163-1175.e1112.

&





Addendum

Nederlandse samenvatting

Curriculum vitae

List of publications

Dankwoord

Nederlandse Samenvatting

Ons brein is een immens complex orgaan dat bestaat uit biljoenen zenuwcellen die samen een netwerk vormen. Zenuwcellen bestaan uit drie compartimenten: het cellichaam, één lange dunne uitloper, het axon, en meerdere vertakte kortere uitlopers, de dendrieten (Hoofdstuk 1, Figuur 1). Zenuwcellen communiceren met elkaar via synapsen: contactplaatsen waar de zenuwprikkel van het axon wordt doorgegeven aan de ontvangende dendriet. Het axon stuurt een signaal door synapsblaasjes gevuld met neurotransmitters vrij te laten, die vervolgens receptoren op de ontvangende dendriet activeren. Daarmee is een zenuwprikkel doorgegeven en wordt een signaalcascade in de ontvangende zenuwcel in gang gezet. Voor een goed functionerend netwerk van zenuwcellen is een juiste balans tussen excitatie en inhibitie cruciaal. Er zijn excitatoire (stimulerende) en inhibitoire (remmende) neurotransmitters die respectievelijk een positief of een negatief signaal geven. Afhankelijk van de hoeveelheid positieve en negatieve signalen ontvangen door de dendriet wordt een zenuwprikkel weer doorgestuurd. Een synaps gebruikt altijd maar één type neurotransmitter en we spreken daarom ook wel van excitatoire en inhibitoire synapsen. De excitatoire neurotransmitter glutamaat activeert glutamaatreceptoren op het zogeheten postsynaptische membraan op de dendriet. Deze receptoren zijn niet willekeurig verdeeld op dit postsynaptische membraan, maar zitten geclusterd daar waar glutamaat wordt vrij gelaten. Hierdoor verloopt het proces van signaaloverdracht efficiënt. Er zijn dan ook vele complexe mechanismen die de distributie van receptoren in het membraan bepalen om de communicatie tussen synapsen goed te laten verlopen. Als communicatie niet goed verloopt doordat deze moleculaire mechanismen verstoord zijn heeft dit grote gevolgen voor het functioneren van het zenuwstelsel. Zo kunnen verstoringen in de activatie van receptoren bijvoorbeeld leiden tot hersenaandoeningen zoals autisme. Het doel van dit proefschrift is het in kaart brengen van hoe de positionering van glutamaatreceptoren bijdraagt aan het functioneren van het zenuwstelsel. In deze samenvatting zal ik dieper ingaan op de moleculaire processen die hierbij betrokken zijn en de belangrijkste bevindingen van dit proefschrift nader toelichten.

Duidelijke en doelgerichte communicatie is essentieel in het dagelijkse leven, zo ook in ons brein. Om het proces van informatie uitwisseling goed te laten plaatsvinden zijn zowel de zender als de ontvanger belangrijk. De focus in dit proefschrift ligt op de ontvanger, ofwel de glutamaatreceptoren in excitatoire synapsen. Er zijn twee type glutamaatreceptoren: ionotrope glutamaatreceptoren (iGluRs) en metabotrope glutamaatreceptoren (mGluRs). Waar iGluRs belangrijk zijn voor het snel doorgeven van signalen, zijn mGluRs met name belangrijk voor de doeltreffendheid van signaaloverdracht op langere termijn en zijn daardoor van cruciaal belang voor leren en geheugen. In **Hoofdstuk 2** worden deze twee type glutamaatreceptoren uitvoerig besproken en in **Hoofdstuk 3** wordt de huidige kennis samengevat over de functionele organisatie van de verschillende mGluR subtypes in synapsen. Tegenwoordig kunnen we met vrienden aan de andere kant van de wereld communiceren door simpelweg met elkaar te bellen. In ons brein, al dan niet minder geavanceerd, werkt dit anders. Om dit te begrijpen moeten we terug in de tijd, naar toen er enkel snel gecommuniceerd kon worden door tegenover elkaar te staan en met elkaar te praten. Dit werkt bij synapsen net zo, in een synaps ligt het axon vlak naast de dendriet waardoor de neurotransmitters de receptoren kunnen bereiken. Of receptoren geactiveerd kunnen worden hangt dus af van hun organisatie in het postsynaptische membraan en hierbij is de nabijheid van de plek waar de

neurotransmitters worden vrij gelaten van belang. Al van eerdere studies weten we dat iGluRs geconcentreerd zitten in het midden van het postsynaptische membraan, recht tegenover de plek waar glutamaat wordt vrijgelaten uit het axon. mGluRs daarentegen, zitten verrijkt in een ring om dit synaptische membraan heen, ook wel de perisynaptische zone genoemd. Hierdoor zijn mGluRs verder verwijderd van de plek waar glutamaat wordt vrijgelaten, wat betekent dat een hogere concentratie glutamaat nodig is om mGluRs te kunnen activeren (Hoofdstuk 1, Figuur 2). Op deze manier bepalen de hoeveelheid zenuwprikkels welk type receptoren er geactiveerd worden, wat de signaalcascade in de ontvangende zenuwcel bepaalt.

In **Hoofdstuk 4** laten we zien dat het ook belangrijk is dat geactiveerde receptoren weer gedeactiveerd worden om overprikkeling te voorkomen. Voor het deactiveren van receptoren is de endocytotische zone cruciaal, dit is een gebied dat mGluRs opneemt en recycleert na activatie. Wij hebben ontdekt dat het eiwit Shank hierin een belangrijke rol speelt, namelijk doordat Shank de endocytotische zone als het ware kan verankeren aan het postsynaptische membraan (Hoofdstuk 7, Figuur 1). Het weghalen van Shank leidt niet alleen tot het ontkoppelen van dit recycle-centrum, maar ook tot overprikkeling van mGluRs en verstoring van de communicatie tussen zenuwcellen, dit kan weer leiden tot neurologische aandoeningen.

Het postsynaptische membraan is ontzettend klein, gemiddeld 500 nanometer in lengte. Dit is 2000x kleiner dan 1 millimeter. Conventionele microscopie technieken hebben een te lage resolutie om de distributie van receptoren binnen dit membraan op nanometer schaal zichtbaar te maken. In **Hoofdstuk 5** gebruiken wij daarom innovatieve superresolutie microscopie technieken die gebruik maken van slimme belichting en eigenschappen van fluorescerende eiwitten om in te zoomen op synapsen en zelfs op individuele receptoren. Door middel van superresolutie microscopie kunnen we in levende zenuwcellen de bewegende receptoren in het postsynaptische membraan volgen met hoge precisie. Dit heeft geleid tot de ontdekking dat mGluRs lokale clusters vormen in de perisynaptische zone, kleine gebieden waar de receptoren ook verhinderd worden in hun beweging. Deze informatie geeft veel weg over mogelijke mechanismen die dit veroorzaken, zoals bijvoorbeeld interacties met andere eiwitten. Door dit inzicht hebben we verder ontdekt welk deel van mGluR essentieel is voor deze clustering in de perisynaptische zone en tegelijkertijd voorkomt dat mGluRs clusteren in het postsynaptische membraan (Hoofdstuk 7, Figuur 2). Dit laatste blijkt erg belangrijk te zijn om overprikkeling van mGluRs en verstoring van signaaloverdracht in synapsen te voorkomen. Daarbij is dit een van de eerste onderzoeken die experimenteel het belang aantoonde van mGluR positionering in het juist functioneren en signaleren van excitatoire synapsen.

In **Hoofdstuk 6** hebben we een techniek, genaamd ORANGE, ontwikkeld die gebruik maakt van de CRISPR-Cas9 techniek om het DNA in het genoom van een zenuwcel aan te passen door een fluorescerend eiwit vast te plakken aan een eiwit naar interesse. Deze techniek hebben we uitvoerig getest voor verscheidene synaptische eiwitten, waaronder receptoren zoals mGluRs (Hoofdstuk 5, Figuur II-K). In hoofdstuk 4 en 5 hebben we extra eiwitten, gekoppeld aan een fluorescerend eiwit, tot expressie gebracht in een zenuwcel. Een groot voordeel van ORANGE is de mogelijkheid om de al aanwezige eiwitten te visualiseren en de functionele organisatie van synapsen in beeld te brengen zonder al te grote aanpassingen.

De onderzoeken in dit proefschrift geven nieuwe inzichten in de moleculaire mechanismen onderliggend aan de functionele organisatie van mGluRs in excitatoire synapsen. De fundamentele kennis verkregen in deze studies draagt bij aan het ophelderen van moleculaire processen in de synaps en het functioneren van het zenuwstelsel van groot belang voor het ontwikkelen van therapieën voor neurologische aandoeningen. Met dit onderzoek zijn we weer een stap dichterbij.

Curriculum Vitae

Nicky Scheefhals was born on September 10th, 1991 in Utrecht, the Netherlands. In 2009, she finished her secondary education (VWO) Nature and Health at Meridiaan College 't Hooghe Landt in Amersfoort. Nicky possesses a natural curiosity and decided to move to San Diego for an academic semester at an International Language School. In 2010 she returned and started the bachelor Biology at the University of Utrecht (UU). Nicky soon learned that she was particularly interested in molecular and cellular neurobiology, and after receiving her bachelor's degree in 2013 she continued her studies with the master Molecular and Cellular Life Sciences at the UU. During this two-year Master's program Nicky carefully selected two laboratories to perform her research internships, each using different but complementary approaches to study fundamental processes in brain functioning. During her first internship Nicky studied the role of scaffolding proteins in the dynamic positioning and trafficking of group I metabotropic glutamate receptors (mGluRs) using advanced microscopy techniques in the group of Prof. dr. Casper Hoogenraad, under supervision of Dr. Harold MacGillavry at the Cell Biology research division at UU. To broaden her horizon Nicky performed her second internship at the Neurobiology division of Biological Science at the University of California, San Diego in the laboratory of Dr. Brenda Bloodgood, investigating the potential role of the immediate early gene *Npas4* in conveying information about the spatial organization of excitatory inputs to the nucleus using electrophysiology. To finalize her master's degree, she wrote a PhD proposal as part of the Graduate Program Quantitative and Computational Life Sciences (Qbio) under supervision of Dr. Harold MacGillavry which was granted by the Netherlands Organization for Scientific Research (NWO) and obtained her master's degree with Cum Laude. Driven by her great interest in understanding the fundamental processes in brain functioning and enthusiasm in studying this using novel and exciting techniques revolutionizing neuroscience research, Nicky started her PhD in 2016 in the lab of Dr. Harold MacGillavry at the department of Cell Biology, Neurobiology and Biophysics of the UU. In her PhD research, she studied the functional organization of metabotropic glutamate receptors at excitatory synapses, which resulted in this dissertation.

List of Publications

Scheefhals, N., Westra, M., and MacGillavry, H.D. (2022) mGluR5 is transiently confined in perisynaptic nanodomains to shape synaptic transmission. Submitted, *under revisions*.

Bodzęta, A.*, Scheefhals, N.*, and MacGillavry, H.D. (2021) Membrane trafficking and positioning of mGluRs at presynaptic and postsynaptic sites of excitatory synapses. *Neuropharmacology* 200, 108799.

Lindhout, F.W., Portegies, S., Kooistra, R., Herstel, L.J., Stucchi, R., Hummel, J.J.A., Scheefhals, N., Katrukha, E.A., Altelaar, M., MacGillavry, H.D., Wierenga, C.J., and Hoogenraad, C.C. (2021) Centrosome-mediated microtubule remodeling during axon formation in human iPSC-derived neurons. *EMBO J.* e106798.

Willems, J.* , de Jong, A. P. H.* , Scheefhals, N., Mertens, E., Catsburg, L. A. E., Poorthuis, R. B., de Winter, F., Verhaagen, J., Meye, F. J., and MacGillavry, H. D. (2020) ORANGE: A CRISPR/Cas9-based genome editing toolbox for epitope tagging of endogenous proteins in neurons. *PLoS Biol.* 18, e3000665.

Scheefhals, N., Catsburg, L. A. E., Westerveld, M. L., Blanpied, T. A., Hoogenraad, C. C., and MacGillavry, H. D. (2019) Shank proteins couple the endocytic zone to the postsynaptic density to control trafficking and signaling of metabotropic glutamate receptor 5. *Cell Rep.* 29, 258-269 e258.

Ormel, P.R.* , Vieira de Sá, R.* , Bodegraven, E.J., Karst, H., Harschnitz, O., Sneeboer, M.A.M., Johansen, L.E., van Dijk, R.E., Scheefhals, N., van Berlekom, A.B., Martínez, E.R., Kling, S., MacGillavry, H.D., van den Berg, L.H., Kahn, R.S., Hol, E.H., de Witte, L.D., and Pasterkamp, R.J. (2018) Microglia innately develop within cerebral organoids. *Nat. Commun.* 9, 4167.

Scheefhals, N., and MacGillavry, H.D. (2018) Functional organization of postsynaptic glutamate receptors. *Mol. Cell. Neurosci.* 91, 82-94.

* *authors contributed equally*



Dankwoord

Een PhD traject is als het beklimmen van een berg. Soms valt de berg tegen, klim je tot waar je kunt en kom je erachter dat het uitzicht halverwege ook al een hoogtepunt is. En wat blijkt ik klimmen toch leuk te vinden, mijn PhD traject heeft mij zoveel mooie en inspirerende momenten gebracht. Nu is het einde van mijn PhD echt in zicht, ik zet de laatste puntjes op de i voor mijn proefschrift en mijn promotiedatum staat vast. De top van de berg komt in mijn vizier, nog een klein stukje omhoog en dan heb ik mijn doel bereikt. De laatste klim is nog even goed doorpakken, maar ik voel vooral ook de adrenaline en euforie: bijna de top bereikt! Living on the edge, ofwel leven op het randje betekend voor mij dat je je eigen uitdaging opzoekt, nieuwe avonturen aan gaat maar vooral ook geniet van het uitzicht onderweg. Blijken die mGluRs toch een mooi rolmodel te zijn! Natuurlijk heb ik dit traject niet alleen afgelegd en heb ik heb ik steun gehad van een heleboel lieve mensen om mij heen.

Harold, mijn co-promotor, bedankt voor alles van begin tot eind – en dat zijn heel wat jaren! Op 2 september 2014 informeerde ik bij Casper over een mogelijke stage plek en schreef ik “I am intrigued by the central nervous system, especially synaptic plasticity and its role in learning and memory..”. Wat een geluk dat ik bij jou terecht kon voor een stage. Ik wist het toen nog niet, maar wat een match was het project en het feit dat je toewerkte naar het starten van je eigen lab met de focus op synaps organisatie. Ik vergeet het moment ook nooit meer dat ik de bacteriekweek uit kwam lopen en je mij vertelde dat Casper en jij vonden dat het Honoursprogramma waarin je de kans kreeg eigen funding op te halen voor een PhD project helemaal iets voor mij was. Bedankt voor het vertrouwen die je toen al in mij had. Waar ik vrij onzeker begon, heeft dit vertrouwen mij geholpen om te ontwikkelen tot de wetenschapper, maar ook persoon die ik nu ben. Ik durf dan ook volmondig te zeggen dat je mentorschap, positiviteit en passie voor de wetenschap ook bij mij het vlammetje hebben aangewakkerd. Toen ik aan mijn studie Biologie begon had ik nooit durven dromen dat ik zo goed op mijn plek terecht zou komen, een té gek project in een prettige en stimulerende omgeving. Bedankt voor je humor, woordgrappen en scherpe opmerkingen – iets waar ik mij wel raad mee wist en een (soms iets te snel?) weerwoord op had. Bedankt voor de motiverende gesprekken, je enorme support en gezelligheid, ik ga de “kom op, nog een laatste biertje” missen op de vrijdagmiddag borrels en conferenties. Dit is geen afscheid, aangezien ik in de wetenschap blijf en alles wat ik geleerd heb nu mag toepassen als postdoc aan het Radboud UMC. Wie weet komen er nog mooie samenwerkingen in de toekomst en kunnen we binnenkort hopelijk proosten met een lekker IPA'tje op de acceptatie van hoofdstuk 5! *Lukas*, ondanks dat je pas sinds kort mijn promotor bent, ben je al vanaf het begin een waardevolle begeleider. Harold had net zijn lab opgestart toen ik aan mijn PhD begon. Ik was de eerste en dus in die zin alleen, maar zo voelde dat niet want jij hebt ons meteen opgenomen in je groep. Iets wat helemaal niet vanzelfsprekend is, maar betuigt van betrokkenheid en laat zien hoe belangrijk samenwerken is. Ik werd uitgenodigd voor de kerstborrel bij je thuis, heel gastvrij en gezellig, waardoor ik mij meteen onderdeel voelde van het departement. Ook heb ik ontzettend veel geleerd van de wekelijkse meetings, van superresolutie microscopie tot aan kritisch denken, maar vooral ook van je onuitputtelijke enthousiasme en nieuwe ideeën. Inspirerend om te zien hoe jij de afgelopen jaren aan je eigen weg hebt getimmerd, recent een VICI hebt binnen gehaald en toewerkt naar (nog meer) revolutionair onderzoek.

Veel dank aan de leden van mijn beoordelings- en promotiecommissie, *Prof. dr. Anna Akhmanova*, *Prof. dr. Sander van den Heuvel*, *Prof. dr. Corette Wierenga*, *Prof. dr. Elly Hol*, *Prof. dr. Helmut Hessels*, *Prof. dr. Peter Burbach* en *Prof. dr. Nael Nadif Kasri*. Bedankt voor het beoordelen van mijn proefschrift en verdediging en met name ook de bijdrage aan deze hele speciale dag. *Nael*, mijn verdediging markeert ook een nieuw begin en ik ben heel blij dat ik de komende 3 jaar als postdoc in je lab mag werken aan een heel gaaf project en mij verder kan gaan ontwikkelen als zelfstandige wetenschapper. Uiteraard niet zonder mooie samenwerkingen en een geweldige groep die mij de afgelopen maanden al warm heeft ontvangen. Ik kijk enorm uit naar deze nieuwe uitdaging en wat de toekomst nog meer gaat brengen.

It was a pleasure to be part of the Cell Biology, Neurobiology and Biophysics department. Even though I always described the place I worked at as the most ugly building at the Uithof, the content of the Kruyt building richly compensated for the outside with its high quality scientific research and facilities. But most of all, the supportive and collaborative atmosphere makes the department very unique. All PI's, thank you for contributing to exciting science in a supportive environment. *Casper*, bedankt dat ik als student aan de slag mocht in je lab, voor de leerzame werkbesprekingen en ondersteuning tijdens het opzetten van mijn PhD project. *Anna*, bedankt voor al je inzet voor het departement, zeker ook tijdens de lockdown en covid tijden. Je passie voor de wetenschap en je alomvattende kennis zijn een groot voorbeeld en ik hechte altijd grote waarde aan je constructieve feedback, waarvoor bedankt. *Corette*, met mijn fascinatie voor synaptische plasticiteit en ontwikkeling van het brein was je voor mij onmisbaar in het departement. Altijd enthousiast, vol nieuwe ideeën en je gaat een goede discussie nooit uit de weg. Tijdens de promotieborrel van Dennis hebben we een goed gesprek gehad over mijn ambities, visie op mijn toekomstige carrière en alles wat daarbij komt kijken. Daar gaf je ook aan altijd mee te willen denken over vervolgstappen en mogelijkheden, bedankt voor je betrokkenheid en ik weet je te vinden! Binnenkort ook in Nijmegen, wat een mooie stap en heel leuk dat we elkaar weer vaker gaan treffen. *Ginny*, it was always nice to chat with you and admire your crazy hippocampus dissection skills during the preparation of the primary neuron cultures. Over the past years you established a wonderful team and published an impressive amount of work, I wish you many more scientific achievements to come. *Sabrina*, *Paul*, *Mike* and *Florian*, thank you for your valuable input during the weekly Monday meetings. Een grote dank gaat ook uit naar *Sander*, *Rob* en *Can*, door het opzetten en begeleiden van het Honors master programma Qbio heb ik de kans gekregen mijn eigen wetenschappelijke ideeën uit te werken in een onderzoeksvoorstel en deze ook uit te voeren tijdens mijn PhD. Ik heb ontzettend veel geleerd tijdens de maandelijkse meetings over computationele biologie en het belang van het integreren van verschillende wetenschappelijke disciplines. It goes without saying that the department highly depends on the great efforts of the technicians and teachers. You keep the department running smoothly, provide support and educate the next generation of scientists to come. *Phebe*, *René*, *Bart*, *Eugene*, *Ilya*, *Wilco*, *Wendy*, *Marjolein*, *Esther*, *Lena*, *Ron*, *Laurens*, and *Jan Andries*, thank you all!

I had such a blast working with all the members of the MacGillavry lab and seeing the lab grow from the start. I can honestly say that we all get along so well and really formed a united team, which I feel is very special! Lieve *Lisa*, het klikte meteen tussen ons – je was nog maar net binnen voor je sollicitatie in het Kruyt en ik was al enthousiast! Mijn eerste indruk



heeft mij niet teleurgesteld, wij werden dikke “deur” maatjes tot ergernis van anderen in het kantoor (sorrrie Dieudonné & Jessica!). Toen je ineens aankwam met je noise cancelling koptelefoon was ik bang dat het voorbij zou zijn met de deur-ventileer-momentjes, maar deze angst was gelukkig ongegrond. Bij jou kon ik altijd terecht om even te sparren, voor een goede kop koffie gemaakt met onze eigen french press, maar vooral ook om even lekker te geiten en lachen (sorrrie Dieudonné & Jessica) wat altijd een zeer welkome afleiding was! Ik heb ontzettend veel bewondering voor hoe structureel jij altijd te werk gaat en nergens gras over laat groeien. Als jij ergens je zinnen op hebt gezet, dan houdt niets of niemand je tegen, een hele mooie eigenschap. Bedankt voor de gezelligheid en goede gesprekken in Lausanne, waar we een paar dagen extra plakten aan de European Synapse meeting. In jou heb ik echt een vriendin gevonden. We zijn beide mama van een pracht dochter, heel bijzonder om dat met je te kunnen delen. Je bent een topper, een luisterend oor en altijd in voor wijn, bier en kaas – wat wil je nog meer! Bedankt ook dat je samen met mij de berg hebt beklommen naar de top en straks naast mij staat als paranimf. *Manon*, wij zijn echt een team vrijwel vanaf het eerste uur. Een maand nadat ik begon aan mijn PhD kwam je bij mij stage lopen en kreeg je de nobele taak om de relatieve lokalisatie van de 3 GluAs in kaart te brengen, een project met heel veel potentie maar écht niet gemakkelijk. Zo is ook de term “een Manonnetje” ontstaan, zelf niet in de gaten hebben hoe goed je bent en hoe tof de data is die je hebt gegenereerd. Gelukkig werd dit al snel bevestigd met de poster prijs die je won tijdens de Dutch Neuroscience Meeting en PhD positie die je aangeboden kreeg aan het einde van je stage. Uitdagende projecten trek je aan (lipides, confinement analyse, ONI), maar jij grijpt het met beide handen aan en gaat er met enorme toewijding mee aan de slag. Ontzettend veel respect heb ik voor je toewijding, doorgrondigheid en ongekende aandacht voor details. In onze samenwerking aan hoofdstuk 5 wist ik zeker dat alles wat jij inbracht geen half werk, maar werk van hoge kwaliteit was. Bedankt voor je waardevolle input en ik hoop dat we binnenkort kunnen proosten op de acceptatie ervan. Ook bedankt voor alle gezelligheid en betrokkenheid. Je bent altijd zo attent, ik ga je baksels missen maar gelukkig mag ik nog altijd een kaartje van je ontvangen – écht lief! *Jelmer*, top prestaties leveren doe jij op meerdere vlakken, zo combineer je meerdere triatlons met uitstekend en innovatief onderzoeker zijn zonder al te veel moeite lijkt het. Jij kan je helemaal vastbijten op het ontwikkelen en optimaliseren van tools met ORANGE als kers op de taart, wat jij echt naar een hoger niveau hebt getild. Inmiddels wordt deze CRISPR-Cas9 knock-in techniek al door meerdere labs over de wereld toegepast en ik kijk dan ook met trots terug op deze samenwerking samen met Arthur. We sluiten samen onze PhD af, 19 oktober ben jij aan de beurt en ik weet zeker dat je het fantastisch gaat doen! Bedankt voor je heerlijke nuchterheid, maar vooral ook gezelligheid tijdens de vele borrels – zo vergeet ik ook nooit meer onze burrito, uh perudo, avond, wat hebben we gelachen! *Anna*, so exciting to have found another mGluR enthusiast in you! It always felt a bit lonely to be in the mGluR team, but we brought the somewhat forgotten (when compared to the AMPA and NMDA receptors) receptor back to life! I really admire your ambition and perseverance. You are such an intelligent scientist, delivering beautiful and thorough work. You are not afraid to set the bar high, emphasized by the fact that Marie Curie is your role model. Be kind to yourself and I am certain that you will achieve your goals and in a few years I can proudly say (which I already do) that I have a co-shared first author paper with you. *Arthur*, je werd geïntroduceerd als oud VU collega (niet zo oud hoor) van Harold met een fantastisch CV die mogelijk geïnteresseerd was om een tweede postdoc te komen doen. Na een leuke eerste

kennismaking werd mij al snel duidelijk dat je een geweldige toevoeging was aan het lab. Je nam echt een mentor rol op je en wist altijd de juiste vragen te stellen tijdens andermans presentaties om zo prioriteiten te stellen in het plan van aanpak en het doel helder voor ogen te krijgen. Heel knap hoe je zelf ook altijd de tijd nam om helder en visueel aantrekkelijk je eigen projecten te presenteren, daar heb ik echt veel van geleerd. Het was heel prettig samenwerken aan het ORANGE project, waar je met ORANGE CAKE nog een geweldig gevolg aan hebt kunnen geven. Je creativiteit met afkortingen, maar vooral ook met het ontwerpen van double knock-in strategieën en “thinking outside the box” is een inspiratie. Je bent een steengoede wetenschapper en het is zonde dat de academie je is verloren, maar je bent begonnen aan een nieuw avontuur waar je een enorme aanwinst bent. *Yolanda*, your positivity and enthusiasm are contagious. You are always so kind and considerate, I really enjoyed having you around. Your first introduction to the department must have been quite intense, meeting everyone all at once during the survival games at the annual labouting. Luckily you were not the only one that fell in the water, fully submerged, and together we laughed about our clumsiness over a warm tea, while the rest was still battling outside. The expertise you brought to the lab was very valuable and I learned a lot from your workshop on electrophysiology. I am very happy that you decided to continue your career in the Netherlands and I am sure I will see you around. *Wouter*, net terug van je stage in Canada begon je vol enthousiasme aan je PhD en toen BAM daar was covid. Volgens mij was je nog geen maand op weg en toen kwam je al thuis te zitten. Je hebt je er geweldig doorheen geslagen, want je enthousiasme is geen greintje minder geworden. Je zit vol goede ideeën en nu het Kruijter weer up and running is maak je maximaal gebruik van je tijd en grijp je elke kans aan om experimenten te doen. Gelukkig maar, want Lisa, Manon, Jelmer en ik zijn allemaal kort na elkaar vertrokken, waardoor jij het stokje van iedereen hebt moeten overnemen. Maar met jouw drive en talent weet ik zeker dat dit helemaal goed gaat komen, je eerste eerste-auteurs paper is zelfs al binnen, te gek! *Niels*, voordat je bij het lab kwam kende ik je al van je mooie werk dat je presenteerde op een poster tijdens de Dutch Neuroscience Meeting, wat ook heeft geleid tot een indrukwekkend paper. Je project over Alzheimer en AMPA receptoren zette je voort in het lab en het was altijd heel interessant en leuk om hierover mee te denken. Het is duidelijk dat jij een enorme passie hebt voor de wetenschap, je werkt hard om je doelen te bereiken maar durft ook je grenzen aan te geven en maakt dit bespreekbaar. Heel veel respect hiervoor en het beste voorbeeld wat je als vader van 3 kunt geven. I would also like to thank all the students for their scientific contribution and for creating a pleasant atmosphere in the lab. *Eline*, bedankt voor je harde en mooie werk, ik heb je stageverslag er nog regelmatig bij gepakt. Mooi om te zien dat je nu als Scientist aan de slag bent.

After a ten minute bike ride, walking into the Kruijter building and into my office N502 always felt very familiar and amicable. Surrounded by many science enthusiasts, but most of all supportive and fun people. Lieve *Robbelien*, lieve vriendin, lieve N502-buddy. De dag beginnen met even kort bijkletsen klinkt vrij onbetekenend, maar was voor mij van grote waarde. Die tien minuutjes waarin we even bij elkaar incheckten en onze planning voor de dag doornamen gaven een boost voor de dag. We delen veel interesses, maar ook zeker een aantal niet; ik heb mijn best gedaan goede zorg te geven aan onze garnalen en vissen maar ik kwam niet veel verder dan ernaar staren. En ja, dan hebben we nog die spraakberichten. Jij bent de enige waar ik een uitzondering voor maak, mijzelf over die drempel trek en



spraakberichten in spreek. En inmiddels zijn dat zelfs spraakberichten van 5, soms wel 10 minuten en vind ik het stiekem nog best leuk ook. Wij weten elkaar altijd te vinden in een heuvel landschap vol pieken en dalen, vol indrukwekkende uitzichten en verraderlijke afgronden, vol avonturen en overwinningen. We hebben weinig woorden nodig om elkaar te begrijpen, ik kan niet genoeg benadrukken hoe belangrijk dat voor mij is. Wat ben jij een fantastisch persoon, ik bewonder je positieve instelling, je vrolijke noot, je zorgzaamheid en onverdeelde aandacht, je ondernemende karakter en heerlijke humor. Je bent geweldig in wat je doet, als wetenschapper maar ook daarbuiten. Je bent een kritische denker, een enorme doorzetter, een echte team player en levert altijd een puik staaltje schrijfwerk. Kortom, een unieke en sterke vrouw! Ik ben maar wat blij dat je van mij een trendsetter hebt gemaakt en we de wondere wereld van het moederschap met elkaar kunnen delen. En of ze het nou willen of niet, Ebbie, Evie en Mila worden beste vriendinnetjes! Ik prijs mij heel gelukkig dat ik je straks aan mijn zijde heb als paranimf, maar ook als vriendin voor het leven. Bedankt voor alles. *Phebe*, je inzet voor de afdeling en de toewijding waarmee jij alles draaiende houdt is onmisbaar. Je ziet velen komen en gaan, maar jij blijft je keihard inzetten en staat voor iedereen klaar. Ik mis je heerlijke directheid nu al, wat hebben we daar ook veel om gelachen. Vol goede energie, ga jij dansend en zingend door het leven, bedankt voor je gezelligheid en ik kom graag een koffie drinken als ik in de buurt ben! *René*, je heerlijke nuchtere en relaxte houding was altijd een fijne toevoeging aan een soms wat gestresst kantoor. Daarentegen, het gekibbel tussen jou en Sybren over vissen en al het andere was een ware comedy serie, jammer dat er geen nieuw seizoen meer komt. Maar jij blijft en wat ben ik blij voor jou, maar vooral ook voor de afdeling! Ik weet niet wat er in het water zit in het Kruij, maar de meisjes nemen het duidelijk over – mooi om te horen hoe trots je over je dochter praat en ik wens je heel veel geluk. *Yuji*, thank you for always taking your time whenever I had a question, you are so friendly. Hidden behind the computer screens I sometimes wasn't even aware you were in, your super focus on work was exceptional. You are also an exceptional, hardworking scientist, and I am so happy to hear that you and Xingxiu moved to San Diego and continue to be excellent scientists. I wish you and *Xingxiu* all the best for the future. And thank all for the wonderful time in office N502.

Thank you to all members of Hoogenraad, Akhmanova, Kapitein, Wierenga, Farías, van Bergen en Henegouwen and Oliveira groups for sharing fantastic science and creating a pleasant work environment. Lieve *Feline*, lieve parel, het duurde niet lang voordat we de deur bij elkaar plat liepen. Voor steun en advies in het uitvoeren van ons onderzoek, voor het delen van lief en leed, voor een koffie break of wandeling naar de spar of vrijdag om 17.00 uur om de ander achter de laptop vandaan te trekken en het weekend in te luiden met een biertje. We dachten altijd met elkaar mee, in het ontwerpen van experimenten, plotten van data en uitvoeren van de juiste statistische analyses. Die wetenschappelijke discussies waren altijd zo leuk en waardevol. Op onze spontane STED sessie na hebben we niet echt samengewerkt, maar toch vormden we samen een team en is mijn onderzoek beter geworden door jouw input. Ik heb enorme bewondering voor jou als wetenschapper, je talent voor wetenschapscommunicatie, kritisch denken, je eigen weg durven te kiezen en ambitie zijn uniek. Helemaal in combinatie met je persoonlijkheid, je bent allesbehalve een suffe wetenschapper, je bent lief, betrokken en een échte gezellige brabo! Zo bijzonder dat ik je parelnimf was en wat ben ik blij dat ik nog altijd bij je terecht kan voor al het bovenstaande. *Dennis*, zonder jou was mijn PhD een stuk saaier en eentoniger (letterlijk) geweest. Je heerlijke

gemopper en stemverheffing als iemand in jouw ogen weer iets absurds zei was onmisbaar aan de lunchtafels en in de wandelgangen. Maar écht, want wat heb ik dat de laatste 2 jaar gemist! Gelukkig mag ik daar nog regelmatig van genieten tijdens een wandeling, lunch of etentje. Deze bourgondische meid verblijd je altijd met je kookkunsten die met gemak tippen aan de lobster roll in San Diego ;). Samen rondstruinen door de kilometers lange poster hallen, verdwalen tussen alle parallelle sessies, maar vooral ook alle uitstapjes in San Diego en ons waanzinnige huis aan Mission bay waren écht een onvergetelijke ervaring! Verdwalen doe je niet meer en je zeiksnor is ook aanzienlijk getrimd, want je hebt je plek helemaal gevonden als docent aan de UVA, heel fijn om te zien. *Anne, Roderick, Sybren* en *Marijn*, bedankt voor alle gezelligheid op werk, conferenties en daarbuiten. Het best uitgewerkte experiment tijdens mijn PhD waren de wine & cheese avonden, wat hebben we gelachen! *Anne* en *Roderick*, bedankt voor de leerzame werkbesprekingen, ik heb veel geleerd van jullie toffe projecten. Te gek om te zien dat jullie je wetenschappelijke talent en enthousiasme nu toepassen in een postdoc, veel succes en al het beste voor de toekomst. *Sybren*, the one and only, je bent een uniek persoon, maar in de beste zin van het woord. Altijd helemaal jezelf, een tikkel(tje) cynisch, maar met een heel goed hart. Bedankt ook voor je aanmoediging, ik ben eindelijk begonnen met rijlessen ;). Hopelijk kruisen onze wegen nog en wie weet zelfs achter het stuur. *Marijn*, bedankt voor je oprechte interesse en je enthousiasme in zo ongeveer alles wat los en vast zit. Ready to take off, zet jij je carrière voort, heel veel succes met je droombaan. *Klara*, jij bent altijd zo vriendelijk en betrokken. Zo fijn dat je altijd de tijd nam om te vragen hoe het met mij ging, bedankt hiervoor! *Daphne*, bedankt voor je gezellige inzet voor het departement en de IB, vele uitjes en borrels zijn te danken aan jou. Veel succes met je PhD! *Eugene, Wilco* and *Mithila* thank you for all the support and valuable input during my time as a master and PhD student. *Amélie*, an excellent and fun scientist that knows how to enjoy a good wine, beer or cheese. You are prove that scientists are not (or don't have to be) boring! Thank you for the good conversations and support. I am so excited that you started your own lab in Amsterdam and I cannot wait to see what the future will bring, they are so lucky to have you! Lets keep sharing our knowledge and love for beers. *Robin*, uitbundig en vrolijk of juist volledig in gedachten verzonken kwam ik je altijd tegen in de gangen van het Kruyt. Je bent écht een fijn en authentiek persoon, en daar bovenop een echte doorzetter en omdenker. Het is ook altijd gezellig en goed om even bij te kletsen als ik je tegen het lijf loop op de Burgemeester Reigerstraat of in de moestuin. En dat gebeurt heel regelmatig, dus ik zeg: tot snel! *Jessica*, wat heb jij een indrukwekkend PhD portfolio. De afgelopen jaren heb je ontzettend hard gewerkt en het is goed te zien dat je nu even een pauze pakt om vervolgens je verdere dromen weer na te jagen. Ik heb ook genoten van het samen organiseren van de labouting, dankjewel hiervoor. *Liu*, I really appreciate your kind and funny personality, all the best for you and your family. *Martin*, bedankt voor je altijd enthousiaste bijdrage aan werkbesprekingen. Je passie voor de wetenschap weet je altijd goed over te brengen en ik weet zeker dat je nog vele jonge onderzoekers zult motiveren en inspireren. *Lotte* en *Carlijn*, jullie vrolijkheid werkte altijd zeer aanstekelijk. Ik wens jullie veel succes met de afronding van je PhD, maar met jullie inzet en doorzettingsvermogen komt dit helemaal goed. *Cynthia*, bedankt voor je support en goede gesprekken. Ik wens je het allerbeste voor de toekomst. *Nazmiye, Chiung-Yi* and *Dipti*, you are such intelligent scientists and above all always so kind and considerate. *Chiung-Yi*, thank you for taking on the challenge of bouldering with me. Best wishes for the future. *Ate, Jian, Marvin, Hai Yin, Elske, Katerina, Sara, Hugo, Giel, Josiah, Janine, Malina, Funso, Joyce, Boris, Emma, Milena, York,*



Peter Jan, Babet, Fangrui, Ruddi, Eitan, Amol, Ankit, Chao, Derk, Ha, Mai Dan, Chun Hei and Max, thank you for all the fun and support!! *Margriet, Sofia, Olga, Philipp, Laura, Elena, Eliana, Kai, Inés, Marta, Maud, Riccardo, Marleen, Sam and Ivar* you have made me feel very appreciated and welcome, first as a student and later when I started my PhD. *Marina, Petra, Bas, Desiree and Max*, thank you for making me feel part of the group and for all the valuable input during the shared work discussions. *Gabriela*, thank you for sharing all the tips and tricks on figure making and it was really fun to have you as an office mate. *Dieudonné* and *Cátia*, the neuron culture gurus! I always admired your passion for science and it is fantastic to see you both continued in science. *Dieudonné*, hopelijk heb je het ons inmiddels vergeven dat het tussen deurtje altijd op een kiertje stond ;).

I greatly enjoyed all the collaborations and valuable input from outside the department. *Paul* and *Renata*, it was my pleasure to contribute to your study on a new cerebral organoid model that innately develops microglia, thank you for the fun and fruitful collaboration. *Thomas Blanpied*, thank you for the discussions, critical reading of chapters 2 and 4 and the great fun at SfN, San Diego. I highly admire your work and am fortunate you mentored my mentor. *Eline Mertens, Rogier Poorthuis, Fred de Winter, Joost Verhaagen and Frank Meye*, thank you for joining team ORANGE and your fantastic contributions.

Wat is het fijn om lieve vrienden en familie om je heen te hebben die je steunen en motiveren tijdens je promotie traject. Samen genieten van het weekend vol met etentjes en uitstapjes, vakanties, spontane avondjes, naar het park of de speeltuin – even niet aan werk hoeven denken, zijn zo belangrijk voor de juiste balans. Lieve vriendinnen van de jaarclub, lieve *Aimee, Alinda, Akke, Bianca, Djoeke, Esmee, Eline, Floor, Juliette, Maartje, Sarah* en *Sophie*, 12 geweldige meiden, 12 jaar aan vriendschap en 12 jaar aan hoogtepunten. Bedankt voor de clubavonden op dinsdag, de etentjes, feestjes en festivals en bovenal de geweldige reizen die we samen hebben gemaakt. Bedankt voor alle mooie momenten, maar ook voor een luisterend oor om hoogte- en dieptepunten mee te delen. Stuk voor stuk zijn jullie ambitieuze meiden, doorzetters en niet bang om nieuwe avonturen aan te gaan. Misschien niet eens bewust, maar doordat we dit met elkaar delen motiveren we elkaar in het bereiken van onze doelen. Voor mij zijn jullie een bron van inspiratie. *Akke*, bedankt dat ik bij jou altijd helemaal mezelf kan zijn, dat je onaangekondigd op mijn stoep staat en ik altijd bij je terecht kan. Lieve *Cheryl*, lieve vriendin en oud-huisgenoot, bedankt voor alle mooie momenten. Op de grond van het lachen chips vretend na een avondje stappen, alle fratsen en avonturen op de vereniging, maar ook alle goede gesprekken en het delen van lief en leed. Allemaal dierbare momenten, het maakt niet uit hoelang we elkaar even niet gezien hebben, wij begrijpen elkaar. Bedankt hiervoor! *Moritz* en *Sandra*, wat hebben wij een te gekke tijd beleefd samen in San Diego en ik ben heel blij dat we elkaar nog steeds opzoeken. *Moritz*, op mijn eerste dag in SD leerde ik je kennen op een feestje in mijn nieuwe appartement. Kapot van de vlucht, ben ik met mijn laatste energie toch nog aangesloten bij de feestvreugde en wat ben ik daar achteraf blij mee. We kwamen erachter dat we super veel gemeen hadden en ik heb echt genoten van alle taco Tuesdays, feestjes en lunch breaks op de campus van UCSD. En hoe leuk dat ik de matchmaker ben geweest tussen jou en *Sandra*, jullie zijn een geweldig en knap stel! Vrienden van de JC A en +I, bedankt voor alle borrels, feestjes en festivals, een heerlijke uitlaatklep! Bijzonder om onderdeel te zijn van zo'n hechte vriendengroep. *Peter* en *Jean*, jullie oprechte betrokkenheid is echt ontzettend waardevol, dankjewel!

Lieve familie, ook al is het vaak maar moeilijk uit te leggen wat ik nou precies doe, jullie stonden altijd paraat als er mijlpalen gevierd moesten worden of om mij aan te moedigen na een tegenslag. *Paul* en *Ineke*, vanaf het begin heb ik mij welkom gevoeld bij jullie. Altijd betrokken, geïnteresseerd en begaan. Bedankt voor de goede gesprekken en interesse in mijn onderzoek. Geweldig om te zien hoe fijn Mila het heeft bij jullie. Jullie vangen haar altijd met ontzettend veel liefde op en ik ben heel blij dat ze zulke fantastische grootouders heeft. Lieve *Iris*, *Davy*, *Lance*, *Suzan*, *Tim*, *Nienke*, *Nick* en *Lucienne*, jullie zijn hele fijne mensen en ik waardeer jullie enorm. En dan de crème de la crème van de familie natuurlijk, de heerlijk kids *Robin*, *Riley* en *Yari*, fantastisch om jullie te zien opgroeien en te zien hoe leuk jullie met Mila spelen, maar ook veel van elkaar leren.

Lieve *Lisa*, sèssstrrrra, waar moet ik beginnen? Er zijn geen woorden die kunnen omvatten hoeveel ik om je geef, hoe ontzettend trots ik op je ben en hoezeer ik altijd onder de indruk ben van alles wat je bereikt. Je bent lief, betrokken, intelligent, geweldig, lekker eigenwijs en heerlijk jezelf. Familie kies je niet uit, maar ik had mij geen beter zusje kunnen wensen. We zijn elkaars uitlaatklep, kunnen elkaar alles zeggen, even flink ruzie maken maar het ook meteen weer bijleggen, samen huilen van het lachen, ga zo maar door. We zijn huisgenootjes en collega's geweest, hebben mooie reizen gemaakt samen met pap en mam, maar ook nog vele city trips met z'n tweetjes, bedankt voor alle mooie momenten samen! Ik koester onze band enorm en het is dan ook niet voor niets dat je de peet tante bent van onze kleine meid Mila. *Nick*, het is ontzettend fijn je bij de familie te hebben. Oder het genot van lekker eten en een (2, 3 of 4..) goed glas wijn hebben we elkaar al goed leren kennen en mooie ervaringen gedeeld. Jullie zijn een mooi stel en vormen een lief gezinnetje met pup Teun. Lieve *Guus* en *Jenny*, het voelt bijna onpersoonlijk om jullie bij naam te noemen want voor mij is het altijd pap en mam. Maar anoniem blijven was geen optie, want mijn grootste dank gaat uit naar jullie. Jullie onvoorwaardelijke liefde en steun hebben ervoor gezorgd dat ik mijn doel heb bereikt en ga promoveren tot doctor. Jullie zijn mijn grootste voorbeeld en alles wat ik van jullie geleerd heb probeer ik toe te passen en door te geven. Ik kan altijd op jullie terugvallen en kom altijd helemaal tot rust als ik bij jullie ben. Jullie zijn mijn meest trouwe supporters en jullie blijven mij verrassen met jullie vrijgevigheid in meerdere opzichten. Iets wat door jullie vaak als vanzelfsprekend wordt beschouwd, maar ik heel speciaal vind. Jullie vertrouwen in mij geeft mij zoveel zelfvertrouwen en daardoor durf ik mijzelf uit te dagen en nieuwe avonturen aan te gaan. Al voordat Mila fan was van Pippi Langkous werd de uitspraak "Ik heb het nog nooit gedaan dus ik denk dat ik het wel kan" al vaak aangehaald. Een mooi motto. Mijn liefde voor kaas, lekker eten en wijn heb ik niet van een vreemde. De ontelbare etentjes, zowel binnen- als buitenshuis, met of zonder wijn arrangementen leveren altijd de meest gezellige avonden op. Als we de slappe lach hebben gehad is wat mij betreft de avond helemaal geslaagd! Ik glimlach ook écht van oor tot oor als ik zie hoe gek jullie zijn op Mila. Heerlijk hoe ze in jullie tuin lekker kan rondstruinen, een tuin die jullie inmiddels hebben omgebouwd tot waar speelparadijs. Samen lachen als ze weer de meest gekke fratsen uit haalt, aandachtig luisteren naar de uitvoerige gesprekken die ze voert, ons hand voor de mond slaan als ze weer oh zo ondeugend is, ons verbazen als ze iets nieuws geleerd heeft of genieten van de genegenheid die ze bij je zoekt met haar knuffeldoekje en speen. Samen genieten van deze mooie momenten is zo fijn en waardevol! Bedankt dat jullie zulke geweldige ouders en grootouders zijn! Tijdens het schrijven van dit dankwoord ben ik mij ook maar weer al te bewust geworden van mijn eigenaardige eigenschap om te gooien

met gezegdes en spreekwoorden, terwijl ik er ook altijd in slaag om ze *nét* (oké toegegeven, soms ook volledig) verkeerd te zeggen of een creatieve combinatie van twee te maken. Dit leidt altijd tot hysterisch gelach aan jullie kant en vooral ook tot herhaling van mijn mooie creatie als een ander het niet goed gehoord heeft of later nog even opgerakeld wordt door de één als dit niet in het bijzijn was van de anderen. Gelukkig was google mijn beste vriend tijdens het schrijven van dit dankwoord en heb ik nu af en toe hard om mezelf kunnen lachen. Ach, een dag niet gelachen is een dag niet geleefd ;).

Lieve *Floris*, jij bent mijn rots, mijn anker in de branding. Nee alle gekheid op een stokje (gniffel), bedankt dat je mij aan mijn jas terug de eetzaal van Unitas in trok toen ik erop stond te vertrekken en mij vervolgens nooit meer hebt losgelaten. Bedankt voor alle gratis kaassoufflés toen je koningsnacht organiseerde, een avond om nooit meer te vergeten, gelukkig hebben we de foto's nog. Bedankt dat je niet bent afgeschrikt en mee ging in mijn enthousiasme en na 2 maanden al samen met mij naar Barcelona ging en de nog vele tripjes en reizen die daarop volgden. Bedankt dat je mijn familie ziet als je eigen, bedankt dat ik bij jou helemaal mezelf kan zijn, bedankt dat je mijn zorgen altijd in perspectief kunt zetten en bedankt dat je mij altijd motiveert en stimuleert in al mijn keuzes en ambities. Bedankt voor je leergierigheid, interessante discussies en dat ik altijd een wandelende Wikipedia en encyclopedie heel dichtbij me heb. Bedankt dat je altijd in mij gelooft, ook als ik dat zelf niet doe en voor alle aanmoediging tijdens mijn promotietraject. Bedankt voor wie je bent. 11 keer bedankt, omdat we 11 jaar samen zijn en 11 inmiddels ons geluksgetal is. Ik kan eindeloos door gaan, maar tot slot dan de 11e en laatste, bedankt dat je de liefste, leukste, gekste, zorgzaamste en allerbeste papa bent voor ons mupke Mila. Liefste *Mila*, jij bent mijn grootste hoogtepunt in mijn klim naar de top. Mila Lily Hamel, geboren op 11-11-2020, de lelie op de achterkant van mijn proefschrift staat symbool voor jou. Ik ben nu al zo trots op wie je bent, maar ook tot wie jij je zal ontplooiën en wie je bent als je oud genoeg bent om dit te lezen. Ik beloof je altijd te steunen en ondersteunen in het zoeken naar je eigen uitdagingen en avonturen. Je af en toe los te laten, hoewel ik mij dat nu nog niet kan voorstellen, om op het randje te leven, zoals mijn ouders, jouw opa en oma, dat ook altijd hebben gedaan. Jouw mama zijn is het mooiste en meeste overweldigende wat mij ooit is overkomen. Ik ben zo dankbaar dat jij in ons leven bent en alle avonturen die we samen als gezin beleven en nog gaan beleven. Daarom, lieve *Floris* en *Mila*, draag ik dit proefschrift op aan jullie.

Hora est!

Nicky Scheefhals



